frontiers | Research Topics

Cell network in antitumor immunity of pediatric and adult solid tumors

Edited by
Ombretta Melaiu and Silvia Pesce

Published in
Frontiers in Immunology

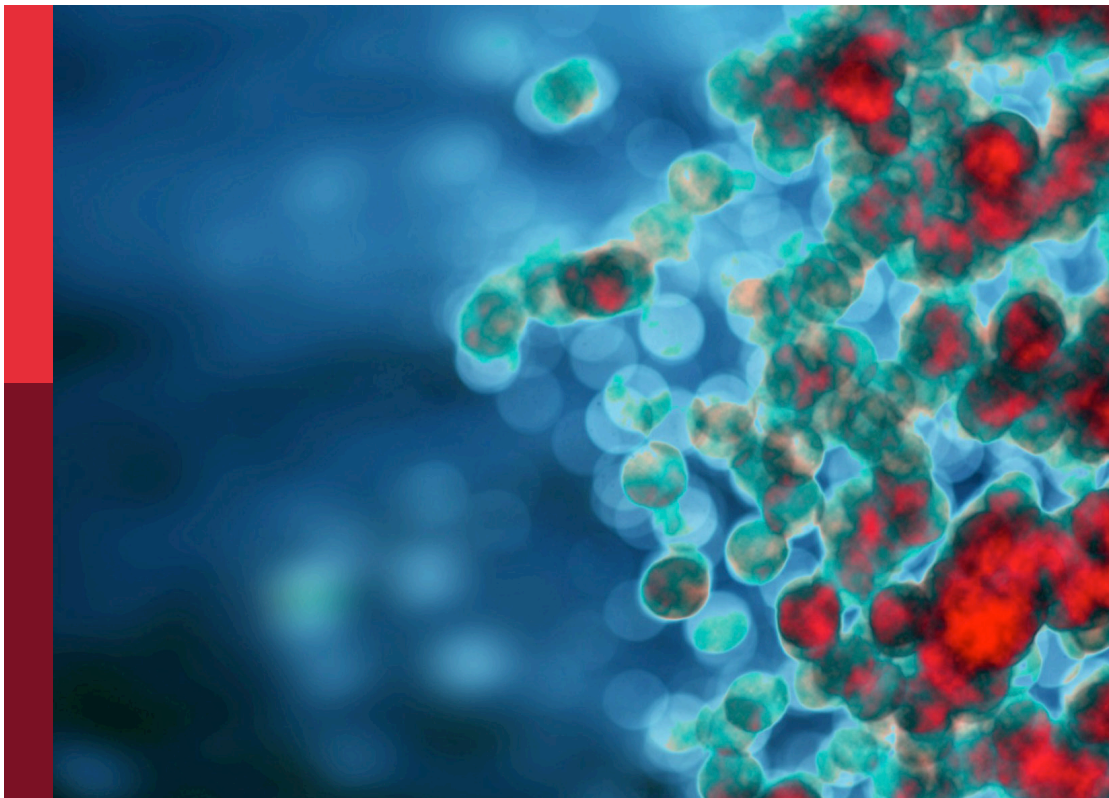

ISSN 1664-8714
ISBN 978-2-8325-2969-0
DOI 10.3389/978-2-8325-2969-0

About Frontiers

Frontiers is more than just an open access publisher of scholarly articles: it is a pioneering approach to the world of academia, radically improving the way scholarly research is managed. The grand vision of Frontiers is a world where all people have an equal opportunity to seek, share and generate knowledge. Frontiers provides immediate and permanent online open access to all its publications, but this alone is not enough to realize our grand goals.

Frontiers journal series

The Frontiers journal series is a multi-tier and interdisciplinary set of open-access, online journals, promising a paradigm shift from the current review, selection and dissemination processes in academic publishing. All Frontiers journals are driven by researchers for researchers; therefore, they constitute a service to the scholarly community. At the same time, the *Frontiers journal series* operates on a revolutionary invention, the tiered publishing system, initially addressing specific communities of scholars, and gradually climbing up to broader public understanding, thus serving the interests of the lay society, too.

Dedication to quality

Each Frontiers article is a landmark of the highest quality, thanks to genuinely collaborative interactions between authors and review editors, who include some of the world's best academicians. Research must be certified by peers before entering a stream of knowledge that may eventually reach the public - and shape society; therefore, Frontiers only applies the most rigorous and unbiased reviews. Frontiers revolutionizes research publishing by freely delivering the most outstanding research, evaluated with no bias from both the academic and social point of view. By applying the most advanced information technologies, Frontiers is catapulting scholarly publishing into a new generation.

What are Frontiers Research Topics?

Frontiers Research Topics are very popular trademarks of the *Frontiers journals series*: they are collections of at least ten articles, all centered on a particular subject. With their unique mix of varied contributions from Original Research to Review Articles, Frontiers Research Topics unify the most influential researchers, the latest key findings and historical advances in a hot research area.

Find out more on how to host your own Frontiers Research Topic or contribute to one as an author by contacting the Frontiers editorial office: frontiersin.org/about/contact

Cell network in antitumor immunity of pediatric and adult solid tumors

Topic editors
Ombretta Melaiu — University of Rome Tor Vergata, Italy
Silvia Pesce — University of Genoa, Italy

Topic coordinator
Elin Bernson — University of Gothenburg, Sweden

Citation
Melaiu, O., Pesce, S., eds. (2023). *Cell network in antitumor immunity of pediatric and adult solid tumors*. Lausanne: Frontiers Media SA.
doi: 10.3389/978-2-8325-2969-0

Table of contents

frontiers | Frontiers in Immunology

TYPE Editorial
PUBLISHED 06 July 2023
DOI 10.3389/fimmu.2023.1246695

OPEN ACCESS

EDITED AND REVIEWED BY
Sabrina Giglio,
University of Cagliari,
Italy

*CORRESPONDENCE
Silvia Pesce
silvia.pesce@unige.it
Ombretta Melaiu
Ombretta.Melaiu@uniroma2.it

†These authors have contributed equally to this work

RECEIVED 24 June 2023
ACCEPTED 28 June 2023
PUBLISHED 06 July 2023

CITATION
Pesce S and Melaiu O (2023) Editorial: Cell network in antitumor immunity of pediatric and adult solid tumors.
Front. Immunol. 14:1246695.
doi: 10.3389/fimmu.2023.1246695

Editorial: Cell network in antitumor immunity of pediatric and adult solid tumors

Silvia Pesce[1*†] and Ombretta Melaiu[2*†]

[1]Department of Experimental Medicine and Centre of Excellence for Biomedical Research, University of Genoa, Genoa, Italy, [2]Department of Clinical Sciences and Translational Medicine, University of Rome Tor Vergata, Rome, Italy

KEYWORDS

tumor microenvironment (TME), tumor-infiltrating immune cells, biomarkes, tumor immunity, immunotherapy

Editorial on the Research Topic
Cell network in antitumor immunity of pediatric and adult solid tumors

The tumor microenvironment (TME) is a highly structured ecosystem composed of cancer cells and a variety of non-cancer cells embedded in an altered and vascularized extracellular matrix. A rich diversity of immune cells, cancer-associated fibroblasts (CAFs), and endothelial cells, previously considered only bystanders in tumorigenesis, are now recognized as key players in neoplasms and thus represent attractive targets for prognostic and therapeutic purposes (1). Tumor progression, for example, is associated with a decrease in cytotoxic T and NK cells, an increase in exhausted $CD8^+$ T cells (2), immunosuppressive $CD4^+$ $FOXP3^+$ Tregs (3), and regulatory B cells (4). In contrast, dendritic cells (DCs) show defective maturation and function (5). Along with immune populations, CAFs are a dominant component of many cancer types. The activation of CAFs in the TME can be the result of several mechanisms, including exposure to inflammatory mediators, changes in extracellular matrix (ECM) composition and stiffness, and altered metabolites (6). In this regard, the crucial role of deregulated metabolic demands in generating a TME supportive of neoplastic progression is becoming increasingly clear (7). Importantly, all these aspects have implications for the efficacy of immunotherapy (as well as chemotherapy and radiotherapy), and a major effort is underway to identify combinatorial therapeutic strategies that take advantage of inhibitors and/or modulators of the various TME components.

This Research Topic was devised to update our current knowledge on the complex interconnectedness of the TME and its influence on disease progression and response to therapy. We have collected a series of articles that provide us with in-depth evaluations of the role of different types of immune and stromal cells in the control of solid tumors, novel immunotherapeutic strategies, and multi-omics approaches that offer further insights into this field. In brief, this Research Topic includes seven original research papers, three case reports, one perspective and two reviews of the current literature.

In recent years, a growing number of studies have investigated the key characteristics of NK and T cells in different disease settings. In this context, the work of Caforio et al. has identified Che1 as a key protein able to promote the viability of tumor cells, but also the expression of the Nectin-1 ligand, resulting in an impaired killing activity of NK cells.

These results suggest how the identification of targets with a dual function, i.e., cancer promoter, and modulator of the immune response, could lead to much more potent therapeutic strategies for eradicating a malignancy. In line with this, Bergantini et al. better explored the pathogenesis of sarcoidosis by analyzing the frequency and phenotype of NK and T cells in two different districts: bronchoalveolar lavage (BAL) and peripheral blood (PB). The authors showed that compared to PB, BALs were mainly infiltrated by a subset of CD56brightCD16neg NK cells and of memory effector T cells. In addition, the more mature BAL-NK cell subset (CD56dim/negCD16$^+$) expressed higher levels of PD1 and activation markers, such as NKp44, CD69 and CD25.

The partially unsuccessful use of immune checkpoint inhibitors (ICIs) in patients with poorly immunogenic neoplasms and highly immunosuppressive TME (8) has led to a growing interest in better characterizing the role of DCs, heterogeneous population playing a central role in the activation and regulation of all immune responses. A detailed evaluation of glioma infiltrating DC subpopulations and their activating/tolerogenic profile was performed by Carenza et al. Their results showed a significant reduction of circulating DCs and a concomitant intratumoral recruitment of all DC subpopulations, which were however functionally impaired. Their drastic functional impairment was even more evident in glioma patients undergoing perioperative steroid treatment, usually administered to control peritumoral edema. This suggests the use of alternative therapeutic strategies to control this symptom.

It is well known that also the intratumoral spatial organization of immune cells and their crosstalk with other cellular components play a crucial role in determining prognosis and response to immunotherapy in cancer patients (9). Timperi et al. reviewed the suppressive crosstalk between newly identified macrophages and CAF subpopulations in a variety of solid tumors and proposed targets that could be used as potential novel therapeutic approaches. Concurrently, the importance of tertiary lymphoid structures (TLS) is another area of great interest (10). Two articles in our Research Topic addressed their role in breast and lung cancers, respectively. A first remarkable observation concerns the differential impact of TLSs maturation status on tumour progression. Indeed, a high number of mature TLSs, as shown by Wang et al., is associated with a better prognosis of breast cancer patients, suggesting that TLSs are privileged sites for local lymphocyte differentiation and antigen presentation. In contrast, Zhao et al. associated the abundance of immature TLS with lack of response to immunotherapy in a lung adenocarcinoma (LUAD) patient, characterized by high FOXP3$^+$ regulatory T cells and increasing levels of the circulating checkpoint proteins BTLA, TIM-3, LAG-3, PD-1, PD-L1, and CTLA4. Consistent with previous findings, Cai et al., in evaluating the efficacy of neoadjuvant chemo-immunotherapy compared with chemotherapy alone, showed that only patients with increased TLS and concomitant infiltration of B and T cells were able to undergo major pathologic response (MPR) when treated with chemotherapy alone. In the remaining cases, the addition of ICIs to chemotherapy was associated with a significantly higher rate of MPR together with a major abundance of CD8$^+$ T cells in the tumor stroma and M1 macrophage density in the tumor center. Interestingly, the importance of adding ICIs has been demonstrated not only in the neoadjuvant setting, but also after multiple lines of adjuvant treatment, as reported by Zhang et al., in a patient with small cell lung cancer.

In cancer immunotherapy, in addition to ICIs designed to augment natural immune responses, other types of neoplasms are being treated with chimeric antigen receptors (CARs), designed to induce new immune responses directed against tumor-expressed targets (11). For CAR T cells to be effective, bridging therapy is often required (12). Saldi et al. demonstrated that an extended radiotherapy approach is an excellent strategy to enhance the effect of CD19-directed CAR T-cell therapy, leading to a complete remission of the disease in a patient with relapsed/refractory diffuse large B-cell lymphoma. However, since the use of CAR T cells can lead to graft-versus-host disease (GvHD) and cytokine release syndrome, there is increasing interest in the engineering of NK cells, which have a higher safety profile. To date, NK cells have been engineered against various CARs or the chimeric NKG2D receptor and have shown promising results in preclinical and clinical models. In addition to NKG2D, other activating receptors may also yield encouraging responses. For example, Cifaldi et al. proposed the use of the never-before-explored DNAM-1 chimeric receptor engineered-NK cells. The authors provide a rationale predicting that this therapeutic tool has several strengths to consider: first and foremost, the fact that, unlike other constructs, NK cells engineered for DNAM-1 are able to specifically target tumor cells that express high levels of PVR and Nectin-2, while tolerating normal cells that usually express low levels of these ligands.

These latest studies highlight another important need: quickly identifying patients who may respond to one treatment over another. Many factors influence for example the effectiveness of immunotherapy, and few biomarkers have been developed so far to assess its benefit accurately (11). In this context, Huang et al. applied integrated analysis to develop a four genes-prognostic signature, called LATPS, for LUAD patients. The LATPS-low subgroup had better survival, and a greater chance of benefiting from immunotherapy, thus representing a promising prognostic tool with clinical utility. Similarly, by studying the role of lactate in LUAD TME, Shang et al. established a gene signature called “LaSig” that can predict survival and response to immunotherapy as well as to cisplatin, erlotinib, gemcitabine and vinblastine in these patients. Using single cell RNAseq data, Xie et al. showed that immune, stromal, and tumor cells of colorectal cancer patients share similar lipid metabolism during their terminal differentiation, that confers an immunosuppressive microenvironment. In addition, through the integration of scRNA-seq and mass-RNA-seq data, they built an immune and clinical risk model with high prognostic power. Finally, Rozenberg et al. reviewed the pathological mechanisms directly involved in the formation and pathogenesis of circulating heterotypic tumor cells (CTCs) emerging as prognostic and therapeutic markers in metastatic malignancies.

In summary, the papers included in this Research Topic represent the latest advances in the field of immuno-oncology. Based on these studies, we can believe and trust that in-depth

exploration of the TME promises to advance tumor treatment research in the next decade.

Author contributions

OM and SP: drafted the article, provided critical inputs, and corrected the manuscript. All authors contributed to the article and approved the submitted version.

Funding

This work was supported by funds from PRIN 2022 DD n. 104 - 02-02-2022 (2022ZFFALH).

Acknowledgments

We express our gratitude to all the authors who have contributed to this Research Topic and to the reviewers for their valuable work. We hope that the reader will find this Research Topic motivating and helpful.

Conflict of interest

The authors declare that the research was conducted in the absence of any commercial or financial relationships that could be construed as a potential conflict of interest.

Publisher's note

References

1. Bejarano L, Jordão MJC, Joyce JA. Therapeutic targeting of the tumor microenvironment. *Cancer Discov* (2021) 11:933–59. doi: 10.1158/2159-8290.CD-20-1808

2. Philip M, Schietinger A. CD8+ T cell differentiation and dysfunction in cancer. *Nat Rev Immunol* (2022) 22:209–23. doi: 10.1038/s41577-021-00574-3

3. Togashi Y, Shitara K, Nishikawa H. Regulatory T cells in cancer immunosuppression - implications for anticancer therapy. *Nat Rev Clin Oncol* (2019) 16:356–71. doi: 10.1038/s41571-019-0175-7

4. Laumont CM, Banville AC, Gilardi M, Hollern DP, Nelson BH. Tumour-infiltrating b cells: immunological mechanisms, clinical impact and therapeutic opportunities. *Nat Rev Cancer* (2022) 22:414–30. doi: 10.1038/s41568-022-00466-1

5. Wculek SK, Cueto FJ, Mujal AM, Melero I, Krummel MF, Sancho D. Dendritic cells in cancer immunology and immunotherapy. *Nat Rev Immunol* (2020) 20:7–24. doi: 10.1038/s41577-019-0210-z

6. Sahai E, Astsaturov I, Cukierman E, DeNardo DG, Egeblad M, Evans RM, et al. A framework for advancing our understanding of cancer-associated fibroblasts. *Nat Rev Cancer* (2020) 20:174–86. doi: 10.1038/s41568-019-0238-1

7. Dey P, Kimmelman AC, DePinho RA. Metabolic codependencies in the tumor microenvironment. *Cancer Discov* (2021) 11:1067–81. doi: 10.1158/2159-8290.CD-20-1211

8. Naimi A, Mohammed RN, Raji A, Chupradit S, Yumashev AV, Suksatan W, et al. Tumor immunotherapies by immune checkpoint inhibitors (ICIs); the pros and cons. *Cell Commun Signal* (2022) 20:44. doi: 10.1186/s12964-022-00854-y

9. Rozenblatt-Rosen O, Regev A, Oberdoerffer P, Nawy T, Hupalowska A, Rood JE, et al. The human tumor atlas network: charting tumor transitions across space and time at single-cell resolution. *Cell* (2020) 181:236–49. doi: 10.1016/j.cell.2020.03.053

10. Zhang Q, Wu S. Tertiary lymphoid structures are critical for cancer prognosis and therapeutic response. *Front Immunol* (2022) 13:1063711. doi: 10.3389/fimmu.2022.1063711

11. Melaiu O, Lucarini V, Giovannoni R, Fruci D, Gemignani F. News on immune checkpoint inhibitors as immunotherapy strategies in adult and pediatric solid tumors. *Semin Cancer Biol* (2022) 79:18–43. doi: 10.1016/j.semcancer.2020.07.001

12. Amini L, Silbert SK, Maude SL, Nastoupil LJ, Ramos CA, Brentjens RJ, et al. Preparing for CAR T cell therapy: patient selection, bridging therapies and lymphodepletion. *Nat Rev Clin Oncol* (2022) 19:342–55. doi: 10.1038/s41571-022-00607-3

frontiers in Immunology

CASE REPORT
published: 31 January 2022
doi: 10.3389/fimmu.2022.794217

Case Report: Sarcoid-Like Reactions and Tertiary Lymphoid Structures Following Dual Checkpoint Inhibition in a Patient with Early-Stage Lung Adenocarcinoma

Xiaoliang Zhao[1†], Dongsheng Yue[1†], Juanjuan Qian[2†], Lei Zhang[2], Jin Song[2], Bin Zhang[1], Chunmei Zhang[2], Leina Sun[1], Yuchen Ma[1], Henghui Zhang[3] and Changli Wang[1*]*

[1] Tianjin Medical University Cancer Institute and Hospital, Tianjin Key Laboratory of Cancer Prevention and Therapy, National Clinical Research Center for Cancer, Tianjin, China, [2] Department of Medicine, Genecast Biotechnology Co., Ltd, Wuxi, China, [3] Beijing Shijitan Hospital, and School of Oncology, Capital Medical University, Beijing, China

Immune checkpoint inhibitor-induced sarcoid-like reactions and tertiary lymphoid structures (TLSs) are increasingly recognized but rarely reported in the same patient. We report a patient with lung adenocarcinoma who displayed sarcoid-like reactions in intrathoracic lymph nodes and tertiary lymphoid structures in surgical tumor after neoadjuvant therapy with nivolumab plus ipilimumab. Pathological examination revealed 50% residual tumor cells after treatment, and the CT evaluation of the primary tumor showed a stable disease. The patient experienced a recurrence eight months after surgery. To identify immune correlates of the limited response to immunotherapy, we conducted genomic and transcriptional assays, multiplex immunoassay, and multiplex immunohistochemistry on the pre- and post-immunotherapy tumor, lymph node, and plasma samples. *TP53* R181C, *KRAS* G12C and *SMAD4* R361H were identified as driver mutations of the tumor. In addition to abundant infiltrated lymphocytes, immunotherapy induced high levels of inhibitory components in post-treatment tissue samples, especially the FOXP3$^+$ regulatory T cells in tumor and PD-L1 expression in the lymph node. Despite abundant TLSs in the post-treatment tumor, most TLSs were immature. Moreover, increasing levels of circulating checkpoint proteins BTLA, TIM-3, LAG-3, PD-1, PD-L1, and CTLA4 were observed during immunotherapy. Collectively, our observations revealed that high levels of immunosuppressive molecules in tumor, lymph nodes and/or in peripheral blood might indicate poor outcomes after immunotherapy, even in the setting of a patient with concurrent sarcoid-like reactions and tertiary lymphoid structures.

Keywords: sarcoid-like reaction, tertiary lymphoid structure, immune checkpoint inhibitor, tumor immune microenvironment, non-small cell lung cancer

OPEN ACCESS

Edited by:
José Mordoh, IIBBA-CONICET Leloir Institute Foundation, Argentina

Reviewed by:
Khaled Murshed, Hamad Medical Corporation, Qatar
Maya Gulubova, Trakia University, Bulgaria

***Correspondence:**
Changli Wang
wangchangli@tjmuch.com
Henghui Zhang
zhhbao@ccmu.edu.cn

†These authors have contributed equally to this work

Specialty section:
This article was submitted to Cancer Immunity and Immunotherapy, a section of the journal Frontiers in Immunology

Received: *13 October 2021*
Accepted: *11 January 2022*
Published: *31 January 2022*

Citation:
Zhao X, Yue D, Qian J, Zhang L, Song J, Zhang B, Zhang C, Sun L, Ma Y, Zhang H and Wang C (2022) Case Report: Sarcoid-Like Reactions and Tertiary Lymphoid Structures Following Dual Checkpoint Inhibition in a Patient with Early-Stage Lung Adenocarcinoma. Front. Immunol. 13:794217. doi: 10.3389/fimmu.2022.794217

INTRODUCTION

Immune checkpoint inhibitors (ICIs), while significantly improving survival in patients with multiple advanced cancers, are associated with a unique set of immune-related adverse events, including sarcoid-like reactions (SLRs). ICI-induced SLRs have been reported most commonly in patients with melanoma and lung cancer, and occur in intrathoracic locations (lung and/or mediastinal lymph nodes) and the skin (1). SLRs are histologically characterized as non-caseating granulomas without malignant cells. Patients may be asymptomatic or may have no severe manifestations, and the reactions can spontaneously resolve without specific treatment or ICI discontinuation (2, 3). The incidence of ICI-induced SLRs remains unclear as the reaction is easily mistaken for disease progression and clinicians usually have low awareness (4). However, SLRs are attracting increasing attention in the neoadjuvant setting for non-small cell lung cancer (NSCLC) due to their influence on clinical treatment planning of curative surgery. In NEOSTAR study, SLR, which was defined as nodal immune flare, was found in 16% (7/44) of patients with early-stage NSCLC after neoadjuvant ICI therapy (5). Another phase II trial reported that 13% of 15 patients with resectable NSCLC developed SLRs after inductive pembrolizumab monotherapy (6). ICI-induced SLRs have been reported to associate with favorable therapeutic response in patients with melanoma (7, 8), while there is little known about the association of SLRs with immunotherapy outcomes in lung cancer patients.

Tertiary lymphoid structures (TLSs) are ectopic lymphoid aggregates that developed at chronic inflammatory sites in non-lymphoid tissues including tumors (9). Mature TLSs are characterized by a T-cell zone and a germinal center with proliferating B cells. Across a variety of tumors, the presence of TLSs is associated with favorable clinical outcomes, despite several reports describing negative prognostication of TLSs (10, 11). The prognostic value of TLSs in NSCLC has been reported in several studies since a decade ago. The high density of follicular B cells or mature dendritic cells in TLSs, and high density of TLSs, were associated with favorable prognosis in NSCLC patients (12–15). Moreover, B cells and mature TLSs are demonstrated to predict therapeutic efficacy of immunotherapy across different tumor types (16–19), arousing the interest in the artificial induction of TLSs in tumor therapy. And in the post-treatment samples of non-small cell lung cancer, the presence of TLSs with a germinal center was shown to correlate with the pathological response to neoadjuvant anti-PD-1 therapy (20). However, the formation mechanism and antitumor effect of TLSs deserve further exploration, and standardized evaluation methods need to be established before TLSs can be used to guide clinical decisions.

Here we report a stage IB NSCLC patient with SLRs and TLSs induced by neoadjuvant nivolumab plus ipilimumab. We examined the immune microenvironment of the tumor and lymph nodes, as well as the dynamics of immune-related proteins in peripheral blood, to reveal the immune features of the patient and explore correlates of the limited response to immunotherapy.

Case Presentation

A 54-year-old non-smoking Chinese woman was referred to our hospital because of a mass which was incidentally discovered by radiological examination during a routine medical checkup. She had no cough, chest tightness or chest pain, and no other abnormalities were found. The patient reported no history of autoimmune disease or family history of tumor. Positron emission tomography-computed tomography (PET-CT) revealed a 39 mm×45 mm×45 mm mass with abnormally increased intake of 18F-fluorodeoxyglucose. And CT-guided biopsy confirmed adenocarcinoma. The patient was diagnosed with stage IB (cT2N0M0) lung adenocarcinoma in August 2018 (**Figure 1A**). Then she started to receive neoadjuvant immune checkpoint inhibitors (ICIs) nivolumab (3 mg/kg, days 1, 15, 29) plus ipilimumab (1 mg/kg, day 1). No immune-related adverse events were found during immunotherapy. One month after the last dose of nivolumab, CT scan revealed enlargement of the primary tumor and multiple lymph nodes (**Figure 1B**). PET-CT showed that the primary lesion diameter increased by approximately 5% compared with that at baseline, and the standard uptake value (SUV) increased from 7.6 to 10.5. Increased hypermetabolic activity was observed in the superior mediastinal vascular space, mediastinal right brachial vein and posterior vena cava, right pulmonary artery, para-aortic arch, subcarina and both pulmonary hila. Preoperative examination showed that the patient's cardiopulmonary function was normal and suitable for surgery. One week later, the patient underwent left upper lobectomy and radical lymph node dissection through video-assisted thoracic surgery (VATS). The size of the excised tumor was 45 mm×43 mm×37 mm, and a total of 16 lymph nodes were removed. One month after surgery, the patient started to receive two cycles of routine chemotherapy, pemetrexed plus carboplatin, every 3 weeks. During chemotherapy, the patient experienced persistent radiating and dull pain in the left posterior chest. Aortic dissection (Stanford B) was found on the first postoperative CT scan after chemotherapy and then the patient underwent endovascular stent-graft placement. However, another aortic dissection in the abdominal aorta was found on the second follow-up CT scan three month later and the patient refused surgery. Eight months after surgery, the patient developed a lung metastasis (**Figure S1**) and began to receive treatment at a local hospital.

Histopathological examination of the resected tumor revealed advanced lung adenocarcinoma, a relatively low ratio of viable tumor cells (50%) and large numbers of infiltrating lymphocytes (**Figure 1B**); all resected lymph nodes were negative for metastases but with extensive histiocytic nodular hyperplasia

Abbreviations: ICI, immune checkpoint inhibitor; SLR, sarcoid-like reaction; TLS, tertiary lymphoid structure; NSCLC, non-small cell lung cancer; PET-CT, positron emission tomography-computed tomography; MAF, mutant allele frequency; mIHC, multiplex immunohistochemistry; NK cell, natural killer cell; Treg cell, regulatory T cell; PD-1, programmed cell death 1; PD-L1, programmed cell death ligand 1; CTLA-4, cytotoxic T-lymphocyte antigen 4; TIM-3, T cell immunoglobulin and mucin domain-containing protein 3; BTLA, B and T lymphocyte attenuator; LAG-3, lymphocyte-activation gene 3; GC, germinal center.

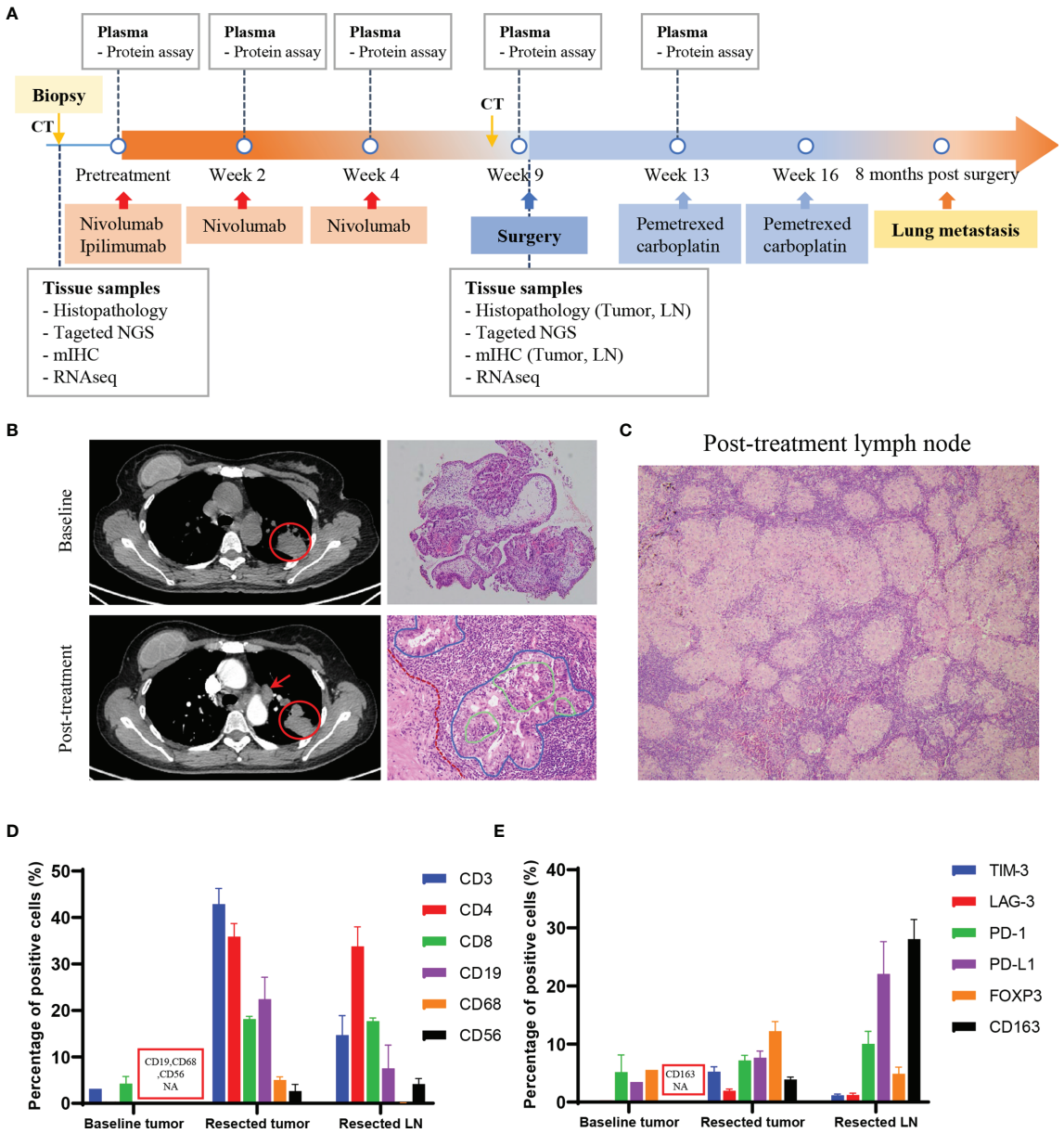

FIGURE 1 | Treatment course of the patient with lung adenocarcinoma. **(A)** Time line of clinical events, along with the time points of sample collection and analyses. **(B)** CT images showed the primary tumor (red circle) and lymph node (red arrow), and the pathological images of the tumor pre- and post-immunotherapy treatment. Red dotted line: fibrosis in the tumor stroma; blue solid line: cancer nest; green solid line: lymphocytes infiltrating into the cancer nest. Magnification: 100×, 200×. **(C)** Pathological image of the post-treatment lymph node showed non-caseating granulomas. Magnification: 100×. **(D, E)** Quantitative results of immune cell markers **(D)** and regulatory or inhibitory markers **(E)** in the baseline biopsy tumor (pre-treatment), resected tumor and resected lymph node (post-treatment) by mIHC assay. For bar graph: *error bar* represents *SEM*. CT, computed tomography; NGS, next-generation sequencing; mIHC, multiplex immunochemistry; LN, lymph node; NA, not available.

(**Figure 1C**). A diagnosis of sarcoid-like reaction in lymph nodes was made for this patient. Driver mutations associated with tumorigenesis were examined by next-generation sequencing (NGS) (**Supplementary Methods**). *TP53* R181C, *KRAS* G12C and *SMAD4* R361H were identified, with the mutant allele frequency (MAF) of 6.9%, 5.5% and 6.2% in the resected tumor and 26%, 23.4% and 34.4% in the tissue obtained by tumor biopsy prior to the onset of immunotherapy. *EGFR* L858R was found in the baseline tumor, but the MAF was 0.59%. *ALK* and *ROS1* rearrangements were not found.

Profiling of Local and Peripheral Immune Characteristics

The local immune microenvironment was explored by multiplex immunohistochemistry (mIHC) assay using the Opal seven-color IHC Kit (PerkinElmer, USA). With three staining panels,

we analyzed the multiple immune components in the pre- and post- immunotherapy tissue samples, including T lymphocytes (CD3, CD4, CD8), B lymphocytes (CD19), macrophages (CD68), natural killer cells (NK cells, CD56) and a series of regulatory (FOXP3, CD163) or inhibitory (PD1, PD-L1, TIM-3, LAG-3) markers (**Figure S2**). For surgical specimens, more than 10 fields of view in 200× magnification of each tissue slide were selected to calculate percentage of the positive cells in all nucleated cells. The average density of positive cells was shown in **Table S1**. Detailed methods were provided in the **Supplementary Material** (**Supplementary Methods**). The quantitative results showed that the post-treatment tumor and lymph node were infiltrated with a large number of lymphocytes (**Figure 1D**) and rich in high levels of inhibitory molecules or checkpoint proteins (**Figure 1E**). Of note, among the inhibitory markers, the $FOXP3^+$ regulatory T cells (Treg) accounted for one-third of helper T cells in tumor tissue (**Figures 1D, E**). Obviously, immunotherapy induced an inflammatory environment in the primary tumor compared to baseline (**Figure 2A**). According to the high infiltration of B lymphocytes, we further observed tertiary lymphoid structures (TLSs) in the post-treatment tumor, characterized by a dense aggregation of $CD3^+$ T lymphocytes and $CD19^+$ B lymphocytes (**Figure 2B**). We scanned the whole tissue section on a hematoxylin and eosin-stained slide and counted the TLSs (**Figure 2C**). A total of 31 TLSs were found, with a density of 0.27 TLS per mm^2, accounting for 3.3% of the whole tissue area. However, there were very few TLSs with a germinal center (GC), suggesting that most TLSs were immature. And we observed high expression of checkpoint proteins, especially PD-L1, in lymph node tissue after immunotherapy (**Figures 2D, E**). The expression of PD-L1 in baseline tumor and post-treatment tumor was relatively low, but was abnormally high in the post-treatment lymph node. Based on the immune microenvironment of the tumor and lymph node, it seems difficult to infer whether immunosuppressive factors predominated in the intense combat between immune system and tumor triggered by ICIs.

Then we explored the changes of peripheral immune factors. Blood samples were collected prior to each cycle of immunotherapy and the radical surgery, and one month after surgery as shown in **Figure 1A**. A total of plasma 59 proteins, including cytokines, chemokines, growth factors, and checkpoint proteins, were simultaneous detected by two ProcartaPlex panels with sandwich ELISA based multiplex immunoassays (**Supplementary Methods**). The results show that all detectable checkpoint proteins were increased during the neoadjuvant immunotherapy (**Figure S3**), such as B and T lymphocyte attenuator (BTLA), T cell immunoglobulin and mucin domain-containing protein 3 (TIM-3), lymphocyte-activation gene 3 (LAG-3), programmed cell death 1 (PD-1), programmed cell death ligand 1 (PD-L1), cytotoxic T-lymphocyte antigen 4 (CTLA4) (**Figures 3A–F**). As accumulating evidence shows that these circulating immune checkpoints are associated with a poor response to immune checkpoint blockade, the ascending concentrations of the checkpoint proteins during treatment might suggest activation of alternative immune evasion tactics of tumor. Moreover, we also examined the expression of these proteins in tumor tissue pre- and post- neoadjuvant immunotherapy by RNA sequencing. In consistent with the findings about plasma proteins, RNA expression of the checkpoint proteins was upregulated in the tumor after immunotherapy (**Figure 3G**).

DISCUSSION

We report the tumor-immune features of an early-stage NSCLC patient with SLRs and TLSs after neoadjuvant nivolumab plus ipilimumab. In addition to abundant infiltrating immune cells, we also found high levels of inhibitory components in post treatment tissue samples, especially the Treg cells in tumor and PD-L1 expression in the lymph node. Despite high number of TLSs, most of them were immature and might not have efficient anti-tumor activity. Moreover, extensively increasing immune checkpoint proteins were found during immunotherapy treatment. Hence, it is suggested that the effect of immunosuppression in this patient is equal or superior to the beneficial antitumor effect induced by ICIs, leading to the limited response to immunotherapy.

It is interesting to find SLRs and TLSs in the same patient treated with ICIs. Although an association of them in immunotherapy setting was suspected, the similar case has not been reported yet. Collectively, the two resections are associated with an inflammatory immune environment, and assumed to correlate with favorable outcomes of melanoma patients treated with immunotherapy (7, 8, 17). However, the patient here didn't benefit from immunotherapy, with a stable disease evaluated by radiology and 50% residual tumor cells by histology after treatment, and had a recurrence 8 months after surgery. According to the previous case reports of 8 SLR patients with NSCLC (21–28), 4 achieved partial response, 2 had progressive disease, and 2 had stable disease after immunotherapy. The association between SLRs and immunotherapy outcomes in lung cancer seems not clear. On the other hand, although total TLS and germinal center-positive (GC+) TLS subset scores were demonstrated to predict survival in resected NSCLC patients (29), most studies suggested that only TLSs with GC were functional, and B cells in immature TLSs could adopt a regulatory phenotype and inhibit immune reactions (30). Moreover, we noted the predominant inhibitory Treg cells in post treatment tumor and PD-L1 expression in the lymph node for their crucial roles in immunosuppression. Treg cells are one of the well-known cell types that can suppress anti-tumor immune response (31). And tumor-infiltrating follicular regulatory T cells, which are primarily located within TLSs and exhibit superior suppressive capacity and *in vivo* persistence as compared with Treg cells, could impair the survival of patients and impede the efficacy of immunotherapy treatment by regulating TLS (32). Nevertheless, a retrospective study showed that high TLS-B cell density could counterbalance the deleterious impact of high Treg cell density on survival of untreated NSCLC patients (33). It is difficult to fully assess TLSs and Treg cells by biopsy before neoadjuvant immunotherapy, while Treg cells in the posttreatment tumor tissue of this patient were deemed to impair anti-tumor immune response. As for the high level of PD-L1 expression in lymph nodes, which has not been reported in ICI-induced SLR

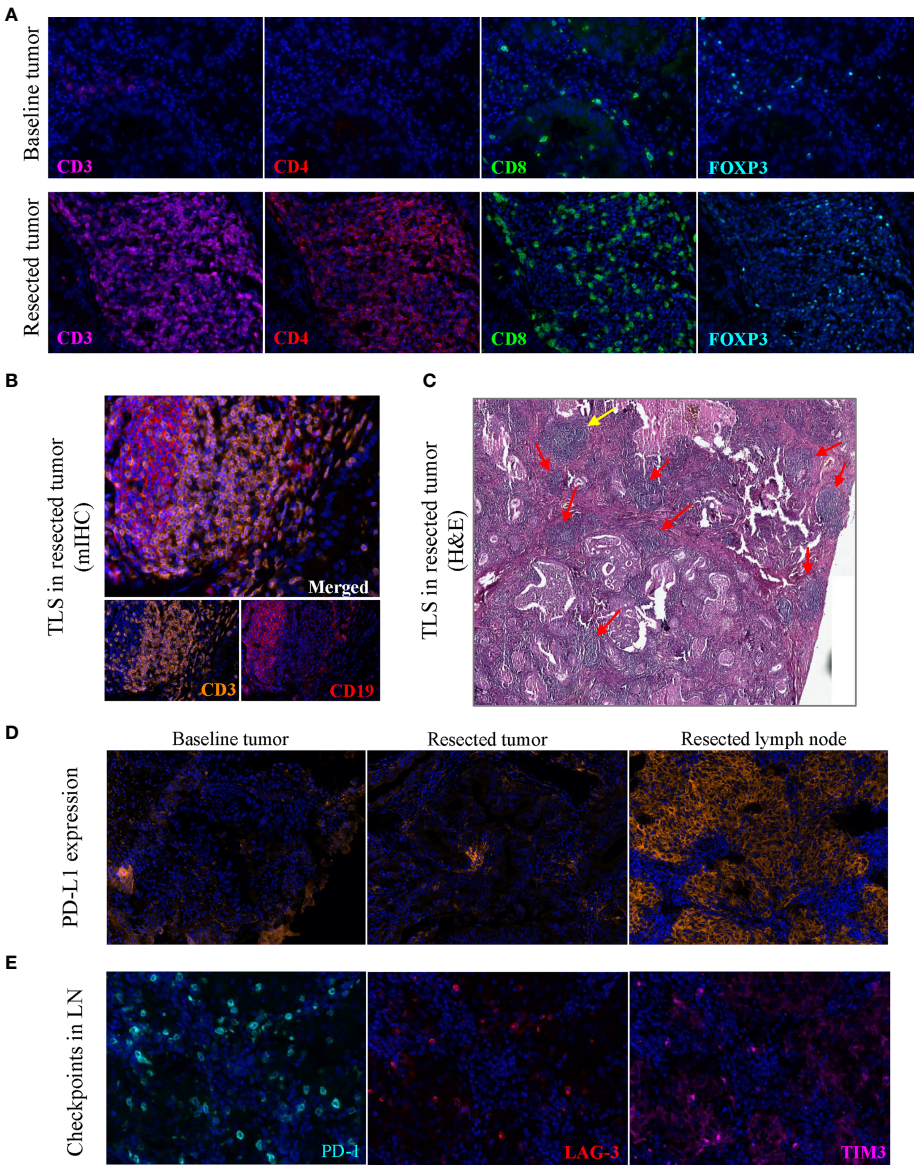

FIGURE 2 | Images of tertiary lymphoid structures and immune cell markers. **(A)** Images showed the abundant $CD3^+$, $CD4^+$, $CD8^+$ and $FOXP3^+$ cells in post-treatment tumor on the same slide, with the markers stained on baseline tumor as a contrast. **(B)** TLS in the post-treatment tumor stained by multiplex immunohistochemistry. **(C)** TLSs on a hematoxylin and eosin-stained section, yellow arrow indicates a mature TLS with a pale area, red arrow indicates immature TLSs. **(D)** PD-L1 expression in the baseline tumor, post-treatment tumor and post-treatment lymph node tissue. **(E)** Immune checkpoint proteins PD-1, LAG-3, TIM3 in the post-treatment lymph node tissue. Original magnification of fluorescence image: 200×. TLS, tertiary lymphoid structure; LN, lymph node; mIHC, multiplex immunohistochemistry.

cases, a recent study showed that lymphatic endothelia PD-L1 expression reduced tumor immunity, inducing apoptosis in tumor-specific CD8+ central memory cells in tumor-draining lymph nodes (34). Therefore, we highlight the importance of investigating inhibitory immune components in microenvironment of tumor and lymph nodes when assessing local immune status.

There is accumulating evidence indicating that high levels of circulating immune checkpoint proteins were associated with poor prognosis in a variety of cancers, such as BTLA and TIM-3 in clear cell renal cell carcinoma (35) and PD-1, PD-L1 and BTLA in pancreatic adenocarcinoma (36). The circulating checkpoint proteins also showed a predictive value in ICI-treated patients. LAG-3 expression on pretreatment peripheral blood cells could identify patients with melanoma who may not benefit from immune checkpoint blockade (37). High levels of LAG-3 and PD-1 in pre-treatment serum samples of melanoma patients may predict resistance to anti-PD-1 treatment and anti-PD-1 plus anti-CTLA4 respectively (38). Moreover, increased tumor infiltrated $TIM3^+$ or $LAG3^+$ T cells also correlated with a

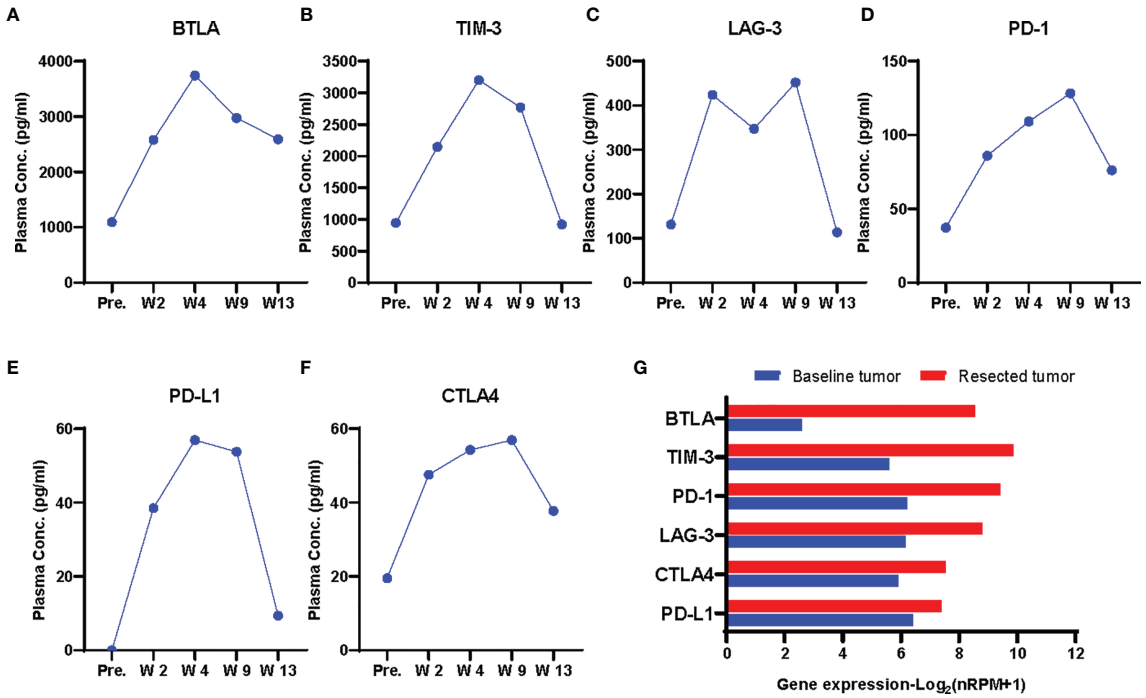

FIGURE 3 | Dynamics of plasma immune checkpoint proteins. **(A–F)** Plasma concentrations of checkpoint proteins BLTA **(A)**, TIM-3 **(B)**, LAG-3 **(C)**, PD-1 **(D)**, PD-L1 **(E)**,CTLA4 **(F)** at each time point. pre., W2, W4, prior to each cycle of immunotherapy; W9, prior to the radical surgery; W13, four weeks after surgery. The proteins were upgregulated during immunotherapy treatment. **(G)** Gene expression of the immune checkpoint proteins in pre- and post-treatment tumor by RNA sequencing.

shorter progression free survival or adaptive resistance to anti-PD-1 therapy (38, 39).

There are several limitations of this study. First, we only have one patient with co-occurrent SLRs and TLSs who did not respond well to neoadjuvant immunotherapy, so the association between the reactions and inhibitory immune components and clinical outcomes remain to be explored in more patients. Second, we did not determine the comprehensive cellular composition of tertiary lymphoid structures in tumor tissue or the main cell types expressing PD-L1 in lymph nodes due to lack of enough sample.

This report presents the special reactions SLR and TLS and immune characteristics of a NSCLC patient during the treatment with neoadjuvant immune checkpoint inhibitors, which may provide a new perspective for exploring the mechanism of immunotherapy and looking for new predictive markers.

DATA AVAILABILITY STATEMENT

The original contributions presented in the study are included in the article/**Supplementary Material**. Further inquiries can be directed to the corresponding authors.

ETHICS STATEMENT

The studies involving human participants were reviewed and approved by the ethics committee of Tianjin Medical University Cancer Institute and Hospital. The patients/participants provided their written informed consent to participate in this study. Written informed consent was obtained from the individual(s) for the publication of any potentially identifiable images or data included in this article.

AUTHOR CONTRIBUTIONS

Conception and design: CW and HZ. Provision of study materials or patients: XZ and DY. Collection and assembly of data: JS, BZ, CZ, LS, and YM. Analysis and interpretation of data: XZ, DY, and JQ. Manuscript writing and revision: JQ and LZ. All authors contributed to the article and approved the submitted version.

FUNDING

This study was supported by the National Key Sci-Tech Special Project of China (2018ZX10302207).

SUPPLEMENTARY MATERIAL

The Supplementary Material for this article can be found online at: https://www.frontiersin.org/articles/10.3389/fimmu.2022.794217/full#supplementary-material

REFERENCES

1. Gkiozos I, Kopitopoulou A, Kalkanis A, Vamvakaris IN, Judson MA, Syrigos KN. Sarcoidosis-Like Reactions Induced by Checkpoint Inhibitors. *J Thorac Oncol* (2018) 13(8):1076–82. doi: 10.1016/j.jtho.2018.04.031
2. Nishino M, Sholl LM, Awad MM, Hatabu H, Armand P, Hodi FS. Sarcoid-Like Granulomatosis of the Lung Related to Immune-Checkpoint Inhibitors: Distinct Clinical and Imaging Features of a Unique Immune-Related Adverse Event. *Cancer Immunol Res* (2018) 6(6):630–5. doi: 10.1158/2326-6066.CIR-17-0715
3. Chanson N, Ramos-Casals M, Pundole X, Suijkerbuijk K, Jose de Barros ESM, Lidar M, et al. Immune Checkpoint Inhibitor-Associated Sarcoidosis: A Usually Benign Disease That Does Not Require Immunotherapy Discontinuation. *Eur J Cancer (Oxford England: 1990)* (2021) 158:208–16. doi: 10.1016/j.ejca.2021.05.041
4. Chorti E, Kanaki T, Zimmer L, Hadaschik E, Ugurel S, Gratsias E, et al. Drug-Induced Sarcoidosis-Like Reaction in Adjuvant Immunotherapy: Increased Rate and Mimicker of Metastasis. *Eur J Cancer* (2020) 131:18–26. doi: 10.1016/j.ejca.2020.02.024
5. Cascone T, Weissferdt A, Godoy MCB, William WN Jr, Leung CH, Lin HY, et al. Nodal Immune Flare Mimics Nodal Disease Progression Following Neoadjuvant Immune Checkpoint Inhibitors in Non-Small Cell Lung Cancer. *Nat Commun* (2021) 12(1):5045. doi: 10.1038/s41467-021-25188-0
6. Eichhorn F, Klotz LV, Kriegsmann M, Bischoff H, Schneider MA, Muley T, et al. Neoadjuvant Anti-Programmed Death-1 Immunotherapy by Pembrolizumab in Resectable Non-Small Cell Lung Cancer: First Clinical Experience. *Lung Cancer* (2021) 153:150–7. doi: 10.1016/j.lungcan.2021.01.018
7. Tetzlaff MT, Nelson KC, Diab A, Staerkel GA, Nagarajan P, Torres-Cabala CA, et al. Granulomatous/sarcoid-Like Lesions Associated With Checkpoint Inhibitors: A Marker of Therapy Response in a Subset of Melanoma Patients. *J Immunother Cancer* (2018) 6(1):14. doi: 10.1186/s40425-018-0323-0
8. Cabanié C, Ammari S, Hans S, Pobel C, Laparra A, Danlos FX, et al. Outcomes of Patients With Cancer and Sarcoid-Like Granulomatosis Associated With Immune Checkpoint Inhibitors: A Case-Control Study. *Eur J Cancer (Oxford England: 1990)* (2021) 156:46–59. doi: 10.1016/j.ejca.2021.07.015
9. Sautes-Fridman C, Petitprez F, Calderaro J, Fridman WH. Tertiary Lymphoid Structures in the Era of Cancer Immunotherapy. *Nat Rev Cancer* (2019) 19 (6):307–25. doi: 10.1038/s41568-019-0144-6
10. Rodriguez AB, Engelhard VH. Insights Into Tumor-Associated Tertiary Lymphoid Structures: Novel Targets for Antitumor Immunity and Cancer Immunotherapy. *Cancer Immunol Res* (2020) 8(11):1338. doi: 10.1158/2326-6066.CIR-20-0432
11. Finkin S, Yuan D, Stein I, Taniguchi K, Weber A, Unger K, et al. Ectopic Lymphoid Structures Function as Microniches for Tumor Progenitor Cells in Hepatocellular Carcinoma. *Nat Immunol* (2015) 16(12):1235–44. doi: 10.1038/ni.3290
12. Germain C, Gnjatic S, Tamzalit F, Knockaert S, Remark R, Goc J, et al. Presence of B Cells in Tertiary Lymphoid Structures Is Associated With a Protective Immunity in Patients With Lung Cancer. *Am J Respir Crit Care Med* (2014) 189(7):832–44. doi: 10.1164/rccm.201309-1611OC
13. Dieu-Nosjean M-C, Antoine M, Danel C, Heudes D, Wislez M, Poulot V, et al. Long-Term Survival for Patients With Non–Small-Cell Lung Cancer With Intratumoral Lymphoid Structures. *J Clin Oncol* (2008) 26(27):4410–17. doi: 10.1200/JCO.2007.15.0284
14. Fukuhara M, Muto S, Inomata S, Yamaguchi H, Mine H, Takagi H, et al. The Clinical Significance of Tertiary Lymphoid Structure and its Relationship With Peripheral Blood Characteristics in Patients With Surgically Resected Non-Small Cell Lung Cancer: A Single-Center, Retrospective Study. *Cancer Immunol Immunother: CII* (2021). doi: 10.1007/s00262-021-03067-3
15. Silina K, Soltermann A, Attar FM, Casanova R, Uckeley ZM, Thut H, et al. Germinal Centers Determine the Prognostic Relevance of Tertiary Lymphoid Structures and Are Impaired by Corticosteroids in Lung Squamous Cell Carcinoma. *Cancer Res* (2018) 78(5):1308–20. doi: 10.1158/0008-5472.CAN-17-1987
16. Petitprez F, de Reynies A, Keung EZ, Chen TW, Sun CM, Calderaro J, et al. B Cells Are Associated With Survival and Immunotherapy Response in Sarcoma. *Nature* (2020) 577(7791):556–60. doi: 10.1038/s41586-019-1906-8
17. Cabrita R, Lauss M, Sanna A, Donia M, Skaarup Larsen M, Mitra S, et al. Tertiary Lymphoid Structures Improve Immunotherapy and Survival in Melanoma. *Nature* (2020) 577(7791):561–5. doi: 10.1038/s41586-019-1914-8
18. Helmink BA, Reddy SM, Gao J, Zhang S, Basar R, Thakur R, et al. B Cells and Tertiary Lymphoid Structures Promote Immunotherapy Response. *Nature* (2020) 577(7791):549–55. doi: 10.1038/s41586-019-1922-8
19. Vanhersecke L, Brunet M, Guégan J-P, Rey C, Bougouin A, Cousin S, et al. Mature Tertiary Lymphoid Structures Predict Immune Checkpoint Inhibitor Efficacy in Solid Tumors Independently of PD-L1 Expression. *Nat Cancer* (2021) 2(8):794–802. doi: 10.1038/s43018-021-00232-6
20. Cottrell TR, Thompson ED, Forde PM, Stein JE, Duffield AS, Anagnostou V, et al. Pathologic Features of Response to Neoadjuvant Anti-PD-1 in Resected Non-Small-Cell Lung Carcinoma: A Proposal for Quantitative Immune-Related Pathologic Response Criteria (irPRC). *Ann Oncol: Off J Eur Soc Med Oncol* (2018) 29(8):1853–60. doi: 10.1093/annonc/mdy218
21. Shinomiya S, Kaira K, Mouri A, Kagamu H. Synchronous Dilemma of Sarcoid-Like Reaction and Drastic Response After PD-1 Blockade Administration in Lung Cancer. *Jpn J Clin Oncol* (2021) 51(7):1179–80. doi: 10.1093/jjco/hyab043
22. Takamori S, Furubayashi N, Taguchi K, Matsubara T, Fujishita T, Ito K, et al. Sarcoid-Like Reaction of the Extrathoracic Lymph Node in a Patient With Lung Adenocarcinoma Treated With Pembrolizumab. *Thorac Cancer* (2021) 12(14):2122–25. doi: 10.1111/1759-7714.14011
23. Noguchi S, Kawachi H, Yoshida H, Fukao A, Terashita S, Ikeue T, et al. Sarcoid-Like Granulomatosis Induced by Nivolumab Treatment in a Lung Cancer Patient. *Case Rep Oncol* (2018) 11(2):562–66. doi: 10.1159/000492383
24. Paolini L, Poli C, Blanchard S, Urban T, Croué A, Rousselet MC, et al. Thoracic and Cutaneous Sarcoid-Like Reaction Associated With Anti-PD-1 Therapy: Longitudinal Monitoring of PD-1 and PD-L1 Expression After Stopping Treatment. *J Immunother Cancer* (2018) 6(1):52. doi: 10.1186/s40425-018-0372-4
25. Sanderson E, Wimaleswaran H, Senko C, White S, McDonald CF. Durvalumab Induced Sarcoid-Like Pulmonary Lymphadenopathy. *Respirol Case Rep* (2020) 8(3):e00542. doi: 10.1002/rcr2.542
26. Suozzi KC, Stahl M, Ko CJ, Chiang A, Gettinger SN, Siegel MD, et al. Immune-Related Sarcoidosis Observed in Combination Ipilimumab and Nivolumab Therapy. *JAAD Case Rep* (2016) 2(3):264–68. doi: 10.1016/j.jdcr.2016.05.002
27. Birnbaum MR, Ma MW, Fleisig S, Packer S, Amin BD, Jacobson M, et al. Nivolumab-Related Cutaneous Sarcoidosis in a Patient With Lung Adenocarcinoma. *JAAD Case Rep* (2017) 3(3):208–11. doi: 10.1016/j.jdcr.2017.02.015
28. Yousuf H, Mekki R, Khan K, Hussain A. Pembrolizumab-Induced Sarcoid-Like Reaction in a Patient With Lung Cancer. *Cureus* (2020) 12(12):e12395. doi: 10.7759/cureus.12395
29. Rakaee M, Kilvaer TK, Jamaly S, Berg T, Paulsen EE, Berglund M, et al. Tertiary Lymphoid Structure Score: A Promising Approach to Refine the TNM Staging in Resected Non-Small Cell Lung Cancer. *Br J Cancer* (2021) 124:626776(10). doi: 10.3389/fimmu.2021.626776
30. Kinker GS, Vitiello GAF, Ferreira WAS, Chaves AS, Cordeiro de Lima VC, Medina TDS. B Cell Orchestration of Anti-Tumor Immune Responses: A Matter of Cell Localization and Communication. *Front Cell Dev Biol* (2021) 9:678127. doi: 10.3389/fcell.2021.678127
31. Tanaka A, Sakaguchi S. Regulatory T Cells in Cancer Immunotherapy. *Cell Res* (2017) 27(1):109–18. doi: 10.1038/cr.2016.151
32. Eschweiler S, Clarke J, Ramírez-Suástegui C, Panwar B, Madrigal A, Chee SJ, et al. Intratumoral Follicular Regulatory T Cells Curtail Anti-PD-1 Treatment Efficacy. *Nat Immunol* (2021) 22(8):1052–63. doi: 10.1038/s41590-021-00958-6
33. Germain C, Devi-Marulkar P, Knockaert S, Biton J, Kaplon H, Letaief L, et al. Tertiary Lymphoid Structure-B Cells Narrow Regulatory T Cells Impact in Lung Cancer Patients. *Front Immunol* (2021) 12:626776. doi: 10.3389/fimmu.2021.626776
34. Cousin N, Cap S, Dihr M, Tacconi C, Detmar M, Dieterich LC. Lymphatic PD-L1 Expression Restricts Tumor-Specific CD8 T-Cell Responses. *Cancer Res* (2021) 81(15):4133–44. doi: 10.1158/0008-5472.CAN-21-0633
35. Wang Q, Zhang J, Tu H, Liang D, Chang DW, Ye Y, et al. Soluble Immune Checkpoint-Related Proteins as Predictors of Tumor Recurrence, Survival, and T Cell Phenotypes in Clear Cell Renal Cell Carcinoma Patients. *J Immunother Cancer* (2019) 7(1):334. doi: 10.1186/s40425-019-0810-y
36. Bian B, Fanale D, Dusetti N, Roque J, Pastor S, Chretien AS, et al. Prognostic Significance of Circulating PD-1, PD-L1, Pan-BTN3As, BTN3A1 and BTLA

in Patients With Pancreatic Adenocarcinoma. *Oncoimmunology* (2019) 8(4): e1561120. doi: 10.1080/2162402X.2018.1561120
37. Shen R, Postow MA, Adamow M, Arora A, Hannum M, Maher C, et al. LAG-3 Expression on Peripheral Blood Cells Identifies Patients With Poorer Outcomes After Immune Checkpoint Blockade. *Sci Trans Med* (2021) 13 (608):eabf5107. doi: 10.1126/scitranslmed.abf5107
38. Hassel JC, Wiecken M, Hülsmeyer I, Roth J, Eurich R, Machiraju D. 1126p Prediction of Clinical Outcome by Soluble Immune Checkpoints and T Cell Subsets in Patients Treated With Immune Checkpoint Blockers for Metastasized Melanoma. *Ann Oncol* (2020) 31:S756–7. doi: 10.1016/j.annonc.2020.08.1249
39. Koyama S, Akbay EA, Li YY, Herter-Sprie GS, Buczkowski KA, Richards WG, et al. Adaptive Resistance to Therapeutic PD-1 Blockade Is Associated With Upregulation of Alternative Immune Checkpoints. *Nat Commun* (2016) 7:10501. doi: 10.1038/ncomms10501

Conflict of Interest: JQ, JS, LZ, and CZ are employed by Genecast Biotechnology Co., Ltd.

The remaining authors declare that the research was conducted in the absence of any commercial or financial relationships that could be construed as a potential conflict of interest.

Publisher's Note: All claims expressed in this article are solely those of the authors and do not necessarily represent those of their affiliated organizations, or those of the publisher, the editors and the reviewers. Any product that may be evaluated in this article, or claim that may be made by its manufacturer, is not guaranteed or endorsed by the publisher.

frontiers | Frontiers in Immunology

ORIGINAL RESEARCH
published: 19 May 2022
doi: 10.3389/fimmu.2022.868155

The Presence of Tertiary Lymphoid Structures Provides New Insight Into the Clinicopathological Features and Prognosis of Patients With Breast Cancer

Bin Wang[1†], Jie Liu[1†], Yin Han[2], Yaotiao Deng[1], Jinze Li[3] and Yu Jiang[1]*

[1] Department of Medical Oncology, Cancer Center, West China Hospital, Sichuan University, Chengdu, China, [2] Department of Pathology, Chengdu Fifth People's Hospital, Chengdu, China, [3] Department of Urology, Institute of Urology, West China Hospital, Sichuan University, Chengdu, China

OPEN ACCESS

Edited by:
Brian J. Czerniecki, Moffitt Cancer Center, United States

Reviewed by:
Anthony B. Rodriguez, University of Virginia, United States
Shahram Salek-Ardakani, Pfizer, United States

***Correspondence:**
Yu Jiang
jiang_yu@scu.edu.cn

[†]These authors have contributed equally to this work and share first authorship

Specialty section:
This article was submitted to Cancer Immunity and Immunotherapy, a section of the journal Frontiers in Immunology

Received: *02 February 2022*
Accepted: *19 April 2022*
Published: *19 May 2022*

Citation:
Wang B, Liu J, Han Y, Deng Y, Li J and Jiang Y (2022) The Presence of Tertiary Lymphoid Structures Provides New Insight Into the Clinicopathological Features and Prognosis of Patients With Breast Cancer. Front. Immunol. 13:868155. doi: 10.3389/fimmu.2022.868155

Background: Tertiary lymphoid structures (TLSs) have been proven to be predictive biomarkers of favorable clinical outcomes and response to immunotherapies in several solid malignancies. Nevertheless, the effect of TLSs in patients with breast cancer (BC) remains controversial. The objective of the current study is to investigate the clinicopathological and prognostic significance of TLSs in BC. Given the unique difficulties for detecting and quantifying TLSs, a TLS-associated gene signature based on The Cancer Genome Atlas (TCGA) BC cohort was used to validate and supplement our results.

Methods: Electronic platforms (PubMed, Web of Science, EMBASE, the Cochrane Library, CNKI, and Wanfang) were searched systematically to identify relevant studies as of January 11, 2022. We calculated combined odds ratios (ORs) with 95% confidence intervals (CIs) to determine the relationship between clinicopathological parameters and TLSs. The pooled hazard ratios (HRs) and 95% CIs were also calculated to evaluate the prognostic significance of TLSs. The TLS signature based on the TCGA BC cohort was applied to validate and supplement our results.

Results: Fifteen studies with 3,898 patients were eligible for enrollment in our study. The combined analysis indicated that the presence of TLSs was related to improved disease-free survival (DFS) (HR = 0.61, 95% CI: 0.41–0.90, $p < 0.05$) and overall survival (OS) (HR = 1.66, 95% CI: 1.26–2.20, $p < 0.001$). Additionally, the presence of TLSs was positively correlated with early tumor TNM stage and high tumor-infiltrating lymphocytes. TLS presence was positively related to human epidermal growth factor receptor 2 (HER-2) and Ki-67 but inversely correlated with the status of estrogen and progesterone receptor. Simultaneously, our study found that tumor immune microenvironment was more favorable in the high-TLS signature group than in the low-TLS signature group. Consistently, BC patients in the high-TLS signature group exhibited better survival

outcomes compared to those in the low-TLS signature group, suggesting that TLSs might be favorable prognostic biomarkers.

Conclusions: TLS presence provides new insight into the clinicopathological features and prognosis of patients with BC, whereas the factors discussed limited the evidence quality of this study. We look forward to consistent methods to define and characterize TLSs, and more high-quality prospective clinical trials designed to validate the value of TLSs alone or in combination with other markers.

Keywords: tertiary lymphoid structures, breast cancer, prognosis, survival, clinicopathological parameters, signature

INTRODUCTION

Breast cancer (BC) has been the most frequently diagnosed malignancy worldwide, and is the main cause of tumor-associated mortality in women (1, 2). Originating from mammary epithelial cells, BC as a kind of heterogeneous disease has divergent histological subtypes and biological characteristics, thus leading to distinct clinical behaviors and treatment sensitivity profiles (3). Although the recent success of immunotherapy has paved the way for various solid or hematological malignancies, most subtypes of BC exhibit little efficacy to immunotherapy with immune checkpoint inhibitors only approved in combination therapy for PD-L1-positive metastatic triple-negative breast cancer (TNBC) (4). Poor immunogenicity, lack of T-cell infiltration, and an immunosuppressive tumor microenvironment (TME) have been identified as major barriers to the success of immunotherapy in BC (4). The interaction between tumor cells and the immune TME is a complex, dynamic, and evolving process; thus, conventional tumor characteristics and biomarkers may not be adequate to predict immunotherapy effectiveness and prognostication. Data across large BC clinical trials supported that the high levels of tumor-infiltrating lymphocytes (TILs) are predictive biomarkers for favorable prognosis and of the response to immunotherapy, particularly in HER-2$^+$ BC and TNBC (5). Besides TILs, recent evidence revealed that spatial organization plays a crucial role in determining prognosis and response to immunotherapy, with tertiary lymphoid structures (TLSs) attracting widespread attention (6, 7).

TLSs are ectopic cellular aggregates in nonlymphoid tissues under conditions of chronic inflammation including tumors, and share similar architectural and functional characteristics with secondary lymphoid organs (SLOs) (8). The architecture of mature TLSs is characterized by B-cell-enriched zones that consists of B-cell follicles surrounded by a network of follicular helper T cells and follicular dendritic cells, T-cell-enriched regions with dendritic cells (DCs), high endothelial venules (HEVs), as well as lymphatic vessels (6, 7). In addition to the relevant number of immune cells, TLSs emphasize the spatial proximity of specialized subsets of immune cells within TLSs. In contrast to SLOs, TLSs represent privileged sites for local lymphocyte differentiation and antigen presentation, which provide an important milieu for both cellular and humoral antitumor immunity (7). Accumulating research has indicated that TLS presence was deeply associated with positive immunoreactivity and favorable clinical outcomes in most types of solid tumors (6). However, some studies evaluated the prognostic value of TLSs limited to small study numbers and subsets of BC, with inconsistent and conflicting results. Although a previous meta-analysis by Zhang et al. suggested that TLSs were related to better prognosis, their result was based on a limited number of studies, with only two or three studies providing survival outcomes (9). Furthermore, all included studies in their meta-analysis showed that TLSs were beneficial for prognosis, but opposite conclusions have been reported in the recent study (10).

Hence, with the publication of new studies regarding this topic, further evaluation of the role of TLSs in BC is necessary. This study including more than 15 articles aimed to comprehensively assess clinicopathological and prognostic values of TLSs in BC, providing higher-level medical evidence for clinical practice. Simultaneously, given the unique difficulties in the detection and quantification of TLSs, the TLS-related gene signature based on the TCGA BC cohort was further used to validate and supplement our results.

MATERIALS AND METHODS

The present study was performed in accordance with the Preferred Reporting Items for Systematic Review and Meta-Analysis (PRISMA) criteria (11). The protocol of this meta-analysis was registered in the PROSPERO (registration number: CRD42022302921).

Search Strategies

Six electronic platforms (PubMed, Web of Science, EMBASE, the Cochrane Library, CNKI, and Wanfang) were searched systematically to identify eligible studies as of January 2022, regardless of any restrictions in the region or language. Random combinations of the following items were applied in our search: "Tertiary Lymphoid Structure OR tertiary lymphoid organ OR Ectopic Lymphoid Tissue OR Ectopic Lymphoid-Like Structure", and "breast neoplasm OR breast cancer OR breast tumor OR breast carcinoma". Additionally, references cited in relevant studies and reviews were manually searched to identify potential studies for inclusion. Two researchers independently

reviewed the literature, and any differences were addressed *via* discussion with a third researcher.

Inclusion and Exclusion Criteria

The eligible studies were selected in accordance with the following criteria: (1) the patients were definitively diagnosed with BC by histopathological examination; (2) TLSs were determined by the hematoxylin and eosin (H&E) staining method or immunohistochemistry (IHC) method based on BC tissues; and (3) studies reported the association of TLS presence with clinicopathological parameters or survival outcomes, including disease-free survival/overall survival (DFS/OS). Exclusion criteria included the following: (1) reviews, editorials, letters, conference abstracts, case reports, or unpublished articles; (2) studies involving animal models or cell lines; (3) studies with unavailable data or insufficient data for analyses; and (4) studies composed of an overlapping patient population.

Data Extraction

All required data were extracted from eligible studies by two investigators independently, which were as follows: (1) first author, publication date, country, sample size, detection methods, TLS location, cutoff criteria, and study design; (2) clinicopathological parameters, including the association between TLSs and age, tumor size, lymph node status, lymphovascular invasion (LVI), histological grade, TNM stage, estrogen receptor (ER) status, progesterone receptor (PR) status, human epidermal growth factor receptor 2 (HER-2) status, and the cell proliferation marker Ki-67 index; and (3) hazard ratios (HRs) and 95% confidence intervals (CIs) of DFS and OS. If survival outcomes were not given explicitly, the HR with 95% CI was retrieved from Kaplan–Meier curves through Engauge Digitizer (version 4.1) software and Tierney's reported method (12).

Quality Evaluation

The quality of the selected studies was independently evaluated by two researchers using the Quality in Prognosis Studies (QUIPS) tool of the Cochrane Prognosis Methods Group, which considers the following domains: (1) study participation, (2) study attrition, (3) prognostic factor measurement, (4) outcome measurement, (5) study confounding, and (6) statistical analysis and reporting (13). Each domain was scored low, moderate, or high risk of bias by answering three to six more detailed questions (**Supplementary Table 1**) (14). Studies were considered of high quality when risk of bias was rated low in at least four of the six domains, and low in both study attrition and study confounding. Any disagreements were resolved by consultation with a third researcher.

Bioinformatics Analysis

The mRNA expression and clinical information of BC patients in this study were downloaded from the TCGA database (https://portal.gdc.cancer.gov/). We applied single-sample Gene Set Enrichment Analysis (ssGSEA) to quantify the enrichment scores of TLS signature-related genes (CCR6, CD1D, CD79B, CETP, EIF1AY, LAT, PTGDS, RBP5, and SKAP1) (15). We separated patients into three groups equally according to the tertile of the TLS score. The ESTIMATE algorithm was used to analyze the immune score, stromal score, ESTIMATE score, and tumor purity to test the effect of the high- and low-TLS signature groups. The enrichment levels of the 29 immune-associated gene sets were quantified by the ssGSEA score (16), and the relative fractions of 22 human immune cell infiltration were accurately calculated by the CIBERSORT deconvolution algorithm (17), further testing the difference between the high- and low-TLS signature groups using Mann–Whitney *U* test. Correlation analysis between TLS scores and major immune checkpoint genes was performed using Spearman's algorithm, and the difference in immune checkpoint genes between these two groups was explored by Mann–Whitney *U* test. The survival differences between two groups were compared using a log-rank test, and visualized by Kaplan–Meier curves.

Statistical Analysis

All calculations were conducted using STATA version 17.0 and R version 4.1.1 with corresponding packages. The pooled odds ratios (ORs) and the corresponding 95% CIs were calculated to assess the association between TLS presence and clinicopathological parameters. The merged HRs with 95% CIs were adopted to evaluate the correlation between TLS presence and prognosis. Heterogeneity between studies was assessed using Cochran's Q and Higgins I^2 tests. $I^2 > 50\%$ and $p < 0.10$ were defined as significant heterogeneity, and the random-effect model was applied; otherwise, the fixed-effect model was utilized. We conducted a subgroup analysis to investigate the heterogeneity cause. Moreover, sensitivity analysis was employed to assess the stability of the pooled outcomes by dropping each study individually. Meanwhile, both Begg's funnel plots and Egger's tests were adopted to evaluate potential publication bias. Statistical significance was defined as a p-value of less than 0.05.

RESULTS

Study Characteristics

As shown in the PRISMA flowchart (**Figure 1**), a total of 494 articles were identified from electronic databases according to the initial search strategy. After preliminary screening and full-text review, 15 studies with a total of 3,898 patients (10, 18–31) were fully in conformity with the screening criteria and were included in this study. The baseline characteristics of the eligible studies are summarized in **Table 1**. The fifteen included studies were retrospective studies published between 2015 and 2021, with a patient population ranging from 60 to 769. Seven studies were performed in Korea (18, 20, 23–25, 27, 28), five in China (19, 22, 29–31), two in Greece (10, 26), and one in Belgium (21). Ten of the 15 included studies reported the correlation between clinicopathological features and TLSs (TNM stage, 4 studies; age, 5 studies; tumor size, 4 studies;

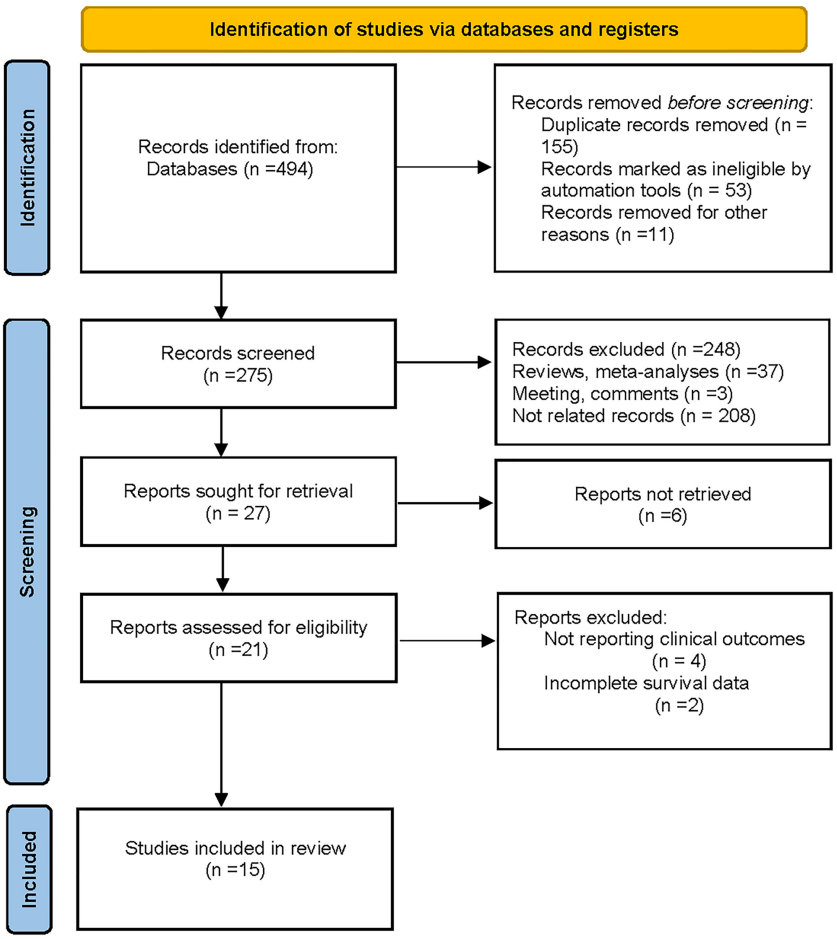

FIGURE 1 | Study search and selection process flow diagram (PRISMA 2020).

lymph node status, 7 studies; LVI, 4 studies; histological grade, 7 studies; TILs, 3 studies; ER, 3 studies; PR, 3 studies; HER-2, 6 studies; Ki-67, 2 studies). Ten of the 15 included studies investigated the prognostic role of TLS presence, with eight assessing DFS and four assessing OS. The study quality assessment results of each study using the QUIPS tool suggested that the methodology of the studies was relatively reliable, and only two studies harbored a high overall risk of bias (**Figure 2**).

Correlation Between TLS Presence and Clinicopathological Parameters

To evaluate the value of TLSs as an effective biomarker, we investigated the relationship between the TLS presence and certain clinicopathological parameters in patients with BC. The results of this analysis are shown in **Figure 3** and **Supplementary Table 2**. The pooled OR revealed that TLS presence was more prevalent in BC patients with earlier tumor TNM stage (OR = 0.17, 95% CI: 0.07–0.46, $p < 0.001$; $I^2 = 68.3\%$, $p = 0.024$) (**Figure 3A**). However, the correlation between TLS presence and age (OR = 0.96, 95% CI: 0.68–1.35, $p = 0.802$; $I^2 = 0\%$, $p = 0.800$), tumor size (OR = 1.08, 95% CI: 0.77–1.51, $p = 0.680$; $I^2 = 0\%$, $p = 0.760$), lymph node status (OR = 0.64, 95% CI: 0.31–1.30, $p = 0.215$; $I^2 = 86.6\%$, $p < 0.001$), LVI (OR = 2.25, 95% CI: 0.59–8.54, $p = 0.236$; $I^2 = 92.4\%$, $p < 0.001$), and histological grade (OR = 1.75, 95% CI: 0.55–5.60, $p = 0.346$; $I^2 = 92.7\%$, $p < 0.001$) was not statistically significant (**Figures 3B–F**). TLSs have recently drawn attention as markers for TILs. The pooled results from three included studies showed that TLS presence was positively associated with TILs in tumors (OR = 8.054, 95% CI: 3.94–16.46, $p < 0.001$; $I^2 = 66.3\%$, $p = 0.051$) (**Figure 3G**). Moreover, a total of 8 studies investigated the correlation of TLS presence with the expression of immunohistochemical markers (ER, PR, HER-2, and Ki-67) (**Figures 3H–K**). The pooled results showed that TLS presence was negatively associated with the expression of ER (OR = 0.28, 95% CI: 0.14–0.54, $p < 0.001$; $I^2 = 55.8\%$, $p = 0.104$) and PR (OR = 0.318, 95% CI: 0.22–0.47, $p < 0.001$; $I^2 = 0\%$, $p = 0.757$). In addition, TLS was correlated with high expression of HER-2 (OR = 3.27, 95% CI: 1.66–6.47, $p = 0.001$; $I^2 = 72.8\%$, $p = 0.002$) and Ki-67 (OR =2.14, 95% CI: 1.27–3.59, $p < 0.004$; $I^2 = 7.5\%$, p = 0.299).

TABLE 1 | Main characteristics of the eligible studies.

Eligible study	Year	Country	Sample size	Median age (range)	Cohort	Detected method	TLS markers	TLS location	Cutoff criteria	Survival outcome	Source of HR	Study design
Lee HJ et al. (25)	2015	Korea	447	NR	HER2+ BC	H&E	NA	Within 5 mm from the invasive or *in situ* carcinoma	None, minimal, moderate, or abundant	DFS	Reported	Retrospective
Figenschau SL et al. (26)	2015	Greece	167	NR	PBC	H&E/IHC	CD3, CD4, CD8, CD20, CD21, BCL-6, and PNAd	Global	Very low, low, medium, and high	DFS, OS	Reported	Retrospective
Lee HJ et al. (27)	2016	Korea	769	47 (23–76)	TNBC	H&E/IHC	MECA-79	In tumor adjacent tissue	None, little, moderate, or abundant	DFS, OS	Reported	Retrospective
Kim A et al. (18)	2016	Korea	204	48 (27–76)	Ductal BC	H&E/IHC	CD3 and CD20	Near to or remote from the invasive or *in situ* carcinoma	Absent, low, moderate, or abundant	NR	Reported	Retrospective
Zhou Z et al. (30)	2016	China	100	49.3 (31–72)	PBC	H&E/IHC	CD3, CD20, CD21, BCL-6, and CD62L	Global	Positive vs. negative	NR	Reported	Retrospective
Song IH et al. (23)	2017	Korea	108	42 (23–70)	TNBC	H&E/IHC	CD3, CD8, and CD20	Global	No, little, moderate, or abundant	DFS	Reported	Retrospective
Park IA et al. (20)	2017	Korea	681	47.4 (23–76)	TNBC	H&E	NA	In the adjacent area of the invasive and *in situ* carcinoma	Absent, low, moderate, or abundant	DFS	Reported	Retrospective
Liu X et al. (19)	2017	China	248	NR	Invasive BC	H&E/IHC	CD3, CD20, and CD23	Within 5 mm from the invasive or *in situ* carcinoma	Positive vs. negative	DFS, OS	Survival curve	Retrospective
Buisseret L et al. (28)	2017	Belgium	189	NR	PBC	H&E/IHC	CD3, CD4, CD8, CD20, and CD23	Global	Positive vs. negative	NR	Reported	Retrospective
Gao S et al. (29)	2017	China	150	48.5 (34–75)	Invasive ductal BC	H&E/IHC	CD3, CD4, CD8, CD20, CD21, CD62L, and, BCL-6	Global	Positive vs. negative	NR	Reported	Retrospective
Lee M et al. (24)	2019	Korea	335	NR	Metastatic BC	H&E	NA	Primary and metastatic sites	Present vs. absent	OS	Reported	Retrospective
Sofopoulos M et al. (10)	2019	Greece	167	53 (26–78)	Invasive ductal BC	H&E/IHC	CD3, CD4, CD8, CD20, CD23, CD31, CD163, and, FOXP3	Within 5 mm from the infiltrative tumor border	Negative, low to moderate, and high	DFS/OS	Survival curve	Retrospective
Chao X et al. (22)	2020	China	60	50 (25–81))	Metaplastic BC	H&E/IHC	CD3 and CD20	Within the invasive border	Absent and present	DFS	Reported	Retrospective
Zhang Y et al. (31)	2020	China	105	52 (30–79)	Invasive ductal BC	H&E/IHC	CD3, CD10, CD20, and CD21	Within 5 mm from the invasive or *in situ* carcinoma	Absent and present	NR	Reported	Retrospective
Noël G et al. (21)	2021	Belgium	168	NR	Invasive ductal BC	H&E/IHC	CD3 and CD20	Global	No, inactive, and active	DFS	Survival curve	Retrospective

BC, breast cancer; TNBC, triple-negative breast cancer; DFS, disease-free survival; OS, overall survival; NR, not reported; NA, not applicable; H&E, hematoxylin and eosin staining; IHC, immunohistochemistry.

FIGURE 2 | Risk of bias graph of included studies. **(A)** Assessment regarding each risk of bias item for each included study. **(B)** Each bias risk item was presented as a percentage for all included studies.

Effect of TLS on Survival Outcomes of Patients With Breast Cancer

To deeply assess the prognostic effect of TLSs in BC patients, a meta-analysis was performed on HRs for DFS and OS. Eight studies with 572 patients examined the relationship between TLS presence and DFS (**Figure 4A**). Because of moderate heterogeneity between included studies (I^2 = 62.3%, p = 0.010), a random-effect model was performed to evaluate the pooled HR and 95% CI of DFS. The merged results suggested that TLS presence was obviously related to a better DFS (HR = 0.61, 95% CI: 0.41–0.90, $p < 0.05$). Four studies including 1,666 patients assessed the association between TLS presence and OS (**Figure 4B**). Since heterogeneity across studies was I^2 = 52.9%, p = 0.038, a random-effect model was adopted for analysis. The merged results indicated that TLS presence was correlated with longer OS (HR = 1.66, 95% CI: 1.26–2.20, $p < 0.001$).

Subgroup Analyses

Limited to the number of studies included, we only performed subgroup analysis for DFS and stratified by median age, ethnicity, sample size, source of data, and detection method (**Table 2**). The DFS rate did not differ between patients with a median age below 50 years and those over 50 years and between sample sizes greater than or less than 300. Subgroup analysis stratified by ethnicity and source of data showed that TLS expression in both Asian and univariate analyses was more prone to be correlated with better DFS (HR = 0.63, 95% CI: 0.54–0.73, $p < 0.001$) with low heterogeneity (I^2 = 43.2%, p = 0.117). Nevertheless, for two studies in Caucasians, the pooled data reached the opposite conclusion (HR = 1.67, 95% CI: 0.29–9.80, p = 0.924) with significant heterogeneity. For subgroup analyses based on the detection method, the results suggested that TLS presence predicted better DFS with detection using

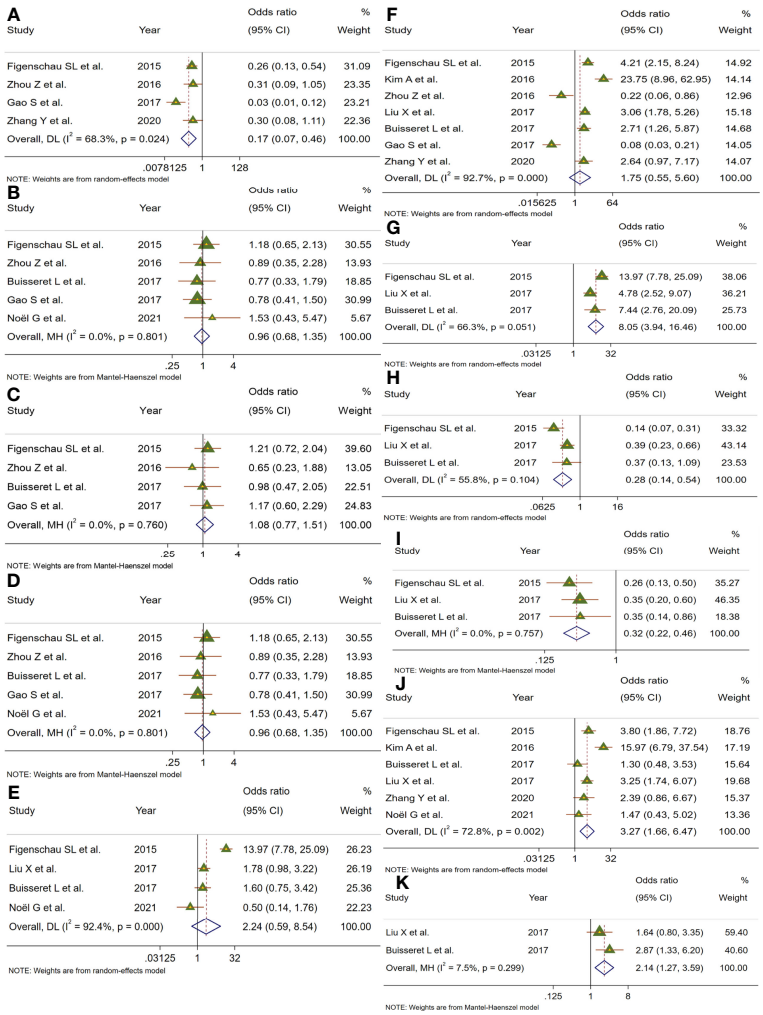

FIGURE 3 | Meta-analysis for the association of TLSs with clinicopathological parameters. Forest plots showed the correlation between TLS presence and **(A)** TNM stage, **(B)** age, **(C)** tumor size, **(D)** lymph node status, **(E)** lymphovascular invasion, **(F)** histological grade, **(G)** TILs, **(H)** ER, **(I)** PR, **(J)** HER-2, and **(K)** Ki-67. Each result was shown by the OR with 95% CI. Diamonds indicated pooled OR with their corresponding 95% CIs.

H&E staining (HR = 0.61, 95% CI: 0.45–0.82, $p < 0.001$), while TLS detected by H&E staining combined with IHC had no statistically significant correlation for DFS (HR = 0.29, 95% CI: 0.26–1.37, $p = 0.224$). Thus, ethnicity, source of data, and/or detection method might be a source of heterogeneity. Moreover, the heterogeneity among studies might be caused by the complex subtypes of BC.

Sensitivity Analysis

Sensitivity analysis was employed to investigate the stability of the pooled survival outcomes by sequentially dropping each study individually (**Figures 5A, B**). The final result indicated that no significant influence of the merged survival outcomes was observed after removing any of the included studies, demonstrating that our results were stable and reliable.

Publication Bias

Both Begg's funnel and Egger's tests were conducted to estimate the potential publication bias. Begg's funnel plots appeared symmetrical (Begg's: $p = 0.386$ for DFS; $p = 0.734$ for OS), and the p-values in Egger's test were 0.701 for DFS and 0.529 for OS, As shown in **Figures 5C, D**. Thus, there was no significant publication bias in studies on TLSs with respect to survival analysis.

Validation Results of the TLS Signature Based on The Cancer Genome Atlas

At present, the major research dilemma for TLSs is lack of standards for detection and quantification. Detecting TLSs through H&E staining and IHC is susceptible to subjective bias and inconvenient for quantifying TLSs. Recently, several gene signatures detecting TLSs identified from transcriptomic analysis

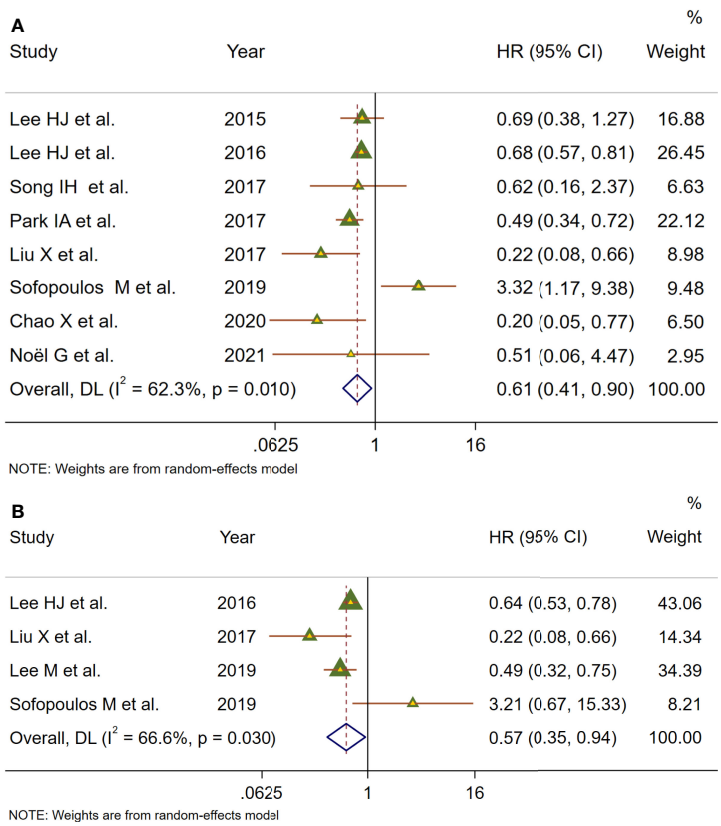

FIGURE 4 | Meta-analysis of the prognostic value of TLS presence in BC patients. **(A)** Forest plots of the association between the TLS presence and disease-free survival. **(B)** Forest plots of the association between the TLS presence and overall survival. An HR <1 suggested that the presence of TLSs was associated with favorable prognosis. Diamonds indicated overall HR with their corresponding 95% CIs.

were proven to be feasible in the quantification of TLSs. The 9-gene TLS signature mainly represented the B cells and T cells in TLSs, which was thought to be more representative of TLS-associated gene expression than the 12-chemokine signature (32). The 9-gene signature has been used for TLS quantification in a variety of solid tumors such as lung adenocarcinoma and melanoma, conveying significant prognostic and predictive value (15, 32). First, we comparatively assessed the differential expression of 9 genes between tumor and normal tissues in the TCGA BC cohort (**Figure S1**). Based on the 9-gene enrichment score, BC patients were separated into a high-TLS signature group (top tertile) and a low-TLS signature group (bottom tertile). We then investigated correlations between the expression of the 9-gene signature and the TME. In the ESTIMATE algorithm, patients in the high-TLS signature group had higher immune, stromal, and ESTIMATE scores and lower tumor purity than patients in the low-TLS signature group (**Figures 6A, B**). As shown in **Figure 6A**, the infiltration degree of immune cell subsets in the high-TLS signature group was significantly higher than that in the low-TLS signature group. The CIBERSORT analysis indicated that the relative proportions of immune cells including B cells, plasma cells, CD8 T cells, CD4 T cells, follicular helper T cells, regulatory T cells (Tregs), NK cells, monocytes, macrophages, activated dendritic cells, mast cells, neutrophils, and eosinophils were significantly different between the high- and low-TLS signature groups (**Figure 6C**). The differences in immune cell proportion indicated that the 9-gene signature can efficiently reflect the enrichment of TLSs in the TME. We next evaluated the correlation between the TLS signature and the expression of immune-related checkpoint genes. Pearson correlation analysis revealed that the TLS signature score was positively correlated with immune-related checkpoint expression. Notably, compared with the low-TLS signature group, the expression of all major checkpoint genes was significantly upregulated in the high-TLS signature group. We then further assessed the prognostic value of the TLS signature in patients with BC. The Kaplan–Meier curve revealed the high-TLS signature group was significantly associated with improved OS.

DISCUSSION

As a complex network composed of a variety of immune subsets, the tumor immune microenvironment exerts a great impact on immunotherapeutic efficacy and prognosis (33). TLSs have

TABLE 2 | Subgroup analysis of the prognostic value of TLSs for DFS in patients with breast cancer.

Subgroup analysis	No. of studies	Effect model	Pooled HR (95%CI)	*p*	Heterogeneity	
					I^2(%)	*p*
DFS						
Total	8	Random	0.61 (0.41, 0.90)	0.013	62.3	0.010
Median age						
<50	3	Fixed	0.64 (0.55, 0.75)	<0.001	13.8	0.314
≥50	3	Random	0.54 (0.08, 3.57)	0.524	87.6	0.000
Ethnicity						
Asian	6	Fixed	0.63 (0.54, 0.73)	<0.001	43.2	0.117
Caucasian	2	Random	1.67 (0.29, 9.80)	0.568	57.0	0.127
Sample size						
<300	5	Random	0.62 (0.35, 1.10)	0.104	75.2	0.003
≥300	3	Fixed	0.64 (0.53, 0.77)	<0.001	15.8	0.305
Source of data						
Univariate	6	Fixed	0.63 (0.54, 0.73)	<0.001	43.2	0.117
K-M curves	2	Random	1.67 (0.29, 9.80)	0.568	57.0	0.127
Detected method						
H&E	3	Random	0.61 (0.45, 0.82)	0.001	56.9	0.128
H&E and IHC	5	Random	0.29 (0.26, 1.37)	0.224	69.2	0.006

HR, hazard ratio; CI, confidence interval; H&E, hematoxylin and eosin staining; IHC, immunohistochemistry.

attracted increasing attention as a unique structure of the TME. TLSs not only are prognostic biomarkers of improved clinical outcome among cancer patients but also shape a local and favorable site for generating antitumor humoral and cellular immune responses (6, 8). However, several studies exploring the impact of TLS on prognosis and tumor progression were limited to small study numbers and subsets of BCs, of which the results are conflicting and lack more comprehensive evaluations. To the best of our knowledge, this is the most comprehensive meta-analysis including 15 articles to assess the clinicopathological and prognostic value of TLSs in BC.

The prognosis of BC is well recognized to be influenced by host- and tumor-associated factors (age, tumor size, histological grade, lymph node, hormone and growth receptor status, etc.) (19). First, we synthesized eleven pieces of research to evaluate the correlation between TLSs and clinicopathological parameters in BC (**Figure 3**). Our results suggested that the presence of TLSs was correlated with early TNM stage. Consistent with this, the

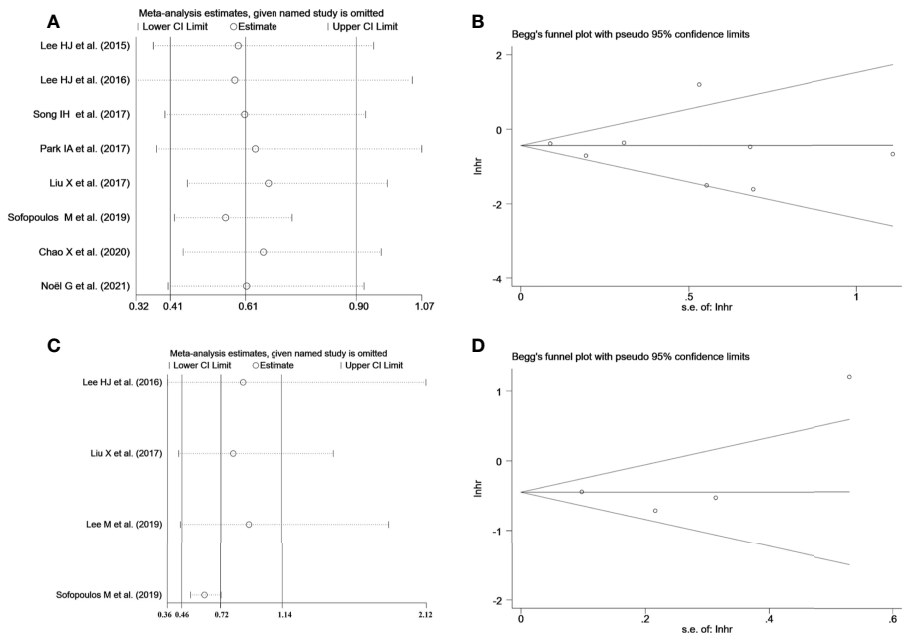

FIGURE 5 | **(A)** Sensitivity analysis between TLS presence and DFS. **(B)** Sensitivity analysis between TLS presence and OS. **(C)** Begg's funnel plot for publication bias of TLS presence on DFS. **(D)** Begg's funnel plot for publication bias of TLS presence on OS.

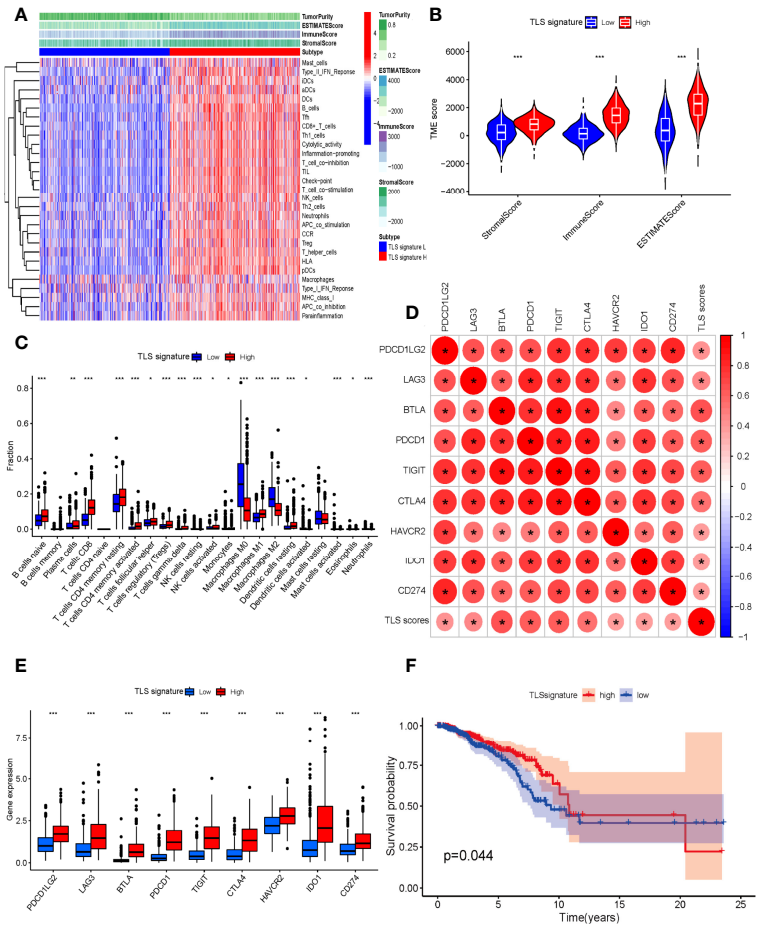

FIGURE 6 | **(A)** Relationship between TLS signature and tumor immune microenvironment. Twenty-nine immune-associated gene sets were quantified by ssGSEA. Tumor purity, estimate scores, stromal scores, and immune scores were evaluated by ESTIMATE. **(B)** Comparison of stromal scores, immune scores, and ESTIMATE scores between the high- and low-TLS signature groups (Mann–Whitney *U* test). **(C)** The relative fractions of 22 human immune cell infiltration in the high- and low-TLS signature groups (Mann–Whitney *U* test). **(D)** The correlation between TLS signature scores and immune-related checkpoint gene expression (Spearman's test). **(E)** Comparison of immune-related checkpoint genes between the high- and low-TLS signature groups (Mann–Whitney *U* test). **(F)** Comparison of OS between the high- and low-TLS signature groups (log-rank test). $^{*}p < 0.05$, $^{**}p < 0.01$, $^{***}p < 0.001$.

density of TLSs was also found to be obviously increased in early TNM stage in oral squamous cell carcinoma and NSCLC (34, 35). A positive association was found between the presence of TLSs and TIL levels in our study, which might be associated with TLS function. Being nonencapsulated and close to tumor tissues compared to draining lymph nodes, TLSs facilitate rapid migration of APCs to TLSs and presentation of antigen peptides to T-cell APCs at the site of the tumor (36). Indeed, some studies also reported that TILs were the strongest independent factor predicting TLSs, but not all cases with high TILs showed TLS formation (37). We also found that TLSs were negatively related to ER and PR status, but were correlated with high expression of HER-2 and Ki-67. These results were in line with previous studies, which revealed that increased TILs are inversely related to the expression of ER or PR, and are positive with HER-2 status, the pathologic complete response rate, and improved survival outcomes (25, 38). In the current study, we did not find the relationship between TLSs and age, tumor size, LVI, or histologic grade.

We then systematically evaluated the prognostic impact of TLS presence on BC patients (**Figure 4**). Our meta-analysis describes that HR = 0.68 for OS and HR = 0.54 for DFS, both of which were statistically significant. The study revealed that patients with TLS presence had better survival outcomes regarding DFS and OS. It was worth noting that that sensitivity analyses revealed that our results were reliable and robust, but moderate heterogeneity between included studies was observed in survival outcomes, which can be caused by different baseline characteristics of individual studies. Therefore, subgroup analyses were performed using median age, ethnicity, sample size, source of data, and detection method to explore the potential heterogeneity (**Table 2**). The results revealed that ethnicity, source of data, and/or detection method may be a source of heterogeneity. Therefore, it is worth noting that TLSs

are hardly accurately identified by H&E staining alone, and IHC with TLS markers is typically necessary to evaluate TLS characteristics. Moreover, the heterogeneity among studies might be due to the complex subtyping of BC. Recent studies have suggested that maturation degrees and distribution of TLSs are critical to determine the impact of TLSs on prognosis. However, due to a lack of data, subgroup analysis could not be conducted to assess the impact of different maturation degrees and distributions of TLSs on survival outcomes. A high proportion of mature TLSs containing GCs was associated with better prognostic outcome than total TLSs, and the prognostic value of TLSs was lost while GC formation was impaired (39, 40). TLSs could localize to the core of tumor tissues called intratumor TLSs and/or the invasive margin of tumor tissues, known as peritumor TLSs (41). Several studies have indicated that the density of peritumor TLSs is associated with improved prognoses, whereas there are a few opposite results. Sofopoulos et al. described that patients with invasive ductal carcinoma having peritumoral TLSs exhibited worse DFS and OS than patients lacking TLSs (10). High levels of tumor-infiltrating Treg cells observed at the peritumoral areas were demonstrated to be correlated with relapse and death in BC patients (42).

Moreover, given the unique difficulties in TLS detection and quantification, we validated and supplemented the results of our analysis by TLS-related gene signature in BC patients (**Figure 6**). Accumulating evidence has confirmed that TLSs are highly associated with immune cell infiltration, which closely have an impact on the development, progression, and prognosis as well as the treatment of BC (43). Hence, the immune score, stromal score, and ESTIMATE score of BC samples were estimated *via* the ESTIMATE algorithm. Higher immune, stromal, or ESTIMATE scores and lower tumor purity were found in patients of the high-TLS signature group than those in the low-TLS signature group. Simultaneously, we observed that most of the 29 immune subsets, which represented immune cell types, functions, and pathways, in the high group were more abundant compared to the low group. Interestingly, the immunosuppressive subsets like Treg cells, which might lead to poor outcomes, were also higher in the high group. Indeed, immunosuppressive cells are also components of TLSs, and associations of TLSs with immunosuppressive cells have been reported in various solid tumors including BC, lung cancer, and melanoma (15, 42, 44). There was evidence that TLSs in combination with "immunoscore" defined by intratumoral immune cells might provide a comprehensive and most powerful prognosticator. Li et al. found that TLSs combined with $CD8^+$ T cells and $CD57^+$ NK cells provided a higher predictive prognostic accuracy (45). It was still noteworthy that all major checkpoint genes were obviously upregulated in the high-TLS signature group compared with the low-TLS signature group, suggesting that patients with high expression of TLS signature were more likely to benefit from immunotherapy. A study by Cabrita et al. observed that TLS-rich tumors in particular were related to significantly increased survival after CTLA4 inhibitor on the basis of the TLS signature (15). TLS-rich tumors were more infiltrated by $CD8^+$ T cells, and these T cells might be depleted, explaining the correlation between immune checkpoint expression and TLSs and why checkpoint inhibitor might result in productive anti-tumor immunity in TLS-rich tumors (46). Intriguingly, checkpoint inhibitor therapy might also promote the formation of TLSs. Analysis of on-treatment tumor biopsies of urothelial carcinoma and melanoma has shown that tumors of responding patients showed a higher number of TLS-associated B cells relative to matched pretherapy samples after neoadjuvant immune checkpoint blockade (8). All these results demonstrated the significant correlations with TLS signature representing the major component of TLSs, which revealed that the 9-gene signature can efficiently reflect TLS enrichment in the TME. Our study also demonstrated that BC patients with a high TLS signature expression displayed improved survival, which showed that TLS signature could act as a favorable prognostic factor for BC patients. Based on the above results and discussion, multiple measures including chemotherapy, immunostimulants, vaccination, and TLS-associated cytokines and chemokines have been applied to explore the induction of TLS formation (40, 47). Considering some immunosuppressive factors such as regulatory T and B cells that impaired the antitumor of TLSs reported from recent studies, therapeutic strategies to induce TLS formation and maturation while inhibiting immunosuppressive factors might create bright prospects for enhancing tumor immunotherapeutic response (48).

This present study as the most comprehensive meta-analysis provides more substantial evidence for clinicopathological and prognostic significance of TLSs in BC. However, important considerations should be emphasized while interpreting the conclusions of this study. The cellular components, locations, and maturation degrees of TLSs might dictate treatment efficacy, tumor recurrence, and patient survival. The heterogeneity of the means used to quantify TLSs further confound their use in the clinic. Because the number of retrieved studies was not sufficient to be analyzed depending on the detection methods, no restriction was placed on the detection methods. Different scoring methods, scoring systems, and thresholds might lead to different results. Other limitations of our study were also noteworthy. First, partial survival data unavailable in the original article were extracted from Kaplan–Meier curves, which are less reliable than data directly acquired from research. Secondly, compared to multivariate analysis, data from univariate analysis may overestimate the effect sizes. Third, all the research data were derived from Asian and Caucasian patients. Accordingly, the global representation of data is insufficient and lacking. Finally, all studies included were retrospectively conducted and might have inherent structural biases. Therefore, prospective randomized trials are required to validate our results in the future.

In conclusion, TLS presence provides new insight into the clinicopathological features and prognosis of patients with BC. The presence of TLSs might have the potential to predict prognosis of BC patients, whereas factors discussed above limited the evidence quality of this study. We look forward to consistent methods to define and characterize TLSs, and more

high-quality prospective clinical trials designed to validate the prognostic and predictive value of TLSs alone or in combination with other markers.

DATA AVAILABILITY STATEMENT

The original contributions presented in the study are included in the article/**Supplementary Material**. Further inquiries can be directed to the corresponding author.

AUTHOR CONTRIBUTIONS

Conception and design: BW, JL, and YJ. Wrote the manuscript: BW and JL. Acquired data: YH, YD, and J-ZL. Analyzed the data: BW. Discussed the results and implications of findings: JL, YD, and YH. Interpretation of data: BW and J-ZL. YJ performed critical evaluation, verification of the manuscript, and supported funding. All authors contributed to the article and approved the submitted version.

FUNDING

This work was funded by the National Natural Science Foundation of China (Grant Number 81903181) and the 1·3·5 Project for Disciplines of excellence–Clinical Research Incubation Project, West China Hospital (Grant Number 2021HXFH019).

ACKNOWLEDGMENTS

We would like to thank American Journal Experts (www.aje.com) for English language editing.

SUPPLEMENTARY MATERIAL

The Supplementary Material for this article can be found online at: https://www.frontiersin.org/articles/10.3389/fimmu.2022.868155/full#supplementary-material

REFERENCES

1. Sung H, Ferlay J, Siegel RL, Laversanne M, Soerjomataram I, Jemal A, et al. Global Cancer Statistics 2020: GLOBOCAN Estimates of Incidence and Mortality Worldwide for 36 Cancers in 185 Countries. *CA Cancer J Clin* (2021) 71(3):209–49. doi: 10.3322/caac.21660
2. Siegel RL, Miller KD, Fuchs HE, Jemal A. Cancer Statistics, 2022. *CA Cancer J Clin* (2022) 72(1):7–33. doi: 10.3322/caac.21708
3. Yamazaki CM, Yamaguchi A, Anami Y, Xiong W, Otani Y, Lee J, et al. Antibody-Drug Conjugates With Dual Payloads for Combating Breast Tumor Heterogeneity and Drug Resistance. *Nat Commun* (2021) 12(1):3528. doi: 10.1038/s41467-021-23793-7
4. Franzoi MA, Romano E, Piccart M. Immunotherapy for Early Breast Cancer: Too Soon, Too Superficial, or Just Right? *Ann Oncol* (2021) 32(3):323–36. doi: 10.1016/j.annonc.2020.11.022
5. Savas P, Salgado R, Denkert C, Sotiriou C, Darcy PK, Smyth MJ, et al. Clinical Relevance of Host Immunity in Breast Cancer: From TILs to the Clinic. *Nat Rev Clin Oncol* (2016) 13(4):228–41. doi: 10.1038/nrclinonc.2015.215
6. Schumacher TN, Thommen DS. Tertiary Lymphoid Structures in Cancer. *Science* (2022) 375(6576):eabf9419. doi: 10.1126/science.abf9419
7. Sautès-Fridman C, Petitprez F, Calderaro J, Fridman WH. Tertiary Lymphoid Structures in the Era of Cancer Immunotherapy. *Nat Rev Cancer* (2019) 19 (6):307–25. doi: 10.1038/s41568-019-0144-6
8. Helmink BA, Reddy SM, Gao J, Zhang S, Basar R, Thakur R, et al. B Cells and Tertiary Lymphoid Structures Promote Immunotherapy Response. *Nature* (2020) 577(7791):549–55. doi: 10.1038/s41586-019-1922-8
9. Zhang NN, Qu FJ, Liu H, Li ZJ, Zhang YC, Han X, et al. Prognostic Impact of Tertiary Lymphoid Structures in Breast Cancer Prognosis: A Systematic Review and Meta-Analysis. *Cancer Cell Int* (2021) 21(1):536. doi: 10.1186/s12935-021-02242-x
10. Sofopoulos M, Fortis SP, Vaxevanis CK, Sotiriadou NN, Arnogiannaki N, Ardavanis A, et al. The Prognostic Significance of Peritumoral Tertiary Lymphoid Structures in Breast Cancer. *Cancer Immunol Immunother* (2019) 68(11):1733–45. doi: 10.1007/s00262-019-02407-8
11. Page MJ, McKenzie JE, Bossuyt PM, Boutron I, Hoffmann TC, Mulrow CD, et al. The PRISMA 2020 Statement: An Updated Guideline for Reporting Systematic Reviews. *Bmj* (2021) 372:n71. doi: 10.1136/bmj.n71
12. Tierney JF, Stewart LA, Ghersi D, Burdett S, Sydes MR. Practical Methods for Incorporating Summary Time-to-Event Data Into Meta-Analysis. *Trials* (2007) 8:16. doi: 10.1186/1745-6215-8-16
13. Hayden JA, van der Windt DA, Cartwright JL, Côté P, Bombardier C. Assessing Bias in Studies of Prognostic Factors. *Ann Intern Med* (2013) 158 (4):280–6. doi: 10.7326/0003-4819-158-4-201302190-00009
14. Hayden JA, Côté P, Bombardier C. Evaluation of the Quality of Prognosis Studies in Systematic Reviews. *Ann Intern Med* (2006) 144(6):427–37. doi: 10.7326/0003-4819-144-6-200603210-00010
15. Cabrita R, Lauss M, Sanna A, Donia M, Skaarup Larsen M, Mitra S, et al. Tertiary Lymphoid Structures Improve Immunotherapy and Survival in Melanoma. *Nature* (2020) 577(7791):561–5. doi: 10.1038/s41586-019-1914-8
16. He Y, Jiang Z, Chen C, Wang X. Classification of Triple-Negative Breast Cancers Based on Immunogenomic Profiling. *J Exp Clin Cancer Res* (2018) 37 (1):327. doi: 10.1186/s13046-018-1002-1
17. Newman AM, Liu CL, Green MR, Gentles AJ, Feng W, Xu Y, et al. Robust Enumeration of Cell Subsets From Tissue Expression Profiles. *Nat Methods* (2015) 12(5):453–7. doi: 10.1038/nmeth.3337
18. Kim A, Heo SH, Kim YA, Gong G, Jin Lee H, et al. An Examination of the Local Cellular Immune Response to Examples of Both Ductal Carcinoma in Situ (DCIS) of the Breast andWith Emphasis on Tertiary Lymphoid Structures and Tumor Infiltrating Lymphoctytes. *Am J Clin Pathol* (2016) 146(1):137–44. doi: 10.1093/ajcp/aqw097
19. Liu X, Tsang JYS, Hlaing T, Hu J, Ni YB, Chan SK, et al. Distinct Tertiary Lymphoid Structure Associations and Their Prognostic Relevance in HER2 Positive and Negative Breast Cancers. *Oncologist* (2017) 22(11):1316–24. doi: 10.1634/theoncologist.2017-0029
20. Park IA, Hwang SH, Song IH, Heo SH, Kim YA, Bang WS, et al. Expression of the MHC Class II in Triple-Negative Breast Cancer Is Associated With Tumor-Infiltrating Lymphocytes and Interferon Signaling. *PLoS One* (2017) 12(8):e0182786. doi: 10.1371/journal.pone.0182786
21. Noël G, Fontsa ML, Garaud S, De Silva P, de Wind A, Van den Eynden GG, et al. Functional Th1-Oriented T Follicular Helper Cells That Infiltrate Human Breast Cancer Promote Effective Adaptive Immunity. *J Clin Invest* (2021) 131(19) e139905. doi: 10.1172/JCI139905

22. Chao X, Liu L, Sun P, Yang X, Li M, Luo R, et al. Immune Parameters Associated With Survival in Metaplastic Breast Cancer. *Breast Cancer Res* (2020) 22(1):92. doi: 10.1186/s13058-020-01330-6
23. Song IH, Heo SH, Bang WS, Park HS, Park IA, Kim YA, et al. Predictive Value of Tertiary Lymphoid Structures Assessed by High Endothelial Venule Counts in the Neoadjuvant Setting of Triple-Negative Breast Cancer. *Cancer Res Treat* (2017) 49(2):399–407. doi: 10.4143/crt.2016.215
24. Lee M, Heo SH, Song IH, Rajayi H, Park HS, Park IA, et al. Presence of Tertiary Lymphoid Structures Determines the Level of Tumor-Infiltrating Lymphocytes in Primary Breast Cancer and Metastasis. *Mod Pathol* (2019) 32 (1):70–80. doi: 10.1038/s41379-018-0113-8
25. Lee HJ, Kim JY, Park IA, Song IH, Yu JH, Ahn JH, et al. Prognostic Significance of Tumor-Infiltrating Lymphocytes and the Tertiary Lymphoid Structures in HER2-Positive Breast Cancer Treated With Adjuvant Trastuzumab. *Am J Clin Pathol* (2015) 144(2):278–88. doi: 10.1309/AJCPIXUYDVZ0RZ3G
26. Figenschau SL, Fismen S, Fenton KA, Fenton C, Mortensen ES. Tertiary Lymphoid Structures Are Associated With Higher Tumor Grade in Primary Operable Breast Cancer Patients. *BMC Cancer* (2015) 15:101. doi: 10.1186/s12885-015-1116-1
27. Lee HJ, Park IA, Song IH, Shin SJ, Kim JY, Yu JH, et al. Tertiary Lymphoid Structures: Prognostic Significance and Relationship With Tumour-Infiltrating Lymphocytes in Triple-Negative Breast Cancer. *J Clin Pathol* (2016) 69(5):422–30. doi: 10.1136/jclinpath-2015-203089
28. Buisseret L, Garaud S, de Wind A, Van den Eynden G, Boisson A, Solinas C, et al. Tumor-Infiltrating Lymphocyte Composition, Organization and PD-1/Pd-L1 Expression Are Linked in Breast Cancer. *Oncoimmunology* (2017) 6(1): e1257452. doi: 10.1080/2162402X.2016.1257452
29. Song G. *Expression and Clinical Significance of CD4 +, CD8 + Lymphocytes and Tertiary Lymphoid Structures in Breast Cancer Tissues [Master Dissertation]*. University of South China (2017). Available at: https://kns.cnki.net/kcms/detail/detail.aspx?dbcode=CMFD&dbname=CMFD201801&filename=1018043053.nh&uniplatform=NZKPT&v=UMw9fuiD7_A2JsvaHbydkh1fSeVOkoZearxyexzNY9v-_WmOyonPOgq2IpSXtskM. [Accessed January 11, 2022].
30. Zhongwei Z. *Expression of Tertiary Lymphoid Structures in Breast Cancer and Its Clinical Significance [[Master Dissertation]]*. University of South China (2016). Available at : https://kns.cnki.net/kcms/detail/detail.aspx?dbcode=CMFD&dbname=CMFD201701&filename=1016317546.nh&uniplatform=NZKPT&v=zWJ5AFRcjn4wyhSUWN0DA3NjhcjAIXOFEJRTYlgCcEvQdJtf18RiCODxwnoDXOK6. [Accessed January 15, 2022].
31. Zhang Y, Gong G, Xu J, Wu S. Formation and Clinical Significance of Tertiary Lymphoid Structures in Invasive Ductal Carcinoma of Breast. *Chin J BioMed Eng* (2020) 26(4):323–7. doi: 10. 3760/cma. j. cnl15668-20200322-00087
32. Feng H, Yang F, Qiao L, Zhou K, Wang J, Zhang J, et al. Prognostic Significance of Gene Signature of Tertiary Lymphoid Structures in Patients With Lung Adenocarcinoma. *Front Oncol* (2021) 11:693234. doi: 10.3389/fonc.2021.693234
33. Lian X, Yang K, Li R, Li M, Zuo J, Zheng B, et al. Immunometabolic Rewiring in Tumorigenesis and Anti-Tumor Immunotherapy. *Mol Cancer* (2022) 21 (1):27. doi: 10.1186/s12943-021-01486-5
34. Wirsing AM, Ervik IK, Seppola M, Uhlin-Hansen L, Steigen SE, Hadler-Olsen E. Presence of High-Endothelial Venules Correlates With a Favorable Immune Microenvironment in Oral Squamous Cell Carcinoma. *Mod Pathol* (2018) 31(6):910–22. doi: 10.1038/s41379-018-0019-5
35. Rakaee M, Kilvaer TK, Jamaly S, Berg T, Paulsen EE, Berglund M, et al. Tertiary Lymphoid Structure Score: A Promising Approach to Refine the TNM Staging in Resected Non-Small Cell Lung Cancer. *Br J Cancer* (2021) 124(10):1680–9. doi: 10.1038/s41416-021-01307-y
36. Tang H, Qiu X, Timmerman C, Fu Y-X. Targeting Tertiary Lymphoid Structures for Tumor Immunotherapy. In: M-C Dieu-Nosjean, editor. *Tertiary Lymphoid Structures: Methods and Protocols*. New York, NY: Springer New York (2018). p. 275–86.
37. Paijens ST, Vledder A, de Bruyn M, Nijman HW. Tumor-Infiltrating Lymphocytes in the Immunotherapy Era. *Cell Mol Immunol* (2021) 18 (4):842–59. doi: 10.1038/s41423-020-00565-9
38. Denkert C, Loibl S, Noske A, Roller M, Müller BM, Komor M, et al. Tumor-Associated Lymphocytes as an Independent Predictor of Response to Neoadjuvant Chemotherapy in Breast Cancer. *J Clin Oncol* (2010) 28 (1):105–13. doi: 10.1200/JCO.2009.23.7370
39. Siliņa K, Soltermann A, Attar FM, Casanova R, Uckeley ZM, Thut H, et al. Germinal Centers Determine the Prognostic Relevance of Tertiary Lymphoid Structures and Are Impaired by Corticosteroids in Lung Squamous Cell Carcinoma. *Cancer Res* (2018) 78(5):1308–20. doi: 10.1158/0008-5472.CAN-17-1987
40. Lauss M, Donia M, Svane IM, Jönsson G. B Cells and Tertiary Lymphoid Structures: Friends or Foes in Cancer Immunotherapy? *Clin Cancer Res* (2021) 28(9):1751–8. doi: 10.1158/1078-0432.CCR-21-1130
41. Zhao H, Wang H, Zhou Q, Ren X. Insights Into Tertiary Lymphoid Structures in the Solid Tumor Microenvironment: Anti-Tumor Mechanism, Functional Regulation, and Immunotherapeutic Strategies. *Cancer Biol Med* (2021) 18 (4):981–91. doi: 10.20892/j.issn.2095-3941.2021.0029
42. Gobert M, Treilleux I, Bendriss-Vermare N, Bachelot T, Goddard-Leon S, Arfi V, et al. Regulatory T Cells Recruited Through CCL22/CCR4 Are Selectively Activated in Lymphoid Infiltrates Surrounding Primary Breast Tumors and Lead to an Adverse Clinical Outcome. *Cancer Res* (2009) 69(5):2000–9. doi: 10.1158/0008-5472.CAN-08-2360
43. Alberts E, Wall I, Calado DP, Grigoriadis A. Immune Crosstalk Between Lymph Nodes and Breast Carcinomas, With a Focus on B Cells. *Front Mol Biosci* (2021) 8:673051. doi: 10.3389/fmolb.2021.673051
44. Joshi NS, Akama-Garren EH, Lu Y, Lee DY, Chang GP, Li A, et al. Regulatory T Cells in Tumor-Associated Tertiary Lymphoid Structures Suppress Anti-Tumor T Cell Responses. *Immunity* (2015) 43(3):579–90. doi: 10.1016/j.immuni.2015.08.006
45. Li Q, Liu X, Wang D, Wang Y, Lu H, Wen S, et al. Prognostic Value of Tertiary Lymphoid Structure and Tumour Infiltrating Lymphocytes in Oral Squamous Cell Carcinoma. *Int J Oral Sci* (2020) 12(1):24. doi: 10.1038/s41368-020-00092-3
46. Petitprez F, de Reyniès A, Keung EZ, Chen TW, Sun CM, Calderaro J, et al. B Cells Are Associated With Survival and Immunotherapy Response in Sarcoma. *Nature* (2020) 577(7791):556–60. doi: 10.1038/s41586-019-1906-8
47. Sautès-Fridman C, Verneau J, Sun CM, Moreira M, Chen TW, Meylan M, et al. Tertiary Lymphoid Structures and B Cells: Clinical Impact and Therapeutic Modulation in Cancer. *Semin Immunol* (2020) 48:101406. doi: 10.1016/j.smim.2020.101406
48. Weinstein AM, Storkus WJ. Therapeutic Lymphoid Organogenesis in the Tumor Microenvironment. *Adv Cancer Res* (2015) 128:197–233. doi: 10.1016/bs.acr.2015.04.003

Conflict of Interest: The authors declare that the research was conducted in the absence of any commercial or financial relationships that could be construed as a potential conflict of interest.

frontiers | Frontiers in Immunology

CASE REPORT
published: 14 July 2022
doi: 10.3389/fimmu.2022.934700

Case Report: Subtotal Lymphoid and Total Marrow Irradiation as Bridge Therapy to CD19-Directed CAR T Cells in a Chemorefractory DLBCL With Leukemic Involvement

Simonetta Saldi[1†], Vincenzo Maria Perriello[2†], Lorenza Falini[2], Loredana Ruggeri[2], Christian Fulcheri[3], Sara Ciardelli[2], Alessandra Innocente[2], Stelvio Ballanti[2], Nicodemo Baffa[4], Leonardo Flenghi[2], Antonio Pierini[1], Cynthia Aristei[2] and Brunangelo Falini[1*]*

[1] Radiation Oncology Section, Department of Medicine and Surgery, University of Perugia, Perugia, Italy, [2] Hematology Section, Department of Medicine and Surgery, Center for Hemato-Oncological Research, University of Perugia, Perugia, Italy, [3] Health Physics Department, Ospedale S. Maria della Misericordia, Perugia, Italy, [4] Nuclear Medicine, Ospedale S. Maria della Misericordia, Perugia, Italy

CAR T cell therapy has transformed the salvage approach for relapsed/refractory diffuse large B-cell lymphoma (R/R DLBCL). Maintaining disease control before CAR T cell infusion during product manufacturing (so-called bridging therapy) is an important step to optimizing outcome. Among possible bridging therapies, radiation therapy (RT) represents a valuable option, particularly when the disease is limited. Here, we report for the first time on a patient with chemorefractory-transformed DLBCL showing nodal, extranodal, and massive bone marrow (BM) lymphoma infiltration associated with leukemic involvement, a successful bridge therapy to CD19-directed CAR T cell therapy by subtotal lymphoid/total marrow irradiation plus thiothepa followed by reinfusion of CD34+ autologous hematopoietic stem cells. Such a novel bridging regimen allowed a significant reduction of nodal and BM tumor volume while improving blood cell count before CAR T cell infusion. The PET-CT scan and BM evaluation performed at 1, 3, and 6 months after treatment showed complete remission of the disease. A relapse occurred at almost 1 year in lymph nodes because of CD19 antigen escape while the BM remained free of disease. This extended radiotherapy approach may be an effective bridging therapy for chemorefractory DLBCL patients eligible for CAR T cells who present with a high tumor burden, including massive BM involvement associated with leukemic involvement. This preliminary evidence is worth confirming in additional patients.

Keywords: CAR (chimeric antigen receptor) T cells, radiotherapy, diffuse large B-cell lymphoma, bridge therapy, gene therapy

OPEN ACCESS

Edited by:
Raffaella Greco,
San Raffaele Hospital (IRCCS), Italy

Reviewed by:
Gabriele Casirati,
Dana–Farber Cancer Institute, United States
Claire Roddie,
University College London, United Kingdom

****Correspondence:***
Vincenzo Maria Perriello
vincenzomaria.perriello@unipg.it
Brunangelo Falini
brunangelo.falini@unipg.it

†These authors have contributed equally to this work

Specialty section:
This article was submitted to Cancer Immunity and Immunotherapy, a section of the journal Frontiers in Immunology

Received: *02 May 2022*
Accepted: *20 June 2022*
Published: *14 July 2022*

Citation:
Saldi S, Perriello VM, Falini L, Ruggeri L, Fulcheri C, Ciardelli S, Innocente A, Ballanti S, Baffa N, Flenghi L, Pierini A, Aristei C and Falini B (2022) Case Report: Subtotal Lymphoid and Total Marrow Irradiation as Bridge Therapy to CD19-Directed CAR T Cells in a Chemorefractory DLBCL With Leukemic Involvement. Front. Immunol. 13:934700. doi: 10.3389/fimmu.2022.934700

INTRODUCTION

Chimeric antigen receptor (CAR) T cells directed against the CD19 B-cell molecule (tisagenlecleucel, axicabtagene, and lisocabtagene) induce long-term complete responses (CRs) in about 40% of relapsed/refractory (R/R) diffuse large B-cell lymphoma (DLBCL) patients (1–3). However, about 60% of cases show no or only temporary response to anti-CD19 CAR T cells because of several factors, including immune escape due to CD19 loss (4) or insufficient CAR T cell expansion/persistence *in vivo* (5).

Another major obstacle to the success of this adoptive T-cell therapy is the inability to control disease progression before CAR T cell infusion, particularly in patients with very high tumor burden, including massive bone marrow (BM) involvement. Bridging approaches to CAR T cells in chemorefractory DLBCL include polatuzumab vedotin (drug-conjugated anti-CD79b monoclonal antibody)-bendamustine-rituximab (6), drug-conjugated monoclonal antibodies directed against CD19 (7), bispecific antibodies (anti CD3/CD20) (7), or radiotherapy (RT) (8–10).

Here, we report on a 49-year-old woman with nodal, left iliopsoas muscle, BM, and subsequent leukemic involvement by chemorefractory DLBCL who was successfully bridged to CAR T cell therapy using subtotal lymphoid irradiation (sTLI) followed by total marrow irradiation (TMI) plus thiothepa and reinfusion of CD34+ autologous hematopoietic stem cells. To our knowledge, this is the first time sTLI/TMI has been adopted as a bridge therapy to allow the infusion of CAR T cells.

CASE PRESENTATION

A 49-year-old woman presented in 2019 because of low back pain, fever, and night sweats. A BM biopsy revealed a massive infiltration by CD5+ DLBCL, probably secondary to low grade B-cell lymphoma not otherwise specified. The FISH analysis showed monoallelic deletion of *TP53* and amplification of the *MYC* gene (range 4–9 signals) in virtually all tumor cells; no rearrangements of *BCL2* and *BCL6* were detected. A positron emission tomography/computed tomography (PET/CT) showed a hypermetabolic uptake by multiple supra- and sub-diaphragmatic lymph nodes, spleen, left iliopsoas muscle and BM. The patient received 5 cycles of R-CHOP (rituximab, cyclophosphamide, doxorubicin, and vincristine) plus 1 cycle of high-dose methotrexate (as prophylaxis for central nervous system involvement) that only led to a partial remission (PR) at PET/CT scan. She then underwent two cycles of salvage chemotherapy with R-DHAOX (rituximab, cytarabine, and oxaliplatin) followed by collection of CD34+ peripheral hematopoietic stem cells. After a FEAM conditioning regimen (fotemustine, etoposide, cytarabine, and melphalan), she underwent an autologous hematopoietic stem cell transplantation (auto-HSCT) without significant response (**Figure 1A**). Therefore, the patient was regarded as eligible for CAR T cell therapy and underwent an apheresis collection of lymphocytes. We opted for sTLI as a bridge to CAR T cells instead of polatuzumab-based regimens because polatuzumab was not yet available from the Italian Drug Agency (AIFA). Moreover, the disease appeared chemorefractory and the patient was radiotherapy-naïve raising the opportunity to obtain a certain degree of response. In particular, 20 Gy was delivered in 10 fractions over 5 days in all PET/TC positive tumor sites (i.e., the left iliopsoas muscle and all the main nodal stations, minus the mediastinum) except for the spleen, which received 11.5 Gy (**Figures 1B, C**). One month later, the disease evolved to leukemia (WBC 3,900/μl [normal: 4,000–9,000/μl], 70% tumor lymphoid cells) and the patient became transfusion dependent due to marked anemia (Hb 7.9 gr/dl [normal: 13 to 17 g/dl]) and thrombocytopenia (platelets, 10,000/μl [normal: 140,000–400,000/μl]). A BM biopsy showed massive involvement by DLBCL expressing CD19 (**Figures 1D–G**). For this reason, the patient received TMI (18 Gy; 1.8 Gy × 2/die for 5 days) (**Figures 1H, I**), followed by thiotepa (5 mg/kg) and an infusion of residual, previously collected autologous CD34+ hematopoietic stem cells (5.5×10^6/kg). Side effects included grade 4 mucositis limited to the mouth and requiring opioids, fever due to *Staphylococcus haemolyticus* sepsis (detected at blood cultures) that was successfully treated with daptomycin, and an asymptomatic increase of HHV6 copies in the peripheral blood for which she received ganciclovir.

After sTLI and TMI therapy, the PET/CT showed the disappearance of all metabolic positive lymphadenopathy but persistence of uptake in the left iliopsoas muscle (**Figure 2A**), while BM biopsy revealed about a 50% reduction of tumor cells. The residual lymphoma B cells expressed CD19 by immunohistochemistry. The blood cell count (BCC) showed: WBC 3,440/μl with the disappearance of circulating lymphoma cells, Hb 8.2 and an increase in platelet number (132,000/μl).

Given the good response to bridging therapy, the patient underwent lymphocyte depletion with fludarabine and cyclophosphamide, followed by a tisagenlecleucel infusion. She received a total of 130×10^6 CD3+ cells, with a 33% CD19-CAR-transduced T cell and a 2:1 CD4:CD8 ratio. After CAR T cell infusion, she experienced a grade 3 cytokine release syndrome (CRS) characterized by fever and hypotension that was successfully treated with tocilizumab (four doses), single dose dexamethasone (20 mg), and supportive therapy. Indeed, PET/CT scans performed 1, 3, and 6 months after tisagenlecleucel showed CR (**Figure 2B**). A prolonged neutropenia was observed with BCC returning to normal at 6 months (WB 4.970/μl, N 45%, L 41%, M 10%, Hb 11 g/dl, PLT 274,000/μl). Notably, despite previous TMI, the patient did not experience prolonged anemia or thrombocytopenia after CAR T cell therapy. CAR T cell expansion, monitored by flow cytometry every week after CAR T infusion, showed high CAR T cell levels in peripheral blood 14 days after infusion (276 CAR T positive cells/microliter) (**Figures 2F, G**). At 3 and 6 months after CAR T cell therapy, very low counts of normal B lymphocytes were detected by flow cytometry (B-cell aplasia), supporting the evidence of long-term CAR T cell persistence. At 11 months of follow-up, PET-CT showed a relapse in the left laterocervical and several retroperitoneal lymph nodes (**Figure 2C**) due to CD19 antigen escape (**Figure 2D**), while the BM biopsy showed a markedly hypocellular marrow without infiltration

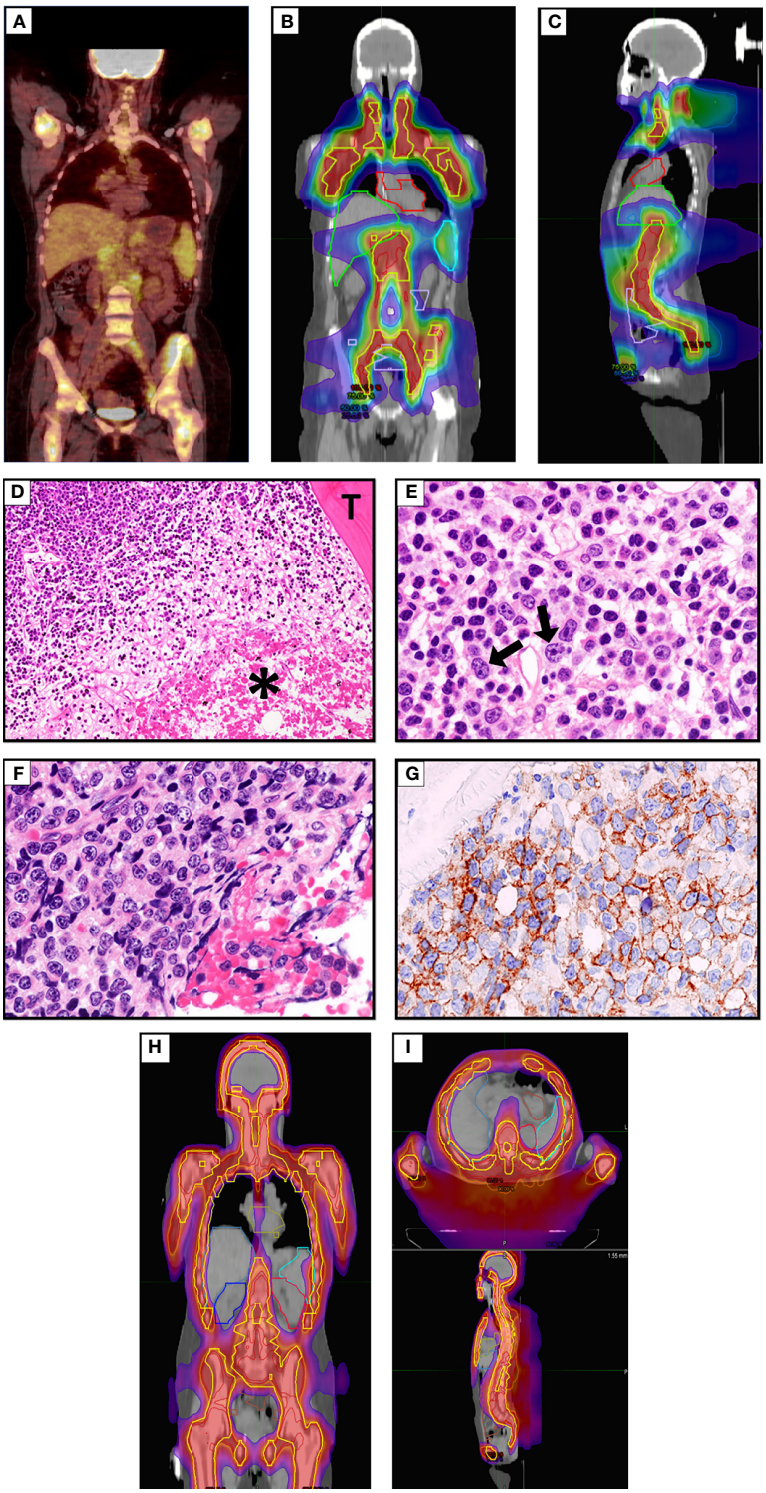

FIGURE 1 | **(A)** FDG-PET/CT coronal maximum intensity projection (MIP) image before sTLI showing avid uptake of BM, multiple lymph nodes and iliopsoas muscle. **(B, C)** sTLI dose distribution color wash **(B)**, coronal view **(C)**, sagittal view. **(D)** Massive BM involvement by DLBCL. The asterisk * indicates a large area of necrosis. T indicates a BM trabecula (Hematoxylin–Eosin; × 100). **(E)** An area from the same section as **(D)** showing infiltration by low grade B-cell lymphoma and occasional large cells (arrows) (Hematoxylin–Eosin; ×400). **(F)** The same section as **(D)** showing another area infiltrated by DLBCL cells (Hematoxylin–Eosin; ×400), that express the CD19 molecule **(G)** (Leica immunoperoxidase staining; ×400). **(H, I)** Total marrow irradiation (TMI) dose distribution color wash **(H)**, coronal view **(I)**, axial and sagittal view.

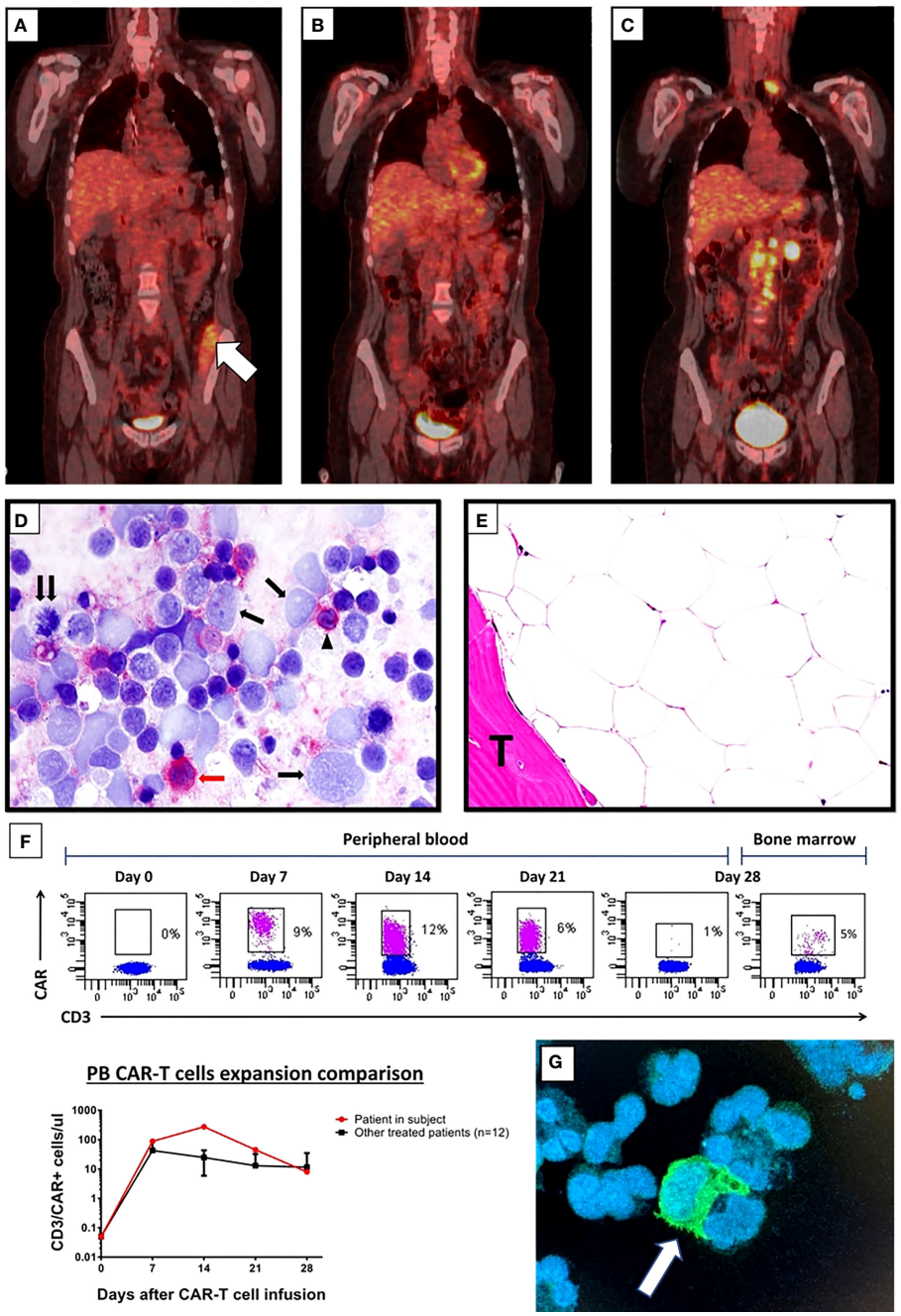

FIGURE 2 | **(A–C)** FDG-PET/CT coronal maximum intensity projection (MIP) image after sTLI/TMI and before CAR T cells; white arrow in **(A)** indicates metabolic uptake in the iliopsoas muscle **(A)** FDG-PET/CT after CD19-directed CAR T cell therapy showing metabolic complete response at 6 months **(B)** and DLBCL relapse at 11 months **(C)**. **(D)** Imprint of latero-cervical lymph node at relapse immunostained for the CD19 CAR target (detected in red). Almost all large lymphoma cells appear CD19-negative (single arrows); the double arrow points to a CD19-negative tumor cell in mitosis. The red arrow indicates a CD19 positive (red) large tumor cell while the arrowhead indicates a CD19 positive (red) normal small B lymphocyte (Alkaline Phosphatase Anti-Alkaline Phosphatase (APAAP) technique; ×400). Negativity of >95% of tumor cells for CD19 was also confirmed in frozen and paraffin sections of the lymph node (not shown). **(E)** BM biopsy taken 11 months after CAR T cell infusion showing a markedly hypocellular marrow without lymphoma infiltration. T indicated BM trabecula. (Hematoxylin–Eosin; ×400). **(F)** Flow cytometry plots showing CAR T cells detected in the CD3+ T-cell subsets in the peripheral blood every week the first month after CAR T cell infusion and in bone marrow aspirate at day 28-disease assessment (top). Comparison of CAR T cell absolute count expansion between the patient in subject and mean of the other treated patients in our center (n = 12) at indicated time points after CAR T cell infusion (bottom). CAR T cells were detected staining anti-CD19 CARs by the biotinylated CD19 CAR detection reagent (Miltenyi) together with anti-biotin-APC. **(G)** Immunofluorescence image stained by biotinylated CD19 CAR detection reagent (Miltenyi) together with anti-FC FITCH conjugated secondary antibody (Thermo-Fisher, green) and DAPI (for cell nuclei, blue) performed on cytospin preparation from the peripheral blood of the patient obtained 14 days after CAR T cell infusion. The white arrow indicates a CAR T cell probably embracing a leukemic B cell.

by lymphoma (**Figure 2E**). Because of her young age and good performance status, she is now being considered for haploidentical HSCT (**Figure 3**, timeline of events).

DISCUSSION AND CONCLUSIONS

Patients with R/R DLBCL frequently require bridge therapy to decrease the tumor burden before CAR T cell infusion (10). In fact, low tumor burden has been associated with improved overall response rate, durability of response at 1 year (2, 11, 12) and lower treatment-related toxicity, mainly CRS (9). Moreover, an increased LDH (13) or a high metabolic tumor volume-MTV on PET/CT (14) in R/R DLBCL treated with axicabtagene, correlated with shorter PFS and OS. Similarly, a high tumor burden was predictive of lower event-free survival in adult B-ALL patients treated with CD19-directed CAR T cells (15). Thus, optimal tumor debulking before CAR T cell infusion can potentially improve the outcome.

To our knowledge, this is the first time that sTLI and TMI have been used as bridging therapies to CAR T cell infusion in a chemorefractory leukemic DLBCL. In general, RT appears particularly attractive as bridging therapy to CAR T cells, especially in patients with highly chemorefractory (10, 16–18) and high tumor burden (19). In one study, bridging RT was superior to bridging chemo-immunotherapy in terms of PFS (10), allowing all patients to receive CAR T cells (axicabtagene) versus 74 and 67% of patients who underwent other forms of bridging therapy. So far, bridging RT has been mainly delivered to limited target volumes, independently of disease extension (10). However, in the present patient, sTLI to all involved areas was used to reduce out-of-field disease progression (10, 20). Although CD19 CAR T cells can eradicate substantial tumor cell infiltration in B-ALL in progressive disease settings, data in DLBCL are limited. Our patient had a high-burden progressive disease (including massive BM and peripheral blood involvement) that in DLBCL has been associated with a lower response to CAR T cells and higher rates of CRS and ICANS. Thus, going ahead with CAR T cell therapy would have probably increased the risk of severe CAR-related toxicities. Based on these considerations, we decided to deliver TMI followed by an infusion of autologous CD34+ hematopoietic stem cells before CAR T cells. Slight B-cell lymphoma contamination of the CD34+ purified hematopoietic stem cells of the patient was disregarded because contaminated cells were expected to be killed by CAR T cells. Despite the fact that the treatment in our patient was very active resulting in a CR of almost one year duration, she unfortunately relapsed because of CD19 escape.

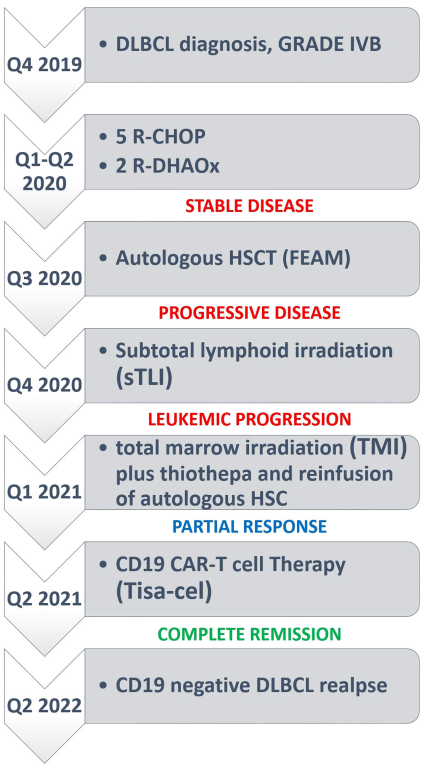

FIGURE 3 | Timelines of events.

The optimal RT dose and fractionation schedule for CAR T cells remain unclear. Commonly used doses are 30 Gy (3 Gy fraction) or 20 Gy (4 Gy fraction), which have been associated with local control in about 80% of patients (8). In a retrospective assessment, diverse schedules (median total dose of 35 Gy in a median of 2.5 Gy fraction) had no impact on PFS (10). Large irradiated volumes in our patient dictated the fractionation schedule, which was derived from our conditioning regimen for haploidentical HSCT with regulatory and effector T cells in AML using TLI plus TMI (21). This "comprehensive" RT allowed bridging to CAR T cells and achieving almost 1 year of CR in an otherwise incurable case. TLI + TMI sculpts radiation doses to lymph nodes, spleen, and bones while reducing them to visceral organs (22, 23). Further clinical and laboratory assessments will help determine whether using this RT approach may be of benefit in patients with high burden disease and improving blood cell count, as in the present case. On the other hand, it remains unclear whether bridging "comprehensive" RT provides better outcomes than irradiating small volumes in candidates for CAR T cell therapy. In fact, the benefits of localized bridging RT may extend beyond the irradiated area by inducing systemic immune-mediated anti-tumor responses, the so-called abscopal effect (24). Local irradiation has been reported to sensitize tumor cells to adoptive T-cell therapy through a number of mechanisms (25–27), including: i) the release of tumor-associated antigens, facilitating their cross-presentation by dendritic cells and antigen-specific T-cell priming; ii) enhancing migration of cytotoxic T lymphocytes to irradiated areas *via* increased release of chemokines; and iii) improving their proliferation and effector function in irradiated sites. Robust CAR T cell expansion and long-time persistence have been associated with enhanced responses and prolonged survival, while poor *in vivo* proliferation has been closely correlated with failure (28).

In conclusion, salvage treatments of R/R DLBCL are rapidly evolving with novel approaches such as bispecific and drug-conjugated antibodies, including polatuzumab combinations. In the near future, the main challenge will be to find the best bridge

therapy for CAR T cells according to patient and disease features. Bridging therapy may not have only the role of controlling the disease during CAR T cell manufacturing but should be part of the treatment, with the aim of further improving the expansion and persistence of adoptive T-cell therapy and, consequently, the outcome. For patients at increased risk of non response/relapse following CD19-directed CAR T cell therapy, as the patient presented here, the role of bridging "comprehensive" radiotherapy, including TLI ± TMI approaches and potentially consolidative allogeneic SCT, should be further evaluated in clinical trials.

DATA AVAILABILITY STATEMENT

The original contributions presented in the study are included in the article/**Supplementary Material**. Further inquiries can be directed to the corresponding authors.

ETHICS STATEMENT

Written informed consent was obtained from the individual(s) for the publication of any potentially identifiable images or data included in this article.

AUTHOR CONTRIBUTIONS

SS, VMP, CA, and BF conceived and designed the study. SS, CF, and CA carried out Radiotherapy. VMP, LFa, AI, SB, LFi, and BF managed the patient. VMP and BF carried out the pathological analysis. LR, SC, and AP carried out the immunophenotype analysis. BF wrote the manuscript. SS, VMP, LF, and CA approved the final draft of the manuscript. All authors listed have made a substantial, direct, and intellectual contribution to the work and approved it for publication.

REFERENCES

1. Neelapu SS, Locke FL, Bartlett NL, Lekakis LJ, Miklos DB, Jacobson CA, et al. Axicabtagene Ciloleucel CAR T-Cell Therapy in Refractory Large B-Cell Lymphoma. *N Engl J Med* (2017) 377(26):2531–44. doi: 10.1056/NEJMoa1707447
2. Abramson JS, Palomba ML, Gordon LI, Lunning MA, Wang M, Arnason J, et al. Lisocabtagene Maraleucel for Patients With Relapsed or Refractory Large B-Cell Lymphomas (TRANSCEND NHL 001): A Multicentre Seamless Design Study. *Lancet* (2020) 396(10254):839–52. doi: 10.1016/S0140-6736(20)31366-0
3. Schuster SJ, Bishop MR, Tam CS, Waller EK, Borchmann P, McGuirk JP, et al. Tisagenlecleucel in Adult Relapsed or Refractory Diffuse Large B-Cell Lymphoma. *N Engl J Med* (2019) 380(1):45–56. doi: 10.1056/NEJMoa1804980
4. Plaks V, Rossi JM, Chou J, Wang L, Poddar S, Han G, et al. CD19 Target Evasion as a Mechanism of Relapse in Large B-Cell Lymphoma Treated With Axicabtagene Ciloleucel. *Blood* (2021) 138(12):1081–5. doi: 10.1182/blood.2021010930
5. Xu X, Sun Q, Liang X, Chen Z, Zhang X, Zhou X, et al. Mechanisms of Relapse After CD19 CAR T-Cell Therapy for Acute Lymphoblastic Leukemia and Its Prevention and Treatment Strategies. *Front Immunol* (2019) 10:2664. doi: 10.3389/fimmu.2019.02664
6. Liebers N, Duell J, Fitzgerald D, Kerkhoff A, Noerenberg D, Kaebisch E, et al. Polatuzumab Vedotin as a Salvage and Bridging Treatment in Relapsed or Refractory Large B-Cell Lymphomas. *Blood Adv* (2021) 5(13):2707–16. doi: 10.1182/bloodadvances.2020004155
7. Logue JM, Chavez JC. How to Sequence Therapies in Diffuse Large B-Cell Lymphoma Post-CAR-T Cell Failure. *Curr Treat Options Oncol* (2021) 22(12):112. doi: 10.1007/s11864-021-00906-4
8. Sim AJ, Jain MD, Figura NB, Chavez JC, Shah BD, Khimani F, et al. Radiation Therapy as a Bridging Strategy for CAR T Cell Therapy With Axicabtagene Ciloleucel in Diffuse Large B-Cell Lymphoma. *Int J Radiat Oncol Biol Phys* (2019) 105(5):1012–21. doi: 10.1016/j.ijrobp.2019.05.065
9. Wright CM, LaRiviere MJ, Baron JA, Uche C, Xiao Y, Arscott WT, et al. Bridging Radiation Therapy Before Commercial Chimeric Antigen Receptor T-Cell Therapy for Relapsed or Refractory Aggressive B-Cell Lymphoma. *Int J Radiat Oncol Biol Phys* (2020) 108(1):178–88. doi: 10.1016/j.ijrobp.2020.05.014
10. Pinnix CC, Gunther JR, Dabaja BS, Strati P, Fang P, Hawkins MC, et al. Bridging Therapy Prior to Axicabtagene Ciloleucel for Relapsed/Refractory Large B-Cell Lymphoma. *Blood Adv* (2020) 4(13):2871–83. doi: 10.1182/bloodadvances.2020001837
11. Locke FL, Ghobadi A, Jacobson CA, Miklos DB, Lekakis LJ, Oluwole OO, et al. Long-Term Safety and Activity of Axicabtagene Ciloleucel in Refractory Large B-Cell Lymphoma (ZUMA-1): A Single-Arm, Multicentre, Phase 1-2 Trial. *Lancet Oncol* (2019) 20(1):31–42. doi: 10.1016/S1470-2045(18)30864-7
12. Locke FL, Rossi JM, Neelapu SS, Jacobson CA, Miklos DB, Ghobadi A, et al. Tumor Burden, Inflammation, and Product Attributes Determine Outcomes of Axicabtagene Ciloleucel in Large B-Cell Lymphoma. *Blood Adv* (2020) 4(19):4898–911. doi: 10.1182/bloodadvances.2020002394
13. Nastoupil LJ, Jain MD, Feng L, Spiegel JY, Ghobadi A, Lin Y, et al. Standard-Of-Care Axicabtagene Ciloleucel for Relapsed or Refractory Large B-Cell Lymphoma: Results From the US Lymphoma CAR T Consortium. *J Clin Oncol* (2020) 38(27):3119–28. doi: 10.1200/JCO.19.02104
14. Dean EA, Mhaskar RS, Lu H, Mousa MS, Krivenko GS, Lazaryan A. High Metabolic Tumor Volume is Associated With Decreased Efficacy of Axicabtagene Ciloleucel in Large B-Cell Lymphoma. *Blood Adv* (2020) 4(14):3268–76. doi: 10.1182/bloodadvances.2020001900
15. Park JH, Riviere I, Gonen M, Wang X, Sénéchal B, Curran KJ, et al. Long-Term Follow-Up of CD19 CAR Therapy in Acute Lymphoblastic Leukemia. *N Engl J Med* (2018) 378(5):449–59. doi: 10.1056/NEJMoa1709919
16. Tseng YD, Chen YH, Catalano PJ, et al. Rates and Durability of Response to Salvage Radiation Therapy Among Patients With Refractory or Relapsed Aggressive non-Hodgkin Lymphoma. *Int J Radiat Oncol Biol Phys* (2015) 91(1):223–31. doi: 10.1016/j.ijrobp.2014.09.041
17. Plastaras JP, Chong EA, Schuster SJ. Don't Get Stuck on the Shoulder: Radiation Oncologists Should Get Into the CAR With T-Cell Therapies. *Int J Radiat Oncol Biol Phys* (2019) 105(5):1022–4. doi: 10.1016/j.ijrobp.2019.09.005
18. Smith EL, Mailankody S, Staehr M, Wang X, Senechal B, Purdon TJ, et al. BCMA-Targeted CAR T-Cell Therapy Plus Radiotherapy for the Treatment of Refractory Myeloma Reveals Potential Synergy. *Cancer Immunol Res* (2019) 7(7):1047–53. doi: 10.1158/2326-6066.CIR-18-0551
19. Qu C, Ping N, Kang L, Liu H, Qin S, Wu Q, et al. Radiation Priming Chimeric Antigen Receptor T-Cell Therapy in Relapsed/Refractory Diffuse Large B-Cell Lymphoma With High Tumor Burden. *J Immunother* (2020) 43(1):32–7. doi: 10.1097/CJI.0000000000000284
20. Imber BS, Sadelain M, DeSelm C, Batlevi C, Brentjens RJ, Dahi PB, et al. Early Experience Using Salvage Radiotherapy for Relapsed/Refractory non-Hodgkin Lymphomas After CD19 Chimeric Antigen Receptor (CAR) T Cell Therapy. *Br J Haematol* (2020) 190(1):45–51. doi: 10.1111/bjh.16541
21. Pierini A, Ruggeri L, Carotti A, Falzetti F, Saldi S, Terenzi A, et al. Haploidentical Age-Adapted Myeloablative Transplant and Regulatory and Effector T Cells for Acute Myeloid Leukemia. *Blood Adv* (2021) 5(5):1199–208. doi: 10.1182/bloodadvances.2020003739

22. Wong JY, Liu A, Schultheiss T, Popplewell L, Stein A, Rosenthal J, et al. Targeted Total Marrow Irradiation Using Three-Dimensional Image-Guided Tomographic Intensity-Modulated Radiation Therapy: An Alternative to Standard Total Body Irradiation. *Biol Blood Marrow Transplant* (2006) 12 (3):306–15. doi: 10.1016/j.bbmt.2005.10.026
23. Stein A, Palmer J, Tsai NC, Al Malki MM, Aldoss I, Ali H, et al. Phase I Trial of Total Marrow and Lymphoid Irradiation Transplantation Conditioning in Patients With Relapsed/Refractory Acute Leukemia. *Biol Blood Marrow Transplant* (2017) 23(4):618–24. doi: 10.1016/j.bbmt.2017.01.067
24. Buchwald ZS, Wynne J, Nasti TH, Zhu S, Mourad WF, Yan W, et al. Radiation, Immune Checkpoint Blockade and the Abscopal Effect: A Critical Review on Timing, Dose and Fractionation. *Front Oncol* (2018) 8:612. doi: 10.3389/fonc.2018.00612
25. Weiss T, Weller M, Guckenberger M. NKG2D-Based CAR T Cells and Radiotherapy Exert Synergistic Efficacy in Glioblastoma. *Cancer Res* (2018) 78(4):1031–43. doi: 10.1158/0008-5472.CAN-17-1788
26. Lai JZ, Zhu YY, Ruan M. Local Irradiation Sensitized Tumors to Adoptive T Cell Therapy *via* Enhancing the Cross-Priming, Homing, and Cytotoxicity of Antigen-Specific CD8 T Cells. *Front Immunol* (2019) 10:2857. doi: 10.3389/fimmu.2019.02857
27. Matsumura S, Wang B, Kawashima N, Braunstein S, Badura M, Cameron TO, et al. Radiation-Induced CXCL16 Release by Breast Cancer Cells Attracts Effector T Cells. *J Immunol* (2008) 181(5):3099–107. doi: 10.4049/jimmunol.181.5.3099
28. Gupta A, Gill S. CAR-T Cell Persistence in the Treatment of Leukemia and Lymphoma. *Leuk Lymphoma* (2021) 62(11):2587–99. doi: 10.1080/10428194.2021.1913146

Conflict of Interest: The authors declare that the research was conducted in the absence of any commercial or financial relationships that could be construed as a potential conflict of interest.

Publisher's Note: All claims expressed in this article are solely those of the authors and do not necessarily represent those of their affiliated organizations, or those of the publisher, the editors and the reviewers. Any product that may be evaluated in this article, or claim that may be made by its manufacturer, is not guaranteed or endorsed by the publisher.

frontiers | Frontiers in Immunology

TYPE Original Research
PUBLISHED 06 October 2022
DOI 10.3389/fimmu.2022.984666

OPEN ACCESS

EDITED BY
Peter J. Siska,
University Medical Center Regensburg, Germany

REVIEWED BY
Roni Rayes,
McGill University, Canada
Dong Xie,
Tongji University, China

*CORRESPONDENCE
Zhiqiang Xue
xuezhiqiang301@126.com

†These authors have contributed equally to this work

SPECIALTY SECTION
This article was submitted to Cancer Immunity and Immunotherapy, a section of the journal Frontiers in Immunology

RECEIVED 02 July 2022
ACCEPTED 23 September 2022
PUBLISHED 06 October 2022

CITATION
Cai W, Jing M, Gu Y, Bei T, Zhao X, Chen S, Wen J, Gao J, Wu C and Xue Z (2022) Tumor microenvironment features decipher the outperformance of neoadjuvant immunochemotherapy over chemotherapy in resectable non-small cell lung cancer.
Front. Immunol. 13:984666.
doi: 10.3389/fimmu.2022.984666

Tumor microenvironment features decipher the outperformance of neoadjuvant immunochemotherapy over chemotherapy in resectable non-small cell lung cancer

Wenhan Cai[1†], Miao Jing[1†], Yajun Gu[2], Ting Bei[2], Xiaochen Zhao[2], Shiqing Chen[2], Jiaxin Wen[1], Jie Gao[3], Chongchong Wu[4] and Zhiqiang Xue[1*]

[1]Department of Thoracic Surgery, the First Medical Center of Chinese PLA General Hospital, Beijing, China, [2]Department of Medical Affairs, 3D Medicines Inc., Shanghai, China, [3]Department of Pathology, the First Medical Center of Chinese PLA General Hospital, Beijing, China, [4]Department of Diagnostic Radiology, the First Medical Center of Chinese PLA General Hospital, Beijing, China

This study evaluated the efficacy of neoadjuvant immunochemotherapy (Io+Chemo) versus chemotherapy alone (Chemo) in resectable non–small cell lung cancer (NSCLC) in a real-world setting. The association of tumor immune microenvironment (TIME) with pathologic response to different neoadjuvant therapies was also explored.Stage I–III NSCLC patients who received Io+Chemo or Chemo alone followed by surgery were included in the study. Tumor tissues collected during surgery were subjected to TIME evaluation using multiplex immunohistochemistry to measure immune cell subsets, including T cells, B cells, NK cells, and macrophages. Fifty-five patients were included, including 24 treated with neoadjuvant Io+Chemo and 31 with Chemo alone. Io+Chemo induced significantly higher major pathologic response (MPR) (75.0% vs. 38.7%, P = 0.0133) and numerically better pathologic complete response (pCR) (33.3% vs. 12.9%, P = 0.1013) than Chemo. Compared with tumors with Chemo, tumors with Io+Chemo demonstrated a significantly higher ratio of M1 macrophage density in the tumor to that in the stroma (P = 0.0446), more abundant $CD8^+$ cells in the stroma (P = 0.0335), and fewer $PD\text{-}L1^+CD68^+$ cells in both tumor and stroma. pCR/MPR patients displayed significantly higher density of $CD3^+$, $CD3^+CD4^+$, $CD20^+$, CD56 bright cell subsets and more tertiary lymphoid structures and significantly lower density of $PD\text{-}L1^+CD68^+$ and $CD3^+CD4^+Foxp3^+$cells in the tumor or stroma. This study favored neoadjuvant Io+Chemo over Chemo and revealed the TIME features underlying the outperformance of Io+Chemo over Chemo.

KEYWORDS

non-small cell lung cancer, PD-(L) 1 blockade, tumor immune microenvironment, neoadjuvant therapy, immunochemotherapy

Introduction

Immunotherapies targeting cytotoxic T lymphocyte-associated protein 4 (CTLA4) and the axis of programmed death 1 (PD-1)/programmed death ligand-1 (PD-L1) have ushered the modern era of oncology. Following the approval of pembrolizumab as the frontline treatment for advanced and metastatic non-small cell lung cancers (NSCLC) patients who are PD-L1 positive, neoadjuvant use of anti-PD-L1/PD-1 antibody has been exploited (1). Increasing trials are currently underway to evaluate the preoperative utility of anti-PD-L1/PD-1 antibody in multiple malignancies, including lung cancer. CheckMate 159 (NCT02259621), a phase II trial, reported a major pathologic response (MPR) rate of 45% in stage I–III NSCLC with nivolumab (2). That rate from other studies of anti-PD-L1/PD-1 antibody decreased, ranging from 13.8% to 40.0% (3–8). More recently, the NADIM trial, which examined the combination of nivolumab with chemotherapy, has reported superior pathologic complete response (pCR) and MPR rates of 82.9% and 63.4%, respectively, and 36-month progression-free survival (PFS) and overall survival (OS) of 81.1% and 91.0%, respectively, among patients with stage IIIA NSCLC, showing great promise of PD-(L)1 blockade plus chemotherapy in shifting the paradigm of NSCLC (9, 10). Similarly, CheckMate 816 showed that neoadjuvant nivolumab plus chemotherapy increased MPR and pCR rate to 36.9% and 24.0%, respectively, in stage IB-IIIA NSCLC, and other trials (clinical trial NO. NCT02572843, NCT02716038, NCT04304248) released remarkably consistent MPR rate running the gamut between ~62% and ~67% and favorable pCR rate as well (11–14).

As a newcomer of "common dominator" for cancer therapy, immunotherapy of PD-(L)1 blockade exerts a distinct mechanism in comparison with chemotherapy. Whereas neoadjuvant chemotherapy aims to preoperatively "debulk" tumors to resectable ones, neoadjuvant PD-(L)1 blockades, termed normalization cancer immunotherapy, exploit strategy based on immune evasion mechanisms to restore antitumor immunity to defend tumor antigens. Anti-PD-(L)1 recovers the functional tumor-specific cytotoxic T cells in the tumor immune microenvironment (TIME). Moreover, neoadjuvant PD-(L)1 blockade leverages the high levels of tumor antigen in the primary tumor to enhance T cell priming (15). At present, extensive studies are unmet to better understand the mechanism actions for these two distinct therapeutic treatments. Particularly, the mechanisms underlying the outperformance of PD-(L)1 blockade plus chemotherapy were poorly studied. The co-effects of this combination on immune response and TIME could be illuminated by analyzing tumor specimens obtained after neoadjuvant treatment, which offered a rich source for in-depth interrogations. Findings from that studies may uncover pathways, mechanisms, and biomolecules that could be co-targeted in new treatment combinations to increase the efficacy of anti–PD-(L)1 drugs (15).

Except for CheckMate 816, few studies evaluated PD-(L) 1 blockade plus chemotherapy and chemotherapy alone in a head-to-head manner. This study investigates the treatment response to neoadjuvant treatment with Io+Chemo in comparison with Chemo alone in a real-world cohort of patients with resectable NSCLC. The associations of post-NAT TIME with treatment and treatment response were also explored, attempting to elucidate the mechanism underlying the effects of neoadjuvant immunotherapy plus chemotherapy.

Materials and methods

Participants and study design

NSCLC patients who received neoadjuvant immunotherapy combined with chemotherapy (Io+Chemo) or chemotherapy alone (Chemo), followed by surgery between October 5, 2018 and June 30, 2021 at the First Medical Center of Chinese PLA General Hospital were retrospectively included if they were aged over 18 years and had resectable stage I–III NSCLC, at least one radiologically measurable target lesion, and an Eastern Cooperative Oncology Group (ECOG) performance status (PS) of 0~1. Patients were excluded for having driver mutations (*EGFR* 19 deletion/L858R and *ALK* fusion), anti-tumor pretreatment, previous exposure to immunosuppressive drugs, autoimmune disease, and organ transplantation. All surgical specimens were subjected to pathologic response and TIME evaluation. This study aimed to investigate the effects of neoadjuvant Io+Chemo and Chemo on NSCLC patients and TIME. The association of post-NAT TIME with pathologic response was also explored (Fig. 1). The research protocol, standard operating procedure (SOP) of data collection, and case report form (CRF) were prospectively designed before the beginning of the study to guarantee the data quality. All procedures performed involving human participants were conducted in accordance with Declaration of Helsinki (as revised in 2013). This study was approved by the ethics committee of the First Medical Center of Chinese PLA General Hospital, and written informed consent was obtained from each patient.

Assessment

Hematoxylin and eosin (H&E) staining was performed on the surgical resection to access pathologic responses to neoadjuvant therapy. An MPR was defined as having less than 10% residual viable tumor cells, and a pCR referred to no

residual tumor cells. Computed tomography (CT) scans were conducted before and after neoadjuvant therapy to access radiologic responses of primary tumors.

Multiplex immunofluorescence staining

Surgical tissue specimens were subjected to the examination of the TIME, which was performed as previously described by 3D Medicines, Inc., a College of American Pathologists (CAP)-accredited and Clinical Laboratory Improvement Amendments (CLIA)-certified laboratory (16). The Akoya OPAL Polaris 7-Color Automation IHC kit (NEL871001KT) was applied to conduct multiplex immunofluorescence (mIF) staining following manufacturer's instructions. Primary antibodies targeting CD163 (Abcam, ab182422, 1:500), CD68 (Abcam, ab213363, 1:1000), PD-1 (CST, D4W2J, 86163S, 1:200), PD-L1 (CST, E1L3N, 13684S, 1:400), CD3 (Dako, A0452, 1:1), CD4 (Abcam, ab133616, 1:100), CD8 (Abcam, ab178089, 1:200), CD56 (Abcam, ab75813, 1:1000), CD20 (Dako, L26, IR604, 1:1), Foxp3 (Abcam, ab20034, 1:100) and pan-CK (Abcam, ab7753, 1:100) or S100 (Abcam, ab52642, 1:200) were sequentially applied to FFPE tissue slides, followed by incubation with secondary antibodies and horseradish peroxidase and tyramide signal amplifying reagent. Nuclei acids were stained with DAPI. Multiplex stained slides were scanned using a Vectra Polaris Quantitative Pathology Imaging System (Akoya Biosciences), which was configured to capture fluorescent spectra at 20 nm wavelength intervals from 440 nm to 780 nm with a fixed exposure time and an absolute magnification of ×200. All scans for each slide were then superimposed to obtain a single image. Unstained and monoplex stained slide images were applied to extract tissue autofluorescence and the spectrum of each fluorophore, respectively. Fluorescence images were imported and analyzed using the AP-TIME image analysis software (3D Medicines Inc.) (17). Tumor parenchyma and stroma were differentiated according to CK staining. The CK positive area with DAPI staining was defined as tumor region, and the CK negative area with DAPI staining was considered as stroma region. The quantities of various cell subsets were expressed as the count number of positively stained cells per square millimeter (cells per mm^2) and as the percentage of positively stained cells in all nucleated cells (%). Total density = (tumor cell counts + stroma cell counts)/(tumor area + stroma area). Total percentage = (tumor cell counts + stroma cell counts)/(tumor total cells + stroma total cells) ×100%. The density and percentage of immune cell subsets in tumor and stroma regions were figured out by detecting signal channel or multiple-channel, namely $CD3^+$, $CD3^+CD4^+$, $CD8^+$, $Foxp3^+$, PD-1^+CD8^+, $CD4^+Foxp3^+$ (Treg), $CD68^+CD163^-$ (M1 macrophage), $CD68^+CD163^+$ (M2 macrophage), PD-$L1^+$ $CD68^+$, CD56 bright (NK cell), CD56 dim (NK cell). The co-occurrence of $CD3^+$ T cells and $CD20^+$ B cells indicates the formation of tertiary lymphoid structures (TLS).

Statistical analysis

The statistical analyses were performed using the Graphpad Prism 9.2 software. Fisher's exact test was used to analyze categorical variables (including NAT efficacy, age, sex, stage, pathology, smoking, and diabetes) between treatment groups. Comparisons between continuous variables with (i.e. BMI) normal distribution were performed using the unpaired t test, and the data with non-normal distribution (i.e. immune cell density) was analyzed by Mann–Whitney U test. $P < 0.05$ was considered statistically significant. The forest plots were built using ggplot2 package (R version 3.6.3). Logistic regression was used to investigate the association between baseline characteristics and pathologic response.

Results

Baseline characteristics

A total of 55 NSCLC patients who received Io+Chemo or Chemo alone before surgery and met the eligibility criteria were included in the study (Figure 1 and Table 1), including 24 in the Io+Chemo group and 31 in the Chemo alone group. Baseline characteristics were balanced between the two treatment groups. The median age of the entire cohort was 61 years (range, 38–72 years). Most patients were male (51/55, 92.73%) and smokers (46/55, 83.64%). Half of the patients had a stage III disease, and lung squamous cell carcinomas (39/55, 70.91%) was the predominant pathologic type.

Addition of immunotherapy to chemotherapy increased the NAT efficacy

Pathologic response of primary tumor from each patient was evaluated for neoadjuvant efficacy. 12 patients achieved a pCR and thirty obtained an MPR. No association was found between pathologic response and baseline characteristics (Supplementary Figure S1). Patients who received Io+Chemo displayed significantly higher MPR rate (75.0% vs. 38.7%, $P = 0.0133$) and numerically increased pCR rate (33.3% vs 12.9%, $P = 0.1013$) than those with Chemo alone (Figure 2). The above data were comparable to the results from the trials, which evaluated the combination of chemotherapy and immunotherapy in resectable NSCLC patients (Supplementary Figure S2) (11–14).

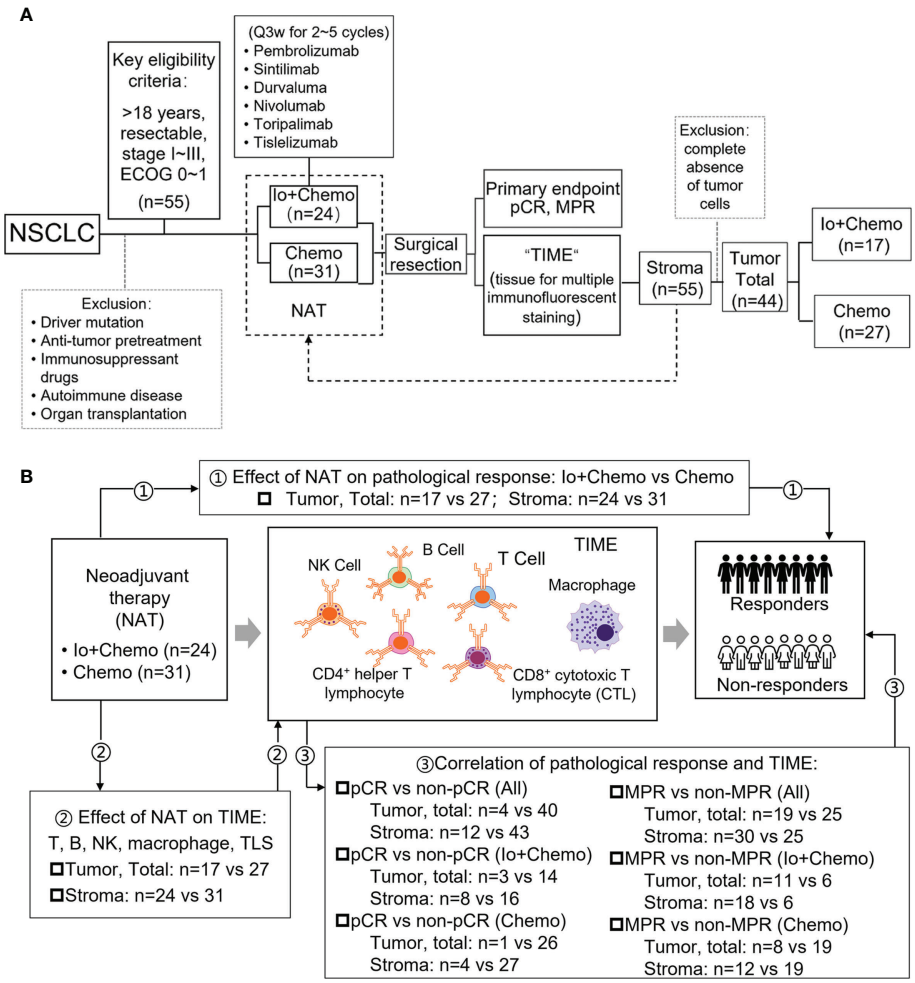

FIGURE 1
Study design examining effects of neoadjuvant therapies on resectable NSCLC patients. **(A)** Study flow chart depicting the study protocol. **(B)** The endpoints explored and sample details in each analyses. NSCLC, non-small cell lung cancer; TIME, tumor immune microenvironment; NAT, neoadjuvant therapy; pCR, pathological complete response; MPR, major pathological response; Io+Chemo, immunochemotherapy; Chemo, chemotherapy; CTL, cytotoxic T lymphocytes. Figure was created with Motifolio Toolkit (Motifolio Inc, Ellicott City, USA). *P <0.05; ns, no statistical significance.

Distinct immune cell infiltration upon neoadjuvant immunochemotherapy and chemotherapy alone

Surgical tissue specimens were subjected to mIF to examine the TIME upon NAT. Of the 55 tissue samples, 11 were identified as tumor-free for a complete absence of tumor cells according to the results of CK and DAPI staining. Thus, immune cell infiltration was evaluated in all 55 cases of tumor stroma and in 44 cases of tumor. The density and percentage of immune cell subsets in TIME were quantified. The $CD8^+$ cell was significantly more abundant in the stroma of the Io+Chemo group than that in the Chemo alone (P = 0.0335, Figure 3A). Compared with the Chemo group, the Io+Chemo group demonstrated a significantly higher M1 macrophage density ($CD68^+CD163^-$ cell subset) ratio in the tumor to that in the stroma (P = 0.0446; Figure 3B). A lower degree of infiltration of PD-$L1^+CD68^+$ cells was seen in both tumor and stroma in the Io+Chemo over in the Chemo (density: tumor, P = 0.0462, stroma, P = 0.0147, total, P = 0.0248; percentage: tumor, P = 0.0537, stroma, P =0.0171, total, P = 0.0156; Figure 3C). Such a decrease in the abundance of PD-$L1^+CD68^+$ cells could be explained by the fact that the PD-L1 on the surface of macrophages was thoroughly blocked by anti-PD-L1 antibodies upon immunotherapy. No difference was found in the infiltration of other immune cell subsets between the two NAT groups (Tables S1, S2).

TABLE 1 Baseline characteristics of NSCLC patients with neoadjuvant therapy.

Characteristics	All (n = 55)	Io+Chemo (n = 24)	Chemo (n = 31)	Io+Chemo vs. Chemo P value
Age, years				0.558
Median (range)	61 (38~72)	58.5 (38~72)	62 (43~72)	
≥65, n (%)	17 (30.91%)	6 (25.00%)	11 (35.48%)	
<65, n (%)	38 (69.09%)	18 (75.00%)	20 (64.52%)	
Sex, n (%)				1.000
Male	51 (92.73%)	22 (91.67%)	29 (93.55%)	
Female	4 (7.27%)	2 (8.33%)	2 (6.45%)	
Stage, n (%) before NAT				0.844
I	13 (23.64%)	5 (20.83%)	8 (25.81%)	
II	12 (21.82%)	6 (25.00%)	6 (19.35%)	
III	30 (54.55%)	13 (54.17%)	17 (54.84%)	
Pathology, n (%)				0.565
Sq	39 (70.91%)	16 (66.67%)	23 (74.19%)	
Non-Sq	16 (29.09%)	8 (33.33%)	8 (25.81%)	
Smoking, n (%)				0.716
Yes	46 (83.64%)	21 (87.50%)	25 (80.65%)	
No	9 (16.36%)	3 (12.50%)	6 (19.35%)	
Diabetes, n (%)				0.643
Yes	5 (9.09%)	3 (12.50%)	2 (6.45%)	
No	50 (90.91%)	21 (87.50%)	29 (93.55%)	
BMI, (kg/m^2)				0.677
Mean ± SD	24.97 ± 3.01	25.17 ± 3.42	24.82 ± 2.71	

Sq, lung squamous cell carcinomas; NAT, neoadjuvant therapy.

The association between pathologic response and TIME upon NAT

We sought to analyze whether pathologic responses were associated with TIME upon NAT and found that patients who achieved pCR showed a significantly lower infiltration of PD-L1$^+$CD68$^+$ (total, P = 0.018) and CD3$^+$CD4$^+$ Foxp3$^+$ cells (stroma, P = 0.0288) and a higher density of CD56$^+$ (stroma CD56 bright, P = 0.0135; stroma CD56 dim, P = 0.0136) and CD20$^+$ cells (stroma, P = 0.0488) in the TIME over the non-pCR

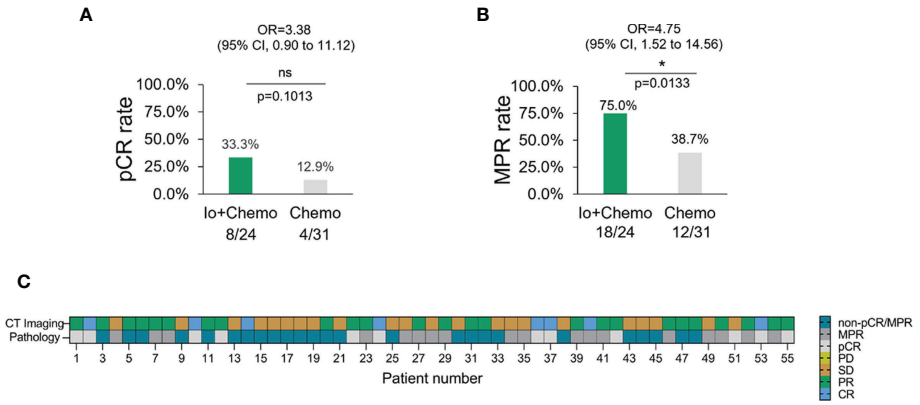

FIGURE 2
The pathologic response in NSCLC patients with different neoadjuvant therapy. **(A)** pCR rate among NSCLC patients with neoadjuvant Io+Chemo or Chemo alone therapy. **(B)** MPR rate among NSCLC patients with neoadjuvant Io+Chemo or Chemo alone therapy. **(C)** Concordance between pathologic and radiologic response. pCR, pathological complete response; MPR, major pathological response; Io+Chemo, immunochemotherapy; Chemo, chemotherapy. CT, computed tomography. *P < 0.05; ns, no statistical significance.

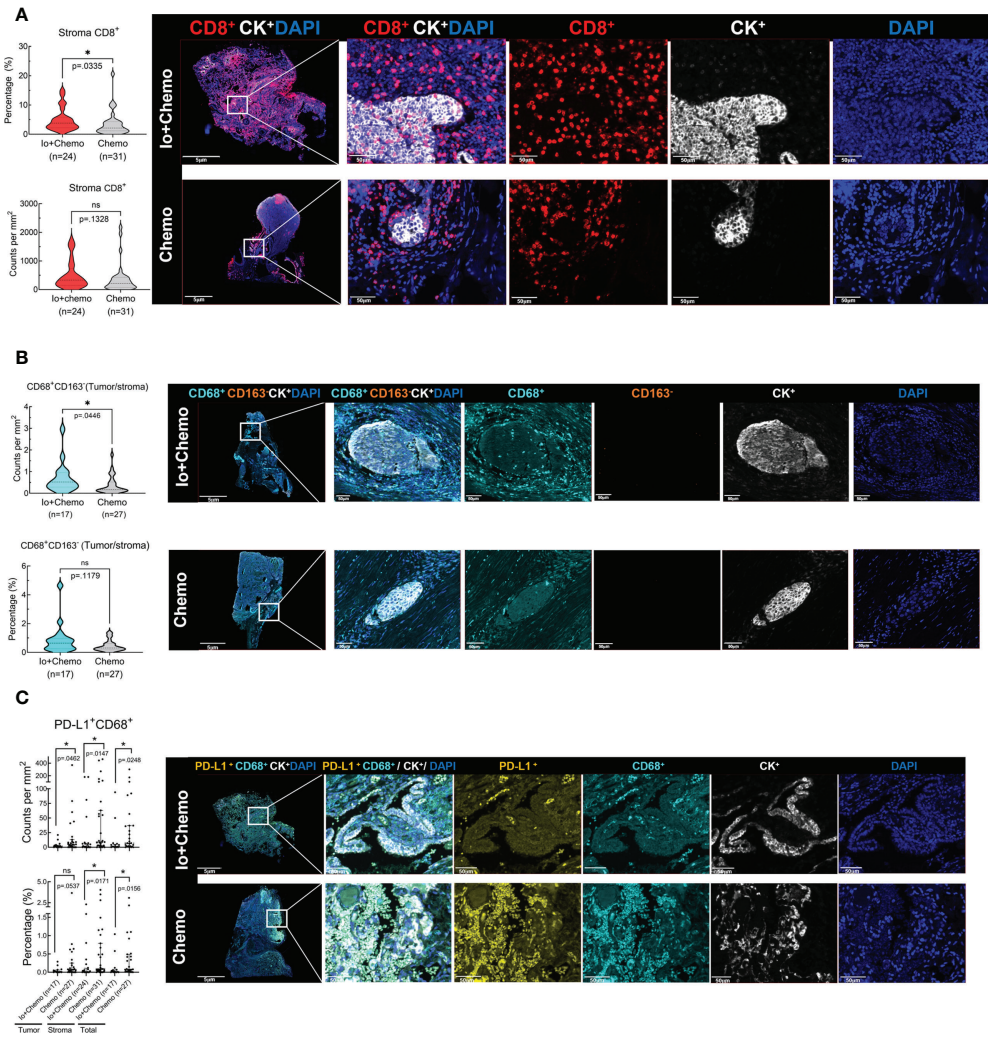

FIGURE 3
The immune cell biomarkers of tumor tissue samples from patients treated with neoadjuvant immunochemotherapy and chemotherapy alone. Multiplex immunofluorescence staining was performed for immune cell biomarkers, as denoted by different colors, in specimens of NSCLC patients treated with neoadjuvant therapy (surgical resection after NAT). The density and percentage of $CD8^+$ **(A)**, $CD68^+CD163^-$ **(B)**, and PD-$L1^+CD68^+$ **(C)** immune cells in the tumor center or stroma were analyzed. Representative images showing the multiplex immunofluorescence staining for identifying the immune cell subsets in the tumor immune microenvironment. Io+Chemo, immunochemotherapy; Chemo, chemotherapy; *P <0.05; ns, no statistical significance.

counterparts (Figures 4A–D). $CD3^+$ (tumor, P = 0.0491; total, P = 0.0218), $CD3^+CD4^+$ (tumor, P = 0.0201; total, P = 0.0305), and $CD20^+$ cells (tumor, P = 0.0425; stroma, P = 0.0214; total, P = 0.0176) and TLS (P = 0.0433) were more abundant in the TIME of MPR patients (Figures 4E–H) over that of the non-MPR patients. No difference was found in the infiltration of other immune cell subsets between the different responding groups (Tables S3–S5).

In patients who received Io+Chemo, no difference was found in immune cell infiltration between the responders and non-responders. A numerically higher density of TLS was observed in the TIME of MPR patients (Figure S3A and Tables S6–S8). While in the patients treated with Chemo, patients who achieved pCR were found to have a significantly lower density of $Foxp3^+$ cells over the non-pCR patients (stroma, P = 0.038). MPR patients showed a significantly higher infiltration of $CD3^+$ cells (Total, P = 0.0448), $CD20^+$ cells (stroma, P = 0.0254), and TLS (P= 0.0063) (Figures S3B–E and Tables S9–S11).

Discussion

In this real-world cohort of stage I-III resectable NSCLC patients, we report that the addition of PD-(L)1 blockade to chemotherapy was associated with an significantly increased

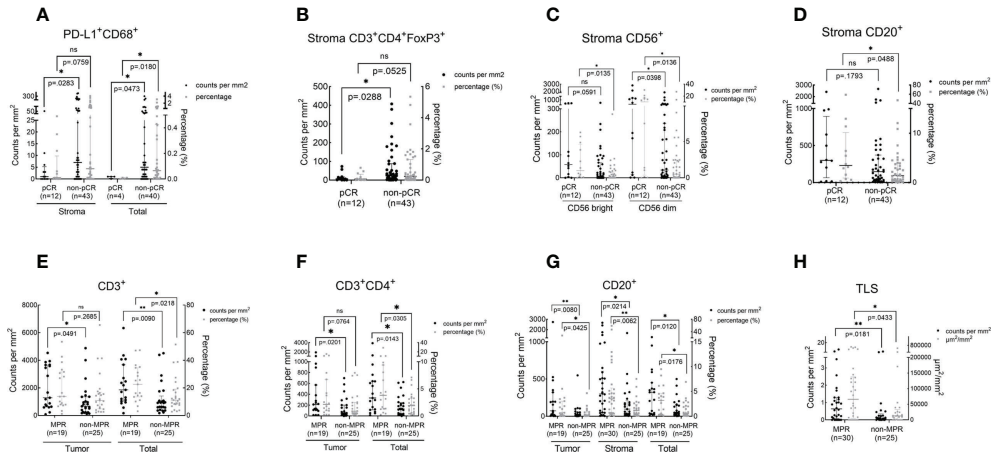

FIGURE 4
The association between immune cell infiltration in the TIME and pathologic response. The scatter plot was shown as median with interquartile range. pCR, pathological complete response; MPR, major pathological response; *P <0.05; *P <0.01; ns, no statistical significance. The density and percentage of PD-L1+CD68+ **(A)**, CD3+CD4+FoxP3+**(B)**, CD56+**(C)**, CD20+**(D, G)**, CD3+**(E)**, CD3+CD4+**(F)** immune cells and TLS **(H)** were statistical different in responders and non-responders. **p<0.01.

MPR rate and a numerically higher pCR rate in comparison to chemotherapy alone (MPR, 75.0% vs. 38.7%; pCR, 33.3% vs. 12.9%), which favored PD-(L)1 blockade plus chemotherapy over chemotherapy alone. mIF analysis of surgical resection specimens revealed that compared with patients subjected to NAT of Chemo alone, patients treated with Io+Chemo showed more abundant $CD8^+$ cells in tumor stroma and a higher ratio of M1 macrophage density in the tumor center to that in the tumor stroma, suggesting the potential mechanism underlying a better response to Io+Chemo than Chemo alone. Among the entire cohort, patients who obtained MPR or pCR displayed significantly increased infiltration of $CD20^+$ B cells, $CD3^+$ T cells, $CD3^+CD4^+$ T cells, $CD56^+$ NK cells, TLS, and lower density of $CD3^+CD4^+Foxp3^+$ nTreg cells and $PD\text{-}L1^+CD68^+$ cells compared with their non-MPR or non-pCR counterparts. In the Chemo alone group, increased infiltrations of $CD20^+$ B cells, $CD3^+$ T cells, and TLS were observed in MPR tumors over non-MPR ones, and a lower degree of infiltration of Foxp3+ cells was seen in the pCR tumors than that in the non-pCR tumors. In the Io+Chemo subgroup, no significant difference was found in the density of immune cell subsets between groups based upon response (Figure 5).

Most recently, CheckMate 816 has reported a significantly increased pathologic response induced by neoadjuvant nivolumab + chemotherapy over chemotherapy alone in stage IB to IIIA resectable NSCLC (11), which was slightly lower than that observed in our real-world cohort. Similarly, multiple single-arm trials released drastically increased MPR and pCR rates achieved from PD-(L)1 blockade plus chemotherapy (11–14). It is getting clear that the combinational strategy incorporating immune checkpoint inhibitors and chemotherapy is becoming the "primary actor" in the neoadjuvant NSCLC scenario. While cellular and molecular mechanism of PD-(L)1 blockade therapy has been studied, little is known about the mechanism underlying the outperformance of the combination of PD-(L)1 blockade with chemotherapy over chemotherapy alone. Our study evaluated the infiltration of immune cell subsets in the TIME utilizing the tumor tissue specimens collected after NAT (surgical specimen). A significantly higher degree of $CD8^+$ T cell infiltration was observed in Io+Chemo than that in Chemo alone, suggesting PD-(L)1 blockade more robustly restored antitumor immunity by promoting cytotoxic T cell activation and proliferation. Consistently, Forde P et al. observed an increased number of T-cell clones in both the tumor and peripheral blood after preoperative treatment of nivolumab, and other research groups also reported similar evidence across multiple tumor types, including lung cancer, ovarian cancer, colorectal cancer, and esophageal squamous cell carcinoma (2, 8, 18, 19).

Moreover, compared with those with Chemo alone, tumors upon Io+Chemo showed a higher ratio of M1 macrophage density in the tumor center to that in the tumor stroma, making it rational to speculate that PD-(L)1 blockade improved the polarization of M1-TAMs and promoted the infiltration of M1-TAMs from tumor stroma to tumor center. This observation was consistent with previous reports that M1-TAMs may elevate antitumor immunity by producing immune-activating cytokines, rendering the patients responsive to immunotherapy (19, 20). Interestingly, we observed a decrease in the abundance of $PD\text{-}L1^+CD68^+$ macrophages in the Io +Chemo-treated tumor stroma over that of Chemo alone. The potential reasons that might give explanations for this

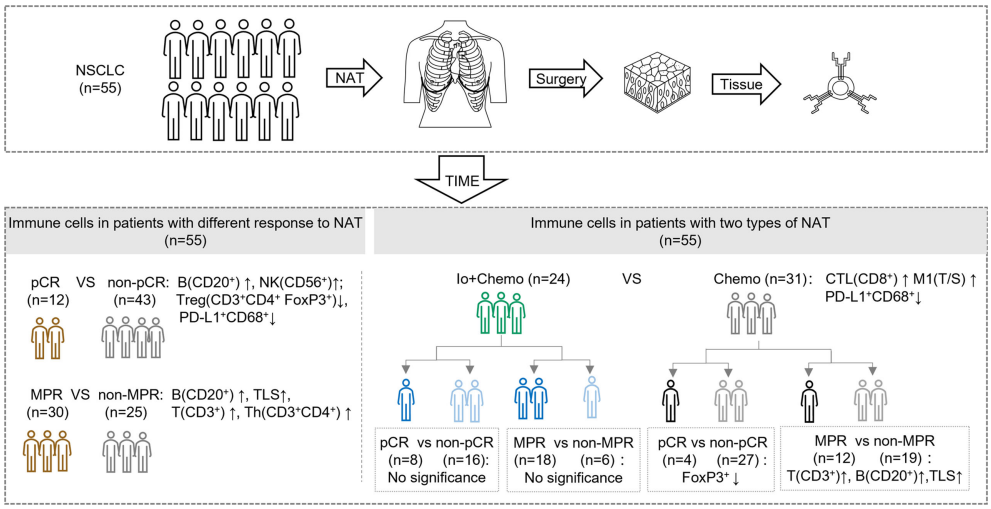

FIGURE 5
Summary of tumor microenvironment in patients with neoadjuvant therapy (NAT). TIME, tumor immune microenvironment; Io+Chemo, immunochemotherapy; Chemo, chemotherapy; pCR, pathological complete response; MPR, major pathological response. TLS, tertiary lymphoid structures; CTL, cytotoxic T lymphocytes; T/S, the ratio of tumor to stroma; M1, $CD68^+CD163^-$ macrophage. No significance means no difference at a given significance value (P <0.05). Figure was created with Motifolio Toolkit (Motifolio Inc, Ellicott City, USA).

phenomenon are the followings. First, PD-L1 that on the surface of microphages might be pre-blocked by anti-PD-L1 antibody (the immunotherapy regimen applied) before performing mIF. Second, we assumed that the immune-chemotherapy enhanced (or restored, if the PD-1/PD-L1 pathway is upregulated) antitumor immunity by altering the molecular characteristics of immune cell subsets to activate antitumor immune pathways, which involved the regulation of PD-L1 expression on macrophages. If the case was the second, it suggests that PD-(L)1 expression might not be the major hurdle for cancer patients who are less responsive to PD-(L)1 blockade. Perhaps the most novel look herein was that the combination of PD-(L)1 blockade with chemotherapy exerted similar effects on the TIME, such as increased infiltrations of $CD8^+$ T cells and promoted polarization of M1 TAMs, as reported in studies investigating mono-immunotherapy of PD-(L)1 blockade. At least, chemotherapy, as a component of the combinatorial therapy regimen, might not have played a rogue role for efficacy.

Based on the evidence that both neoadjuvant immunotherapy and chemotherapy can induce immune responses fine-tuned by stimulation and inhibitory signals pathways (2, 21–24), we further examined the association between pathologic response and TIME regardless of the therapy strategy. In the entire cohort, patients who obtained MPR or pCR displayed significantly increased infiltration of $CD20^+$ B cells, $CD3^+$ T cells, $CD3^+CD4^+$ T cells, $CD56^+$ NK cells, TLS, and decreased infiltration of $CD3^+CD4^+Foxp3^+$ Treg cells and $PD\text{-}L1^+CD68^+$ cells. Thus, we envision that the tumors achieving pathologic response should display an enhanced antitumor immune response by regulating T lymphocytes and B lymphocytes through multiple immune pathways, either induced by chemotherapy or immunotherapy.

We further examined the association between pathologic response and TIME in treatment subgroups. In the Io+Chemo population, no difference was found in immune cell infiltration between the responders and non-responders, which might resulted from a small sample size. A numerically higher density of TLS was observed in the TIME of MPR patients. While in the patients who were treated with Chemo, MPR patients showed a significantly higher infiltration of TLS, $CD3^+$ cells and $CD20^+$ cells. Patients who achieved pCR were found to have a significantly lower density of $FoxP3^+$ cells, which was consistent with previous reports that neoadjuvant chemotherapy increased cytotoxic T Cell, and B cell infiltration and decreased the density of $Foxp3^+$ T cells (23) in the tumor of resectable NSCLC patients (21, 22).

This study was primarily limited by the small size and its retrospective design. Prospective studies with larger sample sizes are warranted to confirm the findings. Another limitation was that pre-surgery biopsy samples were not available, for which the exploration of the predictive value of pre-surgery TIME for efficacy and the comparison of TIME before and after NAT were not feasible.

Conclusions

This real-world study favored neoadjuvant PD-(L)1 blockade plus chemotherapy over chemotherapy alone. We revealed for the first time that compared with chemo alone, Io +Chemo therapy was associated with increased infiltration of $CD8^+$ T cells, and promoted polarization of M1 macrophages. Our findings provided new insights of understanding the mechanisms underlying the outperformance of Io+Chemo over Chemo alone.

Data availability statement

The raw data supporting the conclusions of this article will be made available by the authors, without undue reservation.

Ethics statement

This study was approved by the ethics committee of the First Medical Center of Chinese PLA General Hospital, and written informed consent was obtained from each patient. The patients/participants provided their written informed consent to participate in this study.

Author contributions

WC: Acquisition of data, writing-review and editing. MJ: Methodology, writing-review and editing. YG: Data curation, formal analysis, writing-review and editing. TB: Writing–original draft, writing–review and editing. XZ: Conceptualization, resources, supervision, writing–review and editing. SC: Conceptualization, resources, supervision, writing–review and editing. JW: Resources, data curation, writing-review and editing. JG: Resources, data curation, writing-review and editing. CW: Resources, data curation, writing-review and editing. ZX: Conceptualization, resources, supervision, methodology, project administration, writing–review and editing. All authors contributed to the article and approved the submitted version.

Funding

This work was supported by the National Natural Science Foundation of China (NO. 62076254).

Acknowledgments

We would like to thank all coordinators at the First Medical Center of Chinese PLA General Hospital, China and 3D Medicines Inc., Shanghai, China for supporting this study.

Conflict of interest

YG, TB, XZ and SC are employees of 3D Medicines Inc. The other authors declare no potential conflicts of interest.

Publisher's note

Supplementary material

The Supplementary Material for this article can be found online at: https://www.frontiersin.org/articles/10.3389/fimmu.2022.984666/full#supplementary-material

References

1. (NCCN) NCCN. NCCN clinical practice guidelines in oncology. In: *Non-small cell lung cancer. version 3.* PA, USA: National Comprehensive Cancer Network. (2022).

2. Forde PM, Chaft JE, Smith KN, Anagnostou V, Cottrell TR, Hellmann MD, et al. Neoadjuvant PD-1 blockade in resectable lung cancer. *N Engl J Med* (2018) 378(21):1976–86. doi: 10.1056/NEJMoa1716078

3. Kwiatkowski DJ, Rusch VW, Chaft JE, Johnson BE, Nicholas A, Wistuba II, et al. Neoadjuvant atezolizumab in resectable non-small cell lung cancer (NSCLC): Interim analysis and biomarker data from a multicenter study (LCMC3). *J Clin Oncol* (2019) 37(15_suppl):8503–. doi: 10.1200/JCO.2019.37.15_suppl.8503

4. Gao S, Li N, Gao S, Xue Q, Ying J, Wang S, et al. Neoadjuvant PD-1 inhibitor (Sintilimab) in NSCLC. *J Thorac Oncol* (2020) 15(5):816–26. doi: 10.1016/j.jtho.2020.01.017

5. Tong BC, Gu L, Wang X, Wigle DA, Phillips JD, Harpole DHJr., et al. Perioperative outcomes of pulmonary resection after neoadjuvant pembrolizumab in patients with non–small cell lung cancer. *J Thorac Cardiovasc Surg* (2022) 163 (2):427–36. doi: 10.1016/j.jtcvs.2021.02.099

6. Wislez M, Mazieres J, Lavole A, Zalcman G, Carre O, Egenod T, et al. 1214O neoadjuvant durvalumab in resectable non-small cell lung cancer (NSCLC): Preliminary results from a multicenter study (IFCT-1601 IONESCO). *Ann Oncol* (2020) 31:S794. doi: 10.1016/j.annonc.2020.08.1416

7. Besse B, Adam J, Cozic N, Chaput-Gras N, Planchard D, Mezquita L, et al. 1215O - SC neoadjuvant atezolizumab (A) for resectable non-small cell lung cancer (NSCLC): Results from the phase II PRINCEPS trial. *Ann Oncol* (2020) 31:S794–S5. doi: 10.1016/j.annonc.2020.08.1417

8. Cascone T, William WNJr., Weissferdt A, Leung CH, Lin HY, Pataer A, et al. Neoadjuvant nivolumab or nivolumab plus ipilimumab in operable non-small cell lung cancer: the phase 2 randomized NEOSTAR trial. *Nat Med* (2021) 27(3):504–14. doi: 10.1038/s41591-020-01224-2

9. Provencio M, Nadal E, Insa A, García-Campelo MR, Casal-Rubio J, Dómine M, et al. Neoadjuvant chemotherapy and nivolumab in resectable non-small-cell lung cancer (NADIM): an open-label, multicentre, single-arm, phase 2 trial. *Lancet Oncol* (2020) 21(11):1413–22. doi: 10.1016/S1470-2045(20)30453-8

10. Provencio M, Nadal E, Insa A, Campelo MRG, Pereiro D, Domine M, et al. OA20.01 long term survival in operable stage Iiia Nsclc patients treated with neoadjuvant nivolumab plus chemotherapy - nadim study. *J Thorac Oncol* (2021) 16(10):S883. doi: 10.1016/j.jtho.2021.08.101

11. Forde PM, Spicer J, Lu S, Provencio M, Mitsudomi T, Awad MM, et al. Neoadjuvant nivolumab plus chemotherapy in resectable lung cancer. *New Engl J Med* (2022) 386(21):1973–85. doi: 10.1056/NEJMoa2202170

12. Rothschild SI, Zippelius A, Eboulet EI, Savic Prince S, Betticher D, Bettini A, et al. SAKK 16/14: Durvalumab in addition to neoadjuvant chemotherapy in patients with stage IIIA(N2) non–Small-Cell lung cancer–a multicenter single-arm phase II trial. *J Clin Oncol* (2021) 39(26):2872–80. doi: 10.1200/JCO.21.00276

13. Shu CA, Gainor JF, Awad MM, Chiuzan C, Grigg CM, Pabani A, et al. Neoadjuvant atezolizumab and chemotherapy in patients with resectable non-small-cell lung cancer: An open-label, multicentre, single-arm, phase 2 trial. *Lancet Oncol* (2020) 21(6):786–95. doi: 10.1016/S1470-2045(20)30140-6

14. Zhao Z-R, Yang C-P, Chen S, Yu H, Lin Y-B, Lin Y-B, et al. Phase 2 trial of neoadjuvant toripalimab with chemotherapy for resectable stage III non-small-cell lung cancer. *OncoImmunology* (2021) 10(1):1996000. doi: 10.1080/2162402X.2021.1996000

15. Topalian SL, Taube JM, Pardoll DM. Neoadjuvant checkpoint blockade for cancer immunotherapy. *Science* (2020) 367(6477):eaax0182. doi: 10.1126/science.aax0182

16. Zhang W, Gong C, Peng X, Bi X, Sun Y, Zhou J, et al. Serum concentration of CD137 and tumor infiltration by M1 macrophages predict the response to sintilimab plus bevacizumab biosimilar in advanced hepatocellular carcinoma patients. *Clin Cancer Res* (2022) 28(16):3499–508. doi: 10.1158/1078-0432.CCR-21-3972

17. Cheng G, et al. Artificial intelligence-assisted score analysis for predicting the expression of the immunotherapy biomarker PD-L1 in lung cancer. *Front Immunol* (2022) 13. doi: 10.3389/fimmu.2022.893198

18. Thaker PH, Bradley WH, Leath CAIII, Gunderson Jackson C, Borys N, Anwer K, et al. GEN-1 in combination with neoadjuvant chemotherapy for patients with advanced epithelial ovarian cancer: A phase I dose-escalation study. *Clin Cancer Res* (2021) 27(20):5536–45. doi: 10.1158/1078-0432.CCR-21-0360

19. Yang G, Su X, Yang H, Luo G, Gao C, Zheng Y, et al. Neoadjuvant programmed death-1 blockade plus chemotherapy in locally advanced esophageal squamous cell carcinoma. *Ann Trans Med* (2021) 9(15):1254. doi: 10.21037/atm-21-3352

20. Li X, Liu R, Su X, Pan Y, Han X, Shao C, et al. Harnessing tumor-associated macrophages as aids for cancer immunotherapy. *Mol Cancer* (2019) 18(1):177. doi: 10.1186/s12943-019-1102-3

21. Gaudreau P-O, Negrao MV, Mitchell KG, Reuben A, Corsini EM, Li J, et al. Neoadjuvant chemotherapy increases cytotoxic T cell, tissue resident memory T cell, and b cell infiltration in resectable NSCLC. *J Thorac Oncol* (2021) 16(1):127–39. doi: 10.1016/j.jtho.2020.09.027

22. Parra ER, Villalobos P, Behrens C, Jiang M, Pataer A, Swisher SG, et al. Effect of neoadjuvant chemotherapy on the immune microenvironment in non–small cell lung carcinomas as determined by multiplex immunofluorescence and image analysis approaches. *J ImmunoTher Cancer* (2018) 6(1):48. doi: 10.1186/s40425-018-0368-0

23. Devitt ME, Gade KE, Hall RD, Horton BJ, Stelow EB, Bullock T, et al. The effect of chemotherapy on the tumor immune microenvironment in non-small cell lung cancer (NSCLC): A single-institution retrospective analysis. *J Clin Oncol* (2018) 36(5_suppl):155. doi: 10.1200/JCO.2018.36.5_suppl.155

24. Wang S, Yuan P, Mao B, Li N, Ying J, Tao X, et al. Genomic features and tumor immune microenvironment alteration in NSCLC treated with neoadjuvant PD-1 blockade. *NPJ Precis Oncol* (2022) 6(1):2. doi: 10.1038/s41698-021-00244-6

frontiers | Frontiers in Immunology

TYPE Original Research
PUBLISHED 24 November 2022
DOI 10.3389/fimmu.2022.1064874

OPEN ACCESS

EDITED BY
Fanping Meng,
Fifth Medical Center of the PLA General Hospital, China

REVIEWED BY
Hongyan Huang,
Capital Medical University, China
Xiaofeng Li,
Tianjin Medical University Cancer Institute and Hospital, China

*CORRESPONDENCE
Jian Guan
guanjian5461@163.com
Yongzhong Zhan
171290466@qq.com
Laiyu Liu
liulaiyu@sina.com

†These authors have contributed equally to this work and share first authorship

SPECIALTY SECTION
This article was submitted to Cancer Immunity and Immunotherapy, a section of the journal Frontiers in Immunology

RECEIVED 08 October 2022
ACCEPTED 09 November 2022
PUBLISHED 24 November 2022

CITATION
Huang J, Yuan L, Huang W, Liao L, Zhu X, Wang X, Li J, Liang W, Wu Y, Liu X, Yu D, Zheng Y, Guan J, Zhan Y and Liu L (2022) LATPS, a novel prognostic signature based on tumor microenvironment of lung adenocarcinoma to better predict survival and immunotherapy response. *Front. Immunol.* 13:1064874. doi: 10.3389/fimmu.2022.1064874

LATPS, a novel prognostic signature based on tumor microenvironment of lung adenocarcinoma to better predict survival and immunotherapy response

Jihong Huang[1†], Lu Yuan[1†], Wenqi Huang[1†], Liwei Liao[1], Xiaodi Zhu[1], Xiaoqing Wang[2], Jiaxin Li[1], Wenyu Liang[1], Yuting Wu[3], Xiaocheng Liu[1], Dong Yu[1], Yunna Zheng[1], Jian Guan[2*], Yongzhong Zhan[1*] and Laiyu Liu[1*]

[1]Chronic Airways Diseases Laboratory, Department of Respiratory and Critical Care Medicine, Nanfang Hospital, Southern Medical University, Guangzhou, China, [2]Department of Radiation Oncology, Nanfang Hospital, Southern Medical University, Guangzhou, China, [3]Department of Blood Transfusion, Ganzhou People's Hospital, Ganzhou, China

Background: Clinically, only a minority of patients benefit from immunotherapy and few efficient biomarkers have been identified to distinguish patients who would respond to immunotherapy. The tumor microenvironment (TME) is reported to contribute to immunotherapy response, but details remain unknown. We aimed to construct a prognostic model based on the TME of lung adenocarcinoma (LUAD) to predict the prognosis and immunotherapy efficacy.

Methods: We integrated computational algorithms to describe the immune infiltrative landscape of LUAD patients. With the least absolute shrinkage and selection operator (LASSO) and Cox regression analyses, we developed a LUAD tumor microenvironment prognostic signature (LATPS). Subsequently, the immune characteristics and the benefit of immunotherapy in LATPS-defined subgroups were analyzed. RNA sequencing of tumor samples from 28 lung cancer patients treated with anti-PD-1 therapy was conducted to verify the predictive value of the LATPS.

Results: We constructed the LATPS grounded on four genes, including UBE2T, KRT6A, IRX2, and CD3D. The LATPS-low subgroup had a better overall survival (OS) and tended to have a hot immune phenotype, which was characterized by an elevated abundance of immune cell infiltration and increased activity of immune-related pathways. Additionally, tumor immune dysfunction and exclusion (TIDE) score was markedly decreased in the LATPS-low subgroup, indicating an enhanced opportunity to benefit from immunotherapy. Survival analysis in 28 advanced lung cancer patients treated with an anti-PD-1 regimen

10.3389/fimmu.2022.1064874

at Nanfang hospital revealed that the LATPS-low subgroup had better immunotherapy benefit.

Conclusion: LATPS is an effective predictor to distinguish survival, immune characteristics, and immunotherapy benefit in LUAD patients.

KEYWORDS

immunotherapy, prognosis, immune infiltration, tumor microenvironment, LUAD

Introduction

Immunotherapy has dramatically revolutionized the landscape of non-small cell lung cancer (NSCLC) treatment (1). Among the various immunotherapy, immune checkpoint inhibitors (ICIs) reactivate the immune system to eliminate cancer cells, exhibiting a durable anti-tumor response in NSCLC patients (2, 3). However, not all NSCLC patients respond to ICIs treatment. The overall response rate (ORR) was only about 40% in PD-L1 > 50% cases (4, 5). Multiple reported factors including PD-L1, TMB, and MSI can't efficiently predict immunotherapy response (6). Thus, new biomarkers are urgently needed.

Recently, the tumor microenvironment (TME) was demonstrated to exhibit a strong influence on the response to ICIs treatment (7, 8). Jiang P et al. constructed a tumor immune dysfunction and exclusion (TIDE) model based on the status of T cell dysfunction and exclusion. The TIDE model had a higher accuracy for predicting the immunotherapy response of advanced NSCLC compared with traditional PD-L1 expression and TMB (9). However, the TIDE model needs to conduct whole transcriptome sequencing of the tumor samples. Besides, the TIDE model only focused on the T cells' status, which may not be insufficient to reflect the complexity of the TME in patients with NSCLC.

NSCLC accounts for nearly 85% of lung cancer and lung adenocarcinoma (LUAD) is the most common pathological type, making up approximately 40% of lung cancers (1). Thus, a deeper understanding of the TME might help to discover novel biomarkers for immunotherapy in LUAD. In the present study, we sought to explore the immune landscape in LUAD using the CIBERSORT and ESTIMATE algorithms, screen out differently expressed genes and construct a LUAD tumor microenvironment prognostic signature (LATPS). Subsequently, we explored the clinical value of the LATPS in predicting survival and immunotherapeutic benefits in LUAD patients.

Materials and methods

Patients and data collection

The RNA sequencing data and corresponding clinical annotations were retrieved from The Cancer Genome Atlas (TCGA) database (https://portal.gdc.cancer.gov/). Microarray profiles were downloaded from Gene Expression Omnibus (GEO) (https://www.ncbi.nlm.nih.gov/geo/). We collected 1088 LUAD patients (GSE42127, GSE72094, and TCGA-LUAD) and combined them into a meta cohort after normalization (10) to generate the LATPS.

To evaluate the predictive value of the LATPS for immunotherapy benefits, three independent immunotherapy cohorts, including two NSCLC cohorts who received anti-PD-1 treatment (GSE135222, GSE126044), 28 advanced NSCLC patients with intervention of anti-PD-1 therapy at Nanfang Hospital (Guangzhou, China) from January 2019 to June 2021, were chosen to verify the predictive value of the constructed LATPS for immunotherapy benefits. The detailed clinical characteristics are presented in Supplementary Table 1. In Nanfang Hospital cohort, Patients were eligible for enrolment if they were aged ≥18 years, diagnosed with advanced NSCLC, had an Eastern Cooperative Oncology Group (ECOG) performance status score of 0 or 1. Exclusion criteria included: unstable or untreated central nervous system metastases, uncontrolled infection, ongoing corticosteroid therapy over 10 mg prednisone per day, active autoimmune disease within the past 2 years, discontinued to received ICIs due to serious ICIs-related adverse events (IRAs), and those who lost of follow-ups. The patients were treated with anti-PD-1 therapy every 3 weeks as a cycle. Tumor response was assessed every 2 cycles according to the Response Evaluation Criteria in Solid Tumors (RECIST), version 1.1 (11). Archived formalin-fixed, paraffin embedded (FFPE) tumor samples of the 28 NSCLC patients were collected prior to receiving immunotherapy. Before sample collection, it was

approved by the Ethics Committee of Nanfang Hospital. To validate the survival classification and predictive capability of the LATPS, other four independent LUAD cohorts, including GSE29016 (n=38), GSE31210 (n=226), GSE41271 (n=182), and GSE50081 (n=127) were applied as external validation cohorts.

RNA sequencing and data processing

The RNA was first extracted from FFPE samples and quantified on a Qubit 3.0/4.0, then it was assessed on a 2100 Bioanalyzer. Next, a part of total RNA (50 ng) was used with the SMARTer Stranded Total RNA-Seq Kit v2 according to the low-throughput protocol. We applied the Illumina NovaSeq 6000 Sequencing System to conduct RNA-seq libraries paired-end sequencing after PCR enrichment and purification. To ensure data quality, we used Trimmomatic (12), RSeQC (13), and bowtie2 (14) to preprocess the raw reads and obtain clean reads, which were used for subsequent analyses. Based on default parameters, we used FeatureCounts (15) to evaluate the expression level of each gene. All the sequencing data used in this study passed the quality control, with the data screening threshold set at greater than 3 G, and a uniquely mapping rate greater than 60%.

Identification of differentially expressed genes and functional enrichment analysis

The abundance of infiltrated immune cells in LUAD samples was evaluated based on the LM22 gene signature with the "CIBERSORT" package (16). We used the "ESTIMATE" package to assess the immune and stromal contents of each LUAD sample, which further generated TME scores, including ImmuneScore, StromalScore, and ESTIMATEScore. The ESTIMATEScore was calculated as the sum of ImmuneScore and StromalScore. Higher ESTIMATEScore refers to lower tumor purity (17). According to the CIBERSORT results, we performed consensus clustering with the "ConsensusClusterPlus" package (18). We applied the "km" algorithm based on "euclidean" distance of ConsensusClusterPlus package. Subsequently, an empirical cumulative distribution function (CDF) diagram and a delta area diagram were generated to visualize the clustering results, in which k represented the number of subgroups. We chose k = 3 as the optimal value for the delta area showed a significant reduction and CDF plateaued when k > 3, which classified LUAD patients into three TME subgroups. A consensus matrix was generated to demonstrate the clustering stability of the hierarchical clustering results. Principal component analysis (PCA) was used to visualize the clustering pattern. DEGs among different TME subgroups were identified using the "Limma" package with the screening threshold set at a p-value< 0.05 and an absolute log2FoldChange > 1. "Boruta" package was applied to reduce superfluous genes. We conducted gene ontology (GO) enrichment analysis utilizing the "clusterProfiler" package (19). GO terms with p-value< 0.05 were considered statistically significant.

Constructing the LATPS for patients with LUAD

We screened out 1035 LUAD patients (the total cohort) with matched survival information from the meta cohort. Then, the total cohort was randomly divided into a training cohort and a test cohort at a ratio of 1:1. We used the training cohort to identify prognostic genes and construct the LATPS. Firstly, we used univariate Cox regression analysis to screen out the significant prognostic genes from the DEGs (p-value< 0.01). Secondly, to minimize overfitting (20), we performed LASSO analysis using the "glmnet" package. Finally, after filtration using LASSO analysis, we established the LATPS based on four hub genes filtered by Multivariate Cox regression analysis. Subsequently, we calculated the LATPS score as follows:

$$\text{LATPS score} = \sum_i Coefficient\ of\ gene(i) \times Expression\ of\ gene\ (i)$$

Coefficient of gene (i) represents the regression coefficients of the four hub genes in the Cox model and *Expression of gene (i)* means the expression value of the four hub genes for patients with LUAD. Thereafter, we classified the patients into a LATPS-high subgroup and a LATPS-low subgroup according to the median LATPS scores. Moreover, we conducted survival analysis using "survival" and "survminer" packages. To evaluate the predictive power and capability of the LATPS, Time-dependent receiver operating characteristic (ROC) in the "timeROC" package was analyzed. Furthermore, we performed a prognostic meta-analysis to evaluate the comprehensive predictive significance of LATPS in four validation cohorts (n=573) using the "meta" R package.

Analyzing the predictive value of the LATPS for immunotherapy response

We applied single sample gene set enrichment analysis (ssGSEA) algorithm to quantify the relative abundance of the immune cell infiltration in each LUAD sample using the gene set variation analysis (GSVA) package. Twenty eight immune cell subpopulations gene signatures were obtained from a previous study (21) and the other 24 types of tumor-infiltrating immune cells (TIICs) gene signatures were downloaded from the Immune Cells Abundance Identifier (ImmuCellAI) database. We then performed GSVA to estimate the variation of pathway activity over a sample population in an unsupervised manner

based on the "GSVA" package (22). We obtained the twenty five immune-related pathways gene signatures from a previous study (23). The Spearman method was utilized to analyze the correlation between LATPS score and immune-related pathways or immune cell infiltration level. Results were filtered by setting a p-value< 0.05 as a threshold and were visualized using lollipop plots. Thereafter, we scored LUAD patients using the TIDE algorithm online (http://tide.dfci.harvard.edu/). Additionally, we performed survival and ROC analyses in three independent cohorts who received immunotherapy to investigate the potential value of the LATPS to predict immunotherapy benefits.

Establishing a nomogram signature

We collected clinicopathological factors integrated with transcriptome profile of LUAD patients. Then we performed univariate and multivariate Cox regressions to determine whether the LATPS model was an independent prognostic factor. We employed the "rms" and "foreign" packages to establish a predictive nomogram on the basis of the clinicopathological factors and LATPS score. Subsequently, calibration curve and ROC curve analyses were used to assess the predictive precision of the nomogram.

Statistical analysis

The Mann-Whitney U test was employed to compare continuous variables between two groups. Kruskal–Wallis tests were used to conduct difference comparisons of three or more groups (24). The Chi-squared test was carried out to compare categorical variables between two groups. Survival curve analysis was conducted using the Kaplan–Meier method and log-rank tests were used to identify significant differences among subgroups. A p-value< 0.05 was considered statistically significant. All analyses were processed with R version 4.0.2 and its appropriate packages.

Results

Characterization of immune cell landscape in LUAD

The workflow chart of our study is shown in Figure 1. LUAD samples (n = 1088) from GSE72094, GSE42127, and TGCA-LUAD were combined into one meta-cohort after normalization. Table 1 summarizes the baseline information of the patients with LUAD in different datasets. PCA was applied to visualize the overall expression pattern of the three LUAD cohorts before and after normalization (Supplementary Figures 1A, B). The ESTIMATE algorithm then generated TME scores, including StromalScore, ImmuneScore, and ESTIMATEScore. Survival analyses showed that TME score-high patients had better OS, indicating that the TME may influence the OS of LUAD patients (Figures 2A-C).

To further analyze the immune cell landscape of LUAD patients, we first calculated the abundance of 22 immune cell subpopulations of each LUAD sample using the CIBERSORT algorithm. We then performed unsupervised clustering to categorize LUAD patients into three TME subgroups according to the CIBERSORT results. (Supplementary Figures 2A, B). The consensus matrix showed that when k = 3, there was little crossover between LUAD samples (Supplementary Figure 2C). In addition, PCA indicated a marked difference in immune cell infiltration levels among the TME subgroups (Figure 2D). To explore the clinical significance of the TME subgroups, we performed a survival analysis. As a result, the three TME subgroups showed a significant difference in OS (log-rank test, P<0.001) (Figure 2E).

We next aimed to investigate the distribution of tumor-infiltrating immune cells (TIICs) among TME subgroups. A heatmap was generated to visualize the distribution of TIICs (Figure 2F). TME subgroup A was marked by higher-level infiltration of monocytes, M2 macrophages, activated dendritic cells, resting dendritic cells, resting mast cells, memory B cells, and memory resting $CD4^+$ T cells. TME subgroup B was characterized by higher-level infiltration of plasma cells, $CD8^+$ T cells, memory activated $CD4^+$ T cells, follicular helper T cells, gamma delta T cells, activated natural killer cells, and M1 macrophages. TME subgroup C was featured by a notable elevated regulatory T cell (Treg) and M0 macrophage infiltration. A boxplot further revealed the different distribution of TIICs in the three TME subgroups (Figure 2G). Additionally, we observed a higher StromalScore in TME subgroup A (P<0.05) (Figure 2H), a greater ImmuneScore in TME subgroup B (P<0.05) (Figure 2I), and a lower ESTIMATEScore in TME subgroup C (P<0.05) (Figure 2J), suggesting differences in tumor purity among the three TME subgroups.

Construction of the LATPS

To obtain quantitative indexes of immune cell landscape in LUAD patients, differential expression analysis to identify the transcriptome variations among the TME subgroups was performed using the Limma package, which identified 149 DEGs. Volcano plots were constructed to show the results of pairwise comparison between the TME subgroups (Supplementary Figures 2D-F). We then performed the Boruta method to reduce redundant genes, leaving 146 candidate DEGs. By using the clusterProfiler package, GO enrichment analysis of the DEGs was carried out, and it was found that they were significantly enriched in humoral immune response, T cell activation, and extracellular organization (Supplementary Figures 2G).

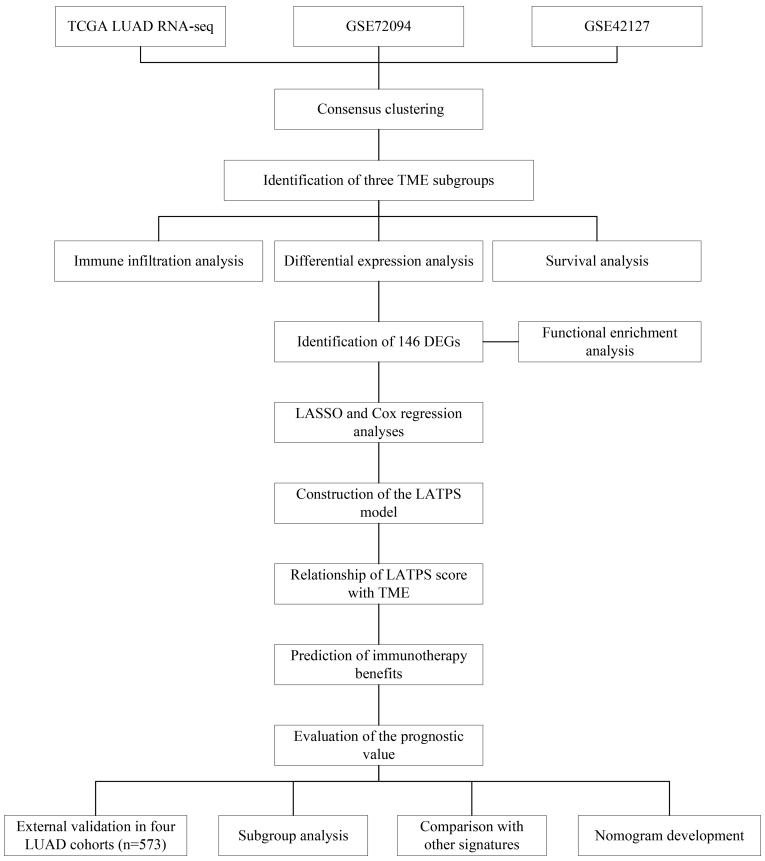

FIGURE 1
The workflow chart of this study.

TABLE 1 Clinical characteristics of patients with LUAD in each dataset.

Characteristics		Dataset		
		GSE42127	GSE72094	TCGA
Platform (%)		GPL6884	GPL15048	IlluminaHiSeq
Patients (n)		133	442	513
Age (%)	≤65	65 (48.9)	127 (28.7)	238 (46.4)
	>65	68 (51.1)	294 (66.5)	256 (49.9)
	NA	0 (0.0)	21 (4.8)	19 (3.7)
Sex (%)	Female	65 (48.9)	240 (54.3)	276 (53.8)
	Male	68 (51.1)	202 (45.7)	237 (46.2)
Stage (%)	I	89 (66.9)	265 (60.0)	274 (53.4)
	II	22 (16.5)	69 (15.6)	121 (23.6)
	III	20 (15.0)	63 (14.3)	84 (16.4)
	IV	1 (0.8)	17 (3.8)	26 (5.1)
	NA	1 (0.8)	28 (6.3)	8 (1.6)
Survival (%)	Alive	90 (67.7)	298 (67.4)	326 (63.5)
	Dead	43 (32.3)	122 (27.6)	187 (36.5)
	NA	0 (0.0)	22 (5.0)	0 (0.0)

NA, not available.

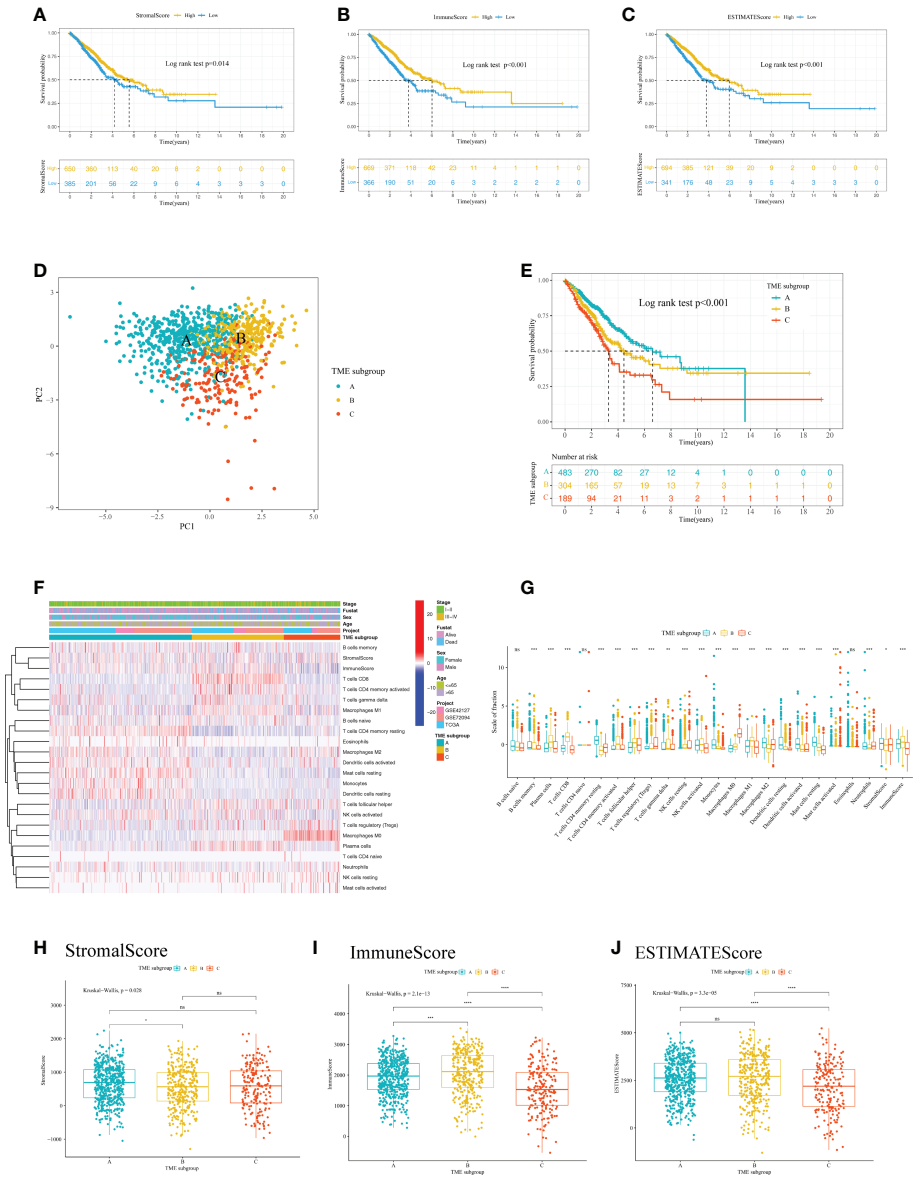

FIGURE 2
Analysis of the immune cell infiltration and TME scores of patients with LUAD. Kaplan–Meier curve analysis of the OS for different levels of **(A)** StromalScore, **(B)** ImmuneScore, and **(C)** ESTIMATEScore. **(D)** PCA for the immune cell infiltration level of the three TME subgroups, showing a remarkable difference in immune cell infiltration levels between different subgroups. **(E)** Kaplan–Meier curve analysis for the OS of patients with LUAD in different TME subgroups. **(F)** Heatmap of the 22 TIICs in different LUAD cohorts. Rows represent TIICs, and columns indicate LUAD samples. **(G)** The fraction of 22 TIICs, StromalScore, and ImmuneScore were compared between different TME subgroups using the Kruskal-Wallis test. The Kruskal–Wallis test was used to compare the statistical difference of **(H)** StromalScore, **(I)** ImmuneScore and **(J)** ESTIMATEScore of the three TME subgroups. *p< 0.05; **p< 0.01; ***p< 0.001; ****p< 0.0001; ns, no significance. LUAD, lung adenocarcinoma; TME, tumor microenvironment; OS, overall survival; PCA, principal component analysis; TIIC, tumor infiltrating immune cell.

Next, LUAD patients with complete prognostic information (the total cohort) were randomly divided into a training cohort (n = 519) and a test cohort (n = 516). There was no statistical difference in clinicopathological parameters between the training and test cohorts (Table 2). Univariate Cox regression analysis was conducted in the training cohort to further explore the prognostic value of the 146 candidate DEGs, which identified 93 genes that were associated significantly with survival (Supplementary Table 2). The top 30 significant genes were shown in Figure 3A.

To avoid overfitting of the candidate genes, LASSO analysis was performed and 12 genes were retained (Figure 3B, C).

TABLE 2 Clinical characteristics of patients with LUAD in different dataset.

Characteristics		Dataset		p value
		Training cohort	Test cohort	
n		519	516	
Age (%)	<=65	207 (39.9)	214 (41.5)	0.736
	>65	306 (59.0)	298 (57.8)	
	NA	6 (1.2)	4 (0.8)	
Sex (%)	Female	270 (52.0)	287 (55.6)	0.272
	Male	249 (48.0)	229 (44.4)	
Stage (%)	I	318 (61.3)	295 (57.2)	0.102
	II	94 (18.1)	114 (22.1)	
	III	72 (13.9)	86 (16.7)	
	IV	27 (5.2)	15 (2.9)	
	NA	8 (1.5)	6 (1.2)	
Survival (%)	Alive	355 (68.4)	341 (66.1)	0.467
	Dead	164 (31.6)	175 (33.9)	

NA, not available.

Multivariate Cox regression analysis was used to establish the prognostic signature and four hub genes, including *UBE2C* (encoding ubiquitin conjugating enzyme E2 C), *KRT6A* (encoding keratin 6A), *IRX2* (encoding iroquois homeobox 2), and *CD3D* (encoding CD3d molecule) were identified (Figure 3D). We scored each patient with LUAD with following formula: LATPS score = *UBE2C**0.177738 + *KRT6A**0.110354 + *IRX2**(-0.112574) + *CD3D**(-0.250127).

Moreover, PCA revealed markedly different distribution patterns of the four hub genes between the LATPS-high and LATPS-low subgroups in the training (Figure 3E and Supplementary Figure 3A), test (Figure 3F and Supplementary Figure 3B), and total cohorts (Figure 3G and Supplementary Figure 3C).

Correlation between the LATPS and the TME

We then sought to explore the immune characteristics of the LATPS-defined subgroups. The ESTIMATE algorithm was used to estimate tumor purity in LUAD samples. Boxplots showed distinct distributions of StromalScore, ImmuneScore, and ESTIMATEScore between the LATPS subgroups (Supplementary Figure 3D-F). Notably, the ImmuneScore was significantly higher in the LATPS-low subgroup (Mann-Whitney U test, P<2.2e−16) (Supplementary Figure 3E). Immune activation and immune infiltration are pivotal components of the immune system; therefore, we evaluated the abundance of immune cells and the activation of immune-related pathways using the GSVA package. The heatmap showed that the LATPS-low patients had a higher infiltration level for most TIICs (Figure 4A). For further validation, a lollipop plot was constructed, which revealed that the LATPS score correlated negatively with the infiltration of most immune cells (Figure 4B).

Additionally, a heatmap showed that the majority of immune-related pathways were significantly enriched in the LATPS-low subgroup, comprising antigen processing and presentation, CTLA4 Signalling, and PDL1 Signalling (Figure 4C). The LATPS score was correlated negatively with the majority of immune-related pathways (Figure 4D). Collectively, these results suggested that the LATPS-low subgroup tended to be a hot immune phenotype and might benefit more from immunotherapy (23).

The role of the LATPS in predicting immunotherapeutic benefits

To further explore whether the LATPS could distinguish potential immunotherapeutic benefits for different subgroups, we scored each LUAD sample using TIDE algorithm and visualized the distribution of the results as waterfall plots (Supplementary Figure 3G-I). A higher TIDE score represents a greater possibility of immune dysfunction and immune evasion, indicating that the patients would receive less benefit from immunotherapy (9). Notably, the LATPS-low patients had a lower TIDE score, suggesting that these patients might achieve a better immunotherapy response (Figure 5A-C).

To verify the above speculation, we assessed the predictive value in NSCLC cohorts receiving anti-PD-1 treatment, including GSE135222, GSE126044 and Nanfang Hospital cohorts. As a result, we could find that LATPS-low patients had better progression-free survival (PFS) in GSE135222 cohort (log-rank test, P=0.017) (Figure 5D) and Nanfang Hospital cohort (log-rank

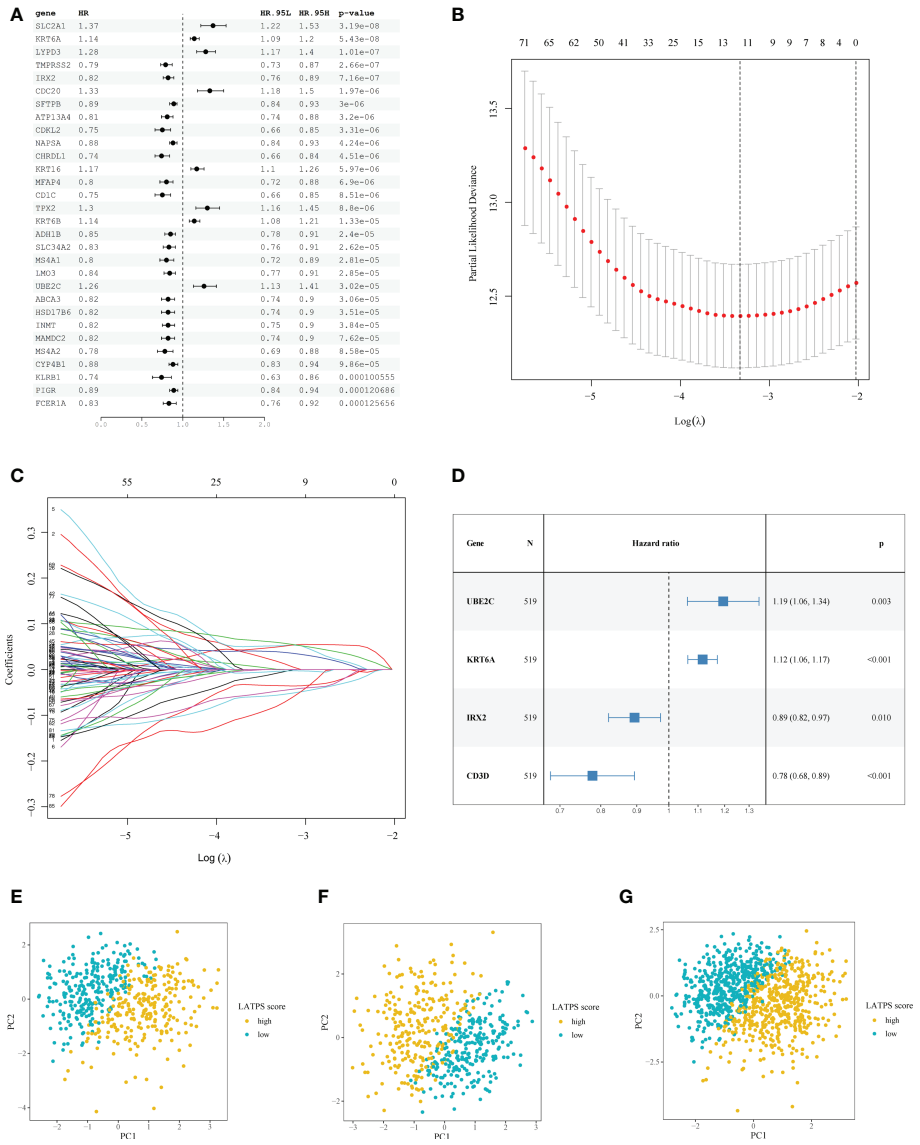

FIGURE 3
Construction of the LATPS. **(A)** Forest plot presenting the top 30 significant genes from the univariate Cox analysis results. **(B)** A coefficient profile plot was generated against the log (lambda) sequence. Selection of the optimal parameter (lambda) in the LASSO model. **(C)** LASSO coefficient profiles of the 93 candidate prognostic genes. **(D)** Forest plot illustrating the multivariate Cox model results. PCA showing the distribution differences between the LATPS-high and LATPS-low subgroups of the **(E)** training, **(F)** test, and **(G)** total cohorts. LATPS, LUAD tumor microenvironment prognostic signature; LASSO, least absolute shrinkage and selection operator; PCA, principal component analysis.

test, P=0.005) (Figure 5F). The AUC of LATPS for predicting immunotherapy benefits was 0.643 at 6 months, 0.702 at 12 months, and 0.858 at 18 months follow-up in GSE135222 cohort (Figure 5E). As for Nanfang Hospital cohort, the AUC was 0.548 at 6 months, 0.656 at 12 months, and 0.700 at 18 months follow-up, respectively (Figure 5G). Moreover, the LATPS score had the potential to distinguish patients with different anti-PD-1 responses (Mann-Whitney U test, P=0.052) (Supplementary Figure 4A). ROC analysis revealed that the LATPS had a promising accuracy to predict immunotherapy response in the GSE126044 cohort, with an AUC of 0.818. (Supplementary Figure 4B). These findings strongly suggested that the LATPS is a promising prognostic biomarker that can predict immunotherapy benefits.

Exploring and validating the prognostic value of the LATPS

To further explore the prognostic value of the LATPS in patients with LUAD, we performed survival analysis in the

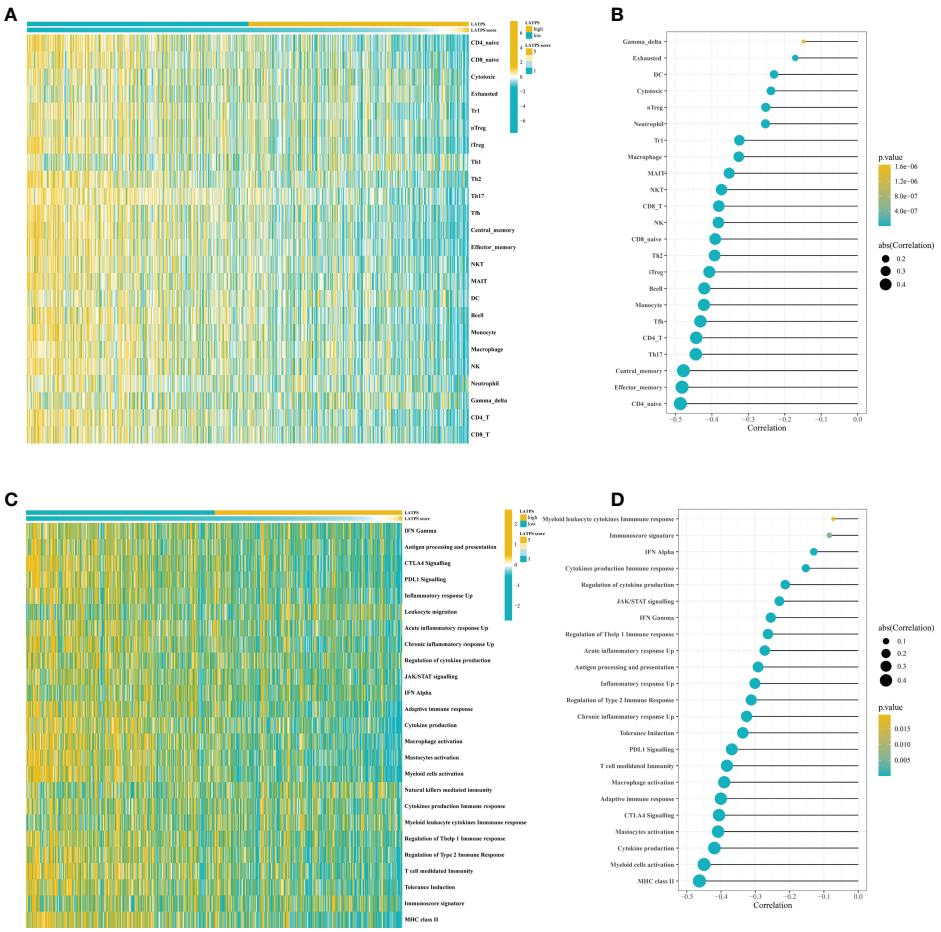

FIGURE 4
The LATPS score is associated with immune cell infiltration and immune activation. **(A)** Heatmap showing the LATPS score and relative abundance of 24 TIICs. **(B)** Lollipop plot showing the correlation between the LATPS score and the ssGSEA scores of 24 TIICs. **(C)** Heatmap presenting the LATPS score and GSVA scores of 25 immune-related pathway gene sets. **(D)** Lollipop plot presenting the correlation between the LATPS score and GSVA scores of 25 immune-related pathway gene sets. LATPS, LUAD tumor microenvironment prognostic signature; TIIC, tumor infiltrating immune cell; ssGSEA, single sample gene set enrichment analysis; GSVA, gene set variation analysis.

training cohort. As it revealed that patients in the LATPS-low subgroup had a significantly better OS (log-rank test, P<0.001) (Figure 6A). We then performed a Time-dependent ROC analysis to evaluate the accuracy of the LATPS. The areas under the curves (AUCs) of this signature for 1-, 3-, and 5-year OS were 0.736, 0.722, and 0.698, respectively (Figure 6B).

We then aimed to interrogate whether the prognostic predictive power of the LATPS is of robustness, the patients were divided into LATPS-high and LATPS-low subgroups in the test cohort according to the median LATPS score used in the training cohort. Consistent with the results in the training cohort, survival analysis showed that the LATPS-low subgroup experienced a better outcome than the LATPS-high subgroup in the test cohort (log-rank test, P< 0.001) (Figure 6C) and the AUC at 1, 3, and 5 years was 0.679, 0.683, and 0.656 in the test cohort (Figure 6D). Meanwhile, we assessed the predictive value of LATPS in internal independent datasets, including the TCGA dataset, GSE42127 dataset, and GSE72094 dataset. The results from the above datasets showed the same trend in OS, with great significance (log-rank test, P< 0.001, P = 0.021, P< 0.001), and the AUC at 1, 3, and 5 years was 0.704, 0.688, and 0.638 in TCGA dataset; 0.800, 0.705, 0.705 in GSE42127 dataset; 0.697, 0.724, and 0.788 in GSE72094 dataset, respectively (Figure 6E-J). Moreover, we performed a prognostic meta-analysis to assess the integrated predictive significance of LATPS. The selected fixed effects model of the meta-analysis showed that the LATPS is a significant predictor of OS in external LUAD patients (HR: 1.86, 95%CI: 1.51-2.30, P< 0.001) (Figure 6K).

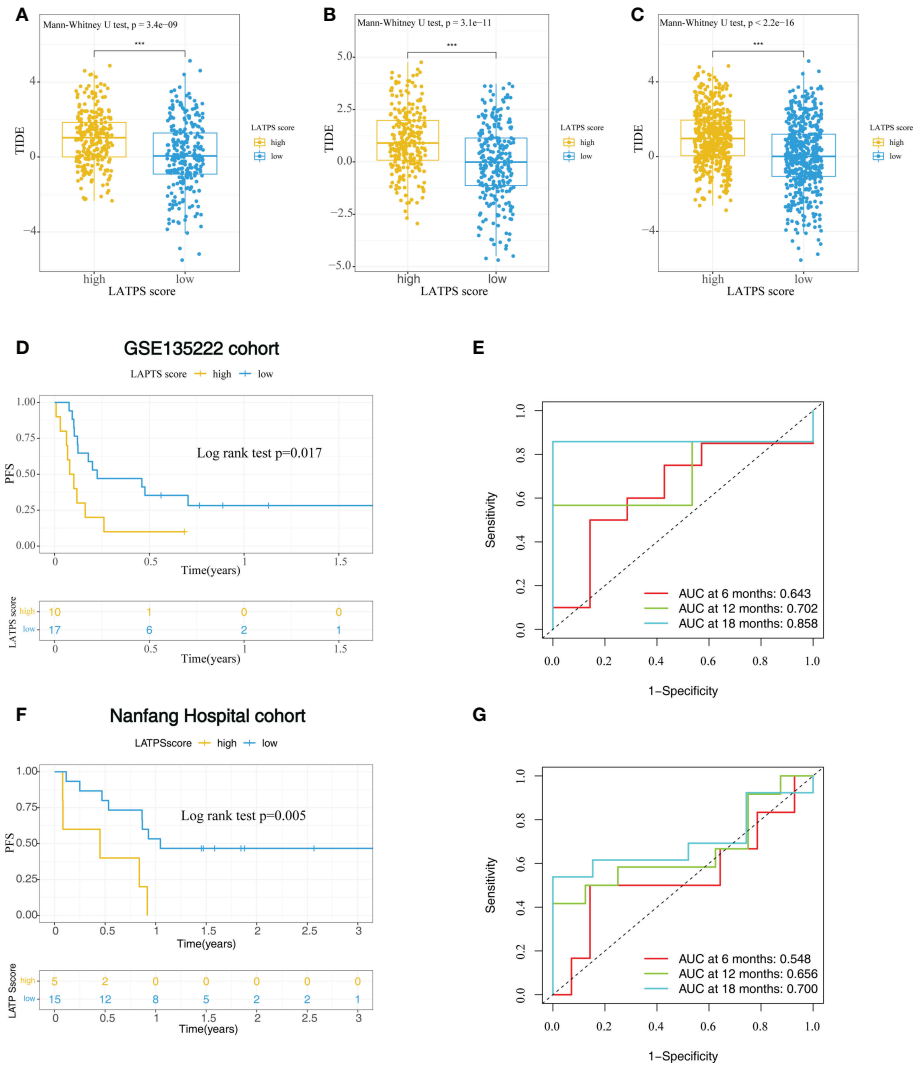

FIGURE 5
The role of the LATPS in the prediction of immunotherapeutic benefits. The relative distribution of TIDE was compared between the LATPS-high and LATPS-low subgroups in the **(A)** training, **(B)** test, and **(C)** total cohorts. **(D, E)** Kaplan–Meier curve and ROC curve analyses of the LATPS for predicting immunotherapy benefits in GSE135222 cohort. **(F, G)** Kaplan–Meier curve and ROC curve analyses of the LATPS for predicting immunotherapy benefits in Nanfang Hospital cohort. LATPS, LUAD tumor microenvironment prognostic signature; ROC, receiver operating characteristic.

The association between the LATPS and clinical characteristics

Next, univariate and multivariate Cox regression analyses were conducted to assess whether the LATPS score could predict patients' prognoses independently. The results indicated that both the stage and LATPS score can independently predict patients' prognoses (Table 3). Time-dependent ROC curves analysis to further compare the predictive capacity between the LATPS score and clinicopathological factors revealed that the LATPS score had a higher AUC than the other factors (Figures 7A-C). This implied that the LATPS can more precisely predict the patient's prognosis than the other clinicopathological factors. Boxplots were generated to describe the distribution of the LATPS score *via* stratification of patients based on age, sex, and stage. Results showed that the LATPS score was notably elevated in males, patients aged below 65 years, and in stage III–IV (Figures 7D-F). Moreover, stratified survival analysis revealed that LATPS-low patients were linked to better OS (Figures 7G-L), which agreed with our result in the training cohort.

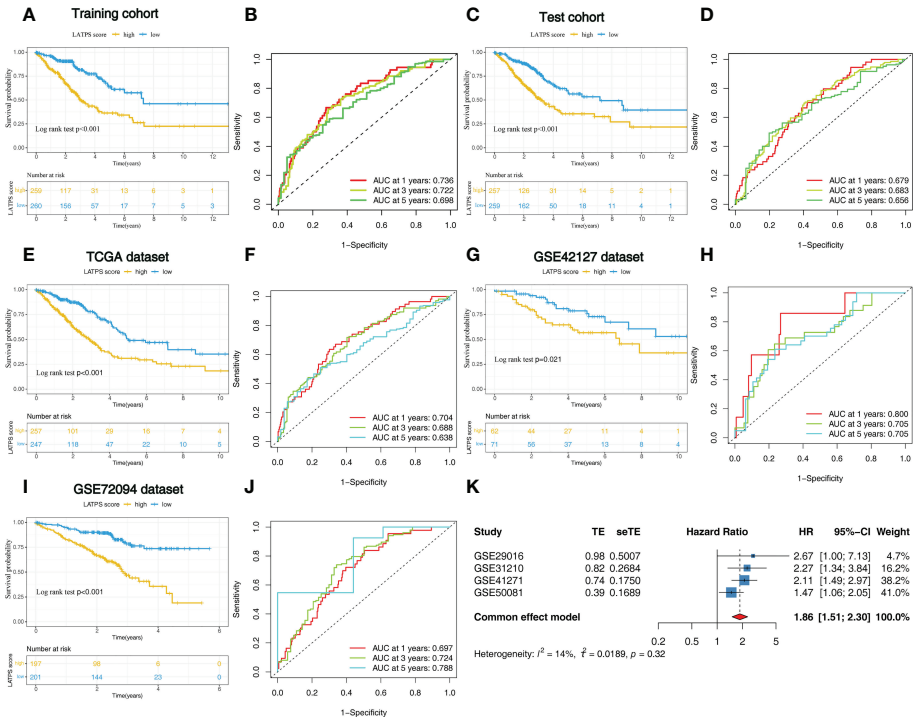

FIGURE 6
Identification of the LATPS in the training, test, and external validation cohorts. **(A, B)** Kaplan–Meier curve and the ROC curve for training cohort. **(C, D)** Kaplan–Meier curve and the ROC curve for test cohort. **(E, F)** Kaplan–Meier curve and the ROC curve for TCGA dataset. **(G, H)** Kaplan–Meier curve and the ROC curve for GSE42127 dataset. **(I, J)** Kaplan–Meier curve and the ROC curve for GSE72094 dataset. **(K)** Results of the prognostic meta-analysis on the basis of four external LUAD cohorts. LATPS, LUAD tumor microenvironment prognostic signature; ROC, receiver operating characteristic.

TABLE 3 Univariate and multivariate Cox regression analysis in training, test, and total cohorts.

Variables	Univariate analysis				Multivariate analysis			
	HR	HR.95L	HR.95H	P value	HR	HR.95L	HR.95H	P value
Training cohort								
Age	1.004	0.989	1.020	0.574	1.002	0.986	1.018	0.841
Sex	1.256	0.921	1.715	0.150	1.081	0.781	1.497	0.637
Stage	1.863	1.615	2.149	0.000	1.745	1.506	2.022	0.000
LATPS score	1.866	1.617	2.153	0.000	1.820	1.559	2.125	0.000
Test cohort								
Age	1.018	1.002	1.034	0.031	1.019	1.004	1.035	0.015
Sex	1.362	1.008	1.839	0.044	1.144	0.837	1.566	0.399
Stage	1.448	1.241	1.690	0.000	1.462	1.248	1.711	0.000
LATPS score	1.570	1.350	1.826	0.000	1.550	1.319	1.822	0.000
Total cohort								
Age	1.011	1.000	1.022	0.056	1.012	1.001	1.023	0.039
Sex	1.296	1.045	1.609	0.018	1.070	0.859	1.332	0.547
Stage	1.655	1.491	1.838	0.000	1.608	1.445	1.788	0.000
LATPS score	1.711	1.542	1.897	0.000	1.700	1.524	1.897	0.000

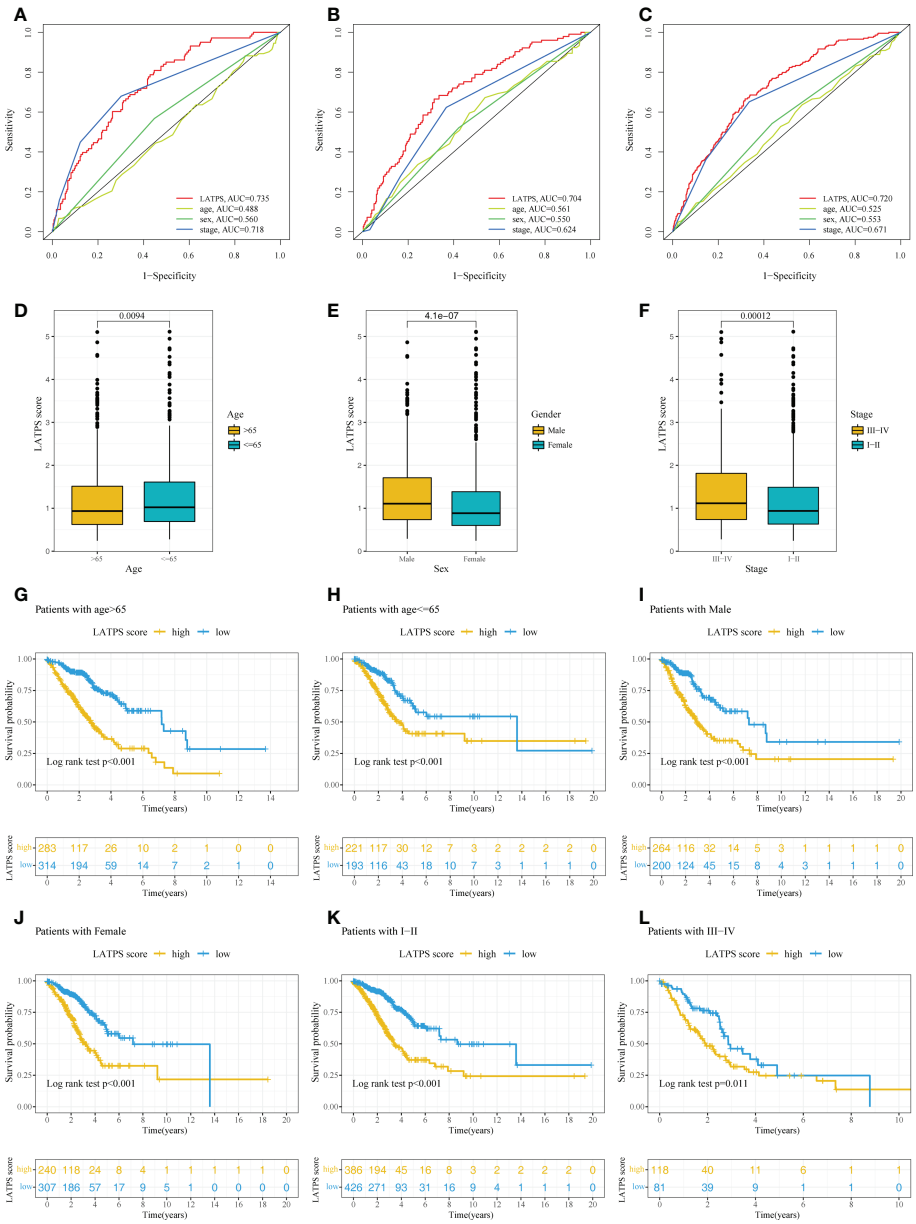

FIGURE 7
Confirmation of the LATPS *via* stratification of patients based on specific demographic and clinical features. Time-dependent ROC curve analysis of the LATPS score and clinicopathological factors to assess the predictive capacity of the LATPS in the **(A)** training, **(B)** test, and **(C)** total cohorts. **(D-F)** Boxplot showing the relationships between the LATPS score and clinicopathologic factors for all patients with LUAD. **(G-L)** Kaplan–Meier curve analysis for patients of **(G)** age > 65, **(H)** age ≤ 65, **(I)** Male, **(J)** Female, **(K)** Stage I–II, **(L)** Stage III–IV in the LATPS-high and LATPS-low subgroups. LATPS, LUAD tumor microenvironment prognostic signature; LUAD, lung adenocarcinoma; ROC, receiver operating characteristic.

Comparison with other published LUAD signatures and construction of a nomogram signature

To further evaluate the survival classification and predictive capacity of LATPS. We not only compared the LATPS with clinicopathological factors but also compared the predictive performance of two TME-based LUAD signatures. Wu signature was an 8-gene signature (25). Yue signature was a signature consisting of 3 genes (26). We applied Kaplan–Meier curve and the ROC curve analyses to assess the predictive efficacy of the above signatures. As a result, (LATPS, Wu signature, and Yue signature) had the same significant trend in survival, for patients in the low-risk group had better OS (log-rank test, P<0.001,p<0.001, p<0.001), and

the AUC was 0.704, 0.715, 0.636 at 1 year; 0.688, 0.692, 0.651 at 3 years; and 0.638, 0.627, 0.569 at 5 years, respectively (Figures 8A-C).

Next, to assess the clinical utility of LATPS, a nomogram signature was established according to the clinicopathological factors and LATPS score in the training cohort. Each patient was scored according to their clinical features and LATPS score to predict survival probability (Figure 8D). Calibration curve analysis revealed that actual and nomogram-predicted OS corresponded well (Figure 8E). ROC curve analysis showed that the nomogram signature had more favorable predictive accuracy than other clinicopathological signatures (Figures 8F-H). Moreover, Calibration curve and ROC curve analyses of the nomogram signature in internal cohorts indicated that the nomogram signature was of favorable predictive capacity for OS (Supplementary Figures 5A-H). Collectively, these results suggested that the LATPS had clinical utility as a prognostic tool.

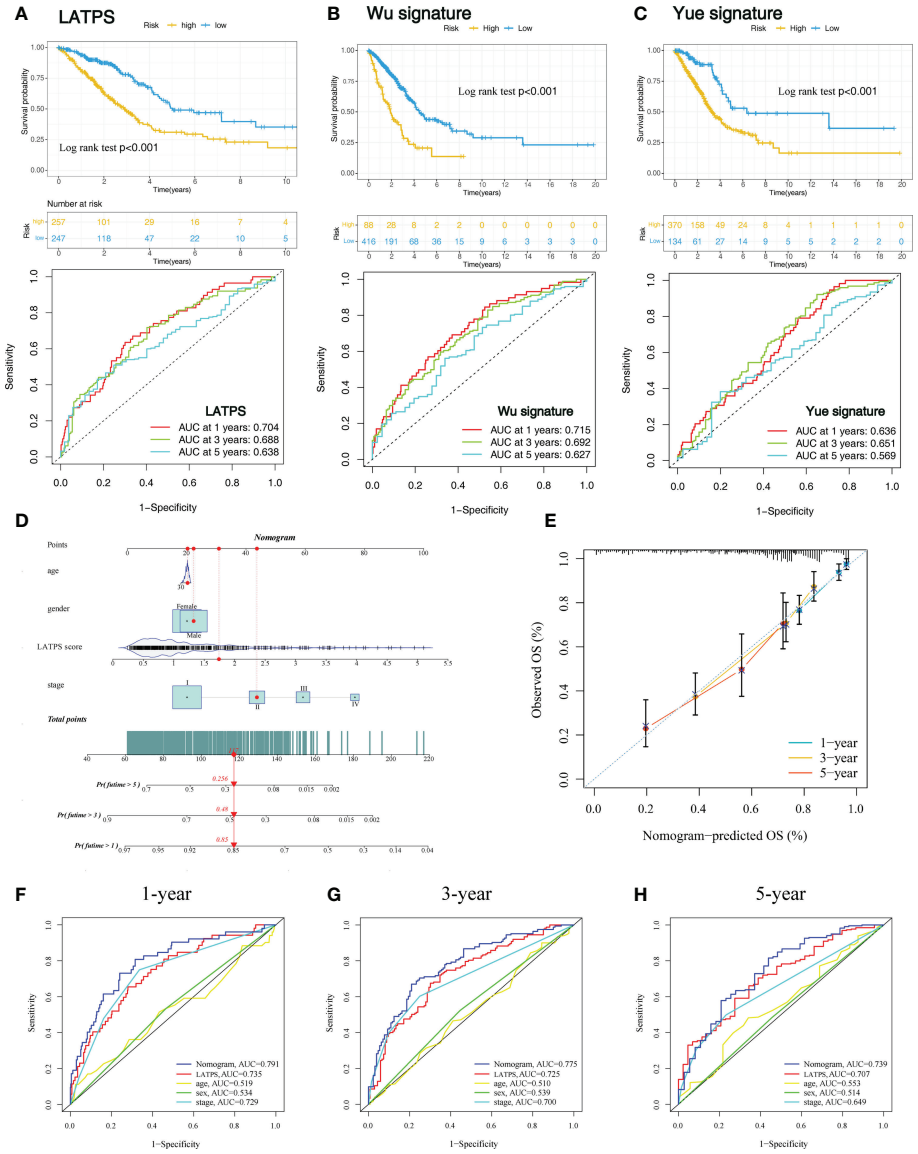

FIGURE 8
Comparison of the LATPS with other published gene signatures and construction of a nomogram. Kaplan–Meier curve and the ROC curve of **(A)** LATPS, **(B)** Wu signature, and **(C)** Yue signature. **(D)** Nomogram based on the LATPS and clinical information of patients with LUAD. **(E)** Calibration curve of the nomogram used for predicting OS at 1, 3, and 5 years. Time-dependent ROC curves analysis of the nomogram and clinicopathological factors in predicting **(F)** 1-, **(G)** 3-, and **(H)** 5-year OS. LATPS, LUAD tumor microenvironment prognostic signature; LUAD, lung adenocarcinoma; OS, overall survival; ROC, receiver operating characteristic.

Discussion

ICIs treatment only benefits a fraction of NSCLC patients with PD-L1 > 1% (5). Nevertheless, the IMpower132 study showed an OS benefit in PD-L1-negative patients treated with ICI therapy (27). Moreover, a previous study revealed that the accuracy of TMB in predicting the immunotherapy response for NSCLC is only about 60% (9). Therefore, conventional PD-L1 expression and TMB may not be enough to distinguish patients who would benefit from ICIs. Jiang P and Daniela ST pointed out that the status of T cells and the infiltration of T cells may be promising biomarkers for NSCLC treated with immunotherapy (9, 28). However, the TME of NSCLC is complicated and heterogeneous, which consists of various immune cells apart from T cells. Furthermore, taking into consideration that LUAD and lung squamous carcinoma (LUSC) were different in the tumor immune landscape (29), a deeper mining of the TME of LUAD may provide new insights for predicting immunotherapy response.

We analyzed the immune landscape in LUAD samples and identified three distinct TME subgroups. Notably, TME subgroup A was associated with the best OS and exhibited a significant increase in the infiltration of memory B cells, memory resting $CD4^+$ T cells, monocytes, M2 macrophages, dendritic cells, and resting mast cells. Besides, TME subgroup B was associated with better prognosis, featured by an elevated infiltration of plasma cells, $CD8^+$ T cells, gamma delta T cells, activated NK cells, M1 macrophages, and a higher ImmuneScore compared with TME subgroup C. Conversely, TME subgroup C was associated with the worst OS and was marked by a greater density of Tregs and M0 macrophages infiltration. Previous studies have shown a high Treg density was associated with poor prognosis in a variety of cancers, including lung cancer (30, 31). Higher infiltration of $CD8^+$ T cells and M1 macrophages was related to better survival outcomes, which agrees with previous studies (32, 33). Thus, the immune cell infiltration pattern played an important role in patient's prognosis, which would provide guidance to predict clinical outcomes.

Clinically, it is difficult to obtain the immune infiltration pattern of each LUAD patient. It needs to perform whole transcriptome sequencing (detect approximately 20,000 genes) of LUAD tumor samples to identify the TME subgroups, which would be expensive and impractical in clinical practice. Thus, we aim to construct a simple and efficient signature to reflect the immune infiltration pattern and predict the survival of LUAD patients based on the identified TME subgroups. Besides, we wanted to unravel the underlying biological characteristics of the three TME subgroups and screen out the key genes that may influence the OS of the distinct TME subgroups. Therefore, we explored the transcriptome variation among the TME subgroups. Subsequently, we identified 146 TME-related DEGs after performing differential expression analysis. GO functional enrichment analysis revealed that the DEGs were mainly associated with immune-related GO terms, including humoral immune response, regulation of cell killing and T cell activation. Studies have demonstrated the abundance and dysfunction of immune cells might affect antitumor immunity and immunotherapy response (9, 34, 35). Thus, our results indicated that imbalances in these immune-related functions or pathways might result in diverse clinical outcomes in patients with LUAD. Based on the expression of the 146 DEGs may help to distinguish different infiltration patterns and provide personalized treatment.

However, in the clinic, it would be impractical to determine the mRNA expression of the 146 TME-related DEGs. Therefore, we utilized computational algorithms to select hub genes and established a LUAD TME prognostic signature (LATPS), comprising four hub prognostic genes (*UBE2C*, *KRT6A*, *IRX2*, and *CD3D*). Reportedly, these four genes correlated with patient survival. Overexpression of *UBE2C* was reported as an independent risk factor associated with dismal outcomes in patients with lung cancer (36, 37). Reportedly, *KRT6A* is associated with cell proliferation and invasion, which drives cancer progression by upregulating glucose-6-phosphate dehydrogenase (G6PD) through MYC signaling pathway (38). Consistent with previous studies, our results revealed that both *UBE2C* and *KRT6A* were LUAD risk factors. Elevated expression of *IRX2* was linked with shorter OS in nasopharyngeal carcinoma (NPC) (39). Interestingly, we identified *IRX2* as a protective factor in LUAD; however, limited studies have focused on the role of *IRX2* in LUAD. For *CD3D*, its higher expression is related to a better outcome in colon cancer (40). Previous studies discovered that *CD3D* correlates highly with lymphocyte infiltration and is regarded as a promising therapeutic target (41, 42). In addition, PCA revealed that the mRNA expression pattern of the four hub genes could categorize patients with LUAD into two different subgroups, implying that there may be a difference in immune infiltration pattern and survival between the LATPS-defined subgroups.

ICIs have revolutionized the treatment of NSCLC and improved outcomes (43, 44). Therefore, understanding the response to immunotherapy may help to predict patients' prognoses. Studies revealed that TIICs of the TME play a crucial role in immunotherapy response (7, 8). Besides, patients with an inflammatory phenotype or an immunity-high phenotype have a better prognosis and are thought to be more likely to benefit from immunotherapy (23, 45). Therefore, we further explored the immune infiltration landscape in the LATPS-defined subgroups. Interestingly, similar to previous studies, patients in the LATPS-low subgroup tended to be a hot immune phenotype, characterized by elevated immune cell infiltration and hyperactivated immune-related pathways. Thus, our results suggested that the LATPS is of potential predictive value in assessing immunotherapy response. Cancer immunotherapy using ICIs functions by blocking inhibitory signaling and reactivating cytotoxic T lymphocytes to attack cancer cells (46). Multiple factors affect immunotherapy

effectiveness and few biomarkers have been developed to accurately assess the benefit of immunotherapy. Jiang P et al. identified the TIDE score, which quantifies two different mechanisms of tumor immune escape, including T cell dysfunction and exclusion. A patient with a lower TIDE score is likely to benefit from immunotherapy. The accuracy of the TIDE score for predicting immunotherapy response in NSCLC was about 80% (9). While the TIDE score was based on small samples of 21 NSCLC patients treated with immunotherapy and it was complicated to calculate, limiting its clinical application. We observed a lower TIDE score in the LATPS-low subgroup, which indicated that the LATPS might be useful for patient selection before ICI treatment.

To verify the predictive value of the LATPS in elevating ICI treatment benefits, we performed survival analysis in immunotherapy cohorts. In the GSE135222 cohort, 27 advanced NSCLC patients received anti-PD-1 therapy. As shown in Figure 5D, patients with lower LATPS score obtained longer PFS (log rank test, $p = 0.017$). In addition, we collected FFPE tumor samples of NSCLC patients treated with anti-PD-1 based therapy at Nanfang Hospital for RNA sequencing analysis. Among them, 20 patients with available survival information. Consistently, the LATPS-low subgroup got longer PFS than the LATPS-high subgroup (log rank test, $p = 0.005$), suggesting that the LATPS could distinguish different outcomes in patients who received immunotherapy. The AUC of LATPS for predicting immunotherapy benefits was higher in the GSE135222 cohort compared with the Nanfang Hospital cohort. Considering the sample size of Nanfang Hospital is smaller than the GSE135222 cohort, which may explain the lower ACU in the Nanfang Hospital cohort. Thus, further large scale immunotherapy cohorts are needed to verify our results. Moreover, ROC curves of the above two cohorts revealed that the LATPS is a potential predictor to predict immunotherapy benefits with an AUC of 0.548 to 0.858. Besides, it was evident that LATPS has better predictive accuracy at longer follow-ups according to the ROC curve analysis.

Subsequently, we further evaluated the clinical value of the LATPS for predicting immunotherapy response. In the GSE126044 NSCLC immunotherapy cohort, patients who responded to anti-PD-1 therapy had lower LATPS scores compared with none responders (Mann-Whitney U test, $p = 0.052$). Although it was not statistically significant, there was a trend that lower LATPS scores were more likely to benefit from immunotherapy. Besides, the GSE126044 was grounded on small numbers of samples, consisting of only 16 patients. Further large immunotherapy cohorts are needed to verify this hypothesis. The TIDE model has been reported to predict the outcome of NSCLC treated with first-line anti-PD1 or anti-CTLA4 antibodies with an AUC of about 0.80 (9). In the GSE126044 cohort, the AUC of LATPS for predicting immunotherapy response was 0.818, which was comparable with the TIDE model. Therefore, our results showed that the LATPS model could serve as a promising biomarker, which would facilitate the development of new avenues for personalized immune-intervention strategies. In addition, The TIDE model mainly focuses on the T cell status, which might be insufficient to reflect the complexity of the TME in LUAD. Besides, whole transcriptome sequencing of tumor samples is needed to generate the TIDE score, which is inconvenient to conduct in the clinic. Our LATPS model comprises only four genes, making it easier than the TIDE model to apply in clinical practice.

Next, we aimed to assess the survival classification and predictive efficacy of LATPS. Survival analysis revealed that LATPS-low patients had better prognoses than the LATPS-high subgroup in the training cohort, indicating that the LATPS was closely linked to LUAD survival. Furthermore, validation of the predictive accuracy of the LATPS using internal cohorts and stratification survival analysis demonstrated that the LATPS can more precisely predict the prognosis of LUAD compared with other clinicopathological factors. Moreover, univariate and multivariate Cox regression analyses identified the LATPS as an independent risk factor to predict patient prognosis, which was confirmed by the prognostic meta-analysis. Collectively, our results showed that the LATPS is a robust and generalizable predictor for survival in LUAD.

We also compared the LATPS with other previously published signatures (Wu signature (25) and Yue signature (26)), which were based on the TME of LUAD patients. ROC analysis demonstrated that the LATPS has a better predictive ability than Yue signature. Meanwhile, LATPS has a lower AUC for predicting OS at 1 and 3 years, but a higher AUC at 5 years compared with Wu signature. However, LATPS is a 4-gene signature, which is easier to conduct than the 8-gene signature (Wu signature) in the clinic. These results indicate that the overall performance of our LATPS is superior to others.

Several studies have constructed prognostic models to predict patients' OS; however, few of them have been applied clinically (33, 47, 48). Nomograms can conveniently and efficiently estimate cancer prognosis, and are used widely in clinical cancer research (49). Thus, we established a nomogram according to the LATPS score and clinicopathological factors, which can be conveniently obtained in the clinic. Calibration curve analysis showed favorable accordance between nomogram-predicted and actual OS in the training cohort. Additionally, ROC curve analysis showed that the nomogram signature had an AUC of 0.791, which was higher than other clinicopathological models. Thus, our results suggested that the LATPS is a promising prognostic tool with clinical utility.

Conclusively, we applied integrated analysis to explore the TME of LUAD and constructed a LATPS, which can serve as a reliable tool to predict the prognosis and immunotherapy benefits of LUAD patients; however, further large scale studies are needed to validate the signature in LUAD cohorts treated with immunotherapy.

Data availability statement

The data presented in the study are deposited in the Figshare database, which is available by visiting https://figshare.com/articles/dataset/Nanfang_hospital_NSCLC_immunotherapy_cohort/21564015. The processed data and R codes used during the current study are available from the corresponding author upon reasonable request.

Ethics statement

The studies involving human participants were reviewed and approved by The Ethics Committee of Nanfang Hospital. The patients/participants provided their written informed consent to participate in this study. Written informed consent was obtained from the individual(s) for the publication of any potentially identifiable images or data included in this article.

Author contributions

Conceptualization and design: LYL, JG, and YZZ. Data collection: XZ, YW, XL, DY, and YNZ. Methodology: XW and LWL. Data analysis: JH and XZ. Software: JH and LY. Generating of the Figure: JL and WL. Writing of the manuscript: JH and WH. Revision of the manuscript: JH, LY, and XZ. All authors contributed to the article and approved the submitted version.

Funding

This work was supported by the National Natural Science Foundation of China [grant number 81870026], the President Foundation of Nanfang Hospital, Southern Medical University [grant number 2020C044], and the Clinical Research Program of Nanfang Hospital, Southern Medical University [grant numbers 2018CR019, 2018CR021, 2020CR025].

Acknowledgments

We appreciated the TCGA, GEO, and ImmuCellAI databases for the availability of the original data used in this study.

Conflict of interest

The authors declare that the research was conducted in the absence of any commercial or financial relationships that could be construed as a potential conflict of interest.

Publisher's note

Supplementary material

The Supplementary Material for this article can be found online at: https://www.frontiersin.org/articles/10.3389/fimmu.2022.1064874/full#supplementary-material

SUPPLEMENTARY FIGURE 1
(A) Principal component analysis showing the distribution differences of different LUAD cohorts before removing batch effects using the ComBat algorithm. **(B)** Principal component analysis showing the distribution differences of different LUAD cohorts after removing batch effects using the ComBat algorithm. LUAD, lung adenocarcinoma.

SUPPLEMENTARY FIGURE 2
(A) Empirical cumulative distribution function diagram and **(B)** delta area diagram showing the results of consistent clustering based on the CIBERSORT results, where k represents the number of subgroups. **(C)** Consensus matrix presenting the clustering stability of hierarchical clustering for k = 3. **(D-F)** Volcano plots showing the DEGs between different TME subgroups. Red dots represent upregulated genes and green dots represent downregulated genes. **(G)** GO enrichment analysis of the 146 DEGs derived from the three TME subgroups. DEGs, differentially expressed genes. TME, tumor environment. GO, gene ontology.

SUPPLEMENTARY FIGURE 3
Principal component analysis showing the distribution differences between the LATPS-high and LATPS-low subgroups of the **(A)** training, **(B)** test, and **(C)** total cohorts. The distribution of **(D)** StromalScore, **(E)** ImmuneScore, and **(F)** ESTIMATEScore between the LATPS-high and LATPS-low subgroups. Statistical significance was assessed using the Mann-Whitney U test. The distribution of TIDE of patients with LUAD patients in the **(G)** training, **(H)** test, and **(I)** total cohorts. LATPS, LUAD tumor microenvironment prognostic signature; TIDE, tumor immune dysfunction and exclusion; LUAD, lung adenocarcinoma.

SUPPLEMENTARY FIGURE 4
(A) Distribution of the LATPS score in patients with different response status to anti-PD-1 therapy of NSCLC in GSE126044. **(B)** ROC analysis of the LATPS to predict an anti-PD-1 response. NSCLC, non-small cell lung cancer; PD-1, programmed cell death 1; ROC, receiver operating characteristic.

SUPPLEMENTARY FIGURE 5
Calibration curve for predicting overall survival at 1, 3, and 5 years in **(A)** test and **(B)** total cohorts. **(C-H)** Time-dependent ROC curves analysis of the nomogram and clinicopathological factors to predict 1-, 3-, and 5-year overall survival in **(C-E)** test and **(F-H)** total cohorts. ROC, receiver operating characteristic.

References

1. Duma N, Santana-Davila R, Molina JR. Non-small cell lung cancer: Epidemiology, screening, diagnosis, and treatment. *Mayo Clin Proc* (2019) 94 (8):1623–40. doi: 10.1016/j.mayocp.2019.01.013

2. Forde PM, Chaft JE, Smith KN, Anagnostou V, Cottrell TR, Hellmann MD, et al. Neoadjuvant PD-1 blockade in resectable lung cancer. *N Engl J Med* (2018) 378(21):1976–86. doi: 10.1056/NEJMoa1716078

3. Steven A, Fisher SA, Robinson BW. Immunotherapy for lung cancer. *Respirology* (2016) 21(5):821–33. doi: 10.1111/resp.12789

4. Li X, Shao C, Shi Y, Han W. Lessons learned from the blockade of immune checkpoints in cancer immunotherapy. *J Hematol Oncol* (2018) 11(1):31. doi: 10.1186/s13045-018-0578-4

5. Reck M, Rodríguez-Abreu D, Robinson AG, Hui R, Csőszi T, Fülöp A, et al. Five-year outcomes with pembrolizumab versus chemotherapy for metastatic non-Small-Cell lung cancer with PD-L1 tumor proportion score ≥ 50. *J Clin Oncol* (2021) 39(21):2339–49. doi: 10.1200/JCO.21.00174

6. Havel J, Chowell D, Chan T. The evolving landscape of biomarkers for checkpoint inhibitor immunotherapy. *Nat Rev Cancer* (2019) 19(3):133–50. doi: 10.1038/s41568-019-0116-x

7. Nishino M, Ramaiya NH, Hatabu H, Hodi FS. Monitoring immune-checkpoint blockade: response evaluation and biomarker development. *Nat Rev Clin Oncol* (2017) 14(11):655–68. doi: 10.1038/nrclinonc.2017.88

8. Binnewies M, Roberts EW, Kersten K, Chan V, Fearon DF, Merad M, et al. Understanding the tumor immune microenvironment (TIME) for effective therapy. *Nat Med* (2018) 24(5):541–50. doi: 10.1038/s41591-018-0014-x

9. Jiang P, Gu S, Pan D, Fu J, Sahu A, Hu X, et al. Signatures of T cell dysfunction and exclusion predict cancer immunotherapy response. *Nat Med* (2018) 24(10):1550–8. doi: 10.1038/s41591-018-0136-1

10. Zhang B, Wu Q, Li B, Wang D, Wang L, Zhou Y, et al. M 6 a regulator-mediated methylation modification patterns and tumor microenvironment infiltration characterization in gastric cancer. *Mol Cancer* (2020) 19(1):53. doi: 10.1186/s12943-020-01170-0

11. Eisenhauer EA, Therasse P, Bogaerts J, Schwartz LH, Sargent D, Ford R, et al. New response evaluation criteria in solid tumours: revised RECIST guideline (version 1.1). *Eur J Cancer* (2009) 45(2):228–47. doi: 10.1016/j.ejca.2008.10.026

12. Bolger AM, Lohse M, Usadel B. Trimmomatic: a flexible trimmer for illumina sequence data. *Bioinformatics* (2014) 30(15):2114–20. doi: 10.1093/bioinformatics/btu170

13. Wang L, Wang S, Li W. RSeQC: quality control of RNA-seq experiments. *Bioinformatics* (2012) 28(16):2184–5. doi: 10.1093/bioinformatics/bts356

14. Langmead B, Salzberg SL. Fast gapped-read alignment with Bowtie2. *Nat Methods* (2012) 9(4):357–9. doi: 10.1038/nmeth.1923

15. Liao Y, Smyth GK, Shi W. featureCounts: an efficient general purpose program for assigning sequence reads to genomic features. *Bioinformatics* (2014) 30(7):923–30. doi: 10.1093/bioinformatics/btt656

16. Newman AM, Liu CL, Green MR, Gentles AJ, Feng W, Xu Y, et al. Robust enumeration of cell subsets from tissue expression profiles. *Nat Methods* (2015) 12 (5):453–7. doi: 10.1038/nmeth.3337

17. Yoshihara K, Shahmoradgoli M, Martínez E, Vegesna R, Kim H, Torres-Garcia W, et al. Inferring tumour purity and stromal and immune cell admixture from expression data. *Nat Commun* (2013) 4:2612. doi: 10.1038/ncomms3612

18. Wilkerson MD, Hayes DN. ConsensusClusterPlus: a class discovery tool with confidence assessments and item tracking. *Bioinformatics* (2010) 26 (12):1572–3. doi: 10.1093/bioinformatics/btq170

19. Yu G, Wang L, Han Y, He Q. clusterProfiler: an r package for comparing biological themes among gene clusters. *OMICS* (2012) 16(5):284–7. doi: 10.1089/omi.2011.0118

20. Simon N, Friedman J, Hastie T, Tibshirani R. Regularization paths for cox's proportional hazards model *via* coordinate descent. *J Stat Softw* (2011) 39(5):1–13. doi: 10.18637/jss.v039.i05

21. Charoentong P, Finotello F, Angelova M, Mayer C, Efremova M, Rieder D, et al. Pan-cancer immunogenomic analyses reveal genotype-immunophenotype relationships and predictors of response to checkpoint blockade. *Cell Rep* (2017) 18 (1):248–62. doi: 10.1016/j.celrep.2016.12.019

22. Hänzelmann S, Castelo R, Guinney J. GSVA: gene set variation analysis for microarray and RNA-seq data. *BMC Bioinf* (2013) 14:7. doi: 10.1186/1471-2105-14-7

23. García-Mulero G, Alonso MH, Pardo J, Santos C, Sanjuan X, Salazar R, et al. Lung metastases share common immune features regardless of primary tumor origin. *J Immunother Cancer* (2020) 8(1):e000491. doi: 10.1136/jitc-2019-000491

24. Hazra A, Gogtay N. Biostatistics series module 3: Comparing groups: Numerical variables. *Indian J Dermatol* (2016) 61(3):251–60. doi: 10.4103/0019-5154.182416

25. Wu J, Li L, Zhang H, Zhao Y, Zhang H, Wu S, et al. A risk model developed based on tumor microenvironment predicts overall survival and associates with tumor immunity of patients with lung adenocarcinoma. *Oncogene* (2021) 40 (26):4413–24. doi: 10.1038/s41388-021-01853-y

26. Yue C, Ma H, Zhou Y. Identification of prognostic gene signature associated with microenvironment of lung adenocarcinoma. *PeerJ* (2019) 7:e8128. doi: 10.7717/peerj.8128

27. Nishio M, Barlesi F, West H, Ball S, Bordoni R, Cobo M, et al. Atezolizumab plus chemotherapy for first-line treatment of nonsquamous NSCLC: Results from the randomized phase 3 IMpower132 trial. *J Thorac Oncol* (2021) 16(4):653–64. doi: 10.1016/j.jtho.2020.11.025

28. Thommen DS, Koelzer VK, Herzig P, Roller A, Trefny M, Dimeloe S, et al. A transcriptionally and functionally distinct PD-1 + CD8 + T cell pool with predictive potential in non-small-cell lung cancer treated with PD-1 blockade. *Nat Med* (2018) 24(7):994–1004. doi: 10.1038/s41591-018-0057-z

29. Faruki H, Mayhew G, Serody J, Hayes D, Perou C, Lai-Goldman M. Lung adenocarcinoma and squamous cell carcinoma gene expression subtypes demonstrate significant differences in tumor immune landscape. *J Thorac Oncol* (2017) 12(6):943–53. doi: 10.1016/j.jtho.2017.03.010

30. Jacobs J, Nierkens S, Figdor C, Vries I, Adema G. Regulatory T cells in melanoma: the final hurdle towards effective immunotherapy? *Lancet Oncol* (2012) 13(1):e32–42. doi: 10.1016/S1470-2045(11)70155-3

31. Ke X, Zhang S, Xu J, Liu G, Zhang L, Xie E, et al. Non-small-cell lung cancer-induced immunosuppression by increased human regulatory T cells *via* Foxp3 promoter demethylation. *Cancer Immunol Immunother* (2016) 65(5):587–99. doi: 10.1007/s00262-016-1825-6

32. Chen Y, Li Z, Zhou G, Sun Y. An immune-related gene prognostic index for head and neck squamous cell carcinoma. *Clin Cancer Res* (2021) 27(1):330–41. doi: 10.1158/1078-0432.CCR-20-2166

33. Yi M, Li A, Zhou L, Chu Q, Luo S, Wu K. Immune signature-based risk stratification and prediction of immune checkpoint inhibitor's efficacy for lung adenocarcinoma. *Cancer Immunol Immunother* (2021) 70(6):1705–19. doi: 10.1007/s00262-020-02817-z

34. Poggio M, Hu T, Pai C, Chu B, Belair C, Chang A, et al. Suppression of exosomal PD-L1 induces systemic anti-tumor immunity and memory. *Cell* (2019) 177(2):414–427.e13. doi: 10.1016/j.cell.2019.02.016

35. Philip M, Schietinger A. CD8 + T cell differentiation and dysfunction in cancer. *Nat Rev Immunol* (2021) 22(4):209–23. doi: 10.1038/s41577-021-00574-3

36. Guo W, Sun S, Guo L, Song P, Xue X, Zhang H, et al. Elevated TOP2A and UBE2C expressions correlate with poor prognosis in patients with surgically resected lung adenocarcinoma: a study based on immunohistochemical analysis and bioinformatics. *J Cancer Res Clin Oncol* (2020) 146(4):821–41. doi: 10.1007/s00432-020-03147-4

37. Wang Y, Shi F, Tao R, Wu J, Gu J, Yang R, et al. The relationship between UBE2C and AGGF1 overexpression and tumor angiogenesis in non-small cell lung cancer. *Cancer Manag Res* (2021) 13:5919–30. doi: 10.2147/CMAR.S320393

38. Che D, Wang M, Sun J, Li B, Xu T, Lu Y, et al. KRT6A promotes lung cancer cell growth and invasion through MYC-regulated pentose phosphate pathway. *Front Cell Dev Biol* (2021) 9:694071. doi: 10.3389/fcell.2021.694071

39. Si J, Si Y, Zhang B, Lan G, Wei J, Huang B, et al. Up-regulation of the IRX2 gene predicts poor prognosis in nasopharyngeal carcinoma. *Int J Clin Exp Pathol* (2018) 11(8):4073–82.

40. Yang Y, Zang Y, Zheng C, Li Z, Gu X, Zhou M, et al. CD3D is associated with immune checkpoints and predicts favorable clinical outcome in colon cancer. *Immunotherapy* (2020) 12(1):25–35. doi: 10.2217/imt-2019-0145

41. Zhu Z, Ye W, Wu X, Lin S, Xu J, Li L, et al. Comprehensive analysis reveals a prognostic and therapeutic biomarker CD3D in the breast carcinoma microenvironment. *Biosci Rep* (2021) 41(1):BSR20202898. doi: 10.1042/BSR20202898

42. Pan Q, Cheng Y, Cheng D. Identification of CD8+ T cell-related genes: Correlations with immune phenotypes and outcomes of liver cancer. *J Immunol Res* (2021) 2021:9960905. doi: 10.1155/2021/9960905

43. Brahmer J, Pardoll D. Immune checkpoint inhibitors: making immunotherapy a reality for the treatment of lung cancer. *Cancer Immunol Res* (2013) 1(2):85–91. doi: 10.1158/2326-6066.CIR-13-0078

44. Smit E, Baas P. Lung cancer in 2015: Bypassing checkpoints, overcoming resistance, and honing in on new targets. *Nat Rev Clin Oncol* (2016) 13(2):75–6. doi: 10.1038/nrclinonc.2015.223

45. He Y, Jiang Z, Chen C, Wang X. Classification of triple-negative breast cancers based on immunogenomic profiling. *J Exp Clin Cancer Res* (2018) 37 (1):327. doi: 10.1186/s13046-018-1002-1

46. Mahoney K, Rennert P, Freeman G. Combination cancer immunotherapy and new immunomodulatory targets. *Nat Rev Drug Discovery* (2015) 14(8):561–84. doi: 10.1038/nrd4591

47. Ren Z, Hu M, Wang Z, Ge J, Zhou X, Zhang G, et al. Ferroptosis-related genes in lung adenocarcinoma: Prognostic signature and immune, drug resistance, mutation analysis. *Front Genet* (2021) 12:672904. doi: 10.3389/fgene.2021.672904

48. Cheng Y, Hou K, Wang Y, Chen Y, Zheng X, Qi J, et al. Identification of prognostic signature and gliclazide as candidate drugs in lung adenocarcinoma. *Front Oncol* (2021) 11:665276. doi: 10.3389/fonc.2021.665276

49. Iasonos A, Schrag D, Raj G, Panageas K. How to build and interpret a nomogram for cancer prognosis. *J Clin Oncol* (2008) 26(8):1364–70. doi: 10.1200/JCO.2007.12.9791

frontiers | Frontiers in Immunology

TYPE Original Research
PUBLISHED 25 November 2022
DOI 10.3389/fimmu.2022.1024925

OPEN ACCESS

EDITED BY
Yutian Zou,
Sun Yat-sen University Cancer Center (SYSUCC), China

REVIEWED BY
Le Liu,
Southern Medical University, China
Son Hai Vu,
Gyeongsang National University, South Korea
Zhangxiang Zhao,
First Affiliated Hospital of Jinan University, China

*CORRESPONDENCE
Shangyong Li
lisy@qdu.edu.cn
Ningning He
heningning@qdu.edu.cn

SPECIALTY SECTION
This article was submitted to Cancer Immunity and Immunotherapy, a section of the journal Frontiers in Immunology

RECEIVED 22 August 2022
ACCEPTED 31 October 2022
PUBLISHED 25 November 2022

CITATION
Shang S, Wang M-z, Xing Z, He N and Li S (2022) Lactate regulators contribute to tumor microenvironment and predict prognosis in lung adenocarcinoma. *Front. Immunol.* 13:1024925. doi: 10.3389/fimmu.2022.1024925

Lactate regulators contribute to tumor microenvironment and predict prognosis in lung adenocarcinoma

Shipeng Shang[1], Mi-zhou Wang[1,2], Zhiyuan Xing[1,3], Ningning He[1*] and Shangyong Li[1*]

[1]School of Basic Medicine, Qingdao University, Qingdao, China, [2]Anesthesia Operating Department, The Affiliated Qingdao Municipal Hospital of Qingdao University, Qingdao, China, [3]Department of Abdominal Tumor Surgery, Qingdao Central Hospital to Qingdao University, Qingdao, China

Background: Lactic acid, as a product of glycolysis, increases tumor cell migration and the invasion of tumor cells in the tumor microenvironment. Besides this, lactic acid promotes the expression of programmed death-1 expression (PD-1) in regulatory T cells, which could cause the failure of PD-1 blockade therapy. However, the implications of lactic acid in the tumor microenvironment of lung adenocarcinoma (LUAD) remain largely unclear.

Methods: We performed unsupervised consensus clustering to identify lactic-associated subtypes using expression profile of lactate regulators in LUAD. Differentially expressed genes (DEGs) associated with lactic-associated subtypes was used to construct lactate signature (LaSig) using LASSO regression algorithm. Immune infiltration analysis was conducted by ESTIMATER and drug sensitivity was estimated by R package called "pRRophetic". The difference between two groups was calculated using Wilcox rank sum test and correlation analysis was calculated using Pearson correlation coefficient.

Results: In this study, we evaluated DNA methylation and the mutation frequency of lactate regulators and found lactate regulators showed low mutation frequency in the TCGA-LUAD cohort, except TP53. At the RNA level, the expression level of lactate regulators was significantly associated with the immune cell component. In particular, expression of LDHA was positively correlated with CD4 T cell, CD8 T cell, M1 macrophages, and the enrichment score of multiple immune pathways. Two clusters were defined using the gene expression level of lactate regulators, and LDHA was significantly upregulated in cluster 1 with poor overall survival. A lactate signature (LaSig) had a robust performance in predicting the survival rate and immunotherapy response of LUAD patients. Moreover, patients in the high

LaSig group may be more likely to benefit from these drugs (Cisplatin, Erlotinib, Gemcitabine, and Vinblastine) than those in the low LaSig group.

Conclusion: In summary, our study explores the role of lactate regulators in guiding the clinical treatment of lung adenocarcinoma and provides additional help to supplement traditional molecular subtypes.

KEYWORDS

lactate regulator, lung adenocarcinoma, cancer prognosis, risk model, immunotherapy

Introduction

The Warburg effect is an important metabolic feature of tumors, and it rapidly generates energy through aerobic glycolysis (1, 2). Unlike normal cells, tumor cells can produce lactic acid with sufficient oxygen to fuel tumor cells, which contributes to the tumor invasion and metastasis (3). In previous studies, lactate production is demonstrated to be closely associated with the growth of a variety of cancers, including lung (4), breast (5), and gastric cancer (6). The lactate dehydrogenase-A (LDHA) enzyme is found to play an essential role in the survival and proliferation of cancer cells (7). Besides this, the antiviral and antitumor functions of natural killer cells were enhanced by LDHA (8).

Lung adenocarcinoma (LUAD) is the most common type of lung cancer and a deadly malignant tumor with high mortality (9). Immunotherapy has become an important therapeutic strategy for LUAD with low response rates because of tumor heterogeneity and adverse events (10, 11). Identifying effectiveness biomarkers is essential to improve the effect of immunotherapy. Currently, a variety of biomarkers are used to evaluate the response of immunotherapy, including tumor mutation burden (12), PD-1, PD-L1, CTLA-4 (13), TIGIT (14), MSI (15), and Neoantigen (16). The complex immune microenvironment is an important factor that leads to the different immunotherapy responses of cancer patients. The significant characteristic of the tumor microenvironment is hypoxia, leading to an elevated level of lactic acid produced by cancer cells. The establishment of an immunosuppressive environment is closely related to metabolites (such as lactic acid), which can promote immune escape in the tumor microenvironment (17). In addition, lactic acid plays a vital role in the tumor microenvironment by regulating T cells and can promote the expression of PD-1, which is of great significance for immunotherapy (18). The increase of lactic acid can promote the activity of myeloid-derived suppressor cells and promote the activity of tumor cells (6). However, the study of lactic acid–related in the tumor environment is still limited. The regulating effect of lactic regulators needs to be analyzed in LUAD.

In this study, we aimed to analyze the relationship between the lactic regulator and the immune environment. The established LaSig scoring tool was used to predict prognosis and immunotherapy response in LUAD. LaSig had robust predictive performance and robustness in prognosis of LUAD and played a role in predicting drug sensitivity. In addition, LaSig can be used as a potential marker to predict prognosis of pan-cancer patients. Our results indicate that the lactic regulator may serve as biomarker of prognosis and immunotherapy response of LUAD.

Methods

Data collection and processing

Lactate-associated genes were collected from GO terms in the Molecular Signatures Database (MiSigDB). TCGA gene expression data, DNA methylation data, somatic mutation data, copy number variation (CNV) data, and clinical information were downloaded from Xena public data hubs (https://xenabrowser.net/).

Gene expression data of the additional LUAD samples were obtained from the Gene Expression Omnibus (GEO) database (including GSE31210 and GSE19188). Ensemble ID was converted to a gene symbol, and expression levels of genes containing more than one ensemble ID were represented by the average value. The gene expression level of TCGA-LUAD was expressed in transcripts per million (TPM). The probes were converted to gene symbols based on the annotation file of the Affymetrix Human Genome U133 Plus 2.0 Array. Immunotherapy-associated data of LUAD samples were downloaded from GSE126044 and GSE135222 (Table 1).

TABLE 1 Relevant information for all data sets in this study.

Dataset	Platform	Number of Samples (Numbers of Cancer tissue)
TCGA-LUAD	Illumina HiSeq	585 (526)
GSE31210	GPL570	246 (246)
GSE19188	GPL570	156 (36)
GSE126044	GPL16791	16 (16)
GSE135222	GPL16791	27 (16)

Unsupervised consensus clustering

To identify lactic-associated subtypes, unsupervised clustering was performed to cluster tumor samples into subtypes according to the expression matrix of lactic-associated genes. A consistency clustering algorithm was performed by using the "ConsensusClusterPlus" R package, and it was repeated 1000 times (19).

Generation of the LaSig score

First, differentially expressed genes (DEGs) between clusters 1 and 2 were identified using the "limma" R package with a threshold of |log2FC|>1 and adjusted p value<.01. Second, LUAD samples were randomly divided into training and testing sets according to a ratio of 2:1. Univariate Cox regression analysis of these genes was performed to look for the survival-associated signatures in LUAD, and genes with p-value<.05 were selected for further analysis. Then, the LASSO regression model and 10-fold cross-validation were performed to reduce the dimensionality and select representative genes by using the "glmnet" R package. Finally, we selected 25 genes, and their coefficients were used to generated the LaSig score by the following formula:

$$\text{LaSig Score} = \sum_{i}^{n} Gene_i * Coef_i$$

where $Gene_i$ and $Coef_i$ represent the expression level and LASSO coefficient of each selected gene, respectively.

Gene set enrichment analysis

GO and KEGG enrichment analysis of DEGs were performed using the "clusterProfiler" R package (20). Seventeen immune pathway–associated genes were collected from The Immunology Database and Analysis Portal (ImmPort) database (https://www.immport.org/). The immune pathway score of LUAD samples was calculated by the "GSVA" R package.

Tumor microenvironment estimation

Subpopulations of 22 immune cells were estimated by using CIBERSORTx (http://cibersort.stanford.edu/) with the gene expression profile of LUAD samples (21). The samples with p<.05 were employed for further analysis.

Analysis of drug sensitivity

An R package called "pRRophetic" was used to estimate drug sensitivity. Fifty percent of cellular growth inhibition (IC_{50}) was used as an indicator of drug sensitivity.

Statistical analysis

The Pearson correlation coefficient was used for correlation analysis. The Wilcox rank sum test was used to calculate the difference between the two groups. The Kaplan–Meier method was used to compare the overall survival of LUAD patients. All statistical analyses were conducted using R (R 4.1.2) software and p<.05 was considered significant.

Result

Multi-omics feature of lactic in LUAD

To evaluate the influence of lactic acid on LUAD, 25 lactic regulators were summarized by KEGG pathway. First, the mutation profiles of LUAD patients were studied, and we found that, except the *TP53*, mutations in 21 lactic regulators were rare in LUAD, ranging from 0% to 3% (Figure 1A). Next, the co-occurrence feature of lactic regulators was analyzed, *SLC5A12* and *LDHB*, *PNKD* and *LDHAL6A* have a co-occurrence relationship (Figure 1B). Besides this, *ACTN3*, *HAGH*, *LDHA*, and *LDHAL6A* were more likely to have copy number gains. Conversely, *TP53*, *LDHAL6B*, and *MIR210* were more likely to have copy number deletions (Figure 1C).

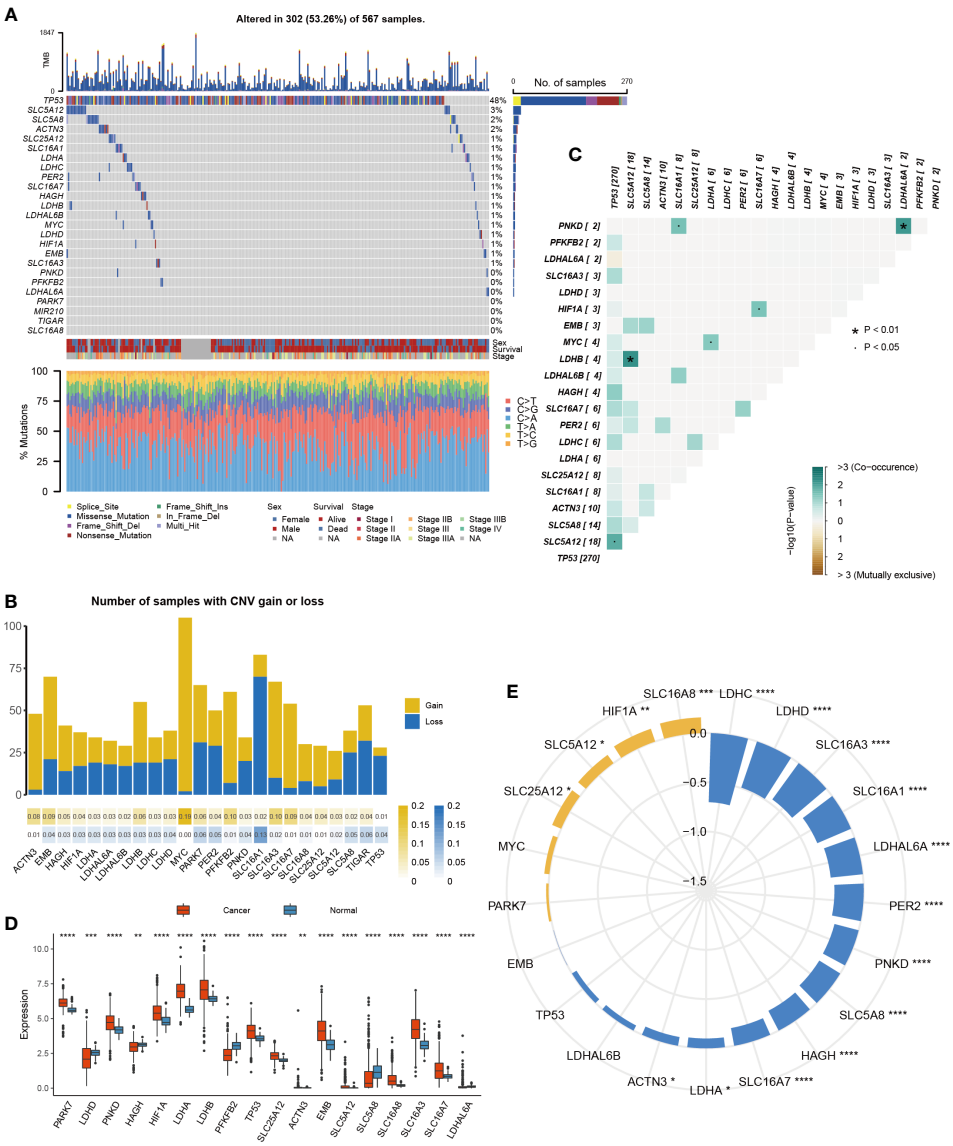

FIGURE 1
Multi-platform features of lactic regulators in LUAD. **(A)** Mutation of lactic regulators in TCGA-LUAD cohort. **(B)** Co-occurrence feature of lactic regulators in TCGA-LUAD cohort. **(C)** Copy number variation frequency of lactic regulators in TCGA-LUAD cohort. Yellow stripe represents copy number gain, and blue stripe represents copy number deletion. **(D)** Comparison of gene expression of lactic regulators between LUAD and normal tissue. **(E)** Correlation of DNA methylation and gene expression of lactic regulators in TCGA-LUAD cohort. Yellow represents positive correlation, and blue represents negative correlation (*P<.05; **p<.01; ***p<.001; ****p<.0001).

The difference in lactic regulators between LUAD and normal lung tissue were studied. Compared with normal tissue samples, 18 of 25 lactic regulators were aberrantly expressed in tumor samples (Figure 1D). To analyze the effect of DNA methylation on gene expression of lactic regulators, correlation between DNA methylation and gene expression was calculated. DNA methylation was negatively correlated with the gene expression level of *ACTN3*, *HAGH*, *LDHA*, *LDHAL6A*, *LDHC*, *LDHD*, *PER2*, *PNKD*, *SLC16A1*, *SLC16A3*, *SLC16A7*, and *SLC5A8* (Figure 1E).

These results reveal the multi-omics characteristics of the lactate regulatory factor in LUAD. At the RNA and epigenetic levels, most of the lactic regulators showed an abnormal pattern in tumor tissue compared with normal tissue, and DNA methylation may affect the gene expression of lactic regulators.

Prognosis and immune characteristics of lactic regulators

To further study the role of lactic regulators in LUAD, a univariate Cox regression model was used to estimate the prognosis value of these lactic regulators. High expression of *LDHA*, *SLC16A1*, *SLC16A3*, and *MIR210* were risk factors of overall survival for LUAD; on the contrary, high expression of *HAGH* and *LDHD* were protective factors (Figure 2A). In addition, *HAGH* and *LDHD* had a relatively strong positive correlation in RNA level.

Recent studies show that lactic acid plays an important regulatory role for immune cells in tumors (22, 23). Therefore, we investigated the relationship between lactic regulators and the

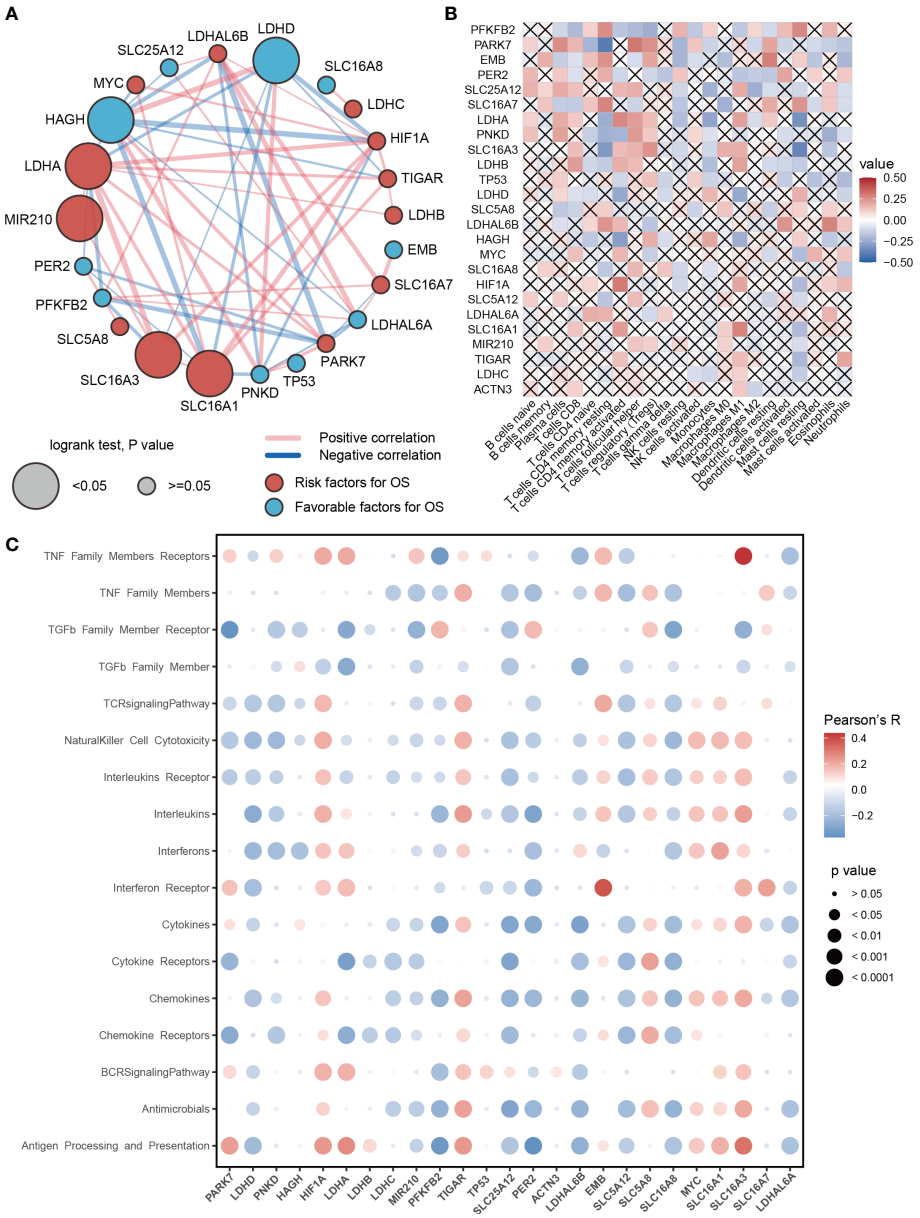

FIGURE 2
Prognosis and immune characteristics of lactic regulators. **(A)** Correlations and prognosis value of DNA lactic regulators in TCGA-LUAD cohort. **(B)** Correlation heat map between lactic regulators and 22 immune cells. Red indicates positive correlation; blue indicates negative correlation; cross indicates p>=.05. **(C)** The correlation between expression level of lactic regulators and immune-associated pathway.

immune cell. The expression level of *PFKFB2* and *PARK7* were associated with the abundance of 2/3 immune cells (Figure 2B). Moreover, lactic regulators were significantly correlated with multiple immune pathways (Figure 2C). The expression level of *EMB* and *SLC16A3* were positively correlated with interferon receptors and members of the TNF family of receptors, respectively. In summary, the expression of *PARK7*, *LDHD*, *PNKD*, *HAGH*, *MIR210*, *PFKFB2*, *PER2*, *SLC5A12*, and *SLC16A8* had a negative correlation with the pathway activity of the T cell receptor signaling pathway. The expression of HIF1A, TIGAR, EMB, SLC5A8, MYC, SLC16A1, and SLC16A7 was positively correlated with the enrichment score of the T-cell receptor signaling pathway

Construction of lactate-associated signatures

Lactic regulators may have important contributions to tumor heterogeneity due to their close links with the immune cell and immune pathway. LUAD samples were clustered into two categories using unsupervised clustering (Figure 3A). There were 13 genes with high expression levels in cluster 1 and 12 genes with high expression levels in cluster 2 (Figure 3B). As shown in Figure 3C, there is a significant difference in survival rate between the two groups. This result suggests that lactic regulators may further influence patient survival by mediating immune pathways.

We collected costimulatory and coinhibitory molecules from the work of Kim et al (24) and compared differences of their expression levels between the two clusters. Multiple costimulatory molecules, such as *CD86*, *CD80*, *CD28*, *CD40*, *CD70*, *TNFSF4*, *TNFRSF9*, *ICOS*, and *TRBV20OR9-2*, showed a higher expression level in cluster 1 (Figure 3D). Multiple coinhibitory molecules, such as *HAVCR2*, *CD274*, *PDCD1LG2*, *PDCD1*, *VSIR*, *CD276*, *TMIGD2*, *PVR*, *CD226*, *TIGIT*, and *CD96*, also showed a higher expression level in cluster 1 (Figure 3E).

The impact of lactic regulators for tumor heterogeneity was further explored, and we identified 4318 DEGs between clusters 1 and 2. These genes were enriched in immune-related terms by using GO analysis and cancer-related terms by using KEGG pathway analysis (including immune response–activating cell surface receptor signaling pathway, neutrophil activation involved in immune response, and Salmonella infection; Figures 4A, B). Univariate Cox regression analysis was used to select a prognosis-associated gene, and expression levels of 1007 genes were found to be significantly associated with survival. Twenty-five key genes were selected to construct LaSig by using a LASSO regression model and tenfold cross-validation in the training set (Figure S1). The formula of LaSig was: (-0.179)*CLEC7A+(0.008)*AP1S3+(0.044)*KRAS+(-0.067)*ATP6V1B2+(0.023)*EXT1+(0.014)*ADM+(0.078)*TLE1+(0.057)*DKK1+(0.011)*SLC16A4+(8.37e-6)*FLNC+(-0.04)*BEX4+(-0.008)*SEC14L4+(-0.023)*AKTIP+(0.084)*PLEK2+(-0.073)*PGS1+(-0.014)*SLC47A1+(-0.112)*MYLIP+(-0.067)*FAM117A+(0.139)*C1QTNF6+(0.143)*MESDC2+(-0.005)*MPEG1+(-0.042)*OSCP1+(0.296)*LDLRAD3+(-0.075)*LRRC10B+(0.011)*FAM83A. In the low LaSig group, the high expression of 12 genes is a risk factor for LUAD, and the high expression of 13 genes is a protective factor. The high LaSig and low risk groups were divided according to the median value of LaSig (cutoff of training and testing sets: 0.117 and 0.007). There was a significant difference in survival between high and low risk groups in the training set, validation set, and GSE19188 (Figures 4E–G). This suggests the role of LaSig in predicting survival of LUAD patients.

To assess the relationship between LaSig and clinical features, we compared the age, gender, and stage of LUAD patients in the high LaSig and low risk groups. We found that T4, N2, M1, and stage have higher LaSig scores (Figure S2). This suggests LaSig may reflect the malignancy degree of the tumor.

Drug sensitivity between high and low LaSig group patients

Chemotherapy is widely used in the treatment of LUAD. However, cancer patients have different drug sensitivity due to tumor heterogeneity. We compared IC_{50} of high and low LaSig group patients to find out whether LaSig score is applicable to personalized treatment strategies. The patients in the high LaSig group were sensitive to Cisplatin, Gemcitabine, and Vinblastine, and the patients in the low LaSig group was more sensitive to Erlotinib in the TCGA, GSE31210, and GSE19188 cohorts (Figure 5). This may provide help in determining therapeutic strategies for LUAD patients.

The role of LaSig in predicting immunotherapy response of LUAD

The above results reveal the close relationship between lactic regulators and the immune microenvironment. We further explored the role of LaSig score in guiding immunotherapy response. First, the human leukocyte antigen had higher expression level in low LaSig than high LaSig (Figure 6A). Second, tumor purity and the immune score of LUAD patients were calculated. LaSig was negatively correlated with tumor purity and positively correlated with immune score in LUAD (Figures 6B, C). Second, to evaluate the role of LaSig score in predicting immunotherapy response, the LaSig score of non–

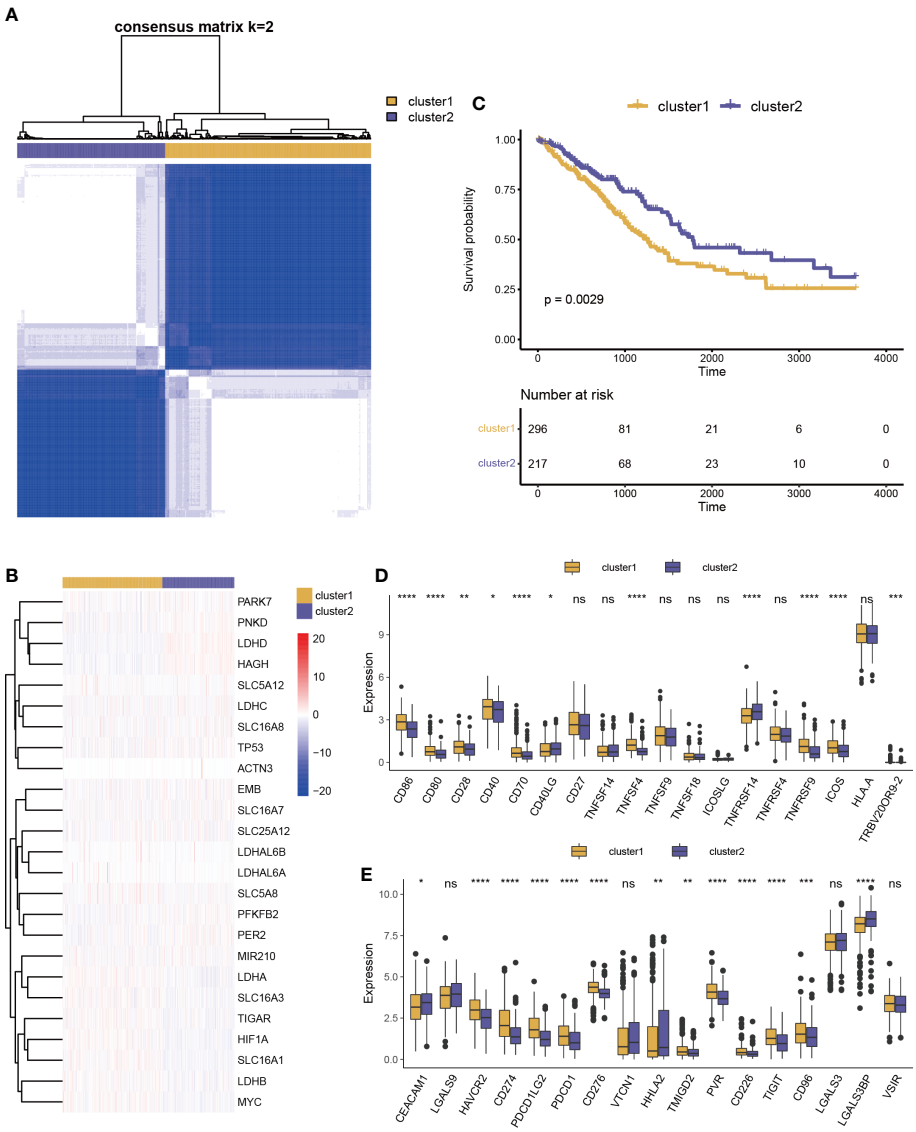

FIGURE 3
Prognosis and immune characteristics of lactic regulators. **(A)** Consensus clustering analysis of lactic regulators for optimal *k* = 2. **(B)** Kaplan–Meier curves of OS for two clusters of patients. **(C)** Heat map of 25 lactic regulators between the two distinct subtypes. **(D, E)** Differential analysis of costimulatory and coinhibitory molecules two clusters (*p<.05; **p<.01; ***p<.001; ****p<.0001).

small cell lung cancer patients treated with anti-PD-1/PD-L1 was calculated. We found that LaSig scores of nonresponders were significantly higher than those of responders (Figure 6D). Besides this, the patients were divided into two groups by using the LaSig score cutoff, and the low LaSig score group had a better prognosis (Figure 6E). These results reveal the potential role of LaSig in predicting immunotherapy.

Exploring the role of LaSig in the pan-cancer cohort

We next studied the role of LaSig in predicting the prognosis of the pan-cancer cohort. LaSig was significantly associated with prognosis in 11 cancer types (Figure 7), including adrenocortical cancer (ACC), bladder cancer (BLCA), cervical cancer (CESC),

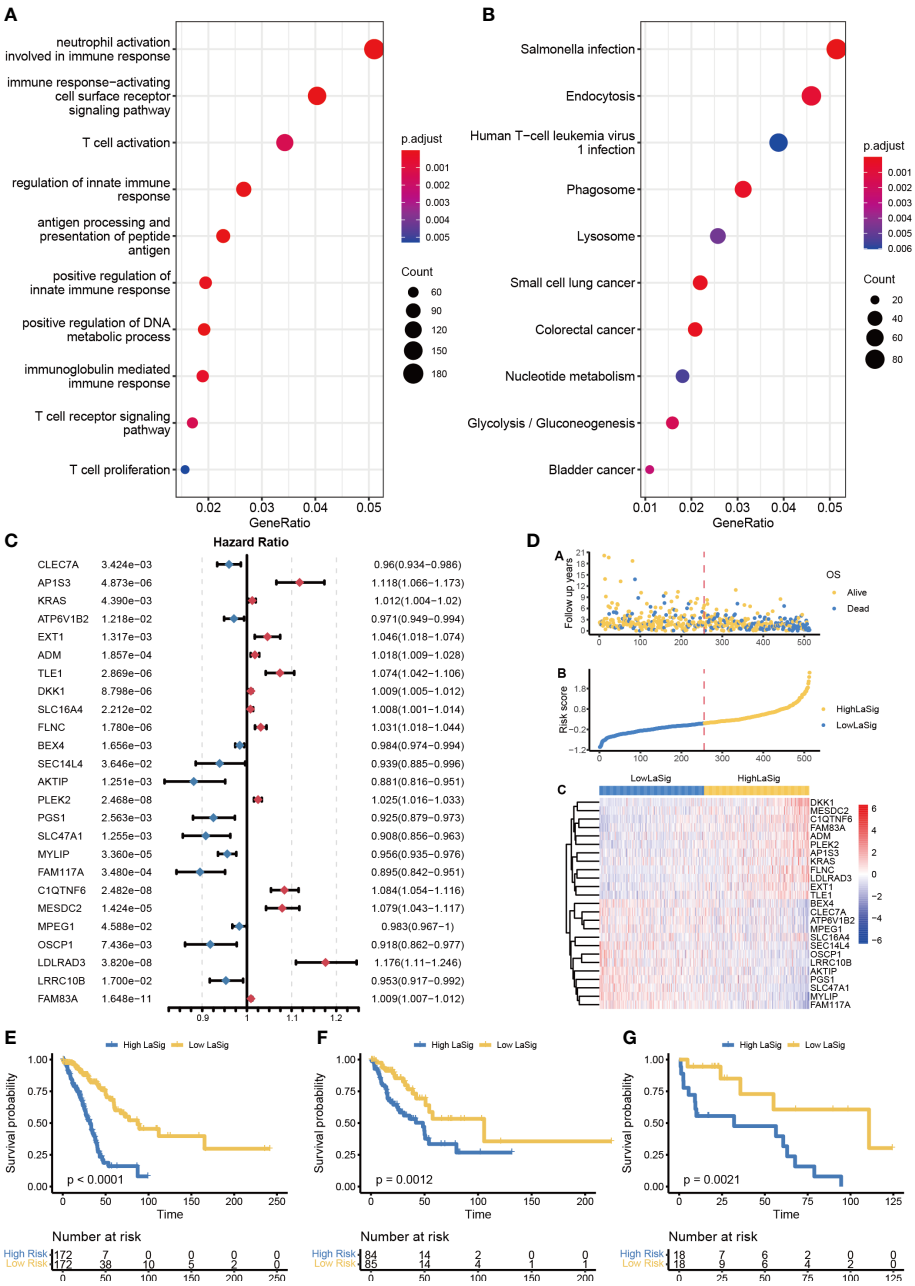

FIGURE 4
Construction of LaSig to predict the prognosis of LUAD patients. **(A, B)** GO and KEGG pathway enrichment analysis of differential expression genes. **(C)** The forest plot of key lactic signatures using univariate Cox regression analysis. **(D)** The distributions of risk scores, OS status, and gene expression of key lactic signatures. **(E–G)** Kaplan–Meier curves of high and low risk groups in training set €, test set **(F)**, and GSE19188-cohort **(G)**.

kidney clear cell carcinoma (KIRC), kidney papillary cell carcinoma (KIRP), mesothelioma (MESO), pancreatic cancer (PAAD), sarcoma (SARC), melanoma (SKCM), thymoma (THYM), and ocular melanomas (UVM). Moreover, LaSig also represented the expression of PD-1, which is significantly positively correlated with the expression of PD-1, including BLCA, kidney chromophobe (KICH), acute myeloid leukemia (LAML), lower grade glioma (LGG), liver cancer (LIHC), LUAD, pancreatic cancer (PAAD), testicular cancer (TGCT) and UVM (Figure S3).

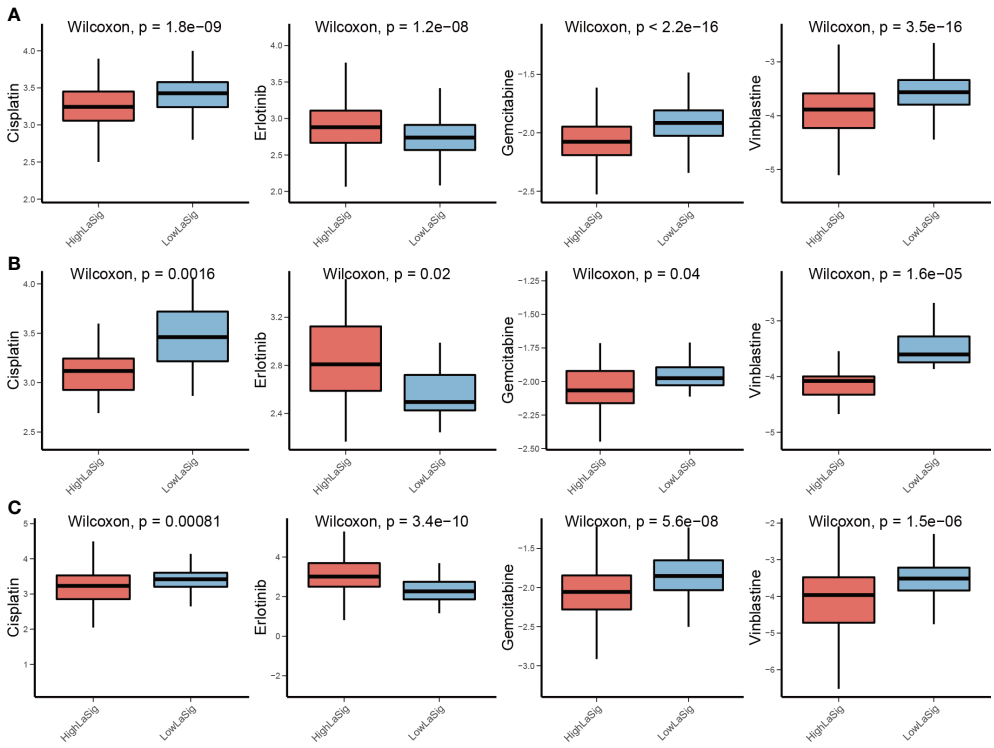

FIGURE 5
Drug sensitivity comparison between LaSig groups. **(A–C)** Difference comparison of IC_{50} of Cisplatin, Erlotinib, Gemcitabine, and Vinblastine between high and low LaSig groups in the TCGA **(A)**, GSE19188 **(B)**, and GSE31210 cohorts **(C)**.

Discussion

Lactic acid has long been considered as metabolic waste of highly proliferating cells. Nevertheless, lactic acid recently has been found to be an important product affecting tumor proliferation and metastasis (25, 26). Lactic acid could regulate T cell migration and effector function and promote the expression of PD-1 (27). However, the impact of lactic acid in the immune microenvironment of LUAD has not been identified clearly. To explore the role of lactate regulators in the immune microenvironment of LUAD can help us understand the effect of lactic acid on LUAD and guide immunotherapy.

In this study, 25 lactate regulators were collected and analyzed in LUAD. The expression level of a large number of lactate regulators in LUAD samples changed. DNA methylation of lactate regulators has a significant negative correlation with the expression of genes, which demonstrates that DNA methylation regulates expression of those genes that were associated with abnormal metabolism of the tumor. The acidification of the tumor microenvironment is an important cause of carcinogenesis processes, including metastasis and immune escape (28). The increase in lactate in the tumor is more consistent with tumor growth and migration.

Lactate regulators are also significantly correlated with immune cells, and PARK7 was negatively correlated with resting memory CD4+ T cell. In addition, the increased levels of extracellular lactate are closely associated with the Notch1/TAZ axis, which can inhibit the activity of cytotoxic T cells and lead to the proliferation and migration of lung cancer cells (29). Thus, PARK7 as a redox-sensitive chaperone may affect the status of the CD4+ T cell.

Two groups were obtained by unsupervised cluster analysis of gene expression levels of lactic acid regulators, which can distinguish prognosis. DEGs were identified between two clusters and mainly enriched in immune- and cancer-related pathways. These results suggest that molecular subtypes based on the expression level of lactate regulators may be an important prognostic feature in cancer patients. We constructed and validated a prognosis risk signature with 25 lactate regulator–related genes, named LaSig, which divided LUAD patients into

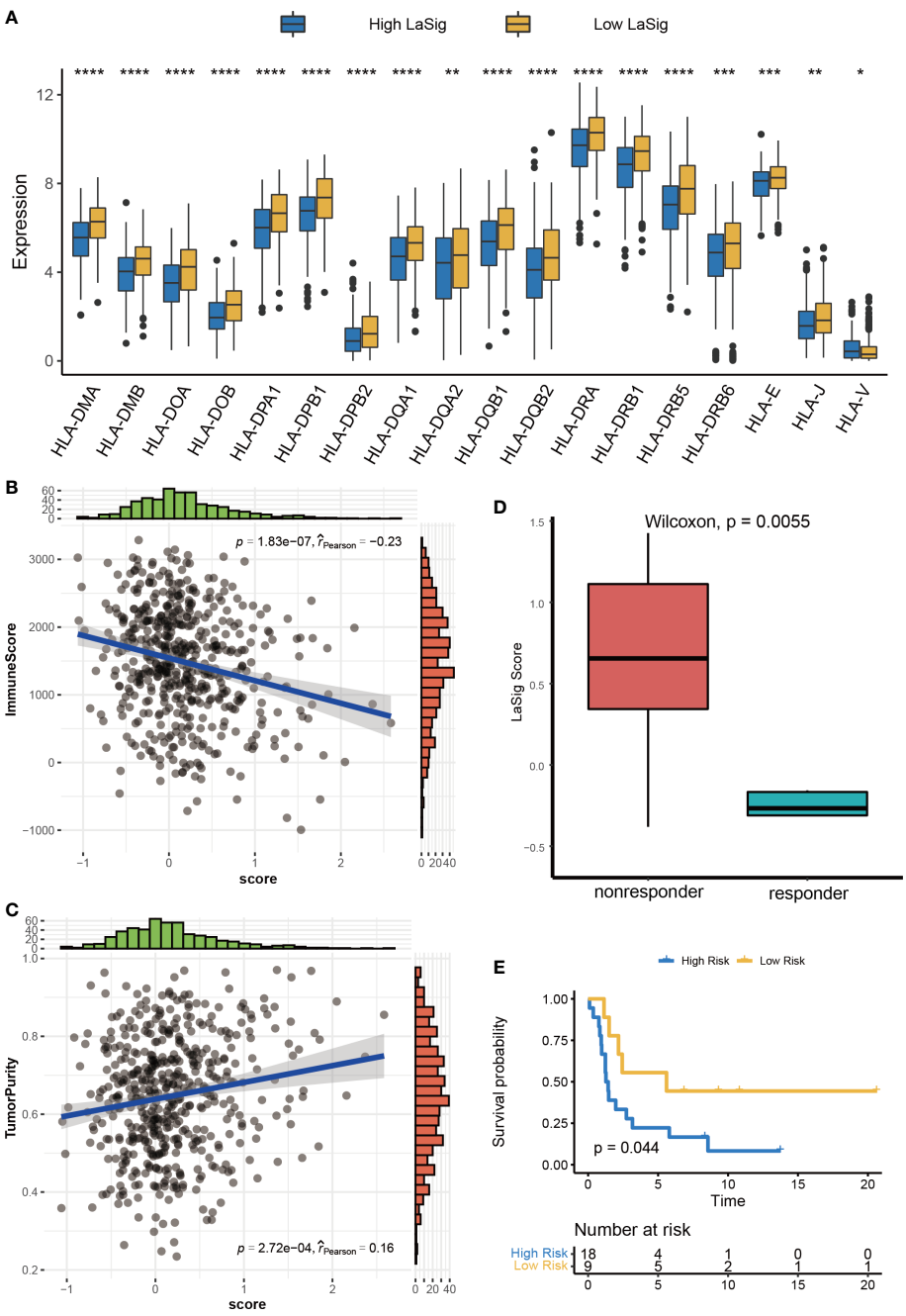

FIGURE 6
Correlation analysis between LaSig and anti-PD-L1 immunotherapy. **(A)** The expression level of human leukocyte antigen in high and low LaSig groups. **(B)** Correlation between LaSig and tumor purity. **(C)** Correlation between LaSig and stromal score. **(D)** LaSig score of patients with different immunotherapy responses. **(E)** Survival analysis of patients with different LaSig groups (*p<.05; **p<.01; ***p<.001; ****p<.0001).

high and low LaSig groups. The level of HLA gene expression and immune score in the low LaSig group were higher than those in the high LaSig control group. Hence, the immunotherapy data set is further used to verify the predictive value of LUAD immunotherapy response. Heterogeneity of the tumor microenvironment is an important factor affecting the treatment of cancer patients, including chemotherapy and immunotherapy. The difference of lactate metabolism is one of the reasons for the heterogeneity of the tumor microenvironment. Alteration of the tumor metabolism may be a potential solution to improve the

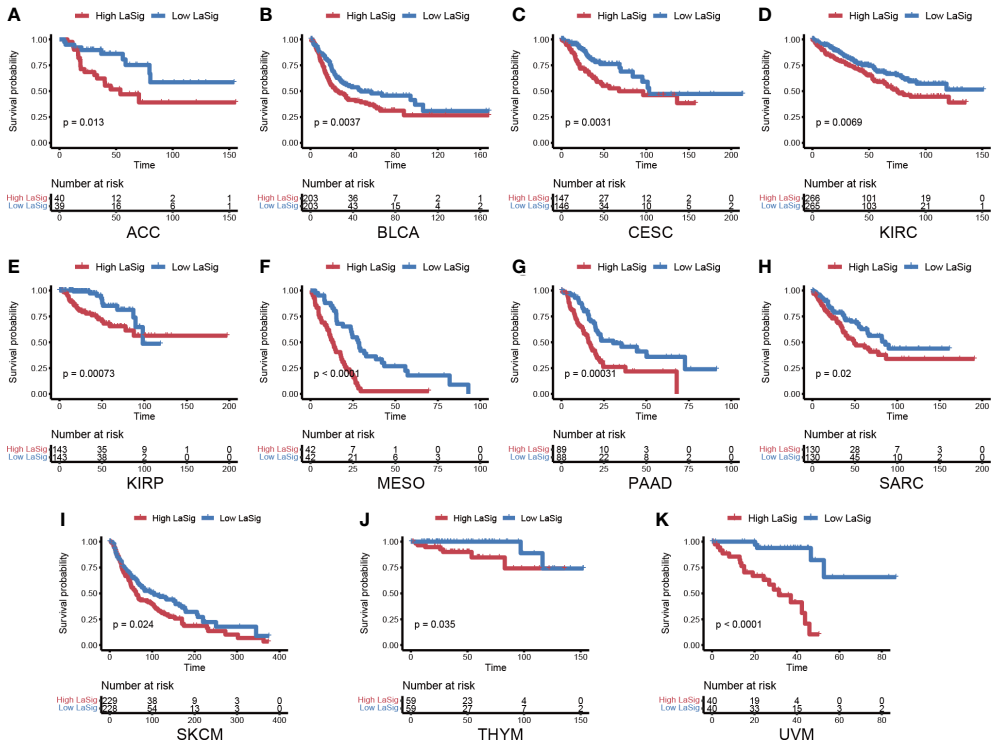

FIGURE 7
The role of LaSig in the pan-cancer cohort. **(A–K)** Survival analysis of LaSig in pan-cancer dataset.

efficacy of immunotherapy. In addition, LaSig also has predictive ability of prognosis in many types of cancer.

Conclusion

In this study, we analyzed the association between lactate regulators and immune cells. The LaSig score was constructed to predict prognosis and immunotherapy response of LUAD. LaSig may become a valuable signature to guide the treatment of LUAD patients. The expression level of lactate regulators is associated with immune cells and the immune checkpoint in the tumor environment. The prognostic risk model based on multiple lactate signature genes provides a new perspective for predicting prognosis and immunotherapy response.

Data availability statement

The datasets presented in this study can be found in online repositories. These datasets were downloaded from TCGA database, GSE31210, GSE19188, GSE126044 and GSE135222.

Author contributions

NH and SL designed and directed all the research. SS performed the experimental analysis and drafted the manuscript. M-ZW revised the manuscript. ZX participated in language editing. All authors contributed to the article and approved the submitted version.

Funding

This study was supported by the Shandong Provincial Youth Entrepreneurship Program for Colleges and Universities (2021KJ075).

Acknowledgments

We thank the members of the research team for their support and guidance.

Conflict of interest

The authors declare that the research was conducted in the absence of any commercial or financial relationships that could be construed as a potential conflict of interest.

Publisher's note

All claims expressed in this article are solely those of the authors and do not necessarily represent those of their affiliated organizations, or those of the publisher, the editors and the reviewers. Any product that may be evaluated in this article, or claim that may be made by its manufacturer, is not guaranteed or endorsed by the publisher.

Supplementary material

The Supplementary Material for this article can be found online at: https://www.frontiersin.org/articles/10.3389/fimmu.2022.1024925/full#supplementary-material

References

1. Vander Heiden MG, Cantley LC, Thompson CB. Understanding the warburg effect: the metabolic requirements of cell proliferation. *Science* (2009) 324 (5930):1029–33. doi: 10.1126/science.1160809

2. Liberti MV, Locasale JW. The warburg effect: How does it benefit cancer cells? *Trends Biochem Sci* (2016) 41(3):211–8. doi: 10.1016/j.tibs.2015.12.001

3. Faubert B, Li KY, Cai L, Hensley CT, Kim J, Zacharias LG, et al. Lactate metabolism in human lung tumors. *Cell* (2017) 171(2):358–71.e9. doi: 10.1016/j.cell.2017.09.019

4. Updegraff BL, Zhou X, Guo Y, Padanad MS, Chen PH, Yang C, et al. Transmembrane protease TMPRSS11B promotes lung cancer growth by enhancing lactate export and glycolytic metabolism. *Cell Rep* (2018) 25(8):2223–33.e6. doi: 10.1016/j.celrep.2018.10.100

5. Brown TP, Bhattacharjee P, Ramachandran S, Sivaprakasam S, Ristic B, Sikder MOF, et al. The lactate receptor GPR81 promotes breast cancer growth *via* a paracrine mechanism involving antigen-presenting cells in the tumor microenvironment. *Oncogene* (2020) 39(16):3292–304. doi: 10.1038/s41388-020-1216-5

6. Yang X, Lu Y, Hang J, Zhang J, Zhang T, Huo Y, et al. Lactate-modulated immunosuppression of myeloid-derived suppressor cells contributes to the radioresistance of pancreatic cancer. *Cancer Immunol Res* (2020) 8(11):1440–51. doi: 10.1158/2326-6066.CIR-20-0111

7. Xie H, Hanai J, Ren JG, Kats L, Burgess K, Bhargava P, et al. Targeting lactate dehydrogenase–a inhibits tumorigenesis and tumor progression in mouse models of lung cancer and impacts tumor-initiating cells. *Cell Metab* (2014) 19(5):795–809. doi: 10.1016/j.cmet.2014.03.003

8. Sheppard S, Santosa EK, Lau CM, Violante S, Giovanelli P, Kim H, et al. Lactate dehydrogenase a-dependent aerobic glycolysis promotes natural killer cell anti-viral and anti-tumor function. *Cell Rep* (2021) 35(9):109210. doi: 10.1016/j.celrep.2021.109210

9. Sung H, Ferlay J, Siegel RL, Laversanne M, Soerjomataram I, Jemal A, et al. Global cancer statistics 2020: GLOBOCAN estimates of incidence and mortality worldwide for 36 cancers in 185 countries. *CA Cancer J Clin* (2021) 71(3):209–49. doi: 10.3322/caac.21660

10. Ma KY, Schonnesen AA, Brock A, Van Den Berg C, Eckhardt SG, Liu Z, et al. Single-cell RNA sequencing of lung adenocarcinoma reveals heterogeneity of immune response-related genes. *JCI Insight* (2019) 4(4):e121387. doi: 10.1172/jci.insight.121387

11. Baxi S, Yang A, Gennarelli RL, Khan N, Wang Z, Boyce L, et al. Immune-related adverse events for anti-PD-1 and anti-PD-L1 drugs: systematic review and meta-analysis. *BMJ* (2018) 360:k793. doi: 10.1136/bmj.k793

12. Jardim DL, Goodman A, de Melo Gagliato D, Kurzrock R. The challenges of tumor mutational burden as an immunotherapy biomarker. *Cancer Cell* (2021) 39 (2):154–73. doi: 10.1016/j.ccell.2020.10.001

13. Gibney GT, Weiner LM, Atkins MB. Predictive biomarkers for checkpoint inhibitor-based immunotherapy. *Lancet Oncol* (2016) 17(12):e542–e51. doi: 10.1016/S1470-2045(16)30406-5

14. Chauvin JM, Zarour HM. TIGIT in cancer immunotherapy. *J Immunother Cancer* (2020) 8(2):e000957. doi: 10.1136/jitc-2020-000957

15. Franke AJ, Skelton WP, Starr JS, Parekh H, Lee JJ, Overman MJ, et al. Immunotherapy for colorectal cancer: A review of current and novel therapeutic approaches. *J Natl Cancer Inst* (2019) 111(11):1131–41. doi: 10.1093/jnci/djz093

16. Chen F, Zou Z, Du J, Su S, Shao J, Meng F, et al. Neoantigen identification strategies enable personalized immunotherapy in refractory solid tumors. *J Clin Invest* (2019) 129(5):2056–70. doi: 10.1172/JCI99538

17. Ngwa VM, Edwards DN, Philip M, Chen J. Microenvironmental metabolism regulates antitumor immunity. *Cancer Res* (2019) 79(16):4003–8. doi: 10.1158/0008-5472.CAN-19-0617

18. Kumagai S, Koyama S, Itahashi K, Tanegashima T, Lin YT, Togashi Y, et al. Lactic acid promotes PD-1 expression in regulatory T cells in highly glycolytic tumor microenvironments. *Cancer Cell* (2022) 40(2):201–18.e9. doi: 10.1016/j.ccell.2022.01.001

19. Wilkerson MD, Hayes DN. ConsensusClusterPlus: A class discovery tool with confidence assessments and item tracking. *Bioinformatics* (2010) 26 (12):1572–3. doi: 10.1093/bioinformatics/btq170

20. Yu G, Wang LG, Han Y, He QY. clusterProfiler: an r package for comparing biological themes among gene clusters. *OMICS* (2012) 16(5):284–7. doi: 10.1089/omi.2011.0118

21. Newman AM, Liu CL, Green MR, Gentles AJ, Feng W, Xu Y, et al. Robust enumeration of cell subsets from tissue expression profiles. *Nat Methods* (2015) 12 (5):453–7. doi: 10.1038/nmeth.3337

22. Bohn T, Rapp S, Luther N, Klein M, Bruehl TJ, Kojima N, et al. Tumor immunoevasion *via* acidosis-dependent induction of regulatory tumor-associated macrophages. *Nat Immunol* (2018) 19(12):1319–29. doi: 10.1038/s41590-018-0226-8

23. Watson MJ, Vignali PDA, Mullett SJ, Overacre-Delgoffe AE, Peralta RM, Grebinoski S, et al. Metabolic support of tumour-infiltrating regulatory T cells by lactic acid. *Nature* (2021) 591(7851):645–51. doi: 10.1038/s41586-020-03045-2

24. Berglund A, Mills M, Putney RM, Hamaidi I, Mule J, Kim S. Methylation of immune synapse genes modulates tumor immunogenicity. *J Clin Invest* (2020) 130 (2):974–80. doi: 10.1172/JCI131234

25. Qian J, Gong ZC, Zhang YN, Wu HH, Zhao J, Wang LT, et al. Lactic acid promotes metastatic niche formation in bone metastasis of colorectal cancer. *Cell Commun Signal* (2021) 19(1):9. doi: 10.1186/s12964-020-00667-x

26. Brown TP, Ganapathy V. Lactate/GPR81 signaling and proton motive force in cancer: Role in angiogenesis, immune escape, nutrition, and warburg phenomenon. *Pharmacol Ther* (2020) 206:107451. doi: 10.1016/j.pharmthera.2019.107451

27. Haas R, Smith J, Rocher-Ros V, Nadkarni S, Montero-Melendez T, D'Acquisto F, et al. Lactate regulates metabolic and pro-inflammatory circuits in control of T cell migration and effector functions. *PloS Biol* (2015) 13(7):e1002202.

28. Chen L, Huang L, Gu Y, Cang W, Sun P, Xiang Y. Lactate-lactylation hands between metabolic reprogramming and immunosuppression. *Int J Mol Sci* (2022) 23(19):11943. doi: 10.3390/ijms231911943

29. Xie M, Fu XG, Jiang K. Notch1/TAZ axis promotes aerobic glycolysis and immune escape in lung cancer. *Cell Death Dis* (2021) 12(9):832. doi: 10.1038/s41419-021-04124-6

frontiers | Frontiers in Immunology

TYPE Case Report
PUBLISHED 30 November 2022
DOI 10.3389/fimmu.2022.1059331

OPEN ACCESS

EDITED BY
Zhijie Wang,
National Cancer Center of China,
China

REVIEWED BY
Bin Zhang,
Dalian Medical University, China
Yosuke Shionoya,
Ainosato At Home Clinic, Japan

*CORRESPONDENCE
Huijuan Cui
chjzryhyy@sina.com

†These authors share first authorship

SPECIALTY SECTION
This article was submitted to Cancer Immunity and Immunotherapy, a section of the journal Frontiers in Immunology

RECEIVED 01 October 2022
ACCEPTED 10 November 2022
PUBLISHED 30 November 2022

CITATION
Zhang X, Zheng J, Niu Y, Xue C, Yu Y, Tan K and Cui H (2022) Long-term survival in extensive-stage small-cell lung cancer treated with different immune checkpoint inhibitors in multiple-line therapies: A case report and literature review.
Front. Immunol. 13:1059331.
doi: 10.3389/fimmu.2022.1059331

Long-term survival in extensive-stage small-cell lung cancer treated with different immune checkpoint inhibitors in multiple-line therapies: A case report and literature review

Xu Zhang[1†], Jiabin Zheng[2†], Yun Niu[3], Chongxiang Xue[1], Yixuan Yu[1], Kexin Tan[1] and Huijuan Cui[2*]

[1]Graduate School, Beijing University of Chinese Medicine, Beijing, China, [2]Department of Integrative Oncology, China-Japan Friendship Hospital, Beijing, China, [3]Department of Pathology, China-Japan Friendship Hospital, Beijing, China

Background: Extensive-stage small-cell lung cancer (ES-SCLC) is highly malignant, is highly prone to recurrence, and has a short survival period. It is very difficult to achieve long-term survival in ES-SCLC, which has not been significantly improved in the last 20 years. For a long time, platinum-based chemotherapy has occupied the core position in the treatment of small-cell lung cancer (SCLC), but there are few options for treatment drugs or regimens, and if disease progression occurs, the options for follow-up regimens are obviously limited. The advent of immunotherapy has changed this situation to some extent, and immunotherapy has shown some effects in improving efficiency and prolonging survival, whether in first- or third-line therapy, but it is still unsatisfactory.

Case presentation: A 57-year-old patient with ES-SCLC experienced disease progression after four lines of treatment including synchronous radiotherapy, chemotherapy, and antiangiogenesis. However, the patient still benefited when switching to the programmed cell death receptor-1 (PD-1) inhibitor toripalimab in combination with chemotherapy in the fifth line. Even after the development of immune resistance, the patient still benefited after switching to tislelizumab in combination with different chemotherapy regimens or alone in the sixth and seventh lines. Following the progression of tislelizumab in combination with chemotherapy, the patient again profited after switching to durvalumab in combination with anlotinib and again achieved a progressive-free survival (PFS) of 11 months. Overall, the patient achieved a total of 45 months of PFS and 50 months of overall survival (OS), with a shocking and exciting 30 months of PFS achieved in the immune combination phase alone.

Conclusion: We report a patient with ES-SCLC who achieved long-term survival after at least eight lines of therapy including chemotherapy,

antiangiogenesis, and different immune checkpoint inhibitors (ICIs). This suggests that long-term survival in SCLC is possible with aggressive, combined, and standardized treatment. Otherwise, immunotherapy postline enablement can still benefit patients, rechallenge after immune resistance is also possible in SCLC, and combination with chemotherapy or antiangiogenic therapy can improve the efficacy and prolong the survival. This will provide new ideas and options for the selection of treatment options for SCLC.

KEYWORDS

ES-SCLC, long-term survival, ICIs, re-challenge, combined regimens

Introduction

Lung cancer, accounting for about 18% of cancer-related deaths, remains the leading cause of cancer-related deaths worldwide (1), of which small-cell lung cancer (SCLC) accounts for only 15% of lung cancer (2). However, SCLC is the most malignant type of lung cancer and has the worst prognosis, with an average overall survival (OS) of only 2–4 months in the natural course (3). On the one hand, due to its rapid proliferation rate and easy early metastasis, two-thirds of patients are in the extensive stage at the initial diagnosis, leading to its high mortality rate (4).

For extensive-stage small-cell lung cancer (ES-SCLC), comprehensive medical treatment is top ranked. SCLC is extremely sensitive to chemotherapy, and chemotherapy has excellent efficacy (2, 5). However, SCLC is very easy to relapse, and the recurrence rate within 1 year after first-line treatment is more than 80% (6). After relapse, the therapeutic effect is limited, and despite years of exploration, no more effective therapeutic drugs have emerged. Even with the advent of immunotherapy in recent years (7–10), there has been a modest improvement in the efficiency and survival of SCLC treatment with an objective response rate (ORR) of only 10% for single-agent immunotherapy in third-line treatment. Even in combination with ipilimumab, the ORR is only 33% and the maximum median progressive-free survival (PFS) is only 2.6 months (9). While in first-line treatment, the median OS was prolonged by less than 3 months compared to chemotherapy, despite an ORR of 68% for immune combination chemotherapy (11). If the disease progresses again after immunotherapy, the follow-up treatment options will also be significantly limited.

Here, we reported a case of a patient with ES-SCLC who received three different immune checkpoint inhibitors (ICIs) in combination with chemotherapy or antiangiogenic targeted therapy after progressing on fourth-line chemotherapy and achieved a total of 45 months of PFS and 50 months of high-quality OS. Such treatment results were very different from clinical reports and brought us a very great surprise.

Case presentation

In January 2018, a 57-year-old Chinese woman was admitted to our hospital for hemoptysis. The patient was in good health and had no history of smoking, a family history of hereditary disease, or tumor. However, the current chest computed tomography (CT) and positron emission tomography (PET)-CT suspected left-sided advanced central-type lung cancer with multiple lymph node metastases in the mediastinum and hilar and pleural effusion (Figure 1). Blood tests show a significant elevation of tumor markers including neuron-specific enolase (NSE) (Figure 2A) and pro-gastrin-releasing peptide (Pro-GRP) (Figure 2B) than the normal. Fortunately, the brain magnetic resonance imaging (MRI) showed no brain metastases. Then, she accepted the fiberoptic bronchoscopy and biopsy at the same time (Figure 2C). Eventually, the diagnosis of ES-SCLC, cT2bN3M1a, stage IVa was given. Immunohistochemical analyses suggested "CD56 (+), CgA (±), Syn (+), CK (AE1/AE3) (perinuclear punctate +), CK5/6 (–), CK7 (-), NapsinA (-), TTF-1 (+), Ki-67 (80%+), and programmed cell death receptor ligand-1 (PD-L1) <5%." The genetic testing demonstrated the tumor mutational burden (TMB) of 1.82 and microsatellite stabilization (MSS).

She was administered four-line systematic chemotherapies including etoposide and carboplatin (EC) (Figure 3), vinorelbine and ifosfamide (NI) followed by anlotinib (Figure 3), irinotecan and pobaplatin (IP) (Figure 3), and albumin paclitaxel combined with cisplatin (TC) (Figure 3). Otherwise, she also got radiotherapy during the initial treatment period. Her disease ultimately progressed while on these systematic therapies, although some lesions shrank or were even partially relieved within a short period.

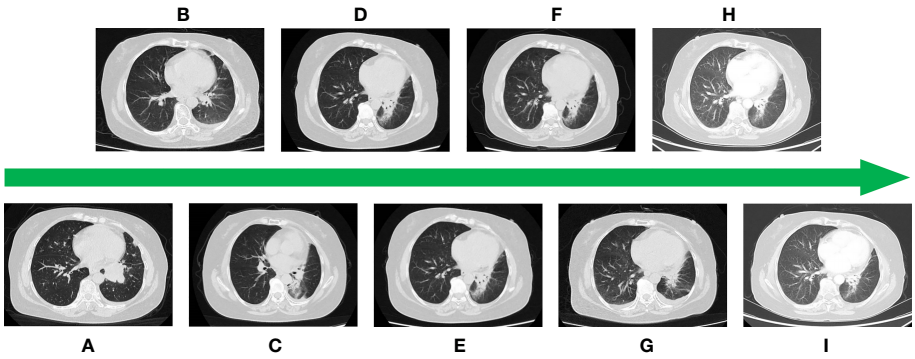

FIGURE 1
(A) CT image at the time of initial diagnosis. **(B)** Image after first-line treatment. **(C)** Image after second-line treatment. **(D)** Image after third-line treatment. **(E)** Image after fourth-line treatment. **(F)** Image after fifth-line treatment. **(G)** Image after sixth-line treatment. **(H)** Image after seventh-line treatment. **(I)** Image after eighth-line treatment.

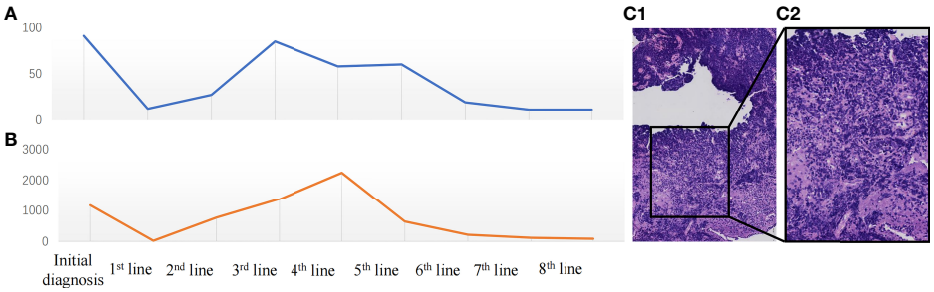

FIGURE 2
(A) Change in neuron-specific enolase (NSE) (ng/ml) during the treatment period. **(B)** Change in pro-gastrin-releasing peptide (Pro-GRP) (pg/ml) during the treatment. **(C)** The microscopic image of the tumor: ×200 (C1), ×400 (C2).

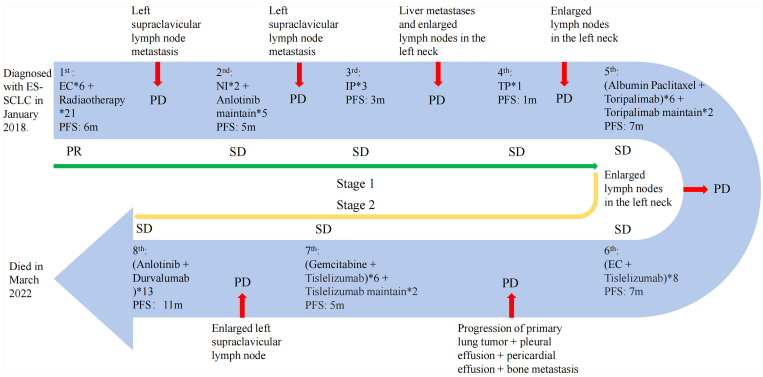

FIGURE 3
The treatment progress of the patient. The first stage includes the first to fourth lines of treatment; the fifth to eighth lines of treatment are the second stage. PR, partial response; PD, progressive disease; SD, stable disease. The efficacy evaluation was judged according to the Response Evaluation Criteria in Solid Tumours (RECIST) (Version 1.1).

10.3389/fimmu.2022.1059331

Notably, the levels of NSE (Figure 2A) and Pro-GRP (Figure 2B) were rising, and the ultrasonography and CT scan showed that the left clavicle lymph nodes were enlarged. Then, she received the fifth-line treatment with albumin paclitaxel plus programmed cell death receptor-1 (PD-1) inhibitor toripalimab (Figure 3). In January 2020, she received radiofrequency ablation treatment for her metastatic supraclavicular fossa lymph node lesion. However, albumin paclitaxel had to be suspended for high brain natriuretic petide (BNP) level and cardiac toxicity. Afterward, she continued receiving toripalimab alone as the maintenance treatment (Figure 3).

In March 2020, the touchable swollen lymph nodes on the left side of the neck revealed that the disease may have progressed. Immediately afterward, she completed ultrasound examination of neck lymph nodes and blood tumor markers, and the disease was judged to have progressed again. Thus, she started the sixth-line treatment with etoposide plus carboplatin and tislelizumab (Figure 3). The following CT scan revealed that the lesion has slightly progressed and she newly acquired pleural and pericardial effusion. Additionally, the bone scan of the body showed multiple bone metastases.

From that time, she received the seventh-line gemcitabine plus tislelizumab (Figure 3). Unfortunately, owing to the coronary heart disease and percutaneous coronary intervention, she delayed receiving the tislelizumab monotherapy then (Figure 3).

With a PFS of 5 months, her left supraclavicular lymph node was evaluated to be larger than before revealed by the CT scan. As a result, a change to PD-L1 agents was determined considering the demand of the patient and her family. Fortunately, she benefited from the eighth-line anlotinib plus durvalumab therapy for up to 11 months (Figure 3). In March 2022, she died of acute heart attack.

Discussion

Although this patient has passed away, it is still exciting to review the complete treatment of this case (Figure 3). To summarize, this patient has several very distinctive features. First, this patient experienced eight lines of treatment and achieved a very long survival without a significant impact on quality of life despite being initially diagnosed with ES-SCLC. Furthermore, this patient could benefit from postline combination immunotherapy despite having received four lines of chemotherapy up front. Even after the development of immune resistance, the benefit continued after switching to a different ICI, with the patient gaining a total of 30 months of PFS during the immunotherapy phase.

In terms of ES-SCLC, the prognosis is poor and survival is short, with a median OS of only 6–10 months even after aggressive and standardized treatment (12), and a 5-year survival rate of less than 2% (13). However, this patient achieved a high-quality long-term survival of almost 50 months after multiple lines of therapy, which is exceedingly rare. A review of the literature revealed that patients with ES-SCLC with better physical status (14, 15), sensitivity to platinum-based drugs and the absence of liver or brain metastases (16), and adherence to active close follow-up may have a better prognosis with the possibility of achieving long-term survival. In these respects, the present patient is in accordance, and this may be one of the reasons for her long-term survival. However, data on long-term survival in ES-SCLC are relatively scarce (17) and are mostly single case reports (18–24), and the specific mechanisms still need to be further explored.

The infiltration of immune cells in the tumor microenvironment (25, 26) and the expression of PD-L1 (27) may be closely related to the efficacy of immunotherapy. Meanwhile, a cohort study found that the infiltration of immune cells in the tumor microenvironment may be crucial for the long-term survival of SCLC, especially the apparent increase in the number of $CD3^+$ T cells, $CD4^+$ T cells, $CD14^+$ T cells, and tumor-infiltrating monocytes and the decrease in suppressor immune cells (28). However, this patient has not been tested for lymphocytes in the immune microenvironment, so there is no direct evidence to support this. However, by reviewing the entire treatment course and outcome of this case, we may be able to refute this hypothesis as well.

Firstly, this patient had excellent efficacy during the immunotherapy phase, although the ICI was only started from the fifth line of treatment. After progressing on fourth-line therapy, the patient first switched to toripalimab in combination with albumin paclitaxel and obtained a PFS of 7 months, with a significantly longer effective time compared to the literature, which may be related to the induction of apoptosis of tumor cells by prior chemotherapeutic agents, increased release of tumor antigenic substances, removal of immunosuppression, modulation of immune response, and remodeling of the immune microenvironment, resulting in immune potentiation (29–34).

After progressing through the fifth line of treatment, the patient switched to the PD-1 inhibitor tislelizumab in combination with different chemotherapy regimens as the sixth and seventh lines of treatment and achieved another 12 months of PFS, again surprising us with such efficacy. A previous study found that after progression on one PD-1 inhibitor in non-small-cell lung cancer (NSCLC), patients can still benefit from swapping to another PD-1 inhibitor (35). As far as we know, however, this is the first report in SCLC. In the case of this patient, we can attribute to the difference in the mechanism of the different drugs. Although both are humanized immunoglobulin G4 (IgG4) monoclonal antibodies that block the binding of PD-1 to PD-L1 or programmed cell death receptor ligand-2 (PD-L2), there are still subtle differences in the mechanism between toripalimab and tislelizumab. Toripalimab binds to PD-1 on the surface of T cells *via* the FG loop (36) while tislelizumab through the CC' loop (37), and the dissociation rate from PD-1 is slower (37), resulting in a higher targeting affinity. In terms of pharmacokinetics, the half-life of tislelizumab is longer than that of toripalimab (38, 39).

In addition, the role of combination chemotherapy cannot be ignored (40–42), as in this case after progression of the tislelizumab combined with EC regimen, seventh-line therapy in combination with gemcitabine resulted in a renewed benefit for the patient and a significantly prolonged PFS compared to chemotherapy alone (43) or immunotherapy. It is also suggested that different chemotherapeutic agents can modify the tumor microenvironment through different mechanisms and add to the effectiveness of immunotherapy (44, 45). Unfortunately, despite the seven lines of treatment, the disease still progressed.

It is reported that when blocking the PD-1/PD-L1 signaling pathway, PD-L1 inhibitors are more effective than PD-1 inhibitors (46). In NSCLC, switching to PD-L1 inhibitor therapy after progression on PD-1 inhibitor therapy still results in disease control rate (DCR) of more than 30% and PFS can be extended by about 3 or 4 months (47–49); patient benefit has also been reported in triple-negative breast cancer (50). This suggests to us that the choice of PD-L1 inhibitor after PD-1 inhibitor progression might be a valid option. However, there are no similar reports in SCLC. In this case, after switching to PD-L1 inhibitor therapy in combination with anlotinib as eighth-line therapy, the patient again benefited with a significant prolongation of PFS for a total of approximately 11 months, which provides clinical evidence for the replacement in SCLC with PD-L1 inhibitors after progression with PD-1 inhibitors. As for the specific grounds for the benefit, we speculate that it is most likely due to the discrepancy in the modes of action between PD-1 and PD-L1 (51, 52).

However, what we still cannot ignore is the combined effect of the antiangiogenic drug anlotinib. ICIs combined with antiangiogenic therapy have been shown to improve the efficacy and prolong PFS and OS (53–56), which may be related to the fact that antiangiogenic drugs can inhibit tumor angiogenesis, reduce the blood supply to the tumor, and alter the tumor microenvironment, thus inhibiting tumor growth. Anlotinib, an essential antiangiogenic agent, has clinically proven efficacy and safety in SCLC (57, 58). The patient achieved a long PFS in this line treatment, significantly longer than reported in the literature (9, 59), which must be attributed to the synergistic effect of the immune combination with antiangiogenesis.

Reviewing the entire course of this patient's treatment, we can observe that the patient obtained a very long and high-quality survival. Especially in the immunotherapy phase, the sequential application of different ICIs and the combination of different regimens brought the possibility of long-term survival for the patient.

In the era of chemotherapy for SCLC, switching to another chemotherapy regimen after progression has become a routine option. While entering the era of immunotherapy, whether it is possible to sequentially apply different ICIs after the progress of one or more ICI therapies has not been reported. However, this case provides objective evidence for the efficacy and safety of immune rechallenge in SCLC.

Conclusion

First, after aggressive and standardized treatment and close follow-up, long-term benefit is still possible, even in SCLC. In addition, immunotherapy remains effective in the later line of treatment. Even if immune resistant, the patient could still benefit again after changing ICIs; and the efficacy could be further improved by combining different treatment regimens. This provides new ideas and options for the treatment process of clinically ES-SCLC.

Data availability statement

The original contributions presented in the study are included in the article/supplementary material. Further inquiries can be directed to the corresponding author.

Ethics statement

Written informed consent was obtained from the individual(s) for the publication of any potentially identifiable images or data included in this article.

Author contributions

XZ and JZ: Collect clinical data, accomplish and revise the paper. YN: Pathology consultation and diagnosis. CX: Revise the paper and organize the paper. YY: Check clinical data and revise the paper. KT: Organize paper. HC: Provide cases, describe the novelty and particularity of the cases, review and revise the content of the article. All authors contributed to the article and approved the submitted version.

Funding

This study was supported by the National High Level Hospital Clinical Research Funding (2022-NHLHCRF-LX-02-0111) and the Capital Health Development Research Project (shoufa 2022-2-4065).

Conflict of interest

The authors declare that the research was conducted in the absence of any commercial or financial relationships that could be construed as a potential conflict of interest.

Publisher's note

References

1. Sung H, Ferlay J, Siegel RL, Laversanne M, Soerjomataram I, Jemal A, et al. Global cancer statistics 2020: GLOBOCAN estimates of incidence and mortality worldwide for 36 cancers in 185 countries. *CA Cancer J Clin* (2021) 71(3):209–49. doi: 10.3322/caac.21660

2. Rudin CM, Brambilla E, Faivre-Finn C, Sage J. Small-cell lung cancer. *Nat Rev Dis Primers.* (2021) 7(1):3. doi: 10.1038/s41572-020-00235-0

3. Yang S, Zhang Z, Wang Q. Emerging therapies for small cell lung cancer. *J Hematol Oncol* (2019) 12(1):47. doi: 10.1186/s13045-019-0736-3

4. Loizidou A, Lim E. Is small cell lung cancer a surgical disease at the present time? *Thorac Surg Clin* (2021) 31(3):317–21. doi: 10.1016/j.thorsurg.2021.04.011

5. Paulus A, Lousberg L, Duysinx B, Sibille A, Duquenne JB, Corhay JL, et al. [Small cell lung cancer : update of therapy]. *Rev Med Liege* (2021) 76(5-6):452–7.

6. Hiddinga BI, Raskin J, Janssens A, Pauwels P, Van Meerbeeck JP. Recent developments in the treatment of small cell lung cancer. *Eur Respir Rev* (2021) 30 (161):210079. doi: 10.1183/16000617.0079-2021

7. Bianco A, D'Agnano V, Matera MG, Della Gravara L, Perrotta F, Rocco D. Immune checkpoint inhibitors: A new landscape for extensive stage small cell lung cancer treatment. *Expert Rev Respir Med* (2021) 15(11):1415-25. doi: 10.1080/17476348.2021.1964362

8. Esposito G, Palumbo G, Carillio G, Manzo A, Montanino A, Sforza V, et al. Immunotherapy in small cell lung cancer. *Cancers (Basel)* (2020) 12(9):2522. doi: 10.3390/cancers12092522

9. Antonia SJ, López-Martin JA, Bendell J, Ott PA, Taylor M, Eder JP, et al. Nivolumab alone and nivolumab plus ipilimumab in recurrent small-cell lung cancer (CheckMate 032): a multicentre, open-label, phase 1/2 trial. *Lancet Oncol* (2016) 17(7):883–95. doi: 10.1016/S1470-2045(16)30098-5

10. Ready N, Farago AF, de Braud F, Atmaca A, Hellmann MD, Schneider JG, et al. Third-line nivolumab monotherapy in recurrent SCLC: CheckMate 032. *J Thorac Oncol* (2019) 14(2):237–44. doi: 10.1016/j.jtho.2018.10.003

11. Paz-Ares L, Dvorkin M, Chen Y, Reinmuth N, Hotta K, Trukhin D, et al. Durvalumab plus platinum–etoposide versus platinum–etoposide in first-line treatment of extensive-stage small-cell lung cancer (CASPIAN): a randomised, controlled, open-label, phase 3 trial. *Lancet* (2019) 394(10212):1929–39. doi: 10.1016/S0140-6736(19)32222-6

12. Zhang S, Li S, Cui Y, Zhao P, Sun X, Cheng Y. Consideration of surrogate endpoints for overall survival associated with first-line immunotherapy in extensive-stage small cell lung cancer. *Front Oncol* (2021) 11:696010. doi: 10.3389/fonc.2021.696010

13. Arriola Aperribay E, Trigo Pérez J, Sánchez Gastaldo A, Navarro Mendivil A, Crama L, Ruiz Gracia P, et al. MA12.03 prognostic value of clinical staging according to TNM in SCLC patients; a real-world SEER database analysis. *J Thorac Oncol* (2021) 16(3):S177-S177. doi: 10.1016/j.jtho.2021.01.255

14. Fujimoto D, Yoshioka H, Kataoka Y, Morimoto T, Kim YH, Tomii K, et al. Efficacy and safety of nivolumab in previously treated patients with non-small cell lung cancer: A multicenter retrospective cohort study. *Lung Cancer.* (2018) 119:14–20. doi: 10.1016/j.lungcan.2018.02.017

15. Rittberg R, Green S, Aquin T, Bucher O, Banerji S, Dawe DE. Effect of hospitalization during first chemotherapy and performance status on small-cell lung cancer outcomes. *Clin Lung Cancer* (2020) 21(5):e388–404. doi: 10.1016/j.cllc.2020.02.013

16. Stratmann JA, Timalsina R, Atmaca A, Rosery V, Frost N, Alt J, et al. Clinical predictors of survival in patients with relapsed/refractory small-cell lung cancer treated with checkpoint inhibitors: A German multicentric real-world analysis. *Ther Adv Med Oncol* (2022) 14:17588359221097191. doi: 10.1177/17588359221097191

17. Steffens CC, Elender C, Hutzschenreuter U, Dille S, Binninger A, Spring L, et al. Treatment and outcome of 432 patients with extensive-stage small cell lung cancer in first, second and third line - results from the prospective German TLK cohort study. *Lung Cancer.* (2019) 130:216–25. doi: 10.1016/j.lungcan.2019.02.026

18. Osawa H, Okauchi S, Ohara G, Kagohashi K, Satoh H. A long-term control of intramedullary thoracic spinal cord metastasis from small cell lung cancer. *Acta Med (Hradec Kralove).* (2018) 61(2):57–9. doi: 10.14712/18059694.2018.52

19. Ramineni G, Bindra BS, Jatwani K, Singh D, Khillan R. A case of long-term survival of 36 months in the setting of extensive-disease small-cell lung cancer. *Cureus* (2019) 11(9):e5605. doi: 10.7759/cureus.5605

20. Kosuda A, Shirahata T, Kudo N, Uehara Y, Miyawaki M, Hagiwara A, et al. Long-term survival of a patient with small cell lung cancer secreting ADH and ACTH simultaneously, following the prolonged use of amrubicin. *Intern Med* (2020) 59(1):107–12. doi: 10.2169/internalmedicine.2838-19

21. Singh PK, Shrestha DK, Singh N, Gupta N. Extensive-disease small cell lung cancer, multiple relapses, five lines of therapy and more than 10-year survival. *BMJ Case Rep* (2020) 13(2):e232607. doi: 10.1136/bcr-2019-232607

22. Vucetic A, Ahmad B, Tang T. Long-term survival in a patient with extensive-stage small cell lung cancer treated with multiple courses of salvage stereotactic radiation after whole brain radiotherapy: A case report. *Oncol Lett* (2022) 24(4):335. doi: 10.3892/ol.2022.13454

23. Wakuda K, Yabe M, Kodama H, Nishioka N, Miyawaki T, Miyawaki E, et al. Long-term outcomes in extensive disease small cell lung cancer patients treated without immune checkpoint inhibitors. *Jpn J Clin Oncol* (2021) 51(12):1736–43. doi: 10.1093/jjco/hyab158

24. Zhang Z, Li Y, Dong Y, Li J, Zhang B, Zhang C, et al. Successful treatment of a patient with multiple-line relapsed extensive-stage small-cell lung cancer receiving penpulimab combined with anlotinib: A case report. *Front Oncol* (2022) 12:846597. doi: 10.3389/fonc.2022.846597

25. Teng MW, Ngiow SF, Ribas A, Smyth MJ. Classifying cancers based on T-cell infiltration and PD-L1. *Cancer Res* (2015) 75(11):2139–45. doi: 10.1158/0008-5472.CAN-15-0255

26. Huang TX, Tan XY, Huang HS, Li YT, Liu BL, Liu KS, et al. Targeting cancer-associated fibroblast-secreted WNT2 restores dendritic cell-mediated antitumour immunity. *Gut.* (2022) 71(2):333–44. doi: 10.1136/gutjnl-2020-322924

27. Yu Y, Zeng D, Ou Q, Liu S, Li A, Chen Y, et al. Association of survival and immune-related biomarkers with immunotherapy in patients with non-small cell lung cancer: A meta-analysis and individual patient-level analysis. *JAMA Netw Open* (2019) 2(7):e196879. doi: 10.1001/jamanetworkopen.2019.6879

28. Muppa P, Parrilha Terra SBS, Sharma A, Mansfield AS, Aubry MC, Bhinge K, et al. Immune cell infiltration may be a key determinant of long-term survival in small cell lung cancer. *J Thorac Oncol* (2019) 14(7):1286–95. doi: 10.1016/j.jtho.2019.03.028

29. Jackaman C, Majewski D, Fox SA, Nowak AK, Nelson DJ. Chemotherapy broadens the range of tumor antigens seen by cytotoxic CD8(+) T cells in vivo. *Cancer Immunol Immunother* (2012) 61(12):2343–56. doi: 10.1007/s00262-012-1307-4

30. Adair SJ, Hogan KT. Treatment of ovarian cancer cell lines with 5-aza-2'-deoxycytidine upregulates the expression of cancer-testis antigens and class I major histocompatibility complex-encoded molecules. *Cancer Immunol Immunother.* (2009) 58(4):589–601. doi: 10.1007/s00262-008-0582-6

31. Zhou J, Wang G, Chen Y, Wang H, Hua Y, Cai Z. Immunogenic cell death in cancer therapy: Present and emerging inducers. *J Cell Mol Med* (2019) 23 (8):4854–65. doi: 10.1111/jcmm.14356

32. Fucikova J, Kepp O, Kasikova L, Petroni G, Yamazaki T, Liu P, et al. Detection of immunogenic cell death and its relevance for cancer therapy. *Cell Death Dis* (2020) 11(11):1013. doi: 10.1038/s41419-020-03221-2

33. Zhou Y, Bastian IN, Long MD, Dow M, Li W, Liu T, et al. Activation of NF-kappaB and p300/CBP potentiates cancer chemoimmunotherapy through induction of MHC-I antigen presentation. *Proc Natl Acad Sci U.S.A.* (2021) 118 (8):e2025840118. doi: 10.1073/pnas.2025840118

34. Wang X, Waschke BC, Woolaver RA, Chen SMY, Chen Z, Wang JH. MHC class I-independent activation of virtual memory CD8 T cells induced by chemotherapeutic agent-treated cancer cells. *Cell Mol Immunol* (2021) 18 (3):723–34. doi: 10.1038/s41423-020-0463-2

35. Fujita K, Uchida N, Kanai O, Okamura M, Nakatani K, Mio T. Retreatment with pembrolizumab in advanced non-small cell lung cancer patients previously treated with nivolumab: emerging reports of 12 cases. *Cancer Chemother Pharmacol* (2018) 81(6):1105–9. doi: 10.1007/s00280-018-3585-9

36. Liu H, Guo L, Zhang J, Zhou Y, Zhou J, Yao J, et al. Glycosylation-independent binding of monoclonal antibody toripalimab to FG loop of PD-1 for tumor immune checkpoint therapy. *MAbs* (2019) 11(4):681–90. doi: 10.1080/19420862.2019.1596513

37. Hong Y, Feng Y, Sun H, Zhang B, Wu H, Zhu Q, et al. Tislelizumab uniquely binds to the CC' loop of PD-1 with slow-dissociated rate and complete PD-L1 blockage. *FEBS Open Bio.* (2021) 11(3):782–92. doi: 10.1002/2211-5463.13102

38. Desai J, Deva S, Lee JS, Lin CC, Yen CJ, Chao Y, et al. Phase IA/IB study of single-agent tislelizumab, an investigational anti-PD-1 antibody, in solid tumors. *J Immunother Cancer.* (2020) 8(1):e000453. doi: 10.1136/jitc-2019-000453

39. Keam SJ. Toripalimab: First global approval. *Drugs* (2019) 79(5):573–8. doi: 10.1007/s40265-019-01076-2

40. Wu J, Zhang A, Li L, Liu S, Yang F, Yang R. Meta-analysis of the efficacy and tolerability of immune checkpoint inhibitors combined with chemotherapy in first-line treatment of small cell lung cancer. *Clin Ther* (2021) 43(3):582–93.e2. doi: 10.1016/j.clinthera.2020.12.017

41. Liu X, Xing H, Zhang H, Liu H, Chen J. Immunotherapy versus standard chemotherapy for treatment of extensive-stage small-cell lung cancer: a systematic review. *Immunotherapy* (2021) 13(12):989–1000. doi: 10.2217/imt-2020-0284

42. Niu Z, Guo S, Cao J, Zhang Y, Guo X, Grossi F, et al. Immune checkpoint inhibitors for treatment of small-cell lung cancer: a systematic review and meta-analysis. *Ann Transl Med* (2021) 9(8):705. doi: 10.21037/atm-21-1423

43. van der Lee I, Smit EF, van Putten JW, Groen HJ, Schlösser NJ, Postmus PE, et al. Single-agent gemcitabine in patients with resistant small-cell lung cancer. *Ann Oncol* (2001) 12(4):557–61. doi: 10.1023/A:1011104509759

44. Heinhuis KM, Ros W, Kok M, Steeghs N, Beijnen JH, Schellens JHM. Enhancing antitumor response by combining immune checkpoint inhibitors with chemotherapy in solid tumors. *Ann Oncol* (2019) 30(2):219–35. doi: 10.1093/annonc/mdy551

45. Hakozaki T, Okuma Y, Kashima J. Re-challenging immune checkpoint inhibitor in a patient with advanced non-small cell lung cancer: a case report. *BMC Cancer.* (2018) 18(1):302. doi: 10.1186/s12885-018-4212-1

46. De Sousa Linhares A, Battin C, Jutz S, Leitner J, Hafner C, Tobias J, et al. Therapeutic PD-L1 antibodies are more effective than PD-1 antibodies in blocking PD-1/PD-L1 signaling. *Sci Rep* (2019) 9(1):11472. doi: 10.1038/s41598-019-47910-1

47. Fujita K, Uchida N, Yamamoto Y, Kanai O, Okamura M, Nakatani K, et al. Retreatment with anti-PD-L1 antibody in advanced non-small cell lung cancer previously treated with anti-PD-1 antibodies. *Anticancer Res* (2019) 39(7):3917–21. doi: 10.21873/anticanres.13543

48. Furuya N, Nishino M, Wakuda K, Ikeda S, Sato T, Ushio R, et al. Real-world efficacy of atezolizumab in non-small cell lung cancer: A multicenter cohort study focused on performance status and retreatment after failure of anti-PD-1 antibody. *Thorac Cancer.* (2021) 12(5):613–8. doi: 10.1111/1759-7714.13824

49. Singh N, Seetharamu N. Complete response with anti-PD-L1 antibody following progression on anti-PD-1 antibody in advanced non-small cell lung cancer. *BMJ Case Rep* (2020) 13(8):e236101. doi: 10.1136/bcr-2020-236101

50. Feng D, Guan Y, Liu M, He S, Zhao W, Yin B, et al. Excellent response to atezolizumab after clinically defined hyperprogression upon previous treatment with pembrolizumab in metastatic triple-negative breast cancer: A case report and review of the literature. *Front Immunol* (2021) 12:608292. doi: 10.3389/fimmu.2021.608292

51. Inman BA, Longo TA, Ramalingam S, Harrison MR. Atezolizumab: A PD-L1-Blocking antibody for bladder cancer. *Clin Cancer Res* (2017) 23(8):1886–90. doi: 10.1158/1078-0432.CCR-16-1417

52. Gelsomino F, Di Federico A, Filippini DM, Dall'Olio FG, Lamberti G, Sperandi F, et al. Overcoming primary resistance to PD-1 inhibitor with anti-PD-L1 agent in squamous-cell NSCLC: Case report. *Clin Lung Cancer.* (2020) 21(2):e45–e8. doi: 10.1016/j.cllc.2019.11.011

53. Reck M, Mok TSK, Nishio M, Jotte RM, Cappuzzo F, Orlandi F, et al. Atezolizumab plus bevacizumab and chemotherapy in non-small-cell lung cancer (IMpower150): key subgroup analyses of patients with EGFR mutations or baseline liver metastases in a randomised, open-label phase 3 trial. *Lancet Respir Med* (2019) 7(5):387–401. doi: 10.1016/S2213-2600(19)30084-0

54. Socinski MA, Nishio M, Jotte RM, Cappuzzo F, Orlandi F, Stroyakovskiy D, et al. IMpower150 final overall survival analyses for atezolizumab plus bevacizumab and chemotherapy in first-line metastatic nonsquamous NSCLC. *J Thorac Oncol* (2021) 16(11):1909–24. doi: 10.1016/j.jtho.2021.07.009

55. Nogami N, Barlesi F, Socinski MA, Reck M, Thomas CA, Cappuzzo F, et al. IMpower150 final exploratory analyses for atezolizumab plus bevacizumab and chemotherapy in key NSCLC patient subgroups with EGFR mutations or metastases in the liver or brain. *J Thorac Oncol* (2022) 17(2):309–23. doi: 10.1016/j.jtho.2021.09.014

56. Bang YJ, Golan T, Dahan L, Fu S, Moreno V, Park K, et al. Ramucirumab and durvalumab for previously treated, advanced non-small-cell lung cancer, gastric/gastro-oesophageal junction adenocarcinoma, or hepatocellular carcinoma: An open-label, phase ia/b study (JVDJ). *Eur J Cancer.* (2020) 137:272–84. doi: 10.1016/j.ejca.2020.06.007

57. Cheng Y, Wang Q, Li K, Shi J, Liu Y, Wu L, et al. Anlotinib vs placebo as third- or further-line treatment for patients with small cell lung cancer: a randomised, double-blind, placebo-controlled phase 2 study. *Br J Cancer.* (2021) 125(3):366–71. doi: 10.1038/s41416-021-01356-3

58. Li Y, Sun Z, Sun W, Wang H, Zu J. Effectiveness and safety of anlotinib monotherapy for patients with extensive-stage small-cell lung cancer who progressed to chemotherapy: A real-world exploratory study. *Clin Med Insights Oncol* (2022) 16:11795549211067184. doi: 10.1177/11795549211067184

59. Liu SV, Reck M, Mansfield AS, Mok T, Scherpereel A, Reinmuth N, et al. Updated overall survival and PD-L1 subgroup analysis of patients with extensive-stage small-cell lung cancer treated with atezolizumab, carboplatin, and etoposide (IMpower133). *J Clin Oncol* (2021) 39(6):619–30. doi: 10.1200/JCO.20.01055

frontiers | Frontiers in Immunology

TYPE Original Research
PUBLISHED 04 January 2023
DOI 10.3389/fimmu.2022.1080556

OPEN ACCESS

EDITED BY
Silvia Pesce,
University of Genoa, Italy

REVIEWED BY
Jean-René Pallandre,
U1098 Interactions Hôte-Greffon-Tumeur &Ingénierie Cellulaire et Génique (INSERM), France
Federica Papaccio,
University of Salerno, Italy
Fabrizio Luppi,
University of Milano Bicocca, Italy

*CORRESPONDENCE
Laura Bergantini
laurabergantini@gmail.com

†These authors have contributed equally to this work

SPECIALTY SECTION
This article was submitted to Cancer Immunity and Immunotherapy, a section of the journal Frontiers in Immunology

RECEIVED 26 October 2022
ACCEPTED 25 November 2022
PUBLISHED 04 January 2023

CITATION
Bergantini L, d'Alessandro M, Del Zotto G, Marcenaro E and Bargagli E (2023) Characterization of natural killer and T cells in bronchoalveolar lavage and peripheral blood of sarcoidosis patients.
Front. Immunol. 13:1080556.
doi: 10.3389/fimmu.2022.1080556

Characterization of natural killer and T cells in bronchoalveolar lavage and peripheral blood of sarcoidosis patients

Laura Bergantini[1*†], Miriana d'Alessandro[1†], Genny Del Zotto[2], Emanuela Marcenaro[3,4] and Elena Bargagli[1]

[1]Respiratory Diseases Unit, Department of Medical Science, Surgery and Neurosciences, University of Siena, Siena, Italy, [2]Department of Research and Diagnostics, IRCCS Istituto Giannina Gaslini, Genova, Italy, [3]Dipartimento di Medicina Sperimentale (DIMES), Università degli Studi di Genova, Genova, Italy, [4]IRCCS Ospedale Policlinico San Martino, Genova, Italy

The characterization of frequency and phenotypes of natural killer (NK) cells and T cells in BAL and peripheral blood of patients with sarcoidosis was evaluated, to discriminate the differential status of these cells in these two compartments. The analysis revealed that $CD56^{bright}CD16^{neg}$ resulted higher in BAL than PB of sarcoidosis and healthy subjects, while $CD56^{dim}CD16^{+}$ showed a different proportion between BAL and PB of both Sarcoidosis patients and HC. Moreover, in comparison with autologous PB, BAL was characterized by a higher expression of activated NK cell markers NKp44, CD69 and CD25. Significantly increased levels of PD-1^{+} NK cells in the BAL of patients were detected. Regarding the maturation of CD4 and CD8, an increase of Effector Memory T cells (T_{EM}) was reported in BAL compared to PB. A better characterization of NK and T cells may lead to an improvement of the pathogenetic mechanisms in sarcoidosis.

KEYWORDS

sarcoidosis, bronchoalveolar lavage, interstitial lung diseases (ILD), natural killer (NK), T cells

Abbreviations: BAL, Bronchoalveolar lavage; ILD, interstitial lung diseases; NK, natural killer; ILCs, Innate lymphoid cells; PB, peripheral blood; HC, Healthy controls; KIRs, killer Ig-like receptors; NCRs, natural cytotoxicity receptors; FVC, forced vital capacity; PFTs, pulmonary function tests; FEV1, forced expiratory volume in the first second; DLco, diffuse lung carbon monoxide; mAbs, monoclonal antibodies; PCA, principal component analysis; T_{EM}, T effector memory; T_{EMRA}, T effector memory RA; T_{CM}, T central Memory.

10.3389/fimmu.2022.1080556

Introduction

Among Interstitial lung diseases of unknown origin, Sarcoidosis is classified as a chronic multisystemic disease that mainly involves the lung of adults and rarely in children (aged 13–15 years), with several clinical presentations and prognosis, characterized by non-necrotizing granulomatous inflammation (1–3).

The pathogenesis of sarcoidosis is already not fully understood due to the heterogeneity of its clinical characteristics and the unpredictable outcome that can be asymptomatic or can evolve into fibrosis with an irreversible process (4). Granulomas comprise several cellular lineages belonging to both innate and adaptive immune responses (5). Among these cell subsets, macrophages that differentiate into epithelioid cells play a key role in the formation and development of granuloma together with $CD4^+$ T helper cells that are interspersed within the granuloma, while other cells such as $CD8^+$ T cells surround the periphery (6, 7). $CD4^+$ and $CD8^+$ T cells characterize granuloma, however, only few studies characterized their functions and subsets at the periphery and into the lung (8, 9).

Bronchoalveolar lavage (BAL) is considered a standard diagnostic procedure in patients with suspicion of interstitial lung diseases (ILD) (10). It involves different cells from the lower respiratory tract, mainly represented by macrophages, lymphocytes, eosinophils, and neutrophils (11). Lymphocytes present in the interstitium of the lung represent the most easily accessible lymphocytes of the human lung (about 5% of the total circulating lymphocyte pool in humans) (11). By clinical data and chest X-ray, the presence of elevated lymphocytes (more than 15%) and CD4/CD8 ratio >3.5 support diagnosis of pulmonary sarcoidosis (12).

The knowledge regards Natural killers (NK) with the other Innate lymphoid cells (ILCs) was recently improved (13, 14). The understanding of NK cell biology has enhanced in terms of maturation, diversity, and adaptive capacities (15).

NK cells provide a first line of defense against infection and cancer (16). They express both inhibitory and activatory receptors. Among inhibitory receptors, killer Ig-like receptors (KIRs), and the CD94/NKG2A heterodimer, recognize major histocompatibility complex (MHC) class I molecules (17). Immune checkpoint PD-1 also belongs to the inhibitory receptors expressed of NK cell surfaces. PD-has recently described on a subset of peripheral blood (PB) NK cells from healthy $HCMV^+$ individuals and NK cells from tumor patients (18–21).

When target cells lack expression of MHC-I molecules, NK cells start their activation with the expression of the natural cytotoxicity receptors (NCRs), i.e. NKp30, NKp44, and NKp46, NKG2D, DNAM-1 and NKG2C (the activating counterpart of NKG2A) (16, 18).

In the last years, the number of studies on NK cell features in the lung increased, showing that the lung contains a high reservoir of NK cells (15). The distribution of the various NK cell populations is similar to that of peripheral blood, with a majority of the more mature NK cells ($CD56^{dim}CD16^+$) and a minority of the immature $CD56^{bright}CD16^{neg}$ NK cells (22, 23).

Only a few works investigated NK cells in Sarcoidosis, and they were mainly focalized on their percentages at a peripheral and alveolar level in comparison with other ILDs for differential diagnosis (1, 24).

In the present study, we analyzed the frequency of NK and T cells and the expression of different NK and T surface markers in BAL and PB samples from sarcoidosis patients, to discriminate the differential status of NK and T cells in these two compartments.

Materials and methods

Study population

BALF and PB cells for each subject were obtained from 13 sarcoidosis patients (mean age 52 ± 14 years). The final diagnosis was performed by a multidisciplinary team at Siena University Hospital, following international criteria.

PB samples from a group of Healthy controls (HCs) were collected. They had no history of autoimmune, cancer, or other relevant diseases that can alter immunologic pathways. All the available variables of HCs were recorded in an electronic database.

The most relevant clinical characteristics are reported in Table 1. At the moment of time sampling, patients were not undergoing any treatments. All subjects gave their informed consent, and the study was approved by the local ethics committee (markerlung 17431).

BAL procedure and handling of cells

BAL and PBMC collection were performed in the laboratory of the Respiratory Diseases Unit, Siena University Hospital (Italy) from January 2019 to December 2020.

BAL was performed as previously described (25). BAL was filtered through sterile gauze. Cytocentrifuge smear was obtained for differential cell count with a Fast Quick - May Grunwald-Giemsa rapid (cat. Nr. 010253, DiaPath, Italy); Remaining cells were centrifuged at 406x*g* for 10 min at 4°C and resuspended in RPMI 1640 medium (Gibco, Paisley, UK). BALF cells were counted and trypan blue exclusion criteria were used for determining cell viability.

PB samples were drawn into a tube containing EDTA anticoagulant (BD Vacutainer® EDTA tubes, BD Biosciences, CA, USA) and processed within eight hours. PBMC was obtained by gradient centrifugation separation (Ficoll Histopaque®-1077, Sigma-Aldrich). Cells obtained from BAL and PB were washed twice, resuspended in 80% RPMI1640, 10%

10.3389/fimmu.2022.1080556

TABLE 1 Demographic, immunologic and functional data of the cohort.

Subjects (n)	13
Male/female	3/10
Age (year)	52 ± 14
Ex Smoker/never smoker (*n*)	6/7
Chest X-ray stages (*n*)	
0	4
I	0
II	6
III, IV	3
Lesions other than lung (*n*)	
Heart	1
Skin	3
Eye	1
Brain	1
Liver	1
BALF cell count (mean ± SD)	
Cellular concentration ($\times 10^6$ cells)	5.8 ± 2.3
Cell/ml ($x10^3$)	96.4 ± 36.5
% of macrophages (%)	77 ± 16
% of lymphocytes (%)	19 ± 15
% of neutrophils (%)	3.3 ± 3.7
% of eosinphils (%)	0.4 ± 0.65
Peripheral cell count (mean ± SD)	
% of monocytes (%)	10.4 ± 2.5
% of lymphocytes (%)	24.2 ± 8.3
% of neutrophils (%)	61.3 ± 8.2
% of eosinphils (%)	3.5 ± 1.7
Biomarkers (mean ± SD)	
ACE (U/l)	62 ± 21
Lysozyme (mg/l)	5.3 ± 1.6
Pulmonary function tests (mean ± SD)	
FEV1%	92.7 ± 17.2
FEV1 ml	2383 ± 640
FVC %	94.4 ± 15
FVC ml	2998 ± 848
DLco (%)	71 ± 13

FBS, and 10% Dimethyl sulfoxide (DMSO) at $2x10^6$ cells per vial, and stored in liquid nitrogen until analysis.

Lung function tests

The following lung function parameters were recorded following standards international recommendation using a Jaeger body plethysmograph with corrections for temperature and barometric pressure. Forced vital capacity (FVC), forced expiratory volume in the first second (FEV1) and diffuse lung carbon monoxide (DLco) were performed and collected as volume (ml) and percentages of predicted values.

Flow cytometry

All mAbs used in flow cytometry for the detection of surface markers are described in Supplementary Table 1. For multiparametric flow cytometric analysis, a standard staining protocol for extracellular markers was used (16). Cells were washed with Wash buffer (HBSS–/– with 2% of FBS), and incubated with antibodies mixed for 30 minutes in the dark at RT. Samples were detected using BD FACS Canto II (BD Biosciences). Titration experiments were defined for determining the optimal concentration. Fluorescence minus one (FMO) controls were used to determine accurate cytofluorimetric analysis following guidelines (26). For the analysis of cells, the total NK cell population was identified based on FSC vs SSC and negative for CD3, CD14, and CD19. CD56 was plotted against CD16 to obtain immature ($CD56^{bright}CD16^{neg}$) and mature ($CD56^{dim/neg}CD16^{+}$) phenotypes of NK cells. On the $CD56^{dim/neg}CD16^{+}$ population a series receptor was evaluated, including NKG2A, NKG2C, CD57, KIR, PD-1, CD25, CD69 and NKp44. For the detection of T Cell maturation, a panel including anti-CD3 APC-Cy7, CD4 FITC, CD62L PE, CD8 Vioblue, and CD45RA PE-Vio770 was used.

Statistical analysis

Means and standard deviations (M ± SD) or medians and quartiles (25th and 75th percentiles) for continuous variables were used. A one-way ANOVA non-parametric test (Kruskal–Wallis test) and Dunn test were performed for the comparison of more than 2 groups. To identify the normal distribution of the variables, the Shapiro–Wilk test was applied. The Chi-squared test was used for categorical variables. Statistical analysis and graphic representation of data were performed by GraphPad Prism 9.0 software (Graphpad Holdings, LLC, San Diego, CA, USA).

A p-value of less than 0.05 was considered statistically significant.

Supervised principal component analysis (PCA) was employed to reduce the dimensionality of data hyperspace and for clusterization of the samples based on their cellular subsets.

For the multivariate analysis, the % of differential surface markers in the overall cohort was used to perform a supervised heatmap analysis; this analysis visualizes the percentages of the differential cellular markers in each enrolled patient. Clusterization was performed based on Spearman rank correlation and K means. The above analyses and corresponding figures were obtained using MORPHEUS (https://software.broadinstitute.org/morpheus/) and ClustVis (http://biit.cs.ut.ee/clustvis) software.

Results

Study population

No statistically significant differences were reported in terms of Sex distribution, age, and smoking habits for HC when compared with sarcoidosis patients. Demographic data (including sex, age, and smoking habits) of sarcoidosis patients are reported in Table 1. As expected, patients were young, prevalently female who had never smoked. At the chest X-ray, three patients report stage III or IV, four patients stage 0, and four patients stage II. Regarding BAL cell count, an increased percentage of lymphocytes was reported, while biomarkers and PFTs values were unaltered.

NK cell analysis of PB and BAL of patients affected by sarcoidosis

As above mentioned, we analyzed a wide number of surface markers on peripheral blood (Sarc-PB) and BAL fluid (Sarc-BAL) NK cells of the selected patients. The results were compared with the peripheral blood of healthy controls (HC-PB). $CD56^{bright}CD16^{neg}$ showed an increased level in BAL than PB of sarcoidosis and healthy subjects. $CD56^{dim/neg}CD16^{+}$ at the same time showed a different proportion between BAL and PB of both Sarcoidosis patients and HC (Figure 1A). Moreover, from the analysis of $CD56^{dim/neg}/CD56^{bright}$ ratio, BAL samples reported significantly lower values of the ratio than PB of HC and Sarcoidosis (2,5 ± 2,4 Sarc-BAL, 26,1 ± 22,9 Sarc-PB, and 14,5 ± 10,6 HC-PB; p=0,0003) (Figure 1A).

In comparison with autologous PB, BAL was characterized by a higher expression of the activation NK cell markers NKp44, CD69, and CD25. In addition, NKG2A was decreased, and its activating counterpart (NKG2C) was increased (Figure 1B).

The levels of markers characterizing terminally differentiated NK cells, such as CD57 and KIRs, were higher in BAL than in the peripheral blood of both patients and HC (Figure 1B).

The inhibitory checkpoint PD-1 showed a similar trend, as it was negative on almost all HD-NK cells, highly positive on a small percentage of Sarc-PB while a highly expressed on a large fraction of BAL-NKs.

T-cell analysis of peripheral blood and Bronchoalveolar lavage of patients affected by sarcoidosis

Due to the crucial immune-pathogenetic role of lymphocytes in granuloma formation of sarcoidosis, analysis of T cell subsets resulted in fundamental to improve the knowledge of pathogenic mechanisms of this disorder.

Interestingly, as expected, a predominance of $CD4^{+}$ T cells was reported in BAL compared to patients' PB, typical of the recruitment of helper T cells into the granuloma. Regarding the maturation of CD4 and CD8, an increase of Effector Memory T cells (T_{EM}) was reported in BAL compared to PB. On the other hand, CD4 and CD8 $T_{EM}RA$ showed decreased percentages in BAL than PB. A decreased level of $CD4^{+}$ naïve T cells was reported. $CD8^{+}$ naive T cells showed the same trend however without reaching significance. Concerning Central Memory T lymphocytes (T_{CM}), only CD8 showed an increased level in BAL than PB (Figures 2A, B).

PCA and Heatmap analysis revealed the same biological behavior among groups

Based on the flow cytometry data, we performed a PCA analysis on all the different cell subgroups detected on the NK and T cell surfaces in BAL and PB. The PCA plot shows that samples with the same biological behavior clustered together, corroborating that the differential cell subsets were characteristic for each condition.

Furthermore, the PB of sarcoidosis patients clusters close to the PB of HC. On the other hand, the BAL samples were located on the opposite side of the PB samples (Figure 3A).

In particular, Unit Variance Scaling is applied to rows and SVD is used to calculate principal components. PC1 and PC2 explain 39.2% and 12.5% of the total variance, respectively (Figure 3A).

Figure 3B showed heatmap analysis performed on cell surface markers of NK and T cells in PB and BAL of sarcoidosis patients and PB of HC based on hierarchical clusterization based on spearman rank correlation. Similar to PCA analysis, the general trend separates samples into three principal groups as indicated by the dendrogram on the top of the matrix and indicated as A, B, and C.

Of note, group A is mainly composed of CD56 cell surface markers, including CD57, NKG2C, and KIR. The B group

10.3389/fimmu.2022.1080556

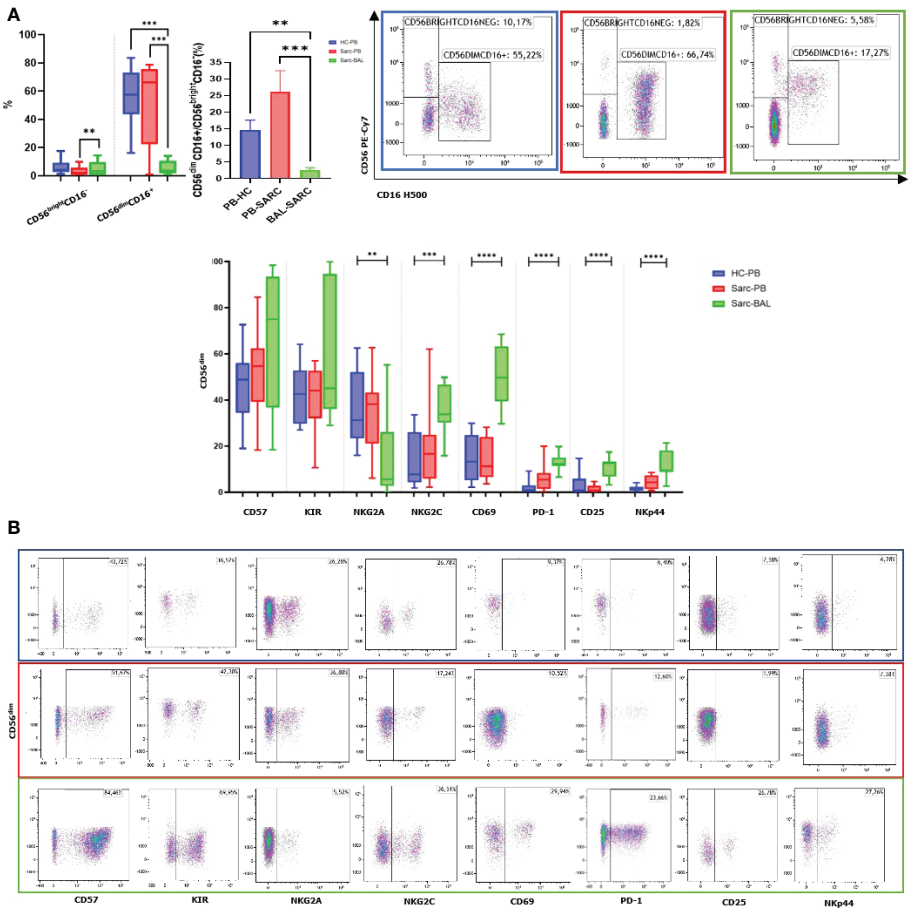

FIGURE 1
(A) Histograms and flow cytometric dot plot of CD56^{bright}CD16^{dim} and CD56$^{dim/neg}$CD16^{+} cell subsets in BAL of sarcoidosis patients and PB of sarcoidosis patients and healthy controls. **(B)** Histograms and flow cytometric dot plot of CD56$^{dim/neg}$CD16^{+} cell subsets expressing CD57, KIR, NKG2A, NKG2C, CD69, PD-1, CD25, and NKp44 in BAL of sarcoidosis patients and PB of sarcoidosis patients and healthy controls. **p<0,01 ***p<0,001 ****p<0,0001.

includes mainly subsets of T cells as T central memory and Naïve T cells.

K means was also applied to detect clusters based on the expression of surface markers (Figure 3B).

The analysis revealed an inverted trend in the expression of several surface markers on the BAL samples with respect to PB of both sarcoidosis and HC group.

Discussion

In this study, an evaluation of different surface cell markers, phenotypically and functionally characterizing NK and T cells, was performed in the BAL and PB of sarcoidosis patients and HCs. Moreover, the lung microenvironment typical of patients affected by sarcoidosis was explored through the analysis of BAL cell subsets. These biological data play an important role in diagnosis and they provide interesting information on the cells in the interstitial space of the lung. From the clinical point of view, the selected patients can be considered representative of a typical sarcoidosis patients' cohort in terms of age and gender distribution as well as of predominance of stage 2 at chest X-ray.

In multivariate analysis, a clear division of the three groups (Sarc-BA, Sarc-PB, and HC-PB) emerged. This result showed that the analyzed NK and T cell subsets greatly differentiate among the three groups, as clearly reported in Figure 3.

Different studies reported that, upon *in vitro* stimulation, there is an increase of IFN-γ and TNF-α produced by immature CD56^{bright} NK cells in BALF of sarcoidosis patients, and this may suggest the involvement of NK cells in granuloma formation (27, 28). Moreover, these studies seem to suggest that the more immature NK cells (CD56^{bright}CD16^{neg}) producing a large amount of Th1 cytokines (IFN-γ and TNF-α) may be involved in the pathogenesis of sarcoidosis (28, 29).

10.3389/fimmu.2022.1080556

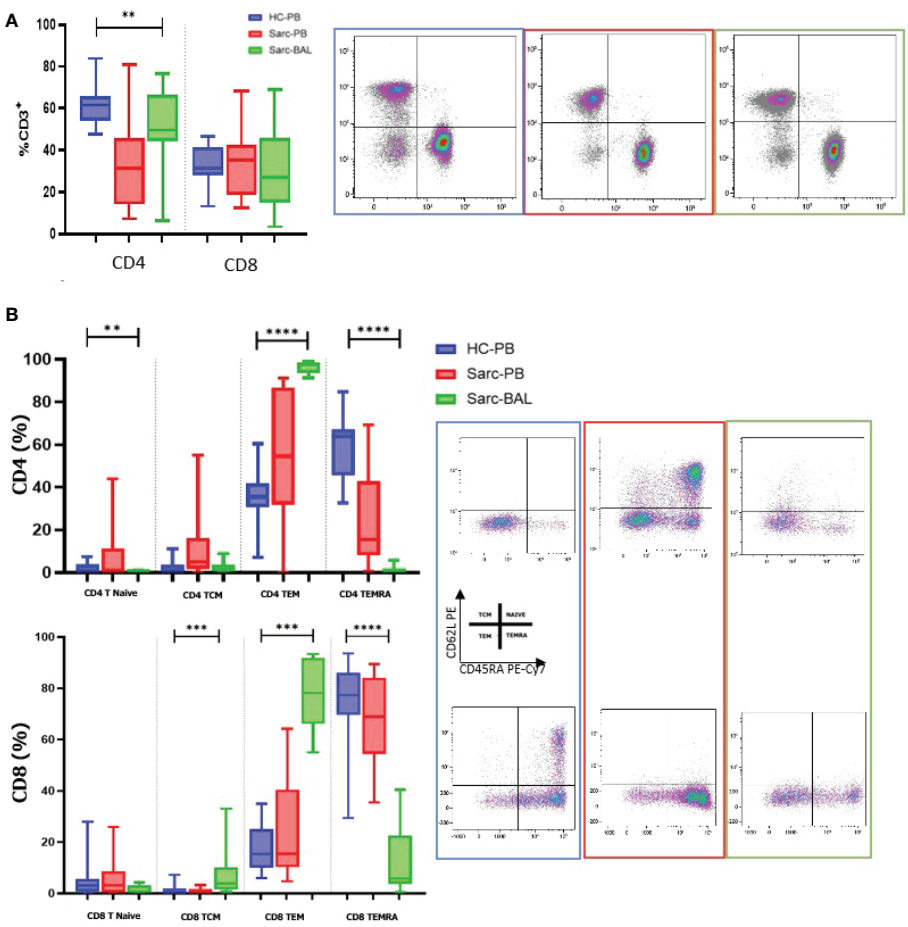

FIGURE 2
(A) Histograms and flow cytometric dot plot of CD4 and CD8 T cell subsets in BAL of sarcoidosis patients and PB of sarcoidosis patients and healthy controls. **(B)** Histograms and flow cytometric dot plot of T Naive, TCM, TEM, and TEMRA of BAL of sarcoidosis patients and in PB of sarcoidosis patients and healthy controls. **p<0,01 ***p<0,001 ****p<0,0001.

In line with the literature, we observed an increased fraction of the immature $CD56^{bright}$ $CD16^{neg}$ NK cell subset and a decrease of the more mature $CD56^{dim/neg}CD16^{+}$ NK phenotype in BAL of patients compared to their PB. Importantly, deep characterization of the $CD56^{dim/neg}CD16^{+}$ NK cell subset in BAL compared to autologous PB showed a large fraction of this more mature NK cell subset expressing KIR and a small percentage of $NKG2A^{+}$ NK subpopulation. Furthermore, in BAL-NK cells were characterized by a high amount of CD57 (a marker of terminal differentiation) and NKG2C, the activating counterpart of NKG2A, generally upregulated during HCMV infection/reactivation. Unfortunately, our study lacks information on patients' HCMV status. Moreover, $CD56^{dim/neg}CD16^{+}$ BAL-NK cells expressed activation markers, such as CD69 (which also represents a tissue-resident marker), NKp44, and CD25.

Regarding CD25, the soluble form "sCD25" was widely used as a serum marker of sarcoidosis active status. Recently it was demonstrated that, in the context of inflammation, $CD56^{dim}$ NK cells expressing CD25 can be activated by IL-2-producing T cells during adaptive immune responses (30, 31). After stimulation with IL-2, NK cells can acquire NKp44, an activating NK cell receptor, involved in the triggering of NK cell cytotoxicity against target cells expressing the relative ligands. NKp44 has never been analyzed before in sarcoidosis patients and it could deserve further investigation.

It is interesting to note that we first described an overexpression of PD-1 in NK cells of BAL samples when compared to the PB of the same patient. In this regard, it has recently been shown that the expression of PD-1 induces an impairment of the function of NK cells towards the target cells expressing the relative ligands (PD-L1/2) thus demonstrating its role as an immune checkpoint also in NK cells (21). Upregulation of PD-1 was also present in PB $CD4^{+}$ T cells of sarcoidosis patients (32, 33).

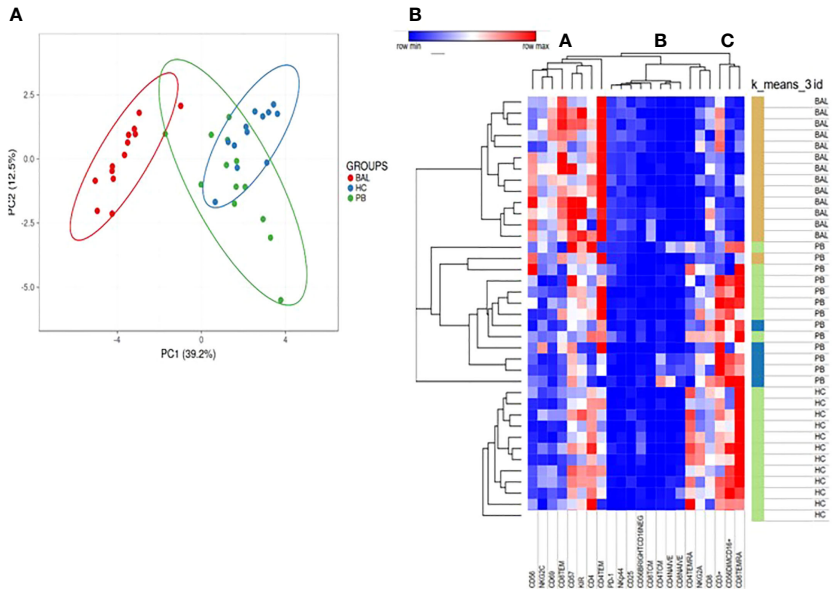

FIGURE 3
(A) For PCA analysis, Unit Variance Scaling is applied to rows; SVD is used to calculate principal components. X and Y axis show principal component 1 (PC1) and principal component 2 (PC2) that explain 39.2% and 12.5% of the total variance, respectively. Prediction ellipses are such that with probability 0.95. **(B)** Heatmap analysis performed on cell surface markers of NK and T cells in PB and BAL of sarcoidosis patients and PB of HC based on hierarchical clusterization based on spearman rank correlation. K means was also applied to detect clusters based on the expression of surface markers.

Braun et al. showed that spontaneous clinical resolution of sarcoidosis corresponds to a reduced percentage of PD-1$^+$ CD4$^+$ T cells, whereas clinical progression to an increase of PD-1$^+$CD4$^+$ T cells suggesting that the blockade of the PD-1 pathway may contribute to the restoration of CD4$^+$ T-Cell Proliferative Capacity in Sarcoidosis patients (32). Moreover, in the same study, an increase in PD-1 levels in BAL compared to PB was also reported exactly as in our cohort of patients. In chronic beryllium diseases, another lung granulomatosis, PD-1 expression on CD4$^+$ T cells directly correlated with the severity of T-cell alveolitis (34).

Although in sarcoidosis the exact role of PD-1 on NK cells was poorly investigated, in other granulomatosis of the lung it has been demonstrated that the PD-1 pathway impaired NK cell functions reducing IFN-γ production and lytic degranulation (35). Further investigation to unravel the role of PD-1 in controlling inflammation in sarcoidosis pathogenesis will be necessary.

In this study, we also evaluated the T cell compartment, in particular: naive, central memory, effector memory, and RA$^+$ effector memory subsets of both CD4$^+$ and CD8$^+$ T cells.

In our study, BAL samples of sarcoidosis patients largely consisted of T_{EM} lymphocytes, belonging both to the helper and the cytotoxic compartment T_{EM} cells represent an immediate defense, whereas T_{CM} cells support the response by proliferating in the secondary lymphoid organs and producing a supply of new effectors (35).

In many studies, it has been shown that lung resident T_{EM} cells can mediate early control of respiratory viral infections but they are inefficient at mediating recall responses in terms of proliferation and accumulation at inflammatory sites (36, 37). In other studies focused on lung malignancies, upregulation of both T_{EM} and T_{CM} was reported with a higher amount of cytokine released compared to T_{EM}RA and T naïve, thus demonstrating their activity in the site of inflammation (38, 39).

In conclusion, in this study, a different NK cell subset distribution was observed at the site of inflammation compared to the PB of sarcoidosis patients (a higher proportion of CD56^{bright} as compared to CD56$^{dim/neg}$ was observed in BAL). In addition, the more mature NK cell subset present in BAL is characterized by overexpression of activation markers, such as CD69, CD25, as well as NKp44, and a large fraction of fully mature NK cells, characterized by the NKG2A$^-$, KIRs$^+$ phenotype. Interestingly, these cells also express high levels of NKG2C and PD-1, as previously described in adult HCMV$^+$ HC (21). The lack of prior research on specific aspects makes our research of interest and useful for further investigation. In this study, the characterization of NK and T- cell subsets in sarcoidosis revealed a distinct phenotype between the bloodstream and lung. Elevated levels of PD-1$^+$ NK cells in the BAL of patients

were observed. Other studies need to determine the functions of these cells. A deeper characterization of these cells can lead to a better understanding of the pathogenetic mechanisms of sarcoidosis.

Data availability statement

The raw data supporting the conclusions of this article will be made available by the authors, without undue reservation.

Ethics statement

The studies involving human participants were reviewed and approved by markerlung 17431. The patients/participants provided their written informed consent to participate in this study.

Author contributions

LB and Md'A: conception and design of the study. GZ and EM: analysis of the data and their interpretation. LB: statistical analysis. LB and Md'A wrote the first draft of the manuscript. EB, EM, and GZ wrote sections of the manuscript. All authors contributed to the manuscript and approved the submitted version.

Funding

This work was supported by the following entities: AIRC IG 2021 – ID. 26037 project – P.I. EM.

Conflict of interest

The authors declare that the research was conducted in the absence of any commercial or financial relationships that could be construed as a potential conflict of interest.

Publisher's note

Supplementary material

The Supplementary Material for this article can be found online at: https://www.frontiersin.org/articles/10.3389/fimmu.2022.1080556/full#supplementary-material

References

1. d'Alessandro M, Carleo A, Cameli P, Bergantini L, Perrone A, Vietri L, et al. BAL biomarkers' panel for differential diagnosis of interstitial lung diseases. *Clin Exp Med* (2020) 20(2):207–16. doi: 10.1007/s10238-020-00608-5

2. Shetty AK, Gedalia A. Childhood sarcoidosis: A rare but fascinating disorder. *Pediatr Rheumatol* (2008) 6(1):16. doi: 10.1186/1546-0096-6-16

3. d'Alessandro M, Bergantini L, Perrone A, Cameli P, Cameli M, Prasse A, et al. Serial investigation of angiotensin-converting enzyme in sarcoidosis patients treated with angiotensin-converting enzyme inhibitor. *Eur J Intern Med* (2020) 78:58–62. doi: 10.1016/j.ejim.2020.04.006

4. Cameli P, Caffarelli C, Refini RM, Bergantini L, d'Alessandro M, Armati M, et al. Hypercalciuria in sarcoidosis: A specific biomarker with clinical utility. *Front Med* (2020) 7:568020. doi: 10.3389/fmed.2020.568020

5. Zhou ER, Arce S. Key players and biomarkers of the adaptive immune system in the pathogenesis of sarcoidosis. *Int J Mol Sci* (2020) 21(19):E7398. doi: 10.3390/ijms21197398

6. McClean CM, Tobin DM. Macrophage form, function, and phenotype in mycobacterial infection: lessons from tuberculosis and other diseases. *Pathog Dis* (2016) 74(7):ftw068. doi: 10.1093/femspd/ftw068

7. d'Alessandro M, Gangi S, Cavallaro D, Bergantini L, Mezzasalma F, Cattelan S, et al. CD103 expression on regulatory and follicular T cells in lymph nodes, bronchoalveolar lavage fluid and peripheral blood of sarcoidosis patients. *Life (Basel).* (2022) 12(5):762. doi: 10.3390/life12050762

8. Salah S, Abad S, Monnet D, Brézin AP. Sarcoidosis. *J Fr Ophtalmol.* (2018) 41 (10):e451–67. doi: 10.1016/j.jfo.2018.10.002

9. d'Alessandro M, Bergantini L, Cameli P, Mezzasalma F, Refini RM, Pieroni M, et al. Adaptive immune system in pulmonary sarcoidosis-comparison of peripheral and alveolar biomarkers. *Clin Exp Immunol* (2021) 205(3):406–16. doi: 10.1111/cei.13635

10. Meyer KC, Raghu G, Baughman RP, Brown KK, Costabel U, du Bois RM, et al. An official American thoracic society clinical practice guideline: The clinical utility of bronchoalveolar lavage cellular analysis in interstitial lung disease. *Am J Respir Crit Care Med* (2012) 185(9):1004–14. doi: 10.1164/rccm.201202-0320ST

11. Harbeck RJ. Immunophenotyping of bronchoalveolar lavage lymphocytes. *Clin Diagn Lab Immunol* (1998) 5(3):271–7. doi: 10.1128/CDLI.5.3.271-277.1998

12. Davidson KR, Ha DM, Schwarz MI, Chan ED. Bronchoalveolar lavage as a diagnostic procedure: a review of known cellular and molecular findings in various lung diseases. *J Thorac Dis* (2020) 12(9):4991–5019. doi: 10.21037/jtd-20-651

13. Cichocki F, Grzywacz B, Miller JS. Human NK cell development: One road or many? *Front Immunol* (2019) 10:2078. doi: 10.3389/fimmu.2019.02078

14. Del Zotto G, Marcenaro E, Vacca P, Sivori S, Pende D, Della Chiesa M, et al. Markers and function of human NK cells in normal and pathological conditions. *Cytometry B Clin Cytom.* (2017) 92(2):100–14. doi: 10.1002/cyto.b.21508

15. Hervier B, Russick J, Cremer I, Vieillard V. NK cells in the human lungs. *Front Immunol* (2019) 10:1263. doi: 10.3389/fimmu.2019.01263

16. Del Zotto G, Antonini F, Pesce S, Moretta F, Moretta L, Marcenaro E. Comprehensive phenotyping of human PB NK cells by flow cytometry. *Cytometry A.* (2020) 97(9):891–9. doi: 10.1002/cyto.a.24001

17. Sun JC, Lanier LL. NK cell development, homeostasis, and function: Parallels with $CD8^+$ T cells. *Nat Rev Immunol* (2011) 11(10):645–57. doi: 10.1038/nri3044

18. Pesce S, Belgrano V, Greppi M, Carlomagno S, Squillario M, Barla A, et al. Different features of tumor-associated NK cells in patients with low-grade or high-

grade peritoneal carcinomatosis. *Front Immunol* (2019) 10:1963. doi: 10.3389/fimmu.2019.01963

19. Di Vito C, Mikulak J, Zaghi E, Pesce S, Marcenaro E, Mavilio D. NK cells to cure cancer. *Semin Immunol* (2019) 41:101272. doi: 10.1016/j.smim.2019.03.004

20. Minetto P, Guo F, Pesce S, Greppi M, Obino V, Ferretti E, et al. Harnessing NK cells for cancer treatment. *Front Immunol* (2019) 10:2836. doi: 10.3389/fimmu.2019.02836

21. Pesce S, Greppi M, Tabellini G, Rampinelli F, Parolini S, Olive D, et al. Identification of a subset of human natural killer cells expressing high levels of programmed death 1: A phenotypic and functional characterization. *J Allergy Clin Immunol* (2017) 139(1):335–46. doi: 10.1016/j.jaci.2016.04.025

22. Björkström NK, Ljunggren HG, Michaëlsson J. Emerging insights into natural killer cells in human peripheral tissues. *Nat Rev Immunol* (2016) 16 (5):310–20. doi: 10.1038/nri.2016.34

23. Lugli E, Marcenaro E, Mavilio D. NK cell subset redistribution during the course of viral infections. *Front Immunol* (2014) 5:390. doi: 10.3389/fimmu.2014.00390

24. Bergantini L, Cameli P, d'Alessandro M, Vagaggini C, Refini RM, Landi C, et al. NK and NKT-like cells in granulomatous and fibrotic lung diseases. *Clin Exp Med* (2019) 19(4):487–94. doi: 10.1007/s10238-019-00578-3

25. d'Alessandro M, Bergantini L, Mezzasalma F, Cavallaro D, Gangi S, Baglioni S, et al. Immune-checkpoint expression on CD4, CD8 and NK cells in blood, bronchoalveolar lavage and lymph nodes of sarcoidosis. *Mol Diagn Ther* (2022) 26 (4):437–49. doi: 10.1007/s40291-022-00596-0

26. Cossarizza A, Chang HD, Radbruch A, Abrignani S, Addo R, Akdis M, et al. Guidelines for the use of flow cytometry and cell sorting in immunological studies (third edition). *Eur J Immunol* (2021) 51(12):2708–3145. doi: 10.1002/eji.202170126

27. Zhang H, Costabel U, Dai H. The role of diverse immune cells in sarcoidosis. *Front Immunol* (2021) 12. doi: 10.3389/fimmu.2021.788502

28. Katchar K, Söderström K, Wahlstrom J, Eklund A, Grunewald J. Characterisation of natural killer cells and CD56+ T-cells in sarcoidosis patients. *Eur Respir J* (2005) 26(1):77–85. doi: 10.1183/09031936.05.00030805

29. Tutor-Ureta P, Citores MJ, Castejón R, Mellor-Pita S, Yebra-Bango M, Romero Y, et al. Prognostic value of neutrophils and NK cells in bronchoalveolar lavage of sarcoidosis. *Cytometry B Clin Cytom.* (2006) 70(6):416–22. doi: 10.1002/cyto.b.20120

30. Abel AM, Yang C, Thakar MS, Malarkannan S. Natural killer cells: Development, maturation, and clinical utilization. *Front Immunol* (2018) 9. doi: 10.3389/fimmu.2018.01869

31. Chase JM, Leong JW, Romee R, Fehniger TA. Cytokine activation induces CD25 expression and a signaling-competent high-affinity IL-2 receptor on CD56dim human NK cells. *Blood.* (2012) 120(21):2159. doi: 10.1182/blood.V120.21.2159.2159

32. Braun NA, Celada LJ, Herazo-Maya JD, Abraham S, Shaginurova G, Sevin CM, et al. Blockade of the programmed death-1 pathway restores sarcoidosis CD4 (+) T-cell proliferative capacity. *Am J Respir Crit Care Med* (2014) 190(5):560–71. doi: 10.1164/rccm.201401-0188OC

33. Hawkins C, Shaginurova G, Shelton DA, Herazo-Maya JD, Oswald-Richter KA, Rotsinger JE, et al. Local and systemic CD4+ T cell exhaustion reverses with clinical resolution of pulmonary sarcoidosis. *J Immunol Res* (2017) 2017:3642832. doi: 10.1155/2017/3642832

34. Palmer BE, Mack DG, Martin AK, Gillespie M, Mroz MM, Maier LA, et al. Up-regulation of programmed death-1 expression on beryllium-specific CD4+ T cells in chronic beryllium disease. *J Immunol* (2008) 180(4):2704–12. doi: 10.4049/jimmunol.180.4.2704

35. Shu CC, Wang JY, Wu MF, Wu CT, Lai HC, Lee LN, et al. Attenuation of lymphocyte immune responses during mycobacterium avium complex-induced lung disease due to increasing expression of programmed death-1 on lymphocytes. *Sci Rep* (2017) 7:42004. doi: 10.1038/srep42004

36. Hogan RJ, Zhong W, Usherwood EJ, Cookenham T, Roberts AD, Woodland DL. Protection from respiratory virus infections can be mediated by antigen-specific CD4(+) T cells that persist in the lungs. *J Exp Med* (2001) 193(8):981–6. doi: 10.1084/jem.193.8.981

37. Hogan RJ, Usherwood EJ, Zhong W, Roberts AA, Dutton RW, Harmsen AG, et al. Activated antigen-specific CD8+ T cells persist in the lungs following recovery from respiratory virus infections. *J Immunol* (2001) 166(3):1813–22. doi: 10.4049/jimmunol.166.3.1813

38. Zhang Y, Li W, Zhai J, Jin Y, Zhang L, Chen C. Phenotypic and functional characterizations of CD8+ T cell populations in malignant pleural effusion. *Exp Cell Res* (2022) 417(1):113212. doi: 10.1016/j.yexcr.2022.113212

39. Holgersen EM, Gandhi S, Zhou Y, Kim J, Vaz B, Bogojeski J, et al. Transcriptome-wide off-target effects of steric-blocking oligonucleotides. *Nucleic Acid Ther* (2021) 31(6):392–403. doi: 10.1089/nat.2020.0921

frontiers | Frontiers in Immunology

TYPE Original Research
PUBLISHED 04 January 2023
DOI 10.3389/fimmu.2022.1003419

OPEN ACCESS

EDITED BY
Silvia Pesce,
University of Genoa, Italy

REVIEWED BY
Lai Wen,
University of Nevada, United States
Xiaorong Zhou,
Nantong University, China

*CORRESPONDENCE
Jun Ye
wzmcyejun@zju.edu.cn
Jianshan Mao
jshmao@zju.edu.cn

†These authors have contributed equally to this work

SPECIALTY SECTION
This article was submitted to Cancer Immunity and Immunotherapy, a section of the journal Frontiers in Immunology

RECEIVED 26 July 2022
ACCEPTED 12 December 2022
PUBLISHED 04 January 2023

CITATION
Xie S, Cai Y, Chen D, Xiang Y, Cai W, Mao J and Ye J (2023) Single-cell transcriptome analysis reveals heterogeneity and convergence of the tumor microenvironment in colorectal cancer.
Front. Immunol. 13:1003419.
doi: 10.3389/fimmu.2022.1003419

Single-cell transcriptome analysis reveals heterogeneity and convergence of the tumor microenvironment in colorectal cancer

Siyuan Xie[1†], Yangke Cai[1†], Delong Chen[2†], Yu Xiang[1,3], Wen Cai[1], Jianshan Mao[1*] and Jun Ye[1*]

[1]Department of Gastroenterology, The Second Affiliated Hospital, Zhejiang University School of Medicine, Hangzhou, Zhejiang, China, [2]Department of Cardiology, The Second Affiliated Hospital, Zhejiang University School of Medicine, Hangzhou, Zhejiang, China, [3]Department of Gastroenterology, Huzhou Central Hospital, Huzhou, Zhejiang, China

Introduction: Colorectal cancer (CRC) ranks second for mortality and third for morbidity among the most commonly diagnosed cancers worldwide. We aimed to investigate the heterogeneity and convergence of tumor microenvironment (TME) in CRC.

Methods: We analyzed the single-cell RNA sequencing data obtained from the Gene Expression Omnibus (GEO) database and identified 8 major cell types and 25 subgroups derived from tumor, para-tumor and peripheral blood.

Results: In this study, we found that there were significant differences in metabolic patterns, immunophenotypes and transcription factor (TF) regulatory patterns among different subgroups of each major cell type. However, subgroups manifested similar lipid metabolic patterns, immunosuppressive functions and TFs module at the end of the differentiation trajectory in CD8+ T cells, myeloid cells and Fibroblasts. Meanwhile, TFs regulated lipid metabolism and immunosuppressive ligand-receptor pairs were detected by tracing the differentiation trajectory. Based on the cell subgroup fractions calculated by CIBERSORTx and bulk RNA-sequencing data from The Cancer Genome Atlas (TCGA), we constructed an immune risk model and clinical risk model of CRC which presented excellent prognostic value.

Conclusion: This study identified that the differentiation was accompanied by remodeling of lipid metabolism and suppression of immune function, which suggest that lipid remodeling may be an important trigger of immunosuppression. More importantly, our work provides a new perspective for understanding the heterogeneity and convergence of the TME and will aid the development of prognosis and immunotherapies of CRC patients.

KEYWORDS

ScRNA-seq, colorectal cancer, tumor microenvironment, CIBERSORTx, prognosis

1 Introduction

Colorectal cancer (CRC) accounts for about 10% of all malignant neoplasms in humans which is the third most common cancer worldwide and its mortality rate (9.4%) was the second highest among malignancies, only after lung cancer. As of 2020, more than 935,000 people worldwide died from CRC or its complications (1). The traditional mode of surgery combined with chemoradiotherapy has not achieved the ideal curative effect (2). In this context, immunotherapy emerged and quickly became the main treatment mode for a variety of tumors, including CRC, and achieved long-term and sustained remission in a small number of patients, however, the majority of patients did not achieve long-term tumor control after a temporary immune response. This indicates that although immunotherapy has great prospects in tumor treatment, there are still considerable deficiencies at present. We believe that the fundamental solution is to improve the understanding of the tumor microenvironment (TME).

TME plays an important role in the occurrence, development and metastasis of tumors, including not only tumor cells, but also immune cells, stromal cells, cytokines, extracellular matrix and other extracellular components (3). There have been extensive studies on the heterogeneity of TME, most of which focus on the heterogeneity of tumor cells, but the heterogeneity of immune cells and stromal cells is still insufficient. In recent years, more and more studies have confirmed that tumor Infiltrating T lymphocytes (TILs) will gradually differentiate into a dysfunctional state which is known as exhaustion under long-term antigen stimulation, which is one of the main obstacles to anti-tumor immunotherapy in the process of tumor development. The exhausted CD8+ T cells (Tex) were characterized by progressive and hierarchical loss of cytokine production, high co-expression of inhibitory receptors (programmed cell death 1 (PD-1), lymphocyte activation gene 3 protein (LAG3), T cell immunoreceptor with immunoglobulin and ITIM domain (TIGIT), etc.), altered expression of key transcription factors and metabolic derangement (4). Meanwhile, immune checkpoint inhibitor therapy has achieved unprecedented clinical success in a variety of cancers particularly PD-1 antibodies (5). T-cell receptor (TCR) persistent activation, transcription factors (including Signal transducer and activator of transcription 3 (STAT3), STAT4, Nuclear factor of activated T-cells, cytoplasmic 1 (NFATC1) and Blimp-1) and epigenetic components (including DNA methylation) were reported to regulate the expression of immune checkpoints (6–8). However, the metabolic reprogramming was associated with the development and maintenance of Tex while the detailed mechanism remained unclear. In addition, tumor associated macrophages (TAMs) and cancer associated fibroblasts (CAFs) have also been reported as potential targets of tumor immunotherapy. They are heterogeneous cell types which contributed to malignancy through production of angiogenic growth factors, extracellular matrix (ECM) remodeling, and immunosuppression (9, 10). The immunotherapy targeted TAMs has been applied in clinic while the minimal monotherapy efficacy was observed (11). Similarly, altered metabolism in the development of TAMs and CAFs has also been reported while the specific mechanism remains unknown. Notably, investigation of heterogeneity and convergence of above cell types in TME may contribute to clarify the relationship between immunosuppression and metabolic remodeling and find potential therapeutic targets.

Single-cell RNA sequencing (scRNA-seq) is a huge innovation and technological progress in the field of life science. It provides us with gene expression information at the level of individual cells and is an indispensable tool to unravel cellular heterogeneity (12). In this study, we obtained scRNA-seq data from the public database, re-identified and annotated cell populations and constructed cell differentiation tracks, identified multiple cell subpopulations, and found that different types of cells always showed similar phenotypes at the end of their differentiation tracks, which was called convergence. While recent studies have attempted to fully elucidate the TME heterogeneity identified by scRNA-seq in human cancers, there are significant deficiencies in the elucidations of convergence in TME. In this study, we not only focus on the heterogeneity of TME, but also identified the convergence and detected common targets of different cell types which may be potential therapeutic targets and help improve the treatment strategy and clinical prognosis of patients with CRC.

2 Materials and methods

2.1 Data acquisition

The scRNA-seq profiles included 10,398 cells from 10 human CRC samples (accession number GSE146771) (13), which were obtained from the Gene Expression Omnibus (GEO, http://www.ncbi.nlm.nih.gov/geo/) database. This dataset contains 5169 cells from tumor cores, 2400 cells from paratumor tissues and 2829 cells from peripheral blood, performed using the SMART-seq2 platform. Normalized matrix files for the dataset were downloaded. The bulk RNA-seq data of CRC samples, including 398 tumor samples and 39 normal samples, were obtained from the The Cancer Genome Atlas (TCGA) database (https://portal.gdc.cancer.gov/). We excluded samples with an overall survival (OS) time< 7 days or insufficient clinical information regarding age, gender, or TNM stage.

2.2 Processing of the CRC scRNA-seq data

The Seurat package in R 4.0.3 was used for quality control (QC) (14). The quality standards were as follows: 1) genes

detected in< 3 cells were excluded; 2) cells with< 50 total detected genes were excluded; 3) cells with ≥ 5% of mitochondria-expressed genes were excluded. For the remaining cells, cell-cycle scores were calculated using Seurat's CellCycleScoring function since the cell cycle phase effect was observed. Batch effects among the patients had already been eliminated by the data donator. The gene expression matrices were further normalized to RNA counts, mitochondrial percentages, and cell cycle scores using the top 3000 variable genes. PCA was used to calculate the significantly available principal components (PCs). We then applied the t-distributed stochastic neighbor-embedding (tSNE) algorithm for dimensionality reduction with 20 initial PCs to perform cluster classification analyses across all cells (15).

2.3 Cell type recognition

We performed differential expression analysis among all genes within cell clusters using Seurat's FindAllMarkers function to identify the marker genes in each cluster (16). An adjusted P-value< 0.05, expression percentage > 0.25, and | log2 [fold change (FC)] | > 0.25 were considered as cutoff criteria for identifying marker genes (Table S1). Subsequently, different cell clusters were determined and annotated by the singleR package according to the composition patterns of the marker genes and were then manually verified and corrected with the CellMarker database. The malignant cells were annotated by correlation with the data donator's cell annotation.

2.4 Pseudotime trajectory analysis

Single-cell pseudotime trajectories were constructed using the Monocle 2 algorithm, an R package designed for single-cell trajectories by Qiu et al (17). This algorithm applies a machine learning technique to reduce the high-dimensional expression profile to a low-dimensional space, visualized as a tSNE plot. Single cells were projected onto this space and ordered into a trajectory with branch points. The dynamic expression heatmap was constructed using the plot_pseudotime_heatmap function. In addition, differential expression analysis between branches was performed using the plot_genes_branched_heatmap function.

2.5 Functional enrichment analysis

Differentially expressed genes (DEGs) analysis was performed using Seurat's FindMarkers function. The following cutoff threshold values were used: adjusted P-value< 0.05 and | log2 [FC]| >1. The DEGs were loaded into Metascape (http://metascape.org), a tool for gene list enrichment analysis (18).

The Gene Set Variation Analysis (GSVA) algorithm was performed to explore the activity variation of biological process and pathways in each cell types. Gene Oncology gene sets "c2.all.v7.4.symbols.gmt" and Kyoto Encyclopedia of Genes and Genomes sets "c5.all.v7.4.symbols.gmt" from Molecular Signatures Database (MSigDB, http://www.gsea-msigdb.org), which were used for functional analyses. The GSVA analysis was performed in R 4.0.3 to calculate the enrichment score of the pathways in each cell and when the P-value was less than 0.05, the enriched gene set was considered to be statistically significant.

2.6 Cell-cell communication analysis

CellChat is a novel toolkit used to infer intercellular communication networks from scRNA-seq data quantitatively (19). Based on the ligand-receptor interactions database for human and pattern recognition approaches, CellChat can predict major signaling inputs and outputs for cells and establish how those cells and signals coordinate their functions. Ligand-receptor pairs with a P-value< 0.05 were filtered to evaluate the relationship between different cell types.

2.7 Gene regulatory network analysis

We used SCENIC (Aibar et al., 2017) (20), an algorithm that can reconstruct transcriptional states and regulatory networks from scRNA-seq data, to evaluate the gene regulatory networks relating to TFs and regulons in individual cells. The gene expression matrix was input into SCENIC and a co-expression matrix was constructed using GENIE3. Direct binding by DNA-motif analysis was identified based on a motif dataset (hg19-500bp-upstream-7species.mc9nr.feather, hg19-tss-centered-10kb-7species.mc9nr.feather) to construct regulons for each TF. Finally, regulon activity was analyzed using AUCell (Area under the Curve), where a default threshold was applied to binarize the specific regulons. Regulon modules were then identified based on the Connection Specificity Index (CSI) to confirm specific associating partners (21). Hierarchical clustering with Euclidean distance was then performed to identify different regulon modules. We then used 0.65 as a cutoff to construct the regulon association network, to investigate the relationship between different regulons.

2.8 Correlation with bulk RNA-seq data

CIBERSORTx is a new machine learning method developed from CIBERSORT for estimating the abundance of cell clusters in bulk RNA-seq data (22). This tool was used to digitally purify the transcriptome of individual cell clusters from the bulk data

without isolating single cells. We extracted the transcripts per million (TPM) normalization datasets of selected cell types including CD8+ T cells, myeloid cells, fibroblasts and epithelial cells to create the signature matrix in 1000 permutations and without batch correction. Then we separated the CRC patients from TCGA database into training and testing cohorts according to a 1:1 ratio using a randomization method based on survival status and used CIBERSORTx to estimate the fraction of each cell cluster in training and testing cohorts respectively. Notably, the bulk RNA-seq data from TCGA was first normalized to TPM values. Furthermore, stepwise multivariate Cox regression was applied to select the optimal coefficient for each cell cluster to construct the risk model in training cohort. The riskscore were then divided into "high risktype" and "low risktype" according to the median risk score which equaled 1.263 in the training cohort. The formula for the model is as follows:

$$\text{Riskscore} = \sum_{i=1}^{n} Coef_i * Fraction_i$$

Finally, we incorporated the riskscore, TNM stage, gender, and age to construct a clinical risk model using stepwise multivariate Cox regression to construct clinical risk model in the training cohort. The clinical riskscores was then divided into "high clinical risktype" and "low clinical risktype" according to the median risk score which equaled 0.900 in the training cohort. The formula for the model is as follows:

$$\text{Clinical Riskscore} = \sum_{i=1}^{n} Coef_i * Factor_i$$

The associations of immune risktype and clinical risk type with OS were analyzed using Kaplan-Meier (KM) survival analysis, with receiver operating characteristic (ROC) curve analysis used to verify the sensitivity and specificity of the model for the training cohort. The immune risk model and clinical risk model was then applied to the testing cohort, and the reliability of the model was verified by KM curve and ROC curve analyses.

2.9 Statistical analyses

Statistical analyses were conducted using R software (version 4.0.3; R Foundation for Statistical Computing, Vienna, Austria). All statistical tests were two-sided, with P-values< 0.05 considered statistically significant.

3 Results

The samples, including tumor, Para-tumor and blood from 10 treatment-naive CRC patients were involved in this study. According to the annotation of SingleR package and CellMarker database, we finally identified 8 major cell types including CD4+ T cells, CD8+ T cells, B cells, myeloid cells, innate lymphoid cells (ILCs), fibroblast cells, endothelial cells, and epithelial cells (Figure 1A). Each cell type was extracted and further grouped for annotation, and finally 25 cell subtypes were identified (Figure 1B). The top five markers identified by the differences in the main cell types were visualized as a bubble plot (Figure 1E). Interestingly, when we traced the tissue origins, it was noted that immune cells, especially Tex, TAMs, dendritic cells (DCs) and fibroblast cells were highly enriched in tumor tissues (Figures 1C). To investigate the network of interactions in the TME, we used CellChat to calculate potential ligand-receptor pairs. Network visualization was performed to visualize the interactions (Figure 1D). Notably, Tex, macrophages, TAMs, and DCs possessed the most interaction pairs with cells from other lineages, revealing the dominant roles in the TME.

3.1 CD8+ T cells

The CD8+ T cells were divided into nine sub-clusters and annotated into four cell types; naïve CD8+ T cells, effector memory CD8+ T cells (Tem), effector CD8+ T cells (Teff) and Tex (Figure 2A). To clarify the function of each cell type, we extracted the marker genes (Table S1) and loaded these into the Metascape (http://metascape.org/) (Figure 2B, C). The pseudotime trajectory revealed that CD8+ T cells became exhausted (Figure 2D), and inhibitory receptors (IRS) expression increased in a stepwise manner (Table S2). We clustered all the transcription factors surrounding the CD8+ T cells by single-cell regulatory network inference and clustering (SCENIC) analysis and divided them into nine modules using a clustering algorithm (Figure 3E; Table S3). Notably, Module 1 transcription factors including Nuclear receptor ROR-gamma (RORC), Nuclear receptor subfamily 1 group D member 1 (NR1D1), Peroxisome proliferator-activated receptor gamma (PPARG) and Sterol regulatory element-binding protein 2 (SREBF2) were significantly activated in Tex (Figure 3F).

3.1.1 Loss of effector function during exhaustion of CD8+ T cells

The loss of Tex effector function is classed into three major categories: (1) upregulation of cell surface IRS, (2) inhibitory soluble factors and environmental factors such as interleukin10 (IL10), IL4, transforming growth factor-beta (TGF-β), and interferon alpha/beta (IFNα/β), and (3) immunosuppressive cells (11). We examined the immune checkpoints in different cell types (Table S1). Notably, IRS, including the inhibitory receptor T-cell immunoglobulin and mucin domain 3 (TIM3), lymphocyte activation gene 3 protein (LAG3), programmed cell death protein 1 (PDCD1), TIGIT, CD27, cytotoxic T-

10.3389/fimmu.2022.1003419

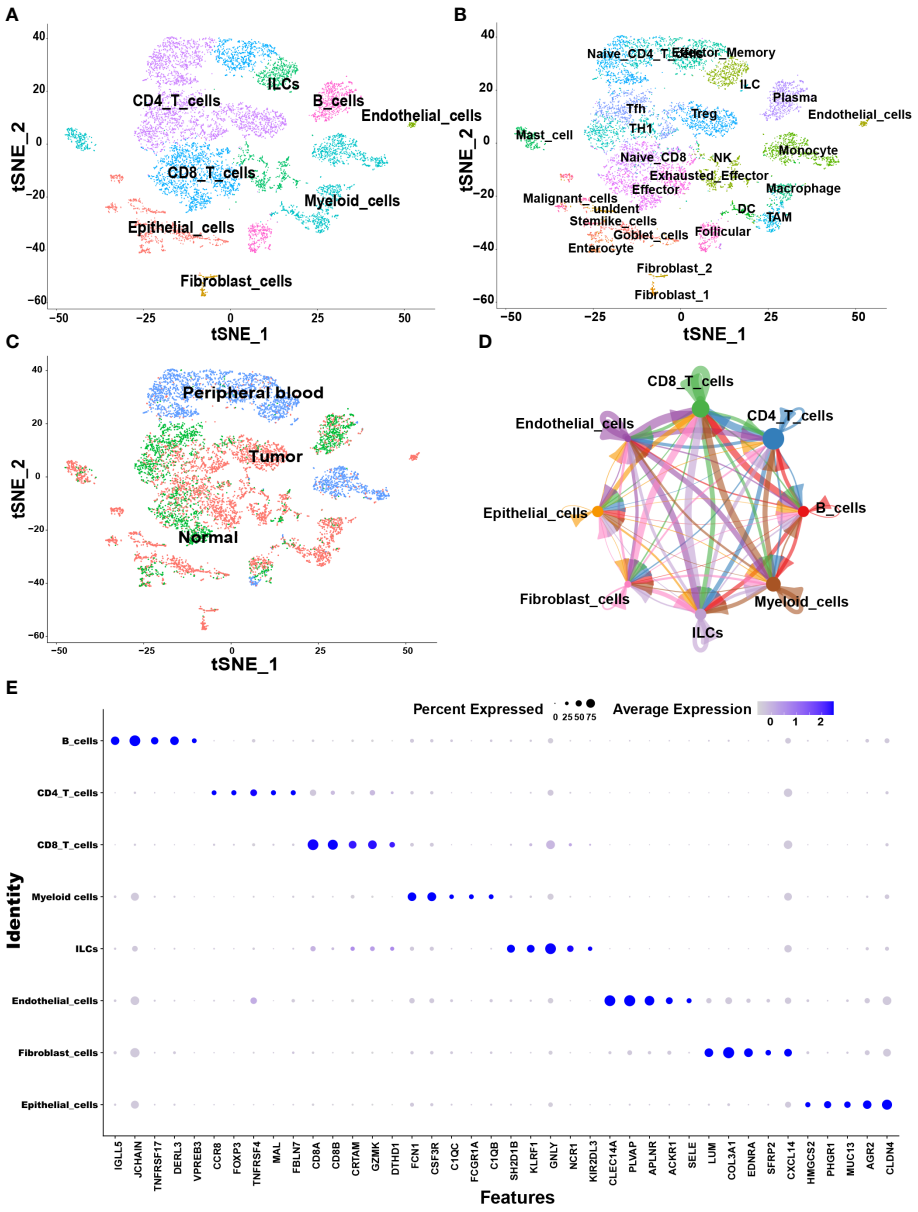

FIGURE 1
Overview of single cells derived from tumors, adjacent tumor tissues, and peripheral blood of CRC patients. **(A–C)** tSNE plots of all the single cells color-coded for **(A)** eight major cell types, **(B)** 25 sub-cell types, **(C)** tissue origins (tumor, adjacent to tumor or blood). **(D)** Interaction network among major cell types constructed by CellChat; circle sizes represent interaction weights; the thicker line indicates more weight and strength of the interactions between variable major cell types. **(E)** Bubble heatmap showing top five marker genes of eight major cell types. Dot size indicates fraction of expressing cells, colored according to expression levels.

lymphocyte protein 4 (CTLA-4), and tumor necrosis factor receptor superfamily member 9 (TNFRSF9), were upregulated in Tex. Enrichment analysis showed that Teff was enriched in numerous proinflammatory pathways such as the IL-2, -3, -17, and -18 signaling pathways, whereas Tex was enriched in IL-4 and -10 immunosuppressive pathways and PD-1 signaling pathways (Figures 2B, C). GSVA analysis confirmed these results (Figure 2G). At the same time, the pseudotime analysis revealed that genes related to IRS were significantly upregulated along with the differentiation such as PD-1 and CTLA-4 (Table S2). The expression of immunosuppressive-related genes such as IL4, IL1RN, and IL4I1 were enhanced, whereas expression of immune activation-related genes such as IL18BP and IL5RA were reduced. This finding agrees with previous results where T cell exhaustion usually manifests as a stepwise loss of effector functions. CellChat analysis was undertaken to determine

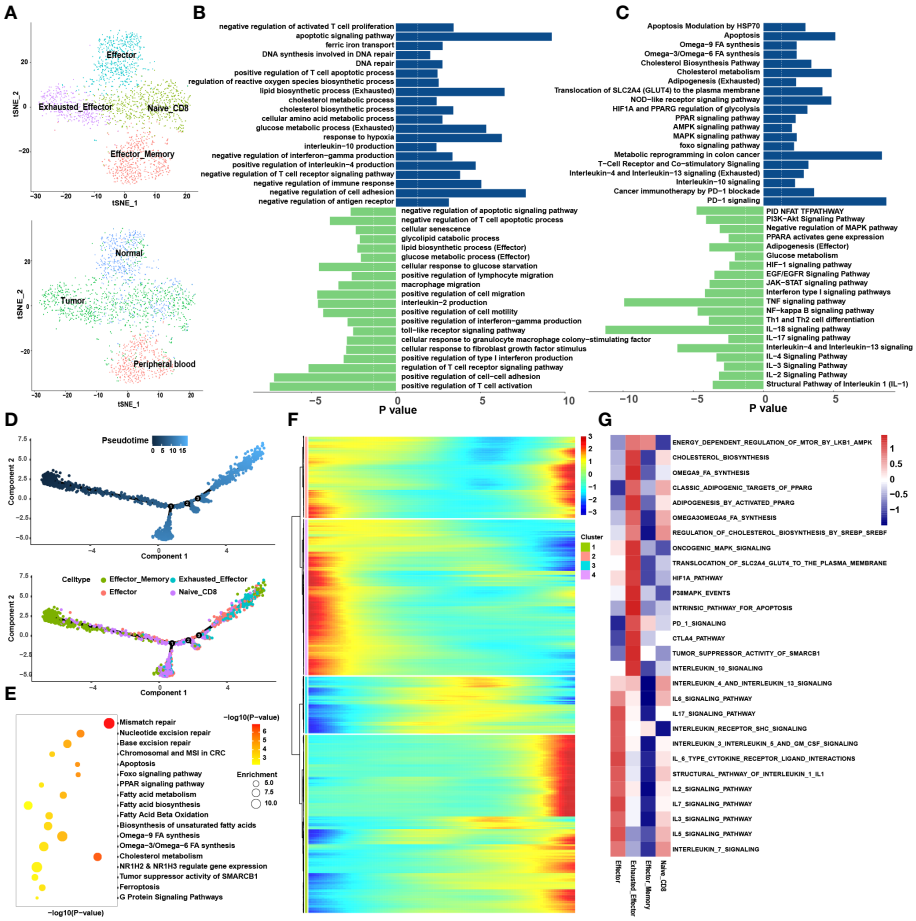

FIGURE 2
CD8+ T cells tend to exhaust in the tumor microenvironment. **(A)** tSNE plots showing 4 sub-cell types of CD8+ T cells (upper) and their tissue origins (lower). **(B)** GO and **(C)** KEGG pathway enrichment analyses of marker genes of Tex (blue color) and Teff (green color). The height of each barplot shows the log10 of P-value calculated using the Metascape database. **(D)** Differentiation trajectory of CD8+ T cells in CRC, color-coded for pseudotime (upper) and sub-cell types (lower). **(E)** Pseudo-heatmap of genes altered in the differentiation process of CD8+ T cells in CRC, divided into four clusters. **(F)** The bubble plot shows the GO and KEGG pathway enrichment analysis of genes in cluster 1 identified in Pseudo-heatmap using the Metascape database. **(G)** The heatmap illustrates the activity of biological process and signaling pathway in each cell type by GSVA.

further the interaction between Tex and other cells in the TME. First, we analyzed the immunosuppressive receptors expressed by Tex, including TIGIT, CTLA-4, ICOS, and PDCD1, and found that different cells produced different ligand-receptor modes (Figure 3A). Endothelial and tumor cells mainly secreted poliovirus receptor (PVR) and NECTIN2, which acted on the TIGIT receptor on the surface of Tex. CD80 and CD86 secreted by DCs and TAMs interacted with CTLA-4. Regulatory T cells (Tregs) mainly secreted CD274 to act on PDCD1. Furthermore, analysis of the PD-L1 pathway regulatory network showed that Tregs were the main senders of PD-L1, with Tex being the main receivers (Figure 3B). Besides, cytokines such as PVR and NECTIN2 also participate in building the tumor immunosuppressive microenvironment. Analysis of the PVR pathway regulatory network showed that tumor and endothelial cells were the main senders, and immunosuppressive cells such as Tex were the receivers (Figure 3D). More interestingly, the fibroblast subgroup served as a mediator in this regulatory network, and this implies that this subgroup could be a potential target for new drugs. The NECTIN2 pathway regulatory network also showed multiple ligand-receptor modes; DCs, endothelial cells, fibroblasts, and TAMs were the main senders, and Tregs, Teff, and Tex were the main receivers (Figure 3C). Because PVR and NECTIN2 can both act on TIGIT, compared to the currently popular PDL1/PDLD1 blockers, TIGIT may not only reverse the exhaustion state of CD8 T cells but may also improve the tumor immunosuppressive microenvironment to a certain extent. Hence, we hypothesized that inhibition of TIGIT could be a new treatment for CRC. Our analyses showed that Tex play

10.3389/fimmu.2022.1003419

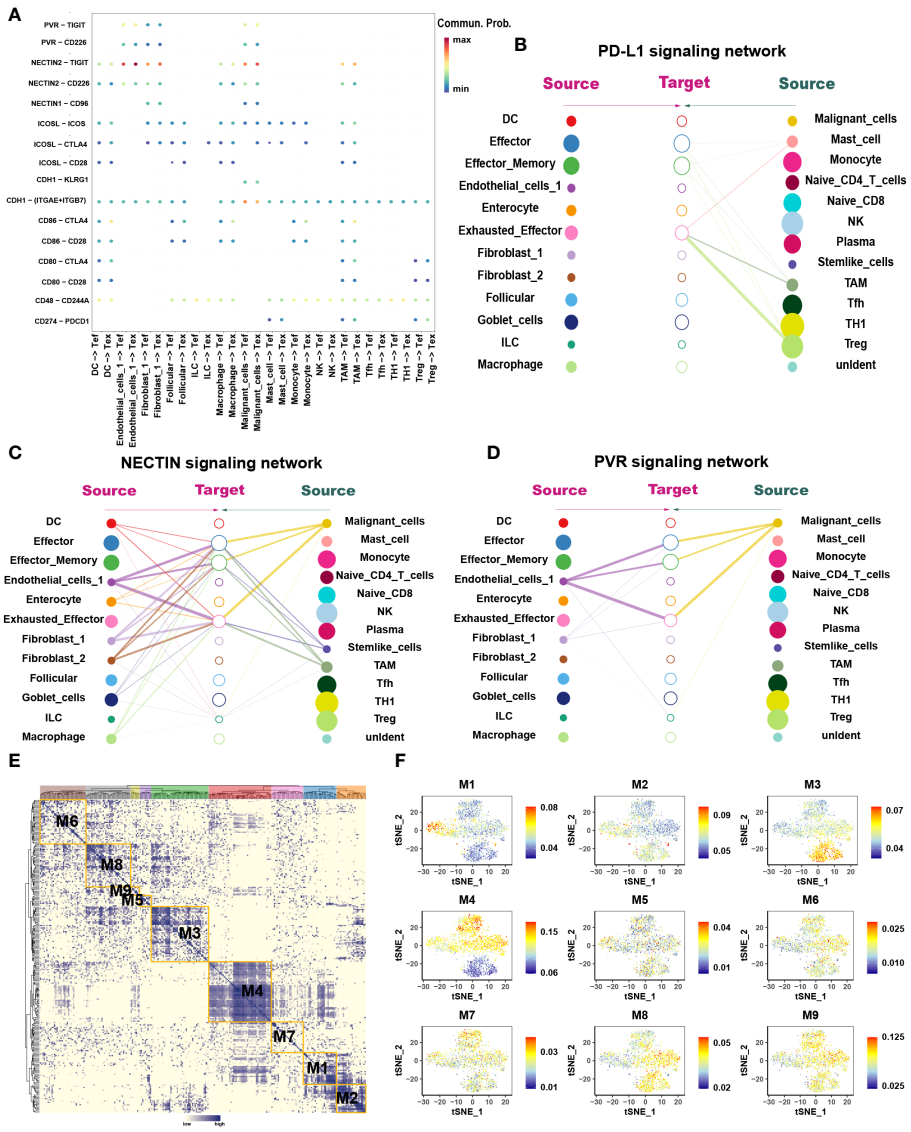

FIGURE 3
The interaction network and transcription regulatory network of CD8+ T cells. **(A)** Summary of selected ligand-receptor interactions between CD8+ T cells and TME-infiltrated cell types detected by CellChat. P-values are represented by the size of each circle. The color gradient indicates the level of interaction; blue and red colors correspond to the smallest and largest values respectively. **(B–D)** Hierarchical plot showing the inferred intercellular communication networks for PD-L1 **(B)**, NECTIN2 **(C)**, and PVR **(D)** signaling, respectively. The interactions are divided into sources and targets and were labeled by solid circle and hollow circle, respectively. The circle sizes in the hierarchical plot are proportional to the number of each cell type and the edge width represents the communication probability. **(E)** Heatmap of 9 identified regulon modules based on the regulon CSI matrix. **(F)** t-SNE map for all CD8+ T cells based on the regulon activity scores (RAS) of the respective regulon modules.

major roles in the immunosuppressive microenvironment, and the depletion of CD8+ T cells is an inevitable outcome in TME.

3.1.2 Metabolic remodeling in the CD8+ T cell exhaustion process

We constructed the differentiation trajectory of CD8+ T cells using pseudotime analysis, in which effector memory CD8+ T cells were present at the initial location of the differentiation trajectory, gradually differentiated into Teff and finally convert into Tex which located at the end of the differentiation trajectory (Figure 2D). As we all know, under chronic inflammation such as during cancer, autoimmunity, and chronic infections, Teff transform into Tex (23). Thus, we identified the DEGs (Table S1) among the Teff and Tex and performed enrichment analysis (Figures 2B, C). It was found that the metabolic patterns of Teff and Tex were significantly different. The glucose metabolic process was enriched in Teff while lipid metabolism processes such as lipid biosynthesis and the cholesterol metabolic pathway

were highly enriched in Tex. GSVA also support this finding (Figure 2G). We extracted genes whose expression increased in the differentiation trajectory and then conducted enrichment analysis. The pathways such as fatty acid biosynthesis and omega-3, -6, and -9 fatty acids (FAs) synthesis were all enriched (Figure 2E). These results implied that the differentiation of T cells was related to lipid metabolism remodeling, and abnormal lipid accumulation may be the energy source for Tex. The DEGs analysis, Pseudotime analysis and GSVA all showed that the PPARG pathway was highly expressed in Tex. A previous study showed activation of the PPAR pathway in the metabolic regulation of lipid and lipoprotein levels (24). Based on these results, we suspect that the lipid metabolism remodeling in Tex is attributed to the activation of the PPARG pathway. To verify this hypothesis, we performed SCENIC analysis to reveal the abnormal transcriptional regulatory network of Tex. Without suspension, PPARG was significantly enriched in Tex. This further demonstrates that the PPARG transcription factor may play an important role in lipid reprogramming in Tex. In addition, we also enriched the RORC, NR1D1, and SREBF2 transcription factors in the M1 module, which are also closely associated with lipid metabolism (25–27). Our results suggested that transcription factors (TFs) such as PPARG and SREBF2 may participate in the metabolic remodeling in Tex and act as latent targets to reverse this process.

3.2 Myeloid cells

Myeloid cells are abundant critical components of the TME which are heterogeneous mixture of cell types having both tumor stimulating and suppressing activities. Analysis of the myeloid cells revealed five distinct sub-clusters: monocytes, macrophages, TAMs, DCs, and mast cells (Figure 4A). Among them, macrophages and TAMs can be activated and polarized into M1 (classically activated) and M2 (selectively activated) phenotypes under the influence of external conditions and stimulus factors. M1 cells usually show pro-inflammatory activity, while M2 cells exhibit tumor-promoting phenotypes characterized by high levels of immunosuppressive markers and anti-inflammatory factors (28).

Interestingly, when traced back to the tissue source, monocytes were present primarily in the blood, while macrophages and TAMs occurred in most tumor tissues (Figure 4A). Pseudotime analysis showed that monocytes differentiated into macrophages when they entered the TME from the blood and finally differentiated into TAMs (Figure 4D).

3.2.1 TAMs are engaged in constructing the immunosuppressive microenvironment

Enrichment analysis revealed that Pathways associated with proinflammation were enriched in macrophages, such as IL-1, -2, -3, -11, -17, -18, -21, TNF alpha and interferon alpha/beta signaling pathways while macrophages also exhibit few M2-like function such as IL-4, -10, and TGF-beta receptor signaling (Figure 4B). In contrast, pathways associated with tumor promotion and immunosuppression were enriched in TAMs such as arachidonic acid metabolism, matrix metalloproteinase (MMP), the vascular endothelial-derived growth factor (VEGF), IL-4, -10, -13 and PD-1 signaling. Few M1-like functional pathways were also present in TAMs such as interferon gamma and TNF signaling pathways. GSVA analysis also disclosed that IFN alpha/beta signaling was enriched in TAMs, while IL-5, -6, -7 and -17 were enriched in macrophages (Figure 4C). In conclusion, macrophages and TAMs exhibit mixed M1 and M2 phenotypes among which macrophages mainly exhibit M1 phenotype, whereas TAMs mainly exhibit M2 phenotype. Combined above results with tissue origination and pseudotime analysis, we speculated that once monocytes from the peripheral blood entered the tumor tissues, they initially differentiated into M1-type macrophages and finally differentiated into M2-type TAMs, alongside enhanced immunosuppressive effects.

SCENIC analysis was performed to determine the changes in TFs during the transformation of macrophages into TAMs (Figures 4F, G). We found that STAT4, NFκB1, NFκB2 and RUNX1 were enriched in macrophages (Table S5) in which STAT4 has been proved to mediates the JAK-STAT-related pathways and participates in the conduction of the IL-12, -21, -23 and -35 signaling pathways (29). NFκB1 and NFκB2 can promote the polarization of macrophages to M1 type (30). Conversely, MAF, ETV5 and EGR2 were highly expressed in TAMs in which MAF regulates the activation of IL-4 pathway and ETV5 is related to blood vessel growth and activation of the IL-10 pathway (31–33). The expression of EGR2 was found to be related to the activation of the IL-4 and TGF-β functional pathways (34, 35).

Finally, we utilized CellChat to investigate the interactions between TAMs and other cell subtypes in TME (Figure 5D). Compared to macrophages, TAMs participated more in constructing the immunosuppressive microenvironment. The immunosuppressive ligands secreted by TAMs, such as CD80, CD86, CD274, ICOSL and NECTIN2 showed evident interactions with other receptors such as CTLA-4, PD-1, ICOS and TIGIT expressed by other cells, especially T cells (Figure 5E–G). In addition to IRS, TAMs also secreted immunosuppressive soluble cytokines such as IL-10 and SPP1 (Figure 5A). Interestingly, TAMs were the main secretors of IL-10, whereas macrophages were the main receivers of IL-10 (Figure 5B). This suggested a possible positive feedback loop between macrophages and TAMs. Once macrophages had differentiated into TAMs, TAMs possibly secrete IL-10 acting on macrophages to promote the differentiation process (Figure 5B). TAMs also secreted SPP1 which have been found mediating macrophage polarization

10.3389/fimmu.2022.1003419

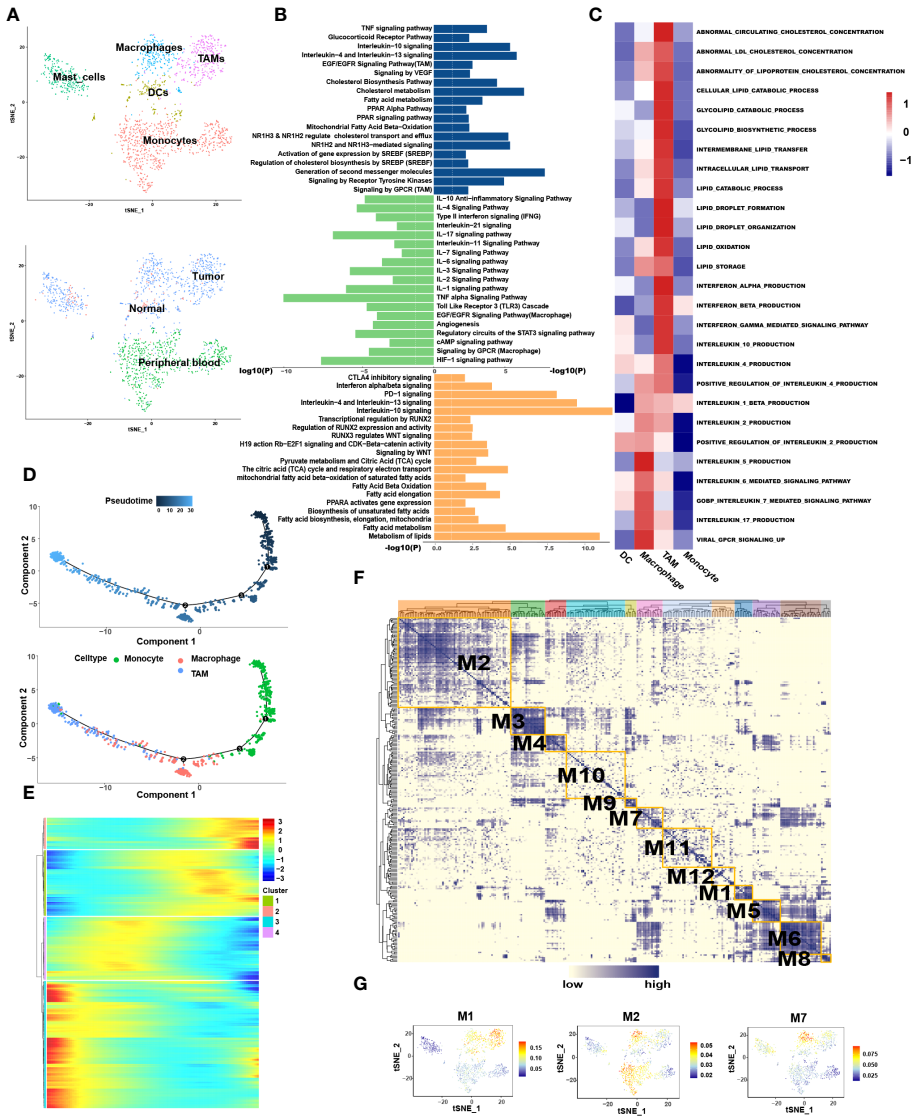

FIGURE 4
Macrophages resulted from M1 polarization, whereas TAMs resulted from M2 polarization in CRC. **(A)** tSNE plots showing 4 sub-cell types of CD8+ T cells (upper) and their tissue origins (lower). **(B)** GO and KEGG pathway enrichment analyses of marker genes of TAMs (blue color), Teff (green color) and DCs (orange color). The height of each barplot shows the log10 of P-value calculated using the Metascape database. **(C)** The heatmap illustrates the activity of biological process and signaling pathway in each cell type by GSVA. **(D)** Differentiation trajectory of monocytes, macrophages and TAMs in CRC, color-coded for pseudotime (upper) and sub-cell types (lower). **(E)** Pseudo-heatmap of genes altered in the differentiation process of monocytes, macrophages, and TAMs in CRC, grouped into four clusters. **(F)** Heatmap of 12 identified regulon modules based on the regulon CSI matrix. **(G)** Selected regulon models which upregulated in TAMs (M1) and Macrophages (M2, M7) showed in t-SNE map for myeloid cells.

and facilitates immune escape in lung adenocarcinoma (36). SPP1 secreted by TAMs could interact with almost all cells in TME, including DCs, Tregs, Tex, fibroblasts, and malignant cells (Figure 5C). Interestingly, TAMs were not only the main secretors of SPP1 but also the main receivers. It may be attributable to the M2 phenotype of TAMs in this study.

3.2.2 Lipid metabolism reprogramming in TAMs

Lipid metabolism associated genes such as PPARA were highly expressed in the TAMs. In order to explore whether there was lipid metabolism remodeling in TAMs similar to that in T cell exhaustion, marker genes of macrophages and TAMs were

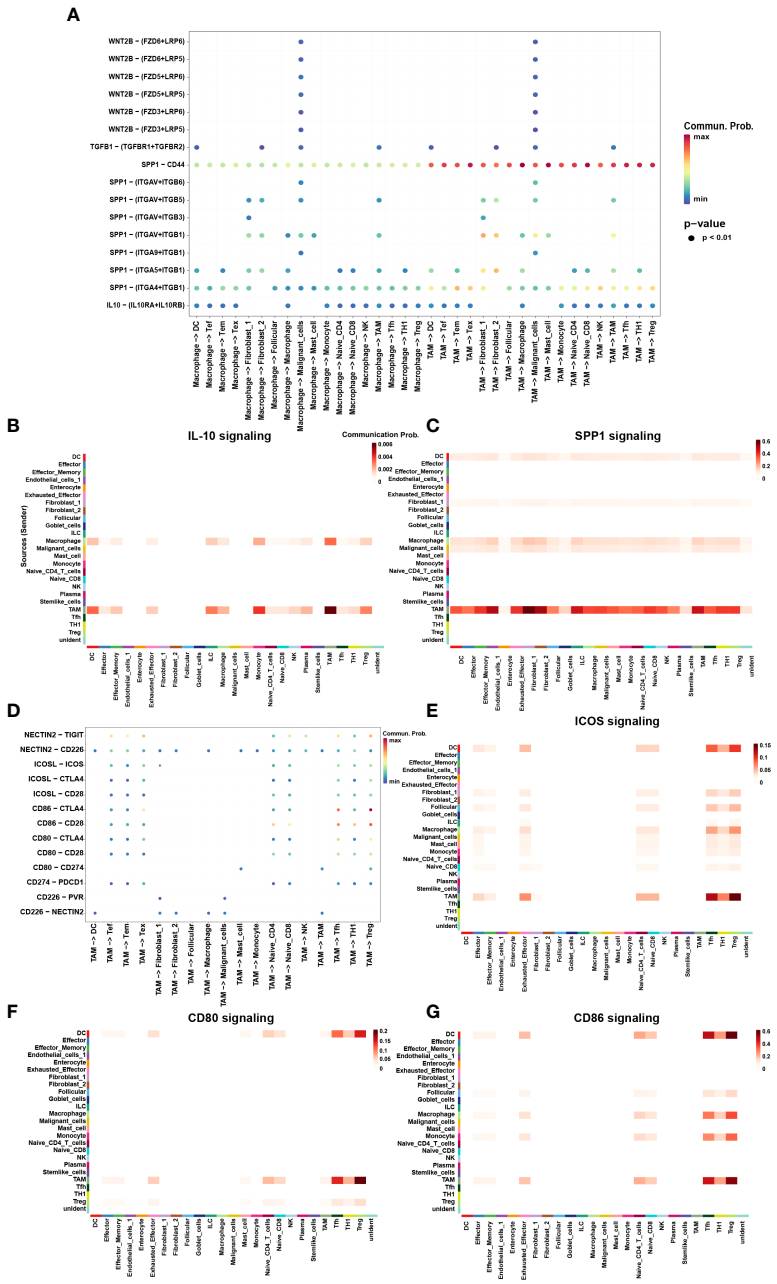

FIGURE 5
The interaction network of macrophages and TAMs. **(A)** Summary of selected soluble factor-receptor interactions among macrophages, TAMs and TME-infiltrated cell types. **(G)** Summary of selected immune checkpoints-receptor interactions between TAMs and TME-infiltrated cell clusters. P-values are represented by the size of each circle. The color gradient indicates the level of interaction; blue and red colors correspond to the smallest and largest values respectively. **(B, C, E–G)** The heatmap plot showed the inferred intercellular communication network for SPP1 **(B)** and IL-10 **(C)**, CD80 **(E)**, CD86 **(F)**, and ICOSL **(G)** signaling of myeloid cells and TME-infiltrated cell clusters, respectively. The interactions are divided into sources (labeled on y-axis) and targets (labeled on x-axis). The color gradient represents the communication probability; white and red colors correspond to the smallest and largest values respectively.

extracted for functional enrichment analysis. The results showed that, compared to macrophages, TAMs are enriched in more lipid metabolic pathways such as cholesterol biosynthesis and fatty acid metabolism, such as the "PPAR Alpha Pathway". "Regulation of cholesterol biosynthesis by sterol regulatory-element binding proteins (SREBP)" and " Oxysterols receptor LXR-beta (NR1H2) and Oxysterols receptor LXR-alpha (NR1H3) Mediated signaling "(Figure 4B). GSVA also further

confirmed enhanced synthesis of cholesterol and lipid droplets in TAMs (Figure 4C). Pseudotime analysis showed that the expression of genes related to lipid output, such as ABCA1 and ABCG1, was gradually enhanced during macrophage differentiation (Table S4). It is reasonable to speculate that the differentiation of macrophages into TAMs is accompanied by lipid metabolism remodeling.

Among the functional pathways enriched in TAMs, three transcription factors attracted our attention, namely SREBF, NR1H2 and NR1H3. Further SCENIC analysis reported the abnormal transcriptional regulatory network in TAMs (Table S5). As shown in Figure 4G, transcription factors in module 1 were significantly activated in TAMs, which include the SREBF and NR1H3. Among them, SREBF functions in the transcriptional regulation of genes involved in the biosynthesis and uptake of lipids, promoting fatty acid synthesis and inducing M2 phenotype of TAMs (37, 38). NR1H2 and NR1H3 act as transcription factors engaged in lipid metabolism synthesis and are important modulators of the SREBP-1c pathway at the transcription level, where they regulate gene expression linked to cholesterol transport and efflux in hepatic lipogenic cells (39). We were particularly interested in the cholesterol efflux function mediated by NR1H2 and NR1H3. Increased cholesterol outflow increased lipid content in the TME to provide nutrition for tumor cell growth and destroyed the lipid raft of TAMs to weaken the Toll-like Receptor 4 (TLR4) signaling pathway (39). It also enhanced the IL-4 pathway, weakened the interferon pathway (40), and has an unexpected role in the polarization of TAMs to M2. We speculated that reprogramming of lipid metabolism in TAMs is involved in the remodeling of immune functions, to a certain extent.

Therefore, SREBF and NR1H3 play important roles in lipid metabolism reprogramming in TAMs. TAMs and Tex have both undergone lipid metabolism remodeling, reflecting the important role of lipid metabolism in the process of T cell exhaustion and TAMs polarization to M2 type. However, there are significant differences between these two kinds of cells, which are mainly manifested in the differences in the transcription regulatory factors. Hence, we suspect that SREBF and NR1H3 may be important targets to prevent or reverse the polarization from TAMs to M2.

3.2.3 DCs exhibit a similar pattern to TAMs in metabolism remodeling and construction of the immunosuppressive microenvironment

DCs are the most potent antigen-presenting cells in the immune system and are central players in the adaptive immune response. DEGs analysis revealed that DCs exhibited highly expressed immunosuppressive cytokines, such as IL-4, -10, and IFNα/β (Table S1). Further enrichment analysis showed that IL-4, -10, and -13, interferon alpha/beta, PD-1, and CTLA-4 inhibitory signaling pathways were enriched in DCs (Figure 4B). CellChat analysis found DCs exhibited a similar pattern to TAMs in secreting immunosuppressive cytokines, especially ICSO (Figure 5E), CD80 (Figure 5F) and CD86 (Figure 5G). These heatmaps indicated that DCs and TAMs were the main secretors participating in the exhaustion process of CD8+ T cells, synergistically promoting the construction of the immunosuppressive microenvironment.

At the same time, enrichment analysis showed that lipid metabolism, fatty acid metabolism, and PPARA signaling pathways were highly enriched in DCs (Figure 4B). Except for aberrant lipid storage, the PPARs pathway also enhances TCA cycle, resulting in citric acid accumulation. These conditions provide the substrate for the *de novo* synthesis of fatty acids and intracellular lipid droplets. Other pathways were also enriched, including Wnt signaling and CDK-beta-catenin activity. Wnt5 has been proved to act on Frizzled (FZD) family receptors on DCs and trigger the activation of downstream PPAR pathways through activation of β-catenin signals to remodel lipid metabolism in melanoma (41) (Figure 4B). Transcriptional regulation by RUNX2 and RUNX3, regulating Wnt signaling was enriched in DCs. SCENIC analysis demonstrated that RUNX2 was highly expressed in DCs (Figure S3D). These results implied that lipid metabolism remodeling in DCs might also depend on the core Wnt/β-catenin/PPAR signaling pathway regulated by the RUNX family.

Based on the above analysis, we speculate that lipid metabolism reprogramming in DCs is involved in reconstructing the immunosuppressive microenvironment.

3.3 Fibroblast cells

We extracted 145 fibroblast cells classified into two clusters: fibroblast-1 and fibroblast-2 (Figures 6A, B). Pseudotime analysis revealed that fibroblast-1 was present at the initial stage of the differentiation trajectory, and fibroblast-2 was present at the end. Interestingly, fibroblast_2 also differentiated into two distinct subtypes, state2 and state3 (Figure 6C).

3.3.1 Similar metabolic and functional remodeling in fibroblasts

Enrichment analysis showed that compared to fibroblast-1, fibroblast-2 is more involved in extracellular matrix (ECM) degradation and promotion of cell motility regulated by MET signaling pathway (Figure 6D). Interestingly, the metabolic patterns between the two clusters are totally different. The pathways related to lipid cholesterol and fatty acid metabolism were significantly enriched in fibroblast-2. In contrast, fibroblast-1 exhibited carbohydrate metabolism pattern (Figure 6E). Furthermore, the two subgroups of fibroblast-2 both exhibited patterns of ECM regulation and lipid metabolism, while the state2 subgroup showed stronger patterns of lipid metabolism remodeling, ECM degradation and promotion of cell motility regulated by MET signaling pathway compared to state3 (Figure 6F). Among these, several

10.3389/fimmu.2022.1003419

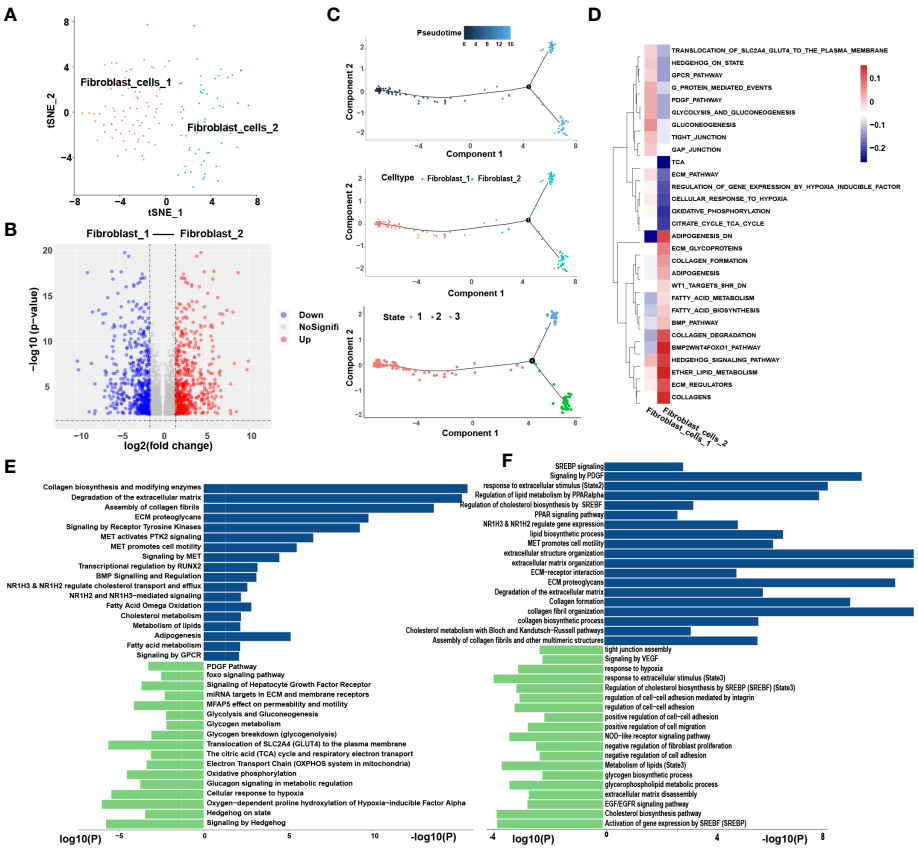

FIGURE 6
Similar metabolic and functional remodeling in fibroblasts. **(A)** tSNE plots showing 2 sub-cell types of fibroblasts. **(B)** The volcano plot illustrated the DEGs of each sub cluster, statistically significant DEGs were defined with p< 0.05 and [logFC] > 1 as the cut-off criterion. **(C)** Differentiation trajectories of fibroblasts color-coded for pseudotime (upper) and sub-cell types (median) and states (lower). **(D)** The heatmap illustrates the activity of biological process and signaling pathway in each cell type by GSVA. **(E)** GO and KEGG pathway enrichment analyses of marker genes of fibroblast-2 (blue) and fibroblast-1 (green). **(F)** Enrichment analyses of marker genes of state2 (blue) and state3 (green) cluster. The height of each barplot shows the log10 of P-value calculated using the Metascape database.

pathways highly enriched in fibroblast-2 aroused our attention, such as"NR1H2&NR1H3 regulate gene expression linked to cholesterol transport and efflux", "NR1H2 and NR1H3 Mediated signaling" and "transcriptional regulation by RUNX2". SCENIC analysis also showed that NR1H2, NR1H3and RUNX were upregulated in fibroblast-2 (Figure S3D). It was highly consistent with that of TAMs. Above results revealed that enhanced lipid metabolism and abnormal lipid accumulation may also occur in the differentiation from fibroblast-1 to fibroblast-2.

3.4 The infiltration of tumor-educated immune cells is associated with a worse prognosis in CRC

We performed digital cytometry analyses using CIBERSORTx to evaluate the abundance of tumor stromal and immune cell subsets analyzed previously in patients from The Cancer Genome Atlas-Colon Adenocarcinoma (TCGA-COAD) data. We established a new risk model using stepwise regression to evaluate the association between cell fractions and prognostic outcomes and identify the optimal coefficient for each subgroup in the training cohort. Finally, we selected sixteen subgroups to construct the model. The formula for the risk model is as follows:

Riskscore=-2.373*Fibroblast_cells.0+9.172*Fibroblast_cells.1 +6.570*Myeloid.cell.0+5.484*Myeloid.cell.1-827.566*Myeloid.cell.2 +9.532*Myeloid.cell.5+18.344*Myeloid.cell.6-.645*Myeloid.cell.7 +16.412*CD8_T_cells.0-0.766*CD8_T_cells.1+7.595*CD8_T_cells. 2+40.164*CD8_T_cells.3+7.233*CD8_T_cells.4-28.620 *CD8_T_cells.5+8.862*CD8_T_cells.7+4.852*CD8_T_cells.8 (The correspondence between each subgroup and sub cell type was applied in Supplementary Table 9).

Then, we evaluated the prognostic value of the risk model for overall survival (OS). Patients in the high-risk group had a significantly worse OS than the low-risk group both in training

and testing cohort ($p<0.001$ and $p=0.03$, respectively) (Figures 7A, B). The model's accuracy was verified using time-dependent receiver operating characteristic (ROC) curves, which confirmed the reliability of the prognoses for both cohorts. The area under the ROC curve for the risk score was 0.823, 0.774, and 0.696 for 1-, 2- and 3-year OS in the training cohort, versus 0.709, 0.709, 0.711 in the testing cohort. (Figures 7C, D). Furthermore, we used a stepwise multivariate Cox regression to construct a new clinical model incorporating riskscore, TNM stage, gender, and age in the training cohort and selected riskscore and TNM stage to construct the model. The formula for the clinical risk model is as follows:

$$\text{Clinical riskscore} = 0.472 \star \text{riskscore} + 0.582 \star \text{stage}$$

Interestingly, riskscore and TNM stage were both independent prognosis factors ($p<0.001$ and $p=0.038$, respectively). The patients were separated into two subgroups according to the median clinical riskscore. KM survival analysis revealed that high clinical risktype had a significantly worse OS than low clinical risktype both in training cohort and testing cohort ($p<0.001$ and $p=0.0012$, respectively) (Figures 7E, F). The areas under the ROC curve for 1-, 2-, and 3-year OS was 0.885, 0.746, and 0.734 for 1-, 2- and 3-year OS in the training cohort, versus 0.827, 0.780, 0.780 in the testing cohort. (Figures 7G, H), which was better than the immune risk model.

We also applied other immune risk model that have been reported and TNM stage for validation. Patients in the high-risk/high-stage (III-IV) group showed a significantly worse OS than the low-risk/low-stage (I-II) group ($p<0.001$ and $p=0.015$, respectively) (Figures S6B, S6A). The area under the ROC curve for the risk score was 0.758, 0.760, and 0.717 for 1-, 2- and 3-year OS for the immune risk model, versus 0.726, 0.636, 0.650 for the TNM stage model (Figures S6D, S6C).

4 Discussion

Currently, the treatment of CRC, especially advanced CRC, still remains challenging. Although ICB has made some progress, only a small number of people benefit from it due to low efficiency, high drug resistance, severe toxicity and potential for relapse. A recent study found that both tumor cells and tumor-infiltrating cells are involved in the development of drug resistance (42). As for the other defects are due to insufficient of systematic cognization of immunotherapy. Recent studies related the heterogeneity identified by scRNA-seq in human cancers to cell types found in murine tumor models and identified many functional sub clusters responsible for the poor immunotherapy response such as CXCL13+BHLHE40+ Th1-like cell population (43), C1QC+SPP1+TAMs (13), XCR1 +CADM1+cDC, CD1A+ CD172A+cDC (44), which provides many valuable insights for the development of clinical strategies. Although recent studies have made significant progress in resolving the problem of heterogeneity, there are obvious shortcomings in elucidating the common features of newly defined immunosuppressive cells such as Tex and TAMs.

In this study, we leverage the advantage of integrated scRNA-seq and bulk RNA-seq as well as a variety of bioinformatics analyses to clarify the heterogeneity and convergence of TME in CRC. Eight main cell types were identified preliminarily and 25 sub cell types were further distinguished after improving the resolution. It was found that the metabolic patterns and immunophenotypes displayed by each cell type were extremely different. However, we were surprised to find that multiple sub cell types manifest similar metabolic patterns and immunosuppressive functions at the end of differentiation trajectory. Meanwhile, we found similar immunosuppressant ligand-receptor pairs in Tex, TAMs, and fibroblast-2 sub cell types by intercellular communication network analysis, and similar TFs regulating lipid metabolic remodeling were found in transcription factor regulatory network analysis.

Since it is impossible to adequately characterize the tumor microenvironment in CRC, we selected several specific cell types, such as CD8+ T cells, myeloid cells and fibroblasts representing the main components of the TME, to illustrate its heterogeneity and convergence. Our key conclusions are as follows:

First, we identified that the immunosuppressive microenvironment of CRC was co-shaped by immune cells, stromal cells and tumor cells. Meanwhile, for each cell type the cells closer to the end of their differentiation trajectory showed more immunosuppressive characteristics, such as exhaustion in CD8+ T cells and polarization to the M2 phenotype in TAMs. In this process, proinflammatory functions were inhibited, whereas immunosuppression functions were enhanced. In addition, the intercellular communication network showed more active secretion of immunosuppressive cytokines by cells closer to the end of their differentiation trajectory. For example, in the regulation of IRS, exhaustion was the inevitable outcome of CD8+ T cells mediated by various cells in the TME. At the same time, different cells manifested different ligand modes. Tumor cells mainly secreted PVR and NECTIN2 to act on the TIGIT receptor. CD80 and CD86 secreted by DCs and TAMs interacted with CTLA-4 and Tregs mainly secreted CD274 to act on PDCD1. Soluble cytokines such as IL-10 and SPP1 were secreted by TAMs. More importantly, there are multiple positive feedback loops among intercellular subgroups. For example, the network analysis of IL-10 implied a potential positive feedback loop between macrophages and TAMs to promote the differentiation process. The positive feedback loop may equally be applied to SPP1 in TAMs to maintain the M2 phenotype. Therefore, we speculate that these inhibitory ligand-receptor pairs and positive feedback loops of cytokines are involved

10.3389/fimmu.2022.1003419

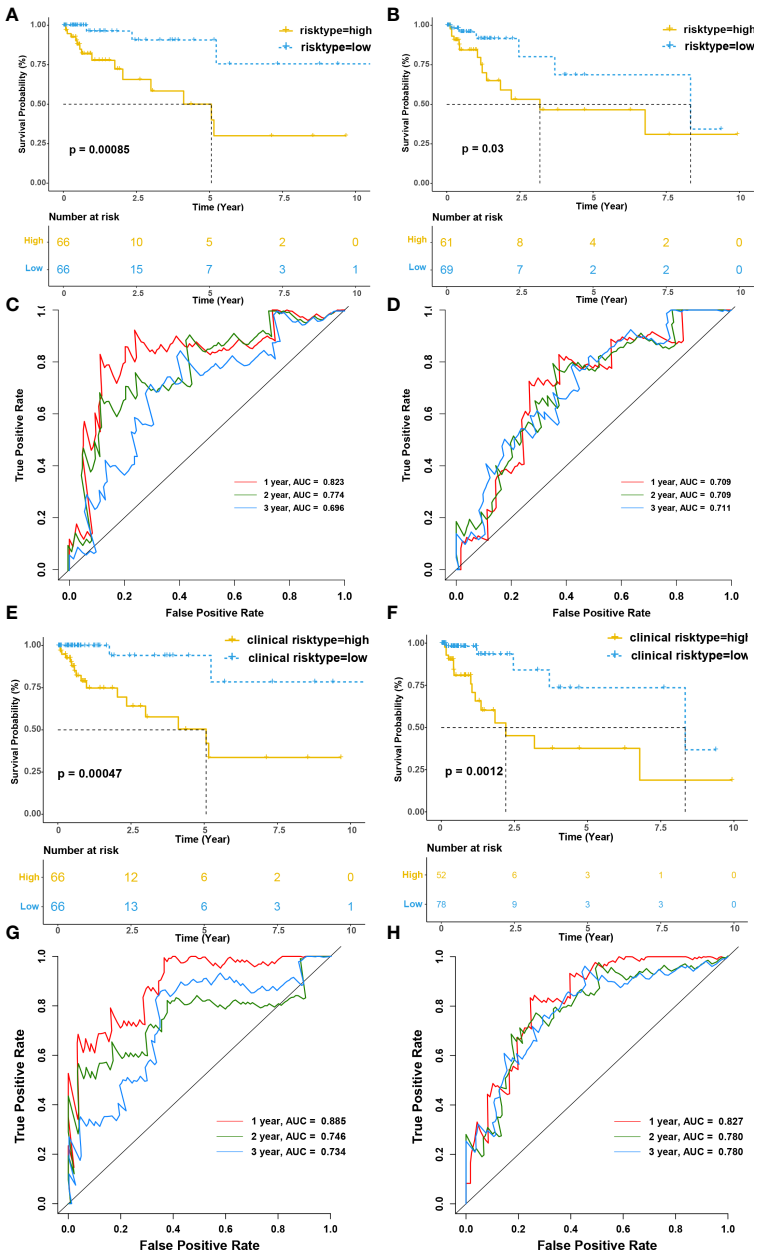

FIGURE 7
Infiltration of tumor-educated immune cells is associated with a worse prognosis in CRC. **(A, B)** Kaplan–Meier survival curves of immune risk model for the training **(A)** and testing cohorts**(B)**, respectively. **(C, D)** The time-dependent ROC curves of immune risk model for 1-, 2- and 3-OS year in the training **(C)** and testing cohorts **(D)**, respectively. The areas under the ROC curve for 1-, 2- and 3- year OS were 0.823, 0.774, and 0.696 in the training cohort and 0.709, 0.709 and 0.711 for 1-, 2- and 3- year OS in the testing cohort. **(E, F)** Kaplan–Meier survival curves of clinical risk model for the training **(E)** and testing cohorts**(F)**, respectively. **(G, H)** The time-dependent ROC curves of clinical risk model for 1-, 2- and 3- OS year in the training **(G)** and testing cohorts **(H)**, respectively. The areas under the ROC curve for 1-, 2- and 3- year OS were 0.823, 0.774, and 0.696 in the training cohort and 0.709, 0.709 and 0.711 for 1-, 2- and 3- year OS in the testing cohort.

in the construction and maintenance of the immunosuppressive microenvironment, and are also important potential targets for our immunotherapy and targeted therapy.

As mentioned above, we mapped the differentiation pathways of each cell type and found that different subgroups of each cell type had different metabolic patterns. Interestingly, although the metabolic patterns of each subgroups within the certain cell types were diverse, those cells close to their terminal differentiation trajectory showed similar metabolic patterns, namely enhanced lipid metabolism and abnormal

accumulation of intracellular lipid. SCENIC analysis revealed that the transcription factors that regulate lipid metabolism remodeling in each cell type partially overlapped. The most representative transcription factors are PPARG, SREBF, NR1H2, and NR1H3. The genes regulated by NR1H2 and NR1H3 were linked to cholesterol transport and efflux, and the outflow of cholesterol could destroy the lipid rafts on cell membranes, attenuating the TLR4 signaling pathway. Furthermore, increased cholesterol outflow also enhanced the IL-4 pathway and attenuated the IFN pathway. This phenomenon implied that enhanced intracellular lipid metabolism might be an important factor in the transformation of immune function, and transcription factors involved in lipid metabolism remodeling in cells may be potential therapeutic targets to reverse immunosuppression.

We applied CIBERSORTx algorithm to quantitatively assess the association between the proportion of cell subgroups in TME and prognosis in CRC. KM survival analysis and ROC curve analysis suggest that our immune risk model is an effective clinical prediction tool, which can improve the accuracy of survival prediction in CRC patients. Furthermore, the clinical risk model constructed by incorporating immune risk type and TNM stage could not only predict the survival prognosis of colorectal cancer patients, but also had significantly better AUC values at 1, 2 and 3 years than immune risk model both in training and testing cohorts. In addition, validation prognostic model showed similar prognostic value to our immune risk model whereas worse than our clinical risk model. This indicates that the risk prognosis model based on cell proportion in TME can supplement the existing clinical prognosis criteria and is a method with great prospects in clinical practice applications.

Currently, conventional RNA sequencing is the mainstream sequencing technology, but its gene expression level is the mixed expression of all cells in the tissue after lysis. Although simple and intuitive, it cannot reflect the gene expression of a single cell or a single cell group. With the further analysis, the accuracy of sequencing is required to be higher and higher. With its high-precision sequencing analysis, scRNA-seq has become a powerful technology in modern medical research, but this technology cannot be applied to most preserved tissue samples and is expensive, so it cannot be used as a routine clinical treatment project. The deconvolution algorithm CIBERSORTx can not only deconstruct ordinary RNA-seq to achieve the secondary utilization of data, but also to some extent make up for the shortcomings of scNA-SEQ tissue samples, such as high requirements, high price and insufficient sample size. More importantly, with the progress of sequencing technology, the cost of ordinary RNA-SEQ will gradually decrease, while the accuracy and data volume of scRNA-seq will continue to improve. Meanwhile, deconvolution algorithms like CIBERSORTx will also continue to improve, which means that in the near future, more and more patients with colorectal cancer can benefit from the high-precision analysis of scRNA-seq while enjoying the low cost of ordinary RNA-seq.

Although the heterogeneity and convergence of CRC microenvironment were further analyzed by using scRNA-seq and constructed an immune risk prognostic model based on CIBERSORTx algorithm and bulk RNA-seq data in this study, there are still some limitations. First of all, our data sources are all public databases, so we cannot obtain all clinical information that is meaningful for the study, such as tumor size, location, differentiation degree, pathological classification, immunohistochemical results, surgical methods, postoperative radiotherapy and chemotherapy, and patients' underlying diseases, etc. This will inevitably lead to the introduction of confounding factors in the construction of the prognostic model, and cause certain deviations in the final results. Secondly, although our single-celled sequencing analysis at the cellular level to reveal the gene expression, and through a variety of biological information analysis method to predict and infer the trajectory, regulation and control of transcription factors, cell differentiation and intercellular communication network, but has not been experimental verification, the follow-up still need further perfect the related experiments *in vivo* and *in vitro* in order to strengthen the reliability of conclusions.

9 Conclusion

This study further revealed the heterogeneity and convergence in TME, especially the high consistent lipid metabolism remodeling and immunosuppressive phenotype during the differentiation of each cell subpopulation, providing a new perspective for the targeted therapy and immunotherapy of colorectal cancer. Meanwhile, CIBERSORTx algorithm was used to integrate scRNA-seq and bulk RNA-seq data to construct immune risk model and clinical risk model, providing reference value for prognostic analysis of colorectal cancer patients. In conclusion, this study provides a new perspective for understanding the heterogeneity and convergence of the TME and will aid the development of immunotherapies to treat CRC.

Data availability statement

Publicly available datasets were analyzed in this study. This data can be found here: Gene Expression Omnibus (GEO, http://www.ncbi.nlm.nih.gov/geo/) database, GSE146771.

Author contributions

JY and JM designed the study and reviewed the literature. SX performed the data analyses and wrote the manuscript for the study. YC and DC downloaded the data from GEO database and participated in the drafting of the manuscript. WC contributed to the reviewing of the literature. YX contributed to the literature research. All authors contributed to the article and approved the submitted version.

Funding

This work was supported by grants from the National Natural Science Foundation of China (No. 81773065); Natural Science Foundation of Zhejiang Province (No. LY21H160023).

Acknowledgments

We would like to thank Dr. Hao Wu for reviewing the manuscript and constructive suggestions.

Conflict of interest

The authors declare that the research was conducted in the absence of any commercial or financial relationships that could be construed as a potential conflict of interest.

Publisher's note

Supplementary material

The Supplementary Material for this article can be found online at: https://www.frontiersin.org/articles/10.3389/fimmu.2022.1003419/full#supplementary-material

References

1. Sung H, Ferlay J, Siegel RL, Laversanne M, Soerjomataram I, Jemal A, et al. Global cancer statistics 2020: GLOBOCAN estimates of incidence and mortality worldwide for 36 cancers in 185 countries. *CA Cancer J Clin* (2021) 71(3):209–49. doi: 10.3322/caac.21660

2. Dekker E, Tanis PJ, Vleugels JLA, Kasi PM, Wallace MB. Colorectal cancer. *Lancet* (2019) 394(10207):1467–80. doi: 10.1016/S0140-6736(19)32319-0

3. Papalexi E, Satija R. Single-cell RNA sequencing to explore immune cell heterogeneity. *Nat Rev Immunol* (2018) 18(1):35–45. doi: 10.1038/nri.2017.76

4. Wherry EJ. T Cell exhaustion. *Nat Immunol* (2011) 12(6):492–9. doi: 10.1038/ni.2035

5. Ribas A, Wolchok JD. Cancer immunotherapy using checkpoint blockade. *Science* (2018) 359(6382):1350–5. doi: 10.1126/science.aar4060

6. Boussiotis VA. Molecular and biochemical aspects of the PD-1 checkpoint pathway. *N Engl J Med* (2016) 375(18):1767–78. doi: 10.1056/NEJMra1514296

7. Lu P, Youngblood BA, Austin JW, Mohammed AU, Butler R, Ahmed R, et al. Blimp-1 represses CD8 T cell expression of PD-1 using a feed-forward transcriptional circuit during acute viral infection. *J Exp Med* (2014) 211(3):515–27. doi: 10.1084/jem.20130208

8. Kao C, Oestreich KJ, Paley MA, Crawford A, Angelosanto JM, Ali MA, et al. Transcription factor T-bet represses expression of the inhibitory receptor PD-1 and sustains virus-specific CD8+ T cell responses during chronic infection. *Nat Immunol* (2011) 12(7):663–71. doi: 10.1038/ni.2046

9. Denardo DG, Ruffell B. Macrophages as regulators of tumour immunity and immunotherapy. *Nat Rev Immunol* (2019) 19(6):369–82. doi: 10.1038/s41577-019-0127-6

10. Sahai E, Astsaturov I, Cukierman E, Denardo D G, Egeblad M, Evans RM, et al. A framework for advancing our understanding of cancer-associated fibroblasts. *Nat Rev Cancer* (2020) 20(3):174–86. doi: 10.1038/s41568-019-0238-1

11. Papadopoulos KP, Gluck L, Martin LP, Olszanski AJ, Tolcher AW, Ngarmchamnanrith G, et al. First-in-Human study of AMG 820, a monoclonal anti-Colony-Stimulating factor 1 receptor antibody, in patients with advanced solid tumors. *Clin Cancer Res* (2017) 23(19):5703–10. doi: 10.1158/1078-0432.Ccr-16-3261

12. González-Silva L, Quevedo L, Varela I. Tumor functional heterogeneity unraveled by scRNA-seq technologies. *Trends Cancer* (2020) 6(1):13–9. doi: 10.1016/j.trecan.2019.11.010

13. Zhang L, Li Z, Skrzypczynska KM, Fang Q, Zhang W, O'brien SA, et al. Single-cell analyses inform mechanisms of myeloid-targeted therapies in colon cancer. *Cell* (2020) 181(2):442–459.e29. doi: 10.1016/j.cell.2020.03.048

14. Butler A, Hoffman P, Smibert P, Papalexi E, Satija R. Integrating single-cell transcriptomic data across different conditions, technologies, and species. *Nat Biotechnol* (2018) 36(5):411–+. doi: 10.1038/nbt.4096

15. Kobak D, Berens P. The art of using t-SNE for single-cell transcriptomics. *Nat Commun* (2019) 10.

16. Zhang XX, Lan YJ, Xu JY, Quan F, Zhao EJ, Deng CY, et al. CellMarker: a manually curated resource of cell markers in human and mouse. *Nucleic Acids Res* (2019) 47(D1):D721–8. doi: 10.1093/nar/gky900

17. Qiu XJ, Mao Q, Tang Y, Wang L, Chawla R, Pliner HA, et al. Reversed graph embedding resolves complex single-cell trajectories. *Nat Methods* (2017) 14 (10):979–+. doi: 10.1038/Nmeth.4402

18. Zhou YY, Zhou B, Pache L, Chang M, Khodabakhshi AH, Tanaseichuk O, et al. Metascape provides a biologist-oriented resource for the analysis of systems-level datasets. *Nat Commun* (2019) 10

19. Jin SQ, Guerrero-Juarez CF, Zhang LH, Chang I, Ramos R, Kuan CH, et al. Inference and analysis of cell-cell communication using CellChat. *Nat Commun* (2021) 12(1)

20. Aibar S, Gonzalez-Blas CB, Moerman T, Van AHT, Imrichova H, Hulselmans G, et al. SCENIC: single-cell regulatory network inference and clustering. *Nat Methods* (2017) 14(11):1083–+. doi: 10.1038/Nmeth.4463

21. Suo SB, Zhu Q, Saadatpour A, Fei LJ, Guo GJ, Yuan GC. Revealing the critical regulators of cell identity in the mouse cell atlas. *Cell Rep* (2018) 25 (6):1436–+. doi: 10.1016/j.celrep.2018.10.045

22. Newman AM, Steen CB, Liu CL, Gentles AJ, Chaudhuri AA, Scherer F, et al. Determining cell type abundance and expression from bulk tissues with digital cytometry. *Nat Biotechnol* (2019) 37(7):773–+. doi: 10.1038/s41587-019-0114-2

23. Crespo J, Sun H, Welling TH, Tian Z, Zou W. T Cell anergy, exhaustion, senescence, and stemness in the tumor microenvironment. *Curr Opin Immunol* (2013) 25(2):214–21. doi: 10.1016/j.coi.2012.12.003

24. Moore KJ, Rosen ED, Fitzgerald ML, Randow F, Andersson LP, Altshuler D, et al. The role of PPAR-gamma in macrophage differentiation and cholesterol uptake. *Nat Med* (2001) 7(1):41–7. doi: 10.1038/83328

25. Kobayashi T, Lam PY, Jiang H, Bednarska K, Gloury R, Murigneux V, et al. Increased lipid metabolism impairs NK cell function and mediates adaptation to the lymphoma environment. *Blood* (2020) 136(26):3004–17. doi: 10.1182/blood.2020005602

26. Musso G, Gambino R, Cassader M. Cholesterol metabolism and the pathogenesis of non-alcoholic steatohepatitis. *Prog Lipid Res* (2013) 52(1):175–91. doi: 10.1016/j.plipres.2012.11.002

27. Yuan X, Dong D, Li Z, Wu B. Rev-erbα activation down-regulates hepatic Pck1 enzyme to lower plasma glucose in mice. *Pharmacol Res* (2019) 141:310–8. doi: 10.3322/caac.21660

28. Olingy CE, Dinh HQ, Hedrick CC. Monocyte heterogeneity and functions in cancer. *J Leukoc Biol* (2019) 106(2):309–22. doi: 10.1002/jlb.4ri0818-311r

29. Meng ZZ, Liu W, Xia Y, Yin HM, Zhang CY, Su D, et al. The pro-inflammatory signalling regulator Stat4 promotes vasculogenesis of great vessels derived from endothelial precursors. *Nat Commun* (2017) 8:14640. doi: 10.1038/ncomms14640

30. Dong C, Zhao G, Zhong M, Yue Y, Wu L, Xiong S. RNA Sequencing and transcriptomal analysis of human monocyte to macrophage differentiation. *Gene* (2013) 519(2):279–87. doi: 10.1016/j.gene.2013.02.015

31. Xu M, Pokrovskii M, Ding Y, Yi R, Au C, Harrison OJ, et al. C-MAF-dependent regulatory T cells mediate immunological tolerance to a gut pathobiont. *Nature* (2018) 554(7692):373–7. doi: 10.1038/nature25500

32. Cheng X, Jin Z, Ji X, Shen X, Feng H, Morgenlander W, et al. ETS variant 5 promotes colorectal cancer angiogenesis by targeting platelet-derived growth factor BB. *Int J Cancer* (2019) 145(1):179–91. doi: 10.1002/ijc.32071

33. Koh B, Hufford MM, Sun X, Kaplan MH. Etv5 regulates IL-10 production in Th cells. *J Immunol* (2017) 198(5):2165–71. doi: 10.4049/jimmunol.1600801

34. Morita K, Okamura T, Sumitomo S, Iwasaki Y, Fujio K, Yamamoto K, et al. Emerging roles of Egr2 and Egr3 in the control of systemic autoimmunity. *Rheumatol (Oxford)* (2016) 55(suppl 2):ii76–81. doi: 10.1093/rheumatology/kew342

35. Veremeyko T, Yung AWY, Anthony DC, Strekalova T, Ponomarev ED. Early growth response gene-2 is essential for M1 and M2 macrophage activation and plasticity by modulation of the transcription factor CEBPβ. *Front Immunol* (2018) 9:2515. doi: 10.3389/fimmu.2018.02515

36. Zhang Y, Du W, Chen Z, Xiang C. Upregulation of PD-L1 by SPP1 mediates macrophage polarization and facilitates immune escape in lung adenocarcinoma. *Exp Cell Res* (2017) 359(2):449–57. doi: 10.1016/j.yexcr.2017.08.028

37. Liu C, Chikina M, Deshpande R, Menk AV, Wang T, Tabib T, et al. Treg cells promote the SREBP1-dependent metabolic fitness of tumor-promoting macrophages *via* repression of CD8(+) T cell-derived interferon-γ. *Immunity* (2019) 51(2):381–397.e6. doi: 10.1016/j.immuni.2019.06.017

38. Shimano H, Sato R. SREBP-regulated lipid metabolism: convergent physiology - divergent pathophysiology. *Nat Rev Endocrinol* (2017) 13(12):710–30. doi: 10.1038/nrendo.2017.91

39. Fang L, Miller YI. Regulation of lipid rafts, angiogenesis and inflammation by AIBP. *Curr Opin Lipidol* (2019) 30(3):218–23. doi: 10.1097/mol.0000000000000596

40. Goossens P, Rodriguez-Vita J, Etzerodt A, Masse M, Rastoin O, Gouirand V, et al. Membrane cholesterol efflux drives tumor-associated macrophage reprogramming and tumor progression. *Cell Metab* (2019) 29(6):1376–1389.e4. doi: 10.1016/j.cmet.2019.02.016

41. Scavo MP, Fucci L, Caldarola L, Mangia A, Azzariti A, Simone G, et al. Frizzled-10 and cancer progression: Is it a new prognostic marker? *Oncotarget* (2018) 9(1):824–30. doi: 10.18632/oncotarget.23159

42. Wu T, Dai Y. Tumor microenvironment and therapeutic response. *Cancer Lett* (2017) 387:61–8. doi: 10.1016/j.canlet.2016.01.043

43. Zhang L, Yu X, Zheng L, Zhang Y, Li Y, Fang Q, et al. Lineage tracking reveals dynamic relationships of T cells in colorectal cancer. *Nature* (2018) 564 (7735):268–72. doi: 10.1038/s41586-018-0694-x

44. Zilionis R, Engblom C, Pfirschke C, Savova V, Zemmour D, Saatcioglu HD, et al. Single-cell transcriptomics of human and mouse lung cancers reveals conserved myeloid populations across individuals and species. *Immunity* (2019) 50(5):1317–1334.e10. doi: 10.1016/j.immuni.2019.03.009

10.3389/fimmu.2022.1003419

Glossary

CRC	colorectal cancer
SCENIC	single-cell regulatory network inference and clustering
TCGA	The Cancer Genome Atlas
HER2	human epidermal growth factor receptor 2
EGFR	epidermal growth factor receptor
TME	tumor microenvironment
Tex	exhausted CD8 T cell
TAM	tumor-associated macrophages
CAF	cancer-associated fibroblasts
ICB	Immune checkpoint blockade
PD-1	programmed cell death 1
CTLA-4	cytotoxic T lymphocyte-associated protein 4
dMMR	mismatch-repair-deficient
MSI-H	microsatellite instability-high
MSI	microsatellite instability
IRS	inhibitory receptors
scRNA-seq	single-cell RNA sequencing
TNM	the tumor
nodes	and metastasis
QC	quality control
ILC	innate lymphoid cell
DC	dendritic cells
BEAM	branch expression analysis modeling
Teff	T effector cell
DEG	differentially expressed genes
AMPK	Adenosine 5’-monophosphate -activated protein kinase
GSVA	gene set variation analysis
FA	fatty acid
SREBP	Sterol regulatory element binding protein
FASN	atty acid synthase
ACC	Acetyl-CoA Carboxylase
HMG-CoA	3-hydroxy-3methylglutary-coenzyme A
ACLY	ATP-citrate lyase
PPAR	peroxisome proliferator-activated receptor
TF	transcription factors
TGF-β	transforming growth factor-beta

(Continued)

CONTINUED

IFNα/β	interferons alpha and beta
TNF	tumor necrosis factor
IL	interleukin
Treg	regulatory T cells
PVR	poliovirus receptor
TIGIT	T cell immunoreceptor with immunoglobulin and ITIM domain
ICOSL/ ICOS	Inducible Co-Stimulator Ligand/Inducible Co-Stimulator
TIM3	the inhibitory receptor T-cell immunoglobulin and mucin domain 3
LAG3	lymphocyte activation gene 3 protein
MSI-L	microsatellite instability-low
VEGF	vascular endothelial-derived growth factor
ZEB1	zinc finger E-box binding homeobox 1
MMP	matrix metalloproteinase
TLR4	Toll-like Receptor 4
TCA	tricarboxylic acid
FZD	Frizzled
GPCR	G-protein-coupled receptor
BMP	bone morphogenetic protein
Dvl	Disheveled
AhR	aryl hydrocarbon receptor
EMT	epithelial–mesenchymal transition
TCGA-COAD	The Cancer Genome Atlas-Colon Adenocarcinoma
OS	overall survival
ROC	receiver operating characteristic
KM	Kaplan-Meier
GEO	Gene Expression Omnibus
PC	principal component
tSNE	t-distributed stochastic neighbor-embedding
CSI	Connection Specificity Index
TPM	transcripts per million
NR1H3	Liver X receptors alpha
NR1H2	Liver X receptors beta

frontiers | Frontiers in Immunology

TYPE Original Research
PUBLISHED 10 January 2023
DOI 10.3389/fimmu.2022.1074762

OPEN ACCESS

EDITED BY
Silvia Pesce,
University of Genoa, Italy

REVIEWED BY
Annalisa Del Prete,
University of Brescia, Italy
Guido Ferlazzo,
University of Messina, Italy

*CORRESPONDENCE
Silvia Della Bella
silvia.dellabella@unimi.it
Domenico Mavilio
domenico.mavilio@unimi.it

†PRESENT ADDRESS
Clelia Peano,
Genomic Research Centre,
Human Technopole, Milan, Italy

‡These authors have contributed equally to this work

§These authors share last authorship

SPECIALTY SECTION
This article was submitted to Cancer Immunity and Immunotherapy, a section of the journal Frontiers in Immunology

RECEIVED 19 October 2022
ACCEPTED 22 December 2022
PUBLISHED 10 January 2023

CITATION
Carenza C, Franzese S, Castagna A, Terzoli S, Simonelli M, Persico P, Bello L, Nibali MC, Pessina F, Kunderfranco P, Peano C, Balin S, Mikulak J, Calcaterra F, Bonecchi R, Savino B, Locati M, Della Bella S and Mavilio D (2023) Perioperative corticosteroid treatment impairs tumor-infiltrating dendritic cells in patients with newly diagnosed adult-type diffuse gliomas.
Front. Immunol. 13:1074762.
doi: 10.3389/fimmu.2022.1074762

Perioperative corticosteroid treatment impairs tumor-infiltrating dendritic cells in patients with newly diagnosed adult-type diffuse gliomas

Claudia Carenza[1,2‡], Sara Franzese[1,2‡], Alessandra Castagna[3], Sara Terzoli[2,4], Matteo Simonelli[4,5], Pasquale Persico[4,5], Lorenzo Bello[6,7], Marco Conti Nibali[6], Federico Pessina[4,8], Paolo Kunderfranco[9], Clelia Peano[10†], Simone Balin[1,2], Joanna Mikulak[2], Francesca Calcaterra[1,2], Raffaella Bonecchi[4,11], Benedetta Savino[1,3], Massimo Locati[1,3], Silvia Della Bella[1,2*§] and Domenico Mavilio[1,2*§]

[1]Department of Medical Biotechnologies and Translational Medicine, University of Milan, Milan, Italy, [2]Laboratory of Clinical and Experimental Immunology, IRCCS Humanitas Research Hospital, Rozzano, Milan, Italy, [3]Laboratory of Leukocyte Biology, IRCCS Humanitas Research Hospital, Rozzano, Milan, Italy, [4]Department of Biomedical Sciences, Humanitas University, Pieve Emanuele, Milan, Italy, [5]Department of Medical Oncology and Hematology, IRCCS Humanitas Research Hospital, Rozzano, Milan, Italy, [6]Unit of Oncological Neurosurgery, IRCCS Istituto Ortopedico Galeazzi, Milan, Italy, [7]Department of Oncology and Hemato-Oncology, University of Milan, Milan, Italy, [8]Department of Neurosurgery, IRCCS Humanitas Research Hospital, Rozzano, Milan, Italy, [9]Bioinformatics Unit, IRCCS Humanitas Research Hospital, Rozzano, Milan, Italy, [10]Institute of Genetic and Biomedical Research, UoS Milan, National Research Council, Rozzano, Milan, Italy, [11]Laboratory of Chemokine Biology, IRCCS Humanitas Research Hospital, Rozzano, Milan, Italy

Introduction: Adult-type diffuse gliomas are malignant primary brain tumors characterized by very poor prognosis. Dendritic cells (DCs) are key in priming antitumor effector functions in cancer, but their role in gliomas remains poorly understood.

Methods: In this study, we characterized tumor-infiltrating DCs (TIDCs) in adult patients with newly diagnosed diffuse gliomas by using multi-parametric flow cytometry and single-cell RNA sequencing.

Results: We demonstrated that different subsets of DCs are present in the glioma microenvironment, whereas they are absent in cancer-free brain parenchyma. The largest cluster of TIDCs was characterized by a transcriptomic profile suggestive of severe functional impairment. Patients undergoing perioperative corticosteroid treatment showed a significant reduction of conventional DC1s, the DC subset with key functions in antitumor immunity. They also showed phenotypic and transcriptional evidence of a more severe functional impairment of TIDCs.

10.3389/fimmu.2022.1074762

Discussion: Overall, the results of this study indicate that functionally impaired DCs are recruited in the glioma microenvironment. They are severely affected by dexamethasone administration, suggesting that the detrimental effects of corticosteroids on DCs may represent one of the mechanisms contributing to the already reported negative prognostic impact of steroids on glioma patient survival.

KEYWORDS

dendritic cells, brain tumors, perioperative corticosteroids, immune suppressive tumor microenvironment, single cell-RNA sequencing

Introduction

Gliomas represent 75% of malignant primary brain tumors in adults, and still remain among the most difficult cancers to treat (1). Their severity relies on a combination of histological features and signature molecular genetic alterations. According to the increasingly recognized role of molecular markers in predicting clinical behavior, the classification of gliomas is rapidly changing. The 2021 WHO classification of central nervous system tumors subdivides adult-type diffuse gliomas into isocitrate dehydrogenase (IDH)-mutant astrocytoma, IDH-mutant and 1p/19q codeleted oligodendroglioma, and IDH-wildtype glioblastoma (2). Although all diffuse gliomas are highly infiltrative and resistant to therapy, IDH-wildtype glioblastomas are characterized by the worst prognosis, with most patients not surviving beyond a year despite standard of care treatment, which consists of maximal safe surgical resection followed by chemoradiation (3).

The urgent need for more efficacious treatments for patients with gliomas, together with the recent progresses of anticancer immunotherapies (4), has renewed the interest in developing novel immunotherapeutic approaches also for gliomas. In this regard, the use of immune checkpoint inhibitors and peptide vaccination have so far failed to improve the survival in these patients, likely because of the low immunogenicity and the highly immunosuppressive tumor microenvironment (TME) that characterize gliomas (5, 6). Among other immunotherapeutic approaches, dendritic cell (DC)-based immunotherapy represents a promising strategy to better control the clinical progression of gliomas (7, 8). Indeed, recent clinical trials demonstrated the ability of DC vaccination protocols to generate potent tumor-specific immune responses *in vivo* and partial benefit on overall and progression-free-survival rates (8). In order to further improve the efficacy of these immunotherapeutic protocols, next generation DC-based vaccines aim at exploiting specific DC subsets able to infiltrate gliomas and to prime/boost cytotoxic T cell-driven anti-cancer immunity (9, 10). Other developing strategies aimed at potentiating the effects of DCs in cancer immunotherapy include the use of DC vaccines in combination with other anticancer therapies, and the reprogramming of tumor-infiltrating DCs towards the promotion of tumor rejection (9, 11, 12). In order to achieve these goals for the treatment of gliomas, a precise characterization of glioma-infiltrating DC subsets, their activatory/tolerogenic profile, and the molecular mechanisms involved in glioma-induced DC tolerogenicity is needed.

DCs are a heterogenous population of professional antigen presenting cells (APCs) that play a central role in the activation and regulation of all immune responses (13). DC-lineage DCs are subdivided into plasmacytoid DCs (pDCs) and conventional DCs (cDCs), which are further divided into cDC1 and cDC2 subsets. pDCs are endowed with the ability to produce high amounts of type I interferon (IFN) in response to viral infections, but in resting conditions they are mainly tolerogenic. Therefore, pDCs in the TME can contribute to tumor-specific tolerance and are associated with a bad prognosis (14). cDC1s are the most efficient DCs in priming cytotoxic T cells due to their high cross-presentation properties, and their presence in the TME is associated with better survival across several types of human cancers (15). cDC2s are mainly specialized in the activation of helper T cells that can be differentially polarized depending on the environmental conditions that sustain cDC2 activation (16). Further subsets of inflammatory DCs can also contribute to the overall shaping of antitumor immune responses exerted by DCs (13). They include monocyte-derived DCs (moDCs), which are rare in human peripheral tissues at the steady-state but rapidly increase during inflammation (13); and 6-sulfo-LacNAc (slan) DCs, which in the blood have a transcriptional profile overlapping with CD16+ non-classical monocytes but in peripheral tissues can acquire typical DC functions (17).

Beyond their belonging to one of these subsets, the behaviour of DCs depends also on their state of activation that is in turn affected by stimuli provided by the tissue microenvironment where DCs reside or are recruited. Upon

exposure to inflammatory stimulation, DCs up-regulate the expression of MHC and costimulatory molecules, secrete pro-inflammatory cytokines, and present antigens to T cells in fully stimulatory conditions. On the other hand, DCs exposed to immunosuppressive environment express low levels of MHC and costimulatory molecules, up-regulate the expression of inhibitory molecules, secrete immunosuppressive cytokines, and present antigens to T cells in tolerogenic conditions (18). Accordingly, in cancer patients DCs are affected by the TME that undergoes profound changes during cancer progression (19, 20). While in the initial stages of cancer DCs activate robust tumor-specific cytotoxic T cells (11), during cancer progression DCs contribute to the tumor escape from immune surveillance by promoting tumor-specific immune tolerance and the development of an immunosuppressive TME (20).

The identification of DC subsets in the TME, together with the characterization of their activatory/tolerogenic profile, has been hampered so far by the low number of DCs in the TME and the lack of DC-specific markers. The recent implementation of high-dimensional single-cell technologies is making possible to define DC features at an unprecedented definition, both at the phenotypic and transcriptomic levels. Accordingly, DCs have started to be deeply characterized in the TME of different types of tumors, providing evidence that tumor immune evasion involves crippling normal DC functions, and that DC heterogeneity and states are conserved across various solid human cancers (21, 22). In the present study, we characterized peripheral blood DCs (PBDCs) and tumor-infiltrating DCs (TIDCs) in newly diagnosed adult-type diffuse glioma patients by using high-dimensional flow cytometry and single cell-RNA sequencing (scRNA-seq) approaches. Our results provide evidence that PBDCs are reduced in glioma patients, and that all subsets of DCs are recruited in the core lesions of glioma but they are functionally impaired. We also observed that the most dramatic reduction and functional impairment of DCs is evident in glioma patients undergoing perioperative steroid treatment to control peritumoral edema.

Methods

Study participants and ethics approval

The study was conducted on 27 newly diagnosed, non-relapsing adult patients with diffuse glioma undergoing surgical resection at the unit of Neuro-Oncology of Humanitas Research Hospital, Rozzano, Milan, Italy. Clinical patient information is provided in Supplementary Table 1. The study protocol was approved by the Institutional Review Boards of Humanitas Research Hospital (ONC-OSS-04-2017; 29/19), and written informed consents were provided by all participants before inclusion in the study in compliance with the Declaration of Helsinki. Twelve age- and sex-matched healthy volunteers were included as controls.

Sample processing and staining

Peripheral blood samples were collected from patients and controls in K2 EDTA BD vacutainer tubes (BD Diagnostics, Franklin Lakes, NJ, USA) and stained with an 18-color DC-dedicated flow cytometry panel of monoclonal antibodies (mAbs) as previously reported (23). 500 µL of whole blood were incubated with ammonium chloride (ACK, Ammonium chloride 0.83% w/v, Potassium Bicarbonate 0.1% w/v, Titriplex 0.004% w/v, Merck KGaA) to lyse erythrocytes and samples were stained with Fixable Viability Stain 780 (BD Biosciences), then washed and stained with the combination of mAbs listed in Supplementary Table 2. Staining conditions for each mAb were preliminarily determined in titration assays, as previously described (24).

Brain tissue samples obtained during surgery were collected, stored at 4°C in supplemented Dulbecco's Modified Eagle Medium (DMEM) high glucose (Lonza) added with 1% Penicillin/Streptomycin and 1% L-Glutamine and digested within 2 hours from excision with type IV Collagenase (1.6 mg/mL) (Merck KGaA) and type I DNase (0.4 mg/mL) (Merck KGaA) in Roswell Park Memorial Institute (RPMI) 1640 medium (Euroclone SpA) at 37°C for 1 hour. Homogenates were then smashed on a 70 µm filter (BD Biosciences), washed with RPMI with the addition of 2% fetal bovine serum (FBS) (Lonza), and collected in 50 mL collection tubes. Samples were then centrifuged at 290 rcf for 7 min, and the pelleted cells were incubated for 2 min with 1 mL of ACK 1X to lyse erythrocytes. Samples were then washed with FACS buffer (Hank's Balanced Salt Solution, HBSS, w/o Ca^{2+} and Mg^{2+}, Lonza, with the addition of 2% FBS), and centrifuged at 290 rcf for 7 min. The samples were then incubated with FACS buffer and Myelin Removal Beads II (Milteny Biotec) and passed through LS Columns (Milteny Biotec) according to manufacturer's instructions. The samples were stained with the same DC-dedicated flow cytometry panel used for peripheral blood samples.

Flow cytometry data acquisition and analysis

All data were acquired on a FACSymphony™ A5 flow cytometer (BD Biosciences). Flow Cytometry Standard (FCS) 3.0 files were imported into FlowJo software version 9.9.6 (FlowJo LLC), and data were compensated by using single-stained antibody-capture beads (CompBeads, BD Biosciences) as previously described (23–25). These data were analyzed by

standard gating strategy, as previously reported (14, 23). Briefly, gated on single, live $CD45^+$ (PB samples) or $CD45^{br}$ (tissue samples) mononuclear cells, DC-lineage DCs were identified within the gate of lineage (CD3, CD19, CD20, CD56)$^-$/$CD14^-$/$CD16^-$/$HLA\text{-}DR^+$ cells. Gated on these cells, pDCs were identified as $CD123^+$/$CD11c^-$ cells; cDCs were identified as $CD11c^+$/$CD123^-$ cells, and further divided into cDC1s and cDC2s based on the expression of CD141 and CD1c, respectively. Inflammatory DCs were identified as lin$^-$/$HLA\text{-}DR^+$/$CD11c^+$ cells that could be positive or negative for CD14 and CD16 expression. They included slanDCs that expressed M-DC8, and moDCs that expressed CD1a. The activation state of each DC subset was examined by assessing the expression of the activatory molecules CD40, CD80 and CD86, and the inhibitory molecules PD-L1, ILT2 and TIM-3. The compensated data were further imported into FlowJo software version 10.7.1 and visualised with a uniform manifold approximation and projection (UMAP). For the UMAP analysis, 2 different concatenated files were created, containing the same number of live $CD45^+$/lin$^-$/$HLA\text{-}DR^+$ cells derived respectively from whole blood of untreated patients (n=12) and whole blood of dex-treated patients (n=11). A unique computational barcode was assigned to each concatenated file. These files were then concatenated in a single file for further visualization in UMAP dot plots (distance function: Euclidean; nearest neighbours: 15; minimum distance: 0.5), based on the expression of the following markers: CD45, CD14, CD16, HLA-DR, CD11c, CD123, CD141, CD1c, M-DC8, CD1a, CD40, CD80, CD86, PD-L1, ILT2, TIM-3. The same analysis was applied also to the cells derived from the tumor, where 2 different concatenated files were created, containing the same number of live $CD45^{br}$/lin$^-$/$HLA\text{-}DR^+$ cells derived respectively from tumour tissue of untreated patients (n=5) and tumor tissue of dex-treated patients (n=3).

ScRNA-seq data processing and analysis

Feature-barcode matrices generated by Savino et al. were down-loaded from Zenodo Repository, where the original data have been deposited (https://zenodo.org/record/6046299#.YgZ6bpbSKN4) and analyzed with R (v3.5.1) toolkit Seurat (v3.0.2). For each sample, Seurat objects were created from feature-barcode matrices. Cells containing > 200 genes and ≤ 10% mitochondrial genes were kept for downstream analysis. Gene expression matrices were then log-normalized with a scale factor of 10,000.

Datasets of each sample were integrated by Seurat data integration pipeline and $CD45^+$ cells were subjected re-clustering, resulting in a total of 28 clusters (resolution level = 1.1). Cluster annotation was performed in silico using SingleR. The cell cluster enriched in DCs (cluster 19) was manually identified based on literature data obtained with scRNA-seq analyses of sorted DC subsets (26) and confirmed by using The Human Protein Atlas database (v20.1). The first 50 DEGs (p_{adj}<0.05) of cluster 19 were then identified by using the 'FindAllMarkers' function in Seurat, with the parameter 'test.use=wilcox' used by default. The aggregated expression scores of these DEGs were calculated on single-cell base using the 'AddModuleScore' function in Seurat. The distribution of DC subsets across different clusters at resolution 0.5 was investigated by analyzing the expression of genes characteristics of classical DC subsets and other subsets recently described on the basis of their transcriptomic profile, including preDCs, migDCs, cDC2A and cDC2B (21, 27–32).

Ingenuity pathway analysis

In order to investigate whether the cluster distribution of TIDCs may reflect DC functional state, we analyzed cell clusters at resolution 0.3 using IPA software program (Qiagen), which analyzes gene expression patterns using a built-in scientific literature-based database. DEGs that were characterized by p_{adj}<0.01, and $|\log_2 FC|$>0.58 were used for IPA analysis in the comparison between clusters 0 and 1, and between clusters 2 and 0. The *core analysis* function included in the software was performed on each cluster, applying the *immune cell* filter. DEGs were interrogated by Diseases and Functions (DFs) and Canonical Pathways (CPs) tools on IPA software. Only statistically significant DFs and CPs characterized by p<0.05 and |z-score|>1.5 were considered. Each gene identifier was mapped to its corresponding gene object in the Ingenuity Pathway Knowledge Base (IPKB).

Statistical analysis

Statistical analysis of flow cytometric results was performed using GraphPad Prism software, version 9.0.0. The normal distribution of data was tested by using Shapiro-Wilk's test. The t-test was used for comparisons between samples. All statistical analyses assumed a two-sided significance level of 0.05.

Results

DC-lineage DC subsets are decreased in the blood of patients with diffuse glioma.

We first analysed PBDCs by using a high-dimensional flow cytometry panel that allows the identification of five distinct DC subsets, namely pDCs, cDC1s, cDC2s, slanDCs, and moDCs (20, 23). Our results showed that the frequency of all subsets of DC-lineage PBDCs were significantly decreased in glioma patients compared with controls (Figure 1A). Among inflammatory DCs,

10.3389/fimmu.2022.1074762

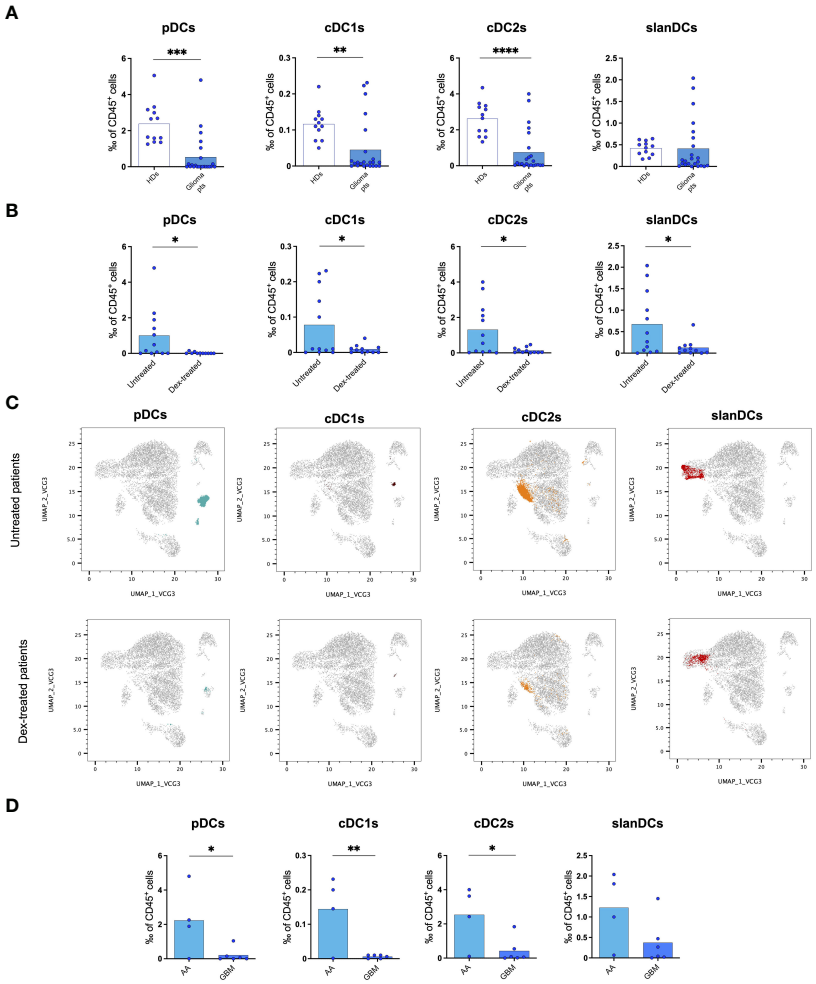

FIGURE 1
Flow cytometric analysis of PBDC subsets showing a reduction of circulating DCs in glioma patients. **(A)** Frequency of PBDC subsets in healthy donors (HDs, n=12) and glioma patients (Glioma pts, n=23). **(B)** Frequency of PBDC subsets in glioma patients either untreated (Untreated, n=12) or treated with dexamethasone (Dex-treated, n=11). Data expressed as per-thousand (‰) of $CD45^+$ cells. Each symbol represents a single sample. In each series, the mean is shown. *p<0.05, **p<0.01, ***p<0.001, ****p<0.0001, calculated using the t-test. **(C)** UMAP plots showing the clustering of PBDC subsets in untreated and dex-treated glioma patients. Each plot shows a single DC subset as identified with manual gating strategy. Viable circulating $CD45^+/lin^-/HLA\text{-}DR^+$ cells of down-sampled, concatenated files obtained from all glioma patients are shown in gray. pDCs are highlighted in dark turquoise, cDC1s in brown, cDC2s in orange, slanDCs in red. **(D)** Frequency of PBDC subsets in untreated IDH-wildtype glioma patients stratified based on histopathological diagnosis (anaplastic astrocytoma: AA, n=4; glioblastoma: GBM, n=6).

slanDCs did not significantly differ in glioma patients compared with controls. moDCs were almost undetectable in all blood samples, as expected (23). Similar results were observed when the absolute count of PBDC subsets was considered.

In order to investigate whether the reduction of PBDCs was associated with perioperative steroid treatment, we analysed PBDC subsets in our glioma patients stratified according to dexamethasone administration (dex-treated *vs* untreated patients). The frequency of all circulating DC subsets, including pDCs, cDC1s, cDC2s and slanDCs, was significantly lower in dex-treated compared with untreated patients (Figure 1B). Similar results were observed when the absolute count of PBDC subsets was considered. PBDC reduction in dex-treated patients was even more evident when DC subsets were visualized in UMAP plots of viable $CD45^+/lin^-/HLA\text{-}DR^+$ cells obtained from down-sampled and concatenated files of all blood samples of dex-treated and untreated glioma patients (Figure 1C).

According to the WHO 2021 classification of primary brain tumors, the majority of our patients subjected to PBDC investigation were affected by glioblastoma IDH-wildtype, the glioma group that accounts for all IDH-wildtype gliomas independently from histopathological diagnosis, and all labelled as WHO grade 4. However, a certain proportion of our patients belonging to this group had a histopathological diagnosis of anaplastic astrocytoma, which in the previous classification (WHO 2016) was labelled as WHO grade 3. In

order to investigate whether the reduction of PBDCs was associated with the histopathological diagnosis of gliomas, we analysed PBDC subsets in untreated patients (to avoid the confounding effect of dexamethasone) further stratified according to their histopathology and observed that, among patients with IDH-wildtype gliomas, the frequency of circulating pDCs, cDC1s and cDC2s was significantly lower in patients with a histopathological diagnosis of glioblastoma compared with those with anaplastic astrocytoma (Figure 1D).

Finally, we investigated the state of activation of PBDCs, and observed that the expression of the activation markers HLA-DR, CD40, CD80 and CD86, and inhibitory molecules PD-L1, ILT2 and TIM-3 on DC subsets did not differ between glioma patients and healthy donors, nor among patients stratified according to dex-treatment or histological diagnosis (data not shown).

All subsets of myeloid DCs infiltrate glioma lesions, whereas they are absent in tumor-free brain parenchyma

We then investigated the presence of TIDCs in glioma lesions by using the same flow cytometric approach used for their circulating counterparts. Three samples of healthy brain tissues obtained from patients affected by gliomas were included as controls. Our results showed that whereas the presence of all DC subsets was negligible in tumour-free brain parenchyma, cDC1s, cDC2s and the inflammatory slanDCs and moDCs, were abundant in the tumor infiltrate of glioma patients, without differences related to tumor histomolecular features. pDCs were detected only in one untreated glioblastoma, IDH-wildtype patient (Figure 2A). When assessing the impact of perioperative steroid treatment on TIDCs, we observed that dex-treated patients showed an overall reduction of TIDCs that was significant in the case of cDC1s, the DC subset with a prominent role in anti-tumor immunity (15) (Figure 2B). These results were even more evident in the UMAP plots of viable $CD45^{br}/lin^{-}/HLA\text{-}DR^{+}$ cells obtained from down-sampled and concatenated files of all tissue samples (Figure 2C).

Because DCs were negligible in tumor-free brain tissue, a comparison of DC phenotype between tumor and healthy brain was not possible. In order to investigate whether the state of activation of TIDCs was affected by perioperative steroid treatment, we also compared the expression of HLA-DR, the costimulatory molecules CD40, CD80 and CD86, and the immune checkpoints PD-L1 and ILT2 on each DC subset between dex-treated and untreated patients. Because of the low number of TIDCs, the analysis was performed on concatenated files of glioma samples. As shown in Figure 2D, we observed that tumor-infiltrating cDC1s, cDC2s, slanDCs and moDCs obtained from dex-treated patients showed a lower expression of HLA-DR and CD40 compared with untreated patients. Dex-induced immunophenotypic changes of pDCs could not be assessed because, as reported above, pDCs were negligible in the tumor infiltrate of dex-treated patients. The expression of the inhibitory molecule TIM-3 could not be assessed on TIDCs, because TIM-3 is cleaved by the collagenase treatment used for glioma tissue processing, as already reported (20).

ScRNA-seq analysis reveals distinct clusters of TIDCs in glioma lesions

After having demonstrated the presence of DCs in glioma core lesions, we characterized their molecular and functional features by analyzing their transcriptomic profile. To this aim, we analyzed scRNA-seq data generated from $CD45^{+}$ cells isolated from 7 core glioma lesions and 2 healthy brain tissue samples obtained from 8 different adult-type diffuse glioma patients, available in Zenodo Repository (https://zenodo.org/record/6046299#.YgZ6bpbSKN4). The Seurat integration procedure was used to remove batch effects. Based on their transcriptomes, unsupervised graph-based clustering partitioned 36,237 cells into 28 distinct clusters. Clusters 25, 26 and 27 were filtered-out because of their small size (less than 20 cells) and excluded from the analysis. We identified cluster 19 as the putative cluster of DCs based on previously reported DC transcriptomic signatures (27). In order to confirm the DC annotation of cluster 19, we selected the first 50 differentially expressed genes (DEGs) between cells included in this cluster and all the others (padj<0.05) (Figure 3A). Based on the information available in the human Blood Atlas (www.proteinatlas.org), we verified that all the 50 DEGs composing the signature were expressed by human DCs and, in particular, 22 of them were enriched in myeloid and/or plasmacytoid DCs (Supplementary Table 3). We then applied to the 50-gene signature the AddModuleScore function from Seurat package, which allows to compare the expression of a specific set of genes among different clusters, and we visualized the expression of this signature on a violin plot (Figure 3B). Taken together, these data confirmed that cluster 19 was the one containing DCs.

To investigate TIDC heterogeneity, we then performed a reclustering of cluster 19, and compared different clustering results for each resolution parameter, from 0 to 0.5. At resolution 0.1, we observed the formation of three main branches, one of which continuing to split up to the resolution 0.5 (Figure 3C). The smallest cluster, stable at resolutions from 0.1 to 0.5, was filtered-out because of its small size and excluded from subsequent analyses. We then focused our analyses on the remaining 4 clusters observed at resolution 0.5. In particular, in order to investigate whether they reflected the distribution of DCs in different subsets, we examined the expression of genes characteristic of DC subsets recently described on the basis of their transcriptomic profiles. Beyond the DC subsets that we

10.3389/fimmu.2022.1074762

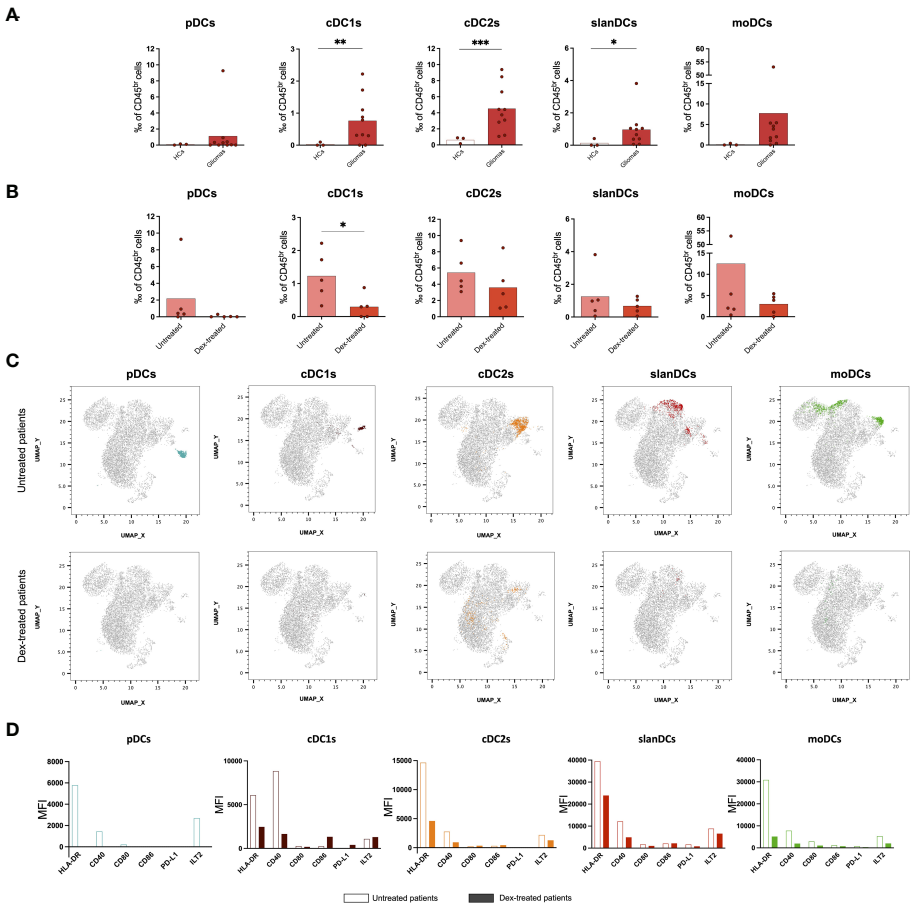

FIGURE 2
Flow cytometric analysis of TIDC subsets showing that perioperative corticosteroid treatment inhibits intratumoral DC recruitment and activation. **(A)** Frequency of DC subsets in healthy tissues (heathy controls: HCs, n=3) and tumor tissues (Gliomas, n=10) obtained from glioma patients. **(B)** Frequency of TIDC subsets in glioma patients either untreated (Untreated, n=5) or treated with dexamethasone (Dex-treated, n=5). Data expressed as per-thousand (‰) of $CD45^{br}$ cells. Each symbol represents a single sample. In each series, the mean is shown. *p<0.05, **p<0.01, ***p<0.001, calculated using the t-test. **(C)** UMAP plots showing the clustering of TIDC subsets in untreated and dex-treated glioma patients. Each plot shows a single DC subset as identified with manual gating strategy. Viable tumor-infiltrating $CD45^{br}/lin^{-}/HLA\text{-}DR^{+}$ cells of down-sampled, concatenated files obtained from all glioma patients are shown in gray. pDCs are highlighted in dark turquoise, cDC1s in brown, cDC2s in orange, slanDCs in red, and moDCs in green. **(D)** Expression of HLA-DR, activatory molecules (CD40, CD80, CD86), and inhibitory molecules (PD-L1, ILT2) on each DC subset, expressed as MFI measured on concatenated files, and compared between untreated and dex-treated glioma patients.

investigated by flow cytometry (namely, pDCs, cDC1s, cDC2s, slanDCs, moDCs), they include preDCs, migratory DCs (migDCs) and the cDC2 subclusters A and B endowed with regulatory and pro-inflammatory properties, respectively (27). Our results confirmed that genes belonging to the gene signature of all DC subsets were indeed expressed by glioma TIDCs (Figure 3D). However, the expression of the genes characteristic of each DC subset was widely spread among the 4 clusters, indicating that none of the clusters of TIDCs corresponded to any defined DC subset. Notably, according to the lack of DCs observed by flow cytometry in healthy brain tissues, cells obtained from healthy brain samples were negligible, indicating that all DCs analysed for transcriptome profiling were derived from core glioma lesions.

The largest cluster of TIDCs has a transcriptomic signature indicative of functional impairment

We further investigated whether the distribution of TIDC clusters in glioma may reflect different DC functional states, as similarly reported in human hepatocarcinoma (33). To this aim, we analysed cell clusters at resolution 0.3 by using the Ingenuity Pathway Analysis (IPA) software, an advanced bioinformatic tool that analyzes gene expression patterns using a built-in scientific literature-based database. We focused on the analysis of DEGs between the two largest clusters, namely clusters 0 and 1. Among 2309 DEGs between the two clusters, 2216 were down-regulated and 93 were up-regulated. By further setting a

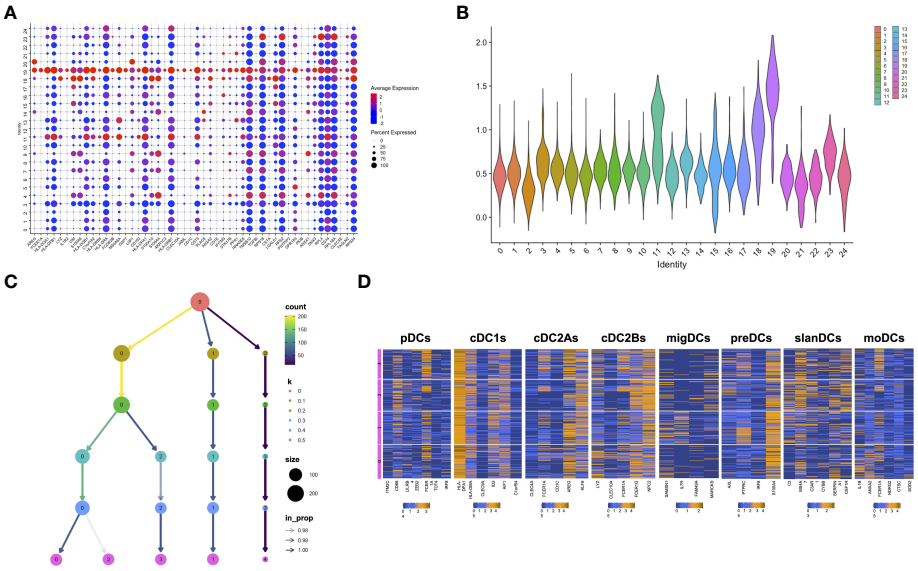

FIGURE 3
scRNAseq confirms the presence and heterogeneity of TIDCs. **(A)** Dot plot showing the first 50 DEGs (p_{adj}<0.05) between cluster 19 and all the other clusters that compose CD45$^+$ cells obtained from 7 tumor tissues and 2 healthy brain tissues from 8 glioma patients. All 50 genes are known to be enriched or expressed by human DCs, thus indicating that cluster 19 is the cluster of DCs. Color scale indicates the average expression level of genes; dot size indicates the percentage of gene-expressing cells in each cluster. **(B)** By applying the AddModuleScore function that allows to compare the expression of a specific set of genes among clusters, the expression of the 50-gene signature characterizing cluster 19 was visualized in a violin plot. **(C)** Reclustering of cluster 19 represented in a clustering tree based on kk-means. Nodes colored according to the value of k and sized according to the number of cells they represent. Edges colored according to the number of cells (from blue representing few to yellow representing many). Cluster labels are randomly assigned by the kk-means algorithm. **(D)** Heatmaps showing the mean expression of genes characteristic of pDCs, cDC1s, cDC2As, cDC2Bs, preDCs, migDCs, slanDCs, and moDCs, in clusters from 0 to 3 at resolution 0.5. Expression values are zero-centered and scaled for each gene. Each gene name is reported on the bottom of each heatmap.

threshold on |log2FC|>0.58, corresponding to a 1.5-fold change, we selected 1935 down-regulated and 80 up-regulated DEGs in cluster 0 compared with cluster 1 (Figure 4A). These genes were used for IPA functional annotation, applying a filter on immune cells. In particular, we applied the Diseases and Functions (DFs) analytics tool to define cellular processes and biological functions predicted to be affected on the basis of relative gene expression changes, and the Canonical Pathways (CPs) tool to predict which pathways were affected. The directional changes in both analyses were predicted by z-score. The analysis of DEGs categorized by DFs indicated that 502 processes and functions were differentially regulated (p<0.05) between cluster 0 and 1. Among these processes and functions, 173 were down-regulated in cluster 0 (as defined based on z-score <-1.5) and only 3 were up-regulated (as defined based on z-score >1.5); the remaining functions lacked z-score, or had a z-score between -1.5 and +1.5 (Supplementary Table 4). The analysis of DEGs categorized by CPs indicated that 191 pathways were differentially regulated (p<0.05) between cluster 0 and 1. Among these pathways, 141 were down-regulated in cluster 0 and 5 were up-regulated (Supplementary Table 5). The results of IPA functional annotation most relevant to TIDC functions in glioma microenvironment are summarized in Figures 4B–E. In particular, the analysis of DEGs categorized by DFs indicated that, based on gene expression, a relevant number of processes and functions relative to cellular migration, adhesion and homing were down-regulated in cluster 0 compared with cluster 1 (Figure 4B). Consistent with this observation, CPs involved in cellular motility, cytoskeleton rearrangement and cell-to-cell interactions were similarly down-regulated in cluster 0 (Figure 4C). In order to gain more insights into the DEGs underlying the down-regulation of these functions and pathways in glioma TIDCs, we examined the DEGs composing the processes and functions reported in Figure 4B and the pathways reported in Figure 4C, and obtained a list of 163 genes (reported in Supplementary Table 6). Supporting the impairment of functions relevant to DC migration and homing, DEGs in this group included genes encoding chemokine receptors or other chemotactic receptors (e.g., CXCR4, SLAMF1, ADGRE5, PTGER4), molecules involved in cytoskeleton rearrangement relevant to cell motility (e.g., S1PR1, MYH9, AKIRIN1, FGD3), metalloproteinases (e.g., MMP7), integrins (e.g., ITGA1, ITGA4, ITGAL), and other adhesion molecules involved in cell-to-cell interactions (e.g., F11R, CD44). Moreover, the analysis of DEGs categorized by DFs also indicated that a high number of processes and functions involved in immune cell activation were down-regulated in cluster 0 compared with cluster 1 (Figure 4D). Consistent with

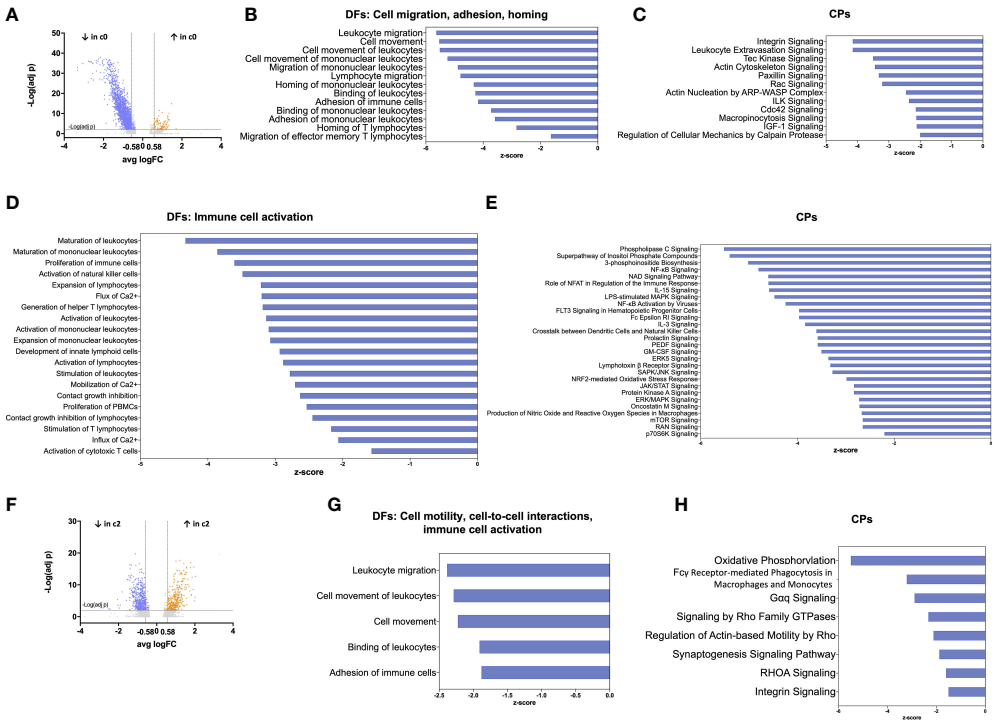

FIGURE 4
Functional annotation of TIDC clusters by IPA analysis reveals impairment of the largest cluster of DCs. **(A)** Volcano plot showing DEGs between cluster 0 (the largest cluster of TIDCs) and cluster 1, at resolution 0.3. Grey dots indicate genes that were not statistically significant (p_{adj}>0.01); orange dots indicate significantly up-regulated genes (with log_2FC>0.58), and blue dots indicate significantly down-regulated genes (with log_2FC<-0.58). **(B)** Bar plot showing DFs of sub-categories related to cell migration, adhesion and homing that were significantly down-regulated in cluster 0 compared with cluster 1. **(C)** Bar plot showing CPs related to DFs shown in **b** that were significantly down-regulated in cluster 0 compared with cluster 1. **(D)** Bar plot showing DFs related to immune cell activation that were significantly down-regulated in cluster 0 compared with cluster 1. **(E)** Bar plots showing CPs related to DFs shown in D that were significantly down-regulated in cluster 0 compared with cluster 1. **(F)** Volcano plot showing DEGs between cluster 2 (mostly composed of cells deriving from *dex-treated* patients) and cluster 0, at resolution 0.3. Grey dots indicate genes that were not statistically significant (p_{adj}>0.01); orange dots indicate significantly up-regulated genes (with log_2FC>0.58), and blue dots indicate significantly down-regulated genes (with log_2FC<-0.58). **(G)** Bar plot showing DFs of sub-categories related to cell motility, cell-to-cell interactions, and immune cell activation that were significantly down-regulated in cluster 2 compared with cluster 0. **(H)** Bar plots showing CPs related to DFs shown in G that were significantly down-regulated in cluster 2 compared with cluster 0. In all the bar plots, the functions or pathways, listed on the left side of the plot, are ranked according to the z-score that predicts a down-regulation (blue, z-score <-1.5).

these observations, CPs relative to receptor signalling, signal transduction, and cytokine-induced responses were significantly down-regulated in cluster 0 (Figure 4E). We then examined the DEGs composing the processes and functions reported in Figure 4D and the pathways reported in Figure 4E and obtained a list of 304 genes (reported in Supplementary Table 7). They included transcripts encoding molecules playing key roles in different steps of DC activation, including signal transduction pathways (e.g., JAK1, STAT4, and several molecules belonging to MAPK, PI and NF-kB pathways), endocytosis and phagocytosis (e.g., FNBP1, CLTC, RAB27A), antigen processing and presentation (e.g., ISG15, AKAP11, ATG5, HLA-DRB5), cytokines and cytokine receptors (e.g., TNFSF14, LTB, IL18R1), molecules involved in DC interactions with other immune cells (e.g., SLAMF6, LY9, CYTIP). These 304 DEGs also included genes involved in cell metabolism and cell proliferation (e.g., BRAF, PIM1, KRAS).

A cluster of TIDCs mainly derived from dex-treated patients has a transcriptomic signature suggestive of further functional impairment

We then focused on the analysis of DEGs between clusters 0 and 2, both originating from the splitting of one single cluster. We observed that cluster 2 was mainly composed of cells deriving from dex-treated patients (78%), whereas these cells were a minority (11%) in cluster 0. Among 967 DEGs between the two clusters, 576 were down-regulated and 391 were up-regulated. By further setting a threshold on |log2FC|>0.58 (corresponding to a 1.5-fold change), we selected 531 down-regulated and 362 up-regulated DEGs in cluster 2 compared with cluster 0 (Figure 4F). These genes were used for IPA functional annotation. The analysis of these genes, categorized by DFs, indicated that 81 processes were differentially regulated

between cluster 2 and 0 (Supplementary Table 8). Among these processes, 8 were down-regulated in cluster 2 compared with cluster 0, whereas the remaining processes lacked z-score, or had a z-score between -1.5 and +1.5. Relevant to TIDC functions in glioma microenvironment, DFs down-regulated in cluster 2 included processes related to cellular motility and cell-to-cell interactions (Figure 4G). The analysis of DEGs categorized by CPs indicated that 83 pathways were differentially regulated between cluster 2 and cluster 0 (Supplementary Table 9). Relevant to TIDC functions in glioma microenvironment, down-regulated CPs in cluster 2 included pathways crucial to signalling, cell-to-cell interactions and phagocytosis (Figure 4H). According to the functions and pathways down-regulated in cluster 2, the 74 DEGs composing the processes and functions reported in Figure 4G and the pathways reported in Figure 4H included transcripts encoding molecules crucially involved in: DC activation and migration pathways (e.g. S100A10, CD63), endocytosis and phagocytosis (e.g. AP2S1, MYO1G, LRP1, FCER1G), antigen processing and presentation (e.g. CTSZ, CALR, LITAF, RAC1), cytokines and cytokine receptors (e.g. TNFSF12, IL4R), cytoskeleton rearrangement relevant to cell motility (e.g. PFN1, ARPC1A, ARPC1B), adhesion molecules involved in cell-to-cell interactions (e.g. ADAM9, GAS6) (Supplementary Table 10). They also included genes involved in cell metabolism and cell proliferation (e.g. G6PC3, SMPD2, CREB3L4, RPS6KB2). As expected, taking into consideration that cluster 2 was mainly composed of cells deriving from dex-treated patients, genes involved in stabilization of glucocorticoid receptor (HSPA1A, HSPA1B) were up-regulated in cluster 2 compared with cluster 0.

Discussion

In this study, we performed a deep characterization of PBDCs and TIDCs in patients with newly diagnosed adult-type diffuse glioma and demonstrated that both the tumor and corticosteroid therapy have profound effects on DCs.

We observed that both cDCs and pDCs are reduced in the blood of glioma patients. These results are in partial agreement with previous studies that reported discordant results, indeed, including reduced, unchanged and increased cDCs and/or pDCs in glioma patients, likely related to different criteria used for patient selection (34, 35). As suggested in other types of cancer, the reduction of PBDCs in our patients may be sustained partly by DC recruitment into the tumor microenvironment, and partly by tumor-derived cytokines, such as VEGF and IL-6 that are produced by glioma cells (26, 36) and inhibit DC maturation in the bone marrow (37). Because only part of the patients enrolled in our study underwent perioperative dexamethasone treatment, we had the opportunity to investigate the impact of corticosteroids on PBDCs in glioma patients. We observed indeed that, compared with untreated patients, dex-treated patients had a significant and marked reduction of all PBDC subsets, thus confirming the high sensitivity of circulating DCs to systemic corticoid administration reported in other settings (38, 39). Notably, we further observed that, among untreated patients with IDH-wildtype gliomas, the reduction of circulating DC-lineage DCs was more marked in patients with a histopathological diagnosis of glioblastoma compared with patients with a histopathological diagnosis of anaplastic astrocytoma. This observation is relevant to the consideration that in several human cancers a more marked PBDC reduction has been described in patients with more advanced disease, possibly related to higher tumor secretion of soluble factors affecting DC generation and distribution (40–44). Although the 2021 WHO classification of central nervous system tumors include all IDH-wildtype diffuse gliomas in the most severe group of glioblastomas independently from their histopathological features[2], it is not yet clear if astrocytomas with molecular but not histopathological features of glioblastomas have exactly the same overall biology and response to treatment as IDH-wildtype gliomas with overt necrosis and/or microvascular proliferation (45). Indeed, our results demonstrating that PBDC counts differ in IDH-wildtype glioma patients stratified based on histopathological diagnosis may suggest that the histopathological grade of these tumors still affects their overall impact on the immune system.

When we moved to the characterization of tissue DCs, first of all we observed that DCs were negligible in healthy brain samples, thus demonstrating the lack of parenchymal DCs in healthy human brain. This finding represents a novelty because the current knowledge on the role of DCs in the central nervous system has been acquired in murine models, so far, showing that DCs in healthy mouse brains are present only in the choroid plexus and in the meninges but not in the brain parenchyma (46).

In our study we further observed that all subsets of DCs were recruited in the core lesions of diffuse gliomas. Notably, this was observed in all patients independently from tumor histomolecular features, indicating that also the most severe type of gliomas retains the ability to recruit DCs in the TME. This observation may provide a possible explanation to the high susceptibility of gliomas to DC vaccines (7, 8), and may suggest the feasibility of targeting TIDCs in these patients with DC reprogramming immunotherapeutic strategies. Notably, the presence of several DC subsets in IDH-wildtype glioblastoma lesions has also been reported by Pombo Antunes and colleagues in a recent study addressing single-cell profiling of myeloid cells by scRNA-seq and cellular indexing of transcriptomes and epitopes (CITE)-seq approaches (47). Indeed, patients with either newly diagnosed or recurrent disease were enrolled, and this fact allowed the observation that TIDCs were far more abundant in recurrent patients. As a consequence, the analysis of TIDCs in

Pombo Antunes' study was performed primarily on recurrent tumors, demonstrating the presence not only of cDC1s, cDC2s and pDCs, but also of more recently identified DC subsets, including cDC2A and cDC2B subtypes, migDCs, and preDCs (47). In this respect, our study confirms and extends these observations, by demonstrating the presence of these same DC subsets in primary tumors, at the immunophenotypic and/or transcriptomic level. In our study we further investigated the functional state of TIDCs. By performing IPA functional annotation that predicts affected cellular functions and pathways based on gene expression, we demonstrated that the most abundant cluster of TIDCs in gliomas was characterized by a transcriptomic signature suggestive of functional impairment. In particular, cellular processes crucial to the primary function of DCs in cancer immunity, namely capturing tumor antigens, migrating to lymph nodes, and activating T cell responses, all resulted down-regulated in the largest cluster of TIDCs. Among the down-regulated genes most relevant to DC functions, we identified CLTC that encodes clathrin, and RAB27A that encodes Rab27a, two molecules that play a key role in DC endocytosis and phagocytosis, respectively (48, 49). The same negative regulation was observed for SLAMF1, a gene encoding the polyfunctional molecule SLAM that, by triggering Nox2 activation, positively regulates DC migration to draining lymph nodes (50). The most abundant cluster of TIDCs was also characterized by a down-regulation of ITGA4 and ITGAL, encoding the integrin-a4 and integrin-aL chains, respectively. These two molecules had been reported as positive prognostic factors in breast cancer (51), likely because of their ability to sustain immune cell infiltration in the tumor, and their role in the formation of the immunological synapses needed for T cell activation. Also AKAP11, member of A-kinase anchoring proteins required for optimal antigen presentation by DCs (52) and ATG5, a key autophagy gene needed for optimal phagosome-to-lysosome fusion and subsequent antigen processing and loading on MHC molecules (53), resulted down-regulated in the largest cluster of glioma TIDCs. Although the list of relevant down-regulated genes may be extended to a huge number of other genes controlling essential DC functions, it is evident from our study that, based on gene expression, a relevant proportion of DCs infiltrating glioma lesions are likely impaired in their ability to efficiently present tumor antigens and activate effective anti-tumor immune responses.

Notably, when we assessed the impact of perioperative corticosteroid treatment on TIDCs, we observed indeed that, compared with untreated glioma patients, dex-treated patients had a significant and marked reduction of tumor-infiltrating cDC1s, the subset most relevant to antitumor immune responses. According to the tolerogenic DC profile induced by dexamethasone *in vitro* (54), dex-treated patients showed an overall reduction in TIDC expression of HLA-DR and CD40 molecules. Moreover, the transcriptomic profile of the cluster enriched in TIDCs obtained from dex-treated patients was characterized by down-regulation of pathways and functions crucial to sustain the role of DCs in cancer immunity, including signal transduction pathways involved in cell activation, and processes involved in antigen presentation and cell migration. These findings are in line with previous studies that characterized the transcriptomic profile of tolerogenic DCs differentiated *in vitro* in the presence of dexamethasone, reporting a down-regulation of DEGs spanning functional families relevant to the ability of DCs to stimulate adaptive immune responses (55). Taken together, our experimental evidence indicates that perioperative steroid treatment reduces the amount and impairs the activity of TIDCs in glioma patients, thus suggesting that these detrimental effects of steroids on DCs may represent one of the mechanisms contributing to the already reported negative prognostic impact of steroids on glioma patient survival (56).

In conclusion, in this study we demonstrated that gliomas have the potential to recruit different DC subsets into the tumor site, but these cells undergo phenotypic and transcriptomic profile changes suggestive of functional DC impairment. This evidence paves the way to the development of new therapeutic strategies aimed at reactivating *in situ* TIDCs and switching their behavior towards promotion of tumor rejection. Moreover, by demonstrating the detrimental effects of perioperative dexamethasone treatment on circulating and glioma-infiltrating DCs, the results of this study support previous clinical evidence that discourages the use of steroids in these patients, suggesting the use of alternative therapeutic strategies for the control of symptomatic peritumoral vasogenic cerebral edema (57).

Data availability statement

The data underlying this article are available in Zenodo, at https://zenodo.org/record/6046299#.YgZ6bpbSKN4. The dataset was derived from sources in the public domain.

Ethics statement

The studies involving human participants were reviewed and approved by Institutional Review Boards of Humanitas Research Hospital (ONC-OSS-04-2017; 29/19). The patients/participants provided their written informed consent to participate in this study.

Author contributions

Data curation and Resources by CC, SF, AC, ST, MS, PP, LB, MN, FP, PK, CP, RB, BS, ML, SDB and DM. Conceptualization and Methodology by CC, SF, AC, ST, MS, PP, LB, MN, FP, PK, CP, RB, BS, ML, SDB and DM. Investigation by CC, SF, AC, ST, PK, CP, BS and Formal Analysis by CC, SF, AC, ST, SDB, PK, JM, FC. Writing – Original Draft by CC, SDB, DM. Writing – Review and Editing by CC, SF, AC, ST, MS, PP, LB, MN, FP, PK, CP, SDB, JM, FC, RB, BS, ML, SDB, DM. Funding Acquisition by ML, DM, SDB. Supervision by MS, LB, ML, SDB, DM. All authors contributed to the article and approved the submitted version.

Funding

This work was supported by Associazione Italiana per la Ricerca sul Cancro (AIRC, IG 14687) and Humanitas Research Hospital (Intramural Research and Clinical Funding Programs 5x1000 2018) grants to DM; AIRC (IG-19213) and Ministero della Salute (RF-2019-12371549) to ML; Department of Medical Biotechnologies and Translational Medicine, University of Milan (2019 and 2020 Intramural Programs) grants to SDB; AIRC (IG 20269) and Ministero dell'Università e della Ricerca (PRIN 20177J4E75) grants to RB; CC and SF were supported by the Doctorate School of Experimental Medicine and Medical Biotechnologies, University of Milan; FC was supported by Fondazione Umberto Veronesi (2020-3274); CC was supported by AIRC (fellowship lotteria vincere insieme per la ricerca 25491); ST was supported by the Data Science in Medicine and Nutrition (DASMEN) Ph.D. program from Humanitas University; JM was supported by type A 2017-PDF-0149 fellowship from the University of Milan.

Conflict of interest

The authors declare that the research was conducted in the absence of any commercial or financial relationships that could be construed as a potential conflict of interest.

Publisher's note

Supplementary material

The Supplementary Material for this article can be found online at: https://www.frontiersin.org/articles/10.3389/fimmu.2022.1074762/full#supplementary-material

References

1. Lapointe S, Perry A, Butowski NA. Primary brain tumours in adults. *Lancet* (2018) 392(10145):432–46. doi: 10.1016/S0140-6736(18)30990-5

2. Louis DN, Perry A, Wesseling P, Brat DJ, Cree IA, Figarella-Branger D, et al. The 2021 WHO classification of tumors of the central nervous system: A summary. *Neuro Oncol* (2021) 23(8):1231–51. doi: 10.1093/neuonc/noab106

3. Weller M, Butowski N, Tran DD, Recht LD, Lim M, Hirte H, et al. Rindopepimut with temozolomide for patients with newly diagnosed, EGFRvIII-expressing glioblastoma (ACT IV): a randomised, double-blind, international phase 3 trial. *Lancet Oncol* (2017) 18(10):1373–85. doi: 10.1016/S1470-2045(17)30517-X

4. Meric-Bernstam F, Larkin J, Tabernero J, Bonini C. Enhancing anti-tumour efficacy with immunotherapy combinations. *Lancet* (2021) 397(10278):1010–22. doi: 10.1016/S0140-6736(20)32598-8

5. Reardon DA, Brandes AA, Omuro A, Mulholland P, Lim M, Wick A, et al. Effect of nivolumab vs bevacizumab in patients with recurrent glioblastoma: The CheckMate 143 phase 3 randomized clinical trial. *JAMA Oncol* (2020) 6(7):1003–10. doi: 10.1001/jamaoncol.2020.1024

6. Locarno CV, Simonelli M, Carenza C, Capucetti A, Stanzani E, Lorenzi E, et al. Role of myeloid cells in the immunosuppressive microenvironment in gliomas. *Immunobiology* (2020) 225(1):151853. doi: 10.1016/j.imbio.2019.10.002

7. Garg AD, Vandenberk L, Koks C, Verschuere T, Boon L, Van Gool SW, et al. Dendritic cell vaccines based on immunogenic cell death elicit danger signals and T cell-driven rejection of high-grade glioma. *Sci Transl Med* (2016) 8(328):1–16. doi: 10.1126/scitranslmed.aae0105

8. Sprooten J, Ceusters J, Coosemans A, Agostinis P, De Vleeschouwer S, Zitvogel L, et al. Trial watch: dendritic cell vaccination for cancer immunotherapy. *Oncoimmunology* (2019) 8(11). doi: 10.1080/2162402X.2019.1638212

9. Anguille S, Smits EL, Lion E, Van Tendeloo VF, Berneman ZN. Clinical use of dendritic cells for cancer therapy. *Lancet Oncol* (2014) 15(7):257–67. doi: 10.1016/S1470-2045(13)70585-0

10. Garg AD, Coulie PG, Van den Eynde BJ, Agostinis P. Integrating next-generation dendritic cell vaccines into the current cancer immunotherapy landscape. *Trends Immunol* (2017) 38(8):577–93. doi: 10.1016/j.it.2017.05.006

11. Palucka K, Banchereau J. Cancer immunotherapy *via* dendritic cells. *Nat Rev Cancer* (2012) 12(4):265–77. doi: 10.1038/nrc3258

12. Qian C, Yang LJ, Cui H. Recent advances in nanotechnology for dendritic cell-based immunotherapy. *Front Pharmacol* (2020) 11:1–9. doi: 10.3389/fphar.2020.00960

13. Collin M, Bigley V. Human dendritic cell subsets: an update. *Immunology* (2018) 154(1):3–20. doi: 10.1111/imm.12888

14. Aspord C, Leccia MT, Charles J, Plumas J. Plasmacytoid dendritic cells support melanoma progression by promoting Th2 and regulatory immunity through OX40L and ICOSL. *Cancer Immunol Res* (2013) 1(6):402–15. doi: 10.1158/2326-6066.CIR-13-0114-T

15. Broz ML, Binnewies M, Boldajipour B, Nelson AE, Pollack JL, Erle DJ, et al. Dissecting the tumor myeloid compartment reveals rare activating antigen-presenting cells critical for T cell immunity. *Cancer Cell* (2014) 26(5):638–52. doi: 10.1016/j.ccell.2014.09.007

16. Yin X, Yu H, Jin X, Li J, Guo H, Shi Q, et al. Human blood CD1c + dendritic cells encompass CD5 high and CD5 low subsets that differ significantly in

phenotype, gene expression, and functions. *J Immunol* (2017) 198(4):1553–64. doi: 10.4049/jimmunol.1600193

17. Micheletti A, Finotti G, Calzetti F, Lonardi S, Zoratti E, Bugatti M, et al. slan/M-DC8+ cells constitute a distinct subset of dendritic cells in human tonsils. *Oncotarget* (2016) 7(1):161–75. doi: 10.18632/oncotarget.6660

18. Ness S, Lin S, Gordon JR. Regulatory dendritic cells, T cell tolerance, and dendritic cell therapy for immunologic disease. *Front Immunol* (2021) 12. doi: 10.3389/fimmu.2021.633436

19. Teng MWL, Galon J, Fridman WH, Smyth MJ. From mice to humans: Developments in cancer immunoediting. *J Clin Invest* (2015) 125(9):3338–46. doi: 10.1172/JCI80004

20. Carenza C, Franzese S, Calcaterra F, Mavilio D, Della Bella S. Comprehensive phenotyping of dendritic cells in cancer patients by flow cytometry. *Cytom Part A* (2021) 99(3):218–30. doi: 10.1002/cyto.a.24245

21. Gerhard GM, Bill R, Messemaker M, Klein AM, Pittet MJ. Tumor-infiltrating dendritic cell states are conserved across solid human cancers. *J Exp Med* (2021) 218(1). doi: 10.1084/jem.20200264

22. Kvedaraite E, Ginhoux F. Human dendritic cells in cancer. *Sci Immunol* (2022) 7(70). doi: 10.1126/sciimmunol.abm9409

23. Carenza C, Calcaterra F, Oriolo F, Di Vito C, Ubezio M, Della Porta MG, et al. Costimulatory molecules and immune checkpoints are differentially expressed on different subsets of dendritic cells. *Front Immunol* (2019) 10:1–15. doi: 10.3389/fimmu.2019.01325

24. Cossarizza A, Chang H-D, Radbruch A, Acs A, Adam D, Adam-Klages S, et al. Guidelines for the use of flow cytometry and cell sorting in immunological studies (second edition). *Eur J Immunol* (2019) 49:1457–973. doi: 10.1002/eji.201970107

25. Giannelli S, Taddeo A, Presicce P, Villa ML, Della Bella S. A six-color flow cytometric assay for the analysis of peripheral blood dendritic cells. *Cytom Part B - Clin Cytom* (2008) 74(6):349–55. doi: 10.1002/cyto.b.20434

26. Salmaggi A, Croci D, Prina P, Cajola L, Pollo B, Marras CE, et al. Production and post-surgical modification of VEGF, tPA and PAI-1 in patients with glioma. *Cancer Biol Ther* (2006) 5(2):204–9. doi: 10.4161/cbt.5.2.2357

27. Villani AC, Satija R, Reynolds G, Sarkizova S, Shekhar K, Fletcher J, et al. Single-cell RNA-seq reveals new types of human blood dendritic cells, monocytes, and progenitors. *Science (80-)* (2017) 356(6335). doi: 10.1126/science.aah4573

28. See P, Dutertre CA, Chen J, Günther P, McGovern N, Irac SE, et al. Mapping the human DC lineage through the integration of high-dimensional techniques. *Science (80-)* (2017) 356(6342). doi: 10.1126/science.aag3009

29. Dutertre CA, Becht E, Irac SE, Khalilnezhad A, Narang V, Khalilnezhad S, et al. Single-cell analysis of human mononuclear phagocytes reveals subset-defining markers and identifies circulating inflammatory dendritic cells. *Immunity* (2019) 51(3):573–89.e8. doi: 10.1016/j.immuni.2019.08.008

30. Brown CC, Gudjonson H, Pritykin Y, Deep D, Lavallée VP, Mendoza A, et al. Transcriptional basis of mouse and human dendritic cell heterogeneity. *Cell* (2019) 179(4):846–63.e24. doi: 10.1016/j.cell.2019.09.035

31. Schinnerling K, García-González P, Aguillón JC. Gene expression profiling of human monocyte-derived dendritic cells - searching for molecular regulators of tolerogenicity. *Front Immunol* (2015) 6:1–10. doi: 10.3389/fimmu.2015.00528

32. van Leeuwen-Kerkhoff N, Lundberg K, Westers TM, Kordasti S, Bontkes HJ, de Gruijl TD, et al. Transcriptional profiling reveals functional dichotomy between human slan + non-classical monocytes and myeloid dendritic cells. *J Leukoc Biol* (2017) 102(4):1055–68. doi: 10.1189/jlb.3MA0117-037R

33. Zhang Q, He Y, Luo N, Patel SJ, Han Y, Gao R, et al. Landscape and dynamics of single immune cells in hepatocellular carcinoma. *Cell* (2019) 179(4):829–845.e20. doi: 10.1016/j.cell.2019.10.003

34. Gousias K, von Ruecker A, Voulgari P, Simon M. Phenotypical analysis, relation to malignancy and prognostic relevance of ICOS + T regulatory and dendritic cells in patients with gliomas. *J Neuroimmunol* (2013) 264(1–2):84–90. doi: 10.1016/j.jneuroim.2013.09.001

35. Wang R, Zhang JL, Wei B, Tian Y, Li ZH, Wang L, et al. Upregulation of plasmacytoid dendritic cells in glioma. *Tumor Biol* (2014) 35(10):9661–6. doi: 10.1007/s13277-014-2211-7

36. Chang CY, Li MC, Liao SL, Huang YL, Shen CC, Pan HC. Prognostic and clinical implication of IL-6 expression in glioblastoma multiforme. *J Clin Neurosci* (2005) 12(8):930–3. doi: 10.1016/j.jocn.2004.11.017

37. Almand B, Resser JR, Lindman B, Nadaf S, Clark JI, Kwon ED, et al. Clinical significance of defective dendritic cell differentiation in cancer. *Clin Cancer Res* (2000) 6(5):1755–66.

38. Shodell M, Shah K, Siegal FP. Circulating human plasmacytoid dendritic cells are highly sensitive to corticosteroid administration. *Lupus* (2003) 12(3):222–30. doi: 10.1191/0961203303lu362xx

39. Bain CR, Draxler DF, Taylor R, Wallace S, Gouldthorpe O, Corcoran TB, et al. The early *in-vivo* effects of a single anti-emetic dose of dexamethasone on innate immune cell gene expression and activation in healthy volunteers. *Anaesthesia* (2018) 73(8):955–66. doi: 10.1111/anae.14306

40. Della Bella S, Nicola S, Brambilla L, Riva A, Ferrucci S, Presicce P, et al. Quantitative and functional defects of dendritic cells in classic kaposi's sarcoma. *Clin Immunol* (2006) 119(3):317–29. doi: 10.1016/j.clim.2006.01.011

41. Sciarra A, Lichtner M, AnnaMaria GA, Mastroianni C, Rossi R, Mengoni F, et al. Characterization of circulating blood dendritic cell subsets DC123+ (lymphoid) and DC11C+ (myeloid) in prostate adenocarcinoma patients. *Prostate* (2007) 67(1):1–7. doi: 10.1016/S0022-5347(18)30842-5

42. Labidi-Galy SI, Treilleux I, Goddard-Leon S, Combes JD, Blay JY, Ray-Coquard I, et al. Plasmacytoid dendritic cells infiltrating ovarian cancer are associated with poor prognosis. *Oncoimmunology* (2012) 1(3):380–2. doi: 10.4161/onci.18801

43. Yamamoto T, Yanagimoto H, Satoi S, Toyokawa H, Yamao J, Kim S, et al. Circulating myeloid dendritic cells as prognostic factors in patients with pancreatic cancer who have undergone surgical resection. *J Surg Res [Internet]* (2012) 173(2):299–308. doi: 10.1016/j.jss.2010.09.027

44. Orsini G, Legitimo A, Failli A, Ferrari P, Nicolini A, Spisni R, et al. Quantification of blood dendritic cells in colorectal cancer patients during the course of disease. *Pathol Oncol Res* (2014) 20(2):267–76. doi: 10.1007/s12253-013-9691-4

45. Horbinski C, Berger T, Packer RJ, Wen PY. Clinical implications of the 2021 edition of the WHO classification of central nervous system tumours. *Nat Rev Neurol* (2022) 0123456789:515–29. doi: 10.1038/s41582-022-00679-w

46. Dunn GP, Okada H. Principles of immunology and its nuances in the central nervous system. *Neuro Oncol* (2015) 17:3–8. doi: 10.1093/neuonc/nov175

47. Pombo Antunes AR, Scheyltjens I, Lodi F, Messiaen J, Antoranz A, Duerinck J, et al. Single-cell profiling of myeloid cells in glioblastoma across species and disease stage reveals macrophage competition and specialization. *Nat Neurosci* (2021) 24(4):595–610. doi: 10.1038/s41593-020-00789-y

48. Kaksonen M, Roux A. Mechanisms of clathrin-mediated endocytosis. *Nat Rev Mol Cell Biol* (2018) 19(5):313–26. doi: 10.1038/nrm.2017.132

49. Jancic C, Savina A, Wasmeier C, Tolmachova T, El-Benna J, Dang PMC, et al. Rab27a regulates phagosomal pH and NADPH oxidase recruitment to dendritic cell phagosomes. *Nat Cell Biol* (2007) 9(4):367–78. doi: 10.1038/ncb1552

50. Wang G, Van Driel BJ, Liao G, O'Keeffe MS, Halibozek PJ, Flipse J, et al. Migration of myeloid cells during inflammation is differentially regulated by the cell surface receptors Slamf1 and Slamf8. *PloS One* (2015) 10(3):1–18. doi: 10.1371/journal.pone.0121968

51. Rojas K, Baliu-Piqué M, Manzano A, Saiz-Ladera C, García-Barberán V, Cimas FJ, et al. In silico transcriptomic mapping of integrins and immune activation in basal-like and HER2+ breast cancer. *Cell Oncol* (2021) 44(3):569–80. doi: 10.1007/s13402-020-00583-9

52. Schillace RV, Miller CL, Carr DW. AKAPs in lipid rafts are required for optimal antigen presentation by dendritic cells. *Immunol Cell Biol* (2011) 89(5):650–8. doi: 10.1038/icb.2010.148

53. Lee HK, Mattei LM, Steinberg BE, Alberts P, Lee YH, Chervonsky A, et al. *In vivo* requirement for Atg5 in antigen presentation by dendritic cells. *Immunity* (2010) 32(2):227–39. doi: 10.1016/j.immuni.2009.12.006

54. Falcón-Beas C, Tittarelli A, Mora-Bau G, Tempio F, Pérez C, Hevia D, et al. Dexamethasone turns tumor antigen-presenting cells into tolerogenic dendritic cells with T cell inhibitory functions. *Immunobiology* (2019) 224(5):697–705. doi: 10.1016/j.imbio.2019.05.011

55. Navarro-Barriuso J, Mansilla MJ, Naranjo-Gómez M, Sánchez-Pla A, Quirant-Sánchez B, Teniente-Serra A, et al. Comparative transcriptomic profile of tolerogenic dendritic cells differentiated with vitamin D3, dexamethasone and rapamycin. *Sci Rep* (2018) 8(1):1–13. doi: 10.1038/s41598-018-33248-7

56. Petrelli F, De Stefani A, Ghidini A, Bruschieri L, Riboldi V, Dottorini L, et al. Steroids use and survival in patients with glioblastoma multiforme: a pooled analysis. *J Neurol* (2021) 268(2):440–7. doi: 10.1007/s00415-020-09731-5

57. Dubinski D, Hattingen E, Senft C, Seifert V, Peters KG, Reiss Y, et al. Controversial roles for dexamethasone in glioblastoma – opportunities for novel vascular targeting therapies. *J Cereb Blood Flow Metab* (2019) 39(8):1460–8. doi: 10.1177/0271678X19859847

frontiers | Frontiers in Immunology

TYPE Review
PUBLISHED 15 March 2023
DOI 10.3389/fimmu.2023.1099921

OPEN ACCESS

EDITED BY
Silvia Pesce,
University of Genoa, Italy

REVIEWED BY
Abhijit Aithal,
University of Nebraska Medical Center, United States
Sabrina Giglio,
University of Cagliari, Italy
Roberto Piñeiro,
Health Research Institute of Santiago de Compostela (IDIS), Spain

*CORRESPONDENCE
Anton Buzdin
buzdin@oncobox.com

†These authors have contributed equally to this work

SPECIALTY SECTION
This article was submitted to Cancer Immunity and Immunotherapy, a section of the journal Frontiers in Immunology

RECEIVED 16 November 2022
ACCEPTED 28 February 2023
PUBLISHED 15 March 2023

CITATION
Rozenberg JM, Buzdin AA, Mohammad T, Rakitina OA, Didych DA, Pleshkan VV and Alekseenko IV (2023) Molecules promoting circulating clusters of cancer cells suggest novel therapeutic targets for treatment of metastatic cancers.
Front. Immunol. 14:1099921.
doi: 10.3389/fimmu.2023.1099921

Molecules promoting circulating clusters of cancer cells suggest novel therapeutic targets for treatment of metastatic cancers

Julian M. Rozenberg[1†], Anton A. Buzdin[1,2,3,4*†], Tharaa Mohammad[1†], Olga A. Rakitina[5], Dmitry A. Didych[6], Victor V. Pleshkan[5,7] and Irina V. Alekseenko[5,7,8]

[1]Laboratory of Translational Bioinformatics, Moscow Institute of Physics and Technology, Dolgoprudny, Russia, [2]PathoBiology Group, European Organization for Research and Treatment of Cancer (EORTC), Brussels, Belgium, [3]Group for Genomic Analysis of Cell Signaling, Shemyakin-Ovchinnikov Institute of Bioorganic Chemistry of the Russian Academy of Sciences, Moscow, Russia, [4]Laboratory for Clinical Genomic Bioinformatics, Sechenov First Moscow State Medical University, Moscow, Russia, [5]Gene Immunooncotherapy Group, Shemyakin-Ovchinnikov Institute of Bioorganic Chemistry of the Russian Academy of Sciences, Moscow, Russia, [6]Laboratory of human genes structure and functions, Shemyakin-Ovchinnikov Institute of Bioorganic Chemistry of the Russian Academy of Sciences, Moscow, Russia, [7]Gene oncotherapy sector, Institute of Molecular Genetics of National Research Centre (Kurchatov Institute), Moscow, Russia, [8]Laboratory of Epigenetics, Institute of Oncogynecology and Mammology, National Medical Research Center for Obstetrics, Gynecology and Perinatology Named after Academician V.I. Kulakov, Ministry of Healthcare of the Russian Federation, Moscow, Russia

Treatment of metastatic disease remains among the most challenging tasks in oncology. One of the early events that predicts a poor prognosis and precedes the development of metastasis is the occurrence of clusters of cancer cells in the blood flow. Moreover, the presence of heterogeneous clusters of cancerous and noncancerous cells in the circulation is even more dangerous. Review of pathological mechanisms and biological molecules directly involved in the formation and pathogenesis of the heterotypic circulating tumor cell (CTC) clusters revealed their common properties, which include increased adhesiveness, combined epithelial-mesenchymal phenotype, CTC-white blood cell interaction, and polyploidy. Several molecules involved in the heterotypic CTC interactions and their metastatic properties, including IL6R, CXCR4 and EPCAM, are targets of approved or experimental anticancer drugs. Accordingly, analysis of patient survival data from the published literature and public datasets revealed that the expression of several molecules affecting the formation of CTC clusters predicts patient survival in multiple cancer types. Thus, targeting of molecules involved in CTC heterotypic interactions might be a valuable strategy for the treatment of metastatic cancers.

KEYWORDS

cancer, metastasis, circulating cancer cell, tumor microenvironment, heterotypic cell interactions

1 Introduction

One of the cancer hallmarks is cancer cells dissemination and metastasis which is a leading cause of cancer associated death (1). Metastasis develops as a consequence of changes within cancer cells that lead to an ability to move through the tissue, survive in the circulation, attach and grow in the distal site, meanwhile escaping immune surveillance (2). Research of the last decades revealed that a key factor which determines the ability of cancer cells to metastasize is pathological interactions with neighboring non-cancerous cells such as fibroblasts, mesenchymal and immune cells, so called cells of tumor microenvironment (TME).

Therefore, development of drugs targeting key molecules involved in the TME interactions that can suppress metastasis is a hot theme of current investigations (3–7).

Cancer associated stromal cells as well as circulating exosomes migrate from the primary tumor to distal sites and change local microenvironment forming so-called pre-metastatic niche permissive for the cancer cells recruitment and growth (8–12). At the same time, cancer cells might disseminate from the primary tumor in the circulation in clusters with cancer associated cells (13–15). These clusters are thought to be relatively rare in the cancer patient population (14, 16, 17), although they have strong metastatic potential (16, 18), and their presence is associated with metastasis and worse prognosis in breast (13, 14, 19), lung cancers (20–22), renal cell carcinoma (23), colorectal cancer (24–26), and others (27).

Our review of current literature revealed that cells involved in the metastasis-promoting heterotypic CTC interactions include platelets, cancer associated fibroblast (CAFs), white blood cells (WBCs), specific population of tumor-associated macrophages, neutrophils and polymorphonuclear myeloid-derived suppressor cells (PMN-MDSCs).

A number of investigations identified several key molecules involved in the heterotypic cell interactions such as IL1R1 (16), IL6, NODA, NOTCH1 (17), CD44 (14), CXCR4 (4), TGFBR2 (4), CDH1 (4, 28), EPCAM (29), ICAM1 (30), CCR1 (31) (Table 1). Their expression promotes formation of CTC clusters and metastasis by inducing adhesion (4, 30, 33), proliferation (16), by metabolic adaptation to oxidative stress (17, 34), and through the epithelial-mesenchymal transition (31, 35). Quite intriguing, in lung cancer most CTCs interacting with WBCs were polyploid (21) thus, implying repression of the mitotic checkpoint, induction of cell survival and migration (36–38).

The analysis of literature and public databases revealed that expression of some genes affecting CTC clusters and metastasis predicts prognosis in many cancer types. Some of these molecules are targeted by the approved or experimental anti-cancer drugs (such as plerixafor for CXCR4 or tocilizumab for IL6R). Altogether, our review suggests the existence of common and cancer tissue specific mechanisms of CTC complex formation with implication for drug development and cancer treatment.

TABLE 1 Genes involved in cancer cell-stromal cell interaction promoting CTC clustering and metastasis.

Cancer type	Target	Target ligand(s)	Interacting cells	Source tissue	Reference
Breast	IL6ST	IL6	neutrophils	Peripheral blood	(16)
Breast	IL1R1	IL1	neutrophils	Peripheral blood	(16)
Breast	VCAM1	ITGA4 ITGB1	neutrophils	Peripheral blood	(16)
Breast	NODAL	CFC1B	PMN-MDSCs	Spheroid cell co-culture	(17)
Breast	NOTCH1	JAG1	PMN-MDSCs	Spheroid cell co-culture	(17)
Breast	CD44	Hyaluronic acid	CAFs	MDA-MB-231 and CD44 positive MCF-7 cells	(14)
Breast	CXCR4	CXCL12	CAFs	MCF10DCIS	(4, 32)
Breast	TGFBR2	TGFB1	CAFs	MCF10DCIS	(4)
Hepatocellular	EPCAM	CAMs	NA	Huh7 organoids in xenograft model	(29)
Lung	ICAM1	ITGAM	PMNs and neutrophils	Lewis lung carcinoma H-59 cells, A549 cells expressing ICAM-1	(30)
Colorectal	IL6R	IL6	Tumor-associated macrophages (TAMs)	Patient blood	(31)
Colorectal	CCR1	CCL2	Tumor-associated macrophages (TAMs)	Patient blood	(31)
Colorectal	CDH1	CDH1, adherent junction protein	NA	Human CRC organoids in xenograft model	(28)

2 Tumor microenvironment promotes formation of the CTC clusters and metastasis

2.1 Interactions with white blood cells

The CTCs can interact with a variety of WBCs in the circulation such as neutrophils (39), PMN-MDSC (17, 40, 41), platelets (31), macrophages (35), and lymphocytes (16).

2.1.1 Interaction with neutrophils

One of the mechanisms of neutrophil mediated metastasis is formation of the neutrophil extracellular traps (NETs) consisting of neutrophil DNA (39). As NETs interact with and provide a niche for CTCs, blocking NET formation by DNAse, e.g. coated with nanoparticles inhibits lung metastasis (39).

Using *in vivo* metastasis models, Spicer et al. have demonstrated a novel role of neutrophils in the early adhesive steps of liver metastasis in the Lewis lung carcinoma mice model (30). Their findings suggest that neutrophils promote cancer cell adhesion within liver sinusoids, thus influencing metastasis. The neutrophil ITGAM/ICAM-1 mediated the adhesion of lipopolysaccharide-activated neutrophils to the cancer cells (30).

In breast cancer, CTCs interact with WBCs and in out of 70 investigated patients with invasive disease, CTCs were found in 34 (49%) patients. Among them, homotypic CTC clusters were found in 14 (20%) patients, out of which 6 (9%) also had CTC-WBC clusters and 4 (6%) had CTC-WBC clusters only (16). On average, about 2 CTCs were found in the CTC-WBC clusters that represented about 10% of all circulating CTCs (16). Most of these WBCs (75%) were myeloid cells, specifically neutrophils and T-cells.

The neutrophil-CTC interactions detected in blood were associated with worse prognosis of patients (16). Neutrophil-CTC clusters promoted cancer cell proliferation *in vitro* and were characterized by higher metastatic potential in mice upon tail vein injection. Analysis of gene expression from either CTC alone or in a complex with neutrophils revealed 41 upregulated genes involved in the DNA replication and cell cycle progression. Further analysis of genes dysregulated in cancer associated neutrophils revealed that TNF-α, Oncostatin M (OSM), IL-1β and IL-6 cytokines are expressed in the neutrophils with corresponding expression of their receptors in CTCs. Reciprocal experiment detected cytokines granulocyte colony-stimulating factor (G-CSF), TGF-β3 and IL-15 in the CTCs with corresponding expression of the receptors in neutrophils. CRISPR-Cas9 mediated knockout of IL6ST and IL1R1 in cancer cells suppressed the growth advantage of the neutrophil-CTC clusters without effect on their frequency (16). In addition, vascular cell adhesion molecule (VCAM1) was identified in a CRISPR-Cas9 screen in the CTC as a molecule required for formation of the neutrophil-CTC clusters (16). Neutrophil recruitment to the primary site and metastasis was dependent on expression of CXCL1/2 in 4T1 breast cancer cells. Among molecules that block cancer cell invasion mediated by neutrophils were also NADPH oxidase, neutrophil elastase inhibitors, and DNAse (39).

2.1.2 Interaction with PMN-MDSCs

Another type of myeloid cell - PMN-MDSCs normally function as suppressors of the immune response and have profound pro-carcinogenic properties promoting angiogenesis, formation of the pre-metastatic niche and cell proliferation (42–45),

It was predicted that PMN-MDSCs interact with CTCs and it was hypothesized (yet to be proven) that PMN-MDSCs shield CTCs from the T-cell mediated destruction (46). At that time, CTCs were usually isolated as CD45 negative cells, thereby clusters of CTC with leukocytes (including PMN-MDSCs) were missed from the analysis.

Indeed, PMN-MDSC clusters with circulating tumor cells were detected in patients with melanoma or breast cancer (17). It was reported that the ratio of cancer and non-cancerous cells in the clusters varied in the range 1:1 to 1:4 in six out of eight patients tested (17).

Interestingly, a previous paper from the same group revealed that aggressive triple negative breast and melanoma cancers overexpress Nodal, an embryonic morphogen of the TGF-β family (47) and a a putative Notch/RBPJ signaling pathway target (48). The patients with aggressive breast cancer had higher levels of Nodal in serum and PMN-MDSCs could promote survival of the CTCs in culture by activating reactive oxygen species (ROS) and Jagged2 response (17). Accordingly, CTCs promote differentiation of the PMN-MDSCs in pro-cancerous "type-2" phenotype by the Nodal signaling (17).

Arnoletti et al. investigated the effect of interactions between the CTCs, MDSCs and T-cells extracted from the portal blood of pancreatic adenocarcinoma patients on CTC and T-cell proliferation, apoptosis and activation. It was demonstrated that MDSCs tended to cooperate with CTCs by repressing T-cells proliferation, although no significant effects on activation and anergy were reported (49).

The mathematical modeling and direct measurements of genomic aberrations in breast cancer CTC clusters isolated by filtration revealed that the fraction of cancer cells in the clusters is in the range of 8%-48% (50). In contrast, isolation of multicellular clusters from the blood of breast cancer patients followed by single cell RNA-seq analysis identified genes associated specifically with clusters, in comparison to single cells, but failed to identify other cell types except platelets (18). In agreement with other studies, cell clusters contributed to metastasis 23 times more actively than the single cells and the presence of clusters in breast and prostate cancers was associated with significantly worse prognosis (18).

The differences in CTC isolation protocols might lead to the differences in cell populations detected within CTC clusters. The latter study (18) utilized HBCTC-Chip coated with cocktail of EPCAM, EGFR and HER2 antibodies (18), whereas Parsortix microfluidic device using Cell Separation Cassettes (GEN3D6.5, ANGLE) was used in the subsequent study that characterized neutrophils-CTC (16), whereas PMN-MDSC-CTCs clusters were isolated by FACS (17, 40, 41).

2.1.3 Interaction with tumor associated macrophages

Interaction of CTCs with tumor associated macrophage (TAMs) seems to promote metastasis. Nanomechanical characterization of tumor associated macrophage-CTC clusters isolated from blood of prostate cancer patients revealed that contact with the macrophages softens and promotes adhesiveness of CTCs, which corresponds to mixed epithelial - mesenchymal phenotype (35). Notably, previous publication of the same group reported softness, deformability, and adhesiveness of single CTCs as markers of aggressive metastatic prostate cancer (51). The presence of TAMs in the invasive front was associated with the mesenchymal phenotype of CTCs and poor prognosis in colorectal cancer (31). Mechanistically, the Il-6 produced by the TAMs induced JAK2/STAT3/miR-506-3p/FoxQ1 signaling in cancer cells, thus promoting epithelial mesenchymal transition (EMT), metastasis and further attraction of macrophages by secretion of CCl2 (31).

2.1.4 Interaction with lymphocytes

We found only one report that mentions interaction of CTCs with lymphocytes (16). However, CTCs are associated with impairments of adaptive immunity. The quantity of CTCs correlates with the presence in peripheral blood of the CD95 (FAS)-positive T-helper cells and stage 3 breast cancer as well as with lower percentage of the CD8+ T-cells with activated T-cell receptor (52, 53), the absence of tumor associated antigen specific TCRs and low TCR heterogeneity (54), and positively associated with intratumoral populations of T-regs (55).

2.2 Interactions with cancer associated fibroblasts

Aside from single CTCs and cancer associated fibroblasts (CAFs), the presence of homotypic and heterotypic clusters of CTCs and CAFs was reported in patients with stages 1-4 of breast cancer (14). In their study, Sharma et al. detected CTCs in 90% and circulating CAFs (cCAFs) in 80% of patients; homotypic CTC clusters were found in 50% and heterotypic - in 25% of patients in treatment naive stages 2-3. Interestingly, only 25% of patients in stage 4 had homotypic clusters and 25% had heterotypic CTC-CAF clusters. The number of cCAFs and CTCs was much higher in patient blood with metastatic breast cancer in comparison to localized cancers whereas nothing was detected in the control group. The effect of cancer treatment on these clusters was not yet addressed (14).

Using MDA-MB-231 cells and CD44-enriched MCF7 cells, authors have been able to demonstrate involvement of the stem cell marker CD44 in the heterotypic clustering and that heterotypic clusters metastasize more efficiently (14). Accordingly, it was shown that tumor suppressor Rb represses CD44 dependent collective invasion, release of breast cancer cells in circulation and lung metastasis (3).

Circulating CAFs and CTCs were also detected in small groups of colorectal and prostate cancer patients (13). Consistent with others, the paper shows images of the distinct multicellular CTC clusters with CAF and with leukocytes, which were obtained by the negative filtration through 10 μm filter (13).

2.3 Interaction with platelets

Activation of the coagulation cascade and formation of platelet-rich thrombus around tumor cells in the vasculature have both been proposed to play major roles in physically shielding CTCs from the stress of blood flow and from lysis by the Natural killer cells (56–58). One of the mechanisms is substitution of cancer cell MHC1 by platelets-derived MHC1 carrying normal peptides thereby protecting cancer cells from both NK and T-cell recognition (59).

Analysis of the single cell gene expression of the CTCs in the pancreatic cancer mouse model revealed that 32% of the circulating cells interact with platelets leading to suppression of epithelial markers and expression changes of many other genes (60).

Accordingly, direct interaction with platelets promotes EMT in cancer cells and either inhibition of NF-kB in cancer cells or inhibition of TGF-β in platelets was sufficient to protect against lung metastasis (61). In turn, disruption of platelets interactions with cancer cell by S-nitrosocaptopril (CapNO) inhibits adhesion to endothelial cells and lung cancer metastasis in immunocompetent mouse models through multiple mechanisms including reduction of Sialyl-Lewis X (Slex) levels in cancer cells and ADP-induced P-selectin in platelets, IL-1b induced VCAM1, ICAM-1, and E-selectin by HUVECs (33).

3 Polyploidy and epithelial-to-mesenchymal transition in CTC clusters

As it is discussed in the previous sections, interaction with TAM (31) or platelets (61) induced metastasis promoting EMT in cancer cells (62). EMT is associated with cancer progression and metastasis (63). During EMT epithelial cells lose contact with epithelial or endothelial cells, change their cytoskeleton and consequentially, become less rigid, acquiring an ability to move (51, 64). In addition, EMT induces stem cell properties in cancer, regulates and is regulated by immunosuppressive cancer microenvironment (65, 66). Notably, cancer stem cells are characterized by mixed epithelial – mesenchymal phenotype (67).

Interestingly, interaction with white blood cells also correlates with mixed Epithelial-mesenchymal phenotype and cancer cells polyploidy (21, 68, 69) that play a key role in cancer resistance to treatment and metastasis (37, 70–72).

The presence of CTC-WBC clusters was associated with worse prognosis in lung (21, 22), breast cancers (19), and hepatocellular carcinoma (73, 74). Remarkably, in lung cancer, CTCs in complex with WBCs were exclusively polyploid (21).

In turn, in glioblastoma, examination of ploidy together with expression of endothelial marker CD31 revealed that pre-operative small triploid CD31 negative CTCs were predictive of inferior prognosis (68).

A recent paper employed the iFISH method combining FISH DNA staining and immunofluorescence (21, 22) to create Atlas of Circulating Rare Cells (69). High throughput imaging analysis of circulating rare cells (CRCs) purified by WBC subtraction categorized cells into 71 subtypes based on the CD45 leukocyte staining, cell size, chromosome 8 ploidy and the presence of a few tumor cell markers including PD-L1 (EPCAM/CK18/PD-L1/AFP/HER2/CA19-9), endothelial CD31, mesenchymal Vimentin and stem cell CD133 markers (69).

Authors presented a set of cell images with polyploid chromosome 8. There were cells double positive for CD31 and Vimentin staining with abnormal chromosomes which can coincide with cytokeratin CK18, and even CD45-/EPCAM+/CD31+/Vim+ "aneuploid mesenchymal epithelial-endothelial fusion clusters" were detected. These observations are consistent with the previous data generated by iFISH linking polyploidy with EMT (21, 75, 76). The presence of CD45 positive cells was detected in the clusters with polyploid or multinuclear cancer cells (21, 69).

Quite importantly, comparison of the total count of CTCs and/or circulating tumor endothelial cells between 31 conditions revealed that CTCs are present in multiple cancers, however, the highest frequency of "CTCs" is observed within the group of non-neoplastic infectious diseases, suggesting that the pure presence of cells with these markers could not be used as a diagnostic test itself (69).

Consistent with the Atlas of Circulating Rare Cells (69), sequencing of CTC clusters and individual circulating cancer cells revealed the mixed epithelial-mesenchymal markers in hepatocellular carcinoma (Vimentin, epithelial: CDH1, EPCAM, ASGR2, Keratin 8, stemness: CD133, POU5F1, NOTCH1 and STAT3) (62) prostate cancer (EPCAM, keratins, E-cad, Vimentin, CD44) (77) and Vimentin in lung cancer (78).

However, two major conceptual questions here currently remain not sufficiently addressed:

(i) How heterotypic interactions of cancer cells with WBCs promote polyploidy?

(ii) How does the combination of ploidy and mesenchymal phenotype enhance metastasis?

Mechanisms of how heterotypic interactions promote mobility and mesenchymal phenotype are described in the subsequent section.

4 Heterotypic interactions within tumor microenvironment are pivotal for CTC cluster formation

Interactions with cells of cancer microenvironment promote EMT, formation of CTC clusters and metastasis (4, 31). Classically, EMT is accompanied by decrease of E-cadherin/N-cadherin ratio (79). A recent publication highlighted a novel role of the E-cadherin (E-cad, encoded by CDH1 gene) expressing cells in breast cancer metastasis (80, 81). It turned out that when cancer cells grow in the presence of CAFs there is a gradient of the E-cad from low at the trailing edge of the invading cancer cells to high E-cad behind it (4). Furthermore, another paper demonstrated that in breast cancer spheroid model stem cells lead the collective invasion co-expressing mesenchymal and epithelial marks (82).

Dermal implants of CAFs with MCF10 cells with low intrinsic metastatic potential promoted this low-high E-cad gradient, the CTC cell clustering and metastasis (4). High throughput RNA expression profiles revealed induction of carcinoembryonic antigen-related cell adhesion molecule 5 (CEACAM5; CAM5) and CEACAM6 (CAM6) in the presence of CAFs. This experiment revealed overexpression of 44 CAF-induced genes, whose expression is associated with poor prognosis in breast cancer. Mechanistically, E-cad, CAM5 and CAM6 interact with each other forming an adherent junction complex on the cell surface. Functional shRNA studies revealed attenuation of lung metastasis upon E-cad, CAM5, or CAM6 depletion. Other excellent functional investigations reported in this paper revealed that CAF produced SDF-1(encoded by CXCL12 gene) and TGF-β that through their cognate receptors CXCR4 and TGFBRII activate SRC kinase phosphorylation/Zeb1 axis altogether mediating tumor cell cluster formation that are also detected as CTC clusters. The caveat of this report for our purposes is that we do not know if fibroblasts travel in the bloodstream with cancer cells. However, this paper clearly demonstrates stromal-cancer cell molecular interactions that regulate the ability of cancer to metastasize (4). Importantly, CRCX4 mediates immunosuppressive tumor microenvironment not only in cancer cells, but also in the SMA positive stromal cells including myofibroblasts and pericytes (32). CRE-Lox mediated knockout of CRCX4 in SMA expressing cells improved survival in mice with breast cancer, and pharmacological inhibition of CRCX4 potentiated activity of immune checkpoint inhibitors in the nude mice bearing human metastatic breast cancer (32).

Similarly, to observation in breast cancer, cells of the collective invasion packs were E-cad positive in lung adenocarcinoma (5). The role of CAFs in the metastasis was demonstrated by the fact that only surrounding CAFs express vimentin and in the vimentin knockout mice, the CAFs motility decreases *in vitro* and *in vivo*. Vimentin was required for the heterotypic cancer cell - CAFs interaction, collective invasion, and lung adenocarcinoma metastasis (5).

Thus, formation of Epithelial-mesenchymal gradient during collective invasion is mediated by cancer cell – stromal cell interaction and pivotal for CTC formation and metastasis (4, 5).

We schematized major findings on CTC interactions and their molecular physiological effects on Figures 1, 2.

5 Expression of molecules involved in the CTC cluster formation and metastasis correlate with cancer survival

As it is discussed in the previous sections, the formation of the CTC clusters and metastasis in particular cancers depend on IL1R1 (16), IL6, NODAL, NOTCH1 (17), CD44 (14), CXCR4 (4), TGFBR2 (4), CDH1 (4, 28), EPCAM (29), ICAM1 (30), and CCR1 (31). Theoretically, these molecules can impact cancer metastasis with little to no information on the mechanisms

10.3389/fimmu.2023.1099921

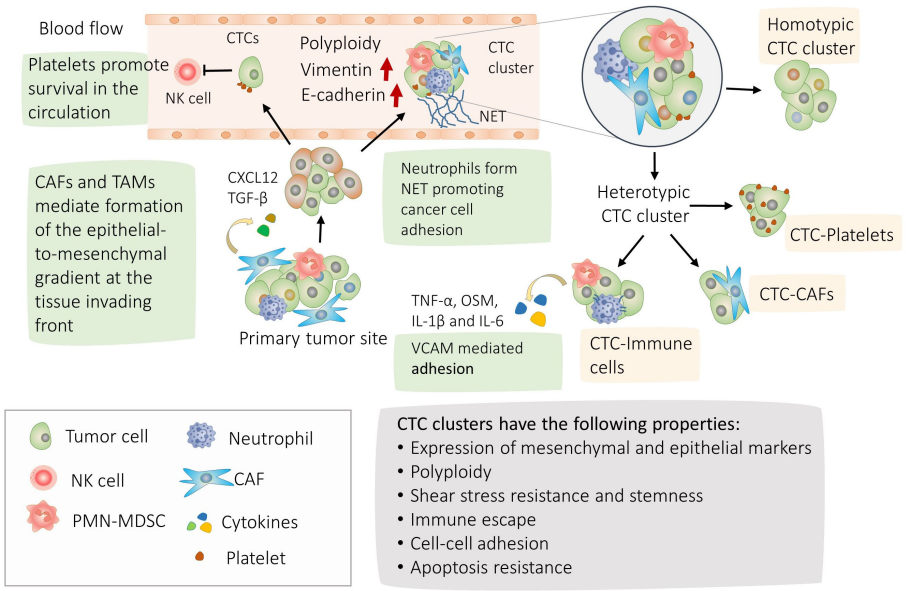

FIGURE 1
Mechanisms of circulating tumor cells (CTC) cluster formation and their properties. Highlighted in green, the process of CTC clusters formation; Tumor cells can separate from adjacent cells with more mobile mesenchymal cells at the leading edge of the invasion and cells with more epithelial properties behind (4, 5). Accordingly, mixed epithelial mesenchymal phenotype and polyploidy are frequently observed in the CTC clusters (21, 22). CTCs and CTC clusters are able to withstand the shear stress in the blood circulation and escape natural killer (NK). CTCs can form homotypic clusters or interact with CAFs, neutrophils, PMN-MDSCs, Tumor associated macrophages (TAM) or platelets forming heterotypic clusters (14, 16, 17). CAFs circulate in the bloodstream in heterotypic CTC clusters and promote cancer cell clustering by secreting CXCL12 and TGF-β (4, 13, 20). During transit and metastasis, platelet-rich thrombus form around CTCs providing protection from shear stress and against lysis by NK cells (56–58). CTC-associated neutrophils express TNF-α, OSM, IL-1β and IL-6 cytokines and their receptors are expressed correspondingly in CTCs. The interaction between CTCs and neutrophils is mediated by VCAM1, whereas TNF-α, OSM, IL-1β, and IL-6 promote proliferation of CTCs (16). In addition, neutrophils promote metastasis by releasing their DNA forming neutrophil extracellular traps (NET) (39). In turn, interaction with polymorphonuclear myeloid derived suppressor cells promote survival of the CTC clusters (17).

involved in CTC cluster formation. To address this possibility, we interrogated a publicly available The Cancer Genome Atlas project (TCGA) database and research papers to examine if high or low expression of molecules that are functionally important for the formation of CTC clusters may characterize patient survival in multiple cancers. For example, it was demonstrated that IL1R1 protein induces CTC proliferation in breast cancer (BRCA) (16), and high *IL1R* gene expression corresponds to inferior prognosis in the TCGA-BRCA cohort (Figure 3A) as well as in many other cancers (Figures 3B, C; Table 2). In turn, high expression of *CXCR4* in BRCA corresponds to better prognosis, smaller yet significant difference between Kaplan-Meier curves predicting better prognosis was observed for lung adenocarcinoma (LUAD) and thyroid cancer (THCA) (Figure 3B, Table 2), whereas no difference was observed in lung squamous cell carcinoma (LUSC).

The clustering analysis separated CTC marker genes into two major groups: (*i*) *CD44, CXCR4, ICAM1, CCR1*, and *IL1R1* where high expression correlated with poor survival for low grade gliomas (LGG), kidney renal clear cell carcinoma (KIRC), for glioblastoma (GBM), kidney renal papillary cell carcinoma (KIRP) or lung squamous cell carcinoma (LUSC) (Figure 3C).

The second gene cluster (*ii*) includes *TGFBR2, IL6ST, IL6R, CDH1*, and *IGFBP5*. In this group we observed a correlation between high expression and better prognosis in KIRC and worse prognosis in KIRP and LGG.

As discussed in the previous sections, molecules included in the analysis promote CTC cluster formation or metastasis in functional studies. Indeed, the results of clustering analysis suggest that high expression of genes from the first cluster predicts a rapid disease progression in multiple cancers. Conversely, the second cluster contains more genes whose expression promotes cancer progression in a cancer specific manner.

However, in some cases focused investigations contradict prediction of patient survival based on the TCGA dataset (Table 3, upper right triangles in Figure 3B depict approximates for HR collected from the literature). Specifically, high expression of stem cell marker *CD44* corresponded to poor prognosis in kidney cancers (KIRC, KIRP) in TCGA data and, accordingly, high CD44 and b-catenin immunostaining correlated with advanced stage, although no significant correlation with survival could be observed in a specific focused study (117). However, other reports communicated a correlation between high CD44 levels and decrease of progression free survival in renal cell carcinoma after treatment with multi-targeted tyrosine kinase inhibitor (84). Consistent with the literature, high *CD44* expression predicts inferior prognosis in LGG and GBM TCGA cohorts (85, 86). The only case of association between *CD44* expression and positive thyroid cancer prognosis contradicts to the literature (87) (Figure 3B).

It was reported that high *CXCR4* expression corresponds to bad prognosis for breast (88), lung (90) and colorectal (118) cancers

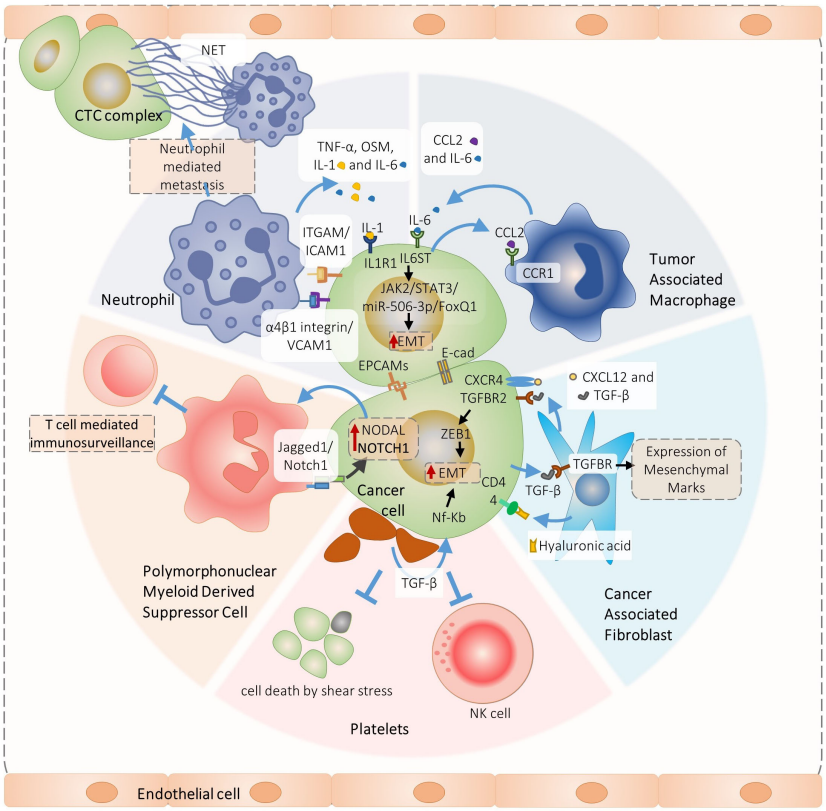

FIGURE 2
Overview of signaling pathways involved in the heterotypic cancer cell interactions pivotal for circulating tumor cells complex formation and metastasis. Specifically, PMN-MDSC-cancer cell interaction promotes ROS-induces Jagged1/Notch1/Nodal signaling that induces CTC cluster formation and metastasis (17), In turn, neutrophil interact with cancer cells *via* ITGAM/ICAM-1 adhesion facilitating interaction with liver sinusoids and metastasis (30). In addition, VCAM1 is required for the neutrophil-CTC cluster formation (29). Neutrophils produce IL1 and IL-6 that promote growth of neutrophils-CTC clusters *via* IL6ST and IL1R1 receptors (16), The Il-6 is also produced by the tumor associated macrophages which induce JAK2/STAT3/miR-506-3p/FoxQ1 signaling in cancer cells promoting epithelial mesenchymal transition (EMT), metastasis and further attraction of macrophages by the CCl2 secretion (31). A similar positive feedback loop is organized by the cancer-associated fibroblasts (CAFs) and cancer cells interactions. The CAFs produce TGF-β and CXCL12 that interact with TGFBR2 and CXCR4 receptors, inducing cancer cell EMT, CTC clusters and metastasis (4). In turn, cancer cells produce TGF-β and induce CAFs myofibroblast differentiation (83).

contradicting TCGA-based findings (Figures 3B, C). It was recently reported that in advanced CD8 negative thyroid cancer, high expression of CXCR4 and its ligand CXCL12 (SDF-1) correlates with bad prognosis, thus contradicting to TCGA data (89).

In contrast, *ICAM1* expression is associated with favorable prognosis in the breast cancer TCGA cohort, consistent with similar survival analysis of NCBI GEO dataset and repression of the lung metastasis in spontaneous breast cancer metastasis model (91) and contradicting another paper reporting pivotal role of the *ICAM1* in the CTC cluster formation, trans-endothelial migration and metastasis in breast cancer (92).

Thus, the positive associations between expression of CD44, CXCR4 and ICAM1 for thyroid, lung and breast cancers in TCGA dataset are not consistent with the literature suggesting that the first cluster is indeed represents genes whose high expression correlates with inferior prognosis consistent with their role in the CTCs biology.

Further we compared TCGA prediction with the literature for a few genes from the second cluster to address the question if they have more tissue specific roles in cancer metastasis.

One of such genes is CDH1 (E-cad protein) whose high expression was a predictor of better prognosis for colorectal cancer in agreement with TCGA data (93, 94). Again, consistent with TCGA data, high protein staining of E-cad in kidney renal papillary cell carcinoma was associated with worse prognosis, and no association was detected for kidney renal clear cell carcinoma (96). Recent analysis of E-cad in the cohort of NSCLC with 66% cases representing squamous cell carcinoma identifies E-cad as a positive prognostic factor consistent with TCGA data (97).

When astrocytomas, oligodendrogliomas and oligoastrocytomas were analyzed, the loss of E-cad immunostaining and hypermethylation of its promoter were associated with worse prognosis contradicting TCGA data, although, gene expression analysis was not performed (95). In contrast, consistent with TCGA data, a positive association between higher E-cad expression and worse prognosis was reported in the low-grade gliomas and in glioblastoma (119, 120).

IL6 receptors IL6ST and IL6R are involved in the CTC heterotypic interactions in breast (16) and colorectal cancers (31). Consistent with the literature, expression of IL6R has strong prognostic value in glioblastoma (98) and in lung adenocarcinoma (99, 100). In contrast,

10.3389/fimmu.2023.1099921

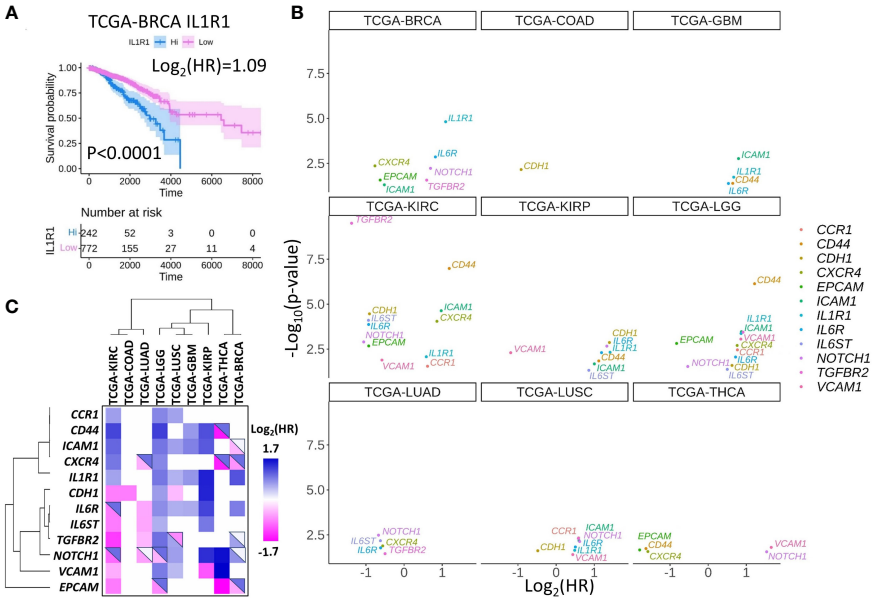

FIGURE 3
Set of selected CTC-associated genes differentially predict survival in several human cancer types. **(A)** An example of Kaplan-Meier curve for breast cancer (BRCA) patients stratified by high or low *IL1R1* expression in tumors. Shaded areas represent 95% confidence intervals. Time is shown in days. **(B)** Hazard ratios (HR) and significance of the differences between Kaplan-Meier curves for patients stratified by the expression of indicated genes for the panel of solid tumors in TCGA database. Only genes with p<0.05 are shown. Note that $\log_2$(HR)<0 for good prognosis corresponding to high gene expression and $\log_2$(HR)>0 for bad prognosis. **(C)** Hazard ratio clustering for gene - cancer combinations revealed two major gene clusters. Top-right triangles depict approximations of the HR collected from the literature. Blue colors represent genes or gene products whose expression is associated with worse prognosis, pink colors represent genes or gene products whose expression is associated with good prognosis while white colors represent cases where the data is controversial.

in kidney clear cell carcinoma we found a contradiction between the literature and TCGA data concerning the biomarker potential of IL6R expression: good predictor according to the literature (101, 102), and poor predictor according to TCGA data. Thus, the role of IL6R expression in cancer can be considered tissue specific.

The member of TGFb receptor family - TGFBR2 is a tumor suppressor in lung cancer, and the loss of TGFBR2 expression is associated with worse prognosis of both squamous cell cancer and adenocarcinoma (107, 108). Accordingly, TGFBR2 mutation predicts lung cancer resistance to checkpoint inhibitors (121). Thus, the literature supports prediction of TCGA dataset regarding the role of TGFBR2 in LUAD progression and contradicts association of high TGFBR2 with negative prognosis in LUSC. In breast cancer, reduced expression of TGFBR2 is associated with worse prognosis contradicting the TCGA data (109) especially in ER positive patients (110), while the report by Gao and coauthors is in line with the TCGA data (111). Theoretically, these contradictions might be connected with the presence of *TGFBR2* mutations which were not investigated in these published reports. Little is known about the influence of the TGFBR2 on glioma survival, however TCGA prediction of the negative association might be valuable since TGBFR2 compensates for inhibition of PDGFR, thereby promoting survival (122).

NOTCH1 activation as measured by the immunostaining against NOTCH intracellular domain correlates with poor prognosis of kidney renal clear cell carcinoma (KIRC) (123). In turn, high total *NOTCH1* immunostaining is associated with progression of kidney renal clear cell carcinoma contradicting TCGA prediction (103, 104). Likewise, in contrast to TCGA data, literature suggests association of NOTCH1 expression and glioma progression by modulating CXCL12/CXCR4 (105, 124).

In contrast, a recent meta-analysis revealed that *NOTCH1* expression does not correlate with overall survival in adenocarcinoma, although DLL4 and HES1 were associated with worse prognosis (125).

Measurements of *VCAM1* in KIRC revealed association of high expression with good prognosis consistent with TCGA data analysis (115, 116). In turn, for KIRP we found no published data that can validate the association of *VCAM1* high expression with good prognosis observed for the TCGA dataset.

EPCAM expression was associated with favorable prognosis of breast cancer in TCGA data, however immunohistochemical analysis has shown that it is associated with worse prognosis specifically in the basal-like and luminal B HER2+ subtypes (113). However, in the HER2 + subtype, *EPCAM* was also reported to be associated with worse prognosis (112). Again, in LGG the protein level of *EPCAM* was associated with poor prognosis, which contradicts to the TCGA trends (113). In thyroid cancers, the presence of EPCAM cleavage product was associated with more aggressive disease progression, although gene expression was not measured in this report (126). Finally, in agreement with the TCGA dataset, high EPCAM expression was associated with better prognosis in kidney cancers (114).

Overall, after comparison of TCGA data with the literature, it is possible to conclude that genes of the first cluster (top, Figure 3B) are mostly predictors of poor prognosis, whereas genes of the

10.3389/fimmu.2023.1099921

TABLE 2 *p*-values and Hazard ratio (HR) levels for survival of patients with high gene expression in tumors depicted in Figures 3B, C.

Gene name	TCGA project ID	p-value	HR	log_2(HR)
CCR1	TCGA-KIRC	0.0283	0.65	-0.61
CCR1	TCGA-LGG	0.0035	0.59	-0.77
CCR1	TCGA-LUSC	0.0047	0.67	-0.59
CD44	TCGA-GBM	0.0408	0.64	-0.64
CD44	TCGA-KIRC	0.0000	0.44	-1.18
CD44	TCGA-KIRP	0.0143	0.46	-1.12
CD44	TCGA-LGG	0.0000	0.43	-1.22
CD44	TCGA-THCA	0.0181	3.10	1.63
CDH1	TCGA-COAD	0.0070	1.89	0.92
CDH1	TCGA-KIRC	0.0000	1.88	0.91
CDH1	TCGA-KIRP	0.0014	0.38	-1.40
CDH1	TCGA-LGG	0.0255	0.65	-0.63
CDH1	TCGA-LUSC	0.0240	1.40	0.48
CXCR4	TCGA-BRCA	0.0044	1.70	0.76
CXCR4	TCGA-KIRC	0.0001	0.55	-0.86
CXCR4	TCGA-LGG	0.0020	0.59	-0.76
CXCR4	TCGA-LUAD	0.0129	1.47	0.56
CXCR4	TCGA-THCA	0.0266	2.99	1.58
EPCAM	TCGA-BRCA	0.0269	1.54	0.63
EPCAM	TCGA-KIRC	0.0021	1.90	0.93
EPCAM	TCGA-LGG	0.0015	1.77	0.83
EPCAM	TCGA-THCA	0.0217	z3.47	1.80
ICAM1	TCGA-BRCA	0.0493	1.43	0.52
ICAM1	TCGA-GBM	0.0017	0.58	-0.80
ICAM1	TCGA-KIRC	0.0000	0.51	-0.97
ICAM1	TCGA-KIRP	0.0214	0.48	-1.06
ICAM1	TCGA-LGG	0.0003	0.55	-0.87
ICAM1	TCGA-LUSC	0.0066	0.66	-0.60
IL1R1	TCGA-BRCA	0.0000	0.47	-1.09
IL1R1	TCGA-GBM	0.0186	0.63	-0.67
IL1R1	TCGA-KIRC	0.0084	0.67	-0.58
IL1R1	TCGA-KIRP	0.0047	0.38	-1.41
IL1R1	TCGA-LGG	0.0004	0.55	-0.86
IL1R1	TCGA-LUSC	0.0226	0.71	-0.49
IL6R	TCGA-BRCA	0.0014	0.57	-0.82
IL6R	TCGA-GBM	0.0415	0.69	-0.53
IL6R	TCGA-KIRC	0.0001	1.91	0.93
IL6R	TCGA-KIRP	0.0050	0.44	-1.19
IL6R	TCGA-LGG	0.0088	0.61	-0.72

(Continued)

TABLE 2 Continued

Gene name	TCGA project ID	p-value	HR	log_2(HR)
IL6R	TCGA-LUAD	0.0166	1.53	0.62
IL6R	TCGA-LUSC	0.0148	0.70	-0.50
IL6ST	TCGA-KIRC	0.0001	1.91	0.93
IL6ST	TCGA-KIRP	0.0474	0.55	-0.86
IL6ST	TCGA-LGG	0.0422	0.71	-0.50
IL6ST	TCGA-LUAD	0.0067	1.54	0.62
NOTCH1	TCGA-BRCA	0.0060	0.62	-0.69
NOTCH1	TCGA-KIRC	0.0013	2.08	1.06
NOTCH1	TCGA-KIRP	0.0021	0.40	-1.33
NOTCH1	TCGA-LGG	0.0292	1.45	0.54
NOTCH1	TCGA-LUAD	0.0033	1.59	0.67
NOTCH1	TCGA-LUSC	0.0074	0.65	-0.62
NOTCH1	TCGA-THCA	0.0275	0.35	-1.53
TGFBR2	TCGA-BRCA	0.0271	0.66	-0.59
TGFBR2	TCGA-KIRC	0.0000	2.60	1.38
TGFBR2	TCGA-LGG	0.0004	0.53	-0.91
TGFBR2	TCGA-LUAD	0.0350	1.41	0.50
TGFBR2	TCGA-LUSC	0.0050	0.67	-0.58
VCAM1	TCGA-KIRC	0.0121	1.49	0.58
VCAM1	TCGA-KIRP	0.0050	2.28	1.19
VCAM1	TCGA-LGG	0.0012	0.56	-0.84
VCAM1	TCGA-LUSC	0.0392	0.74	-0.44
VCAM1	TCGA-THCA	0.0187	0.32	-1.62

second cluster (bottom, Figure 3B) predict survival in a cancer type-specific manner (Figure 3B).

For interrogation of TCGA expression and survival data, we used standard analytic tools from the TCGA project portal GDC (127, 128). The discrepancies between results of TCGA data analysis and the literature could originate from different experimental methods used to assess gene expression, or different cohorts of patients and different treatment regimens among others. Thus, results of positive or negative gene association with patient survival require independent verification to identify or to confirm reliable biomarkers of disease progression and potential targets for drug development.

6 Molecules involved in the CTC heterotypic interaction and known drug targets

Analysis of the TCGA data and the literature revealed that high expression of molecules involved in the CTC heterotypic interactions predicts survival in many cancer types. Accordingly, as it is discussed in the previous sections, these molecules are pivotal for metastasis and therefore sometimes represent targets of clinically approved or experimental cancer drugs. Specifically, results of TCGA dataset analysis suggest poor prognosis for IL6 overexpressing low grade gliomas and glioblastomas. Indeed, pre-clinical data demonstrated that IL6 blockade combined with CD40 stimulation sensitized glioblastoma to immune checkpoint inhibitors and improved survival (129, 130). Likewise, pre-clinical investigations revealed that targeting of the IL6 signaling might be beneficial for other cancers as well, where bad prognosis is associated with high IL6 level such as renal cell carcinoma (131, 132), non-small cell lung cancer (133), and breast cancer (134). We found a single, currently suspended clinical trial of the IL6R antibody tocilizumab for gliomas and glioblastoma treatment (NCT04729959), trials for metastatic breast cancer (NCT03135171), non-small lung cancer among others (NCT04940299, Table 4). Targeting of IL-6 improves immunotherapy outcome in mice models (155, 156). However, IL6-specific antibody siltuximab demonstrated no efficiency against renal cell carcinoma (157) and prostate cancer (158).

IL1R1 expression predicts poor survival in nearly the same set of cancer types as IL6R. There are multiple clinical trials testing IL1R agonist an anti-rheumatoid arthritis drug anakinra against multiple myeloma (136), metastatic breast cancer, and colorectal

10.3389/fimmu.2023.1099921

TABLE 3 Comparison between prediction of patient survival based on TCGA dataset and review of published literature.

Gene ID	Cancer type	Literature reported HR for patients with high level of gene or corresponding protein in the tumors.	TCGA calculated HR for patients with high expression of gene in the tumors	Reference
CD44	Renal cell carcinoma	high	high	(84)
CD44	Low grade glioma	high	high	(85, 86)
CD44	Thyroid	high	low	(87)
CXCR4	Breast	high	low	(88)
CXCR4	Thyroid (CD8 low)	high	low	(89)
CXCR4	Lung	high	low	(90)
ICAM1	Breast	low	low	(91)
ICAM1	Breast	high	low	(92)
CDH1	Colorectal	low	low	(93, 94)
CDH1	Low grade glioma	high	high	(95)
CDH1	Kidney renal papillary cell carcinoma	high	high	(96)
CDH1	Squamous cell carcinoma	low	low	(97)
IL6R	Glioblastoma	high	high	(98)
IL6R	Lung adenocarcinoma	low	low	(99, 100)
IL6R	Kidney renal clear cell carcinoma	high	low	(101, 102)
NOTCH1	Kidney renal clear cell carcinoma	high	low	(103, 104)
NOTCH1	Low grade glioma	high	low	(105, 106)
TGFBR2	Lung adenocarcinoma	low	low	(107, 108)
TGFBR2	Lung squamous cell carcinoma	low	high	(107, 108)
TGFBR2	Breast cancer	low	high	(109, 110)
TGFBR2	Breast cancer	high	high	(111)
EPCAM	Breast cancer	high	low	(112)
EPCAM	Low grade glioma	high	low	(113)
EPCAM	Kidney renal clear cell carcinoma	low	low	(114)
EPCAM	Kidney renal papillary cell carcinoma	low	low	(114)
VCAM1	Kidney renal clear cell carcinoma	low	low	(115, 116)

cancer (159), listed in Table 4. However, we didn't find any specific records for gliomas, lung or kidney cancers. Still, several preclinical investigations have shown that targeting of IL1 signaling in GBM (137, 138), LGG (139) kidney (140) and lung cancer (141) suggest its potential clinical usefulness.

Expression of adhesion molecule ICAM1 also predicts poor prognosis for several cancer types, closely mimicking the effects observed for the *IL1R1* and *IL6R* genes. Specifically, low ICAM1 expression corresponds to better survival in GBM. Indeed, bispecific CAR-T cells against EPCAM and ICAM1 elicited good response in

TABLE 4 Potential off-label applications of drugs targeting molecules involved in the heterotypic CTCs interactions.

CTC cancer type	Target	Target ligand(s)	Drug	Current therapeutic applications	Potential therapeutic applications	References and clinical trials
Breast, Colorectal	IL6ST IL6R	IL6	Siltuximab, tocilizumab	Castleman disease, Rheumatoid arthritis, GBM, LGG, LUSC, BRCA		(129, 130, 133–135) NCT04729959 NCT04940299 NCT03135171
Breast	IL1R1	IL1	anakinra	rheumatoid arthritus, MM, BRCA, colorectal cancer	GBM, LGG, KIRP, KIRC LUSC	(136–141) NCT00635154 NCT01802970 NCT02090101
Breast	IL1R1	IL1	isoanakinra	Solid cancers	GBM, LGG, KIRP, KIRC LUSC	NCT04121442 NCT00072111
Breast	CD44	Hyaluronic acid	RG7356	NA	Solid cancers, AML, GBM	(142–145)
Breast	CXCR4	CXCL12	Ulocuplumab	Multiple myeloma	THCA	(146)
Breast	CXCR4	CXCL12	AMD3100/Plerixafor X4P-001	hematopoietic stem cell (HSC) mobilizer, colorectal cancer, glioblastoma	THCA	(147)
Breast	CXCR4	CXCL12	X4P-001	Triple negative Breast cancer	THCA	NCT05103917
Breast	CXCR4	CXCL12	MB1707	Advanced cancers, NSCLC, breast cancer	THCA	NCT05465590
Breast	TGFBR2	TGFB1	Vactosertib	Solid cancers	LGG, LUSC, BRCA	(148, 149)
Hepatocellular	EPCAM	CAMs	catumaxomab (anti-EpCAM x anti-CD3), bladder, ovarian cancers	malignant ascites	GBM	(150–153)
Lung	ICAM1	ITGAM	Lifitegrast LFA-1/ICAM-1 antagonists	dry eye disease	GBM, LGG, KIRP, KIRC	(153, 154)

MM, multiple myeloma; AML, acute myeloid leukemia.

GBM mice model (153), consistent with other preclinical studies (160, 161). Similarly, CAR-T cells targeted against ICAM1 were successfully tested in mice models of gastric (162), thyroid (163, 164), and triple negative breast cancer (165).

ICAM-1 conjugated with a cytotoxic drug was extensively tested for multiple myeloma (166) and another bispecific anti-CD38-ICAM-1 drug for multiple myeloma is under development (167). The vaccine targeting ICAM-1 is also at the early stage of clinical investigation against ICAM-1 overexpressing bladder cancers (168) or lung cancer (NCT02043665). However, so far, we did not find reports on ICAM-1 targeted therapies clinically tested against gliomas and kidney cancers.

A stem cell marker CD44 predicts poor prognosis in renal cancers and in gliomas. The CD44-specific antibody RG7356 in clinical trials showed moderate efficiency in solid tumors (142) and in acute myeloid leukemia (169). There is also multiple evidence suggesting potential efficiency of CD44 targeting for the treatment of GBM, although additional clinical validation is clearly needed (143–145).

Catumaxomab (genetically engineered bivalent anti-EPCAM and anti-CD3 antibody) is approved for the treatment of malignant ascites (150) and it has been also used experimentally for the treatment of bladder (151) and ovarian (152) cancers. Bispecific CAR-T simultaneously targeting EPCAM and ICAM-1 demonstrated promising results in mice models of gastric and pancreatic cancers (153).

Anti-CXCR4 antibody demonstrated efficiency in multiple myeloma in combination with lenalidomide or bortezomib plus dexamethasone (146), and several related clinical trials are ongoing. A CXCR4 inhibitor AMD3100/Plerixafor was approved by FDA as a hematopoietic stem cell mobilizer and it was recently tested in humans against pancreatic and colorectal cancers as the potential inducer of the immune response (147). Also, preclinical studies showed that inhibition of the CXCR4 might be potentially efficient against other cancers including GBM (170, 171), and the first human clinical trial of plerixafor as an adjunct to combined chemoradiotherapy was conducted in newly diagnosed GBM patients (172) achieving median overall survival of ~21 months. This is a significant improvement over ~17 months period characteristic for the standard chemoradiotherapy (173).

Finally, gamma secretase inhibitors showed therapeutic effects only in CNS tumors and desmoids (174). Targeting of TGF-β receptor is also in development and in clinical trials (148). In turn, anti-VCAM antibodies dramatically reduced pancreatic ductal adenocarcinoma progression in mice models (175, 176).

In Table 4, we summarized drugs targeting molecules involved in the CTC heterotypic interactions.

7 Conclusions

Analysis of the literature describing factors leading to formation of CTC clusters revealed three major features. *First* - the presence of either heterotypic or homotypic CTC aggregates often means unfavorable prognosis and predicts metastasis in many cancer types. Targeting the formation of such clusters is a valuable strategy for metastasis suppression (4, 6, 17). *Second* - cells carry mesenchymal (Vimentin) and epithelial (E-cad) markers together, which is a hallmark of intermediate epithelial associated with stemness of cancer cells (177, 178). *Third* - in turn, intermediate Mesenchymal- Epithelial state frequently coincides with polyploidy as it was shown in lung and colorectal cancers (179, 180). In lung cancer, polyploidy was accompanied by the interaction with WBCs, which were identified as neutrophils or PMN-MDSCs.

It is well established that both polyploidy/mixed EMT phenotype and immunosuppressive PMN-MDSC and TAM contribute to cancer progression, however, how the interaction between them mediates metastatic advantage is yet to be investigated.

Taken together, these findings highlight common mechanisms of metastasis with implication for drug development and cancer treatment.

Author contributions

JMR wrote the text, edited figures and performed data analysis, TM wrote the text and prepared figures, AAB conceptualization and text writing and editing, JMR, AAB and TM These authors contributed equally to this work and share first authorship. OAR, DAD, VVP, and IVA collected related literature, compiled data and wrote the manuscript. All authors contributed to the article and approved the submitted version.

Funding

This study was supported by Russian Science Foundation (project No. 22-15-00483), https://rscf.ru/en/project/22-15-00483/.

Conflict of interest

The authors declare that the research was conducted in the absence of any commercial or financial relationships that could be construed as a potential conflict of interest.

Publisher's note

References

1. Hanahan D. Hallmarks of cancer: New dimensions. *Cancer Discovery* (2022) 12 (1):31–46. doi: 10.1158/2159-8290.CD-21-1059

2. Blomberg OS, Spagnuolo L, de Visser KE. Immune regulation of metastasis: Mechanistic insights and therapeutic opportunities. *Dis Model Mech* (2018) 11(10). doi: 10.1242/dmm.036236

3. Kim K-J, Godarova A, Seedle K, Kim M-H, Ince TA, Wells SI, et al. Rb Suppresses collective invasion, circulation and metastasis of breast cancer cells in CD44-dependent manner. *PloS One* (2013) 8(12):e80590. doi: 10.1371/journal.pone.0080590

4. Matsumura Y, Ito Y, Mezawa Y, Sulidan K, Daigo Y, Hiraga T, et al. Stromal fibroblasts induce metastatic tumor cell clusters *via* epithelial-mesenchymal plasticity. *Life Sci Alliance* (2019) 2(4). doi: 10.26508/lsa.201900425

5. Richardson AM, Havel LS, Koyen AE, Konen JM, Shupe J, Wiles WG, et al. Vimentin is required for lung adenocarcinoma metastasis *via* heterotypic tumor cell-Cancer-Associated fibroblast interactions during collective invasion. *Clin Cancer Res* (2018) 24(2):420–32. doi: 10.1158/1078-0432.CCR-17-1776

6. Gkountela S, Castro-Giner F, Szczerba BM, Vetter M, Landin J, Scherrer R, et al. Circulating tumor cell clustering shapes DNA methylation to enable metastasis seeding. *Cell* (2019) 176(1–2):98–112.e14. doi: 10.1016/j.cell.2018.11.046

7. Rozenberg JM, Zvereva S, Dalina A, Blatov I, Zubarev I, Luppov D, et al. Dual role of p73 in cancer microenvironment and DNA damage response. *Cells* (2021) 10(12). doi: 10.3390/cells10123516

8. Herrera M, Galindo-Pumariño C, García-Barberán V, Peña C. A snapshot of the tumor microenvironment in colorectal cancer: The liquid biopsy. *Int J Mol Sci* (2019) 20(23). doi: 10.3390/ijms20236016

9. Nakamura M, Suetsugu A, Hasegawa K, Satake T, Kunisada T, Shimizu M, et al. Color-coded imaging distinguishes cancer cells, stromal cells, and recombinant cancer-stromal cells in the tumor microenvironment during metastasis. *Anticancer Res* (2018) 38(8):4417–23. doi: 10.21873/anticanres.12743

10. Shtam T, Naryzhny S, Kopylov A, Petrenko E, Samsonov R, Kamyshinsky R, et al. Functional properties of circulating exosomes mediated by surface-attached plasma proteins. *J Hematol* (2018) 7(4):149–53. doi: 10.14740/jh412w

11. Shtam T, Naryzhny S, Samsonov R, Karasik D, Mizgirev I, Kopylov A, et al. Plasma exosomes stimulate breast cancer metastasis through surface interactions and activation of FAK signaling. *Breast Cancer Res Treat* (2019) 174(1):129–41. doi: 10.1007/s10549-018-5043-0

12. Costa-Silva B, Aiello NM, Ocean AJ, Singh S, Zhang H, Thakur BK, et al. Pancreatic cancer exosomes initiate pre-metastatic niche formation in the liver. *Nat Cell Biol* (2015) 17(6):816–26. doi: 10.1038/ncb3169

13. Ao Z, Shah SH, Machlin LM, Parajuli R, Miller PC, Rawal S, et al. Identification of cancer-associated fibroblasts in circulating blood from patients with metastatic breast cancer. *Cancer Res* (2015) 75(22):4681–7. doi: 10.1158/0008-5472.CAN-15-1633

14. Sharma U, Medina-Saenz K, Miller PC, Troness B, Spartz A, Sandoval-Leon A, et al. Heterotypic clustering of circulating tumor cells and circulating cancer-associated fibroblasts facilitates breast cancer metastasis. *Breast Cancer Res Treat* (2021) 189 (1):63–80. doi: 10.1007/s10549-021-06299-0

15. Chen Q, Zou J, He Y, Pan Y, Yang G, Zhao H, et al. A narrative review of circulating tumor cells clusters: A key morphology of cancer cells in circulation promote hematogenous metastasis. *Front Oncol* (2022) 12:944487. doi: 10.3389/fonc.2022.944487

16. Szczerba BM, Castro-Giner F, Vetter M, Krol I, Gkountela S, Landin J, et al. Neutrophils escort circulating tumour cells to enable cell cycle progression. *Nature* (2019) 566(7745):553–7. doi: 10.1038/s41586-019-0915-y

17. Sprouse ML, Welte T, Boral D, Liu HN, Yin W, Vishnoi M, et al. PMN-MDSCs enhance CTC metastatic properties through reciprocal interactions *via* ROS/Notch/Nodal signaling. *Int J Mol Sci* (2019) 20(8). doi: 10.3390/ijms20081916

18. Aceto N, Bardia A, Miyamoto DT, Donaldson MC, Wittner BS, Spencer JA, et al. Circulating tumor cell clusters are oligoclonal precursors of breast cancer metastasis. *Cell* (2014) 158(5):1110–22. doi: 10.1016/j.cell.2014.07.013

19. Jansson S, Bendahl P-O, Larsson A-M, Aaltonen KE, Rydén L. Prognostic impact of circulating tumor cell apoptosis and clusters in serial blood samples from patients with metastatic breast cancer in a prospective observational cohort. *BMC Cancer*. (2016) 16:433. doi: 10.1186/s12885-016-2406-y

20. Duda DG, Duyverman AMMJ, Kohno M, Snuderl M, Steller EJA, Fukumura D, et al. Malignant cells facilitate lung metastasis by bringing their own soil. *Proc Natl Acad Sci USA* (2010) 107(50):21677–82. doi: 10.1073/pnas.1016234107

21. Li Z, Fan L, Wu Y, Niu Y, Zhang X, Wang B, et al. Analysis of the prognostic role and biological characteristics of circulating tumor cell-associated white blood cell clusters in non-small cell lung cancer. *J Thorac Dis* (2022) 14(5):1544–55. doi: 10.21037/jtd-22-423

22. Zhu H-H, Liu Y-T, Feng Y, Zhang L-N, Zhang T-M, Dong G-L, et al. Circulating tumor cells (CTCs)/circulating tumor endothelial cells (CTECs) and their subtypes in small cell lung cancer: Predictors for response and prognosis. *Thorac Cancer*. (2021) 12 (20):2749–57. doi: 10.1111/1759-7714.14120

23. Guan Y, Xu F, Tian J, Gao K, Wan Z, Wang Y, et al. The prognostic value of circulating tumour cells (CTCs) and CTC white blood cell clusters in patients with renal cell carcinoma. *BMC Cancer*. (2021) 21(1):826. doi: 10.1186/s12885-021-08463-7

24. Xu Y, Zhang Q, Xu Z, Xie Q, Ding W, Liu H, et al. Association of circulating tumor cell-white blood cell clusters with survival outcomes in patients with colorectal cancer after curative intent surgery. *Res Sq*. (2022). doi: 10.21203/rs.3.rs-1969451/v1

25. Chu H-Y, Yang C-Y, Yeh P-H, Hsu C-J, Chang L-W, Chan W-J, et al. Highly correlated recurrence prognosis in patients with metastatic colorectal cancer by synergistic consideration of circulating tumor Cells/Microemboli and tumor markers CEA/CA19-9. *Cells* (2021) 10(5). doi: 10.3390/cells10051149

26. Kozuka M, Battaglin F, Jayachandran P, Wang J, Arai H, Soni S, et al. Clinical significance of circulating tumor cell induced epithelial-mesenchymal transition in patients with metastatic colorectal cancer by single-cell RNA-sequencing. *Cancers (Basel)* (2021) 13(19). doi: 10.3390/cancers13194862

27. Herath S, Razavi Bazaz S, Monkman J, Ebrahimi Warkiani M, Richard D, O'Byrne K, et al. Circulating tumor cell clusters: Insights into tumour dissemination and metastasis. *Expert Rev Mol Diagn*. (2020) 20(11):1139–47. doi: 10.1080/14737159.2020.1846523

28. Mizukoshi K, Okazawa Y, Haeno H, Koyama Y, Sulidan K, Komiyama H, et al. Metastatic seeding of human colon cancer cell clusters expressing the hybrid epithelial/mesenchymal state. *Int J Cancer*. (2020) 146(9):2547–62. doi: 10.1002/ijc.32672

29. Hu C-L, Zhang Y-J, Zhang X-F, Fei X, Zhang H, Li C-G, et al. 3D culture of circulating tumor cells for evaluating early recurrence and metastasis in patients with hepatocellular carcinoma. *Onco Targets Ther* (2021) 14:2673–88. doi: 10.2147/OTT.S298427

30. Spicer JD, McDonald B, Cools-Lartigue JJ, Chow SC, Giannias B, Kubes P, et al. Neutrophils promote liver metastasis *via* mac-1-mediated interactions with circulating tumor cells. *Cancer Res* (2012) 72(16):3919–27. doi: 10.1158/0008-5472.CAN-11-2393

31. Wei C, Yang C, Wang S, Shi D, Zhang C, Lin X, et al. Crosstalk between cancer cells and tumor associated macrophages is required for mesenchymal circulating tumor cell-mediated colorectal cancer metastasis. *Mol Cancer*. (2019) 18(1):64. doi: 10.1186/s12943-019-0976-4

32. Chen IX, Chauhan VP, Posada J, Ng MR, Wu MW, Adstamongkonkul P, et al. Blocking CXCR4 alleviates desmoplasia, increases T-lymphocyte infiltration, and improves immunotherapy in metastatic breast cancer. *Proc Natl Acad Sci USA* (2019) 116(10):4558–66. doi: 10.1073/pnas.1815515116

33. Lu Y, Lian S, Ye Y, Yu T, Liang H, Cheng Y, et al. S-nitrosocaptopril prevents cancer metastasis *in vivo* by creating the hostile bloodstream microenvironment against circulating tumor cells. *Pharmacol Res* (2019) 139:535–49. doi: 10.1016/j.phrs.2018.10.020

34. Giesing M, Suchy B, Driesel G, Molitor D. Clinical utility of antioxidant gene expression levels in circulating cancer cell clusters for the detection of prostate cancer in patients with prostate-specific antigen levels of 4-10 ng/mL and disease prognostication after radical prostatectomy. *BJU Int* (2010) 105(7):1000–10. doi: 10.1111/j.1464-410X.2009.08920.x

35. Osmulski PA, Cunsolo A, Chen M, Qian Y, Lin C-L, Hung C-N, et al. Contacts with macrophages promote an aggressive nanomechanical phenotype of circulating tumor cells in prostate cancer. *Cancer Res* (2021) 81(15):4110–23. doi: 10.1158/0008-5472.CAN-20-3595

36. Alhaddad L, Pustovalova M, Blokhina T, Chuprov-Netochin R, Osipov AN, Leonov S. IR-surviving NSCLC cells exhibit different patterns of molecular and cellular reactions relating to the multifraction irradiation regimen and p53-family proteins expression. *Cancers (Basel)* (2021) 13(11). doi: 10.3390/cancers13112669

37. Zhao Q, Zhang K, Li Z, Zhang H, Fu F, Fu J, et al. High migration and invasion ability of pgccs and their daughter cells associated with the nuclear localization of S100A10 modified by sumoylation. *Front Cell Dev Biol* (2021) 9:696871. doi: 10.3389/fcell.2021.696871

38. Rozenberg JM, Zvereva S, Dalina A, Blatov I, Zubarev I, Luppov D, et al. The p53 family member p73 in the regulation of cell stress response. *Biol Direct*. (2021) 16(1):23. doi: 10.1186/s13062-021-00307-5

39. Park J, Wysocki RW, Amoozgar Z, Maiorino L, Fein MR, Jorns J, et al. Cancer cells induce metastasis-supporting neutrophil extracellular DNA traps. *Sci Transl Med* (2016) 8(361):361ra138. doi: 10.1126/scitranslmed.aag1711

40. Vishnoi M, Peddibhotla S, Yin W, T Scamardo A, George GC, Hong DS, et al. The isolation and characterization of CTC subsets related to breast cancer dormancy. *Sci Rep* (2015) 5:17533. doi: 10.1038/srep17533

41. Vishnoi M, Boral D, Liu H, Sprouse ML, Yin W, Goswami-Sewell D, et al. Targeting USP7 identifies a metastasis-competent state within bone marrow-resident melanoma CTCs. *Cancer Res* (2018) 78(18):5349–62. doi: 10.1158/0008-5472.CAN-18-0644

42. Zeng X, Liao G, Li S, Liu H, Zhao X, Li S, et al. Eliminating METTL1-mediated accumulation of PMN-MDSCs prevents hepatocellular carcinoma recurrence after radiofrequency ablation. *Hepatology* (2022). doi: 10.1002/hep.32585

43. Lu X, Lu X. Enhancing immune checkpoint blockade therapy of genitourinary malignancies by co-targeting PMN-MDSCs. *Biochim Biophys Acta Rev Cancer*. (2022) 1877(3):188702. doi: 10.1016/j.bbcan.2022.188702

44. Zhou J, Nefedova Y, Lei A, Gabrilovich D. Neutrophils and PMN-MDSC: Their biological role and interaction with stromal cells. *Semin Immunol* (2018) 35:19–28. doi: 10.1016/j.smim.2017.12.004

45. Gabrilovich DI. Myeloid-derived suppressor cells. *Cancer Immunol Res* (2017) 5 (1):3–8. doi: 10.1158/2326-6066.CIR-16-0297

46. Liu Q, Liao Q, Zhao Y. Myeloid-derived suppressor cells (MDSC) facilitate distant metastasis of malignancies by shielding circulating tumor cells (CTC) from immune surveillance. *Med Hypotheses*. (2016) 87:34–9. doi: 10.1016/j.mehy.2015.12.007

47. Boral D, Vishnoi M, HN L, Yin W, Sprouse ML, Scamardo A, et al. Molecular characterization of breast cancer CTCs associated with brain metastasis. *Nat Commun* (2017) 8(1):196. doi: 10.1038/s41467-017-00196-1

48. Raya A, Kawakami Y, Rodriguez-Esteban C, Buscher D, Koth CM, Itoh T, et al. Notch activity induces nodal expression and mediates the establishment of left-right asymmetry in vertebrate embryos. *Genes Dev* (2003) 17(10):1213–8. doi: 10.1101/gad.1084403

49. Arnoletti JP, Fanaian N, Reza J, Sause R, Almodovar AJ, Srivastava M, et al. Pancreatic and bile duct cancer circulating tumor cells (CTC) form immune-resistant multi-cell type clusters in the portal venous circulation. *Cancer Biol Ther* (2018) 19 (10):887–97. doi: 10.1080/15384047.2018.1480292

50. Silvestri M, Reduzzi C, Feliciello G, Vismara M, Schamberger T, Köstler C, et al. Detection of genomically aberrant cells within circulating tumor microemboli (CTMs) isolated from early-stage breast cancer patients. *Cancers (Basel)* (2021) 13(6). doi: 10.3390/cancers13061409

51. Osmulski P, Mahalingam D, Gaczynska ME, Liu J, Huang S, Horning AM, et al. Nanomechanical biomarkers of single circulating tumor cells for detection of castration resistant prostate cancer. *Prostate* (2014) 74(13):1297–307. doi: 10.1002/pros.22846

52. Gruber I, Landenberger N, Staebler A, Hahn M, Wallwiener D, Fehm T. Relationship between circulating tumor cells and peripheral T-cells in patients with primary breast cancer. *Anticancer Res* (2013) 33(5):2233–8.

53. Mego M, Gao H, Cohen EN, Anfossi S, Giordano A, Sanda T, et al. Circulating tumor cells (CTC) are associated with defects in adaptive immunity in patients with inflammatory breast cancer. *J Cancer*. (2016) 7(9):1095–104. doi: 10.7150/jca.13098

54. Muraro E, Del Ben F, Turetta M, Cesselli D, Bulfoni M, Zamarchi R, et al. Clinical relevance of the combined analysis of circulating tumor cells and anti-tumor T-cell immunity in metastatic breast cancer patients. *Front Oncol* (2022) 12:983887. doi: 10.3389/fonc.2022.983887

55. Xue D, Xia T, Wang J, Chong M, Wang S, Zhang C. Role of regulatory T cells and CD8+ T lymphocytes in the dissemination of circulating tumor cells in primary invasive breast cancer. *Oncol Lett* (2018) 16(3):3045–53. doi: 10.3892/ol.2018.8993

56. Palumbo JS, Talmage KE, Massari JV, La Jeunesse CM, Flick MJ, Kombrinck KW, et al. Platelets and fibrin(ogen) increase metastatic potential by impeding natural killer cell-mediated elimination of tumor cells. *Blood* (2005) 105(1):178–85. doi: 10.1182/blood-2004-06-2272

57. Erpenbeck L, Schön MP. Deadly allies: the fatal interplay between platelets and metastasizing cancer cells. *Blood* (2010) 115(17):3427–36. doi: 10.1182/blood-2009-10-247296

58. Contursi A, Sacco A, Grande R, Dovizio M, Patrignani P. Platelets as crucial partners for tumor metastasis: from mechanistic aspects to pharmacological targeting. *Cell Mol Life Sci* (2017) 74(19):3491–507. doi: 10.1007/s00018-017-2536-7

59. Placke T, Örgel M, Schaller M, Jung G, Rammensee H-G, Kopp H-G, et al. Platelet-derived MHC class I confers a pseudonormal phenotype to cancer cells that subverts the antitumor reactivity of natural killer immune cells. *Cancer Res* (2012) 72 (2):440–8. doi: 10.1158/0008-5472.CAN-11-1872

60. Ting DT, Wittner BS, Ligorio M, Vincent Jordan N, Shah AM, Miyamoto DT, et al. Single-cell RNA sequencing identifies extracellular matrix gene expression by pancreatic circulating tumor cells. *Cell Rep* (2014) 8(6):1905–18. doi: 10.1016/j.celrep.2014.08.029

61. Labelle M, Begum S, Hynes RO. Direct signaling between platelets and cancer cells induces an epithelial-mesenchymal-like transition and promotes metastasis. *Cancer Cell* (2011) 20(5):576–90. doi: 10.1016/j.ccr.2011.09.009

62. Chen VL, Huang Q, Harouaka R, Du Y, Lok AS, Parikh ND, et al. A dual-filtration system for single-cell sequencing of circulating tumor cells and clusters in HCC. *Hepatol Commun* (2022) 6(6):1482–91. doi: 10.1002/hep4.1900

63. Teeuwssen M, Fodde R. Cell heterogeneity and phenotypic plasticity in metastasis formation: The case of colon cancer. *Cancers (Basel)* (2019) 11(9). doi: 10.3390/cancers11091368

64. Zeisberg M, Neilson EG. Biomarkers for epithelial-mesenchymal transitions. *J Clin Invest*. (2009) 119(6):1429–37. doi: 10.1172/JCI36183

65. Guen VJ, Chavarria TE, Kröger C, Ye X, Weinberg RA, Lees JA. EMT programs promote basal mammary stem cell and tumor-initiating cell stemness by inducing primary ciliogenesis and hedgehog signaling. *Proc Natl Acad Sci USA* (2017) 114(49): E10532–9. doi: 10.1073/pnas.1711534114

66. Taki M, Abiko K, Ukita M, Murakami R, Yamanoi K, Yamaguchi K, et al. Tumor immune microenvironment during epithelial-mesenchymal transition. *Clin Cancer Res* (2021) 27(17):4669–79. doi: 10.1158/1078-0432.CCR-20-4459

67. Majc B, Sever T, Zarić M, Breznik B, Turk B, Lah TT. Epithelial-to-mesenchymal transition as the driver of changing carcinoma and glioblastoma microenvironment. *Biochim Biophys Acta Mol Cell Res* (2020) 1867(10):118782. doi: 10.1016/j.bbamcr.2020.118782

68. Li M, Gao F, Ren X, Dong G, Chen H, Lin AY, et al. Nonhematogenic circulating aneuploid cells confer inferior prognosis and therapeutic resistance in gliomas. *Cancer Sci* (2022) 113(10):3535–46. doi: 10.1111/cas.15516

69. Hu B, Gong Y, Wang Y, Xie J, Cheng J, Huang Q. Comprehensive atlas of circulating rare cells detected by SE-iFISH and image scanning platform in patients with various diseases. *Front Oncol* (2022) 12:821454. doi: 10.3389/fonc.2022.821454

70. Mirzayans R, Andrais B, Murray D. Roles of polyploid/multinucleated giant cancer cells in metastasis and disease relapse following anticancer treatment. *Cancers (Basel)* (2018) 10(4). doi: 10.3390/cancers10040118

71. Fei F, Zhang D, Yang Z, Wang S, Wang X, Wu Z, et al. The number of polyploid giant cancer cells and epithelial-mesenchymal transition-related proteins are associated with invasion and metastasis in human breast cancer. *J Exp Clin Cancer Res* (2015) 34:158. doi: 10.1186/s13046-015-0277-8

72. Alhaddad L, Chuprov-Netochin R, Pustovalova M, Osipov AN, Leonov S. Polyploid/Multinucleated giant and slow-cycling cancer cell enrichment in response to X-ray irradiation of human glioblastoma multiforme cells differing in radioresistance and TP53/PTEN status. *Int J Mol Sci* (2023) 24(2). doi: 10.3390/ijms24021228

73. Luo Q, Wang C, Peng B, Pu X, Cai L, Liao H, et al. Circulating tumor-Cell-Associated white blood cell clusters in peripheral blood indicate poor prognosis in patients with hepatocellular carcinoma. *Front Oncol* (2020) 10:1758. doi: 10.3389/fonc.2020.01758

74. Wang C, Luo Q, Huang W, Zhang C, Liao H, Chen K, et al. Correlation between circulating tumor cell DNA genomic alterations and mesenchymal CTCs or CTC-associated white blood cell clusters in hepatocellular carcinoma. *Front Oncol* (2021) 11:686365. doi: 10.3389/fonc.2021.686365

75. Lin PP, Gires O, Wang DD, Li L, Wang H. Comprehensive *in situ* co-detection of aneuploid circulating endothelial and tumor cells. *Sci Rep* (2017) 7(1):9789. doi: 10.1038/s41598-017-10763-7

76. Ye Z, Ding Y, Chen Z, Li Z, Ma S, Xu Z, et al. Detecting and phenotyping of aneuploid circulating tumor cells in patients with various malignancies. *Cancer Biol Ther* (2019) 20(4):546–51. doi: 10.1080/15384047.2018.1538000

77. Boya M, Ozkaya-Ahmadov T, Swain BE, Chu C-H, Asmare N, Civelekoglu O, et al. High throughput, label-free isolation of circulating tumor cell clusters in meshed microwells. *Nat Commun* (2022) 13(1):3385. doi: 10.1038/s41467-022-31009-9

78. Hou J-M, Krebs M, Ward T, Sloane R, Priest L, Hughes A, et al. Circulating tumor cells as a window on metastasis biology in lung cancer. *Am J Pathol* (2011) 178 (3):989–96. doi: 10.1016/j.ajpath.2010.12.003

79. Mendonsa AM, Na T-Y. Gumbiner BM. *E-cadherin contact inhibition cancer. Oncogene.* (2018) 37(35):4769–80. doi: 10.1038/s41388-018-0304-2

80. Padmanaban V, Krol I, Suhail Y, Szczerba BM, Aceto N, Bader JS, et al. E-cadherin is required for metastasis in multiple models of breast cancer. *Nature* (2019) 573(7774):439–44. doi: 10.1038/s41586-019-1526-3

81. Na T-Y, Schecterson L, Mendonsa AM, Gumbiner BM. The functional activity of e-cadherin controls tumor cell metastasis at multiple steps. *Proc Natl Acad Sci USA* (2020) 117(11):5931–7. doi: 10.1073/pnas.1918167117

82. Quan Q, Wang X, Lu C, Ma W, Wang Y, Xia G, et al. Cancer stem-like cells with hybrid epithelial/mesenchymal phenotype leading the collective invasion. *Cancer Sci* (2020) 111(2):467–76. doi: 10.1111/cas.14285

83. Tan H-X, Cao Z-B, He T-T, Huang T, Xiang C-L, Liu Y. TGFβ1 is essential for MSCs-CAFs differentiation and promotes HCT116 cells migration and invasion *via* JAK/STAT3 signaling. *Onco Targets Ther* (2019) 12:5323–34. doi: 10.2147/OTT.S178618

84. Sekino Y, Takemoto K, Murata D, Babasaki T, Kobatake K, Kitano H, et al. CD44 is involved in sunitinib resistance and poor progression-free survival after sunitinib treatment of renal cell carcinoma. *Anticancer Res* (2021) 41(10):4875–83. doi: 10.21873/anticanres.15301

85. Dong Q, Li Q, Wang M, Hu J, Dai J, Niu L, et al. Elevated CD44 expression predicts poor prognosis in patients with low-grade glioma. *Oncol Lett* (2019) 18 (4):3698–704. doi: 10.3892/ol.2019.10728

86. Si D, Yin F, Peng J, Zhang G. High expression of CD44 predicts a poor prognosis in glioblastomas. *Cancer Manag Res* (2020) 12:769–75. doi: 10.2147/CMAR.S233423

87. Kim HM, Koo JS. Immunohistochemical analysis of cancer stem cell marker expression in papillary thyroid cancer. *Front Endocrinol (Lausanne).* (2019) 10:523. doi: 10.3389/fendo.2019.00523

88. Mukherjee D, Zhao J. The role of chemokine receptor CXCR4 in breast cancer metastasis. *Am J Cancer Res* (2013) 3(1):46–57.

89. Wilhelm A, Lemmenmeier I, Lalos A, Posabella A, Kancherla V, Piscuoglio S, et al. The prognostic significance of CXCR4 and SDF-1 in differentiated thyroid cancer depends on CD8+ density. *BMC Endocr Disord* (2022) 22(1):292. doi: 10.1186/s12902-022-01204-2

90. Qiu L, Xu Y, Xu H, Yu B. The clinicopathological and prognostic value of CXCR4 expression in patients with lung cancer: A meta-analysis. *BMC Cancer.* (2022) 22(1):681. doi: 10.1186/s12885-022-09756-1

91. Regev O, Kizner M, Roncato F, Dadiani M, Saini M, Castro-Giner F, et al. ICAM-1 on breast cancer cells suppresses lung metastasis but is dispensable for tumor growth and killing by cytotoxic T cells. *Front Immunol* (2022) 13:849701. doi: 10.3389/fimmu.2022.849701

92. Taftaf R, Liu X, Singh S, Jia Y, Dashzeveg NK, Hoffmann AD, et al. ICAM1 initiates CTC cluster formation and trans-endothelial migration in lung metastasis of breast cancer. *Nat Commun* (2021) 12(1):4867. doi: 10.1038/s41467-021-25189-z

93. Gao M, Zhang X, Li D, He P, Tian W, Zeng B. Expression analysis and clinical significance of eIF4E, VEGF-c, e-cadherin and MMP-2 in colorectal adenocarcinoma. *Oncotarget* (2016) 7(51):85502–14. doi: 10.18632/oncotarget.13453

94. Chang K, Jiang L, Sun Y, Li H. Effect of e-cadherin on prognosis of colorectal cancer: A meta-analysis update. *Mol Diagn Ther* (2022) 26(4):397–409. doi: 10.1007/s40291-022-00593-3

95. D'Urso PI, D'Urso OF, Storelli C, Catapano G, Gianfreda CD, Montinaro A, et al. Retrospective protein expression and epigenetic inactivation studies of CDH1 in patients affected by low-grade glioma. *J Neurooncol.* (2011) 104(1):113–8. doi: 10.1007/s11060-010-0481-5

96. Burandt E, Lübbersmeyer F, Gorbokon N, Büscheck F, Luebke AM, Menz A, et al. E-cadherin expression in human tumors: a tissue microarray study on 10,851 tumors. *biomark Res* (2021) 9(1):44. doi: 10.1186/s40364-021-00299-4

97. Gkogkou P, Peponi E, Ntaskagiannis D, Murray S, Demou A, Sainis I, et al. E-cadherin and syndecan-1 expression in patients with advanced non-small cell lung cancer treated with chemoradiotherapy. *In Vivo.* (2020) 34(1):453–9. doi: 10.21873/invivo.11795

98. Jiang Y, Han S, Cheng W, Wang Z, Wu A. NFAT1-regulated IL6 signalling contributes to aggressive phenotypes of glioma. *Cell Commun Signal* (2017) 15(1):54. doi: 10.1186/s12964-017-0210-1

99. Sun G, Wang T, Shi M, Zhou H, Wang J, Huang Z, et al. Low expression of IL6R predicts poor prognosis for lung adenocarcinoma. *Ann Transl Med* (2021) 9(13):1057. doi: 10.21037/atm-21-36

100. Xu B, Chen Q, Yue C, Lan L, Jiang J, Shen Y, et al. Prognostic value of IL-6R mRNA in lung adenocarcinoma and squamous cell carcinoma. *Oncol Lett* (2018) 16 (3):2935–48. doi: 10.3892/ol.2018.9044

101. Fu Q, Chang Y, An H, Fu H, Zhu Y, Xu L, et al. Prognostic value of interleukin-6 and interleukin-6 receptor in organ-confined clear-cell renal cell carcinoma: A 5-year conditional cancer-specific survival analysis. *Br J Cancer* (2015) 113(11):1581–9. doi: 10.1038/bjc.2015.379

102. Pilskog M, Bostad L, Edelmann RJ, Akslen LA, Beisland C, Straume O. Tumour cell expression of interleukin 6 receptor α is associated with response rates in patients treated with sunitinib for metastatic clear cell renal cell carcinoma. *J Pathol Clin Res* (2018) 4(2):114–23. doi: 10.1002/cjp2.96

103. Zhuang Z, Lin J, Huang Y, Lin T, Zheng Z, Ma X. Notch 1 is a valuable therapeutic target against cell survival and proliferation in clear cell renal cell carcinoma. *Oncol Lett* (2017) 14(3):3437–44. doi: 10.3892/ol.2017.6587

104. Ai Q, Ma X, Huang Q, Liu S, Shi T, Zhang C, et al. High-level expression of Notch1 increased the risk of metastasis in T1 stage clear cell renal cell carcinoma. *PloS One* (2012) 7(4):e35022. doi: 10.1371/journal.pone.0035022

105. Yi L, Zhou X, Li T, Liu P, Hai L, Tong L, et al. Notch1 signaling pathway promotes invasion, self-renewal and growth of glioma initiating cells *via* modulating chemokine system CXCL12/CXCR4. *J Exp Clin Cancer Res* (2019) 38(1):339. doi: 10.1186/s13046-019-1319-4

106. Li J, Cui Y, Gao G, Zhao Z, Zhang H, Wang X. Notch1 is an independent prognostic factor for patients with glioma. *J Surg Oncol* (2011) 103(8):813–7. doi: 10.1002/jso.21851

107. Malkoski SP, Haeger SM, Cleaver TG, Rodriguez KJ, Li H, Lu S-L, et al. Loss of transforming growth factor beta type II receptor increases aggressive tumor behavior and reduces survival in lung adenocarcinoma and squamous cell carcinoma. *Clin Cancer Res* (2012) 18(8):2173–83. doi: 10.1158/1078-0432.CCR-11-2557

108. Nolan K, Tippimanchai D, Verzosa G, Zhao W, Li H, Phillip S, et al. Reduced TGFBR2 expression in NSCLC drives IL-17A dependent inflammation *via* γδT cells. *J Thorac Oncol* (2017) 12(8):S1537. doi: 10.1016/j.jtho.2017.06.023

109. Wei C-Y, Tan Q-X, Zhu X, Qin Q-H, Zhu F-B, Mo Q-G, et al. Expression of CDKN1A/p21 and TGFBR2 in breast cancer and their prognostic significance. *Int J Clin Exp Pathol* (2015) 8(11):14619–29.

110. Busch S, Sims AH, Stål O, Fernö M, Landberg G. Loss of tgfβ receptor type 2 expression impairs estrogen response and confers tamoxifen resistance. *Cancer Res* (2015) 75(7):1457–69. doi: 10.1158/0008-5472.CAN-14-1583

111. Gao N, Zhai Q, Li Y, Huang K, Bian D, Wang X, et al. Clinical implications of tβrii expression in breast cancer. *PloS One* (2015) 10(11):e0141412. doi: 10.1371/journal.pone.0141412

112. Soysal SD, Muenst S, Barbie T, Fleming T, Gao F, Spizzo G, et al. EpCAM expression varies significantly and is differentially associated with prognosis in the luminal b HER2(+), basal-like, and HER2 intrinsic subtypes of breast cancer. *Br J Cancer.* (2013) 108(7):1480–7. doi: 10.1038/bjc.2013.80

113. Chen X, Ma W-Y, Xu S-C, Liang Y, Fu Y-B, Pang B, et al. The overexpression of epithelial cell adhesion molecule (EpCAM) in glioma. *J Neurooncol.* (2014) 119(1):39–47. doi: 10.1007/s11060-014-1459-5

114. Zimpfer A, Maruschke M, Rehn S, Kundt G, Litzenberger A, Dammert F, et al. Prognostic and diagnostic implications of epithelial cell adhesion/activating molecule (EpCAM) expression in renal tumours: A retrospective clinicopathological study of 948 cases using tissue microarrays. *BJU Int* (2014) 114(2):296–302. doi: 10.1111/bju.12487

115. Labrousse-Arias D, Martínez-Alonso E, Corral-Escariz M, Bienes-Martínez R, Berridy J, Serrano-Oviedo L, et al. VHL promotes immune response against renal cell carcinoma *via* NF-κB-dependent regulation of VCAM-1. *J Cell Biol* (2017) 216(3):835–47. doi: 10.1083/jcb.201608024

116. Shioi K, Komiya A, Hattori K, Huang Y, Sano F, Murakami T, et al. Vascular cell adhesion molecule 1 predicts cancer-free survival in clear cell renal carcinoma patients. *Clin Cancer Res* (2006) 12(24):7339–46. doi: 10.1158/1078-0432.CCR-06-1737

117. Agrawal A, Datta C, Panda CK, Pal DK. Association of beta-catenin and CD44 in the development of renal cell carcinoma. *Urologia* (2021) 88(2):125–9. doi: 10.1177/0391560320980672

118. Ottaiano A, Santorsola M, Del Prete P, Perri F, Scala S, Caraglia M, et al. Prognostic significance of CXCR4 in colorectal cancer: An updated meta-analysis and critical appraisal. *Cancers (Basel)* (2021) 13(13):3284. doi: 10.3390/cancers13133284

119. Bourkoula E, Mangoni D, Ius T, Pucer A, Isola M, Musiello D, et al. Glioma-associated stem cells: a novel class of tumor-supporting cells able to predict prognosis of human low-grade gliomas. *Stem Cells* (2014) 32(5):1239–53. doi: 10.1002/stem.1605

120. Lewis-Tuffin LJ, Rodriguez F, Giannini C, Scheithauer B, Necela BM, Sarkaria JN, et al. Misregulated e-cadherin expression associated with an aggressive brain tumor phenotype. *PloS One* (2010) 5(10):e13665. doi: 10.1371/journal.pone.0013665

121. Li T, Wang H, Xu J, Li C, Zhang Y, Wang G, et al. TGFBR2 mutation predicts resistance to immune checkpoint inhibitors in patients with non-small cell lung cancer. *Ther Adv Med Oncol* (2021) 13:17588359211038476. doi: 10.1177/17588359211038477

122. Song K, Yuan Y, Lin Y, Wang Y-X, Zhou J, Gai Q-J, et al. ERBB3, IGF1R, and TGFBR2 expression correlate with PDGFR expression in glioblastoma and participate in PDGFR inhibitor resistance of glioblastoma cells. *Am J Cancer Res* (2018) 5:792–809.

123. An H, Zhu Y, Xu L, Chen L, Lin Z, Xu J. Notch1 predicts recurrence and survival of patients with clear-cell renal cell carcinoma after surgical resection. *Urology* (2015) 85(2):483.e9–483.e14. doi: 10.1016/j.urology.2014.10.022

124. D'Amico M, De Amicis F. Aberrant notch signaling in gliomas: a potential landscape of actionable converging targets for combination approach in therapies resistance. *Cancer Drug Resist* (2022) 5(4):939–53. doi: 10.20517/cdr.2022.46

125. Yuan X, Wu H, Xu H, Han N, Chu Q, Yu S, et al. Meta-analysis reveals the correlation of notch signaling with non-small cell lung cancer progression and prognosis. *Sci Rep* (2015) 5:10338. doi: 10.1038/srep10338

126. Ralhan R, Cao J, Lim T, Macmillan C, Freeman JL, Walfish PG. EpCAM nuclear localization identifies aggressive thyroid cancer and is a marker for poor prognosis. *BMC Cancer.* (2010) 10:331. doi: 10.1186/1471-2407-10-331

127. Love MI, Huber W, Anders S. Moderated estimation of fold change and dispersion for RNA-seq data with DESeq2. *Genome Biol* (2014) 15(12):550. doi: 10.1186/s13059-014-0550-8

128. Page RDM. Tree view: An application to display phylogenetic trees on personal computers. *Bioinformatics* (1996) 12(4):357–8. doi: 10.1093/bioinformatics/12.4.357

129. Yang F, He Z, Duan H, Zhang D, Li J, Yang H, et al. Synergistic immunotherapy of glioblastoma by dual targeting of IL-6 and CD40. *Nat Commun* (2021) 12(1):3424. doi: 10.1038/s41467-021-23832-3

130. Lamano JB, Lamano JB, Li YD, DiDomenico JD, Choy W, Veliceasa D, et al. Glioblastoma-derived IL6 induces immunosuppressive peripheral myeloid cell PD-L1 and promotes tumor growth. *Clin Cancer Res* (2019) 25(12):3643–57. doi: 10.1158/1078-0432.CCR-18-2402

131. Ishibashi K, Koguchi T, Matsuoka K, Onagi A, Tanji R, Takinami-Honda R, et al. Interleukin-6 induces drug resistance in renal cell carcinoma. *Fukushima J Med Sci* (2018) 64(3):103–10. doi: 10.5387/fms.2018-15

132. Gudbrandsdottir G, Aarstad HH, Bostad L, Hjelle KM, Aarstad HJ, Bruserud Ø, et al. Serum levels of the IL-6 family of cytokines predict prognosis in renal cell carcinoma (RCC). *Cancer Immunol Immunother.* (2021) 70(1):19–30. doi: 10.1007/s00262-020-02655-z

133. Ogawa H, Koyanagi-Aoi M, Otani K, Zen Y, Maniwa Y, Aoi T. Interleukin-6 blockade attenuates lung cancer tissue construction integrated by cancer stem cells. *Sci Rep* (2017) 7(1):12317. doi: 10.1038/s41598-017-12017-y

134. Chung AW, Kozielski AJ, Qian W, Zhou J, Anselme AC, Chan AA, et al. Tocilizumab overcomes chemotherapy resistance in mesenchymal stem-like breast cancer by negating autocrine IL-1A induction of IL-6. *NPJ Breast Cancer.* (2022) 8(1):30. doi: 10.1038/s41523-021-00371-0

135. Li L, Li Z, Lu C, Li J, Zhang K, Lin C, et al. Ibrutinib reverses IL-6-induced osimertinib resistance through inhibition of laminin α5/FAK signaling. *Commun Biol* (2022) 5(1):155. doi: 10.1038/s42003-022-03111-7

136. Lust JA, Lacy MQ, Zeldenrust SR, Witzig TE, Moon-Tasson LL, Dinarello CA, et al. Reduction in c-reactive protein indicates successful targeting of the IL-1/IL-6 axis resulting in improved survival in early stage multiple myeloma. *Am J Hematol* (2016) 91(6):571–4. doi: 10.1002/ajh.24352

137. Chen Z, Giotti B, Kaluzova M, Herting CJ, Pinero G, Vallcorba MP, et al. A paracrine circuit of IL-1β/IL-1R1 between myeloid and tumor cells drives glioblastoma progression. *BioRxiv* (2022). doi: 10.1101/2022.04.03.486888

138. Tarassishin L, Lim J, Weatherly DB, Angeletti RH, Lee SC. Interleukin-1-induced changes in the glioblastoma secretome suggest its role in tumor progression. *J Proteomics.* (2014) 99:152–68. doi: 10.1016/j.jprot.2014.01.024

139. Tarassishin L, Casper D, Lee SC. Aberrant expression of interleukin-1β and inflammasome activation in human malignant gliomas. *PloS One* (2014) 9(7):e103432. doi: 10.1371/journal.pone.0103432

140. Aggen DH, Ager CR, Obradovic AZ, Chowdhury N, Ghasemzadeh A, Mao W, et al. Blocking IL1 beta promotes tumor regression and remodeling of the myeloid compartment in a renal cell carcinoma model: Multidimensional analyses. *Clin Cancer Res* (2021) 27(2):608–21. doi: 10.1158/1078-0432.CCR-20-1610

141. Zhang J, Veeramachaneni N. Targeting interleukin-1β and inflammation in lung cancer. *biomark Res* (2022) 10(1):5. doi: 10.1186/s40364-021-00341-5

142. Menke-van der Houven van Oordt CW, Gomez-Roca C, van Herpen C, Coveler AL, Mahalingam D, Verheul HMW, et al. First-in-human phase I clinical trial of RG7356, an anti-CD44 humanized antibody, in patients with advanced, CD44-expressing solid tumors. *Oncotarget* (2016) 7(48):80046–58. doi: 10.18632/oncotarget.11098

143. Yeh M, Wang Y-Y, Yoo JY, Oh C, Otani Y, Kang JM, et al. MicroRNA-138 suppresses glioblastoma proliferation through downregulation of CD44. *Sci Rep* (2021) 11(1):9219. doi: 10.1038/s41598-021-88615-8

144. Xiao Y, Yang K, Wang Z, Zhao M, Deng Y, Ji W, et al. CD44-mediated poor prognosis in glioma is associated with M2-polarization of tumor-associated macrophages and immunosuppression. *Front Surg* (2021) 8:775194. doi: 10.3389/fsurg.2021.775194

145. Lubanska D, Alrashed S, Mason GT, Nadeem F, Awada A, DiPasquale M, et al. Impairing proliferation of glioblastoma multiforme with CD44+ selective conjugated polymer nanoparticles. *Sci Rep* (2022) 12(1):12078. doi: 10.1038/s41598-022-15244-0

146. Ghobrial IM, Liu C-J, Redd RA, Perez RP, Baz R, Zavidij O, et al. A phase Ib/II trial of the first-in-Class anti-CXCR4 antibody ulocuplumab in combination with lenalidomide or bortezomib plus dexamethasone in relapsed multiple myeloma. *Clin Cancer Res* (2020) 26(2):344–53. doi: 10.1158/1078-0432.CCR-19-0647

147. Biasci D, Smoragiewicz M, Connell CM, Wang Z, Gao Y, Thaventhiran JED, et al. CXCR4 inhibition in human pancreatic and colorectal cancers induces an integrated immune response. *Proc Natl Acad Sci USA* (2020) 117(46):28960–70. doi: 10.1073/pnas.2013644117

148. Kim B-G, Malek E, Choi SH, Ignatz-Hoover JJ, Driscoll JJ. Novel therapies emerging in oncology to target the TGF-β pathway. *J Hematol Oncol* (2021) 14(1):55. doi: 10.1186/s13045-021-01053-x

149. Teixeira AF, Ten Dijke P, Zhu H-J. On-target anti-TGF-β therapies are not succeeding in clinical cancer treatments: What are remaining challenges? *Front Cell Dev Biol* (2020) 8:605. doi: 10.3389/fcell.2020.00605

150. Jäger M, Schoberth A, Ruf P, Hess J, Hennig M, Schmalfeldt B, et al. Immunomonitoring results of a phase II/III study of malignant ascites patients treated with the trifunctional antibody catumaxomab (anti-EpCAM x anti-CD3). *Cancer Res* (2012) 72(1):24–32. doi: 10.1158/0008-5472.CAN-11-2235

151. Ruf P, Bauer HW, Schoberth A, Kellermann C, Lindhofer H. First time intravesically administered trifunctional antibody catumaxomab in patients with recurrent non-muscle invasive bladder cancer indicates high tolerability and local immunological activity. *Cancer Immunol Immunother.* (2021) 70(9):2727–35. doi: 10.1007/s00262-021-02930-7

152. Sehouli J, Reinthaller A, Marth C, Reimer D, Reimer T, Stummvoll W, et al. Intra- and postoperative catumaxomab in patients with epithelial ovarian cancer: Safety and two-year efficacy results from a multicentre, single-arm, phase II study. *Br J Cancer.* (2014) 111(8):1519–25. doi: 10.1038/bjc.2014.443

153. Yang Y, McCloskey JE, Yang H, Puc J, Alcaina Y, Vedvyas Y, et al. Bispecific CAR T cells against EpCAM and inducible ICAM-1 overcome antigen heterogeneity and generate superior antitumor responses. *Cancer Immunol Res* (2021) 9(10):1158–74. doi: 10.1158/2326-6066.CIR-21-0062

154. Haber SL, Benson V, Buckway CJ, Gonzales JM, Romanet D, Scholes B. Lifitegrast: a novel drug for patients with dry eye disease. *Ther Adv Ophthalmol* (2019) 11:2515841419870366. doi: 10.1177/2515841419870366

155. Hailemichael Y, Johnson DH, Abdel-Wahab N, Foo WC, Bentebibel S-E, Daher M, et al. Interleukin-6 blockade abrogates immunotherapy toxicity and promotes tumor immunity. *Cancer Cell* (2022) 40(5):509–523.e6. doi: 10.1016/j.ccell.2022.04.004

156. Bent EH, Millán-Barea LR, Zhuang I, Goulet DR, Fröse J, Hemann MT. Microenvironmental IL-6 inhibits anti-cancer immune responses generated by cytotoxic chemotherapy. *Nat Commun* (2021) 12(1):6218. doi: 10.1038/s41467-021-26407-4

157. Rossi JF, Négrier S, James ND, Kocak I, Hawkins R, Davis H, et al. A phase I/II study of siltuximab (CNTO 328), an anti-interleukin-6 monoclonal antibody, in

metastatic renal cell cancer. *Br J Cancer* (2010) 103(8):1154–62. doi: 10.1038/sj.bjc.6605872

158. Fizazi K, De Bono JS, Flechon A, Heidenreich A, Voog E, Davis NB, et al. Randomised phase II study of siltuximab (CNTO 328), an anti-IL-6 monoclonal antibody, in combination with mitoxantrone/prednisone versus mitoxantrone/prednisone alone in metastatic castration-resistant prostate cancer. *Eur J Cancer* (2012) 48(1):85–93. doi: 10.1016/j.ejca.2011.10.014

159. Gottschlich A, Endres S, Kobold S. Therapeutic strategies for targeting IL-1 in cancer. *Cancers (Basel)* (2021) 13(3):477. doi: 10.3390/cancers13030477

160. Piao Y, Henry V, Tiao N, Park SY, Martinez-Ledesma J, Dong JW, et al. Targeting intercellular adhesion molecule-1 prolongs survival in mice bearing bevacizumab-resistant glioblastoma. *Oncotarget* (2017) 8(57):96970–83. doi: 10.18632/oncotarget.18859

161. Yoo K-C, Kang J-H, Choi M-Y, Suh Y, Zhao Y, Kim M-J, et al. Soluble ICAM-1 a pivotal communicator between tumors and macrophages, promotes mesenchymal shift of glioblastoma. *Adv Sci (Weinh).* (2022) 9(2):e2102768. doi: 10.1002/advs.202102768

162. Jung M, Yang Y, McCloskey JE, Zaman M, Vedvyas Y, Zhang X, et al. Chimeric antigen receptor T cell therapy targeting ICAM-1 in gastric cancer. *Mol Ther Oncolytics.* (2020) 18:587–601. doi: 10.1016/j.omto.2020.08.009

163. Min IM, Shevlin E, Vedvyas Y, Zaman M, Wyrwas B, Scognamiglio T, et al. CAR T therapy targeting ICAM-1 eliminates advanced human thyroid tumors. *Clin Cancer Res* (2017) 23(24):7569–83. doi: 10.1158/1078-0432.CCR-17-2008

164. Gray KD, McCloskey JE, Vedvyas Y, Kalloo OR, Eshaky SE, Yang Y, et al. PD1 blockade enhances ICAM1-directed CAR T therapeutic efficacy in advanced thyroid cancer. *Clin Cancer Res* (2020) 26(22):6003–16. doi: 10.1158/1078-0432.CCR-20-1523

165. Wei H, Wang Z, Kuang Y, Wu Z, Zhao S, Zhang Z, et al. Intercellular adhesion molecule-1 as target for CAR-T-Cell therapy of triple-negative breast cancer. *Front Immunol* (2020) 11:573823. doi: 10.3389/fimmu.2020.573823

166. Sherbenou DW, Su Y, Behrens CR, Aftab BT, Perez de Acha O, Murnane M, et al. Potent activity of an anti-ICAM1 antibody-drug conjugate against multiple myeloma. *Clin Cancer Res* (2020) 26(22):6028–38. doi: 10.1158/1078-0432.CCR-20-0400

167. Chen X, Wong OK, Post L. CD38 x ICAM1 bispecific antibody is a novel approach for treating multiple myeloma and lymphoma. *Blood* (2021) 138(Supplement 1):2413–3. doi: 10.1182/blood-2021-146041

168. Annels NE, Mansfield D, Arif M, Ballesteros-Merino C, Simpson GR, Denyer M, et al. Phase I trial of an ICAM-1-Targeted immunotherapeutic-coxsackievirus A21 (CVA21) as an oncolytic agent against non muscle-invasive bladder cancer. *Clin Cancer Res* (2019) 25(19):5818–31. doi: 10.1158/1078-0432.CCR-18-4022

169. Vey N, Delaunay J, Martinelli G, Fiedler W, Raffoux E, Prebet T, et al. Phase I clinical study of RG7356, an anti-CD44 humanized antibody, in patients with acute myeloid leukemia. *Oncotarget* (2016) 7(22):32532–42. doi: 10.18632/oncotarget.8687

170. Cornelison RC, Brennan CE, Kingsmore KM, Munson JM. Convective forces increase CXCR4-dependent glioblastoma cell invasion in GL261 murine model. *Sci Rep* (2018) 8(1):17057. doi: 10.1038/s41598-018-35141-9

171. Daniele S, La Pietra V, Piccarducci R, Pietrobono D, Cavallini C, D'Amore VM, et al. CXCR4 antagonism sensitizes cancer cells to novel indole-based MDM2/4 inhibitors in glioblastoma multiforme. *Eur J Pharmacol* (2021) 897:173936. doi: 10.1016/j.ejphar.2021.173936

172. Thomas RP, Nagpal S, Iv M, Soltys SG, Bertrand S, Pelpola JS, et al. Macrophage exclusion after radiation therapy (MERT): A first in human phase I/II trial using a CXCR4 inhibitor in glioblastoma. *Clin Cancer Res* (2019) 25(23):6948–57. doi: 10.1158/1078-0432.CCR-19-1421

173. Brown NF, Ottaviani D, Tazare J, Gregson J, Kitchen N, Brandner S, et al. Survival outcomes and prognostic factors in glioblastoma. *Cancers (Basel)* (2022) 14(13):3161. doi: 10.3390/cancers14133161

174. McCaw TR, Inga E, Chen H, Jaskula-Sztul R, Dudeja V, Bibb JA, et al. Gamma secretase inhibitors in cancer: A current perspective on clinical performance. *Oncologist* (2021) 26(4):e608–21. doi: 10.1002/onco.13627

175. Sano M, Takahashi R, Ijichi H, Ishigaki K, Yamada T, Miyabayashi K, et al. Blocking VCAM-1 inhibits pancreatic tumour progression and cancer-associated thrombosis/thromboembolism. *Gut* (2021) 70(9):1713–23. doi: 10.1136/gutjnl-2020-320608

176. Takahashi R, Ijichi H, Sano M, Miyabayashi K, Mohri D, Kim J, et al. Soluble VCAM-1 promotes gemcitabine resistance *via* macrophage infiltration and predicts therapeutic response in pancreatic cancer. *Sci Rep* (2020) 10(1):21194. doi: 10.1038/s41598-020-78320-3

177. Grosse-Wilde A, Fouquier d'Hérouël A, McIntosh E, Ertaylan G, Skupin A, Kuestner RE, et al. Stemness of the hybrid Epithelial/Mesenchymal state in breast cancer and its association with poor survival. *PloS One* (2015) 10:e0126522. doi: 10.1371/journal.pone.0126522

178. Kuburich NA, den Hollander P, Pietz JT, Mani SA. Vimentin and cytokeratin: Good alone, bad together. *Semin Cancer Biol* (2022) 86(Pt 3):816–26. doi: 10.1016/j.semcancer.2021.12.006

179. Rohnalter V, Roth K, Finkernagel F, Adhikary T, Obert J, Dorzweiler K, et al. A multi-stage process including transient polyploidization and EMT precedes the emergence of chemoresistent ovarian carcinoma cells with a dedifferentiated and pro-inflammatory secretory phenotype. *Oncotarget* (2015) 6(37):40005–25. doi: 10.18632/oncotarget.5552

180. Wang X, Zheng M, Fei F, Li C, Du J, Liu K, et al. EMT-related protein expression in polyploid giant cancer cells and their daughter cells with different passages after triptolide treatment. *Med Oncol* (2019) 36(9):82. doi: 10.1007/s12032-019-1303-z

frontiers | Frontiers in Immunology

TYPE Mini Review
PUBLISHED 05 June 2023
DOI 10.3389/fimmu.2023.1194642

OPEN ACCESS

EDITED BY
Silvia Pesce,
University of Genoa, Italy

REVIEWED BY
Stéphanie Corgnac,
Institut Gustave Roussy, France
Paola Allavena,
University of Milan, Italy

*CORRESPONDENCE
Eleonora Timperi
eleonora.timperi@curie.fr
Emanuela Romano
emanuela.romano@curie.fr

RECEIVED 27 March 2023
ACCEPTED 19 May 2023
PUBLISHED 05 June 2023

CITATION
Timperi E and Romano E (2023) Stromal circuits involving tumor-associated macrophages and cancer-associated fibroblasts. *Front. Immunol.* 14:1194642. doi: 10.3389/fimmu.2023.1194642

Stromal circuits involving tumor-associated macrophages and cancer-associated fibroblasts

Eleonora Timperi[1]* and Emanuela Romano[1,2]*

[1]Department of Immunology, INSERM U932, Université Paris Sciences et Lettres (PSL) Research University, Institut Curie, Paris, France, [2]Department of Medical Oncology, Center for Cancer Immunotherapy, Institut Curie, Paris, France

The tumor associated macrophages (TAM) represent one of most abundant subpopulations across several solid cancers and their number/frequency is associated with a poor clinical outcome. It has been clearly demonstrated that stromal cells, such as the cancer associated fibroblasts (CAFs), may orchestrate TAM recruitment, survival and reprogramming. Today, single cell-RNA sequencing (sc-RNA seq) technologies allowed a more granular knowledge about TAMs and CAFs phenotypical and functional programs. In this mini-review we discuss the recent discoveries in the sc-RNA seq field focusing on TAM and CAF identity and their crosstalk in the tumor microenvironment (TME) of solid cancers.

KEYWORDS

cancer associated fibroblasts (CAF), tumor associated macrophages (TAM), solid tumors, single cell RNA analysis, monocytes

1 Introduction

The advent of sc-technologies has fast-revolutionized our understanding about macrophage phenotype, function, and plasticity in several diseases, including cancer. The binary view of macrophage states: M1 and M2, has dominated the field until recently. M1 (pro-inflammatory) versus M2 (alternative or anti-inflammatory) profiles were derived by *in vitro* observations in human and mice (1). M1- macrophages, obtained *in vitro* by type 1 cytokines such as IFN-γ (and/or TNF-α) showed efficient phagocytosis, high levels of pro-inflammatory cytokines (i.e. IFN-γ, IL-12, TNF-α) and chemokines (i.e. CCL2, CXCL10). Conversely, the generation of M2-macrophages, was mainly induced by type 2 cytokines like IL-4 and/or IL-13 (1). M2-like macrophages are characterized by increased wound healing activity, reduced phagocytosis and T cell antigen presentation capacity (2, 3). Recent sc- discoveries revealed that human macrophages are highly heterogeneous at the steady state and in pathological conditions, suggesting the importance of a context- and tissue-dependent approach to appreciate their biological properties.

Abbreviations: sc, single cell; TAM, tumor associated macrophages; TR, tissue resident; TRM, tissue resident macrophages; CAF, cancer associated fibroblasts; CSF-1, colony stimulating growth factor 1; ECM, extracellular matrix.

2 TAM: tissue resident macrophages and monocyte-derived TAM in tumor niches

TAM are one of the most abundant population in solid cancers (4). TAM density is linked to poor patient outcome in prostate (PCA), breast (BC), bladder, head and neck (HN), glioma, melanoma, thyroid, lung (NSCLC), hepatocellular (HCC) cancers, and non-Hodgkin lymphoma (5–10). Collectively, TAM may originate from tissue-resident macrophages (TRM) and circulating monocytes (mono)-derived cells. This review will describe recent discoveries on the aspects linked to the TAM origin.

All the organs in the body are populated by (TRM), key players in mounting the first-line of defense against pathogens, preserving vascular tone and integrity, in addition to clearance foreign bodies (11). Embryonically generated-TRM preserve the organ homeostasis at steady state. In response to inflammation, TRM may be originated by circulating monocytes. The contribution by peripheral monocytes could be driven by the inability of TRM to generate macrophages with specific effector functions in the tissue, because of the limited TRM self-renewal intrinsic capacity (11). Upon infections or inflammation, bone-marrow- adult derived cells could be recruited at the tissue and replaced embryonic-TRM. Among many inflammatory triggers (i.e. infections), cancer-associated inflammation may be considered a key perturbator of the frequency of TRM across multiple cancer subtypes. Indeed, circulating monocytes may be recruited by the engagement of various chemoattractant pathway by the interplay of stromal components like CCL2-CCR2, CCL20-CCR6, CCL5-CCR5, CCL8- CXCR4-CXCL12 etc (12). At the tumor site, monocytes undergo gene reprogramming and acquire similar properties of embryonically originated macrophages, depending on specific tissue factors (2, 13–15). Chronic inflammation of different etiology can give rise to the differentiation of recently recruited monocytes towards TAM at the tissue site.

So far, sc-RNA seq technologies have contributed to defining i) the theoretical origin of TAM; ii) TAM heterogeneity; iii) TAM molecular features iv) TAM functional and metabolic states. This large effort has contributed to understand which molecular programs are conserved among cancer types and which programs could be tumor tissue-specific.

3 TAM in the era of single cell RNA-sequencing technology

Most of the sc-datasets showed the APOE (apolipoprotein) gene as a TAM marker. Numerous studies, including our, demonstrated the selective APOE expression by TAM from tumor lesions compared with macrophages from normal-tissue (NT) counterparts (16–18). Despite tissue resident (TR) or monocytic origin of TAM, they may collectively share a core transcriptomic signature comprising: APOE, complement component genes (i.e. C1QA, C1QB, C1QC), and cathepsin (CTSB, CTSD) across several cancer types (16, 18–21).

3.1 TR-derived TAM

TAM derived from TRM were described in several cancer tissues. In human colorectal cancer (CRC), C1QC+ TR-TAMs were identified, showing high complement components (C1QA, C1QC etc.), high levels of HLA-DR molecules and high phagocytic score (20). Importantly, Cheng et al, collecting sc-RNA data from 15 different cancer subtypes, reported that C1QC+ TAM showed a lower connectivity with CD14+ monocytes suggesting their TR origin (19). Of note, the folate receptor-β (FOLR2) has been recently discovered and described as TR marker. In HCC FOLR2+ TAM exhibited fetal-liver features and displayed onco-fetal reprogramming (22), supporting their resident origin. TR FOLR2+ macrophages have been also identified (16) in breast cancer (BC) lesions and in healthy mammary tissues; they were associated with high CD8+ T cell infiltration and better prognosis. Additionally, mannose receptor C, type 1 (MRC1) and perivascular markers like Lymphatic Vessel Endothelial Hyaluronan Receptor 1 (LYVE1) and stabilin-1 (STAB1) were expressed by the FOLR2+ TR-TAMs. In agreement with the expression of perivascular markers, fetal-derived mammary gland macrophages display periductal and perivascular localization (23). In accordance, Cheng et al, demonstrated highest similarities between LVYE1+ TRM and FOLR2+ TR-TAMs. Since LYVE1+ macrophages were identified in multiple cancers and preferentially enriched in NT counterpart (19), the authors suggested that the enrichment of LVYE1+ TRM in adjacent NT may function as the potential pool for the FOLR2+ TAMs. Many observations suggested therefore a protective role for TRM in some cancers, however, other findings proposed that in lung and pancreas lesions, TRM played a key role in tumor initiation (24, 25). In non-small lung cancer TR alveolar TAM may induce epithelial-mesenchymal transition (EMT), regulatory T cell activation and promoting pro-tumorigenic fibroblast-TRM crosstalk, finally fostering tumor progression and invasiveness (25).

3.2 Mono-derived TAM

Tumor-infiltrating mono-derived TAM were described in a variety of human and murine cancer models. Müller and collaborators have been pioneers in dissecting the transcriptomic properties of mono-derived TAMs in gliomas. They demonstrated the co-existence of CX3C motif chemokine receptor 1 (CX3CR1)-blood-derived TAM, CX3CR1+ blood-derived TAM and lastly CD11b+CX3CR1+HLADRlow as TR microglia (26). Corroborating studies by Friebel and collaborators have defined TAM heterogeneity in primary gliomas and brain-derived metastasis. They demonstrated a mono-derived TAM cluster expressing CD163, CD206 and one expressing high level of Cell Adhesion Molecule 1 (CADM1) and CX3CR1 (27). In line, a study in BC identified CADM1 as marker of mono-derived TAM (16). Collectively, all these studies proposed CX3CR1 and CADM1 as mono-derived TAM markers (28).

The lipid-associated TREM2 (Triggering Receptor Expressed on Myeloid Cells 2) receptor has been recently associated to mono-

derived TAM in many cancer subtypes (17, 28–32). Its expression was detected together with APOE, APOC1 (apolipoprotein C1), FABP5 (fatty acid binding protein) and LIPA (Lipase A), genes involved in lipid transport and metabolism and highly detected in breast, sarcoma, colon, lung and other cancers (17, 28–31). Our work and that of others (17, 33) suggested that TREM2+ TAMs bear close transcriptomic profile to a Lipid Associated Macrophage (LAM) subpopulation, highly enriched in the adipose tissue of obese patients and in mice fed with high fat diet (34). These LAM were described as mono-derived cells (17, 33). Lipid-associated molecular profiles were highly enriched in several tumors and associated with a detrimental role in cancer progression. For example, Masetti et al, have demonstrated that MARCO+ TAM expressed high lipid-content and lipid-associated molecular signatures in prostate cancer, similarly lipid-laden TAMs have been discovered by Di Conza et al. (35, 36). Lipid loaded TAM or/and LAM were associated with poor prognosis and outcome (17, 33, 35, 36) suggesting a protumor role for lipids. Intriguingly, several groups have demonstrated that the abrogation of TREM2 activity in mice, by *Trem2* KO models or by Trem2 antibody-based blocked therapies, induced tumor growth delay and synergistic effect on T cell restoration functions concomitantly with anti-PD-1 blockade in many mouse models (CRC, sarcoma) (28). Although the mechanism of Trem2-/- KO or blockade activity seems to be T cell dependent, it remains to be elucidated the blocking effect of Trem2 as lipid marker in cancers. Overall these studies demonstrated a pro-tumoral role for mono-derived TREM2 TAM.

Another mono-derived marker commonly identified is the SPP1 (Osteopontin) gene (37). Of note, Zhang and colleagues demonstrated that a subset of SPP1+ TAMs may be developed from tumor-infiltrating mono-like precursors in CRC lesions (20). SPP1+ TAMs were described in 8 cancer subtypes: BC, PCA, Lung, CRC, Uterine corpus endometrial, Nasopharyngeal, Ovarian and Thyroid carcinoma, preferentially expressing an angiogenic signature (19). Some of them expressed high levels of MARCO gene, and Zhang et al, demonstrated that IL-1β and VEGF were able to upregulate its expression under hypoxic conditions (20). Collectively, SPP1 mono-derived TAM were associated with protumor and M2-like signatures, proposing a protumor role for these cells. Conversely to the observations above, mono-derived SPP1+ TAM have been recently identified associated to protective CXCL13+ T cell responses and highly correlated with plasma B cells, indicating a protective SPP1+ TAM role in human lung cancer (30). The large contribution of sc-datasets in identifying several TAM clusters highlighted the importance of having a consensus annotation. A big effort has been done by Mulder et al, in providing a robust online-available platform with the aim to harmonize the annotations of macrophages in healthy and pathological states. The authors have generated a monocyte-macrophage compendium widely distributed across multiple tissues. Some TAMs were exclusively expanded in cancer and inflamed tissues and generally enriched in neoplastic lesions (37). In pursuing the effort of collecting shared TAM features, Cheng and colleagues have demonstrated that - in a large cohort of 15 different cancer subtypes - TAM subsets could be concomitantly identified across cancer subtypes. However, the similarity analysis failed to exactly cluster TAMs with the same identity. These observations indicated that TAM exhibited high levels of complexity and heterogeneity, highlighting the crucial role for the local tissue microenvironment in shaping the TAM phenotype (14, 22) (Figure 1).

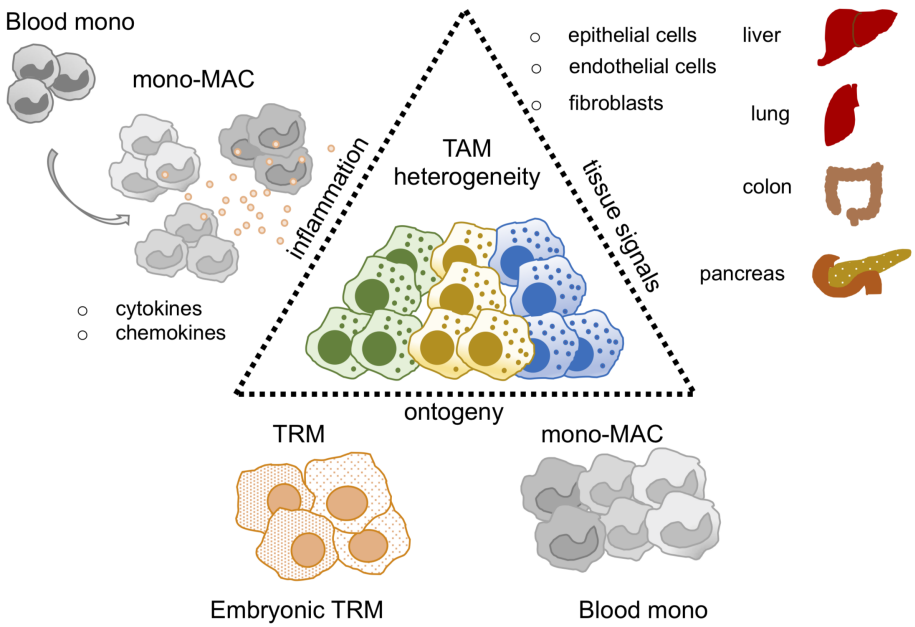

FIGURE 1
TAM heterogeneity in the sc-RNAseq era. Thanks to sc-RNAseq studies TAM heterogeneity has been revised. Key factors described to shape the TAM identity are: i) tissue signals, mediated by epithelial, endothelial and fibroblast cells represented in each organ of interest, ii) ontogeny, TAM may derive from tissue resident macrophages (TRM) or blood monocytes (Blood mono), iii) inflammation, it may influence and balance the recruitment of blood mono at tumor site perturbing TRM/blood monocyte ratio in the tumor.

4 Introduction to CAFs

The TME is a complex ecosystem where the malignant cells coexist with immune and stromal cells (fibroblasts and endothelial cells). CAFs represent the predominant cell type. CAFs play tumorigenic roles by promoting cancer cell survival and proliferation, inducing angiogenesis and extracellular matrix (ECM) remodeling. CAF subsets have been described to modulate immune responses, inducing regulatory T cell programs, T cell suppressive activities and recruiting myeloid cells at the tumor site (38). The peptidase inhibitor 16 (PI16) gene is considered a universal fibroblast marker, mostly expressed by normal fibroblasts (NFs) from NT areas (39). Conversely, CAFs expressed specific markers, less or not expressed by NFs, such as alfa-SMA (a-SMA), fibroblast activated protein (FAP), fibroblast specific protein-1 (FSP1), platelet derived growth factor receptor (PDGFR-α-β and podoplanin (PDPN) (40–44).

4.1 CAF in the era of single cell RNA-sequencing technology

FAP+ CAFs showed an activated phenotype compared to NFs and they were strongly enriched in tumor lesions compared with NT (38). Activated FAP+ CAF expressed pathways involved in collagen activation, ECM, metalloproteinase-related genes, adhesion and wound-healing signatures (45).

Thanks to the sc-RNA studies FAP+ CAFs have been deeply phenotyping, and different groups have observed highly heterogeneity of this subpopulation in NSCLC (30, 46–49), bladder (50), pancreas (51, 52), BC (53), liver (54) and HN (55) tumors.

Öhlund and colleagues have described that FAP^{high} CAFs comprised matrix-producing myo-fibroblastic phenotype (myCAF) and immunomodulatory secretome or inflammatory CAFs (iCAF) in human PCA and pancreatic mouse model. iCAF were able to produce high levels of IL-6, IL-11, leukemia inhibitory factor (LIF), and chemokines (CXCL1, CXCL2) while myCAF, detected closer to the tumor lesions, expressed high levels of α-SMA and ACTA2 genes, CTGF and COL1A1 (TGF-β-response genes) (51). Kieffer at al., have corroborated these observations in BC, distinguishing ANTRX1+ myCAF from ANTXR1- iCAFs. myCAF comprised ecm-myCAF, TGFβ-myCAF, and wound-myCAF involved respectively in extracellular matrix organization pathway, TGF-β pathway, collagen fibril organization and wound healing pathway. Whilst iCAF included subsets deputized to cytokine/chemokines production: detoxCAF (closer to NFs phenotype), IL-iCAF (deputized to cytokine/chemokines productions) and IFN-iCAF (involved in cytokine-mediated response to interferon-gamma genes) (53). The authors demonstrated that myCAFs correlated with non-responder patients to immune checkpoint blockade (ICB) therapies, demonstrating a role of FAP+ CAF in contributing to primary resistance to immunotherapy. Another study demonstrated the presence of leucine-rich-repeat-containing protein 15 (LRRC15+) myCAFs able to directly suppress CD8 T cell function and limit responsiveness to ICB (52). myCAF and iCAF subsets were accordingly identified in triple negative breast cancer (TNBC) and CRC (56, 57). Generally, these data suggested iCAF distal from the tumor lesion and with secretory ability, while myCAF, described in close proximity to the tumor site, showed activated and contractility genes (51, 56, 57). Of interest, Grout et al, dissected NSCLC stromal TME. They identified alcohol dehydrogenase 1B (ADH1B) positive CAFs, carrying low activation state and highly producing CCL19, they were spread throughout the stroma and supported a T-cell permissive TME. In contrast, MYH11+αSMA+ CAFs expressing myosin heavy chain 11 (MYH11) gene, ACTA2, and intermediate levels of CD34 were localized as a single layer encapsulating the tumor nest and orchestrating T-cell exclusion. Both ADH1B+ and MYH11+αSMA+ and CAFs characterized early stage of the disease. At advanced stages other two clusters were identified: FAP+ CAFs expressed high levels of periostin (POSTN), Leucine Rich Repeat Containing 15 (LRRC15), and Gremlin1 (GREM1) genes and FAP+ αSMA+ CAFs. Intriguingly, while FAP+ αSMA+ orchestrated T-cell exclusion, FAP+ CAF showed T-cell permissive TME (47). This study has elucidated the importance of different CAF subpopulations at displaying T-cell permissive or excluding TME. Still remains to understand which factors influence CAF subtypes. Of remarkable interest for the immunologists was the discovery of antigen-presenting CAFs (apCAFs) in mouse and human PCA ductal adenocarcinoma. Elyada et al, showed that apCAFs expressed high levels of MHC-class II genes (H2-Ab1) and CD74 gene, however they did not express classic costimulatory molecules. They expressed markers regulating the immune system like BCAM (CD239), F11R (member of Immunoglobulin genes), IRF5 (interferon stimulating factor 5) and STAT1, known to mediate MHC expression in response to IFN-γ. These MHC class II–expressing CAFs showed the capacity to activate CD4+ T cells in an antigen-specific manner, corroborating their putative immune-modulatory aptitude (58). Rapidly, our view about CAFs and their heterogeneity has changed. The coexistence of myCAF and iCAF in the TME suggests a compartmentalization, both in terms of localization (close or distant to the tumor nest) and functions that may dictate the localization and the phenotype/function of tumor-infiltrating immune cells. Due to the availability of numerous sc-RNA seq datasets and given the deep-phenotyping of CAFs and TAM in many cancer studies, CAF-TAM interactions and their cross-talks has been reviewed.

4.2 CAF and TAM crosstalk in the TME

At steady-state the connection between fibroblasts and macrophages is documented by the ability of NFs to produce colony stimulating growth factor 1 (CSF-1), lineage-specific growth factor, crucial for the proliferation and survival of macrophages. Zhou et al., have demonstrated that microenvironmental sensing by fibroblasts may control macrophage population size by producing CSF-1 (59). CAFs and

TAMs may interact via the CSF1-CSF1R axis also in the TME (60). So far, it has been collectively demonstrated that CAFs may secrete several factors well-known to influence the recruitment and activation state of myeloid cells including: IL-1β, IL-8, IL-6, IL-33, IL-10, Chi3L1, CXCL1, CXCL2, CXCL5, CXCL6, CXCL8, CXCL9, CXCL10, CXCL16, CXCL12/SDF1, CCL2/MCP-1, CCL3, CCL5/Rantes, CCL7, CCL20, CCL26, TGF-β, prostaglandin (PGE2), indoleamine-2,3-dioxygenase (IDO), LIF, VEGF, tumor necrosis factor (TNF), and nitric oxide (NO) (61–63). CAFs may recruit monocyte at the tumor site by CCL2-CCR2 pathway. FAP+ CAFs were identified as a major source of CCL2 in intrahepatic cholangiocarcinoma (64). The CCL2-CCR2 axis was also linked to tumor progression in a spontaneous model of lymphoma; accordingly, genetic ablation of Ccr2 inhibited tumor growth (65). CAFs may promote skin carcinogenesis by maintaining CCL2 mediated monocyte/macrophage infiltration and chronic inflammation (66). CAF derived-CXCL16 chemokine may also recruit mono promoting stromal activation and then tumor progression in TNBC (67). CXCL14 may be produced by CAFs, therefore amplifying mono recruitment at tumor site and acting as stimulator of prostate tumor growth (68). Among the pathways involved in the mono recruitment, CXCL12 is well studied. CAFs produce high levels of CXCL12 in the TME and CXCL12-CXCR4 CAF-TAM axis is responsible for mono recruitment at the tissue (69). In line, targeting the CXCL12 pathway from FAP+ CAFs synergized with anti–PD-L1 immunotherapy in PCA (70). In bladder cancer CXCL12-CXCR4 iCAF-TAM crosstalk was described (50). Our study, in accordance with other studies, demonstrated that iCAF, highly enriched in TNBC, were the major source of CXCL12, resulting the key cells sustaining the recruitment of CXCR4+ monocyte in TNBC (17). In keeping with our observations in TNBC, Wu and colleagues demonstrated that iCAF-TAM crosstalk strongly associated with cytotoxic T-lymphocyte dysfunction in TNBC (57). Overall, the recruitment of monocytes via the CXCL12-CXCR4 axis was associated with tumor progression. iCAF-TAM axis mainly involved the complement cascade activation pathway by the interactions of complement C5-C5AR1. C5 pathway is an important chemotactic factor for the recruitment of immunosuppressive myeloid cells ultimately suppressing T-cell activities (71). A cross-talk between C3-C3aR iCAF-TAM axis has been additionally elucidated in melanoma, HN and BC (60). These data suggested that CD34+ PDPN+ and PDGFR-α+ iCAFs were highly producers of C3, C2, and C4b complement components, additionally to CXCL12, CSF-1 and CCL8 factors. CD34+ CAFs, by producing C3 and by the C3a conversion into an activated form in the TME, allowed the recruitment of C3aR+ circulating monocytes. By confocal microscopy analysis, C3aR+ TAMs were proximally located to CD34+ CAFs, indicative of a generation of supportive protumor niche by iCAF-TAM interactions (60). Globally these data suggested a pro-tumoral role for the complement components in recruiting circulating monocytes and favor immune suppression. These data supported a recent hypothesis that iCAF, rather than myCAF, may play a fundamental role in promoting tumor progression by recruiting monocytes at the tumor site via local inflammation. Among the pathways responsible of CAF monocyte reprogramming IL-6/STAT3 is well studied. CAF-derived IL6 leads to myeloid immunosuppression phenotype by STAT3 activation. Inhibiting IL-6 pathway or STAT3 activation by blocking CAF-TAM interactions decreased immunosuppression in PCA (72) and HCC (73) was observed. STAT3 activation is also mediated by LIF and IL-11. LIF pathway leaded to immunosuppressive signature on TAMs by decreasing CXCL9 expression and preventing cytotoxic CD8+ T-cell recruitment, impairing anti-PD1 response (74). In a model of BC CAF-derived Chi3L1 induced mono recruitment and M2-like TAM reprogramming by inducing CD206 and ARG1 expression.

Cytokines as IL-8, IL-33, IL-10, TGF-β and CCL2 secreted by CAFs promoted the recruitment of monocytes at tumor site and the M2-like protumor phenotype (66, 75, 76). Collectively, many studies have demonstrated CAF-mediated mechanisms inducing M2-like TAM phenotype (17, 77–80). Of note, Mazur et al., explained the mechanisms by which the FAP protein could interact with TAM. The authors have demonstrated that FAP is crucial for the CAF interaction with class A scavenger receptor (SR-A or CD204) expressed by TAM, mainly by cleaving type I collagen resulting in increased TAM adhesion (81). A protumor niche generated by the interactions between FAP+ CAF and SPP1 + TAM has been identified in CRC. The abundance of both FAP+ CAFs and SPP1+ TAMs was correlated with worst patient survival. Interestingly, FAP+ CAFs and SPP1+ TAMs were found in close proximity in the TME communicating by TGFβ-ACVRL1/ACVR1/B pathway, CCL3-CCR5 axis and RARRES2-CMKLR1 pathway. The latter involved in the recruitment of CMKLR1+ monocyte/TAM at the tumor site. These were described as pro-tumoral pathways in the tumor promotion and progression.

Since both FAP+ CAFs and SPP1+ TAMs were enriched in genes linked to ECM the authors suggested that this myCAF-TAM axis may facilitate the generation of desmoplastic structures in CRC (82). In agreement, a positive correlation between FAP+ CAF and SPP1+ mono-derived TAM was found in NSCLC cohort (47). Our study in TNBC demonstrated also a protumor niche between FAP+ CAF and mono-derived LAM. We have demonstrated by *in vitro* assays that FAP+ CAF were able to induce a LAM-like suppressive phenotype characterized by the induction of APOE, APOC1, FABP5, ACP5 and TREM2 genes. LAM-differentiated cells were able to inhibit T cell proliferation and activation state orchestrating suppressive functions (17). In keeping with these studies, a work collecting 10 cancer subtypes has demonstrated the existence of CAFs generated from endothelial cells by endothelial-mesenchymal transition (EndMT) (CAF-EndMT). They exhibited concomitant expression of CD44+CD31+ and ACTA2, in addition to regulator of G Protein Signaling 5 (RGS5), plasmalemmal vesicle-associated protein (PLVAP) and von willebrand factor (VWF) genes. The authors identified CD44+ CAF EndMT - Spp1+ TAM interactions in promoting EndMT process and angiogenesis leading to poor prognosis in cancer patients (45) (Figure 2).

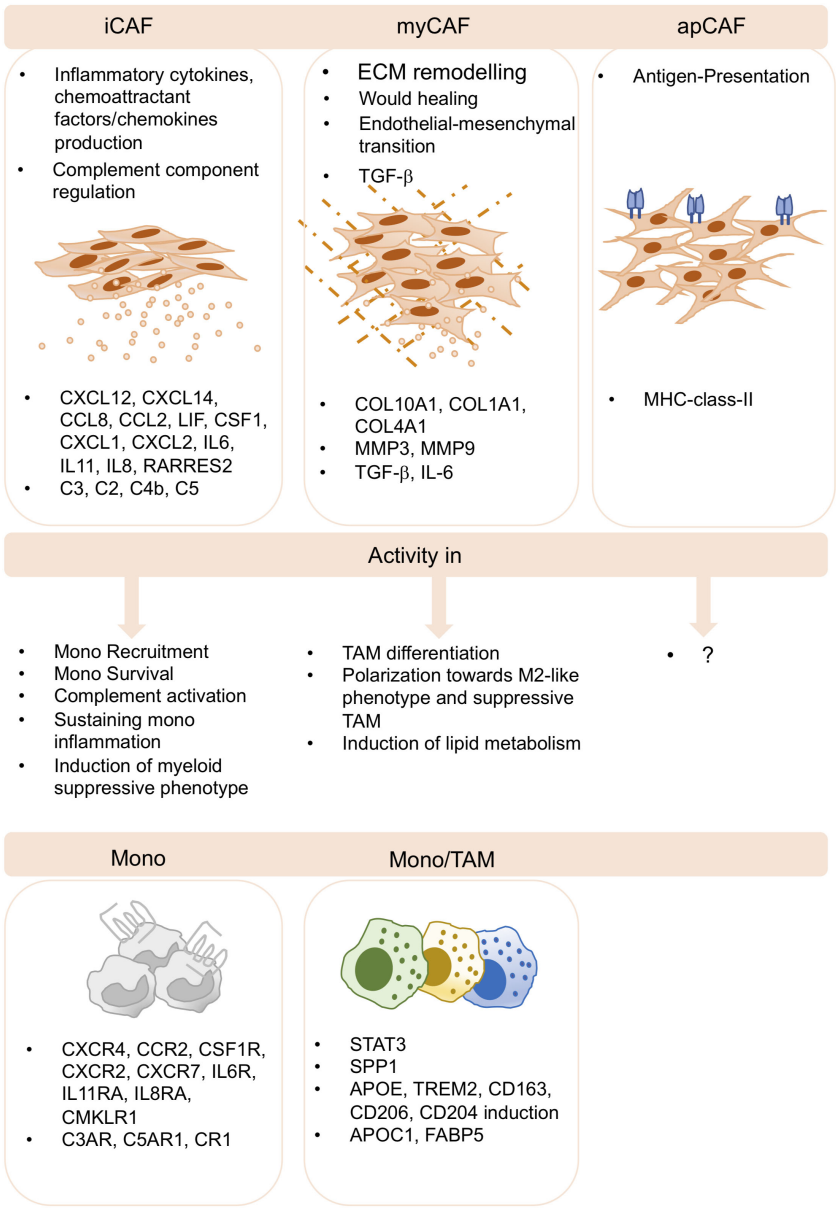

FIGURE 2
CAF-TAM interactions in the TME. Inflammatory CAF (iCAF), myofibroblasts CAF (myCAF) and antigen presenting CAF (apCAF) have been described by several sc-studies and across cancer subtypes. iCAF produces inflammatory cytokines and chemokines and they produce complement components. They play key roles in monocyte recruitment, inflammation, complement activation and in the induction of suppressive functions of myeloid cells. myCAF are involved in extracellular matrix remodeling, wound healing, endothelial-to-mesenchymal transition, and produce TGF-b. They induce M2-like phenotype, differentiation and polarization of suppressive TAM and the induction of lipid metabolism. apCAF have been described, however, no specific functions associated to TAM biology have been reported to date.

5 Discussion

This review gathers evidence from key studies that highlight the suppressive crosstalk between newly identified TAM and CAF subpopulations across different solid cancers and explores the suppressive modules that could provide potential targets of new therapeutic approaches.

Author contributions

ET and ER wrote and conceptualized the review, ET and ER reviewed the literature on single cell studies on tumor-associated macrophages and cancer associated fibroblasts. All authors contributed to the article and approved the submitted version.

Funding

This work was supported by the following grants to ER: Foundation ARC (grant no. AAP SIGN'IT 2019), Fonds Amgen France pour la Science et l'Humain; CIC IGR-Curie 1428; ANR-10-IDEX-0001-02 PSL; and ANR- 11-LABX-0043. ET was supported by a postdoctoral fellowship abroad from the AIRC (2018/2020-number: 20934).

Conflict of interest

ER reports grants from Fonds Amgen France pour la Science et l'Humain during the conduct of the study.

ET declares that the research was conducted in the absence of any commercial or financial relationships that could be construed as a potential conflict of interest.

Publisher's note

References

1. Murray PJ. Macrophage polarization. *Annu Rev Physiol* (2017) 79:541–66. doi: 10.1146/annurev-physiol-022516-034339

2. Sica A, Mantovani A. Macrophage plasticity and polarization: *in vivo* veritas. *J Clin Invest* (2012) 122:787–95. doi: 10.1172/JCI59643

3. Locati M, Curtale G, Mantovani A. Diversity, mechanisms, and significance of macrophage plasticity. *Annu Rev Pathol* (2020) 15:123–47. doi: 10.1146/annurev-pathmechdis-012418-012718

4. Cassetta L, Pollard JW. Targeting macrophages: therapeutic approaches in cancer. *Nat Rev Drug Discovery* (2018) 17:887–904. doi: 10.1038/nrd.2018.169

5. Zhao X, Qu J, Sun Y, Wang J, Liu X, Wang F, et al. Prognostic significance of tumor-associated macrophages in breast cancer: a meta-analysis of the literature. *Oncotarget* (2017) 8:30576–86. doi: 10.18632/oncotarget.15736

6. Yin S, Huang J, Li Z, Zhang J, Luo J, Lu C, et al. The prognostic and clinicopathological significance of tumor-associated macrophages in patients with gastric cancer: a meta-analysis. *PloS One* (2017) 12:e0170042. doi: 10.1371/journal.pone.0170042

7. Cortese N, Carriero R, Laghi L, Mantovani A, Marchesi F. Prognostic significance of tumor-associated macrophages: past, present and future. *Semin Immunol* (2020) 48:101408. doi: 10.1016/j.smim.2020.101408

8. Bingle L, Brown NJ, Lewis CE. The role of tumour-associated macrophages in tumour progression: implications for new anticancer therapies. *J Pathol* (2002) 196:254–65. doi: 10.1002/path.1027

9. Yuan X, Zhang J, Li D, Mao Y, Mo F, Du W, et al. Prognostic significance of tumor-associated macrophages in ovarian cancer: a meta-analysis. *Gynecol Oncol* (2017) 147:181–7. doi: 10.1016/j.ygyno.2017.07.007

10. Zhang J, Chang L, Zhang X, Zhou Z, Gao Y. Meta-analysis of the prognostic and clinical value of tumor-associated macrophages in hepatocellular carcinoma. *J Investig Surg Off J Acad Surg Res* (2021) 34:297–306. doi: 10.1080/08941939.2019.1631411

11. Park MD, Silvin A, Ginhoux F, Merad M. Macrophages in health and disease. *Cell* (2022) 185:4259–79. doi: 10.1016/j.cell.2022.10.007

12. Argyle D, Kitamura T. Targeting macrophage-recruiting chemokines as a novel therapeutic strategy to prevent the progression of solid tumors. *Front Immunol* (2018) 9:2629. doi: 10.3389/fimmu.2018.02629

13. Amit I, Winter DR, Jung S. The role of the local environment and epigenetics in shaping macrophage identity and their effect on tissue homeostasis. *Nat Immunol* (2016) 17:18–25. doi: 10.1038/ni.3325

14. Gosselin D, Link VM, Romanoski CE, Fonseca GJ, Eichenfield DZ, Spann NJ, et al. Environment drives selection and function of enhancers controlling tissue-specific macrophage identities. *Cell* (2014) 159:1327–40. doi: 10.1016/j.cell.2014.11.023

15. Okabe Y, Medzhitov R. Tissue-specific signals control reversible program of localization and functional polarization of macrophages. *Cell* (2014) 157:832–44. doi: 10.1016/j.cell.2014.04.016

16. Nalio Ramos R, Missolo-Koussou Y, Gerber-Ferder Y, Bromley CP, Bugatti M, Núñez NG, et al. Tissue-resident FOLR2+ macrophages associate with CD8+ T cell infiltration in human breast cancer. *Cell* (2022) 185:1189–1207.e25. doi: 10.1016/j.cell.2022.02.021

17. Timperi E, Gueguen P, Molgora M, Magagna I, Kieffer Y, Lopez-Lastra S, et al. Lipid-associated macrophages are induced by cancer-associated fibroblasts and mediate immune suppression in breast cancer. *Cancer Res* (2022) 82:3291–306. doi: 10.1158/0008-5472.CAN-22-1427

18. Azizi E, Carr AJ, Plitas G, Cornish AE, Konopacki C, Prabhakaran S, et al. Single-cell map of diverse immune phenotypes in the breast tumor microenvironment. *Cell* (2018) 174:1293–1308.e36. doi: 10.1016/j.cell.2018.05.060

19. Cheng S, Li Z, Gao R, Xing B, Gao Y, Yang Y, et al. A pan-cancer single-cell transcriptional atlas of tumor infiltrating myeloid cells. *Cell* (2021) 184:792–809.e23. doi: 10.1016/j.cell.2021.01.010

20. Zhang L, Li Z, Skrzypczynska KM, Fang Q, Zhang W, O'Brien SA, et al. Single-cell analyses inform mechanisms of myeloid-targeted therapies in colon cancer. *Cell* (2020) 181:442–459.e29. doi: 10.1016/j.cell.2020.03.048

21. Zilionis R, Engblom C, Pfirschke C, Savova V, Zemmour D, Saatcioglu HD, et al. Single-cell transcriptomics of human and mouse lung cancers reveals conserved myeloid populations across individuals and species. *Immunity* (2019) 50:1317–1334.e10. doi: 10.1016/j.immuni.2019.03.009

22. Sharma A, Seow JJW, Dutertre C-A, Pai R, Blériot C, Mishra A, et al. Onco-fetal reprogramming of endothelial cells drives immunosuppressive macrophages in hepatocellular carcinoma. *Cell* (2020) 183:377–394.e21. doi: 10.1016/j.cell.2020.08.040

23. Jäppinen N, Félix I, Lokka E, Tyystjärvi S, Pynttäri A, Lahtela T, et al. Fetal-derived macrophages dominate in adult mammary glands. *Nat Commun* (2019) 10:281. doi: 10.1038/s41467-018-08065-1

24. Zhu Y, Herndon JM, Sojka DK, Kim K-W, Knolhoff BL, Zuo C, et al. Tissue-resident macrophages in pancreatic ductal adenocarcinoma originate from embryonic hematopoiesis and promote tumor progression. *Immunity* (2017) 47:323–338.e6. doi: 10.1016/j.immuni.2017.07.014

25. Casanova-Acebes M, Dalla E, Leader AM, LeBerichel J, Nikolic J, Morales BM, et al. Tissue-resident macrophages provide a pro-tumorigenic niche to early NSCLC cells. *Nature* (2021) 595:578–84. doi: 10.1038/s41586-021-03651-8

26. Müller S, Kohanbash G, Liu SJ, Alvarado B, Carrera D, Bhaduri A, et al. Single-cell profiling of human gliomas reveals macrophage ontogeny as a basis for regional differences in macrophage activation in the tumor microenvironment. *Genome Biol* (2017) 18:234. doi: 10.1186/s13059-017-1362-4

27. Friebel E, Kapolou K, Unger S, Núñez NG, Utz S, Rushing EJ, et al. Single-cell mapping of human brain cancer reveals tumor-specific instruction of tissue-invading leukocytes. *Cell* (2020) 181:1626–1642.e20. doi: 10.1016/j.cell.2020.04.055

28. Molgora M, Esaulova E, Vermi W, Hou J, Chen Y, Luo J, et al. TREM2 modulation remodels the tumor myeloid landscape enhancing anti-PD-1 immunotherapy. *Cell* (2020) 182:886–900.e17. doi: 10.1016/j.cell.2020.07.013

29. Lavin Y, Kobayashi S, Leader A, Amir E-AD, Elefant N, Bigenwald C, et al. Innate immune landscape in early lung adenocarcinoma by paired single-cell analyses. *Cell* (2017) 169:750–765.e17. doi: 10.1016/j.cell.2017.04.014

30. Leader AM, Grout JA, Maier BB, Nabet BY, Park MD, Tabachnikova A, et al. Single-cell analysis of human non-small cell lung cancer lesions refines tumor classification and patient stratification. *Cancer Cell* (2021) 39:1594–1609.e12. doi: 10.1016/j.ccell.2021.10.009

31. Katzenelenbogen Y, Sheban F, Yalin A, Yofe I, Svetlichnyy D, Jaitin DA, et al. Coupled scRNA-seq and intracellular protein activity reveal an immunosuppressive role of TREM2 in cancer. *Cell* (2020) 182:872–885.e19. doi: 10.1016/j.cell.2020.06.032

32. Binnewies M, Pollack JL, Rudolph J, Dash S, Abushawish M, Lee T, et al. Targeting TREM2 on tumor-associated macrophages enhances immunotherapy. *Cell Rep* (2021) 37:109844. doi: 10.1016/j.celrep.2021.109844

33. Wu SZ, Al-Eryani G, Roden DL, Junankar S, Harvey K, Andersson A, et al. A single-cell and spatially resolved atlas of human breast cancers. *Nat Genet* (2021) 53:1334–47. doi: 10.1038/s41588-021-00911-1

34. Jaitin DA, Adlung L, Thaiss CA, Weiner A, Li B, Descamps H, et al. Lipid-associated macrophages control metabolic homeostasis in a Trem2-dependent manner. *Cell* (2019) 178:686–698.e14. doi: 10.1016/j.cell.2019.05.054

35. Di Conza G, Tsai C-H, Gallart-Ayala H, Yu Y-R, Franco F, Zaffalon L, et al. Tumor-induced reshuffling of lipid composition on the endoplasmic reticulum membrane sustains macrophage survival and pro-tumorigenic activity. *Nat Immunol* (2021) 22:1403–15. doi: 10.1038/s41590-021-01047-4

36. Masetti M, Carriero R, Portale F, Marelli G, Morina N, Pandini M, et al. Lipid-loaded tumor-associated macrophages sustain tumor growth and invasiveness in prostate cancer. *J Exp Med* (2022) 219:e20210564. doi: 10.1084/jem.20210564

37. Mulder K, Patel AA, Kong WT, Piot C, Halitzki E, Dunsmore G, et al. Cross-tissue single-cell landscape of human monocytes and macrophages in health and disease. *Immunity* (2021) 54:1883–1900.e5. doi: 10.1016/j.immuni.2021.07.007

38. Costa A, Kieffer Y, Scholer-Dahirel A, Pelon F, Bourachot B, Cardon M, et al. Fibroblast heterogeneity and immunosuppressive environment in human breast cancer. *Cancer Cell* (2018) 33:463–479.e10. doi: 10.1016/j.ccell.2018.01.011

39. Buechler MB, Pradhan RN, Krishnamurty AT, Cox C, Calviello AK, Wang AW, et al. Cross-tissue organization of the fibroblast lineage. *Nature* (2021) 593:575–9. doi: 10.1038/s41586-021-03549-5

40. Östman A. PDGF receptors in tumor stroma: biological effects and associations with prognosis and response to treatment. *Adv Drug Delivery Rev* (2017) 121:117–23. doi: 10.1016/j.addr.2017.09.022

41. Primac I, Maquoi E, Blacher S, Heljasvaara R, Van Deun J, Smeland HY, et al. Stromal integrin α11 regulates PDGFR-β signaling and promotes breast cancer progression. *J Clin Invest* (2019) 129:4609–28. doi: 10.1172/JCI125890

42. Strutz F, Okada H, Lo CW, Danoff T, Carone RL, Tomaszewski JE, et al. Identification and characterization of a fibroblast marker: FSP1. *J Cell Biol* (1995) 130:393–405. doi: 10.1083/jcb.130.2.393

43. Park JE, Lenter MC, Zimmermann RN, Garin-Chesa P, Old LJ, Rettig WJ. Fibroblast activation protein, a dual specificity serine protease expressed in reactive human tumor stromal fibroblasts. *J Biol Chem* (1999) 274:36505–12. doi: 10.1074/jbc.274.51.36505

44. Sugimoto H, Mundel TM, Kieran MW, Kalluri R. Identification of fibroblast heterogeneity in the tumor microenvironment. *Cancer Biol Ther* (2006) 5:1640–6. doi: 10.4161/cbt.5.12.3354

45. Luo H, Xia X, Huang L-B, An H, Cao M, Kim GD, et al. Pan-cancer single-cell analysis reveals the heterogeneity and plasticity of cancer-associated fibroblasts in the tumor microenvironment. *Nat Commun* (2022) 13:6619. doi: 10.1038/s41467-022-34395-2

46. Kim N, Kim HK, Lee K, Hong Y, Cho JH, Choi JW, et al. Single-cell RNA sequencing demonstrates the molecular and cellular reprogramming of metastatic lung adenocarcinoma. *Nat Commun* (2020) 11:2285. doi: 10.1038/s41467-020-16164-1

47. Grout JA, Sirven P, Leader AM, Maskey S, Hector E, Puisieux I, et al. Spatial positioning and matrix programs of cancer-associated fibroblasts promote T-cell exclusion in human lung tumors. *Cancer Discovery* (2022) 12:2606–25. doi: 10.1158/2159-8290.CD-21-1714

48. Lambrechts D, Wauters E, Boeckx B, Aibar S, Nittner D, Burton O, et al. Phenotype molding of stromal cells in the lung tumor microenvironment. *Nat Med* (2018) 24:1277–89. doi: 10.1038/s41591-018-0096-5

49. Laughney AM, Hu J, Campbell NR, Bakhoum SF, Setty M, Lavallée V-P, et al. Regenerative lineages and immune-mediated pruning in lung cancer metastasis. *Nat Med* (2020) 26:259–69. doi: 10.1038/s41591-019-0750-6

50. Chen Z, Zhou L, Liu L, Hou Y, Xiong M, Yang Y, et al. Single-cell RNA sequencing highlights the role of inflammatory cancer-associated fibroblasts in bladder urothelial carcinoma. *Nat Commun* (2020) 11:5077. doi: 10.1038/s41467-020-18916-5

51. Öhlund D, Handly-Santana A, Biffi G, Elyada E, Almeida AS, Ponz-Sarvise M, et al. Distinct populations of inflammatory fibroblasts and myofibroblasts in pancreatic cancer. *J Exp Med* (2017) 214:579–96. doi: 10.1084/jem.20162024

52. Krishnamurty AT, Shyer JA, Thai M, Gandham V, Buechler MB, Yang YA, et al. LRRC15+ myofibroblasts dictate the stromal setpoint to suppress tumour immunity. *Nature* (2022) 611:148–54. doi: 10.1038/s41586-022-05272-1

53. Kieffer Y, Hocine HR, Gentric G, Pelon F, Bernard C, Bourachot B, et al. Single-cell analysis reveals fibroblast clusters linked to immunotherapy resistance in cancer. *Cancer Discovery* (2020) 10:1330–51. doi: 10.1158/2159-8290.CD-19-1384

54. Affo S, Nair A, Brundu F, Ravichandra A, Bhattacharjee S, Matsuda M, et al. Promotion of cholangiocarcinoma growth by diverse cancer-associated fibroblast subpopulations. *Cancer Cell* (2021) 39:866–882.e11. doi: 10.1016/j.ccell.2021.03.012

55. Puram SV, Tirosh I, Parikh AS, Patel AP, Yizhak K, Gillespie S, et al. Single-cell transcriptomic analysis of primary and metastatic tumor ecosystems in head and neck cancer. *Cell* (2017) 171:1611–1624.e24. doi: 10.1016/j.cell.2017.10.044

56. Pelka K, Hofree M, Chen JH, Sarkizova S, Pirl JD, Jorgji V, et al. Spatially organized multicellular immune hubs in human colorectal cancer. *Cell* (2021) 184:4734–4752.e20. doi: 10.1016/j.cell.2021.08.003

57. Wu SZ, Roden DL, Wang C, Holliday H, Harvey K, Cazet AS, et al. Stromal cell diversity associated with immune evasion in human triple-negative breast cancer. *EMBO J* (2020) 39:e104063. doi: 10.15252/embj.2019104063

58. Elyada E, Bolisetty M, Laise P, Flynn WF, Courtois ET, Burkhart RA, et al. Cross-species single-cell analysis of pancreatic ductal adenocarcinoma reveals antigen-presenting cancer-associated fibroblasts. *Cancer Discovery* (2019) 9:1102–23. doi: 10.1158/2159-8290.CD-19-0094

59. Zhou X, Franklin RA, Adler M, Carter TS, Condiff E, Adams TS, et al. Microenvironmental sensing by fibroblasts controls macrophage population size. *Proc Natl Acad Sci U.S.A.* (2022) 119:e2205360119. doi: 10.1073/pnas.2205360119

60. Davidson S, Efremova M, Riedel A, Mahata B, Pramanik J, Huuhtanen J, et al. Single-cell RNA sequencing reveals a dynamic stromal niche that supports tumor growth. *Cell Rep* (2020) 31:107628. doi: 10.1016/j.celrep.2020.107628

61. Lazennec G, Richmond A. Chemokines and chemokine receptors: new insights into cancer-related inflammation. *Trends Mol Med* (2010) 16:133–44. doi: 10.1016/j.molmed.2010.01.003

62. Barrett RL, Puré E. Cancer-associated fibroblasts and their influence on tumor immunity and immunotherapy. *eLife* (2020) 9:e57243. doi: 10.7554/eLife.57243

63. Ziani L, Safta-Saadoun TB, Gourbeix J, Cavalcanti A, Robert C, Favre G, et al. Melanoma-associated fibroblasts decrease tumor cell susceptibility to NK cell-mediated killing through matrix-metalloproteinases secretion. *Oncotarget* (2017) 8:19780–94. doi: 10.18632/oncotarget.15540

64. Yang X, Lin Y, Shi Y, Li B, Liu W, Yin W, et al. FAP promotes immunosuppression by cancer-associated fibroblasts in the tumor microenvironment via STAT3-CCL2 signaling. *Cancer Res* (2016) 76:4124–35. doi: 10.1158/0008-5472.CAN-15-2973

65. Ren G, Zhao X, Wang Y, Zhang X, Chen X, Xu C, et al. CCR2-dependent recruitment of macrophages by tumor-educated mesenchymal stromal cells promotes tumor development and is mimicked by TNFα. *Cell Stem Cell* (2012) 11:812–24. doi: 10.1016/j.stem.2012.08.013

66. Zhang J, Chen L, Xiao M, Wang C, Qin Z. FSP1+ fibroblasts promote skin carcinogenesis by maintaining MCP-1-mediated macrophage infiltration and chronic inflammation. *Am J Pathol* (2011) 178:382–90. doi: 10.1016/j.ajpath.2010.11.017

67. Allaoui R, Bergenfelz C, Mohlin S, Hagerling C, Salari K, Werb Z, et al. Cancer-associated fibroblast-secreted CXCL16 attracts monocytes to promote stroma activation in triple-negative breast cancers. *Nat Commun* (2016) 7:13050. doi: 10.1038/ncomms13050

68. Augsten M, Hägglöf C, Olsson E, Stolz C, Tsagozis P, Levchenko T, et al. CXCL14 is an autocrine growth factor for fibroblasts and acts as a multi-modal stimulator of prostate tumor growth. *Proc Natl Acad Sci U.S.A.* (2009) 106:3414–9. doi: 10.1073/pnas.0813144106

69. Gok Yavuz B, Gunaydin G, Gedik ME, Kosemehmetoglu K, Karakoc D, Ozgur F, et al. Cancer associated fibroblasts sculpt tumour microenvironment by recruiting monocytes and inducing immunosuppressive PD-1+ TAMs. *Sci Rep* (2019) 9:3172. doi: 10.1038/s41598-019-39553-z

70. Feig C, Jones JO, Kraman M, Wells RJB, Deonarine A, Chan DS, et al. Targeting CXCL12 from FAP-expressing carcinoma-associated fibroblasts synergizes with anti-PD-L1 immunotherapy in pancreatic cancer. *Proc Natl Acad Sci U.S.A.* (2013) 110:20212–7. doi: 10.1073/pnas.1320318110

71. Markiewski MM, DeAngelis RA, Benencia F, Ricklin-Lichtsteiner SK, Koutoulaki A, Gerard C, et al. Modulation of the antitumor immune response by complement. *Nat Immunol* (2008) 9:1225–35. doi: 10.1038/ni.1655

72. Mace TA, Ameen Z, Collins A, Wojcik S, Mair M, Young GS, et al. Pancreatic cancer-associated stellate cells promote differentiation of myeloid-derived suppressor cells in a STAT3-dependent manner. *Cancer Res* (2013) 73:3007–18. doi: 10.1158/0008-5472.CAN-12-4601

73. Deng Y, Cheng J, Fu B, Liu W, Chen G, Zhang Q, et al. Hepatic carcinoma-associated fibroblasts enhance immune suppression by facilitating the generation of myeloid-derived suppressor cells. *Oncogene* (2017) 36:1090–101. doi: 10.1038/onc.2016.273

74. Pascual-García M, Bonfill-Teixidor E, Planas-Rigol E, Rubio-Perez C, Iurlaro R, Arias A, et al. LIF regulates CXCL9 in tumor-associated macrophages and prevents CD8+ T cell tumor-infiltration impairing anti-PD1 therapy. *Nat Commun* (2019) 10:2416. doi: 10.1038/s41467-019-10369-9

75. Zhang R, Qi F, Zhao F, Li G, Shao S, Zhang X, et al. Cancer-associated fibroblasts enhance tumor-associated macrophages enrichment and suppress NK cells function in colorectal cancer. *Cell Death Dis* (2019) 10:273. doi: 10.1038/s41419-019-1435-2

76. Shani O, Vorobyov T, Monteran L, Lavie D, Cohen N, Raz Y, et al. Fibroblast-derived IL33 facilitates breast cancer metastasis by modifying the immune microenvironment and driving type 2 immunity. *Cancer Res* (2020) 80:5317–29. doi: 10.1158/0008-5472.CAN-20-2116

77. Erez N, Truitt M, Olson P, Arron ST, Hanahan D. Cancer-associated fibroblasts are activated in incipient neoplasia to orchestrate tumor-promoting inflammation in an NF-kappaB-Dependent manner. *Cancer Cell* (2010) 17:135–47. doi: 10.1016/j.ccr.2009.12.041

78. Chen S, Morine Y, Tokuda K, Yamada S, Saito Y, Nishi M, et al. Cancer –associated fibroblast–induced M2–polarized macrophages promote hepatocellular carcinoma progression via the plasminogen activator inhibitor–1 pathway. *Int J Oncol* (2021) 59:59. doi: 10.3892/ijo.2021.5239

79. Louault K, Porras T, Lee M-H, Muthugounder S, Kennedy RJ, Blavier L, et al. Fibroblasts and macrophages cooperate to create a pro-tumorigenic and immune resistant environment via activation of TGF-β/IL-6 pathway in neuroblastoma. *Oncoimmunology* (2022) 11:2146860. doi: 10.1080/2162402X.2022.2146860

80. Comito G, Giannoni E, Segura CP, Barcellos-de-Souza P, Raspollini MR, Baroni G, et al. Cancer-associated fibroblasts and M2-polarized macrophages synergize during prostate carcinoma progression. *Oncogene* (2014) 33:2423–31. doi: 10.1038/onc.2013.191

81. Mazur A, Holthoff E, Vadali S, Kelly T, Post SR. Cleavage of type I collagen by fibroblast activation protein-α enhances class a scavenger receptor mediated macrophage adhesion. *PloS One* (2016) 11:e0150287. doi: 10.1371/journal.pone.0150287

82. Qi J, Sun H, Zhang Y, Wang Z, Xun Z, Li Z, et al. Single-cell and spatial analysis reveal interaction of FAP+ fibroblasts and SPP1+ macrophages in colorectal cancer. *Nat Commun* (2022) 13:1742. doi: 10.1038/s41467-022-29366-6

frontiers | Frontiers in Immunology

TYPE Perspective
PUBLISHED 08 June 2023
DOI 10.3389/fimmu.2023.1197053

OPEN ACCESS

EDITED BY
John-Maher,
King's College London, United Kingdom

REVIEWED BY
Roberta Castriconi,
University of Genoa, Italy

*CORRESPONDENCE
Loredana Cifaldi
cifaldi@med.uniroma2.it

RECEIVED 30 March 2023
ACCEPTED 26 May 2023
PUBLISHED 08 June 2023

CITATION
Cifaldi L, Melaiu O, Giovannoni R, Benvenuto M, Focaccetti C, Nardozi D, Barillari G and Bei R (2023) DNAM-1 chimeric receptor-engineered NK cells: a new frontier for CAR-NK cell-based immunotherapy.
Front. Immunol. 14:1197053.
doi: 10.3389/fimmu.2023.1197053

DNAM-1 chimeric receptor-engineered NK cells: a new frontier for CAR-NK cell-based immunotherapy

Loredana Cifaldi[1]*, Ombretta Melaiu[1], Roberto Giovannoni[2], Monica Benvenuto[1,3], Chiara Focaccetti[1], Daniela Nardozi[1], Giovanni Barillari[1] and Roberto Bei[1]

[1]Department of Clinical Sciences and Translational Medicine, University of Rome "Tor Vergata", Rome, Italy, [2]Department of Biology, University of Pisa, Pisa, Italy, [3]Departmental Faculty of Medicine, Saint Camillus International University of Health and Medical Sciences, Rome, Italy

DNAM-1 is a major NK cell activating receptor and, together with NKG2D and NCRs, by binding specific ligands, strongly contributes to mediating the killing of tumor or virus-infected cells. DNAM-1 specifically recognizes PVR and Nectin-2 ligands that are expressed on some virus-infected cells and on a broad spectrum of tumor cells of both hematological and solid malignancies. So far, while NK cells engineered for different antigen chimeric receptors (CARs) or chimeric NKG2D receptor have been extensively tested in preclinical and clinical studies, the use of DNAM-1 chimeric receptor-engineered NK cells has been proposed only in our recent proof-of-concept study and deserves further development. The aim of this perspective study is to describe the rationale for using this novel tool as a new anti-cancer immunotherapy.

KEYWORDS

CAR-NK cells, solid tumors, DNAM-1, NK cell-based immunotherapy, NK cell engineering

Introduction

NK cells are cytotoxic lymphocytes belonging to innate immunity that, by a complex array of activating and inhibitory receptors, are tolerant versus healthy cells and can recognize and kill virus-infected and transformed cells through the release of cytolytic granules and cytotoxic cytokines (1). The peculiar ability to elicit a potent response against target cells is due to the expression by NK cells of a repertoire of activating receptors such as NKG2D, the accessory molecule DNAX (DNAM-1, CD226), and natural cytotoxicity receptors (NCRs) including NKp30, NKp44, and NKp46 (2, 3). Of note, ligands for NKG2D and DNAM-1 are poorly expressed in normal cells [proteinatlas.org, Genotype-Tissue Expression (GTEx) from The Cancer Genome Atlas (TCGA) database and (4)] and highly expressed in virus-infected and transformed cells (5, 6). Furthermore, NK cells, through the expression of FcγRIIIA (CD16) receptor, are responsible for the antibody-

dependent cellular cytotoxicity (ADCC) (7), which is a crucial function in the clinical context of all immunotherapies involving monoclonal antibodies (mAb) (8).

In addition to their cytotoxic function, NK cells play a crucial role in regulating the maturation and activation state of other immune cells, through sophisticated cross-talks and biological mechanisms that further support their use in immunotherapy (9).

In contrast, it is noteworthy that NK cells in cancer patients show impaired functions accompanied by a poor ability to infiltrate the tumor microenvironment (TME), as tumor cells adopt different various immune evasion mechanisms (10–17). Therefore, the adoptive transfer of *ex vivo* expanded and activated allogeneic NK cells for immunotherapy turns out to be a strategic clinical adoption to help cancer patients to fight tumor cells, thus attracting increasing interest in the past decade (18).

Primary allogeneic and alloreactive NK cells, from healthy donors with a favorable immunoglobulin-like receptor (KIR)-human leukocyte antigen (HLA) mismatch (19), can be harvested from several sources such as peripheral blood (20), umbilical cord blood (21) or be derived by induced pluripotent stem cells (iPSC) (22, 23). Compared with the therapeutic use of T cells, that of allogeneic NK cells has several advantages: this has progressively stimulated the improvement of previously limited *ex vivo* amplification methods of NK cells and designs for the expression of various chimeric antigen receptors (CARs) and NKG2D chimeric receptor (24, 25) suitable for clinical use (ClinilTrial.gov and Supplementary Table S1).

In this context, one should consider that T and NK cells are often dysfunctional in cancer patients, limiting the use of autologous cells for engineered manipulation (26). Noticeably, NK cells display greater antitumor effects in allogeneic settings than in autologous ones (20, 27). However, the use of allogeneic T or CAR-T cells presents limitations related to severe haploidentical mismatch conditions necessary to reduce the risk of graft-versus-host disease (GvHD) and cytokine release syndrome (28–30). In contrast, allogeneic NK cells do not cause GvHD (31–33) and display a low risk of proliferation in transfused patients and, thus a major safety, as compared with infused T cells. Finally, the high availability of allogeneic NK cells, their low cost compared to CAR-T cells, and the possibility of cryopreserving them for further administration allowing the treatment of many patients from a single NK cell donor, entitles their clinical use for several types of cancers (34, 35).

So far, the successful use of NK cells engineered for several CARs and for NKG2D chimeric receptor in the hematological and solid tumor settings has been widely reported (ClinicalTrial.gov Supplementary Table S1). Based on the success of CD19-targeted CAR-T cells (36), approved by U.S. Food and Drug Administration (FDA), the first CAR-NK cells were engineered with chimeric anti-CD19 single chain fragment variable (scFv) for the cure of hematologic malignancies (21). Currently, the use of CAR- or NKG2D chimeric receptor-engineered NK cells has been extended to different type of cancers; however, the number of clinical trials evaluating their efficacy against solid tumors is far lower than against hematologic malignancies (14 versus 29, as reported in Supplementary Table S1). This represents a clinical gap that needs to be filled. CAR-T or CAR-NK cells have generally shown greater efficacy in hematologic malignancies than in solid tumors, mainly for the following reasons: (i) firstly, the accessibility of CAR-T or CAR-NK cells to tumor cells is significantly different between solid and hematological tumors, depending on cell morphology (absence or presence of cell-cell adhesions) and body distribution; (ii) secondly, solid tumor cells are less sensitive to cytotoxic lymphocytes, as the immune suppression mechanisms occurring in TME constitute a barrier to lymphocyte infiltration. Therefore, in order to improve the efficacy of the adoptive transfer of CAR-NK cells for immunotherapy of solid tumors, the search for more specific tumor target molecules, accompanied by mechanisms that overcome the barriers of TME, still needs to be extensively explored (37).

Aiming to fill this gap, recently we have provided promising *in vitro* results on the efficacy of never before explored DNAM-1-chimeric receptor-engineered NK cells against neuroblastoma (NB) (38). This proof-of-concept study is prompting us at optimizing the DNAM-1-based chimeric construct with the aim of developing highly efficient DNAM-1 chimeric receptor-engineered NK cells to be employed in preclinical studies and prospective clinical trials primarily directed against solid tumors.

DNAM-1

Human DNAX accessory molecule-1 (DNAM-1, CD226) is constitutively expressed in T, NK cells, and some myeloid cells. It is a type I transmembrane glycoprotein containing a leader sequence of 18 amino acid (aa), two extracellular Ig-like C2-set domains of 230 aa, a transmembrane domain of 28 aa and a cytoplasmic region of 60 aa. Together with other activating receptors, such as NKG2D and NCRs (39), DNAM-1 triggers powerful activating signals that promote NK cell-mediated cytotoxicity and cytokine secretion (40, 41). DNAM-1 mediates activation signals through the engagement with two ligands such as PVR (poliovirus receptor, CD155) and Nectin-2 (poliovirus receptor-related 2 protein, PVRL2, also known as CD112) (5). Furthermore, through cis-binding to the integrin LFA-1 upon the engagement of LFA-1 with ICAM-1 (42), DNAM-1 undergoes phosphorylation at conserved amino acid residues in its cytoplasmic domain such as tyrosine 322 [Y322 in human and Y319 in mouse, (42)] and serine 326 (40) *via* Src family kinase Fyn and protein kinase C, respectively (43). The coordinated expression of DNAM-1 and LFA-1 is also crucial for NK cell education (44).

Adequate expression of DNAM-1 enables NK cells to recognize and kill hematopoietic malignancies such as acute myeloid leukemia (AML) (45), multiple myeloma (MM) (39), and solid tumor cells such as melanoma (46) and NB (47), thus contributing to a favorable prognosis (45, 48). In contrast, DNAM-1 expression is impaired in AML cancer patients and its loss has been correlated with the tumor severity (49).

PVR and Nectin-2 in cancer patients

Both PVR and Nectin-2 ligands are closely linked to tumorigenesis. Indeed, in addition to being expressed in virus-infected cells (43), these ligands are overexpressed in several hematological and solid tumors (5, 50–52). Noticeably, these ligands, in particular PVR, are potential prognostic markers in AML (53, 54), MM (55), hepatocellular carcinoma (56), and bladder urothelial carcinoma (BLCA) (57). As we have previously reported, PVR expression is directly under the control of p53 at promoter level (47), whilst the transcriptional regulation of Nectin-2 remains more widely to be explored (58). Furthermore, PVR and Nectin-2 are both upregulated by Toll-like receptors agonists in dendritic cells (59, 60) and by DNA-damage response in multiple myeloma cells (61) or in Ag-activated T lymphocytes (62). In addition, PVR is upregulated by IFN-γ in NB cell lines (63) and epigenetic modulations in malignant lymphocytes (64), while it is downregulated by the human immunodeficiency virus type 1 Nef and Vpu proteins (65) and the human cytomegalovirus UL141 protein (66).

The activating signal mediated by DNAM-1 following the engagement of the ligands PVR or Nectin-2 is counteracted by the competing binding of inhibitory receptors such as TIGIT (T-cell immunoglobulin and ITIM domain) (67), TACTILE (T cell activation, increased late expression, also known as CD96) (68) and PVRIG (69) for the same ligands. In particular, PVR is recognized by TIGIT and TACTILE (70, 71), while Nectin-2 is recognized by TIGIT and PVRIG (69, 70). For this reason, TIGIT, TACTILE and PVRIG have been considered targets for checkpoint blockade immunotherapy (72). Of note, the high expression levels of PVR, typical of various tumor types, revealed its hypothetical proto-oncogenic role, leading researchers to develop therapeutic strategies that directly target PVR (73).

DNAM-1 chimeric receptor-engineered NK cells

Adoptive transfer of activated NK cells expressing higher and more stable levels of DNAM-1, might be a useful clinical approach to help cancer patients to fight tumor cells. The DNAM-1 chimeric receptor could confer a dual advantage to NK cells: (i) specific recognition of ligands such as PVR and Nectin-2, which are highly expressed in tumor cells, but importantly absent or poorly expressed in normal cells, and (ii) its overexpression, which should result in a favorable molecular imbalance with respect to the normal expression of competing receptors (TIGIT, TACTILE, PVRIG), leading to its increased binding to PVR and Nectin-2. In addition, its function could be strategically improved by in-frame expression of costimulatory molecules that support cytotoxic activity and overcome TME immune escape mechanisms. We previously reported a proof-of-concept study on the activity of DNAM-1-chimeric receptor-engineered NK cells obtained by transient transfection of primary human NK cells for a DNAM-1-chimeric receptor (38). Specifically, we compared four different constructs, including the full-length DNAM-1 receptor, and three different DNAM-1-based chimeric receptors providing the expression of DNAM-1 in frame with costimulatory molecules such as 2B4 and CD3ζ, and we showed that the DNAM-1-CD3ζ construct, which recapitulates a first generation of DNAM-1 chimeric receptor, yielded the best results in terms of expression of DNAM-1 chimeric receptor and NK cell functions. Furthermore, DNAM-1-CD3ζ engineered NK cells were particularly more effective to recognize and kill two NB cell lines, LAN-5 and SMS-KCNR, treated with Nutlin-3a, an MDM2 targeting drug with immunomodulatory effects on the upregulation of ligands for NK cell-activating receptors, including PVR and Nectin-2 (47). Therefore, the combined use of DNAM-1-CD3ζ engineered NK cells with Nutlin-3a in tumors that retain p53-wt, such as most forms of NB, with the exception of some cases of relapse (74), may represent a novel therapeutic approach for solid tumors.

In-silico analysis of PVR and Nectin-2 in solid tumor patients

The widely reported high expression of both PVR and Nectin-2 in solid tumor cells and very low expression in normal cells [protein.atlas.gov and GTEx from TCGA database], was the main reason for choosing to engineer NK cells with a DNAM-1 chimeric receptor. In order to further explore the expression of both PVR and Nectin-2 in solid tumors, and to prospectively propose the adoptive transfer of DNAM-1 chimeric receptor-engineered NK cells also in adult solid malignancies, we performed an *in-silico* bioinformatic analysis by using GEPIA2 (www.gepia2.cancer-pku.cn, Figure 1). Specifically, we queried this online tool providing data concerning gene expression and tumor stage/grade, to compare the expression of selected genes between tumor and normal tissues, based on TCGA. Interestingly, we found that the expression profile of both PVR and Nectin-2 resulted higher in several tumor samples than in paired normal tissues across a broad spectrum of solid tumors. In particular, the expression of PVR was significantly higher in colon adenocarcinoma (COAD), esophageal carcinoma (ESCA), head and neck squamous cell carcinoma (HNSC), pancreatic adenocarcinoma (PAAD), rectum adenocarcinoma (READ), stomach adenocarcinoma (STAD) and thymoma (THYM), while that of Nectin-2 was significantly higher in bladder urothelial carcinoma (BLCA), breast invasive carcinoma (BRCA), COAD, lymphoid neoplasm diffuse large B-cell lymphoma (DLBC), glioblastoma multiforme (GBM), brain lower grade glioma (LGG), ovarian serous cystadenocarcinoma (OV), PAAD, READ, STAD, THYM and uterine corpus endometrial carcinoma (UCEC) (Figure 1A). In addition, the higher expression of PVR or Nectin-2 correlated with the advanced stage of different forms of solid tumors. In particular, PVR higher expression correlated with the advanced stage of adrenocortical carcinoma (ACC), BLCA, liver hepatocellular carcinoma (LIHC), lung adenocarcinoma (LUAD), lung squamous cell carcinoma (LUSC) (Figure 1B), while that of Nectin-2 correlated with the advanced stage of ACC, BLCA, HNSC, testicular germ cell tumors (TGCT), skin cutaneous melanoma

(SKCM) and UCEC (Figure 1C). These data indicate that the high expression of PVR and Nectin-2 in tumor cells compared to normal cells affects several solid tumors, supporting the hypothesis of a wide prospective clinical use of DNAM-1 chimeric receptor-engineered NK cells.

Furthermore, we used the R2 Genomics Analysis and Visualization Platform (https://hgserver1.amc.nl/cgi-bin/r2/main.cgi?open_page=login) to investigate the prognostic value of PVR and Nectin-2 ligands in a variety of tumor types. We found that higher expression of PVR significantly correlated with lower patient overall survival in ACC, BLCA, COAD, ESCA, HNSC, kidney renal clear cell carcinoma (KIRC), kidney renal papillary cell carcinoma (KIRP), LUAD, LUSC, mesothelioma (MESO), OV, prostate adenocarcinoma (PRAD), SKCM, STAD and uveal melanoma (UVM) (Supplementary Figure 1A). By contrast, the lower expression of PVR significantly correlated with lower patient survival in BRCA, PAAD, READ and THYM (Supplementary Figure 1B), in agreement with published data from a cohort of patients with a pediatric form of solid tumor such as NB (75). Similarly, the higher expression of Nectin-2 correlated with lower patient overall survival in KIRC, KIRP, GBM, HNSC, LIHC, LUAD, LUSC, MESO, OV, READ, SKCM, UCEC and uterine carcinosarcoma (UCS) (Supplementary Figure 2A). By contrast, the lower expression of Nectin-2 correlated with lower patient overall survival in BRCA, COAD, ESCA, PRAD, STAD and UVM (Supplementary Figure 2B). These data suggest that the expression levels of both PVR and Nectin-2 can correlate differently with patient overall survival, depending on the kind of solid tumors.

Clinical perspective

With a view to finding an optimized off-the-shelf product for cellular immunotherapeutic approaches, we foresee that DNAM-1 chimeric receptor engineered-NK cells have several strengths that

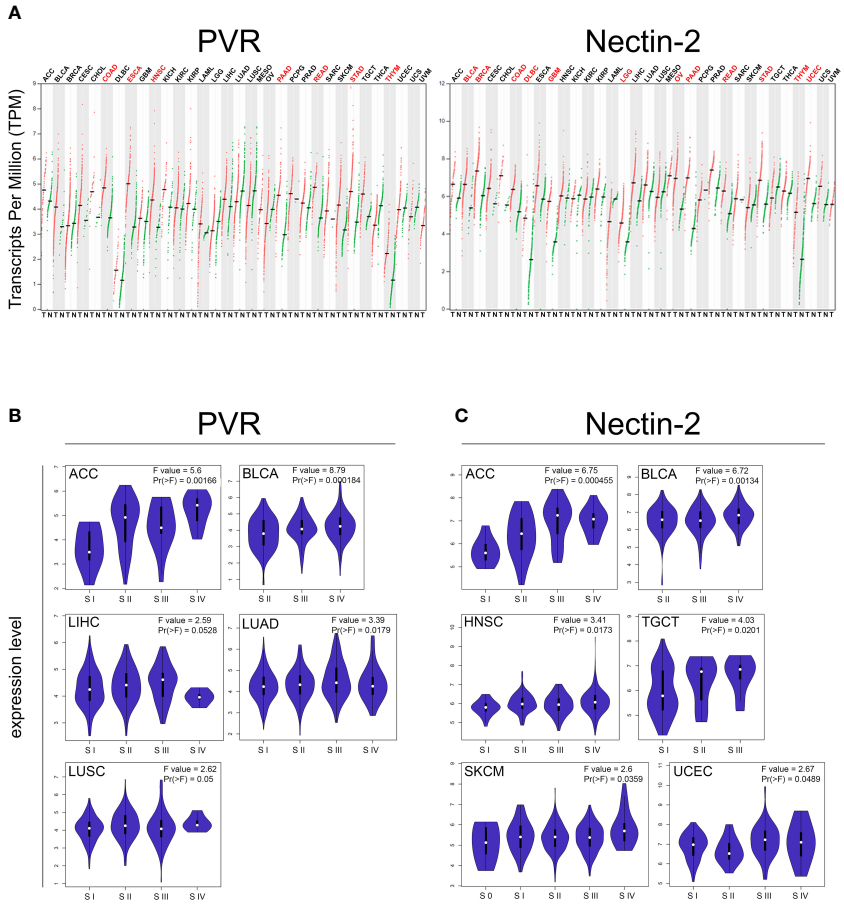

FIGURE 1
In-silico bioinformatics analysis of *PVR* and *NECTIN2* gene expression by GEPIA2 web-tool based on The Cancer Genome Atlas (TCGA) database. **(A)** Dot plot profiling of PVR (top) and Nectin-2 (down) differential expression levels in 33 cancer types, derived from TCGA database, compared to the normal, derived from TCGA or Genotype-Tissue Expression (GTEx). Each dot represents a distinct tumor (red) or normal sample (green) while each column represents a different tumor type (tumor labels and sample sizes are reported in Supplementary Table 2). The transcript per million (TPM) value, shown in ordinate, is used to display the relative gene expression. Tumor labels are indicated in red when there is a significant difference between tumor (T) versus normal (N) tissues. Data were analyzed by ANOVA test. |log2FC| > 1 and FDR < 0.05 were considered as differentially expressed. **(B, C)** Violin plots showing the expression level of PVR **(B)** and Nectin-2 **(C)** among different pathologic stages (S) of indicated solid tumors. F-value indicates the statistical value of the F test; Pr (> F) indicates *p* value. A *p* value of < 0.05 was considered statistically significant.

should be taken into account. NK cells engineered for a chimeric form of an activating receptor such as DNAM-1 are likely to specifically target tumor cells which express high levels of PVR and Nectin-2 (Figure 1), while should be tolerant of normal cells expressing low levels of PVR and Nectin-2 [protein.atlas.org, GTEx from TCGA database and (4)]. This represents an advantage over many types of single-chain antibody-based CAR-engineered lymphocytes designed to target proteins expressed not only by tumor cells but also, at high physiological levels, by various normal cells such as CD19 and B220 (B lymphocytes and follicular dendritic cells), disialoganglioside or GD2 (neurons, skin melanocytes and peripheral nerves), human epidermal growth factor receptor 2 or HER2 (many tissues), prostate-specific membrane antigen or PSMA (kidneys, small intestine and salivary glands), etc. This non-selective tumor specificity is often the cause of high toxicity and adverse effects due to the cytotoxic reaction mediated by CAR-lymphocytes against normal tissues. So far, with a restricted expression in normal tissues and overexpression in many types of solid tumors, B7-H3 resulted a more promising therapeutic target compared to the others (76). DNAM-1 ligands PVR and Nectin-2 have been described to be absent or very scarcely expressed in normal tissue [proteinatlas.org and (73, 77)], so their targeting should hypothetically not be toxic; however, the differential expression of DNAM-1 ligands in cancer versus normal cells does not exclude a possible toxicity mediated by DNAM-1 chimeric receptor-engineered NK cells, which should be carefully explored by preclinical studies.

For a hypothetic good manufacturing practice (GMP) production and clinical use of DNAM-1 chimeric receptor-engineered NK cells, primary NK cells should be isolated through leukapheresis by the blood of a HLA-matched unrelated healthy donor, *ex vivo* expanded and activated, engineered for the expression of DNAM-1 chimeric receptor, expanded to be infused in cancer patients or be cryopreserved for future use (Figure 2). Different modes of administration should be considered, depending on the type and location of the tumor in the body, such as intravenous or local injection. DNAM-1 chimeric receptor, expressed at stable and high levels, should strongly compete for the binding of PVR and Nectin-2 with the agonist receptors TIGIT, TACTILE and PVRIG, thus favoring activating cytotoxic signals over inhibitory ones. The high expression of PVR and Nectin-2 in tumor cells could make them strongly susceptible to DNAM-1 chimeric receptor-engineered NK cell-mediated recognition and killing. Within days after the injection of DNAM-1 chimeric receptor-engineered NK cells, tumor cell death could occur at the tumor site and lead the patient to an objective clinical response, depending on the aggressiveness and size of primary or secondary tumor masses. To avoid recurrence, the number of administrations of DNAM-1 chimeric receptor-engineered NK cells should be carefully planned, depending on the characteristics of the tumor,

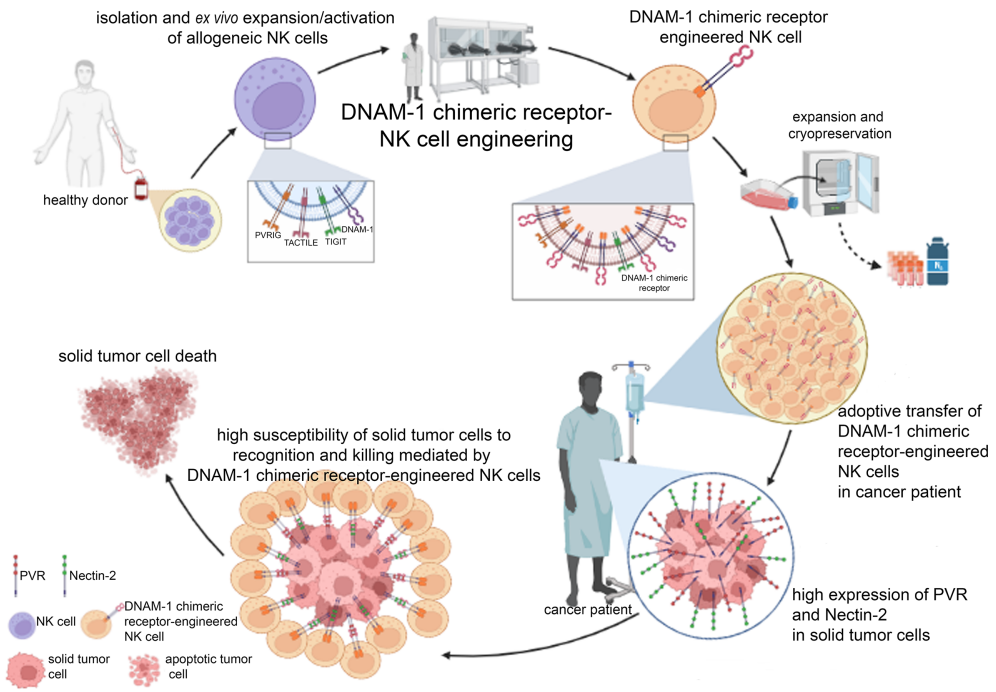

FIGURE 2
Clinical perspective of the GMP manufacturing and clinical use of DNAM-1 chimeric receptor-engineered NK cells. After leukapheresis of a healthy HLA-related donor, mature alloreactive NK cells can be isolated to be firstly *ex vivo* expanded and activated and then engineered for the expression of DNAM-1 chimeric receptor. Large quantities of DNAM-1 chimeric receptor-engineered NK cells can be obtained to be infused in cancer patient or cryopreserved for future use. The high expression of PVR and Nectin-2 specifically in tumor cells should facilitate their recognition mainly by DNAM-1 chimeric receptor compared to competing receptors (TIGIT, TACTILE and PVRIG), thus promoting tumor cell death. The figure was created with Biorender (https://biorender.com/).

such as location, extent, stage, or presence of metastasis. To enhance the anticancer efficiency, the use of DNAM-1 chimeric receptor-engineered NK cells could be combined with that of current anticancer cytotoxic drugs (78, 79), activating cytokines or mAbs recognizing immune checkpoint molecules (80). Ideally, the administration of DNAM-1 chimeric receptor-engineered NK cells should be also considered after surgical removal of solid tumor masses to avoid the risk of developing the minimal residual disease (MRD).

Conclusion

The adoptive transfer of DNAM-1 chimeric receptor-engineered NK cells is expected to represent an innovative strategic clinical tool to help cancer patients in fighting solid tumors. Therefore, the development of preclinical and clinical studies aimed at obtaining stable, nontoxic, highly antitumor cytotoxic DNAM-1 chimeric receptor-engineered NK cells, in high quantities for cryopreservation and immediate future use, applicable to a broad spectrum of solid tumors, deserves further exploration.

Data availability statement

The original contributions presented in the study are included in the article/Supplementary Materials, further inquiries can be directed to the corresponding author/s.

Author contributions

All authors listed have made a substantial, direct, and intellectual contribution to the work and approved it for publication.

Funding

This study was funded by grants from Ministero dell'Università e della Ricerca, PRIN 2020 (BeiR20Prin, CUP: E85F22000060006 to RB).

Conflict of interest

The authors declare that the research was conducted in the absence of any commercial or financial relationships that could be construed as a potential conflict of interest.

Publisher's note

All claims expressed in this article are solely those of the authors and do not necessarily represent those of their affiliated organizations, or those of the publisher, the editors and the reviewers. Any product that may be evaluated in this article, or claim that may be made by its manufacturer, is not guaranteed or endorsed by the publisher.

Supplementary material

The Supplementary Material for this article can be found online at: https://www.frontiersin.org/articles/10.3389/fimmu.2023.1197053/full#supplementary-material

SUPPLEMENTARY FIGURE 1
Overall survival probability of patients with the indicated solid tumor type (tumor labelling is explained in Supplementary Table 2) in each graph carrying high (blue line) or low (red line) *PVR* gene expression. High *PVR* gene expression can correlate with a worse (A) or favorable overall survival (B). Statistically significant *p* values are indicated.

SUPPLEMENTARY FIGURE 2
Overall survival probability of patients with the indicated solid tumor type (tumor labelling is explained in Supplementary Table 2 in each graph carrying high (blue line) or low (red line) *NECTIN2* gene expression. High *NECTIN2* gene expression can correlate with a worse (A) or favorable overall survival (B). Statistically significant *p* values are indicated.

References

1. Lanier LL. Up on the tightrope: natural killer cell activation and inhibition. *Nat Immunol* (2008) 9:495–502. doi: 10.1038/ni1581

2. Lanier LL. NK cell receptors. *Annu Rev Immunol* (1998) 16:359–93. doi: 10.1146/annurev.immunol.16.1.359

3. Biassoni R, Cantoni C, Pende D, Sivori S, Parolini S, Vitale M, et al. Human natural killer cell receptors and co-receptors. *Immunol Rev* (2001) 181:203–14. doi: 10.1034/j.1600-065x.2001.1810117.x

4. Uhlen M, Fagerberg L, Hallstrom BM, Lindskog C, Oksvold P, Mardinoglu A, et al. Proteomics. tissue-based map of the human proteome. *Science* (2015) 347:1260419. doi: 10.1126/science.1260419

5. Bottino C, Castriconi R, Pende D, Rivera P, Nanni M, Carnemolla B, et al. Identification of PVR (CD155) and nectin-2 (CD112) as cell surface ligands for the human DNAM-1 (CD226) activating molecule. *J Exp Med* (2003) 198:557–67. doi: 10.1084/jem.20030788

6. Xiong P, Sang HW, Zhu M. Critical roles of co-activation receptor DNAX accessory molecule-1 in natural killer cell immunity. *Immunology* (2015) 146:369–78. doi: 10.1111/imm.12516

7. Wang W, Erbe AK, Hank JA, Morris ZS, Sondel PM. NK cell-mediated antibody-dependent cellular cytotoxicity in cancer immunotherapy. *Front Immunol* (2015) 6:368. doi: 10.3389/fimmu.2015.00368

8. Li F, Liu S. Focusing on NK cells and ADCC: a promising immunotherapy approach in targeted therapy for HER2-positive breast cancer. *Front Immunol* (2022) 13:1083462. doi: 10.3389/fimmu.2022.1083462

9. Lucarini V, Melaiu O, Tempora P, D'Amico S, Locatelli F, Fruci D. Dendritic cells: behind the scenes of T-cell infiltration into the tumor microenvironment. *Cancers (Basel)* (2021) 13(3):433. doi: 10.3390/cancers13030433

10. Melaiu O, Lucarini V, Cifaldi L, Fruci D. Influence of the tumor microenvironment on NK cell function in solid tumors. *Front Immunol* (2019) 10:3038. doi: 10.3389/fimmu.2019.03038

11. Cozar B, Greppi M, Carpentier S, Narni-Mancinelli E, Chiossone L, Vivier E. Tumor-infiltrating natural killer cells. *Cancer Discovery* (2021) 11:34–44. doi: 10.1158/2159-8290.CD-20-0655

12. Demaria O, Cornen S, Daeron M, Morel Y, Medzhitov R, Vivier E. Harnessing innate immunity in cancer therapy. *Nature* (2019) 574:45–56. doi: 10.1038/s41586-019-1593-5

13. Lavin Y, Kobayashi S, Leader A, Amir ED, Elefant N, Bigenwald C, et al. Innate immune landscape in early lung adenocarcinoma by paired single-cell analyses. *Cell* (2017) 169:750–765 e717. doi: 10.1016/j.cell.2017.04.014

14. Tumino N, Nava Lauson CB, Tiberti S, Besi F, Martini S, Fiore PF, et al. The tumor microenvironment drives NK cell metabolic dysfunction leading to impaired antitumor activity. *Int J Cancer* (2023) 152:1698–706. doi: 10.1002/ijc.34389

15. Gemelli M, Noonan DM, Carlini V, Pelosi G, Barberis M, Ricotta R, et al. Overcoming resistance to checkpoint inhibitors: natural killer cells in non-small cell lung cancer. *Front Oncol* (2022) 12:886440. doi: 10.3389/fonc.2022.886440

16. Albini A, Noonan DM. Decidual-like NK cell polarization: from cancer killing to cancer nurturing. *Cancer Discov* (2021) 11:28–33. doi: 10.1158/2159-8290.CD-20-0796

17. Bruno A, Mortara L, Baci D, Noonan DM, Albini A. Myeloid derived suppressor cells interactions with natural killer cells and pro-angiogenic activities: roles in tumor progression. *Front Immunol* (2019) 10:771. doi: 10.3389/fimmu.2019.00771

18. Davis ZB, Felices M, Verneris MR, Miller JS. Natural killer cell adoptive transfer therapy: exploiting the first line of defense against cancer. *Cancer J* (2015) 21:486–91. doi: 10.1097/PPO.0000000000000156

19. Velardi A, Ruggeri L. Alessandro; moretta; moretta, l. NK cells: a lesson from mismatched hematopoietic transplantation. *Trends Immunol* (2002) 23:438–444. doi: 10.1016/s1471-4906(02)02284-6

20. Veluchamy JP, Kok N, van der Vliet HJ, Verheul HMW, de Gruijl TD, Spanholtz J. The rise of allogeneic natural killer cells as a platform for cancer immunotherapy: recent innovations and future developments. *Front Immunol* (2017) 8:631. doi: 10.3389/fimmu.2017.00631

21. Liu E, Marin D, Banerjee P, Macapinlac HA, Thompson P, Basar R, et al. Use of CAR-transduced natural killer cells in CD19-positive lymphoid tumors. *N Engl J Med* (2020) 382:545–53. doi: 10.1056/NEJMoa1910607

22. Goldenson BH, Hor P, Kaufman DS. iPSC-derived natural killer cell therapies - expansion and targeting. *Front Immunol* (2022) 13:841107. doi: 10.3389/fimmu.2022.841107

23. Maddineni S, Silberstein JL, Sunwoo JB. Emerging NK cell therapies for cancer and the promise of next generation engineering of iPSC-derived NK cells. *J Immunother Cancer* (2022) 10(5):e004693. doi: 10.1136/jitc-2022-004693

24. Lapteva N, Szmania SM, van Rhee F, Rooney CM. Clinical grade purification and expansion of natural killer cells. *Crit Rev Oncog* (2014) 19:121–32. doi: 10.1615/critrevoncog.2014010931

25. Kundu S, Gurney M, O'Dwyer M. Generating natural killer cells for adoptive transfer: expanding horizons. *Cytotherapy* (2021) 23:559–66. doi: 10.1016/j.jcyt.2020.12.002

26. Zhang W, Zhao Z, Li F. Natural killer cell dysfunction in cancer and new strategies to utilize NK cell potential for cancer immunotherapy. *Mol Immunol* (2022) 144:58–70. doi: 10.1016/j.molimm.2022.02.015

27. Liang S, Xu K, Niu L, Wang X, Liang Y, Zhang M, et al. Comparison of autogeneic and allogeneic natural killer cells immunotherapy on the clinical outcome of recurrent breast cancer. *Onco Targets Ther* (2017) 10:4273–81. doi: 10.2147/OTT.S139986

28. Sanber K, Savani B, Jain T. Graft-versus-host disease risk after chimeric antigen receptor T-cell therapy: the diametric opposition of T cells. *Br J Haematol* (2021) 195:660–8. doi: 10.1111/bjh.17544

29. Lu H, Zhao X, Li Z, Hu Y, Wang H. From CAR-T cells to CAR-NK cells: a developing immunotherapy method for hematological malignancies. *Front Oncol* (2021) 11:720501. doi: 10.3389/fonc.2021.720501

30. Kalos M, June CH. Adoptive T cell transfer for cancer immunotherapy in the era of synthetic biology. *Immunity* (2013) 39:49–60. doi: 10.1016/j.immuni.2013.07.002

31. Asai O, Longo DL, Tian ZG, Hornung RL, Taub DD, Ruscetti FW, et al. Suppression of graft-versus-host disease and amplification of graft-versus-tumor effects by activated natural killer cells after allogeneic bone marrow transplantation. *J Clin Invest* (1998) 101:1835–42. doi: 10.1172/JCI1268

32. Gill S, Olson JA, Negrin RS. Natural killer cells in allogeneic transplantation: effect on engraftment, graft- versus-tumor, and graft-versus-host responses. *Biol Blood Marrow Transplant* (2009) 15:765–76. doi: 10.1016/j.bbmt.2009.01.019

33. Geller MA, Miller JS. Use of allogeneic NK cells for cancer immunotherapy. *Immunotherapy* (2011) 3:1445–59. doi: 10.2217/imt.11.131

34. Heipertz EL, Zynda ER, Stav-Noraas TE, Hungler AD, Boucher SE, Kaur N, et al. Current perspectives on "Off-The-Shelf" allogeneic NK and CAR-NK cell therapies. *Front Immunol* (2021) 12:732135. doi: 10.3389/fimmu.2021.732135

35. Kennedy PR, Felices M, Miller JS. Challenges to the broad application of allogeneic natural killer cell immunotherapy of cancer. *Stem Cell Res Ther* (2022) 13:165. doi: 10.1186/s13287-022-02769-4

36. Davila ML, Brentjens RJ. CD19-targeted CAR T cells as novel cancer immunotherapy for relapsed or refractory b-cell acute lymphoblastic leukemia. *Clin Adv Hematol Oncol* (2016) 14:802–8.

37. Maalej KM, Merhi M, Inchakalody VP, Mestiri S, Alam M, Maccalli C, et al. CAR-cell therapy in the era of solid tumor treatment: current challenges and emerging therapeutic advances. *Mol Cancer* (2023) 22:20. doi: 10.1186/s12943-023-01723-z

38. Focaccetti C, Benvenuto M, Pighi C, Vitelli A, Napolitano F, Cotugno N, et al. DNAM-1-chimeric receptor-engineered NK cells, combined with nutlin-3a, more effectively fight neuroblastoma cells *in vitro*: a proof-of-concept study. *Front Immunol* (2022) 13:886319. doi: 10.3389/fimmu.2022.886319

39. El-Sherbiny YM, Meade JL, Holmes TD, McGonagle D, Mackie SL, Morgan AW, et al. The requirement for DNAM-1, NKG2D, and NKp46 in the natural killer cell-mediated killing of myeloma cells. *Cancer Res* (2007) 67:8444–9. doi: 10.1158/0008-5472.CAN-06-4230

40. Shibuya A, Campbell D, Hannum C, Yssel H, Franz-Bacon K, McClanahan T, et al. DNAM-1, a novel adhesion molecule involved in the cytolytic function of T lymphocytes. *Immunity* (1996) 4:573–81. doi: 10.1016/s1074-7613(00)70060-4

41. Tahara-Hanaoka S, Shibuya K, Onoda Y, Zhang H, Yamazaki S, Miyamoto A, et al. Functional characterization of DNAM-1 (CD226) interaction with its ligands PVR(CD155) and nectin-2 (PRR-2/CD112). *Int Immunol* (2004) 16:533–8. doi: 10.1093/intimm/dxh059

42. Shibuya K, Lanier LL, Phillips JH, Ochs HD, Shimizu K, Nakayama E, et al. Physical and functional association of LFA-1 with DNAM-1 adhesion molecule. *Immunity* (1999) 11:615–23. doi: 10.1016/s1074-7613(00)80136-3

43. Cifaldi L, Doria M, Cotugno N, Zicari S, Cancrini C, Palma P, et al. DNAM-1 activating receptor and its ligands: how do viruses affect the NK cell-mediated immune surveillance during the various phases of infection? *Int J Mol Sci* (2019) 20(15):3715. doi: 10.3390/ijms20153715

44. Enqvist M, Ask EH, Forslund E, Carlsten M, Abrahamsen G, Beziat V, et al. Coordinated expression of DNAM-1 and LFA-1 in educated NK cells. *J Immunol* (2015) 194:4518–27. doi: 10.4049/jimmunol.1401972

45. Chashchina A, Marklin M, Hinterleitner C, Salih HR, Heitmann JS, Klimovich B. DNAM-1/CD226 is functionally expressed on acute myeloid leukemia (AML) cells and is associated with favorable prognosis. *Sci Rep* (2021) 11:18012. doi: 10.1038/s41598-021-97400-6

46. Lakshmikanth T, Burke S, Ali TH, Kimpfler S, Ursini F, Ruggeri L, et al. NCRs and DNAM-1 mediate NK cell recognition and lysis of human and mouse melanoma cell lines *in vitro* and *in vivo*. *J Clin Invest* (2009) 119:1251–63. doi: 10.1172/JCI36022

47. Veneziani I, Infante P, Ferretti E, Melaiu O, Battistelli C, Lucarini V, et al. Nutlin-3a enhances natural killer cell-mediated killing of neuroblastoma by restoring p53-dependent expression of ligands for NKG2D and DNAM-1 receptors. *Cancer Immunol Res* (2021) 9:170–83. doi: 10.1158/2326-6066.CIR-20-0313

48. Guillamon CF, Martinez-Sanchez MV, Gimeno L, Mrowiec A, Martinez-Garcia J, Server-Pastor G, et al. NK cell education in tumor immune surveillance: DNAM-1/KIR receptor ratios as predictive biomarkers for solid tumor outcome. *Cancer Immunol Res* (2018) 6:1537–47. doi: 10.1158/2326-6066.CIR-18-0022

49. Sanchez-Correa B, Gayoso I, Bergua JM, Casado JG, Morgado S, Solana R, et al. Decreased expression of DNAM-1 on NK cells from acute myeloid leukemia patients. *Immunol Cell Biol* (2012) 90:109–15. doi: 10.1038/icb.2011.15

50. Sloan KE, Eustace BK, Stewart JK, Zehetmeier C, Torella C, Simeone M, et al. CD155/PVR plays a key role in cell motility during tumor cell invasion and migration. *BMC Cancer* (2004) 4:73. doi: 10.1186/1471-2407-4-73

51. Gao J, Zheng Q, Xin N, Wang W, Zhao C. CD155, an onco-immunologic molecule in human tumors. *Cancer Sci* (2017) 108:1934–8. doi: 10.1111/cas.13324

52. Casado JG, Pawelec G, Morgado S, Sanchez-Correa B, Delgado E, Gayoso I, et al. Expression of adhesion molecules and ligands for activating and costimulatory receptors involved in cell-mediated cytotoxicity in a large panel of human melanoma cell lines. *Cancer Immunol Immunother* (2009) 58:1517–26. doi: 10.1007/s00262-009-0682-y

53. Stamm H, Klingler F, Grossjohann EM, Muschhammer J, Vettorazzi E, Heuser M, et al. Immune checkpoints PVR and PVRL2 are prognostic markers in AML and their blockade represents a new therapeutic option. *Oncogene* (2018) 37:5269–80. doi: 10.1038/s41388-018-0288-y

54. Hattori N, Kawaguchi Y, Sasaki Y, Shimada S, Murai S, Abe M, et al. Monitoring TIGIT/DNAM-1 and PVR/PVRL2 immune checkpoint expression levels in allogeneic stem cell transplantation for acute myeloid leukemia. *Biol Blood Marrow Transplant* (2019) 25:861–7. doi: 10.1016/j.bbmt.2019.01.013

55. Lee BH, Kim JH, Kang KW, Lee SR, Park Y, Sung HJ, et al. PVR (CD155) expression as a potential prognostic marker in multiple myeloma. *Biomedicines* (2022) 10(5):1099. doi: 10.3390/biomedicines10051099

56. Liu WF, Quan B, Li M, Zhang F, Hu KS, Yin X. PVR-a prognostic biomarker correlated with immune cell infiltration in hepatocellular carcinoma. *Diagnostics (Basel)* (2022) 12(12):2953. doi: 10.3390/diagnostics12122953

57. Luo C, Ye W, Hu J, Othmane B, Li H, Chen J, et al. Poliovirus receptor (CD155)-related risk signature predicts the prognosis of bladder cancer. *Front Oncol* (2021) 11:660273. doi: 10.3389/fonc.2021.660273

58. Molfetta R, Zingoni A, Santoni A, Paolini R. Post-translational mechanisms regulating NK cell activating receptors and their ligands in cancer: potential targets for therapeutic intervention. *Front Immunol* (2019) 10:2557. doi: 10.3389/fimmu.2019.02557

59. Kamran N, Takai Y, Miyoshi J, Biswas SK, Wong JS, Gasser S. Toll-like receptor ligands induce expression of the costimulatory molecule CD155 on antigen-presenting cells. *PloS One* (2013) 8:e54406. doi: 10.1371/journal.pone.0054406

60. Pende D, Castriconi R, Romagnani P, Spaggiari GM, Marcenaro S, Dondero A, et al. Expression of the DNAM-1 ligands, nectin-2 (CD112) and poliovirus receptor

(CD155), on dendritic cells: relevance for natural killer-dendritic cell interaction. *Blood* (2006) 107:2030–6. doi: 10.1182/blood-2005-07-2696

61. Soriani A, Zingoni A, Cerboni C, Iannitto ML, Ricciardi MR, Di Gialleonardo V, et al. ATM-ATR-dependent up-regulation of DNAM-1 and NKG2D ligands on multiple myeloma cells by therapeutic agents results in enhanced NK-cell susceptibility and is associated with a senescent phenotype. *Blood* (2009) 113:3503–11. doi: 10.1182/blood-2008-08-173914

62. Ardolino M, Zingoni A, Cerboni C, Cecere F, Soriani A, Iannitto ML, et al. DNAM-1 ligand expression on Ag-stimulated T lymphocytes is mediated by ROS-dependent activation of DNA-damage response: relevance for NK-T cell interaction. *Blood* (2011) 117:4778–86. doi: 10.1182/blood-2010-08-300954

63. Marrella A, Dondero A, Aiello M, Casu B, Olive D, Regis S, et al. Cell-laden hydrogel as a clinical-relevant 3D model for analyzing neuroblastoma growth, immunophenotype, and susceptibility to therapies. *Front Immunol* (2019) 10:1876. doi: 10.3389/fimmu.2019.01876

64. Wang W, Gao L, Wang X, Kang H, Li Y, Wang L, et al. Modulation of the poliovirus receptor expression in malignant lymphocytes by epigenetic alterations. *J Immunother* (2011) 34:353–61. doi: 10.1097/CJI.0b013e3182188017

65. Matusali G, Potesta M, Santoni A, Cerboni C, Doria M. The human immunodeficiency virus type 1 nef and vpu proteins downregulate the natural killer cell-activating ligand PVR. *J Virol* (2012) 86:4496–504. doi: 10.1128/JVI.05788-11

66. Tomasec P, Wang EC, Davison AJ, Vojtesek B, Armstrong M, Griffin C, et al. Downregulation of natural killer cell-activating ligand CD155 by human cytomegalovirus UL141. *Nat Immunol* (2005) 6:181–8. doi: 10.1038/ni1156

67. Zhang Q, Bi J, Zheng X, Chen Y, Wang H, Wu W, et al. Blockade of the checkpoint receptor TIGIT prevents NK cell exhaustion and elicits potent anti-tumor immunity. *Nat Immunol* (2018) 19:723–32. doi: 10.1038/s41590-018-0132-0

68. Georgiev H, Ravens I, Papadogianni G, Bernhardt G. Coming of age: CD96 emerges as modulator of immune responses. *Front Immunol* (2018) 9:1072. doi: 10.3389/fimmu.2018.01072

69. Zhu Y, Paniccia A, Schulick AC, Chen W, Koenig MR, Byers JT, et al. Identification of CD112R as a novel checkpoint for human T cells. *J Exp Med* (2016) 213:167–76. doi: 10.1084/jem.20150785

70. Stanietsky N, Simic H, Arapovic J, Toporik A, Levy O, Novik A, et al. The interaction of TIGIT with PVR and PVRL2 inhibits human NK cell cytotoxicity. *Proc Natl Acad Sci U.S.A.* (2009) 106:17858–63. doi: 10.1073/pnas.0903474106

71. Fuchs A, Cella M, Giurisato E, Shaw AS, Colonna M. Cutting edge: CD96 (tactile) promotes NK cell-target cell adhesion by interacting with the poliovirus receptor (CD155). *J Immunol* (2004) 172:3994–8. doi: 10.4049/jimmunol.172.7.3994

72. Sanchez-Correa B, Valhondo I, Hassouneh F, Lopez-Sejas N, Pera A, Bergua JM, et al. DNAM-1 and the TIGIT/PVRIG/TACTILE axis: novel immune checkpoints for natural killer cell-based cancer immunotherapy. *Cancers (Basel)* (2019) 11(6):877. doi: 10.3390/cancers11060877

73. Kucan Brlic P, Lenac Rovis T, Cinamon G, Tsukerman P, Mandelboim O, Jonjic S. Targeting PVR (CD155) and its receptors in anti-tumor therapy. *Cell Mol Immunol* (2019) 16:40–52. doi: 10.1038/s41423-018-0168-y

74. Carr-Wilkinson J, O'Toole K, Wood KM, Challen CC, Baker AG, Board JR, et al. High frequency of p53/MDM2/p14ARF pathway abnormalities in relapsed neuroblastoma. *Clin Cancer Res* (2010) 16:1108–18. doi: 10.1158/1078-0432.CCR-09-1865

75. Dondero A, Morini M, Cangelosi D, Mazzocco K, Serra M, Spaggiari GM, et al. Multiparametric flow cytometry highlights B7-H3 as a novel diagnostic/therapeutic target in GD2neg/low neuroblastoma variants. *J Immunother Cancer* (2021) 9(4): e002293. doi: 10.1136/jitc-2020-002293

76. Li G, Wang H, Wu H, Chen J. B7-H3-targeted CAR-T cell therapy for solid tumors. *Int Rev Immunol* (2022) 41:625–37. doi: 10.1080/08830185.2022.2102619

77. Oshima T, Sato S, Kato J, Ito Y, Watanabe T, Tsuji I, et al. Nectin-2 is a potential target for antibody therapy of breast and ovarian cancers. *Mol Cancer* (2013) 12:60. doi: 10.1186/1476-4598-12-60

78. Cifaldi L, Locatelli F, Marasco E, Moretta L, Pistoia V. Boosting natural killer cell-based immunotherapy with anticancer drugs: a perspective. *Trends Mol Med* (2017) 23:1156–75. doi: 10.1016/j.molmed.2017.10.002

79. Miyazato K, Hayakawa Y. Pharmacological targeting of natural killer cells for cancer immunotherapy. *Cancer Sci* (2020) 111:1869–75. doi: 10.1111/cas.14418

80. Khan M, Arooj S, Wang H. NK cell-based immune checkpoint inhibition. *Front Immunol* (2020) 11:167. doi: 10.3389/fimmu.2020.00167

frontiers | Frontiers in Immunology

TYPE Original Research
PUBLISHED 26 June 2023
DOI 10.3389/fimmu.2023.1191908

OPEN ACCESS

EDITED BY
Ombretta Melaiu,
University of Rome Tor Vergata, Italy

REVIEWED BY
Emanuela Marcenaro,
University of Genoa, Italy
Emilie Narni-Mancinelli,
INSERM U1104 Centre d'immunologie de Marseille-Luminy (CIML), France

*CORRESPONDENCE
Paola Vacca
paola.vacca@opbg.net
Valentina Folgiero
valentina.folgiero@opbg.net

†These authors share last authorship

RECEIVED 22 March 2023
ACCEPTED 06 June 2023
PUBLISHED 26 June 2023

CITATION
Caforio M, Tumino N, Sorino C, Manni I, Di Giovenale S, Piaggio G, Iezzi S, Strimpakos G, Mattei E, Moretta L, Fanciulli M, Vacca P, Locatelli F and Folgiero V (2023) AATF/Che-1 RNA polymerase II binding protein overexpression reduces the anti-tumor NK-cell cytotoxicity through activating receptors modulation.
Front. Immunol. 14:1191908.
doi: 10.3389/fimmu.2023.1191908

AATF/Che-1 RNA polymerase II binding protein overexpression reduces the anti-tumor NK-cell cytotoxicity through activating receptors modulation

Matteo Caforio[1], Nicola Tumino[2], Cristina Sorino[3], Isabella Manni[3], Stefano Di Giovenale[3], Giulia Piaggio[3], Simona Iezzi[3], Georgios Strimpakos[4], Elisabetta Mattei[5], Lorenzo Moretta[6], M. Fanciulli[3], Paola Vacca[2]*, Franco Locatelli[1,7]† and Valentina Folgiero[1]*†

[1]Department of Pediatric Hematology and Oncology, Cell and Gene Therapy, Bambino Gesù Children's Hospital, Istituto di Ricerca e Cura a Carattere Scientifico (IRCCS), Rome, Italy, [2]Immunology Research Area, Innate Lymphoid Cells Unit, Bambino Gesù Children's Hospital Istituto di Ricerca e Cura a Carattere Scientifico (IRCCS), Rome, Italy, [3]Stabilimento Allevamento Fornitore e Utilizzatore (SAFU) Laboratory, Department of Research, Advanced Diagnostic, Technological Innovation, Regina Elena National Cancer Institute Istituto di Ricerca e Cura a Carattere Scientifico (IRCCS), Rome, Italy, [4]National Research Council (CNR), Institute of Biochemistry and Cell Biology, Monterotondo, Rome, Italy, [5]Consiglio Nazionale delle Ricerche (CNR)-Institute of Cell Biology and Neurobiology, Istituto di Ricerca e Cura a Carattere Scientifico (IRCCS) Fondazione Santa Lucia, Rome, Italy, [6]Tumor Immunology Unit , Children Hospital Bambino Gesù, RomaLM, Rome, Italy, [7]Department of Life Sciences and Public Health, Catholic University of the Sacred Heart, Rome, Italy

Introduction: AATF/Che-1 over-expression in different tumors is well known and its effect on tumorigenicity is mainly due to its central role demonstrated in the oncogenic pathways of solid tumors, where it controls proliferation and viability. The effect exerted by tumors overexpressing Che-1 on the immune response has not yet been investigated.

Methods: Starting from ChIP-sequencing data we confirmed Che-1 enrichment on Nectin-1 promoter. Several co-cultures experiments between NK-cells and tumor cells transduced by lentiviral vectors carrying Che-1-interfering sequence, analyzed by flow-cytometry have allowed a detailed characterization of NK receptors and tumor ligands expression.

Results: Here, we show that Che-1 is able to modulate the expression of Nectin-1 ligand at the transcriptional level, leading to the impairment of killing activity of NK-cells. Nectin-1 down-modulation induces a modification in NK-cell ligands expression able to interact with activating receptors and to stimulate NK-cell function. In addition, NK-cells from Che-1 transgenic mice, confirming a reduced expression of activating receptors, exhibit impaired activation and a preferential immature status.

Discussion: The critical equilibrium between NK-cell ligand expression on tumor cells and the interaction with NK cell receptors is affected by Che-1 over-

expression and partially restored by Che-1 interference. The evidence of a new role for Che-1 as regulator of anti-tumor immunity supports the necessity to develop approaches able to target this molecule which shows a dual tumorigenic function as cancer promoter and immune response modulator.

KEYWORDS

Che-1, Nectin 1, NK cells, immune response, NK killing activity

Introduction

Strategies aimed at affecting the ability of tumor cells to escape from the immune surveillance represent a promising approach in support of current therapies (1–3). Acute lymphoblastic leukemia (ALL) exploits various mechanisms to avoid immune recognition and destruction by the immune system, affecting the phenotypic and functional characteristics of innate and adaptive immune cells (4, 5). A developing leukemia impairs key components of the immune system responsible for anticancer response, particularly in patients poorly responding to treatment or experiencing relapse (6). Among the interactions between leukemia cells and immune system cell populations, the one involving natural killer (NK)-cells is emerging as central in ALL immune-surveillance (7–11). NK-cells are innate lymphoid cells that recognize and kill virus-infected or malignant target cells (12, 13). The NK-cells ability to lyse transformed cells in the absence of antigen-specificity makes them important candidates for treatment of different cancers (14). The ability of NK-cells to kill ALL blasts depends on the balance between the activating and inhibitory receptors on NK-cells, as well as on the presence of their corresponding ligands on ALL cells (8, 15). Many studies have reported down-regulation of activating receptors in peripheral blood NK-cells of patients with hematological malignancies (16–19). NKG2D is an activating immune-receptor expressed on NK-cells able to bind MHC class I-related proteins (MICA and MICB) and ULBP proteins poorly expressed by normal cells, but frequently upregulated in tumor cells (20–22). DNAM-1 receptor has a major costimulatory function exerted through the binding with PVR and Nectin-2 (CD112) ligands on target cells (23–25). ALL blasts escape from NK-cell-mediated killing, predominantly by downregulating the ligands of NK-cell-activating receptors. However, it is of note that also inhibitory receptors act as essential immune check-points (8, 15, 20, 26, 27). Among the NK-cell ligands, Nectins belong to a family of cell-adhesion molecules that can also serve as virus receptors (28, 29). Their expression could represent a potential cancer biomarker, since they are overexpressed on a variety of tumor cells of different origin and can be recognized by activating and inhibitory paired-receptors expressed on NK-cells (30, 31). Tumor cell survival can benefit from modulation of the expression levels of Nectins, thereby influencing subsequent Nectin-mediated signaling, leading to dampened immune response (28, 32). In particular, Nectin-1 (CD111), normally expressed in various epithelial tissues, shows lower expression in tumors of epithelial origin, suggesting a role in reduced cell-cell adhesion, which favors both invasiveness and metastasis (33, 34). In different tumor contexts, such as that of pediatric and adult brain tumors, Nectin-1 was found upregulated (35). A similar modulation was observed also for Nectin-2 (CD112) that, when overexpressed, facilitates tumor cell proliferation, increases invasiveness and migration (36, 37). Thus, the expression of Nectin family proteins can be exploited by tumor cells to evade tumor immune surveillance (28).

Whether an RNA polymerase II binding protein can be involved in immune response is still an unexplored field. AATF/Che-1 (Che-1) has a consolidated role in tumorigenesis of solid tumors and is now clearly involved in the c-Myc-directed oncogenesis in pediatric B-Cell ALL (BCP-ALL) (38). Although ubiquitously expressed, Che-1 overexpression in tumor cells exerts a different contribution in specific oncogenic transcriptional machineries, inducing the expression of cancer genes or upregulating the expression of genes controlling survival functions as cell proliferation (39–42). Che-1-dependent modulation of genes expressing ligands involved in stimulation of the immune system is a field still poorly investigated, although it could offer clues for the identification of new mechanisms of action explaining the meaning of its overexpression in the tumor context. In cancer therapy, it is now evident that targeting pathways of tumorigenesis has limited efficacy, while targeting the cross-talk between tumor and immune cells can strongly improve the current therapies. In this context, we hypothesized that Che-1 could favor tumorigenesis by controlling the expression of membrane-located ligands able to inactivate the anti-tumor immune response. Here, we show that the modulation of Che-1 expression in tumor cells affects the NK-cell-mediated anti-tumor activity by influencing the Nectin-mediated tumor immune surveillance pathways.

Materials and methods

Cell lines

LAL-B cell line was obtained by Epstein barr transduction of bone marrow mononuclear cells derived by BCP-ALL patient (Aut. N. 495 11/04/2019). NALM-6 cell line was bought from ATCC (CRL-3273);. NALM-18 cell line was kindly provided by Dr Pende D. (IRCCS San Martino, Genoa, Italy). All cell lines were cultured in

RPMI-1640 medium supplemented with 10% FBS (Euroclone, IT), 1% penicillin/streptomycin (Euroclone, IT) and 1% L-glutamine (Euroclone, IT).

All cell lines were tested for mycoplasma contamination by PCR with the following primers:

Forward 5'-ACTCCTACGGGAGGCAGCAGTA-3'

Reverse 5'-TCGACCATCTGTCACTCTGTTAAC-3'

Antibodies

- Rabbit anti-human AATF/Che-1 antibody (Cat# A301-031A Bethyl, USA)
- Rabbit anti-human Che-1 antibody (43)
- Rabbit anti-P-Erk 1/2 antibody (#9101 Cell Signaling, Euroclone, IT)
- Rabbit anti-Erk 1/2 antibody (#9102 Cell Signaling, Euroclone, IT)
- Rabbit anti-p21 antibody (#2947 Cell Signaling, Euroclone, IT)
- Mouse anti-β-actin antibody (clone AC-15, Sigma – Aldrich, Merck, IT)
- HRP-conjugated anti-Gapdh antibody (MAB-10578, Immunological Sciences, SIC, IT)
- PE-Vio615-conjugated anti-human CD111 antibody (Clone # REA1210, Miltenji Biotech, DE)
- PE-Vio770-conjugated mouse anti-human CD19 antibody (Clone# LT19, Milteniyi Biotec, DE)
- BV421-conjugated mouse anti-human CD19 antibody (Clone# HIB19, BD Biosciences, CA-USA)
- BUV395-conjugated mouse anti-human CD3 antibody (Clone SP34-2, BD Biosciences, CA-USA)
- BV605-conjugated mouse anti-human CD314 (NKG2D) antibody (Clone# 1D11, BD Biosciences, CA-USA)
- FITC-conjugated mouse anti-human CD19 antibody (Clone# CB19, Immunological Science, SIC, IT
- PE-Cy7-conjugated mouse anti-human CD226 (DNAM) antibody (Clone# 11A8, BioLegend, CA-USA)
- APC-conjugated rat anti-human CD96 (TACTILE) antibody (Clone# 3.3, BioLegend, CA-USA)
- PE-Vio615-conjugated anti-human CD111 (Nectin-1) antibody (Clone# REA1210, Milteniyi Biotec, DE)
- APC-conjugated mouse anti-human CD112 (CD112) (Clone# R2.477, Invitrogen, IT)
- AlexaFluor-647-conjugated mouse anti-human CD155 (PVR) antibody (Clone# TX24, BD Biosciences, CA-USA)
- eFluor450-conjugated anti-human CD336 (NKp44) antibody (Clone # 44.189 eBioscience Thermo FIsher Scientific, IT)
- BV510-conjugated mouse anti-human CD337 (NKp30) antibody (Clone# p30-15, BD Biosciences, CA- USA)
- APC-conjugated mouse anti-human CD335 (NKp46) antibody (Clone# 9E2, Milteniyi Biotec, DE)
- APC-conjugated mouse anti-human ULBP4 antibody (Clone# 709116, R&D biosystems, BioTechne, IT)
- PE-conjugated mouse anti-human ULBP2-5-6 antibody (Clone# 165903, R&D biosystems, BioTechne, IT)
- PE-conjugated mouse anti-human ULBP1 antibody (Clone# 170818, R&D biosystems, BioTechne, IT)
- BV421-conjugated mouse anti-CD107a antibody (Clone# H4A3, BD Biosciences, CA- USA)
- PE-conjugated anti-human IFNγ antibody (Clone# REA600, Milteniyi Biotec, DE)
- PE-Vio770-conjugated anti-human TNFα antibody (Clone# cA2, Milteniyi Biotec, DE)
- BUV786-conjugated mouse anti-human CD16 (Clone# 3G8, BD Biosciences, CA-USA)
- APC-conjugated mouse anti-human CD45 antibody (Clone# HI30, Immunological Sciences, SIC, IT)
- FITC-conjugated anti-mouse CD19 (MAB-519F, Immunological Science, SIC, IT)
- BUV395-conjugated anti-mouse CD3 (Clone#17A2, BD Biosciences, CA-USA)
- APC-vio770-conjugated anti-mouse NK1.1 antibody (Clone# PK136, Milteniyi Biotec, DE).
- APC-conjugated anti-mouse CD314 (NKG2D) antibody (Clone# REA1175, Milteniyi Biotec, DE)
- BV711-conjugated rat anti-mouse CD155 (DNAM) antibody (Clone# TX56, BioLegend, CA-USA)
- PE-conjugated hamster anti-mouse CD27 (Clone# LG.3A10, BioLegend, CA-USA)
- PE-cy7-conjugated anti-mouse CD11b (Clone# M1/70, eBioscience, ThermoFIsher scientific, IT)
- Anti-human CD314 (NKG2D) antibody, pure (Clone# BAT221, Miltenji Biotec, DE)
- Anti-human CD226 (DNAM) IgM F5, kindly provided by Dr D. Pende

Chromatin immunoprecipitation assay

Chromatin immunoprecipitation (ChIP) experiments were performed as previously described by Bruno T. et al., 2006 (44) using anti-AATF/Che-1 antibody (Bethyl, USA). Immunoprecipitations with no specific immunoglobulins (Santa Cruz Biotechnology) were performed as negative controls. For quantitative ChIP analysis (ChIP-qRT), 1 µl of purified DNA was used for amplification on a 7500 Fast Real-Time PCR System (Applied Biosystems) using a SYBER Green 2× qPCR Master Mix (Primerdesign, UK). The following human promoter-specific primers were employed in RT–PCR amplifications:

Nectin 1 promoter forward 5' – TGCCGGCGATCCGCAACA ATG – 3'

Nectin 1 promoter reverse 5' – TTAACGCTAACCCCTCC CCTC – 3'

Che-1 interference

siRNA experiments of Che-1 expression were performed by transfecting a specific pool of three double–stranded RNA oligonucleotides targeting Che-1 (cat. n. 1299003– HSS120157 HSS120158 and HSS120159) or a control sequence (siControl, cat. n. 12935300), purchased from Thermo Fisher Scientific. Transfections were carried out by nucleofection of NALM-6 and LAL-B cells using Amaxa 4D-Nucleofector X Kit L (Lonza, IT) by following the manufacturer's instructions.

Western blotting

Cells were treated as described in Bruno T. et al., 2006 (44). Samples were separated by electrophoresis and transferred onto nitrocellulose membranes. After a blocking step in 5% non-fat-dried milk in 0.1% Tween-PBS, membranes were incubated with primary antibodies overnight at 4°C. After three washes in 0.1% Tween-PBS, membranes were incubated with the appropriate HRP-linked secondary antibodies (Bio-Rad, IT) at room temperature for 45 min, washed with 0.1% Tween-PBS and analyzed by chemi-luminescence (GE Healthcare Life Science, IT). Images were acquired using Alliance Mini HD6 system by UVITEC Ltd, Cambridge, equipped with UVI1D Software (UVITEC, 14–630275). The primary antibodies used were: anti-Che-1 (43), and anti-β-actin (Sigma – Aldrich, Merck, IT).

RNA isolation and quantitative real-time PCR

Total RNA from NALM-6 and LAL-B cells was isolated using EuroGOLD TriFast reagent (Euroclone, IT) according to the manufacturer's instructions. The first-strand cDNA was synthesized with random primers and M-MLV reverse transcriptase (Life Technologies, MA). The cDNA was used for quantitative real-time PCR (qRT–PCR) experiments carried out in a 7500 Fast Real-Time PCR System (Applied Biosystems, CA). ΔΔCt values were normalized with those obtained from the amplification of the endogenous β-actin gene. The following human-specific primers were employed in RT–PCR amplifications:

Nectin 1 forward 5'- GGATGACAAGGTCCTGGTGG- 3'
Nectin 1 reverse 5'- ACTGCACGTTGAGAGTGAGG- 3'
β - actin forward 5' - GACAGGATGCAGAAGGAGATTACT - 3'
β - actin reverse 5' - TGATCCACATCTGCTGGAAGGT - 3'

Lentiviral transduction

Lentiviral vectors pLV-TH (shControl), pLV-shChe-1 TH (45) were produced as previously described (shChe-1 sequence: nucleotides 824–842). Lentiviral stocks were titrated following standard protocols (45), and, routinely, a viral titer of 10^6 transducing units per ml (TU/ml) was achieved. Supernatants were collected and employed to infect NALM-6 cells ($1x10^6$ cells) in retronectin (Takara Shuzo, JP) pre-coated (7mg/ml) non-tissue culture 24-well plates. Samples were centrifuged at 2000g for 90 minutes. Infection proceeded for 48 hours. Infected cells were harvested and tested for GFP-expression through flow-cytometry analysis.

Flow-cytometry

Infected NALM-6 and NALM-18 cells lines were collected and analyzed by flow cytometry with PE-Vio615-conjugated anti-CD111 antibody (Miltenji Biotech, DE).

Human NK-cell isolation

Human NK-cells were isolated from PBMC of healthy donors with the RosetteSep NK-cell enrichment mixture method (Stem-Cell Technologies, IT). NK-cells with purity greater than 90% were stimulated with 100 IU/mL of recombinant human IL2 (PeproTech, FR) for 48 hours at 37°C. NK-cells were maintained in culture with NK MACS medium supplemented with 5% human serum and 1% NK MACS supplement (Miltenyi Biotech, DE).

NK cells cytotoxicity assay

Cell cytotoxicity assays were performed using as target NALM-6 cell line or K562 cell line and as effector cells NK-cells at different Effector/Target (E/T) cell ratios. Killed cells were evaluated after 4 hours. At the end of the co-culture, the assay was stopped by chilling cells on ice, and Propidium Iodide (PI) was added to each sample immediately before acquisition in order to identify the percentage of target cell lysis, as previously described (Ingegnere T Front Immunol 2019). For each set of experiments, all the acquisitions (5,000 target cells/sample) were performed within 20 min. Experiments aimed to study the involvement of DNAM-1 and NKG2D in NK-cell cytotoxicity against NALM-6 siChe-1 cells were performed after 30 minutes inoculation of NK-cells with F5 anti DNAM-1 or anti- NKG2D (BAT221) antibodies.

NK-cells co-culture assay

For NK receptors expression detection, NK-cells were plated at 1×10^5 cells in 96-well plates. NALM-6 cells were added at the indicated ratios. Following 16 hours of incubation at 37°C, NK and NALM-6 cells were collected and assessed by flow-cytometry. BV421 or PE-Vio770-conjugated anti-CD19 with GFP expression were used for target cells exclusion. NK-cells (CD19-/GFP-) were evaluated by BV605-conjugated anti-CD314 (NKG2D), PE-Cy7-conjugated anti-CD226 (DNAM), APC-conjugated anti-CD96 (TACTILE). For Ligands expression detection, NALM-6 cells were plated at 1×10^5 cells in 96-well plates. NK-cells were added at the indicated ratios. Following 16 hours of incubation at 37°C, NK and NALM-6 cells were collected and assessed by flow-

cytometry. BV421 or PE-Vio770-conjugated anti-CD19 with GFP expression were used for target cells selection. NALM-6 siCtrl or siChe-1 (CD19+/GFP+) were evaluated by PE-Vio615-conjugated anti-CD111 (Nectin-1), APC-conjugated anti-CD112 (Nectin-2) and AlexaFluor-647-conjugated anti-CD155 (PVR).

NK-cells degranulation assay

For degranulation assay NK-cells were plated at 1×10^5 cells/well in 96-wells plates. NALM-6 cells were added at the indicated ratio and incubated for 3 hours. After one hour the cells were treated with Golgi Stop (BD Biosciences, CA-USA). Thereafter, cells were labeled with PE-Vio770-conjugated anti-CD19, and BV421-conjugated anti-CD107a antibody (BD Biosciences, California, USA) for 20 min at 4°C, followed by flow-cytometric analysis. For intra-cytoplasmatic evaluation of IFNγ and TNFα, cells were fixed and permeabilized with Fix/perm buffer (eBioscience, ThermoFisher scientific, IT) and then labeled with PE-Conjugated anti-IFNγ and PE-Vio770-conjugated anti-TNFα, BUV786-conjugated anti-CD16, APC-conjugated anti-CD45 for 20min at 4°C.

Transgenic mouse strain generation

All animal studies were approved by the Institutional Animal Care of the Regina Elena National Cancer Institute and by the Government Committee of National Minister of Health and were conducted according with EU Directive 2010/63/EU for animal experiments.

To generate Eμ-Che-1 transgenic mice (C57Bl/6xDBA2 strain) Che-1 was fused to an immunoglobulin enhancer Eμ. After genomic DNA extraction of tail biopsies, the positive founder animals were identified by PCR using the following primers specific for the transgenes:

oligonucleotide up: 5'-CTTCATACCATCCTCTGTGCTTC-3'

oligonucleotide down: 5'-GCTTTTCTAGAGGTGG TTTTGC -3'

Eμ-Che-1 transgenic mice were interbred with MITO-Luc reporter mice (46) to obtain Eμ-Che-1/MITO-Luc (MITO/Che1+/+).

After genomic DNA extraction of tail biopsies, the positive founder animals were identified by PCR using the following primers specific for the transgenes:

oligonucleotide up: 5'-TGTAGACAAGGAAACAACAAA-GCCTGGTGGCC-3'

oligonucleotide down: 5'-GGCGTCTTCCATTTTACC AACAG-TACCGG-3'

MITO/Che+/+ and MITO/Che1+/- used as negative control were subjected to longitudinal *in vivo* imaging sessions at 11 weeks of age.

In vivo imaging

For *in vivo* Bioluminescence imaging (BLI), mice were anesthetized and 75 mg/kg of d-luciferin (Caliper Life Sciences, PerkinElmer, USA) was injected intra-peritoneally. Ten minutes later, quantification of light emission was acquired for 5 min. Signal was detected using the IVIS Lumina II CCD camera system and analyzed with the Living Image2.20 software package (Caliper Life Sciences, PerkinElmer, USA). Photon emission was measured in specific regions of interest (ROIs). Data were expressed as photon/second/cm2/steradiant (p/s/cm2/sr). The intensity of bioluminescence was color coded for imaging purposes; the scale used in each experiment is reported in each figure.

NK-cells extraction from murine spleen

Murine spleen cells were extracted from MITO/Che1+/+ and MITO/Che1+/- mouse models, and mononuclear cells were obtained from murine spleen cells using FICOLL method. The expression of Murine NK receptors were evaluated through flow-cytometric analysis. We analyzed NK-cells selecting CD3-/CD19- using FITC-conjugated anti-CD19 and BUV395-conjugated anti-CD3. Then from CD3-/CD19- cells we selected NK1.1 positive cells using APC-vio770-Conjugated anti-NK1.1. Murine NK cells were evaluated for NKG2D and DNAM expression using APC-conjugated anti-NKG2D and BV711-conjugated anti-DNAM.

For murine NK activity we selected NK-cells through the same gating strategy used for NK receptor evaluation. NK-cells activity was evaluated using CD27 and CD11b expression using PE-conjugated anti-CD27 and PE-cy7-conjugated anti-CD11b antibodies..

Statistical analysis

All statistical tests were carried out using GraphPad Prism version 5.0 for Windows, GraphPad Software, San Diego California, USA (www.graphpad.com). Probability values generated by Student's t-test considered to be statistically significant are *P ≤ 0.05; **P ≤ 0.01; ***P ≤ 0.001

Results

Che-1 transcriptionally controls Nectin-1 expression

In order to find evidence of Che-1 involvement in anti-tumor immune response, we analyzed the Chromatin immune-precipitation-sequencing (ChIP-seq) data (38) obtained in the primary BCP-ALL cell line (LAL-B), to identify a possible enrichment of Che-1 on the promoter sequence of genes belonging to immune check-point regulation. Data analysis revealed the presence of Che-1 on Nectin-1 promoter (Figure 1A) as confirmed by ChIP-assay performed in LAL-B cell line and in NALM-6, another BCP-ALL cell line (Figure 1B). To understand the mechanism of regulation between the two molecules, we down-modulated the expression of Che-1 for 72 hours in the LAL-B and NALM-6 cell lines (Figure 1C left panel) and evaluated Nectin-1

10.3389/fimmu.2023.1191908

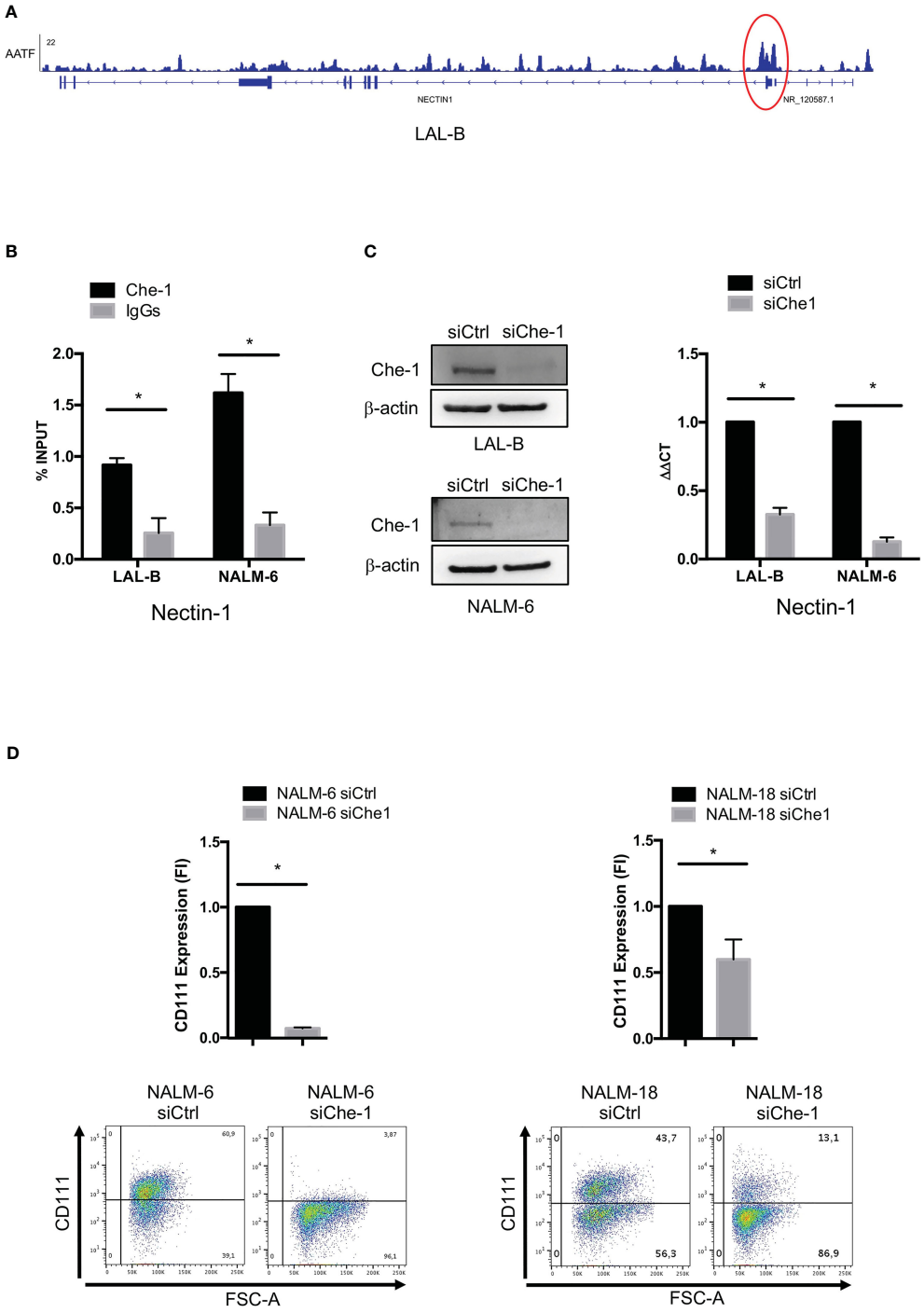

FIGURE 1
Che-1 transcriptionally controls Nectin-1 (CD111) expression. **(A)** Genome Browser screenshot of ChIP-seq signal on Nectin-1 promoter extracted by ChIP-seq assay previously performed in LAL-B cell line (38). **(B)** ChIP assay performed in LAL-B and NALM-6 cell lines showing Che1 enrichment on Nectin-1 promoter. **(C)** Left: Western Blot for Che-1 expression in LAL-B and NALM-6 cell lines upon Che-1 interference. Right: Real-time-PCR for Nectin-1 sequence in LAL-B and NALM-6 cells interfered with Che-1 expression. **(D)** Nectin-1 (CD111) evaluation by flow cytometry in NALM-6 and NALM-18 cell lines transduced with siChe-1 or siCTRL lentiviral vector (n=3); Graph: flow-cytometry of CD111 expression in one representative plot of CD111 expression out of 3 performed. (*P ≤ 0.05; **P ≤ 0.01; ***P ≤ 0.001).

gene modulation. We found that Nectin-1 resulted down-regulated upon 72 hours of Che-1 interference (Figure 1C right panel). In NALM-6 cell line, by lentiviral transduction, we inhibited Che-1 expression (NALM-6 siChe-1)as shown in Supplementary Figure 1A, and analyzed the surface expression of Nectin-1 protein by flow-cytometry analysis. We show that Che-1 interference resulted in Nectin-1 down-modulation, when compared with the controls in which cells were transduced with non-target lentiviral vector (NALM-6 siCtrl). The same result was obtained in NALM-18 BCP-ALL cell line (Figure 1D). These data

confirm that Che-1 sustains its tumorigenic function also by controlling the immune check-point ligands expression on blast cell membrane.

Che-1 overexpression impairs NK-cell killing activity

Since Nectin-1 appears to play an increasing role in tumor immune response (47), we studied its mechanism of action by analyzing NK-cell function. We performed co-culture experiments of NK-cells obtained from peripheral blood of healthy donors with NALM-6 siChe-1 cells or NALM-6 siCtrl cells, as negative control. Cytotoxicity assay demonstrated that NK-cells showed a reduced killing activity when in co-culture with Che-1-overexpressing NALM-6 cell line that is rescued when in co-culture with Che-1-depleted cell line (Figure 2A). Degranulation assay, performed by evaluating CD107a expression on NK-cells, confirmed that Che-1 silenced cells resulted more susceptible to NK-cell degranulation activity when compared with the control condition. Of note, this occurred also at 5:1 and 2,5:1 Effector: Target (E:T) ratio in which NK-cells are quantitatively favored (Supplementary Figure 2A). We further investigated whether this phenomenon reflected an increased capability of NK-cells of releasing effector molecules (IFNγ and TNFα) under the same experimental conditions. Flow-cytometry analysis revealed that the intracellular amount of these two cytokines was significantly increased after co-culture with Che-1 down-regulated cells as compared to the control one (Figure 2B). To deeper understand the effect exerted by Che-1 on NK-cell function, we measured NK proliferation by p-Erk1/2 expression. After a 24-hour co-culture with NALM-6-siCtrl, NK-cell proliferation was strongly reduced if compared with siChe-1 condition where p-Erk1/2 comes-back to the level expressed by NK-cell cultured alone. In addition p21, used as marker of cell cycle arrest, showed high expression level in NK-cells co-cultured with NALM-s siCtrl if compared with siChe condition, confirming the control exerted by Che-1 overexpressing cells on NK-cells proliferation (Figure 2C). In order to better understand the mechanism of action responsible of this functional effect, we performed longer co-culture experiments (16 hours), to study the expression of ligands either in the presence or in the absence of Che-1.

As shown in Figure 2D, in siChe-1 experimental condition, we confirmed that Nectin-1 expression was reduced after 16h of co-culture. Conversely, Nectin-2 expression was increased (Figure 2E), suggesting a possible mechanism of compensation in the blast cells. This is supported by the known trans-interaction mechanism occurring among the Nectin family members (48). Our hypothesis was that up-regulation of Nectin-2 could result in binding of DNAM-1 receptor on NK-cells leading to their activation. This hypothesis is also supported by the lower expression of PVR on siChe-1 cells (Figure 2F). A second interesting effect was observed in the modulation of ULBP molecules on siChe-1 cells. In particular, among the members of ULBP family, we observed in NALM-6 siChe-1 cells an increase of ULBP4 expression (Figure 2G) (49), while ULBP1, 2, 5, 6 were down-modulated (Supplementary Figures 2B, C). Therefore, data on ligand modulation revealed that Che-1 can re-modulate ligand expression on blast cell membrane through the transcriptional inhibition of Nectin-1.

NKG2D and DNAM-1 receptors are involved in Che-1-driven NK-cells inhibition

The modulation of ligand expression due to Che-1 interference prompted us to investigate also the possible effect exerted on NK-cell receptor expression and function. Starting from the paired Nectin-1 receptor, TACTILE, we observed an increase in the level of expression of TACTILE on NK-cells co-cultured with siChe-1 cells probably due to siChe-1-dependent reduced expression of its preferred ligand, Nectin-1 (Figure 3A).

In addition, based on the previous result (Figure 2E) in which PVR expression was impaired in NK-cells co-cultured with siChe-1 NALM-6, we also assessed DNAM-1 expression on NK-cells. Notably, DNAM-1 expression was not modified by Che-1 expression modulation (Figure 3B). This result could be due to a strong up-regulation of Nectin-2 (Figure 2E) occurring upon siChe-1-mediated Nectin-1 inhibition. Similarly to TACTILE, also NKG2D expression was increased on NK-cells upon 16 hours of co-culture with NALM-6 siChe-1 as compared to control cells (Figure 3C). The others NK receptors belonging to the NCR family (NKp30, NKp44 and NKp46) are not affected as shown in Supplementary Figures 3A–C.

To further understand whether these two pathways could be responsible of NK-cell re-activation after Che-1 depletion, we evaluated the NK-cell cytolytic activity under the same previous experimental conditions, either in the presence or in the absence of NKG2D and DNAM-1 monoclonal antibodies (mAbs). These masking mAbs are able to block the interactions between NK activating receptors and their ligands (20, 50). As shown in Figure 3D, mAb-mediated masking of DNAM-1 or NKG2D inhibited NK-cell degranulation against siChe-1 NALM-6 cell line. These results suggest that Che-1 exerts its inhibitory function on the immune response by affecting the two principal pathways sustaining NK-cell cytolytic activity.

Che-1-dependent NKG2D and DNAM-1 down-modulation *in vivo*

In order to investigate the physiological effect of Che-1 over-expression, we generated a transgenic model where Che-1 was fused with an immunoglobulin enhancer (Eμ), to select the B-cell compartment. Figure 4A shows that Che-1 is expressed in two out of nine clones. Taking advantage of the MITO-luc reporter mouse model, previously generated in our lab (46), we crossed them with the EμChe-1 transgenic model with the aim to obtain mice over-expressing Che-1 in the lymphoid organs using a system that allows to monitor cellular proliferation. As expected, MITO/Che-$1^{+/+}$ mice showed high proliferation rate monitored as spleen

10.3389/fimmu.2023.1191908

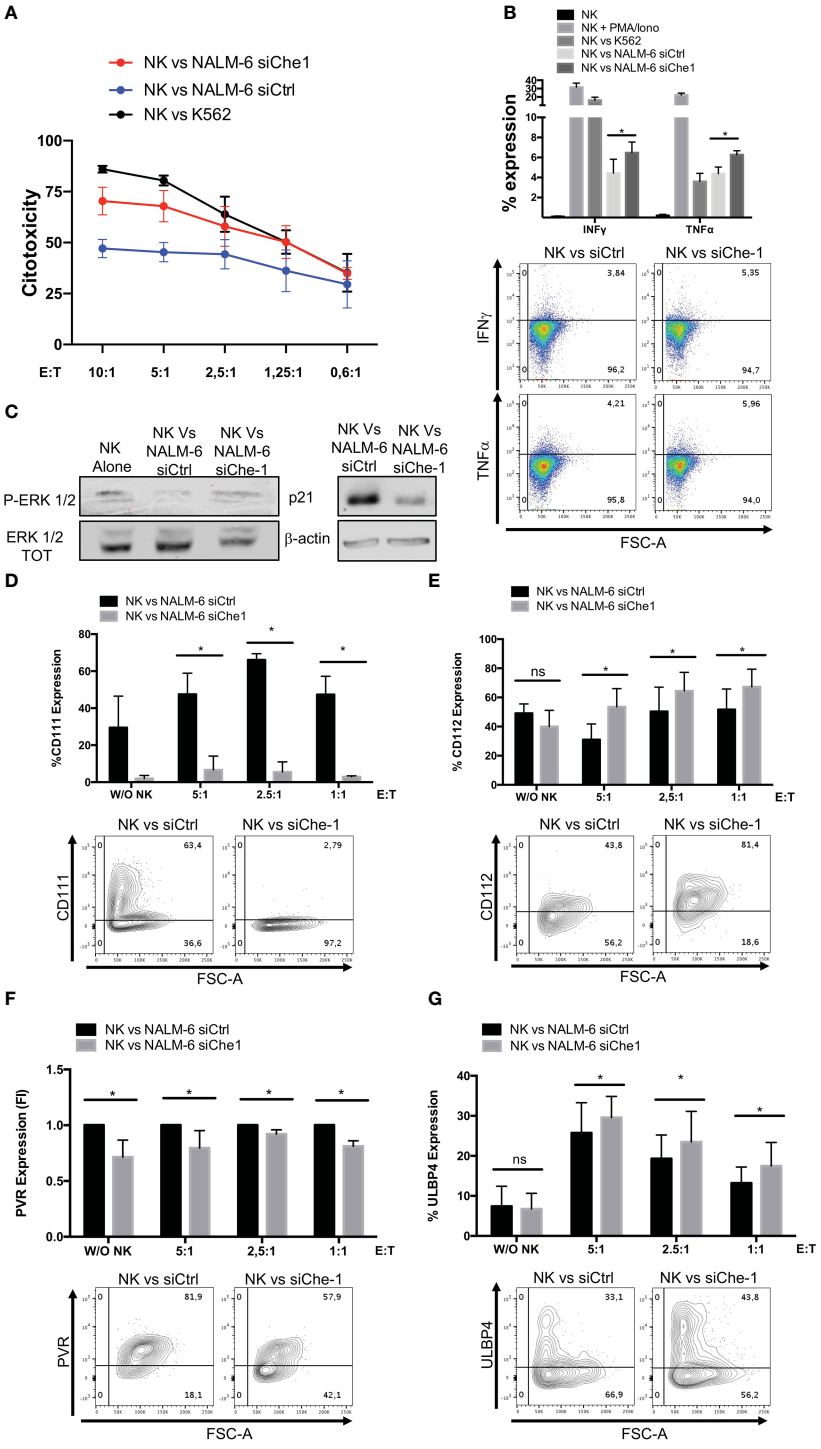

FIGURE 2
Che-1-dependent Nectin-1 down-modulation modifies NK-cell ligand expression. **(A)** Citotoxicity assay of NK-cells (CD19-/GFP-) after a 4-hours-culture with NALM-6 siCtrl or siChe-1 at different Effector : Target (E:T) ratio (10:1, 5:1, 2,5:1, 1,25:1, 0,6:1) (n=3). K562 cell line used as positive control condition **(B)** Graph: flow-cytometry of intra-cytoplasmatic IFNγ and TNFα % of expression in NK-cells co-cultured for 4 hours with NALM-6 siCtrl or siChe-1 E:T 1:1 (n=3). NK-cells alone, stimulated with PMA/Ionomycin (PMA 25ng/ml; Ionomycin 1μg/ml) and co-cultured with K562 were used as control conditions. One representative plot of IFNγ and TNFα expression out of 3 performed. **(C)** One representative p-Erk 1/2 and p21 WB of 3 performed in NK-cells sorted upon 24 hours of co-culture with NALM-6 siCtrl and siChe-1. NK-cell alone sample was used as p-Erk 1/2 basal level. Anti-Erk 1/2 Total (TOT) and anti Actin antibodies were used as loading control. **(D)** Graph: flow cytometry of CD111 (CD19+/GFP+) after a 16-hour co-culture with NK-cells at different E:T ratio (5:1, 2,5:1, 1:1) (n=3). One representative plot of CD111 expression out of 3 performed. Basal CD111 expression was measured in w/o NK cell condition **(E)** Graph: CD112 evaluation by flow-cytometry of NALM-6 siCtrl and siChe-1 (CD19+/GFP+) after a 16-hour co-culture with NK-cells at different E:T ratio (5:1, 2,5:1, 1:1) (n=3). One representative plot of CD112 expression out of 3 performed. Basal CD112 expression was measured in w/o NK cell condition **(F)** Graph: flow-cytometry of NALM-6 siCtrl and siChe-1 (CD19+/GFP+) after a 16-hour co-culture with NK-cells at different E:T ratio (5:1, 2,5:1, 1:1) (n=3). One representative plot of PVR expression out of 3 performed. Basal PVR expression was measured in w/o NK cell condition **(G)** Graph: flow-cytometry of ULBP4 of NALM-6 siCtrl and siChe-1 (CD19+/GFP+) after a 16-hour co-culture with NK-cells at different E:T ratio (5:1, 2,5:1, 1:1) (n=3). One representative plot of ULBP4 expression out of 3 performed. Basal ULBP4 expression was measured in w/o NK cell condition. (*P ≤ 0.05; **P ≤ 0.01; ***P ≤ 0.001; ns, not significant).

10.3389/fimmu.2023.1191908

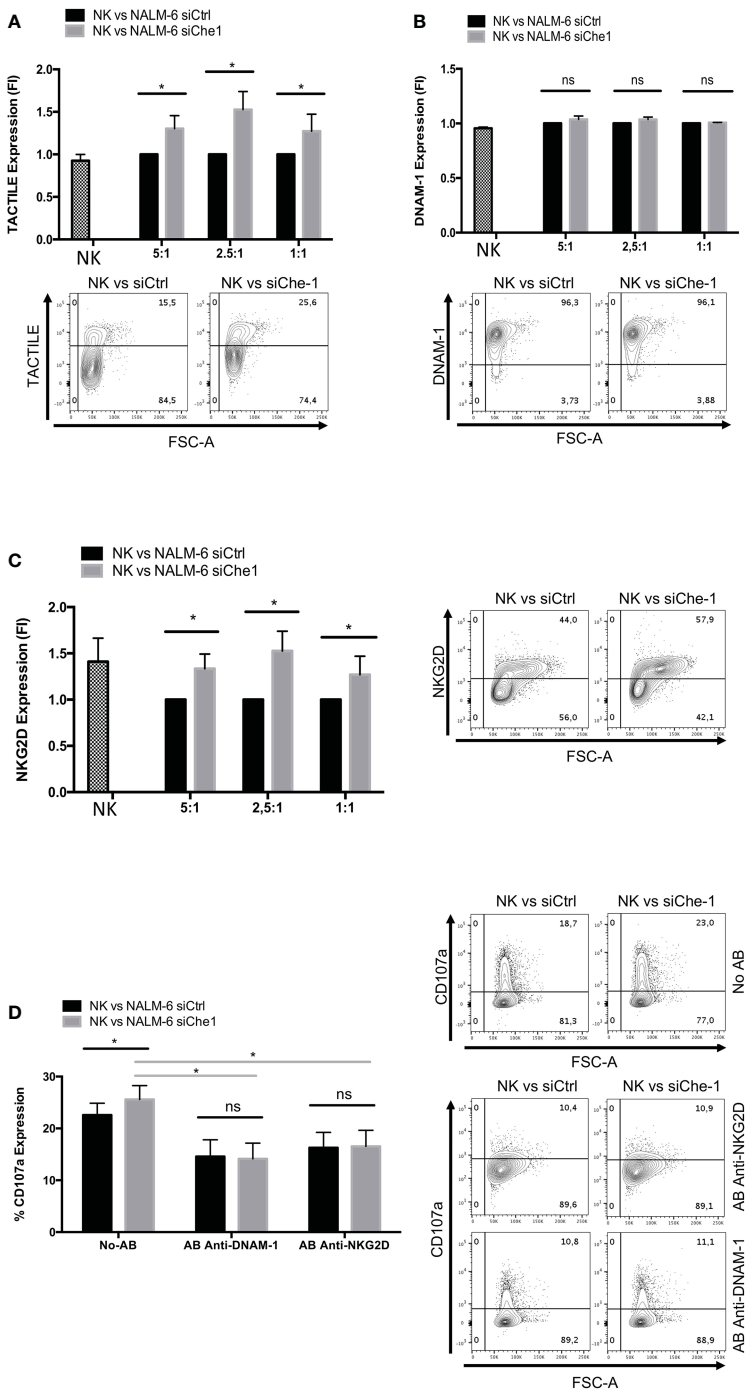

FIGURE 3
NKG2D and DNAM-1 NK receptors are induced when in co-culture with Che-1 interfered cells. **(A)** Graph: flow-cytometry of TACTILE expression, measured as Fold of Induction (FI), of NK-cells (CD19-/GFP-) after a 16-hour co-culture with NALM-6 siCtrl and siChe-1 NK-cells at different E:T ratio (5:1, 2,5:1, 1:1) (n=3). One representative plot of TACTILE expression out of 3 performed. Basal TACTILE expression was measured in NK alone condition **(B)** Graph: of DNAM-1 expression, measured as FI of in flow-cytometry NK-cells (CD19-/GFP) after a 16-hour co-culture with NALM-6 siCtrl and siChe-1 NK-cells at different E:T ratio (5:1, 2,5:1, 1:1) (n=3). One representative plot of DNAM-1 expression out of 3 performed. Basal DNAM-1 expression was measured in NK alone condition **(C)** Graph: NKG2D expression by flow-cytometry measured as FI in NK-cells (CD19-/GFP-) after 16-hour of co-culture with NALM-6 siCtrl and siChe-1 NK-cells at different E:T ratio (5:1, 2,5:1, 1:1) (n=3). One representative plot of NKG2D expression out of 3 performed. Basal NKG2D expression was measured in NK alone condition **(D)** Graph: CD107a evaluation by flow-cytometry of NK-cells (CD19-/GFP-) after a 4 hours of co-culture with NALM-6 siCtrl or siChe-1 at 1:1 E:T ratio in presence of anti-NKG2D or anti-DNAM-1 masking antibodies, respectively, to block interaction with their ligands. (n=3). One Representative plot of CD107a expression of 3 performed. (*P ≤ 0.05; **P ≤ 0.01; ***P ≤ 0.001; ns, not significant).

10.3389/fimmu.2023.1191908

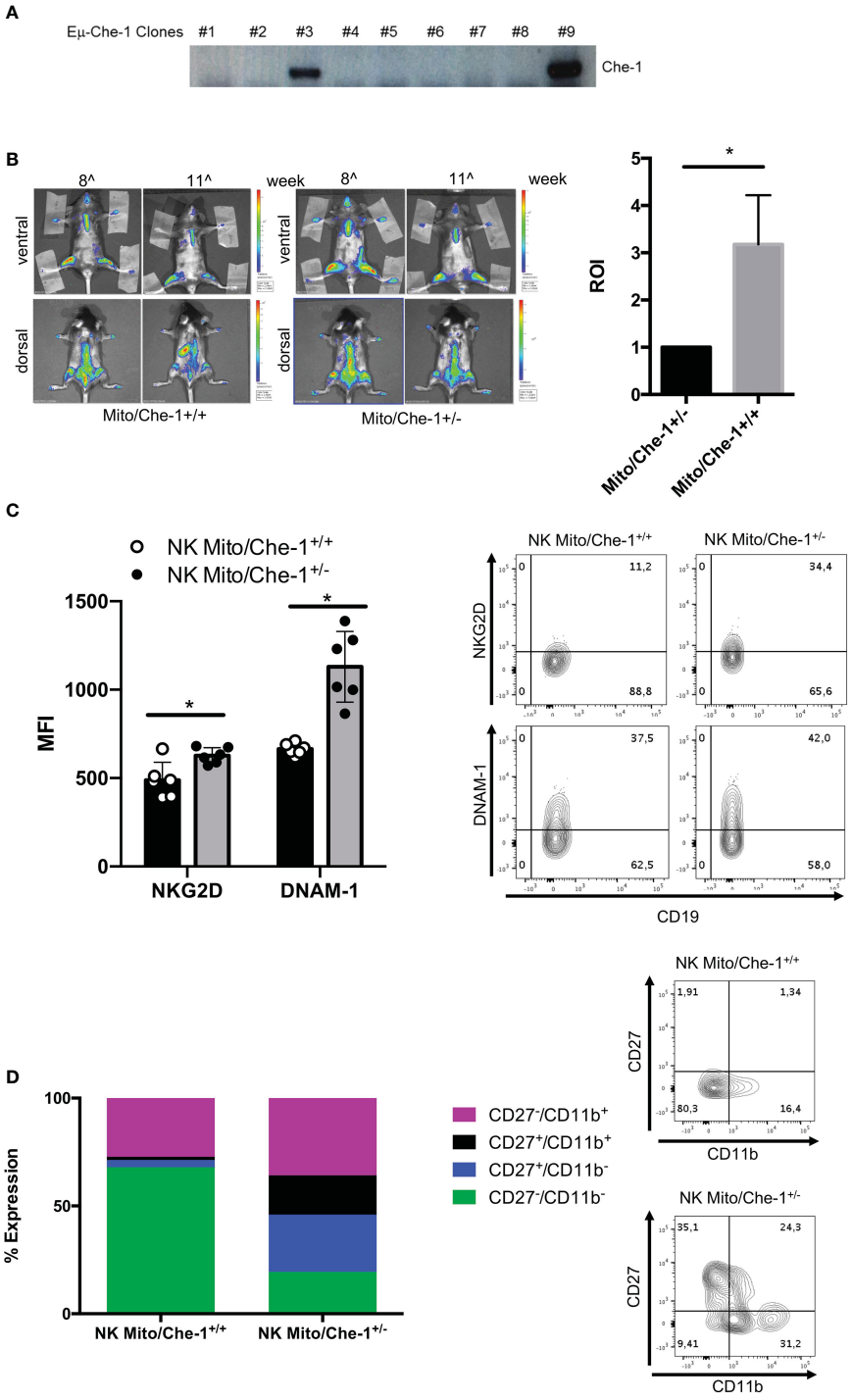

FIGURE 4
In vivo evaluation of Che-1-dependent NK inactivation. **(A)** PCR showing genotyping of Eμ-Che-1 transgenic mice. **(B)** Left: Bio-imaging of MITO/Che-$1^{+/+}$ and MITO/Che-$1^{+/-}$ mice at 11 weeks of age (n=6). Right: graph quantifies spleen luminescence at week 11 (n=6). **(C)**. % of expression of NKG2D and DNAM-1 in NK-cells extracted from spleens of MITO/Che-$1^{+/+}$ and MITO/Che-$1^{+/-}$ mice at week 11 by flow-cytometry (n=3). One representative plot of both receptors out of 3 performed. **(D)** CD27/CD11b evaluation in spleen-derived NK cells: $CD27^-/CD11b^+$ used to detect cytolytic compartment; $CD27^+/CD11b^-$ and $CD27^+/CD11b^+$ for the cytokine production compartment; $CD27^-/CD11b^+$ to measure the maturation status (n=3). One representative plot of the 3 subgroups out of three performed. *P ≤ 0.05; **P ≤ 0.01; ***P ≤ 0.001.

luminescence demonstrating that Che-1 is strongly involved in B-cell proliferation even in a non-tumoral context. Conversely, MITO/Che-$1^{+/-}$ mice, not carrying Che-1 overexpression, showed a sharply reduced proliferation rate and were used as negative control (Figure 4B). In addition, we evaluated the relation between Che-1 over-expression and NK-cells in this *in vivo* setting where the MITO-Luc system allows to monitor the hyper-proliferative status due to Che-1 overexpression. Figure 4C shows that spleen-derived

NK-cells from MITO/Che-1$^{+/-}$ display higher NKG2D and DNAM-1 expression as compared with MITO/Che-1$^{+/+}$ mice, thus confirming the *in vitro* data using human NK-cells. Furthermore, assessment of the murine NK-cell activation status through the analysis of CD27/CD11b expression (51) revealed that in the MITO/Che-1$^{+/+}$ mice the NK-cells were poorly activated as compared to MITO/Che-1$^{+/-}$ mice (Figure 4D). Indeed, both CD27^{-}/CD11b^{+} cytolytic NK-cells and CD27^{+} CD11b^{+} or CD11b^{-} NK-cells (mainly releasing cytokines) were reduced in MITO/Che-1$^{+/+}$ mice. These data confirm the *in vitro* data, showing a reduced NK-cell activation when co-cultured with Che-1 overexpressing cells. In conclusion, the population of immature NK-cells identified by CD27^{-}/CD11b^{-} is higher in MITO/Che-1$^{+/+}$ mice than in MITO/Che-1$^{+/-}$ mice, suggesting that Che-1 overexpression exerts a control on NK-cell development and function.

Discussion

There is increasing evidence regarding the Che-1 over-expression in tumors and its pivotal role in the transcriptional machinery to cooperate in tumorigenic pathways (39, 41). Che-1 characterization in hematological tumors of adults like multiple myeloma, and of pediatric ones such as BCP-ALL was recently defined. In a previous work (38) we demonstrated that Che-1 over-expression is a crucial inducer of blast cell proliferation. We showed that Che-1 is a member of the c-Myc controlled oncogenic pathway and its down-regulation can interfere with c-Myc-dependent regulation of BCP-ALL tumorigenesis. Despite the numerous experimental evidences of the tumorigenic role of Che-1, the effect of its over-expression on the tumor microenvironment has not been investigated. Data obtained by ChIP-seq experiments in a primary BCP-ALL cell line captured our attention showing Che-1 connection with molecules involved in immune response. The discovery of Che-1 enrichment on Nectin-1 promoter suggested to further investigate its mechanism of action. Since NK-cells represent a first line of defenses against tumor growth and metastasis, it is important to study mechanisms which may interfere with anti-tumor immune responses to allow the development of new immunotherapeutic strategies able to rescue anti-tumor function.

This study demonstrates a new mechanism through which tumor cells may increase their ability to escape immune surveillance by modifying the interactions between ligands on tumor cells and the corresponding receptors on NK-cells. The role of Nectin-1 in the tumor context is still poorly investigated; however, we demonstrated that silencing of Che-1 on tumor cells resulted in down-regulation of Nectin-1, while inducing Nectin-2 overexpression as a result of the heterophilic trans-interaction occurring among Nectin family members. We speculate that this effect may be the starting point of a recalibrated ligand expression pattern able to modulate activating NK receptors and, as a consequence, NK-cell anti-tumor activity. The recruitment of NK-cells is attractive in cancer treatment and a key function of NK-cell therapy is widely appreciated as the therapeutic targeting of NK-cell ligands. In addition, regarding the paucity in healthy tissues, ligands for activating NK receptors may represent valid target antigens on malignant cells for antibody-based approaches. The blockade of the interactions between NKG2D and its ligands could lead to reduced anti-tumor response. In support of these results, our *in vivo* experiments confirm a reduced expression of activating receptors on NK-cells from Che-1 transgenic mice. These cells exhibit an impaired activation and a preferential immature status.

Our study demonstrates that Che-1 is upstream of the mechanism orchestrating the re-modulation of NK-ligand expression, thus proposing Che-1 as an efficient bi-specific target able to affect tumor cell viability and, at the same time, to favor NK-mediated immune responses. The difficulty encountered in the last years to develop an approach able to target Che-1 in view of its nuclear localization could now be overcome by the delivery of CRISPR/Cas-9 RNP complex to down-regulate its expression (52). Delivery through gold-nanoparticles is able to guarantee tumor cell entrance in solid and hematological cancers allowing the validation of the system's efficacy in pre-clinical murine tumor models.

Data availability statement

The original contributions presented in the study are included in the article/Supplementary Material, further inquiries can be directed to the corresponding author/s.

Ethics statement

The animal study was reviewed and approved by the Institutional Animal Care of the Regina Elena National Cancer Institute and by the Government Committee of National Minister of Health and were conducted according with EU Directive 2010/63/EU for animal experiments.

Author contributions

MC and NT conceived and performed the experiments, analyzed the data and contributed to the drafting of the manuscript. CS, SI, IM, GS and SG conceived and performed the experiments and analyzed the data. GP, EM, MF and LM contributed to the study design and provided intellectual input; VF and PV conceived the study, designed the experiments and drafted the manuscript. FL provided intellectual input, analyzed the data, supervised study conduction and critically revised the manuscript. All authors contributed to the article and approved the submitted version.

Funding

This work was supported by Fondazione Associazione Italiana per la Ricerca sul Cancro (MFAG-ID 20098 to VF; 5x1000-ID

21147 to LM); Italian Ministry of Health with Current Research Funds 2023 to VF.

Acknowledgments

We are grateful to Dr. Daniela Pende who kindly provided F5 (anti-DNAM-1 IgM) and to Dr Loredana Cifaldi for inspiring discussion of experimental data.

Conflict of interest

The authors declare that the research was conducted in the absence of any commercial or financial relationships that could be construed as a potential conflict of interest.

Publisher's note

Supplementary material

The Supplementary Material for this article can be found online at: https://www.frontiersin.org/articles/10.3389/fimmu.2023.1191908/full#supplementary-material

SUPPLEMENTARY FIGURE 1
Che-1 depletion by lentiviral transduction. **(A)** WB analysis of NALM-6 and NALM-18 cell lines transduced with siCtrl or siChe-1 sequences-carrying lentiviral plasmids to inhibit Che-1 expression. Gapdh antibody was used as loading control.

SUPPLEMENTARY FIGURE 2
siChe-1-dependent CD107a and ULBP family members modulation. **(A)** CD107a expression of NK-cells (CD19-/GFP-) by flow cytometry after a 4-hours-culture with NALM-6 siCtrl or siChe-1 at different Effector : Target (E:T) ratio (n=3). One Representative plot of CD107a expression of 3 performe. NK alone, Nk-cells stimulated with PMA/Ionomycyn and co-cultured were used as control cinditions (Left) (**B** Graph: flow-cytometry of ULBP1 expression of NALM-6 siCtrl and siChe-1 (CD19+/GFP+) after 16 hours of co-culture with NK-cells at different E:T ratio (n=3). One representative plot of ULBP1 expression out of 3 performed. Basal ULBP1 expression was measured in w/o NK cell condition **(C)** Graph: flow-cytometry of ULBP2-5-6 expression of NALM-6 siCtrl and siChe-1 (CD19+/GFP+) after 16-hour co-culture with NK-cells at different E:T ratio (n=3). One representative plot of ULBP2-5-6 expression out of 3 performed. Basal ULBP2-5-6 expression was measured in w/o NK cell condition.

SUPPLEMENTARY FIGURE 3
Natural Citotoxicity Receptors (NCR) expression. **(A)** NKp30, **(B)** NKp44 and **(C)** NKp46 evaluation by flow cytometry of NK-cells(CD19-/GFP-) after a 16-hour co-culture with NALM-6 siCtrl and siChe-1 at different E:T ratio.

References

1. Beatty GL, Gladney WL. Immune escape mechanisms as a guide for cancer immunotherapy. *Clin Cancer Res* (2015) 21:687–92. doi: 10.1158/1078-0432.CCR-14-1860

2. Vinay DS, Ryan EP, Pawelec G, Talib WH, Stagg J, Elkord E, et al. Immune evasion in cancer: mechanistic basis and therapeutic strategies. *Semin Cancer Biol* (2015) 35(Suppl):S185–98. doi: 10.1016/j.semcancer.2015.03.004

3. Disis ML. Immune regulation of cancer. *J Clin Oncol* (2010) 28:4531–8. doi: 10.1200/JCO.2009.27.2146

4. Pastorczak A, Domka K, Fidyt K, Poprzeczko M, Firczuk M. Mechanisms of immune evasion in acute lymphoblastic leukemia. *Cancers (Basel)* (2021) 13:1536. doi: 10.3390/cancers13071536

5. Hunter R, Imbach KJ, Zhou C, Dougan J, Hamilton JAG, Chen KZ, et al. B-cell acute lymphoblastic leukemia promotes an immune suppressive microenvironment that can be overcome by IL-12. *Sci Rep* (2022) 12:11870–022. doi: 10.1038/s41598-022-16152-z

6. Kang SH, Hwang HJ, Yoo JW, Kim H, Choi ES, Hwang S, et al. Expression of immune checkpoint receptors on T-cells and their ligands on leukemia blasts in childhood acute leukemia. *Anticancer Res* (2019) 39:5531–9. doi: 10.21873/anticanres.13746

7. Malhotra A, Shanker A. NK cells: immune cross-talk and therapeutic implications. *Immunotherapy* (2011) 3:1143–66. doi: 10.2217/imt.11.102

8. Pende D, Marcenaro S, Falco M, Martini S, Bernardo ME, Montagna D, et al. Anti-leukemia activity of alloreactive NK cells in KIR ligand-mismatched haploidentical HSCT for pediatric patients: evaluation of the functional role of activating KIR and redefinition of inhibitory KIR specificity. *Blood* (2009) 113:3119–29. doi: 10.1182/blood-2008-06-164103

9. Carlsten M, Jaras M. Natural killer cells in myeloid malignancies: immune surveillance, NK cell dysfunction, and pharmacological opportunities to bolster the endogenous NK cells. *Front Immunol* (2019) 10:2357. doi: 10.3389/fimmu.2019.02357

10. Sportoletti P, De Falco F, Del Papa B, Baldoni S, Guarente V, Marra A, et al. NK cells in chronic lymphocytic leukemia and their therapeutic implications. *Int J Mol Sci* (2021) 22:6665. doi: 10.3390/ijms22136665

11. Paul S, Lal G. The molecular mechanism of natural killer cells function and its importance in cancer immunotherapy. *Front Immunol* (2017) 8:1124. doi: 10.3389/fimmu.2017.01124

12. Moretta L, Montaldo E, Vacca P, Del Zotto G, Moretta F, Merli P, et al. Human natural killer cells: origin, receptors, function, and clinical applications. *Int Arch Allergy Immunol* (2014) 164:253–64. doi: 10.1159/000365632

13. Sivori S, Pende D, Quatrini L, Pietra G, Della Chiesa M, Vacca P, et al. NK cells and ILCs in tumor immunotherapy. *Mol Aspects Med* (2021) 80:100870. doi: 10.1016/j.mam.2020.100870

14. Valipour B, Velaei K, Abedelahi A, Karimipour M, Darabi M, Charoudeh HN. NK cells: an attractive candidate for cancer therapy. *J Cell Physiol* (2019) 234:19352–65. doi: 10.1002/jcp.28657

15. Sivori S, Vacca P, Del Zotto G, Munari E, Mingari MC, Moretta L. Human NK cells: surface receptors, inhibitory checkpoints, and translational applications. *Cell Mol Immunol* (2019) 16:430–41. doi: 10.1038/s41423-019-0206-4

16. Viel S, Charrier E, Marcais A, Rouzaire P, Bienvenu J, Karlin L, et al. Monitoring NK cell activity in patients with hematological malignancies. *Oncoimmunology* (2013) 2:e26011. doi: 10.4161/onci.26011

17. Valenzuela-Vazquez L, Nunez-Enriquez JC, Sanchez-Herrera J, Medina-Sanson A, Perez-Saldivar ML, Jimenez-Hernandez E, et al. NK cells with decreased expression of multiple activating receptors is a dominant phenotype in pediatric patients with acute lymphoblastic leukemia. *Front Oncol* (2022) 12:1023510. doi: 10.3389/fonc.2022.1023510

18. Lee LJ, Hassan N, Idris SZ, Subbiah SK, Seow HF, Mohtaruddin N, et al. Differential regulation of NK cell receptors in acute lymphoblastic leukemia. *J Immunol Res* (2022) 2022:7972039. doi: 10.1155/2022/7972039

19. Gismondi A, Stabile H, Nisti P, Santoni A. Effector functions of natural killer cell subsets in the control of hematological malignancies. *Front Immunol* (2015) 6:567. doi: 10.3389/fimmu.2015.00567

20. Pende D, Spaggiari GM, Marcenaro S, Martini S, Rivera P, Capobianco A, et al. Analysis of the receptor-ligand interactions in the natural killer-mediated lysis of freshly isolated myeloid or lymphoblastic leukemias: evidence for the involvement of the poliovirus receptor (CD155) and nectin-2 (CD112). *Blood* (2005) 105:2066–73. doi: 10.1182/blood-2004-09-3548

21. Fan J, Shi J, Zhang Y, Liu J, An C, Zhu H, et al. NKG2D discriminates diverse ligands through selectively mechano-regulated ligand conformational changes. *EMBO J* (2022) 41:e107739. doi: 10.15252/embj.2021107739

22. Cho H, Chung J, Kim S, Braunschweig T, Kang TH, Kim J, et al. MICA/B and ULBP1 NKG2D ligands are independent predictors of good prognosis in cervical cancer. *BMC Cancer* (2014) 14:957–2407. doi: 10.1186/1471-2407-14-957

23. Shibuya A, Campbell D, Hannum C, Yssel H, Franz-Bacon K, McClanahan T, et al. DNAM-1, a novel adhesion molecule involved in the cytolytic function of T lymphocytes. *Immunity* (1996) 4:573–81. doi: 10.1016/s1074-7613(00)70060-4

24. Pende D, Bottino C, Castriconi R, Cantoni C, Marcenaro S, Rivera P, et al. PVR (CD155) and nectin-2 (CD112) as ligands of the human DNAM-1 (CD226) activating receptor: involvement in tumor cell lysis. *Mol Immunol* (2005) 42:463–9. doi: 10.1016/j.molimm.2004.07.028

25. de Andrade LF, Smyth MJ, Martinet L. DNAM-1 control of natural killer cells functions through nectin and nectin-like proteins. *Immunol Cell Biol* (2014) 92:237–44. doi: 10.1038/icb.2013.95

26. Velardi A, Ruggeri L, Alessandro, Moretta, Moretta L. NK cells: a lesson from mismatched hematopoietic transplantation. *Trends Immunol* (2002) 23:438–44. doi: 10.1016/s1471-4906(02)02284-6

27. Sivori S, Della Chiesa M, Carlomagno S, Quatrini L, Munari E, Vacca P, et al. Inhibitory receptors and checkpoints in human NK cells, implications for the immunotherapy of cancer. *Front Immunol* (2020) 11:2156. doi: 10.3389/fimmu.2020.02156

28. Duraivelan K, Samanta D. Emerging roles of the nectin family of cell adhesion molecules in tumour-associated pathways. *Biochim Biophys Acta Rev Cancer* (2021) 1876:188589. doi: 10.1016/j.bbcan.2021.188589

29. Cifaldi L, Doria M, Cotugno N, Zicari S, Cancrini C, Palma P, et al. DNAM-1 activating receptor and its ligands: how do viruses affect the NK cell-mediated immune surveillance during the various phases of infection? *Int J Mol Sci* (2019) 20:3715. doi: 10.3390/ijms20153715

30. Sanchez-Correa B, Valhondo I, Hassouneh F, Lopez-Sejas N, Pera A, Bergua JM, et al. DNAM-1 and the TIGIT/PVRIG/TACTILE axis: novel immune checkpoints for natural killer cell-based cancer immunotherapy. *Cancers (Basel)* (2019) 11:877. doi: 10.3390/cancers11060877

31. Pasero C, Gravis G, Granjeaud S, Guerin M, Thomassin-Piana J, Rocchi P, et al. Highly effective NK cells are associated with good prognosis in patients with metastatic prostate cancer. *Oncotarget* (2015) 6:14360–73. doi: 10.18632/oncotarget.3965

32. Lozano E, Mena M, Diaz T, Martin-Antonio B, Leon S, Rodriguez-Lobato L, et al. Nectin-2 expression on malignant plasma cells is associated with better response to TIGIT blockade in multiple myeloma. *Clin Cancer Res* (2020) 26:4688–98. doi: 10.1158/1078-0432.CCR-19-3673

33. Guzman G, Oh S, Shukla D, Valyi-Nagy T. Nectin-1 expression in the normal and neoplastic human uterine cervix. *Arch Pathol Lab Med* (2006) 130:1193–5. doi: 10.5858/2006-130-1193-NEITNA

34. Matsushima H, Utani A, Endo H, Matsuura H, Kakuta M, Nakamura Y, et al. The expression of nectin-1alpha in normal human skin and various skin tumours. *Br J Dermatol* (2003) 148:755–62. doi: 10.1046/j.1365-2133.2003.05225.x

35. Friedman GK, Bernstock JD, Chen D, Nan L, Moore BP, Kelly VM, et al. Enhanced sensitivity of patient-derived pediatric high-grade brain tumor xenografts to oncolytic HSV-1 virotherapy correlates with nectin-1 expression. *Sci Rep* (2018) 8:13930–018. doi: 10.1038/s41598-018-32353-x

36. Oshima T, Sato S, Kato J, Ito Y, Watanabe T, Tsuji I, et al. Nectin-2 is a potential target for antibody therapy of breast and ovarian cancers. *Mol Cancer* (2013) 12:60–4598. doi: 10.1186/1476-4598-12-60

37. Li M, Qiao D, Pu J, Wang W, Zhu W, Liu H. Elevated nectin-2 expression is involved in esophageal squamous cell carcinoma by promoting cell migration and invasion. *Oncol Lett* (2018) 15:4731–6. doi: 10.3892/ol.2018.7953

38. Folgiero V, Sorino C, Pallocca M, De Nicola F, Goeman F, Bertaina V, et al. Che-1 is targeted by c-myc to sustain proliferation in pre-b-cell acute lymphoblastic leukemia. *EMBO Rep* (2018) 19:e44871. doi: 10.15252/embr.201744871

39. Bruno T, Desantis A, Bossi G, Di Agostino S, Sorino C, De Nicola F, et al. Che-1 promotes tumor cell survival by sustaining mutant p53 transcription and inhibiting DNA damage response activation. *Cancer Cell* (2010) 18:122–34. doi: 10.1016/j.ccr.2010.05.027

40. Desantis A, Bruno T, Catena V, De Nicola F, Goeman F, Iezzi S, et al. Che-1-induced inhibition of mTOR pathway enables stress-induced autophagy. *EMBO J* (2015) 34:1214–30. doi: 10.15252/embj.201489920

41. Bruno T, Valerio M, Casadei L, De Nicola F, Goeman F, Pallocca M, et al. Che-1 sustains hypoxic response of colorectal cancer cells by affecting hif-1alpha stabilization. *J Exp Clin Cancer Res* (2017) 36:32–017. doi: 10.1186/s13046-017-0497-1

42. Passananti C, Floridi A, Fanciulli M. Che-1/AATF, a multivalent adaptor connecting transcriptional regulation, checkpoint control, and apoptosis. *Biochem Cell Biol* (2007) 85:477–83. doi: 10.1139/O07-062

43. Fanciulli M, Bruno T, Di Padova M, De Angelis R, Iezzi S, Iacobini C, et al. Identification of a novel partner of RNA polymerase II subunit 11, che-1, which interacts with and affects the growth suppression function of Rb. *FASEB J* (2000) 14:904–12. doi: 10.1096/fasebj.14.7.904

44. Bruno T, De Nicola F, Iezzi S, Lecis D, D'Angelo C, Di Padova M, et al. Che-1 phosphorylation by ATM/ATR and Chk2 kinases activates p53 transcription and the G2/M checkpoint. *Cancer Cell* (2006) 10:473–86. doi: 10.1016/j.ccr.2006.10.012

45. Wiznerowicz M, Trono D. Conditional suppression of cellular genes: lentivirus vector-mediated drug-inducible RNA interference. *J Virol* (2003) 77:8957–61. doi: 10.1128/jvi.77.16.8957-8951.2003

46. Goeman F, Manni I, Artuso S, Ramachandran B, Toietta G, Bossi G, et al. Molecular imaging of nuclear factor-y transcriptional activity maps proliferation sites in live animals. *Mol Biol Cell* (2012) 23:1467–74. doi: 10.1091/mbc.E12-01-0039

47. Chan CJ, Andrews DM, Smyth MJ. Receptors that interact with nectin and nectin-like proteins in the immunosurveillance and immunotherapy of cancer. *Curr Opin Immunol* (2012) 24:246–51. doi: 10.1016/j.coi.2012.01.009

48. Samanta D, Ramagopal UA, Rubinstein R, Vigdorovich V, Nathenson SG, Almo SC. Structure of nectin-2 reveals determinants of homophilic and heterophilic interactions that control cell-cell adhesion. *Proc Natl Acad Sci USA* (2012) 109:14836–40. doi: 10.1073/pnas.1212912109

49. Xu Y, Zhou L, Zong J, Ye Y, Chen G, Chen Y, et al. Decreased expression of the NKG2D ligand ULBP4 may be an indicator of poor prognosis in patients with nasopharyngeal carcinoma. *Oncotarget* (2017) 8:42007–19. doi: 10.18632/oncotarget.14917

50. Bottino C, Castriconi R, Pende D, Rivera P, Nanni M, Carnemolla B, et al. Identification of PVR (CD155) and nectin-2 (CD112) as cell surface ligands for the human DNAM-1 (CD226) activating molecule. *J Exp Med* (2003) 198:557–67. doi: 10.1084/jem.20030788

51. Chiossone L, Chaix J, Fuseri N, Roth C, Vivier E, Walzer T. Maturation of mouse NK cells is a 4-stage developmental program. *Blood* (2009) 113:5488–96. doi: 10.1182/blood-2008-10-187179

52. Cheng Q, Xia J, Wang K, Zhang Y, Chen Y, Zhong Q, et al. CRISPR/Cas9 ribonucleoprotein (RNP) complex enables higher viability of transfected cells in genome editing of acute myeloid cells. *Ann Transl Med* (2022) 10:862–22. doi: 10.21037/atm-22-3279

Frontiers in Immunology

Explores novel approaches and diagnoses to treat immune disorders.

The official journal of the International Union of Immunological Societies (IUIS) and the most cited in its field, leading the way for research across basic, translational and clinical immunology.

Discover the latest Research Topics

See more →

Frontiers

Avenue du Tribunal-Fédéral 34
1005 Lausanne, Switzerland
frontiersin.org

Contact us

+41 (0)21 510 17 00
frontiersin.org/about/contact